

Topics in Current Chemistry Collections

Chunhai Fan
Yonggang Ke *Editors*

DNA Nanotechnology

From Structure to Functionality

 Springer

Topics in Current Chemistry Collections

Journal Editors

Massimo Olivucci, Siena, Italy and Bowling Green, USA

Wai-Yeung Wong, Hong Kong, China

Series Editors

Hagan Bayley, Oxford, UK

Greg Hughes, Codexis Inc, USA

Christopher A. Hunter, Cambridge, UK

Seong-Ju Hwang, Seoul, South Korea

Kazuaki Ishihara, Nagoya, Japan

Barbara Kirchner, Bonn, Germany

Michael J. Krische, Austin, USA

Delmar Larsen, Davis, USA

Jean-Marie Lehn, Strasbourg, France

Rafael Luque, Córdoba, Spain

Jay S. Siegel, Tianjin, China

Joachim Thiem, Hamburg, Germany

Margherita Venturi, Bologna, Italy

Chi-Huey Wong, Taipei, Taiwan

Henry N.C. Wong, Hong Kong, China

Vivian Wing-Wah Yam, Hong Kong, China

Chunhua Yan, Beijing, China

Shu-Li You, Shanghai, China

Aims and Scope

The series *Topics in Current Chemistry Collections* presents critical reviews from the journal *Topics in Current Chemistry* organized in topical volumes. The scope of coverage is all areas of chemical science including the interfaces with related disciplines such as biology, medicine and materials science.

The goal of each thematic volume is to give the non-specialist reader, whether in academia or industry, a comprehensive insight into an area where new research is emerging which is of interest to a larger scientific audience.

Each review within the volume critically surveys one aspect of that topic and places it within the context of the volume as a whole. The most significant developments of the last 5 to 10 years are presented using selected examples to illustrate the principles discussed. The coverage is not intended to be an exhaustive summary of the field or include large quantities of data, but should rather be conceptual, concentrating on the methodological thinking that will allow the non-specialist reader to understand the information presented.

Contributions also offer an outlook on potential future developments in the field.

More information about this series at <http://www.springer.com/series/14181>

Chunhai Fan • Yonggang Ke
Editors

DNA Nanotechnology

From Structure to Functionality

With contributions from

Ying Bao • Jie Chen • Jinyi Dong • Jinwei Duan • Jinglin Fu
Xiaoyi Fu • Oleg Gang • Alexandra Hoff • Ezry St. Iago-McRae
Min Ji • Guoliang Ke • Megan E. Kizer • Gezhi Kong • Yuhan Kong
Hua Kuang • Jungyeon Lee • Feng Li • Xiao Hua Liang • Huajie Liu
Jiliang Liu • Yizhen Liu • Ningning Ma • Hong-min Meng
Brian Minevich • David Ng • Sung Won Oh • Fangqi Peng • Lixia Shi
Yun Tan • Weiyang Tang • Leilei Tian • Ye Tian • Fuan Wang
Guan A. Wang • Hong Wang • Huimin Wang • Lihua Wang
Maggie Wang • Qiangbin Wang • Xing Wang • Zhicheng Wang
Zixiang Wei • Itamar Willner • Pia Winterwerber • Yuzhou Wu
Fan Xiao • Hang Xing • Mengyi Xiong • Chuanlai Xu • Xuemei Xu
Qi Yang • Fei Zhang • Ting Zhang • Xiao-Bing Zhang • Dan Zhao
Sisi Zhao • Yuan Zhao • Weiye Zhong • Chao Zhou • Ying Zhu



Springer

Editors

Chunhai Fan
School of Chemistry
and Chemical Engineering
Shanghai Jiao Tong University
Shanghai, China

Yonggang Ke
The Wallace H. Coulter Department
of Biomedical Engineering
Emory University
Atlanta, GA, USA

Partly previously published in *Topics in Current Chemistry (Z) Volume 378 (2020)*.

ISSN 2367-4067

Topics in Current Chemistry Collections

ISBN 978-3-030-54805-6

© Springer Nature Switzerland AG 2020

Chapter “DNA-Programmed Chemical Synthesis of Polymers and Inorganic Nanomaterials” is licensed under the terms of the Creative Commons Attribution 4.0 International License (<http://creativecommons.org/licenses/by/4.0/>). For further details see license information in the chapters.

This work is subject to copyright. All rights are reserved by the Publisher, whether the whole or part of the material is concerned, specifically the rights of translation, reprinting, reuse of illustrations, recitation, broadcasting, reproduction on microfilms or in any other physical way, and transmission or information storage and retrieval, electronic adaptation, computer software, or by similar or dissimilar methodology now known or hereafter developed.

The use of general descriptive names, registered names, trademarks, service marks, etc. in this publication does not imply, even in the absence of a specific statement, that such names are exempt from the relevant protective laws and regulations and therefore free for general use.

The publisher, the authors, and the editors are safe to assume that the advice and information in this book are believed to be true and accurate at the date of publication. Neither the publisher nor the authors or the editors give a warranty, expressed or implied, with respect to the material contained herein or for any errors or omissions that may have been made. The publisher remains neutral with regard to jurisdictional claims in published maps and institutional affiliations.

This Springer imprint is published by the registered company Springer Nature Switzerland AG
The registered company address is: Gewerbestrasse 11, 6330 Cham, Switzerland

Contents

Preface	vii
Towards Active Self-Assembly Through DNA Nanotechnology	1
Jinyi Dong, Chao Zhou and Qiangbin Wang: Topics in Current Chemistry (Z) 2020, 378:33 (12, March 2020) https://doi.org/10.1007/s41061-020-0297-5	
Tailoring DNA Self-assembly to Build Hydrogels	27
Jie Chen, Ying Zhu, Huajie Liu and Lihua Wang: Topics in Current Chemistry (Z) 2020, 378:32 (7, March 2020) https://doi.org/10.1007/s41061-020-0295-7	
DNA-Programmed Chemical Synthesis of Polymers and Inorganic Nanomaterials	57
Xuemei Xu, Pia Winterwerber, David Ng and Yuzhou Wu: Topics in Current Chemistry (Z) 2020, 378:31 (7, March 2020) https://doi.org/10.1007/s41061-020-0292-x	
Engineering Functional DNA–Protein Conjugates for Biosensing, Biomedical, and Nanoassembly Applications	83
Dan Zhao, Yuhan Kong, Sisi Zhao and Hang Xing: Topics in Current Chemistry (Z) 2020, 378:41 (24, May 2020) https://doi.org/10.1007/s41061-020-00305-7	
DNA-Scaffolded Proximity Assembly and Confinement of Multienzyme Reactions	125
Jinglin Fu, Zhicheng Wang, Xiao Hua Liang, Sung Won Oh, Ezry St. Iago-McRae and Ting Zhang: Topics in Current Chemistry (Z) 2020, 378:38 (4, April 2020) https://doi.org/10.1007/s41061-020-0299-3	
Directional Assembly of Nanoparticles by DNA Shapes: Towards Designed Architectures and Functionality	157
Ningning Ma, Brian Minevich, Jiliang Liu, Min Ji, Ye Tian and Oleg Gang: Topics in Current Chemistry (Z) 2020, 378:36 (27, March 2020) https://doi.org/10.1007/s41061-020-0301-0	

Oligonucleotide–Polymer Conjugates: From Molecular Basics to Practical Application	191
Fan Xiao, Zixiang Wei, Maggie Wang, Alexandra Hoff, Ying Bao and Leilei Tian: Topics in Current Chemistry (Z) 2020, 378:24, (17, February 2020) https://doi.org/10.1007/s41061-020-0286-8	
Biotechnological and Therapeutic Applications of Natural Nucleic Acid Structural Motifs	235
Jinwei Duan, Xing Wang and Megan E. Kizer: Topics in Current Chemistry (Z) 2020,378:26 (18, February 2020) https://doi.org/10.1007/s41061-020-0290-z	
DNA-Driven Nanoparticle Assemblies for Biosensing and Bioimaging	267
Yuan Zhao, Lixia Shi, Hua Kuang and Chuanlai Xu: Topics in Current Chemistry (Z) 2020, 378:18 (3, February 2020) https://doi.org/10.1007/s41061-020-0282-z	
Aptamer-Functionalized DNA Nanostructures for Biological Applications	301
Xiaoyi Fu, Fangqi Peng, Jungyeon Lee, Qi Yang, Fei Zhang, Mengyi Xiong,Gezhi Kong, Hong-min Meng, Guoliang Ke and Xiao-Bing Zhang: Topics in Current Chemistry (Z) 2020, 378:21 (7, February 2020) https://doi.org/10.1007/s41061-020-0283-y	
High-performance biosensing based on autonomous enzyme-free DNA circuits	345
Hong Wang, Huimin Wang, Itamar Willner and Fuan Wang: Topics in Current Chemistry (Z) 2020, 378:20 (3, February 2020) https://doi.org/10.1007/s41061-020-0284-x	
DNA Strand Displacement Reaction: A Powerful Tool for Discriminating Single Nucleotide Variants	377
Weiyang Tang, Weiye Zhong, Yun Tan, Guan A. Wang, Feng Li and Yizhen Liu: Topics in Current Chemistry (Z) 2020, 378:10 (2, January 2020) https://doi.org/10.1007/s41061-019-0274-z	

Preface

The double helix structure of deoxyribonucleic acid (DNA) was discovered in 1953 by James D. Watson and Francis H. C. Crick [1]. Thirty years later, Nadrian C. Seeman proposed the concept of utilizing the highly specific Watson-Crick base-pairing to construct self-assembled DNA nanostructures [2]. Since then, the vital role of DNA in the development of novel materials has been explored by many prominent researchers throughout the following decades. In 2006, Paul W. K. Rothemund pioneered DNA origami technique [3], which ushered in a new era of DNA nanotechnology. Up to date, DNA nanotechnology has enabled precise construction of nanomaterials with various patterns and different components in a highly programmable manner, which can be further used in many applications such as nanophotonics and theranostics. This topical collection addresses the recent advances in the field of DNA nanotechnology, focusing on the two essential issues of structure design and functionality.

Zhou and colleagues discussed dynamic DNA assembly systems from the perspective of free energy change in the reaction process, including passive assembly–disassembly systems, autonomous assembly systems, sophisticated artificial metabolism and time-clocking oscillation systems ([1 Towards Active Self-Assembly Through DNA Nanotechnology](#)). H. Liu and colleagues summarized the progress in the field of DNA hydrogels, including the gelation mechanisms, various synthetic strategies and applications of DNA hydrogels ([2 Tailoring DNA Self-assembly to Build Hydrogels](#)).

DNA nanotechnology has dramatically contributed to nanoscale materials of various components, such as biomolecules, polymers and nanoparticles. The contribution by Y. Wu and colleagues summarized recent advances in nanomaterials synthesis of polymers and inorganic nanomaterials using DNA nanostructures as scaffolds, and discussed the current challenges and future outlook ([3 DNA-Programmed Chemical Synthesis of Polymers and Inorganic Nanomaterials](#)). H. Xing and co-workers reviewed the research progress of synthetic DNA–protein conjugates over the past decades, by summarizing DNA–protein conjugation chemistries and the applications ([4 Engineering Functional DNA–Protein Conjugates for Biosensing, Biomedical, and Nanoassembly Applications](#)). J. Fu and

colleagues discussed the recent progress in the field of DNA scaffold-directed assembly of multienzyme reactions, including proximity assembly, confinement, biomimetic substrate channeling and regulation circuits, as well as bioconjugation techniques of hybrid DNA–protein structures (5 [DNA-Scaffolded Proximity Assembly and Confinement of Multienzyme Reactions](#)). The contribution by Y. Tian and O. Gang covered the progress in the development of the self-assembly of nanoparticles using DNA shapes, and discussed a broad range of applications of these architectures (6 [Directional Assembly of Nanoparticles by DNA Shapes: Towards Designed Architectures and Functionality](#)). The contribution by Y. Bao and L. Tian categorized oligonucleotide–polymer conjugates by the structures of the polymer blocks, and discuss the synthesis, purification, and applications for each category (7 [Oligonucleotide–Polymer Conjugates: From Molecular Basics to Practical Application](#)).

DNA-based nanoplatfoms have shown great promise in numerous biological or biomedical applications. The contribution by J. Duan, X. Wang and M. E. Kizer discussed the structural characteristics, biological prevalence, and function of both DNA and RNA structural motifs found in natural biological systems, and highlighted the biotechnological and therapeutic applications of these structural motifs, including catalytic nucleic acids, non-coding RNA, aptamers, G-quadruplexes, i-motifs, and Holliday junctions (8 [Biotechnological and Therapeutic Applications of Natural Nucleic Acid Structural Motifs](#)). Y. Zhao and colleagues analyzed the progress of DNA-driven nanoparticle assemblies for biosensing and bioimaging, focusing on the discussion of the tunable configurations and tailorable optical properties of these spatial structures (9 [DNA-Driven Nanoparticle Assemblies for Biosensing and Bioimaging](#)). The contribution by G. Ke and colleagues introduced the features of aptamer-functionalized DNA nanostructures, and discussed the recent progress, challenges and future directions in biological applications of these nanostructures (10 [Aptamer-Functionalized DNA Nanostructures for Biological Applications](#)). F. Wang and colleagues introduced various autonomous enzyme-free DNA circuits, explained their underlying molecular reaction mechanisms, and discussed their biosensing applications in terms of sensing performance, challenges and outlook (11 [High-performance biosensing based on autonomous enzyme-free DNA circuits](#)). F. Li and Y. Liu offer a systematic survey of current emerging strategies using DNA strand displacement to detect single-nucleotide variants (SNVs), with an emphasis on the molecular mechanisms and their applicability to in vitro diagnostics (12 [DNA Strand Displacement Reaction: A Powerful Tool for Discriminating Single Nucleotide Variants](#)).

We are greatly indebted to all contributing authors, reviewers, and editorial staff of this topical collection for their effort and support. Contributions in this topical collection include the pioneering works published decades ago, as well as state-of-the-art reports published over the recent three years, covering from molecular basics to practical applications. We hope this comprehensive collection can present the readers both a historical overview and cutting-edge advancements in the booming field of DNA Nanotechnology.

Reference

- [1] Watson JD, Crick FHC (1953) Molecular structure of nucleic acids: a structure for deoxyribose nucleic acid. *Nature* 171, 737–738.
- [2] Seeman, NC (1982) Nucleic Acid Junctions and Lattices. *J. Theor. Biol.* 99, 237–247.
- [3] Rothemund PWK (2006) Folding DNA to create nanoscale shapes and patterns. *Nature* 440, 297–302.



Chunhai Fan

School of Chemistry and Chemical Engineering, Shanghai Jiao Tong University, Shanghai, China



Yonggang Ke

The Wallace H. Coulter Department of Biomedical Engineering, Emory University, Atlanta, USA



Towards Active Self-Assembly Through DNA Nanotechnology

Jinyi Dong^{1,2} · Chao Zhou¹  · Qiangbin Wang¹

Received: 29 October 2019 / Accepted: 3 March 2020 / Published online: 12 March 2020
© Springer Nature Switzerland AG 2020

Abstract

Self-assembly, which is ubiquitous in living systems, also stimulates countless synthetic molecular self-assembling systems. Most synthetic self-assemblies are realized by passive processes, going from high-energy states to thermodynamic equilibrium. Conversely, living systems work out of equilibrium, meaning they are energy-consuming, dissipative and active. In recently years, chemists have made extensive efforts to design artificial active self-assembly systems, which will be pivotal to emulating and understanding life. Among various strategies, emerging approaches based on DNA nanotechnology have attracted a lot of attention. Structural- as well as dynamic-DNA-nanotechnology offer diverse tools with which to design building blocks and to shape their assembly behaviors. To achieve active self-assembly, a synergy of diverse DNA techniques is essential, including structural design, controllable assembly–disassembly, autonomous assembly, molecular circuits, biochemical oscillators, and so on. In this review, we introduce progress towards, or related to, active assembly via DNA nanotechnology. Dynamic DNA assembly systems ranging from passive assembly–disassembly systems, to autonomous assembly systems to sophisticated artificial metabolism and time-clocking oscillation systems will be discussed. We catalogue these systems from the perspective of free energy change with the reaction process. We end the review with a brief outlook and discussion.

Keywords DNA nanotechnology · DNA origami · Self-assembly · Out-of-equilibrium assembly · Active assembly

Chapter 1 was originally published as Dong, J., Zhou, C. & Wang, Q. Topics in Current Chemistry (2020) 378: 33. <https://doi.org/10.1007/s41061-020-0297-5>.

✉ Chao Zhou
czhou2018@sinano.ac.cn

✉ Qiangbin Wang
qbwang2008@sinano.ac.cn

Extended author information available on the last page of the article

1 Introduction

Fascinated by the mystery of life, scientists are currently busy looking for extraterrestrial life and trying to create artificial life in the laboratory [1, 2]. One of the most amazing aspects of life is that all living things are formed by self-assembly, which is a fundamental biological design process through which an organized structure seems to be constructed from a disordered collection of smaller parts. Self-assembly can be classified into two types. One is passive and obeys an equilibrium thermodynamic: the system starts from a relatively higher free energy state and reaches a thermodynamic equilibrium state by minimizing free energy. Most artificial self-assembly systems follow this framework. The other type works out of equilibrium, meaning it is energy-consuming and dissipative; in other words, active. Life adopts the latter strategy to organize numerous molecules into the filaments, membranes and organelles that make up cells and carry out myriad complex biochemical reactions [3–5]. By continually consuming energy in endless assembly and disassembly cycles, life continually responds and adapts to the environment via complex biochemical reaction networks. To realize active self-assembly working like living systems could be seen as the Holy Grail in this field, since it is extremely important for understanding and emulating life. Although a formidable challenge, extensive efforts have been made towards this goal in recent years [6–11].

Among various strategies for designing self-assembly systems, DNA nanotechnology is particularly impressive. DNA molecules, as sequenced polymers and nanoscale materials, could be programmed to form nanoscale motifs as building blocks for self-assembly simply by exploiting Watson–Crick base pairs. Since Seeman proposed this concept in the 1980s [12], the field has seen dramatic progress in recent decades. Self-assembled DNA architectures, like DNA tiles [13], DNA origami [14], DNA bricks [15], wireframe structures [16] and even crystals [17, 18], have been prepared readily and successfully by manipulating the hybridization of DNA strands. On the other hand, dynamic DNA nanotechnology offers a toolbox for designing reconfigurable structures, controlling kinetics of assembly, building DNA-based chemical reaction networks [19–21], etc. All these achievements indicate that DNA nanotechnology could be a promising approach towards the goal of life-like self-assembly, or, at least, to mimic some aspects of living systems. Thanks to its high programmability and simplicity, active DNA assembly has been introduced recently in a few exciting successful demonstrations [9–11]. We believe this offers great encouragement to the fields of both DNA nanotechnology and self-assembly. Therefore, we decided to write this review to introduce what DNA nanotechnology has achieved so far towards this goal.

In this review, we would like to talk about active self-assembly systems using DNA nanotechnology. To achieve this goal, a synergy of diverse DNA techniques is essential, including structural design, controllable assembly–disassembly, autonomous assembly, molecular circuits, biochemical oscillators, and so on. Here, we focus mainly on dynamic DNA self-assembly. From the perspective of

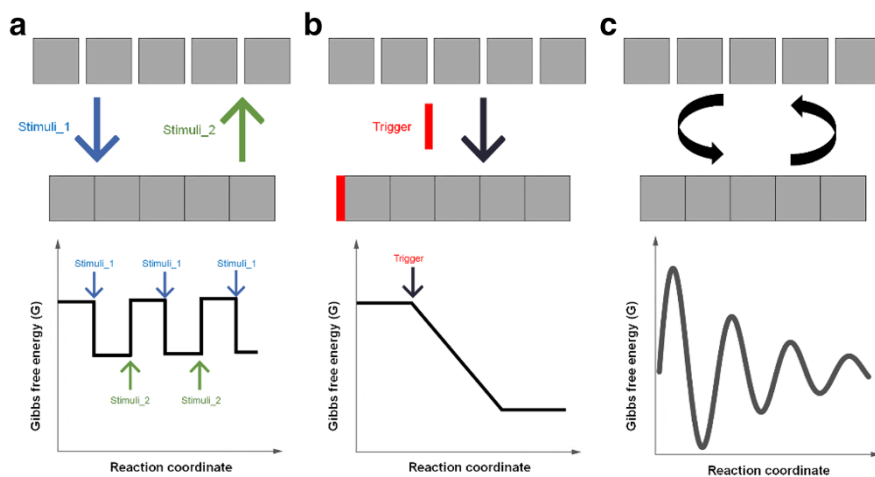


Fig. 1 Three models of dynamic self-assembly and their Gibbs free energy change during the process. **a** Passive assembly–disassembly. **b** Trigger-initiated autonomous assembly. **c** Energy-dissipative oscillating assembly

energy change with the reaction process, such systems can be divided into three major types (Fig. 1). We start from the most fundamental passive assembly–disassembly systems, which were realized by switching between two equilibrium states (Fig. 1a), and subsequently introduce autonomous assembly systems that rely on triggers to initiate the system and, therefore, direct the system from a high energy state to an equilibrium state (Fig. 1b). Finally, we discuss several successful demonstrations of active assembly systems developed very recently, mainly including an assembly system with a cascade of transformations [9], a time-clocking oscillation system [10] (Fig. 1c) and a mesoscale artificial metabolism system [11]. We end the review with a brief discussion and outlook. It should be noted that the term of ‘active assembly’ has been used for various connotations under different circumstances. In a broad sense, it can be used for self-assembly systems that can respond to external stimuli, more like ‘dynamic’. Here, we use the term in its narrowest sense, meaning that self-assembly is energy-consuming and dissipative, like the self-assembly in living organisms.

2 Passive Assembly–Disassembly of DNA

Switchable assembly–disassembly is the simplest dynamic DNA assembly system, as well as the most fundamental component for constructing complicated active assembly systems. In this section, we introduce DNA-based passive assembly–disassembly systems. The energy change of a passive assembly–disassembly system is normally as follows: in the initial state, the system remains at equilibrium; upon some external energy input or environmental change, the equilibrium is disturbed and the system reaches a new equilibrium state under the new circumstance; by

retrieving the input or switching back the environment, the system goes back to its initial equilibrium state (Fig. 1a).

One critical factor for determining the thermodynamic equilibrium state of a system is temperature. Walther et al. [22] reported the thermally controlled assembly–disassembly of a DNA origami filament system. The building block is a cuboid made of DNA origami that is pre-assembled via a thermal annealing process. Such DNA origami cuboids could further assemble into micrometer filaments via the hybridization of connecting DNA strands (blue ends in Fig. 2) at the sides of cuboids. The ligation based on DNA hybridization could be denatured at a relatively higher temperature, which induces disassembly of the filaments. Therefore, this assembly and disassembly process could be controlled by tuning the temperature. The temperature window could be tuned by adjusting the affinities of the DNA connectors. It should be noted that this temperature dependent assembly–disassembly process does not destroy the DNA origami building blocks due to the high thermal stability of DNA origami (melting temperature normally higher than 50 °C). Dietz et al. [23] introduced a non-base-pairing, shape-complementary strategy for engineering the interface of DNA origami. This provides a robust means of higher-order assembly as well as allowing dynamic control. The interface affinity is affected by both temperature and cation concentrations, thus both factors could be used to control the dynamic assembly–disassembly of high-order DNA origami assemblies.

DNA can also sense other environmental factors for designing assembly–disassembly system, for example, pH. To this end, a pH-sensitive connection between DNA building blocks is necessary. A DNA duplex based on Watson–Crick base-pairing can interact with a single-stranded DNA through pH-sensitive parallel Hoogsteen base-pairing to form a triplex. This duplex–triplex transition is highly

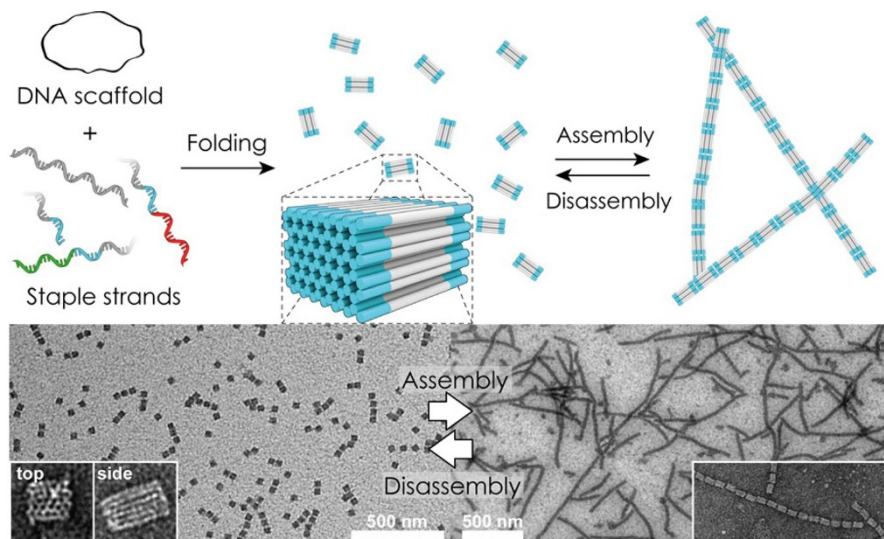


Fig. 2 Temperature controlled assembly–disassembly of DNA origami filaments Reproduced with permission from Ref. [22]. Copyright © 2016, American Chemical Society

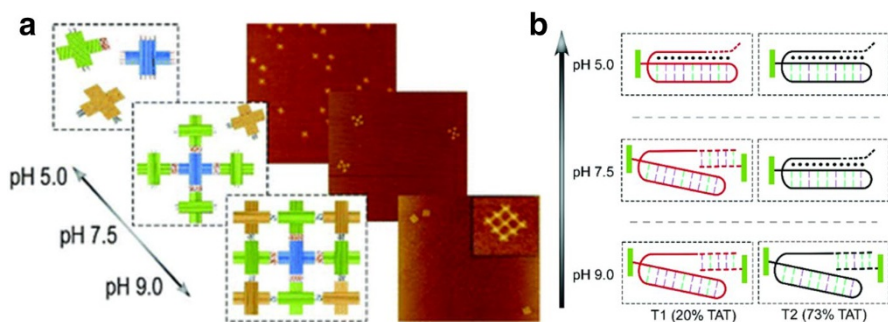


Fig. 3 pH-controlled stepwise assembly–disassembly of DNA origami nanostructures. **a** The reversible stepwise assembly–disassembly of DNA origami at different pH values. **b** Linkers that work at different pH based on duplex–triplex transition. Reproduced with permission from Ref. [24]. Copyright © 2019, the Royal Chemical Society

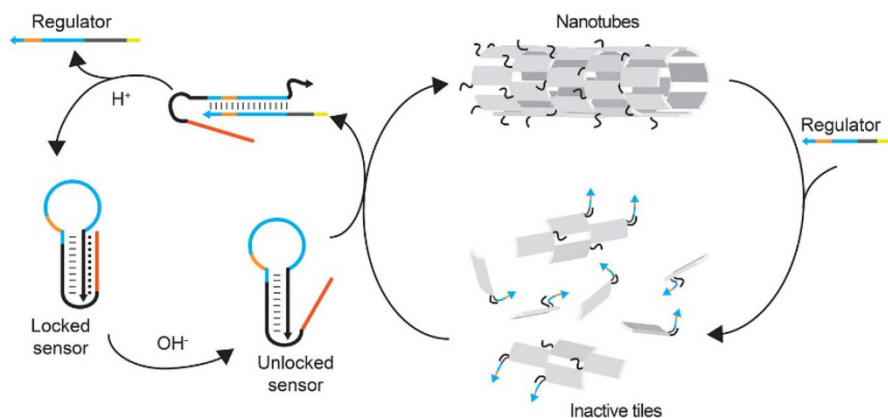


Fig. 4 Reversible self-assembly of DNA nanotubes through intermediate DNA regulator strands. Left side pH sensing device that can release and sequester regulator strands. Right part Regulator intervened assembly–disassembly of DNA tiles. Reproduced with permission from Ref. [28]. Copyright © 2017, American Chemical Society

pH-dependent and could be regulated to sense different pH by tuning the ratio of C–G–C to T–A–T. Employing this strategy, Wang et al. [24] reported the pH-controlled, stepwise assembly–disassembly system of DNA origami (Fig. 3). The DNA triplex connection between DNA structures could be programmed to form and break at certain pH values, enabling stepwise assembly and disassembly of up to nine DNA origami pieces. Similarly, other responsive DNA motifs, e.g., pH-sensitive i-motif [25], K^+ responsive G-quadruplex [26], cation-dependent DNazyme [27], etc., have also been used as the bridge between DNA nanostructures for constructing assembly–disassembly systems.

This pH manipulation can also work in an indirect manner. Franco et al. [28] introduced a system that employ the duplex–triplex transition as a pH sensor that can

release or sequester regulator DNA strands (Fig. 4). Here, these authors employed DNA double crossover tile assembly as the model. This DNA double crossover tile assembly, which was developed by Rothmund et al. [29], has been used widely for investigating dynamic self-assembly. The regulator DNA strands can activate or deactivate tile-based DNA nanotube assembly by interacting with the sticky ends through toehold-mediated strand-displacement reactions. At high pH, the pH sensor sequesters the regulator strands and enables the assembly of DNA tiles into micrometer nanotubes. At low pH, the pH sensor releases the regulator strands. The regulator strands disrupt the connection among DNA tiles via strand-displacement and the nanotubes then disassemble into small tiles. This idea of bridging an upstream regulatory unit and downstream DNA assembly through intermediate DNA strands gives more possibility and flexibility to the design of complex DNA assembly. A similar strategy is also employed for achieving active self-assembly system, which we will introduce below in the section on “Active DNA Self-Assembly System”.

DNA nanostructures could be placed on lipid membranes by conjugated cholesterol moieties. The lipid membranes confine the DNA structures to the surfaces while also providing fluidity. The thermodynamic behavior of DNA nanostructures on fluid soft lipid bilayers will differ from those in solution. The assembly–disassembly process of DNA can be performed on artificial lipid membranes as well as on cell surfaces. These dynamic processes could be directly monitored with various tools, such as high-speed atomic force microscopy (AFM). Endo et al. [30] reported a light-controlled DNA origami assembly–disassembly system on supported lipid bilayers (Fig. 5a). They used pseudo-complementary photo-responsive DNA modified by azobenzene molecules as the linkers of two DNA origami units. Under visible light, the trans-form azobenzene moieties help maintain DNA hybridization and thus bring two DNA origami units together to form dimers. With UV light irradiation, the trans-azobenzene moieties switch to the cis-form and thus dissociate the

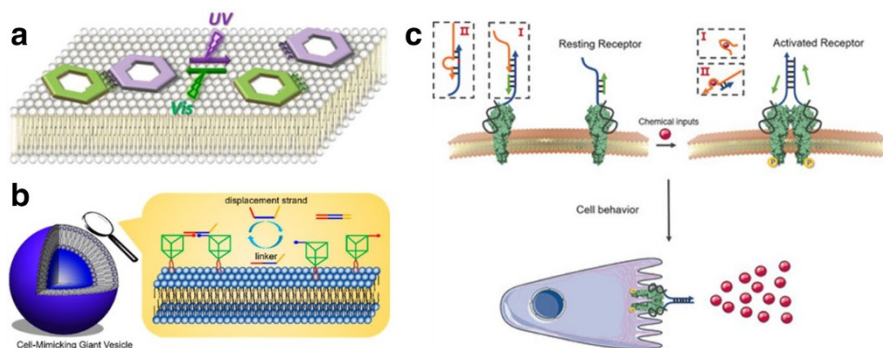


Fig. 5 Dynamic DNA assembly on artificial and cell membranes. **a** Photo-controlled DNA origami association–disassociation on supported lipid bilayer. **b** DNA nanoprisms assembly–disassembly on the surface of cell-mimicking giant vesicles. **c** Dynamic DNA association for controlling the cell membrane receptor dimerization and cell behaviors **a** Reproduced with permission from Ref. [30]. Copyright © 2014, American Chemical Society; **b** reproduced with permission from Ref. [31]. Copyright © 2017, American Chemical Society; **c** reproduced with permission from ref [32]. Copyright © 2018, John Wiley and Sons

DNA origami dimers. The supported lipid bilayer offers a platform to visualize the process by high-speed AFM. Tan et al. [31] reported the assembly–disassembly of DNA nanoprisms driven by strand-displacement reactions on cell-mimicking giant vesicles, and visualized the process by fluorescence microscopy (Fig. 5b). DNA strands can also be attached to specific cell membrane receptors. Thereby, assembly and disassembly could be used for inducing cell membrane receptor dimerization or clustering, thus regulating downstream signalling to control cell behaviors (Fig. 5c) [32].

3 Trigger-Initiated Autonomous DNA Self-Assembly

Active assembly is always autonomous although autonomous assembly is not necessarily active. To some extent, designing autonomous assembly could be regarded as a preliminary to achieving active assembly. In the previous section, we focused on the switch between the assembled state and the disassembled state, which requires alternative external interference to change thermodynamic equilibrium states. In this section, we pay attention to the process of assembling individual units into higher-order assemblies, and how to make this process proceed autonomously. In principle, the autonomous assembly system starts from a meta-stable non-equilibrium state. Upon a trigger that disturbs this meta-stable state, the system reaches its equilibrium state in an autonomous manner. Once the process is initiated by a trigger, no further external intervention is needed (Fig. 1b).

3.1 Hybridization Chain Reaction-Based self-Assembly

One classical demonstration of autonomous DNA assembly is the hybridization chain reaction (HCR) that was first developed by Dirks and Pierce (Fig. 6) [33]. HCR is based on the toehold-mediated strand invasion of stable hairpin structures with long stem duplexes. The HCR system consists of two types of DNA hairpins, H1 and H2, with single-stranded toehold extensions at the 5' and 3' ends of the hairpins, respectively (Fig. 6a). Ingeniously, the loop region of H1 contains the complement of H2 toehold, while the H2 loop is complementary to H1 toehold, and the double-strand stems of H1 and H2 are identical. Due to the long double-strand stem region, the two hairpins coexist metastably. When a trigger molecule with the appropriate sequence is added (complementary to the toehold and adjacent stem sequence), one of the hairpins is opened by toehold-mediated strand displacement, allowing the loop sequence to become freely accessible. This loop sequence can now be attached to the toehold of another hairpin, triggering a chain reaction in which multiple H1 and H2 molecules bind to each other to form long double-stranded polymers.

The initiator of HCR could be encoded as other signals as long as they can interact with strands to open the H1 hairpin. For example, encoding an ATP aptamer to the toehold could initiate the HCR with ATP molecules. The HCR is particularly useful for biological imaging since it could work as a molecular

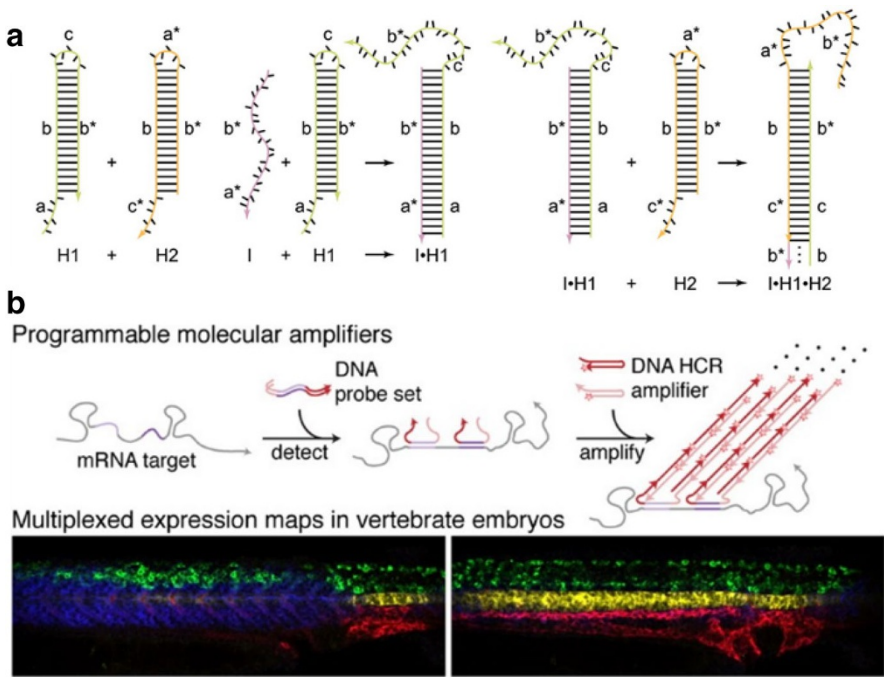


Fig. 6 The hybridization chain reaction (HCR). **a** Principle of HCR. **b** In-situ HCR for multiplexed imaging of mRNA in zebrafish embryos **a** Reproduced with permission from Ref. [33]. Copyright © 2004, National Academy of Sciences; **b** reproduced with permission from Ref. [34]. Copyright © 2010, Springer Nature

amplifier in diverse settings. With three generations of development, Pierce et al. [34] presented in situ HCR as a powerful tool for multiplexed and quantitative bioimaging with high sensitivity and low background (Fig. 6b). Tan et al. [35] developed aptamer-tethered DNA nanotrains with fluorescence as carriers; drug fluorescence quenching, real-time signaling of behaviors of drugs and nanotrains at target cells can be performed.

A variant of HCR uses four-way branch migration for the construction of hybridization polymerization systems (Fig. 7) [36]. In this case, the reaction between H1 and H2 is initiated by the introduction of the DNA duplex with three toeholds. The overhangs a^* and x of the complex hybrid with the complementary overhangs a and x^* of the hairpin H1 to produce a movable Holliday junction (state 1 in Fig. 7). By four-way branch migration, this structure transforms into state 2, and the hairpin H1 unfolds to expose the toehold domain, c . The toeholds c and y are available for hairpin loop H2 to bind to, creating another Holliday junction intermediate (state 3). The configuration relaxes to that of state 4, with two new domains, x and a^* , being used for loop H1 binding. The sequence of the hybridization is repeated cyclically, resulting in a long-nicked duplex strand. Incorporating this autonomous polymerization into DNA-cross-linked

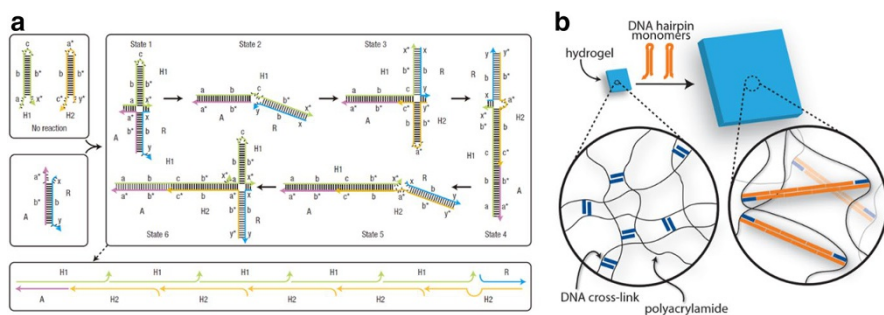


Fig. 7 Autonomous polymerization powered by four-way junction branch migration. **a** Principle of polymerization. **b** Swelling of DNA-cross-linked polyacrylamide hydrogels by the autonomous polymerizations **a** Reproduced with permission from Ref. [36]. Copyright © 2007, Springer Nature; **b** reproduced with permission from Ref. [37]. Copyright © 2017, American Association for the Advancement of Science

polyacrylamide hydrogels, Schulman et al. [37] realized up to 100-fold volumetric hydrogel swelling by successively extending DNA cross-links by autonomous polymerizations.

The principle of HCR could be applied for more complicated autonomous DNA assembly. Fan et al. [38] adapted the concept of HCR in high-order DNA assembly systems (Fig. 8). They designed DNA hairpin tiles (DHTs) that could be opened by initiator strands. Unlike single-stranded hairpin strands, DHTs can be encoded with structural information and therefore endow the system with much more designability and hierarchical complexity. The DHT motif is a double-crossover structure, in which two double helices are arranged in parallel and ligated by a pair of crossover junctions. Fan and colleagues first showed the DHTs could be polymerized into long filaments of low dispersity in a chain-growth way. They then programmed this chain-growth copolymerization to form two-dimensional nanoplatelets. To this end, they changed the distance of two crossover junctions between two associated DHT monomers. In the one-dimensional polymerization, the distance of two intermolecular crossover junctions is about 2.5 helical turns, whereas it was increased to 3 helical turns in 2D chain-growth assembly. This subtle adjustment changed the angle of the two associated DHT monomers. Specifically, the DHT monomers bind to opposite sides of the chain-growth strands. Combining this altered chain-growth copolymerization with DNA overhang associations, the DHTs can assemble into 2D nanoplatelets. Nie et al. [39] showed that two HCRs could be synchronized for assembling nanoladders. With one HCR plus one T-junction cohesion, they also prepared closed nanorings.

3.2 DNA Catalytic Self-Assembly

Another widely explored way of directing meta-stable non-equilibrium systems to equilibrium is catalysis. The first DNA catalytic system was developed by Zhang et al. [40]. As illustrated in Fig. 9a, substrate complex S and fuel strand F react to form waste product W and release oligomers SB and OB as signals and/

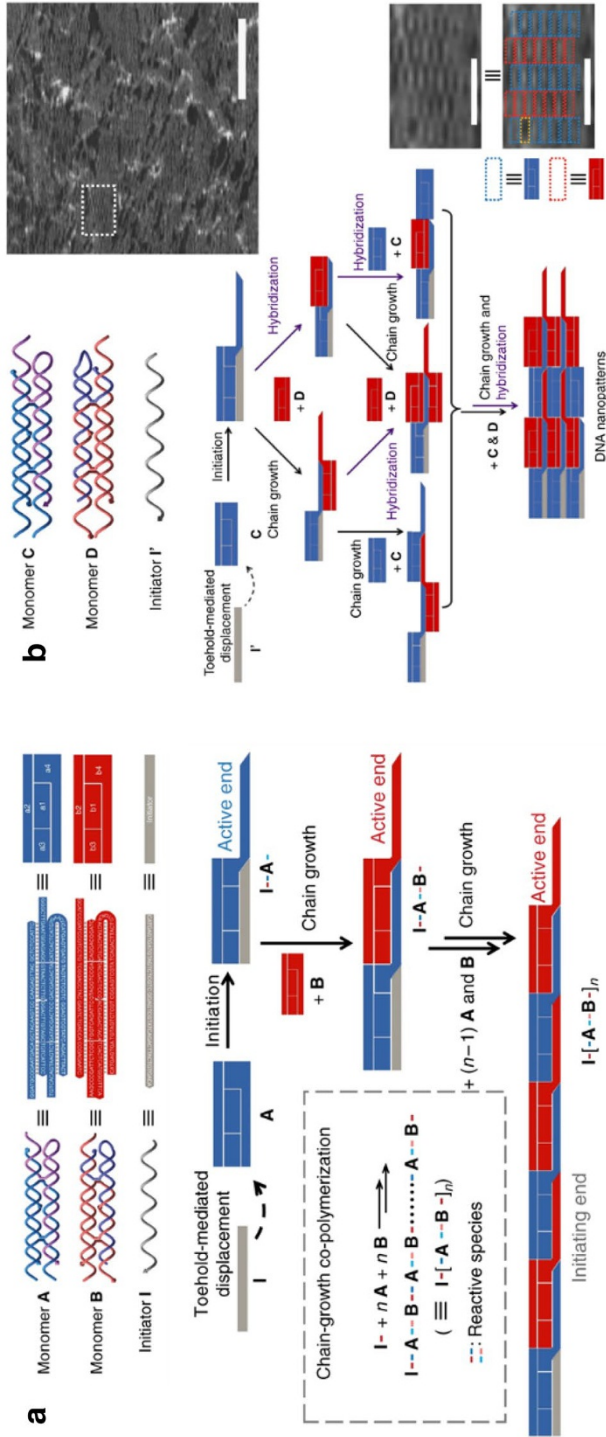


Fig. 8 **a** One- and **b** two-dimensional chain-growth copolymerization of DNA hairpin tiles (DHTs). Bar 50 nm Reproduced with permission from Ref. [38]. Copyright © 2019, Springer Nature

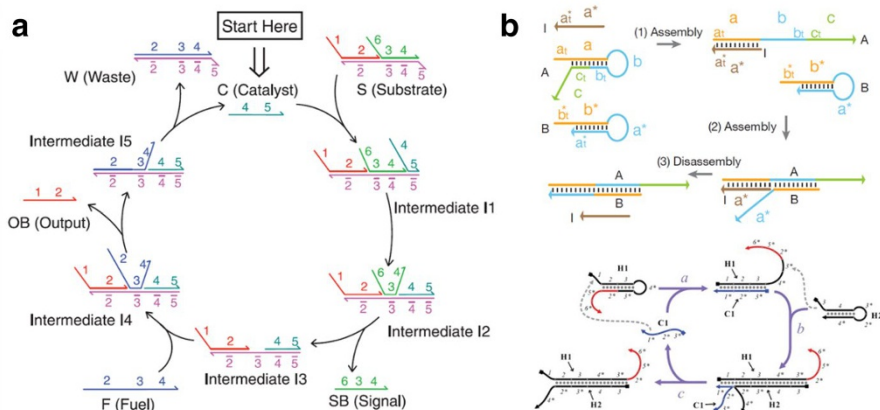


Fig. 9 DNA catalysis system. **a** The first entropy-driven DNA catalysis system that can output two single strands as outputs or downstream signals. **b** The catalytic hairpin assembly that directs the hybridization of two hairpin strands **a** Reproduced with permission from Ref. [40]. Copyright © 2007, American Association for the Advancement of Science; **b** reproduced with permission from Ref. [41]. Copyright © 2008, Springer Nature and Ref. [42] Copyright © 2011, Oxford University Press

or outputs. The reaction is driven by entropy due to the increase in the number of components from two to three. With addition of the catalyst C, SB can be released from intermediate I2 and the hidden toehold becomes exposed. This toehold provides an attachment site for F, which then drives the reaction to completion by toehold-initiated strand invasion. The concept of DNA catalysis has been further adapted to a system termed ‘chain hybridization assembly (CHA)’ (Fig. 9b) [41, 42]. Like HCR, CHA starts from two pre-formed hairpin strands that have complementary strands. The hybridization of these two hairpins is initiated by a short strand to open the first hairpin and therefore disclose the toehold. Different from HCR, CHA stops after hybridization of the two hairpins and releases the initiator strand. Therefore, the initiator strand here functions only as a catalyst.

An entropy-driven DNA catalysis system could be utilized to initiate autonomous DNA tile self-assembly as upstream molecular circuits (Fig. 10) [43]. Here, the DNA double crossover precursor tiles are deactivated by replacing one of the long single-stranded regions with two strands that cover the sticky ends and protect the tiles from hierarchical assembly. These two protecting strands could be displaced by deprotector strands via strand-displacement reactions, while the deprotector strands are stored in the DNA catalysis circuits. Upon addition of DNA catalyst, the upstream control circuit is turned on, and starts to release deprotector strands successively (Fig. 10a), thereby the double crossover tiles are activated and assembled into micrometer filaments autonomously (Fig. 10b). There are many challenges in coupling a DNA catalytic circuit with downstream self-assembly. One such challenge is leakage of the DNA catalytic circuit, meaning a small number of deprotector strands could leak from the substrates. To solve this, DNA sink complexes could be introduced as a competitive threshold for the deprotectors (Fig. 10c).

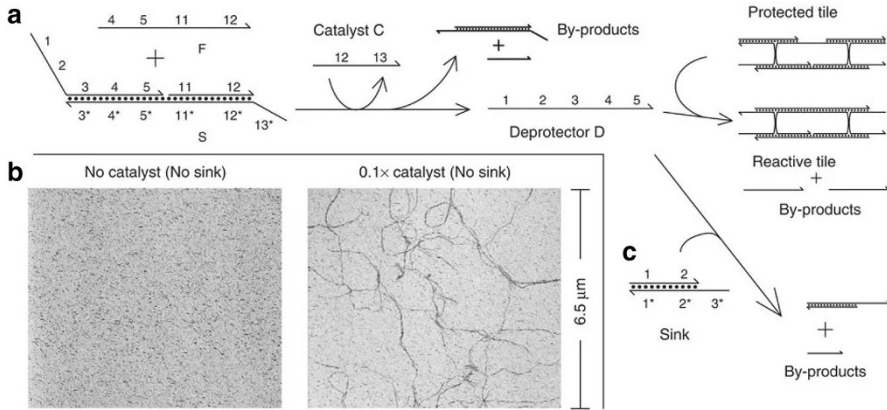


Fig. 10 DNA catalytic circuit controlling autonomous DNA tile self-assembly. **a** The entropy-driven DNA catalysis system that produces the deprotector strands. **b** Atomic force microscopy (AFM) results from the integrated reaction network. DNA nanotubes can assemble in the presence of catalyst. **c** The sink complex acts as a competition threshold for the deprotector to prevent the release of a small amount of deprotector, which will result in DNA nanotube assembly. Reproduced with permission from Ref. [43]. Copyright © 2013, Springer Nature

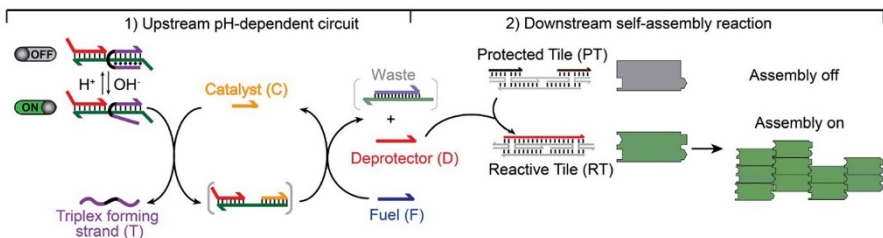


Fig. 11 pH-controlled assembly of DNA tiles. The upstream circuit (1) is a pH-dependent DNA catalytic module, and the downstream self-assembly reaction (2) the self-assembly of DNA double crossover tiles. Reproduced with permission from Ref. [44]. Copyright © 2014, American Chemical Society

The modularity of integrating upstream DNA circuit and downstream self-assembly offers the possibility of designing versatile autonomous self-assembly. Ricci et al. [44] developed a pH-dependent circuit for controlling self-assembly of the same DNA double crossover tiles (Fig. 11). These latter authors re-engineered the three-strand substrate to be responsive to pH by introducing a triplex based on Hoogsteen interactions. The substrate was only accessible to the DNA catalyst at basic pH. Therefore, the generation of deprotector strands could be turned on and off by pH. Ultimately, downstream tile assembly is controlled successfully by the upstream pH-dependent circuit.

CHA may provide an alternative means of catalyzing autonomous assembly. Yang et al. [45] made pioneering efforts in this regard. Unlike DNA catalytic circuits, the CHA does not export a single strand as output. Instead, it simply recombines two individual hairpin strands into one hybridized duplex. Therefore, the

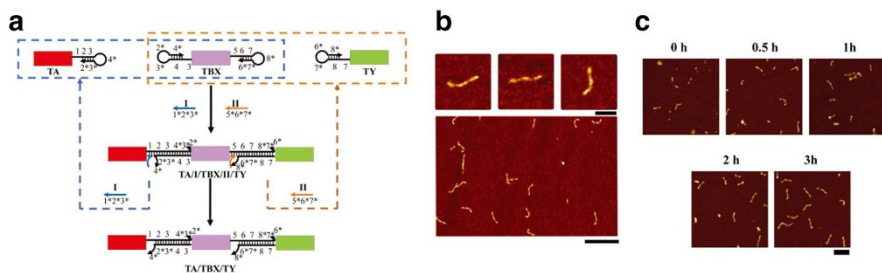


Fig. 12 Chain hybridization assembly (CHA)-driven DNA self-assembly. **a** Self-assembly process of the DNA tile trimer. **b** AFM image of the three-tile assembly product. **c** Kinetic evaluation of the formation of trimer tiles by AFM at different reaction times (0, 0.5, 1, 2, and 3 h). Bars **b** 50 nm, **c** 100 nm. Reproduced with permission from Ref. [45]. Copyright © 2019, John Wiley and Sons

hairpin strands could be employed directly as linkers of DNA building blocks, and CHA could then be used to control assembly. Yang et al. [45] integrated the CHA reactions with DNA tiles and explored them as a means of assembling nanostructures dynamically (Fig. 12). They used DNA tiles (double crossover tiles as well as DNA origami) as artificial “carriages”, hairpin structures modified on DNA tiles as “couplers”, and initiators as “wrenches” to initiate the CHA to actively self-assemble train-shaped DNA nanostructures of controlled length.

3.3 Seed-Guided Self-Assembly

The HCR and DNA catalysis provide tools for solving the problem of how to initiate self-assembly. Another important aspect of controlling self-assembly is to determine when and where to initiate self-assembly. Winfree et al. [46] demonstrated the concept of using pre-assembly DNA origami to efficiently seed and nucleate the growth of DNA tiles (Fig. 13). They used a rectangular DNA origami, which can present up to 32 DNA tile adapters at one side. The tile adapters could recruit desired DNA tiles using sequence-specific sticky ends. Under certain circumstances, DNA double crossover tiles assemble only when the seeds are present, and the growth of DNA tiles started from the tile adapters of DNA origami seeds.

Schulman et al. [47] further developed the seed-directed self-assembly system, designing nanotube origami as the seed to nucleate the assembly of DNA tiles (Fig. 14). Under a thermal annealing process, DNA origami seeds and tiles first formed. DNA tiles would then grow from the nucleated seeds following an isothermal self-assembly pathway (Fig. 14a). In their subsequent work, Schulman and colleagues demonstrated that this growth process could be terminated by rigid or flexible caps that block the growth interfaces (Fig. 14b); based on this, they demonstrated that DNA nanotubes can grow to connect pairs of molecular landmarks with micrometer separation distances and relative orientations [48]. With DNA origami seeds as molecular landmarks, DNA tile nanotubes grow and then join end to end to form stable connections. This process relies simply on diffusion of the free ends and does not need external guidance.

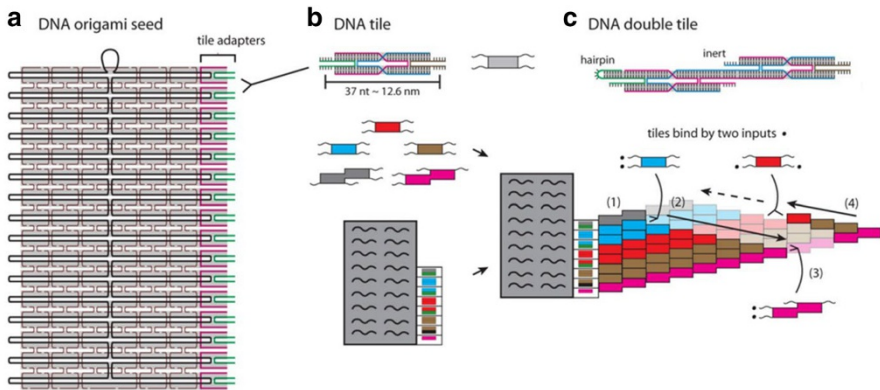


Fig. 13 Molecular design and self-assembly scheme. **a** The DNA origami seed consists of 32 tile adapter strands (*pink* and *green*) that bind at specific locations. **b** Each DNA tile consists of four strands that self-assemble into a molecule with a double-stranded core and four single-stranded 5-nt sticky ends. **c** Each DNA double tile, structurally equivalent to two fused tiles, consists of six strands that display four active sticky ends; two helix arms end either with a hairpin or with an inactive (*inert*) sticky end whose sequence matches no other sticky end. Reproduced with permission from Ref. [46]. Copyright © 2009, National Academy of Sciences

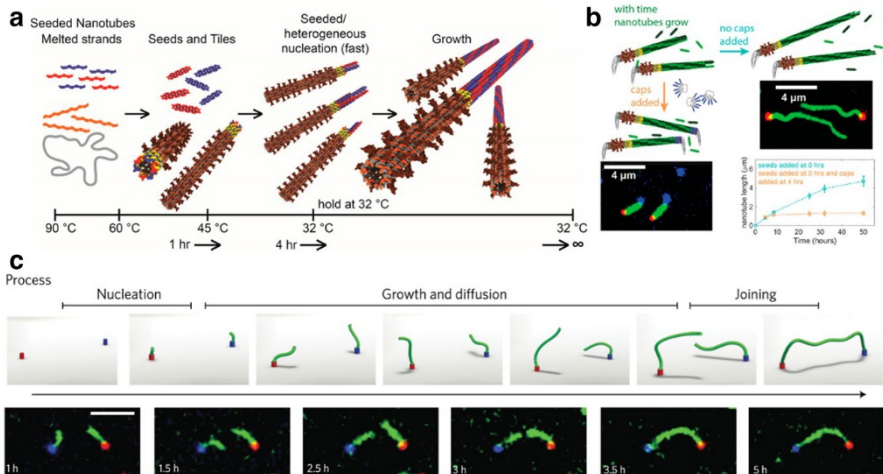


Fig. 14 Seed-mediated growth of DNA nanotubes. **a** Illustration of nucleation-growth process. **b** Termination of nanotube growth. **c** Connection of molecular landmarks by seed-mediated DNA nanotube growth. Bar 5 μm . **a**, **b** Reproduced with permission from Ref. [47]. Copyright © 2017, American Chemical Society; **c** reproduced with permission from Ref. [48]. Copyright © 2017, Springer Nature

It should be noted that nucleation and growth would happen even without the origami seeds. However, nucleation from tiles would be much slower since it requires overcoming a significant energy barrier. From this viewpoint, the seeds not only provide spatiotemporal starting points for self-assembly but also play a role as initiators to lower energy barrier and guide the system to equilibrium.

4 Active DNA Self-Assembly System

The above-mentioned systems all follow the equilibrium thermodynamic framework. In this section we talk about active self-assembly systems with much more complexity. To date, there have been only a few successful demonstrations, most of which were published very recently. Here, we introduce three kinds of system: (1) a self-assembled nanoarray with a cascade of transformations for information-relay systems; (2) a biochemical oscillator controlled dynamic assembly system; and (3) an artificial metabolism system. Each has its own characteristics and could be seen as an out-of-equilibrium active assembly from some aspects. Each can also be regarded as a demonstration of active assembly at different scales, from nanoscale to micrometer and mesoscale.

4.1 Self-Assembled Information-Relay System

The ability to faithfully deliver information in a cascaded and controlled fashion has worked wonders for civilization and biology. Researchers are eager to control the flow of information within a network at nanometer-to-micrometer scale. Song et al. [9] used a DNA “antijunction” as a basic unit to construct limited-size nanoarrays that transmit information from one side to the other in the form of structural transformation (Fig. 15). In a typical diamond-shaped unit, its four adjacent elements share a joint, so that all cells are connected to each other by a four-armed connection, which is a branched DNA motif that can be opened and closed like scissors. In principle, when one antijunction unit changes conformation, the scissor joints communicate this motion to the adjacent units, which then also undergo the same conformational change. This change can be passed to the neighbors’ neighbors and so on, until the entire array adopts the new conformation. Thus, Song and colleagues demonstrated the dynamic reconfiguration of DNA relay arrays. By adding and removing trigger strands, they can switch pre-assembled nanoarrays between different conformations and monitor the process in real time. In addition, they also showed that the conversion path was highly programmable. First, the starting point of transformation depends on where the trigger strands invade and lock the joints. Second, continuous transformation can be stopped and resumed by removing and replacing or locking and unlocking internal units. Finally, the transformation pathway can be controlled by designing odd-shaped nanoarrays with tight corners and adding trigger strands in a stepwise manner.

From the viewpoint of energy change, this self-assembled array is quite interesting. If we focus only on the start and the end states, it seems to be a trigger-initiated system. However, if we look into the landscape change during the relay process, it is very different. The system undergoes an energy oscillating process from the start state to the end state (Fig. 15e) given the alternate generation and disappearance of high-energy antijunction motifs (orange box in the figures).

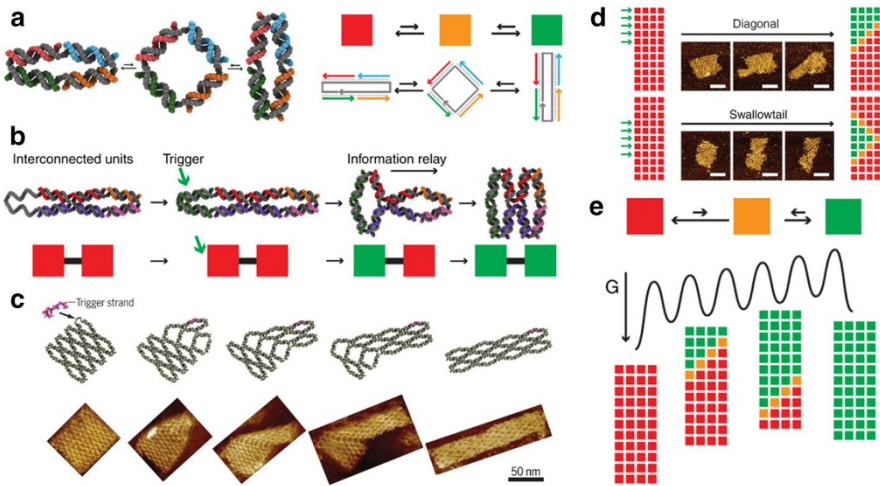


Fig. 15 Molecular information-relay arrays assembled by DNA. **a** A dynamic DNA antijunction that can switch between two stable conformations, through an unstable open conformation. Diagrams for a DNA antijunction: stable conformations red and green, and unstable conformation orange. **b** Transformation of an antijunction unit can be induced by addition of a trigger strand. The information is passed from the converted unit to its closest neighbors, causing them to undergo subsequent transformation. **c** Information relay in DNA “domino” nanoarrays. The molecular DNA nanoarray transforms in a step-by-step relay process, initiated by the hybridization of a trigger strand to a single unit. **d** Control of initiation of transformation via selection addition of green triggers. **e** Free energy landscape during the domino-like cascade transformations. Reproduced with permission from Ref. [9]. Copyright © 2017, American Association for the Advancement of Science

4.2 Biochemical Oscillator Controlled Dynamic Assembly System

The cytoskeleton consists of three major unbalanced supramolecular assemblies that continuously polymerize and depolymerize: microtubules [49], actin filaments [50] and intermediate filaments [51]. The microtubules—the largest of these structures—are mechanically stiff, highly dynamic, and alternate between stable growth and rapid depolymerization. The active assembly of microtubules represents advanced spatiotemporal control. In living organisms, high spatiotemporal ordering is realized by regulatory networks that are prototypes of chemical fuels, energy-dissipating self-assembly with dynamic and adaptive properties.

One of the most important elements of the regulatory network is called the biochemical oscillator, which controls the timing of cellular processes and provide circadian rhythms. Such chemical oscillation could be produced in non-living systems. The BZ reaction is the first example of a chemical oscillator that exhibits imbalances, such as bistability, as well as macroscopic oscillations and synchronization [52, 53]. When appropriate negative feedback is introduced, the well-stirred setup becomes susceptible to stimulation (that is, an input above a certain threshold will cause the output to peak before returning to the initial steady state) or to become oscillating. However, the susceptibility of the chemical oscillator makes it extremely difficult to make it compatible with other systems.

In organisms, long-duration time control is heavily dependent on gene expression. Instead of building pure chemical oscillators, Kim and Winfree [54] built an *in vitro* transcriptional oscillator by employing biological enzymes (Fig. 16a). They devised a ‘two-switch negative-feedback oscillator’. The biological oscillator is composed of nucleic acid strands (RNA and DNA) and enzymes (T7 RNA polymerase and RNase H). As depicted in Fig. 16, there are two switches (SW21 and SW12) in the oscillator as RNA ‘genelets’, each of which could produce single-stranded RNAs (rI2 and rA1) transcribed by T7 RNA polymerase. The activation and inhibition of these genelets could be regulated by DNA reaction networks involving the produced RNAs (Fig. 16b). In short, the produced RNAs can remove DNA strands from the promoter region by forming RNA–DNA hybrids. As a result, with the production and increasing concentration of RNAs, the generation of RNAs is inhibited. At the same time, the RNase H in the system continuously digests the RNAs and releases the DNA strands of the promoter, inducing re-activation of the genelets. The synergy of two such genelets enables the ‘two-switch negative-feedback oscillator,’ which exhibits sustained RNA concentration oscillations. This biochemical oscillator is programmable and compatible with the self-assembled DNA system. Simmel et al. [55] investigated and compared the effect on the oscillators of different strategies of load tweezer-like DNA nanomachines (Fig. 16c). One optimized strategy involved an extra transcription circuit as an insulator genelet. The insulators make the system more robust by isolating the oscillators and the loads, amplifying signals from the oscillators and thus allowing relatively high loads.

Integrating the structural DNA nanotechnology, the dynamic DNA nanotechnology as well as the biochemical oscillator, Franco et al. [10] demonstrated the active oscillating self-assembly of DNA tubular structures, a preliminary analogue to the dynamic growing and shrinking of microtubules (Fig. 17). They chose the DNA double crossover tile self-assembly we introduced earlier in this review. DNA tiles with sticky ends can self-assemble isothermally into nanotube filaments with diameters ranging from 7 to 20 nm. In their system, they added short segments to the sticky ends as toeholds, which could mediate the RNA invaders to break the inter-tile connections by strand-displacement reactions. The generation of RNA invaders is controlled by the biochemical oscillator and the insulator. In addition to playing the role of toehold, the intrusion of a single sticky end region weakens the interaction between the tiles, causing the nanostructures to collapse. Tiles bound to the RNA invader become ‘inactive’. Meanwhile, the RNase H sustainedly digests the RNA invader and converts the inactive tiles to become active. The active tiles re-assemble into nanotubes autonomously. Therefore, the concentration oscillating of RNA invaders actually controls the active assembly and disassembly of nanotubes by the interplay of digestion and generation. They observed the time clocking growth and shrinking of filaments over a time scale of hours.

Integrating these elements to make them work synergistically is not easy. One of the challenges is to match the kinetics of different elements. The oscillating period should match the rate of tile assembly, which is relatively slow. Since enzyme activities are hard to control, the oscillator can be modulated only by tuning the concentrations of oligonucleotides and enzymes. In addition, the oscillator operates in a closed system, so the system faces reduced enzymatic activity, accumulation of

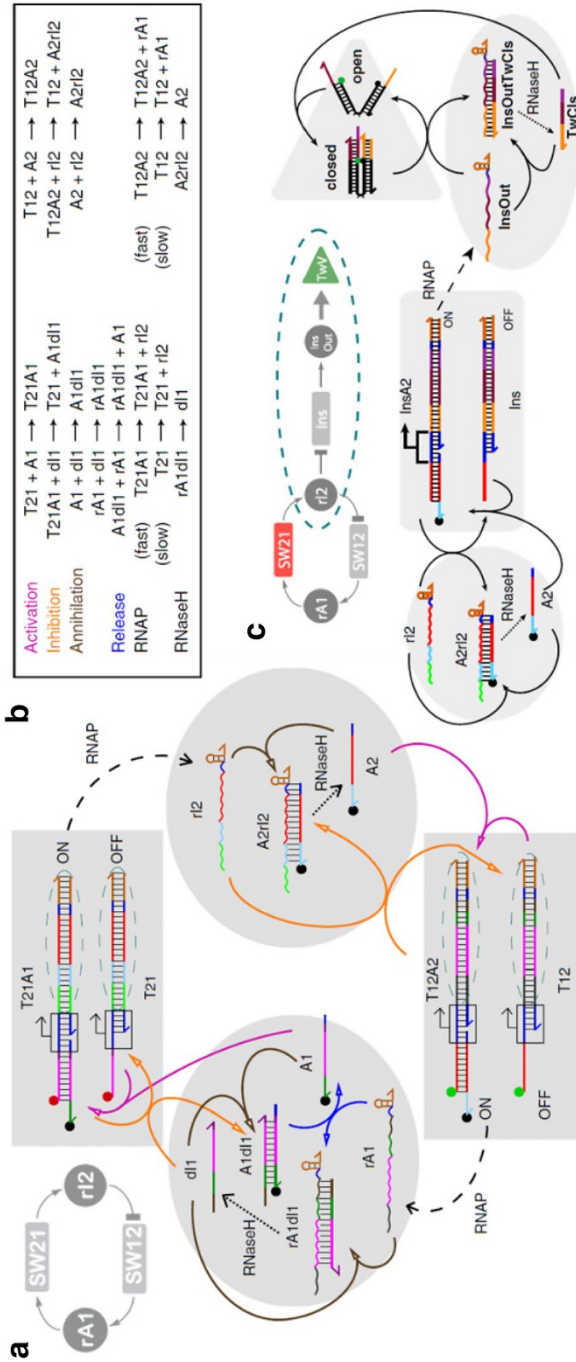


Fig. 16 Schematics of a biological oscillator system that can be coupled to high loads. **a** Topology of the oscillator and its biochemical reactions. **b** List of interactions between oscillator-component species. **c** Driving DNA tweezers with the Oscillator. Transcription of Ins releases InsOut which opens DNA tweezers previously closed by TwCis **a**, **b** Reproduced with permission from Ref. [54]. Copyright © 2011, John Wiley and Sons; **c** Reproduced with permission from Ref. [55]. Copyright © 2011, National Academy of Sciences

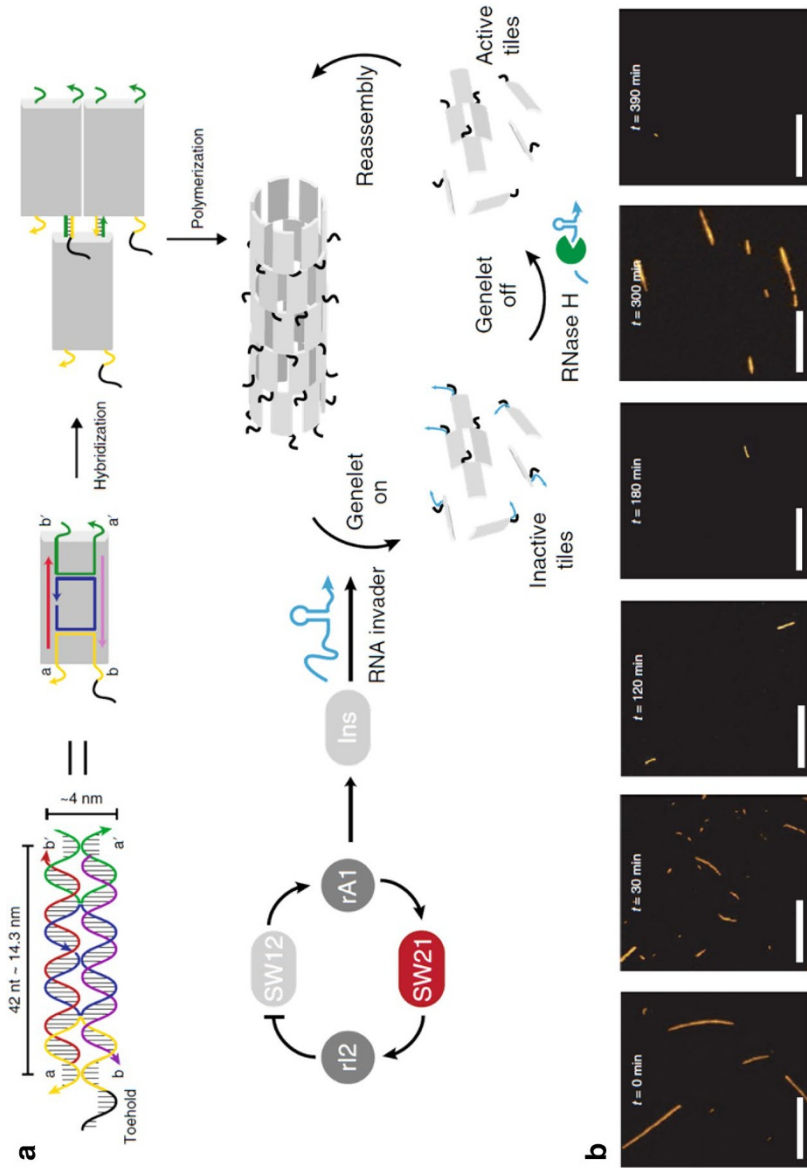


Fig. 17 Biochemical oscillator controlled dynamic assembly of DNA nanotubes. **a** DNA tiles self-assemble into DNA nanotubes. **b** Representative fluorescence microscopy images of nanotube samples at different points in time. Bar 10 μm Reproduced with permission from Ref. [10]. Copyright © 2019, Springer Nature

incompletely degraded RNA, and consumption of NTPs. With all these challenges in mind, Franco et al. [10] achieved a system in which nanotube assembly can be controlled by the oscillator to exhibit one or two large-amplitude oscillations.

4.3 Artificial Metabolism System

The above-mentioned dynamic DNA assembly systems work at the molecular or supramolecular level, and rely on the careful design of building blocks and their precise interactions. Conversely, Luo et al. [11] created a DNA-based dissipative assembly system that works at the mesoscale. Instead of using DNA for the assembly of DNA motifs or nanostructures, they employed DNA as source material for the generation of a hydrogel. By manipulation of the sequential generation and degradation of the DNA hydrogel with a built-in spatiotemporal feedback, they realized an artificial metabolism system. To realize this concept, they engineered a mechanism termed DASH (DNA-based Assembly and Synthesis of Hierarchical materials) that mimics how nature uses metabolism to build structural hierarchy materials through biochemical synthesis and dissipative assembly processes (Fig. 18).

The anabolic generation pathway of DASH (Fig. 18a) consists of two processes: biochemical synthesis of DNA with the help of an enzyme-based rolling circle amplification (RCA) reaction and the assembly of DNA into pre-defined patterns by gelation in a microfluidic device. With this pathway, the continuously generated DNA molecules flow into the microfluidic chamber and form programmed patterns with DNA gelation (Fig. 18b–d) in a dissipative manner. The catabolic degeneration process happens simultaneously along with the anabolic pathway. This is achieved by the enzymatic DNA-hydrolyzing reactions. These two pathways are executed synchronously without any external manipulation. In a three-inlet microfluidic device, the growth and decay of DASH patterns could be controlled by a spatiotemporal feedback mechanism (Fig. 18e). With this artificial metabolism system, Luo et al. [11] further realized emergent locomotion and racing behaviors (Fig. 18f).

5 Discussion and Perspective

Biological cells typically reconfigure their shapes using dynamic signals and regulatory networks that direct the self-assembly process in time and space by sensing, processing, and transmitting information from the environment through molecular components. Bio-inspired out-of-equilibrium systems will set the scene for the next generation of molecular materials with active, adaptive, autonomous, emergent and intelligent behavior. Indeed, life provides the best demonstrations of complex and functional out-of-equilibrium systems: cells keep track of time, communicate, move, adapt, evolve and replicate continuously. Stirred by the understanding of biological principles, artificial out-of-equilibrium systems are emerging in many fields of soft matter science.

Through the route of DNA nanotechnology, much compelling effort has been made towards life-mimicking active assembly. The dynamic control of DNA assembly has been realized by different means with spatial and temporal programmability. However,

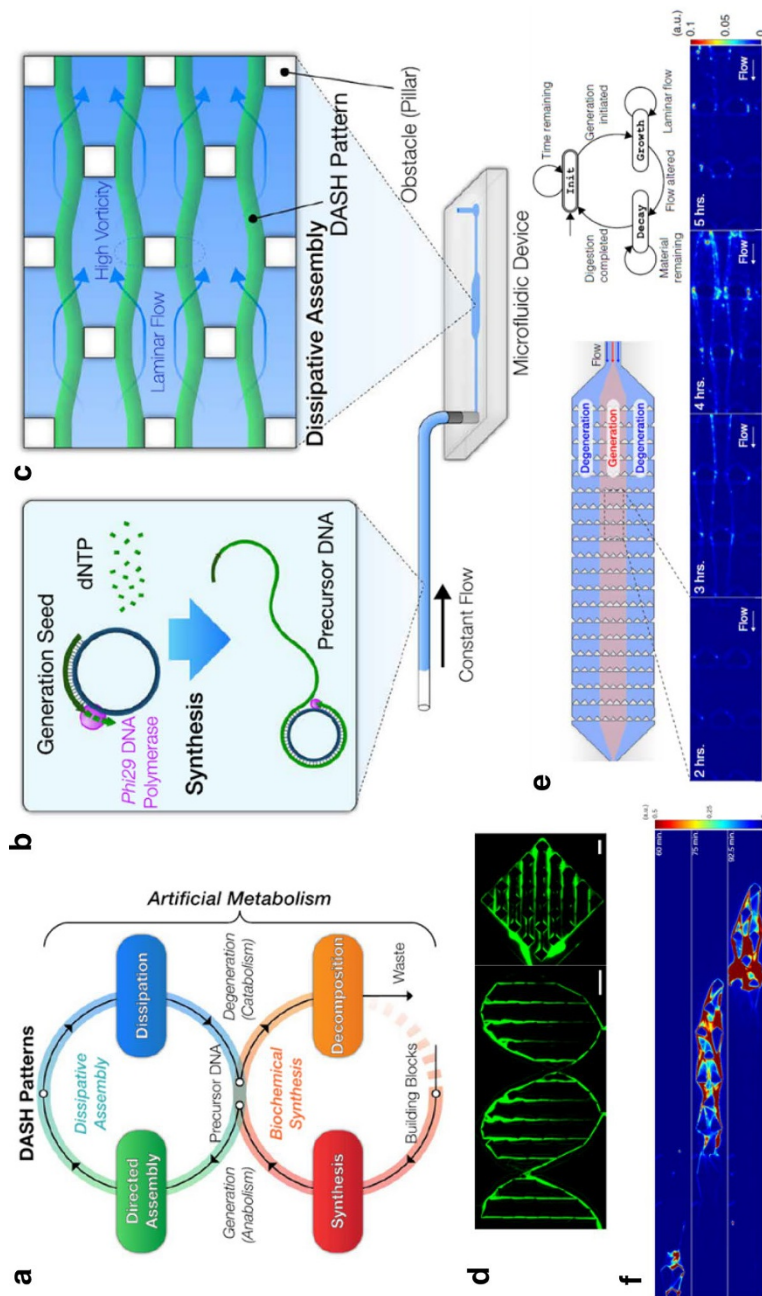


Fig. 18 DNA-based assembly and synthesis of hierarchical materials. **a** Scheme of the artificial metabolism system. **b** Synthesis of precursor DNA by rolling circle amplification (RCA). **c** Formation of DASH (DNA-based Assembly and Synthesis of Hierarchical materials) patterns by dissipative assembly using the flow with obstacles in microfluidic devices. **d** Exemplary DASH patterns formed by DNA hydrogel. **e** Dynamic DASH patterns formed by sequential generation and degeneration of DNA hydrogels. **f** Emergent locomotion and racing behavior powered by dynamic DASH patterns. Reproduced with permission from Ref. [11]. Copyright © 2019, American Association for the Advancement of Science

compared with what happens in living organisms, the development of artificial out-of-equilibrium active systems are still at a very early stage.

The most important and obvious gap is complexity. In addition, the response time of current DNA dynamic systems is significantly slower than the inherent fluctuation time of dynamic biological events, indicating that the response speed of the dynamic DNA structure has large room for improvement. Moreover, the ability to achieve gradual and continuous control over a wide range of states remains a huge challenge. The simplicity and programmability of DNA nanotechnology give us a feasible means to emulate and, in turn, better understand life. While combining these techniques with other materials, and applying design guidelines from DNA systems to other systems may bring more opportunities to achieve bigger successes.

Living organisms decay towards a thermodynamic equilibrium state only when they die. In contrast, the sustainability of artificial out-of-equilibrium systems is still far from satisfactory. There are many thorny issues to be solved to make artificial systems more sustainable. In living systems, energy and precursor materials are supplied continuously at regulated rates, and molecular wastes are recycled or cleaned effectively. In contrast, in an artificial system, energy and precursor materials are normally added at the beginning of the reaction and are consumed irreversibly while wastes accumulate. A possible direction may be to perform artificial systems *in vivo*. Establishing the interfaces between cellular signals and artificial active assembly may solve some of these problems. On the other hand, the coupling of these two systems may provide the means of applying external regulation to life.

To date, the most successful demonstrations have been based on biological enzymes and the use of ATP as fuel. ATP is the molecular unit of currency for energy transfer in life, driving numerous biological motors in a cell by the universal chemical reactions of converting ATP to ADP or AMP. A human-made molecule that can play similar roles, and a set of molecular machines driven by such molecules would be extremely exciting.

Acknowledgements The authors acknowledge the financial support of the National Natural Science Foundation of China (no. 21977112), Natural Science Foundation of Jiangsu Province (BK20190227) and Chinese Academy of Sciences (Y9BES11, Y9AAS110).

Compliance with Ethical Standards

Conflict of interest On behalf of all authors, Chao Zhou and Qiangbin Wang states that there is no conflict of interest.

References

1. Gibson DG, Glass JI, Lartigue C, Noskov VN, Chuang RY, Algire MA, Benders GA, Montague MG, Ma L, Moodie MM, Merryman C, Vashee S, Krishnakumar R, Assad-Garcia N, Andrews-Pfannkoch C, Denisova EA, Young L, Qi ZQ, Segall-Shapiro TH, Calvey CH, Parmar PP, Hutchison CA 3rd, Smith HO, Venter JC (2010) Creation of a bacterial cell controlled by a chemically synthesized genome. *Science* 329(5987):52–56. <https://doi.org/10.1126/science.1190719>
2. Des Marais DJ, Nuth JA 3rd, Allamandola LJ, Boss AP, Farmer JD, Hoehler TM, Jakosky BM, Meadows VS, Pohorille A, Runnegar B, Spormann AM (2008) The NASA astrobiology roadmap. *Astrobiology* 8(4):715–730. <https://doi.org/10.1089/ast.2008.0819>
3. Kaneko K (2006) *Life: an introduction to complex systems biology*. Springer, Berlin

4. Hess B, Mikhailov A (1994) Self-organization in living cells. *Science* 264(5156):223–225
5. Bhalla US, Iyengar R (1999) Emergent properties of networks of biological signaling pathways. *Science* 283(5400):381–387
6. Ashkenasy G, Hermans TM, Otto S, Taylor AF (2017) Systems chemistry. *Chem Soc Rev* 46(9):2543–2554. <https://doi.org/10.1039/c7cs00117g>
7. Merindol R, Walther A (2017) Materials learning from life: concepts for active, adaptive and autonomous molecular systems. *Chem Soc Rev* 46(18):5588–5619. <https://doi.org/10.1039/c6cs00738d>
8. van Roekel HW, Rosier BJ, Meijer LH, Hilbers PA, Markvoort AJ, Huck WT, de Greef TF (2015) Programmable chemical reaction networks: emulating regulatory functions in living cells using a bottom-up approach. *Chem Soc Rev* 44(21):7465–7483. <https://doi.org/10.1039/c5cs00361j>
9. Song J, Li Z, Wang P, Meyer T, Mao C, Ke Y (2017) Reconfiguration of DNA molecular arrays driven by information relay. *Science* 357:6349. <https://doi.org/10.1126/science.aan3377>
10. Green LN, Subramanian HKK, Mardanlou V, Kim J, Hariadi RF, Franco E (2019) Autonomous dynamic control of DNA nanostructure self-assembly. *Nat Chem* 11(6):510–520. <https://doi.org/10.1038/s41557-019-0251-8>
11. Hamada S, Yancey KG, Pardo Y, Gan M, Vanatta M, An D, Hu Y, Derrien TL, Ruiz R, Liu P, Sabin J, Luo D (2019) Dynamic DNA material with emergent locomotion behavior powered by artificial metabolism. *Sci Robot* 4:29. <https://doi.org/10.1126/scirobotics.aaw3512>
12. Seeman NC (1982) Nucleic acid junctions and lattices. *J Theor Biol* 99(2):237–247. [https://doi.org/10.1016/0022-5193\(82\)90002-9](https://doi.org/10.1016/0022-5193(82)90002-9)
13. Yan H, Park SH, Finkelstein G, Reif JH, LaBean TH (2003) DNA-templated self-assembly of protein arrays and highly conductive nanowires. *Science* 301(5641):1882–1884. <https://doi.org/10.1126/science.1089389>
14. Rothmund PW (2006) Folding DNA to create nanoscale shapes and patterns. *Nature* 440(7082):297–302. <https://doi.org/10.1038/nature04586>
15. Ong LL, Hanikel N, Yaghi OK, Grun C, Strauss MT, Bron P, Lai-Kee-Him J, Schueder F, Wang B, Wang P, Kishi JY, Myhrvold C, Zhu A, Jungmann R, Bellot G, Ke Y, Yin P (2017) Programmable self-assembly of three-dimensional nanostructures from 10,000 unique components. *Nature* 552(7683):72–77. <https://doi.org/10.1038/nature24648>
16. Wang W, Chen SL, An B, Huang K, Bai TX, Xu MY, Bellot G, Ke YG, Xiang Y, Wei B (2019) Complex wireframe DNA nanostructures from simple building blocks. *Nat Commun* 10(1):1067. <https://doi.org/10.1038/s41467-019-08647-7>
17. Zheng J, Birktoft JJ, Chen Y, Wang T, Sha R, Constantinou PE, Ginell SL, Mao C, Seeman NC (2009) From molecular to macroscopic via the rational design of a self-assembled 3D DNA crystal. *Nature* 461(7260):74–77. <https://doi.org/10.1038/nature08274>
18. Zhang T, Hartl C, Frank K, Heuer-Jungemann A, Fischer S, Nickels PC, Nickel B, Liedl T (2018) 3D DNA origami crystals. *Adv Mater* 30:e1800273. <https://doi.org/10.1002/adma.201800273>
19. Zhang Y, Pan V, Li X, Yang X, Li H, Wang P, Ke Y (2019) Dynamic DNA structures. *Small* 15(26):e1900228. <https://doi.org/10.1002/smll.201900228>
20. Simmel FC, Yurke B, Singh HR (2019) Principles and applications of nucleic acid strand displacement reactions. *Chem Rev* 119(10):6326–6369. <https://doi.org/10.1021/acs.chemrev.8b00580>
21. Zhang DY, Seelig G (2011) Dynamic DNA nanotechnology using strand-displacement reactions. *Nat Chem* 3(2):103–113. <https://doi.org/10.1038/nchem.957>
22. Tigges T, Heuser T, Tiwari R, Walther A (2016) 3D DNA origami cuboids as monodisperse patchy nanoparticles for switchable hierarchical self-assembly. *Nano Lett* 16(12):7870–7874. <https://doi.org/10.1021/acs.nanolett.6b04146>
23. Wagenbauer KF, Sigl C, Dietz H (2017) Gigadalton-scale shape-programmable DNA assemblies. *Nature* 552(7683):78–83. <https://doi.org/10.1038/nature24651>
24. Yang S, Liu W, Wang R (2019) Control of the stepwise assembly–disassembly of DNA origami nanoclusters by pH stimuli–responsive DNA triplexes. *Nanoscale* 11(39):18026–18030. <https://doi.org/10.1039/C9NR05047G>
25. Dong Y, Yang Z, Liu D (2014) DNA nanotechnology based on i-motif structures. *Acc Chem Res* 47(6):1853–1860. <https://doi.org/10.1021/ar500073a>
26. Yang S, Liu W, Nixon R, Wang R (2018) Metal-ion responsive reversible assembly of DNA origami dimers: G-quadruplex induced intermolecular interaction. *Nanoscale* 10(8):3626–3630. <https://doi.org/10.1039/c7nr09458b>
27. Wu N, Willner I (2016) DNAzyme-controlled cleavage of dimer and trimer origami tiles. *Nano Lett* 16(4):2867–2872. <https://doi.org/10.1021/acs.nanolett.6b00789>

28. Green LN, Amodio A, Subramanian HKK, Ricci F, Franco E (2017) pH-driven reversible self-assembly of micron-scale DNA scaffolds. *Nano Lett* 17(12):7283–7288. <https://doi.org/10.1021/acs.nanolett.7b02787>
29. Rothmund PWK, Ekani-Nkodo A, Papadakis N, Kumar A, Fygenson DK, Winfree E (2004) Design and characterization of programmable DNA nanotubes. *J Am Chem Soc* 126(50):16344–16352. <https://doi.org/10.1021/ja0443191>
30. Suzuki Y, Endo M, Yang Y, Sugiyama H (2014) Dynamic assembly/disassembly processes of photoresponsive DNA origami nanostructures directly visualized on a lipid membrane surface. *J Am Chem Soc* 136(5):1714–1717. <https://doi.org/10.1021/ja4109819>
31. Peng RZ, Wang HJ, Lyu YF, Xu LJ, Liu H, Kuai HL, Liu Q, Tan WH (2017) Facile assembly/disassembly of DNA nanostructures anchored on cell-mimicking giant vesicles. *J Am Chem Soc* 139(36):12410–12413. <https://doi.org/10.1021/jacs.7b07485>
32. Li H, Wang M, Shi T, Yang S, Zhang J, Wang HH, Nie Z (2018) A DNA-mediated chemically induced dimerization (D-CID) nanodevice for nongenetic receptor engineering to control cell behavior. *Angew Chem Int Ed* 57(32):10226–10230. <https://doi.org/10.1002/anie.201806155>
33. Dirks RM, Pierce NA (2004) Triggered amplification by hybridization chain reaction. *Proc Natl Acad Sci USA* 101(43):15275–15278. <https://doi.org/10.1073/pnas.0407024101>
34. Choi HMT, Chang JY, Trinh LA, Padilla JE, Fraser SE, Pierce NA (2010) Programmable in situ amplification for multiplexed imaging of mrna expression. *Nat Biotechnol* 28(11):1208–1212. <https://doi.org/10.1038/nbt.1692>
35. Zhu G, Zheng J, Song E, Donovan M, Zhang K, Liu C, Tan W (2013) Self-assembled, aptamer-tethered DNA nanotrains for targeted transport of molecular drugs in cancer theranostics. *Proc Natl Acad Sci USA* 110(20):7998–8003. <https://doi.org/10.1073/pnas.1220817110>
36. Venkataraman S, Dirks RM, Rothmund PW, Winfree E, Pierce NA (2007) An autonomous polymerization motor powered by DNA hybridization. *Nat Nanotechnol* 2(8):490–494. <https://doi.org/10.1038/nnano.2007.225>
37. Cangialosi A, Yoon C, Liu J, Huang Q, Guo J, Nguyen TD, Gracias DH, Schulman R (2017) DNA sequence-directed shape change of photopatterned hydrogels via high-degree swelling. *Science* 357(6356):1126–1130. <https://doi.org/10.1126/science.aan3925>
38. Zhang H, Wang Y, Zhang H, Liu X, Lee A, Huang Q, Wang F, Chao J, Liu H, Li J, Shi J, Zuo X, Wang L, Wang L, Cao X, Bustamante C, Tian Z, Fan C (2019) Programming chain-growth copolymerization of DNA hairpin tiles for in-vitro hierarchical supramolecular organization. *Nat Commun* 10(1):1006. <https://doi.org/10.1038/s41467-019-09004-4>
39. Nie Z, Wang P, Tian C, Mao C (2014) Synchronization of two assembly processes to build responsive DNA nanostructures. *Angew Chem Int Ed* 53(32):8402–8405. <https://doi.org/10.1002/anie.201404307>
40. Zhang DY, Turberfield AJ, Yurke B, Winfree E (2007) Engineering entropy-driven reactions and networks catalyzed by DNA. *Science* 318(5853):1121–1125. <https://doi.org/10.1126/science.1148532>
41. Yin P, Choi HM, Calvert CR, Pierce NA (2008) Programming biomolecular self-assembly pathways. *Nature* 451(7176):318–322. <https://doi.org/10.1038/nature06451>
42. Li B, Ellington AD, Chen X (2011) Rational, modular adaptation of enzyme-free DNA circuits to multiple detection methods. *Nucleic Acids Res* 39(16):e110. <https://doi.org/10.1093/nar/gkr504>
43. Zhang DY, Hariadi RF, Choi HMT, Winfree E (2013) Integrating DNA strand-displacement circuitry with DNA tile self-assembly. *Nat Commun* 4:1965. <https://doi.org/10.1038/ncomms2965>
44. Amodio A, Zhao B, Porchetta A, Idili A, Castronovo M, Fan CH, Ricci F (2014) Rational design of pH-controlled DNA strand displacement. *J Am Chem Soc* 136(47):16469–16472. <https://doi.org/10.1021/ja508213d>
45. Xing C, Dai J, Huang Y, Lin Y, Zhang KL, Lu C, Yang H (2019) Active self-assembly of train-shaped DNA nanostructures via catalytic hairpin assembly reactions. *Small* 15(27):e1901795. <https://doi.org/10.1002/smll.201901795>
46. Barish RD, Schulman R, Rothmund PWK, Winfree E (2009) An information-bearing seed for nucleating algorithmic self-assembly. *Proc Natl Acad Sci USA* 106(15):6054–6059. <https://doi.org/10.1073/pnas.0808736106>
47. Agrawal DK, Jiang R, Reinhart S, Mohammed AM, Jorgenson TD, Schulman R (2017) Terminating DNA tile assembly with nanostructured caps. *ACS Nano* 11(10):9770–9779. <https://doi.org/10.1021/acsnano.7b02256>

48. Mohammed AM, Sulc P, Zenk J, Schulman R (2017) Self-assembling DNA nanotubes to connect molecular landmarks. *Nat Nanotechnol* 12(4):312–316. <https://doi.org/10.1038/nnano.2016.277>
49. Kirschner M, Mitchison T (1986) Beyond self-assembly: From microtubules to morphogenesis. *Cell* 45(3):329–342. [https://doi.org/10.1016/0092-8674\(86\)90318-1](https://doi.org/10.1016/0092-8674(86)90318-1)
50. Pollard TD, Borisy GG (2003) Cellular motility driven by assembly and disassembly of actin filaments. *Cell* 112(4):453–465. [https://doi.org/10.1016/s0092-8674\(03\)00120-x](https://doi.org/10.1016/s0092-8674(03)00120-x)
51. Lazarides E (1980) Intermediate filaments as mechanical integrators of cellular space. *Nature* 283(5744):249–256. <https://doi.org/10.1038/283249a0>
52. Zaikin AN, Zhabotinsky AM (1970) Concentration wave propagation in two-dimensional liquid-phase self-oscillating system. *Nature* 225(5232):535–537. <https://doi.org/10.1038/225535b0>
53. Epstein IR, Showalter K (1996) Nonlinear chemical dynamics: oscillations, patterns, and chaos. *J Phys Chem* 100(31):13132–13147. <https://doi.org/10.1021/jp953547m>
54. Kim J, Winfree E (2011) Synthetic in vitro transcriptional oscillators. *Mol Syst Biol* 7:465. <https://doi.org/10.1038/msb.2010.119>
55. Franco E, Friedrichs E, Kim J, Jungmann R, Murray R, Winfree E, Simmel FC (2011) Timing molecular motion and production with a synthetic transcriptional clock. *Proc Natl Acad Sci USA* 108(40):E784–793. <https://doi.org/10.1073/pnas.1100060108>

Publisher's Note Springer Nature remains neutral with regard to jurisdictional claims in published maps and institutional affiliations.

Affiliations

Jinyi Dong^{1,2} · Chao Zhou¹  · Qiangbin Wang¹

¹ CAS Key Laboratory of Nano-Bio Interfaces, Division of Nanobiomedicine and i-Lab, Suzhou Institute of Nano-Tech and Nano-Bionics, Chinese Academy of Sciences, Suzhou 215123, People's Republic of China

² School of Physical Science and Technology, ShanghaiTech University, Shanghai 201210, People's Republic of China



REVIEW

Tailoring DNA Self-assembly to Build Hydrogels

Jie Chen^{1,2} · Ying Zhu^{1,3} · Huajie Liu⁴ · Lihua Wang^{1,3}

Received: 9 November 2019 / Accepted: 23 February 2020 / Published online: 7 March 2020
© Springer Nature Switzerland AG 2020

Abstract

DNA hydrogels are crosslinked polymeric networks in which DNA is used as the backbone or the crosslinker. These hydrogels are novel biofunctional materials that possess the biological character of DNA and the framed structure of hydrogels. Compared with other kinds of hydrogels, DNA hydrogels exhibit not only high mechanical strength and controllable morphologies but also good recognition ability, designable responsiveness, and programmability. The DNA used in this type of hydrogel acts as a building block for self-assembly or as a responsive element due to its sequence recognition ability and switchable structural transitions, respectively. In this review, we describe recent developments in the field of DNA hydrogels and discuss the role played by DNA in these hydrogels. Various synthetic strategies for and a range of applications of DNA hydrogels are detailed.

Keywords DNA nanotechnology · DNA hydrogels · Biofunctional materials · Self-assembly

Chapter 2 was originally published as Chen, J., Zhu, Y., Liu, H. & Wang, L. Topics in Current Chemistry (2020) 378: 32. <https://doi.org/10.1007/s41061-020-0295-7>.

✉ Huajie Liu
liuhuajie@tongji.edu.cn

✉ Lihua Wang
wanglihua@zjlab.org.cn

- ¹ Division of Physical Biology, CAS Key Laboratory of Interfacial Physics and Technology, Shanghai Institute of Applied Physics, Chinese Academy of Sciences, Shanghai 201800, China
- ² University of Chinese Academy of Sciences, Beijing 100049, China
- ³ Zhangjiang Laboratory, Shanghai Advanced Research Institute, Chinese Academy of Sciences, Shanghai 201210, China
- ⁴ School of Chemical Science and Engineering, Shanghai Research Institute for Intelligent Autonomous Systems, Key Laboratory of Advanced Civil Engineering Materials of Ministry of Education, Tongji University, Shanghai 200092, China

1 Introduction

Hydrogels are a class of soft materials with high water contents and three-dimensional (3D) crosslinked networks [1]. The chemical characteristics of the polymeric chains in hydrogels can be tailored to make them biocompatible and responsive to specific stimuli (e.g., heat, light, or certain molecules). Due to their unique structural and mechanical properties, hydrogels are probably the most widely used artificial materials in biomedical applications [2] such as bio-sensing [3], drug delivery [4], and tissue engineering [5]. Traditionally, artificial hydrogels are constructed by crosslinking hydrophilic synthetic polymers to form networks. Though the rapid growth of polymer chemistry has enabled the functionalization of hydrogels to suit specific requirements, it remains challenging to customize the structural anisotropy of hydrogels, configure their chains, and program their polymerization [5].

Linear DNA strands, which are famous for their ability to store genetic information [6], can be used as biopolymers in hydrogels, given that DNA hybridization—which obeys strict base-pairing rules—is inherently a sequence-specific self-assembly process. In 1982, Seeman suggested an unusual idea: that artificial DNA nanostructures could be created from branched DNA building blocks [7]. In such an approach, synthetic single-stranded DNAs with designed sequences recognize complementary strands and form predictable structures [8, 9]. New techniques such as DNA origami and spherical DNA have driven the rapid growth of this field in recent years [10, 11]. Similarly, programmable hybridization can lead to the random crosslinking of DNA strands in three dimensions to form hydrogels. Compared with synthetic polymer-based hydrogels, DNA hydrogels have a number of advantages, such as specific molecular recognition, multifunctionality, and excellent biocompatibility [12]. Other notable features of DNA hydrogels that can be achieved through the artful design of DNA sequences include responsiveness to multiple stimuli and tunable mechanical properties [13].

The idea of controlling sol–gel transitions using DNA can be traced back to 1987, when DNA duplexes were covalently interconnected using chemical crosslinkers for the first time [14]. Almost 10 years later, a different strategy involving the crosslinking of synthetic polymers through DNA hybridization emerged, which opened the door to hybrid DNA hydrogel synthesis [15]. However, DNA hydrogels did not attract much attention before the early 2000s, largely because nanotechnology was still in its infancy. This situation changed with the emergence of pure DNA hydrogels, as first reported by the groups of Luo and Liu [16–18]. Their creative work illustrated the infinite variety of DNA interactions that were possible (in contrast to the interactions of synthetic polymers), facilitating the synthesis of smart hydrogels. This research field has grown rapidly over the past decade [12]. Both pure and hybrid DNA hydrogels are now cutting-edge materials for next-generation biomedical and intelligent applications.

In this review, we focus on recent progress in the field of DNA hydrogels fabricated by base–base recognition mechanisms. DNA hydrogels that are formed by physical interwinding are not included in this review, but they are reviewed

elsewhere [12]. We consider different design principles and construction strategies, starting with conventional DNA hybridization strategies in which stable hydrogels are directly formed through sequence-specific hybridization. We then describe enzyme-assisted hybridization strategies and show that nonduplex DNA conformations such as i-motifs and G-quadruplexes can also form networks. Finally, we discuss emerging approaches in order to highlight the future directions for research in this field.

2 Conventional DNA Hybridization Strategies

2.1 Unbranched DNA Strands for Crosslinking Synthetic Polymers

By modifying single-stranded DNA (ssDNA) on synthetic linear polymer chains, it is possible to crosslink polymers to form 3D networks. DNA overhangs on the polymer act as side chains that can be used to connect polymers. Most hybrid DNA hydrogels are fabricated in this manner.

In 1996, Nagahara and Matsuda were the first to utilize this idea to construct a DNA–polyacrylamide hybrid hydrogel [15]. They designed two kinds of acrydite-modified single-stranded DNAs that were separately incorporated into polyacrylamide chains to obtain oligoT–polyacrylamide and oligoA–polyacrylamide. Next, they constructed two types of DNA–polyacrylamide hybrid hydrogels: one was formed by using polyA ssDNA to crosslink the oligoT–polyacrylamide (type I, Fig. 1a); the other was formed through the intermolecular crosslinking of oligoT–polyacrylamide and oligoA–polyacrylamide (type II, Fig. 1b).

To further exploit the advantages of DNA, Lin et al. demonstrated a DNA-crosslinked polyacrylamide hydrogel in which the DNA crosslinker strand incorporated a “toehold” region. Using DNA strand-displacement reactions, the crosslinks could then be eliminated through the addition of a removal strand, facilitating a

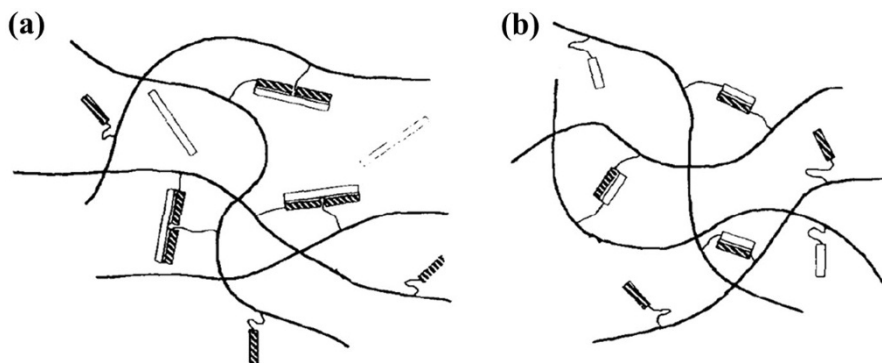


Fig. 1 DNA hydrogels formed by the hybridization of two types of single-stranded DNAs. **a** Schematic of DNA hydrogel formation through the addition of extra ssDNA to crosslink two different ssDNA-modified polymer chains. **b** Schematic of DNA hydrogel formation through the complementary hybridization of ssDNA on polymer chains. Reproduced with permission from [15]

gel-sol transition [19]. Then Lin et al. created a DNA-crosslinked hydrogel with reversible stiffness that utilized a DNA crosslinker which was designed to respond to a specific DNA “fuel” strand [20]. Moreover, Simmel and coworkers constructed a DNA-switchable gel that could be used for quantum dot delivery (Fig. 2a). The particles were released by adding DNA “release” strands that induced hydrogel delinking. The delinked gel could then be relinked by adding the crosslinking strand [21].

A series of hydrogels based on the hybridization of different types of single-stranded DNAs have been constructed and used for sensing and bioassays—for instance, in the detection of miRNAs used for clinical diagnostics. Yuan and Chai proposed a SERS platform for target miRNA detection. In the mechanism for that platform, the target miRNA induces the release of DNA via DNA displacement reactions, and the released DNA induces the dissociation of the 3D hydrogel network. This causes a Raman reporter (TB) to leak out, triggering a strong Raman signal [22]. Based on a similar principle involving a DNA hybrid hydrogel, Ding and coworkers manufactured an electrochemical biosensing platform for miR-21 detection (Fig. 2b) [23]. Li and colleagues developed a portable glucometer readout system for the detection of multiple endogenous miRNAs (Fig. 2c) [24].

Aside from schemes in which the signal is activated by the dissociation of the hydrogel, there are also schemes in which hydrogel formation induces signal enhancement or modification. Tang and colleagues designed a biosensor based on a DNA–polyacrylamide hybrid hydrogel in which Hg^{2+} activated a Mg^{2+} -specific DNAzyme that

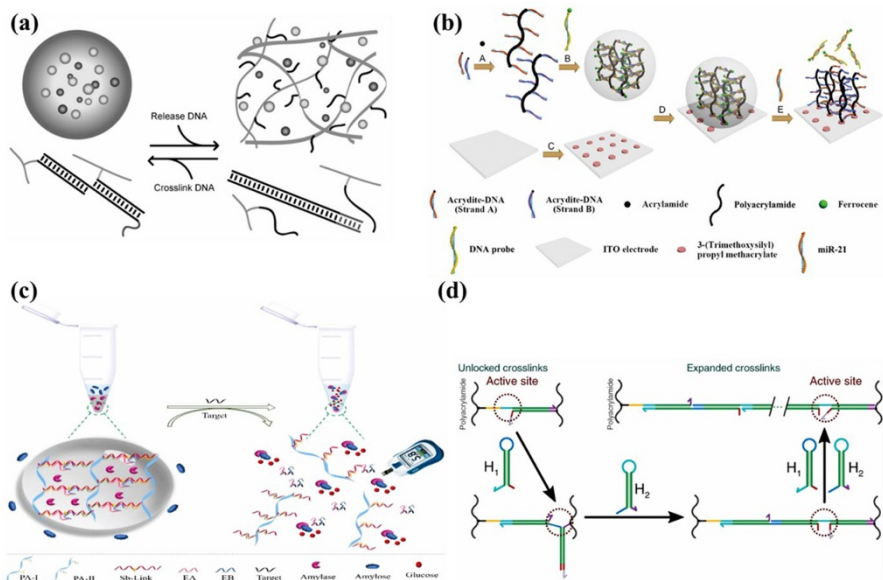


Fig. 2 Applications of DNA/RNA-responsive hydrogels. **a** Schematic of a DNA-switchable gel used for nanoparticle delivery. **b** Schematic of an electrochemical DNA hydrogel biosensor employed for the detection of miR-21. **c** Schematic of a DNA hydrogel used as a sensing platform for target miRNA detection. **d** Schematic of a DNA hydrogel that changes size upon hairpin monomer incorporation. Reproduced with permission from [21, 23, 24, 30]

produced a single-stranded DNA, which in turn initiated a hybridization chain reaction (HCR) between two hairpin-modified polymer chains that induced DNA–polyacrylamide hybrid hydrogel formation on an electrode, activating the signal [25]. Using the same principle (i.e., the initiation of a HCR between two hairpin-modified polymer chains induces the formation of a DNA hybrid hydrogel), Jie and colleagues developed a versatile DNA-hydrogel-amplified fluorescence platform for the detection of a miRNA [26]. In another scheme, the single-stranded DNA used as a crosslinker was premodified with a liposome, and this DNA-modified liposome was used to crosslink DNA-grafted polyacrylamide copolymers, yielding a DNA hydrogel [27].

Moreover, It is worth noting that until very recently, HCR was only used to form hydrogels via the crosslinking of hairpin-DNA-modified polyacrylamides [28]. However, in 2017, Schulman and colleagues designed a system in which HCR was used to successively extend the DNA crosslinker of a DNA-hybrid hydrogel with specific DNA molecules, leading to a hundredfold increase in the volume of the hydrogel [29]. Using the same hydrogel expansion mechanism, Schulman and Fern subsequently developed a new DNA-responsive system. In this system, low concentrations of biomolecular input molecules interact with molecular controllers instead of the hydrogel polymer. These molecular controllers recognize the inputs and then perform appropriate processing and amplification, leading to a strong output signal that triggers large-scale responses in the hydrogel (Fig. 2d) [30].

In all of the above schemes, the DNA strands need to interact directly with the DNA crosslinker to modify the DNA hydrogel network, as the schemes are based on strand displacement reactions. Therefore, to induce large-scale changes in the properties of the hydrogel, a high concentration of external DNA must be added to the system. To avoid this problem, Collins and coworkers exploited Cas12a, a CRISPR (clustered regularly interspaced short palindromic repeats)-associated nuclease, to actuate hydrogels crosslinked by DNA bridges. This scheme only required a low concentration of external DNA to induce changes to the hydrogel network. The mechanism used was as follows. Firstly, Cas12a binds to gRNA to form a gRNA–Cas12a complex. When the target double-stranded DNA is added, the single-stranded deoxyribonuclease (ssDNase) activity of Cas12a is activated; Cas12a indiscriminately cleaves any single-stranded DNA (ssDNA) nearby. Therefore, upon exposure to the gRNA–Cas12a and the target dsDNA, the single-stranded DNA used as the crosslinker in the hydrogel is degraded, dissociating the hydrogel network [31]. This represents a new type of DNA-responsive hydrogel based on sequence recognition of the gRNA and enzymatic cleavage of the Cas12a in the gRNA–Cas12a complex rather than strand displacement or structural changes to DNA crosslinkers. Because of the high specificity and programmability of the CRISPR-Cas12a enzyme system, this type of DNA-responsive hydrogel could be exploited as a smart drug-delivery system or diagnostic tool [32].

2.2 Pure DNA Hydrogels Based on Sticky End Complementary Hybridization

In contrast to the formation of hydrogels based on the direct hybridization of single DNA strands, another conventional DNA hybridization strategy involves the use

of branched DNA sticky end complementary hybridization. This principle has been adopted to prepare pure DNA hydrogels that only consist of whole DNA.

In 2011, Liu and coworkers created a DNA hydrogel through the sticky end complementary hybridization of two DNA building blocks (Fig. 3a). Two kinds of DNA building blocks are used in this system: Y-scaffold DNA (Y-DNA) and a DNA linker (L-DNA). The Y-DNA has three arms, each with a sticky end, and is formed through the self-assembly of three types of single-stranded DNA. The L-DNA is a linear double-stranded DNA containing two sticky ends at both ends of the DNA. The sticky ends of the L-DNA hybridize with the complementary sticky ends of the Y-DNA. The hydrogel is obtained by mixing the Y-DNA and the L-DNA in an appropriate molar ratio. It should be noted that the sticky ends of this system contrast with those of the X-DNA system created by Luo [16], in which the sticky ends are palindromic sequences. Instead, in the system designed by Liu and coworkers, palindromic sequences are avoided as much as possible to suppress self-linking. Therefore, the resulting DNA hydrogel is homogeneous. The thermal response of this DNA hydrogel is dependent on the length and the composition of the sticky ends [18]. Including restriction sites on the L-DNA allows it to be cleaved by the corresponding restriction enzyme, leading to the disruption of the hydrogel network. Thus, this enzyme-triggered DNA hydrogel could be used to envelop and then, when triggered, release single cells (Fig. 3b) [33]. A series of DNA hydrogels

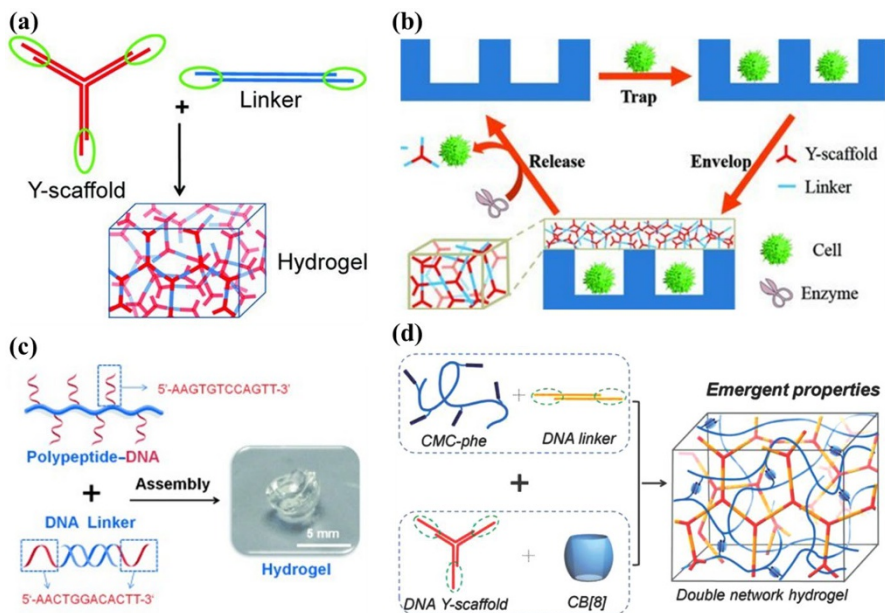


Fig. 3 DNA hydrogel schemes based on sticky end complementary hybridization, and some applications of them. **a** Schematic of DNA hydrogel formation via Y-scaffold and linker self-assembly. **b** Schematic of a DNA hydrogel that dissociates in response to a specific restriction enzyme; this hydrogel could be used to envelop and (when triggered) release cells. **c** Schematic of polypeptide-DNA hydrogel formation through the hybridization of the sticky ends in the DNA linker with the ssDNA on the polypeptide. **d** Schematic of a double-network hydrogel. Reproduced with permission from [18, 33, 35, 36]

based on the same strategy were then reported by Liu's group. For example, a new type of DNA–polypeptide hydrogel was developed [34]. After a series of improvements, they created a supramolecular polypeptide-DNA hydrogel that could be used as a bioink in 3D bioprinting (Fig. 3c) [35]. In addition, responsive double-network (i.e., dual crosslinked) hydrogels were constructed based on cucurbit[8]uril hydrogel networks (Fig. 3d) [36]. A DNA hydrogel with modifiable macroscopic mechanical properties was prepared using an i-motif sequence in the linear linker [37], a hydrogel based on DNA-modified magnetic nanoparticles was created [38], and a tissue-like DNA supramolecular hydrogel permitting cell migration was fabricated [39]. A polypeptide-DNA supramolecular hydrogel with rheological properties that could be modified without changing the network topology and crosslinker was also developed [40]. Moreover, the microrheology of a DNA hydrogel formed from Y-shaped DNA building blocks was studied in detail using diffusing-wave spectroscopy (DWS) [41].

An X-shaped DNA crosslinker with four arms that have sticky ends was designed for the fabrication of multifunctional hydrogels in 2015 (Fig. 4a). To prepare this X-shaped DNA linker, two kinds of Y-shaped DNA were prepared through the self-assembly of two groups of three types of single-stranded DNA, respectively. Upon mixing the two kinds of Y-shaped DNA equally, they assembled to form the X-shaped DNA crosslinker. Two of the arms of the X-shaped DNA serve as crosslinking sites, while the other two are free sticky ends that can be used for further modifications through precise DNA hybridization. Therefore, different functional groups can be attached to the hydrogel network in a specified ratio via reliable DNA hybridization [42]. Using this multiarm DNA crosslinker, Ignatius and coworkers reported the preparation of a multifunctional DNA–protein hybrid hydrogel from modified human serum albumin. The specific multicomponent loading of this

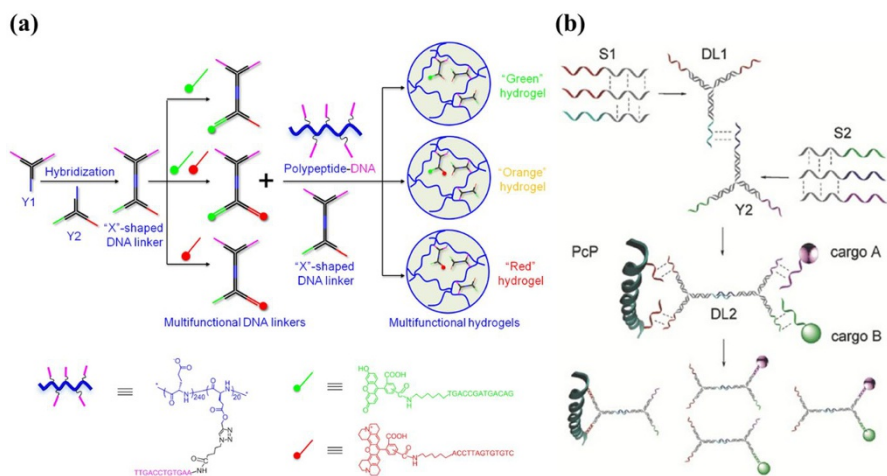


Fig. 4 X-shaped DNA used as a multiarm DNA crosslinker for DNA hydrogel formation. **a** Schematic of the use of rationally designed multifunctional DNA linkers to construct a multifunctional polypeptide-DNA hydrogel. **b** Schematic of the preparation of a protein-DNA hydrogel that is capable of loading and releasing multifunctional cargos. Reproduced with permission from [42, 43]

hydrogel with bioactive cargos and the spatiotemporally controlled release of those cargos from the hydrogel were demonstrated (Fig. 4b) [43].

Moreover, using the Y-DNA and L-DNA model for DNA hydrogel construction, Willner and colleagues demonstrated a Y-shaped DNA structure that was modified with Ag nanoclusters (Ag-NCs) at a specific loop domain in the Y-scaffold. Addition of a DNA linker resulted in the crosslinking of the Y-scaffold to form a three-dimensional hydrogel network containing fluorescent Ag-NCs [44]. Minteer and colleagues used a similar approach to entrap glucose oxidase in a DNA hydrogel, thus producing an enzymatic biobattery [45]. Later, they constructed DNA redox hydrogels by coimmobilizing redox mediators and glucose oxidoreductase enzymes in DNA hydrogels [46]. Similar hydrogels could also be used directly for biotherapy without the need for any chemical modification. For instance, DNA hydrogels in which the linear linker bears unmethylated cytosine-phosphate-guanine (CpG) dinucleotides can be used for tumor vaccinations [47]. This type of hydrogel could also be applied as an ophthalmic therapeutic delivery system [48].

There are other DNA hydrogel design strategies based on sticky end complementary hybridization too. For instance, Takakura and Nishikawa reported a self-gelling and injectable DNA hydrogel based on polypod-like DNA (polypodna) that self-assembled under physiological conditions. This concept was used to create a DNA hydrogel bearing unmethylated cytosine-phosphate-guanine (CpG) dinucleotides that could be used to stimulate innate immunity [49]. Afterwards, Nishikawa employed this method to construct a series of DNA hydrogels for biotherapy. Among them, Nishikawa and coworkers developed a Takumi-based DNA hydrogel (Fig. 5a) [50]. In order to further expand the applications of this hydrogel and improve its therapeutic effects, the hydrogel was mixed with chitosan to improve its sustained release characteristics [51]. Oral delivery of CpG DNA was achieved by coating the hydrogel with chitosan [52]. An enhanced immune response was realized by generating a hydrogel incorporating cholesterol-modified DNA [53]. They also achieved

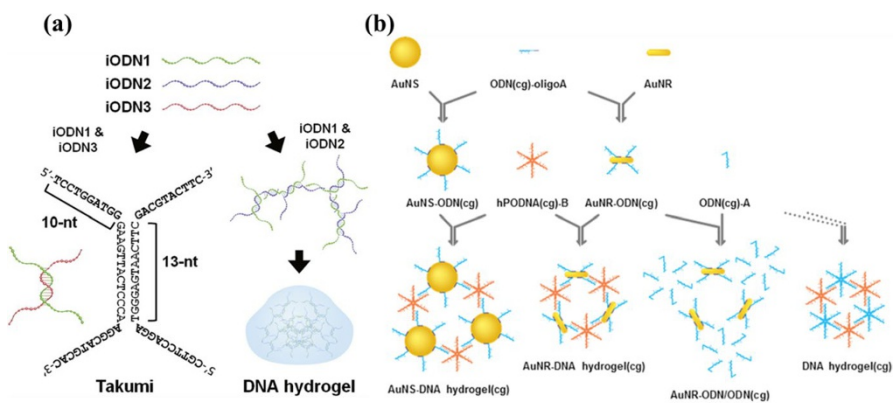


Fig. 5 DNA hydrogels formed through the self-assembly of polypod-like DNA (polypodna). **a** Schematic of the formation of Takumi and a Takumi-based DNA hydrogel. **b** Schematic of the synthesis of AuNS-DNA and AuNR-DNA hydrogels based on hexapodna self-assembly. Reproduced with permission from [50, 54]

a composite-type immunostimulatory DNA hydrogel by mixing appropriately designed hexapod-like DNA (hexapodna)-bearing CpG sequences with oligodeoxynucleotide-modified gold nanoparticles (Fig. 5b). When the hydrogel was irradiated with laser light, hexapodna was released, which stimulated immune cells with its CpG sequences [54]. Filetici and Francesco reported a re-entrant DNA hydrogel based on tetravalent DNA nanostars [55]. They systematically characterized the viscosity and the linear viscoelastic moduli for two different tetravalent DNA nanostar hydrogels [56]. In addition, the relationship between the structure of the tetravalent DNA nanostar hydrogel and its nonequilibrium dynamics was explored [57]. Kelley used a DNA three-way junction (TWJ) nanostructure and DNA-templated quantum dots (QDs) to construct a self-assembled quantum dot DNA hydrogel [58]. A gold nanoparticle (NP) DNA hydrogel based on a DNA three-way junction nanostructure was also developed [59]. Ding constructed a DNA hydrogel with two kinds of X-shaped DNA polymers: 1 and 2. When the two X-shaped DNA polymers were mixed, complementary hybridization of their sticky ends occurred, yielding the DNA hydrogel [60].

As well as schemes that use complex DNA-based systems, short linear double-stranded DNA (dsDNA) equipped with sticky ends has also been used as a building block to form hydrogels (Fig. 6a) [61]. A thermoresponsive DNA hydrogel was used to monitor the diffusion of guest molecules [62]. In a slightly different system, short linear double-stranded DNA (dsDNA) equipped with sticky ends was used to crosslink the main chains of a hydrogel, which were long linear double-stranded DNAs. Therefore, the determinant of hydrogel formation was the crosslinking strand (Fig. 6b, c) [63]. Adopting a similar strategy, Nakatani developed a specific DNA-strand-responsive DNA hydrogel based on a well-designed DNA circuit. The sol–gel phase transition of the DNA hydrogel was realized by adding different DNA strands (Fig. 6d) [64].

Moreover, in contrast to schemes that require multiple types of single-stranded DNA, it is also possible to use just one kind of DNA to construct a DNA hydrogel. Such one-strand (OS) hydrogels can be created using a single DNA strand with multiple domains, where each domain is a self-complementary palindromic sequence. The hydrogel is then formed in a single-step process in which individual strands are crosslinked together by the complementary domains (Fig. 6e). This DNA hydrogel formation method is simple and programmable [65].

3 DNA Hydrogels Formed Using Enzymes

3.1 DNA Hydrogels Formed Using Ligase

Adopting conventional DNA hybridization strategies to construct DNA hydrogels requires sufficiently long sticky ends to stabilize the crosslinker. Ligase can join DNA fragments with complementary sticky ends and can repair nicks in double-stranded DNA with 3'-hydroxyl and 5'-phosphate ends. Therefore, ligase can be used to covalently crosslink such DNA with complementary sticky ends to form hydrogels. In 2006, Luo and coworkers reported that a pure DNA hydrogel had been

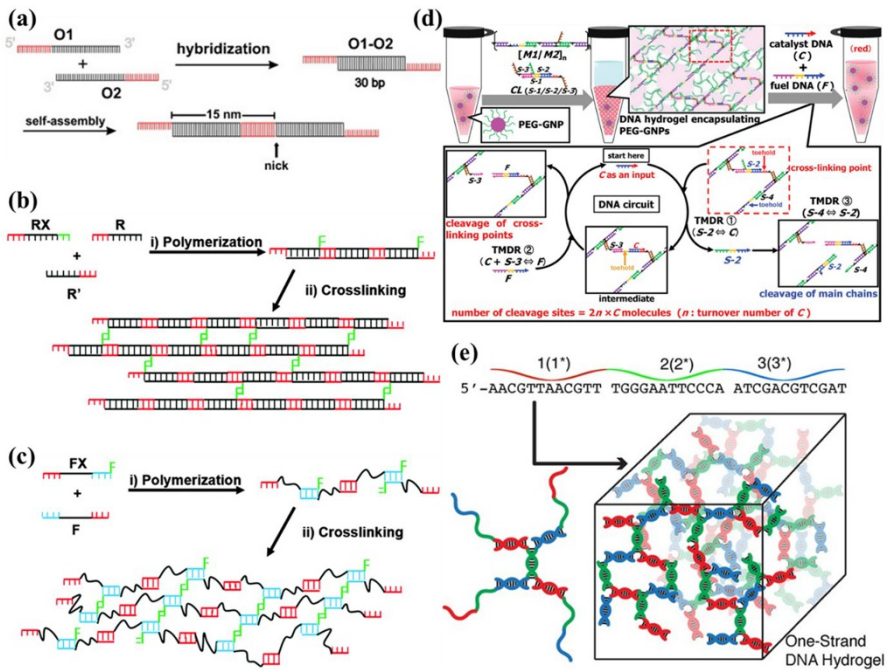


Fig. 6 DNA hydrogels formed via short dsDNA or one-stranded ssDNA self-assembly. **a** Schematic of a hydrogel formed by short linear double-stranded DNA self-assembly. **b** Schematic of a hydrogel formed by the hybridization of sticky ends, leading to rigid double-helix DNA chain crosslinking. **c** Schematic of a hydrogel formed by the hybridization of sticky ends, leading to the crosslinking of flexible DNA chains bearing ssDNA segments. **d** An artfully designed DNA circuit system that was used to create a dynamically programmed DNA hydrogel. **e** Schematic of a hydrogel formed through one-strand DNA self-assembly. Reproduced with permission from [61, 63–65]

constructed entirely from branched DNA for the first time. To obtain this pure DNA hydrogel, the authors designed and synthesized three types of branched DNA monomers: X-DNA, Y-DNA, and T-DNA. Each arm of these branched DNA monomers was a complementary sticky end containing palindromic sequences. Thus, due to the presence of the self-complementary sticky ends, the branched DNA monomers could be assembled via subsequent ligation with T4 DNA ligase into large-scale 3D-structured DNA hydrogels. The authors found that the X-DNA-based hydrogel had better mechanical properties, was more resistant to degradation, and exhibited better sustained release characteristics than the Y-DNA-based hydrogel and the T-DNA-based hydrogel [16].

Subsequently, Luo's group invented a cell-free protein-producing hydrogel system by incorporating actual plasmid DNA genes into a hydrogel. Similarly to the X-DNA hydrogel system mentioned above, this hydrogel was constructed by mixing X-DNA and linear plasmids in a predetermined molar ratio and then applying T4 DNA ligase to form the hydrogel for protein expression [66]. They then scaled up this protein-producing hydrogel by combining it with microfluidic devices, which

resulted in a high generation rate [67]. A similar method can be used to create a hydrogel for mRNA generation. Um and coworkers created a pseudo-eukaryotic nucleus (PEN) which contained a DNA hydrogel that was formed using a target gene with X-shaped DNA via ligation performed by T4 DNA ligase (Fig. 7a). When taken up by a cell, the hydrogel generated mRNA transcripts for protein translation [68]. Moreover, a similar approach was used to create a nanoscale DNA hydrogel that was constructed to produce siRNA and interfere with protein expression in a cell (Fig. 7b) [69]. In addition to using it to integrate a target gene in order to produce proteins and RNA, Takakura and Nishikawa used the sole X-DNA hydrogel system model to develop a highly immunostimulatory DNA hydrogel by connecting X-DNA incorporating six highly potent unmethylated cytosine-phosphate-guanine (CpG) dinucleotide motifs using T4 DNA ligase. They found that this CpG DNA hydrogel was an ideal system for drug delivery [70]. In 2015, Park assembled gold nanoparticles (AuNPs) in a nanoscale DNA hydrogel (Fig. 7c), generating a carrier for anticancer drugs such as doxorubicin (Dox). When excited by near-infrared (NIR) laser light, the AuNPs in the DNA hydrogel generate heat due to the photo-thermal effect, leading to the disintegration of the DNA hydrogel network through thermal denaturation and the release of the Dox. Thus, a DNA hydrogel permitting photo-thermo-chemo combination therapy was realized [71]. A similar strategy was also achieved using gold nanorods (AuNRs) [72]. Other applications of this hydrogel formation model have also been reported. For instance, nano/microscale DNA

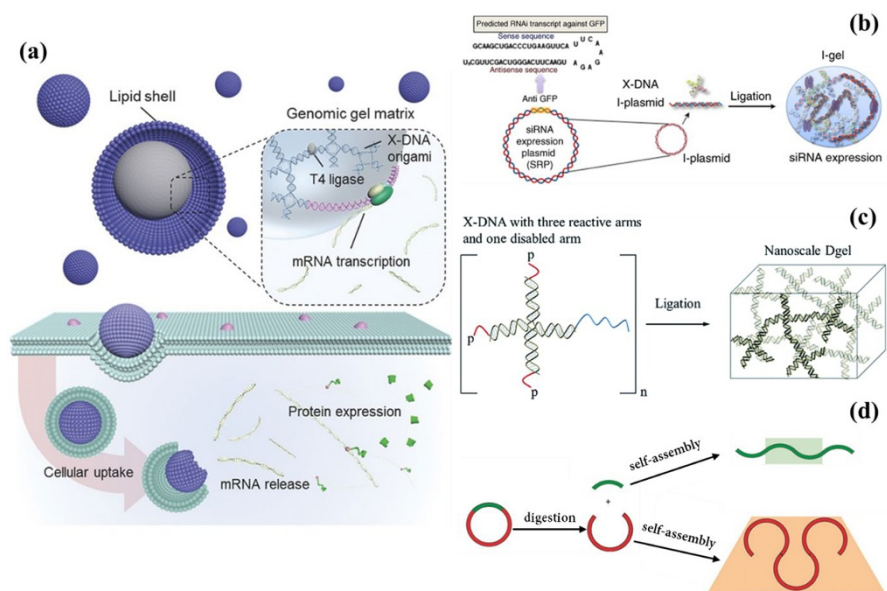


Fig. 7 DNA hydrogels formed with the assistance of ligase. **a** Schematic of a gene-containing DNA hydrogel in a pseudo-eukaryotic nucleus (PEN) for mRNA transcription. **b** Schematic of the principle of a DNA hydrogel used for RNA interference. **c** Schematic of the construction of a nanoscale DNA hydrogel. **d** Schematic of the formation of a DNA hydrogel from the plasmid pUC19. Reproduced with permission from [16, 69, 71, 77]

hydrogels were fabricated in lipid strata [73] and in multi-inlet microfluidic channels [74]. In addition, a nanostructured DNA hydrogel was used as a template to prepare an energy storage device [75] and a supercapacitor electrode [76].

Linear double-stranded DNA obtained from plasmid DNA by enzymatic digestion is also a desirable DNA building block for DNA hydrogels. In this case, hydrogel formation is achieved via the formation of covalent bonds between individual building blocks during enzymatic ligation. The plasmid pUC19 was cleaved by two kinds of endonuclease, yielding two fragments—two types of linear double-stranded DNA with sticky ends containing self-complementary palindromic sequences. These two fragments were separated and then used to form a DNA hydrogel under the direction of the ligase (Fig. 7d) [77].

3.2 DNA Hydrogels Formed Using Polymerase

Polymerase chain reaction (PCR) products that self-assemble to form DNA hydrogels can be realized through the rational design of primer sequences. Luo and colleagues performed PCR using psoralen-crosslinked thermostable Y-shaped DNA as a primer to generate a DNA hydrogel. Because the Y-shaped DNA branches maintained their branched structure during the PCR, they could be used as crosslinking points during hydrogel fabrication (Fig. 8a) [78]. In 2017, Romesberg and coworkers developed bottlebrush primers constructed from 2'-azido-A DNA, alkyne-pUC-F (forward DNA primer), and alkyne-pUC-R (reverse DNA primer) using a chemical click reaction. They then applied DNA polymerase and the bottlebrush primers in a PCR to amplify pUC19, which resulted in a DNA hydrogel (Fig. 8b) [79].

Another polymerase can be used to facilitate DNA self-assembly into hydrogels. That polymerase is terminal deoxynucleotidyl transferase (TdT), which catalyzes the repetitive addition of dNTP to the 3'-OH ends of a primer without the need for a template [80]. An X-shaped DNA motif was used as the primer to produce a hydrogel. This X-shaped DNA motif can elongate in four directions, and X-shaped DNA motifs with poly-A and poly-T tails can be obtained by adding dATP and dTTP, respectively. The hydrogel was formed by hybridizing the X-shaped DNA motifs with poly-T and poly-A tails (Fig. 8c) [81, 82].

4 DNA Hydrogels Based on Special DNA Structures

4.1 DNA Hydrogels Based on an i-Motif or DNA Triplex

i-motifs are pH-sensitive DNA structures that can be obtained by folding cytosine-rich strands in an acidic environment [13]. In 2009, Liu and coworkers invented a pure DNA hydrogel that was formed by directly inducing crosslinking between i-motif structures (Fig. 9a). To construct this hydrogel, Y-shaped DNA was first prepared from three types of single-stranded DNAs. Each arm of the resulting Y-shaped DNA included interlocking domains that enabled the generation of intermolecular i-motif structures. In an alkaline environment, the interlocking

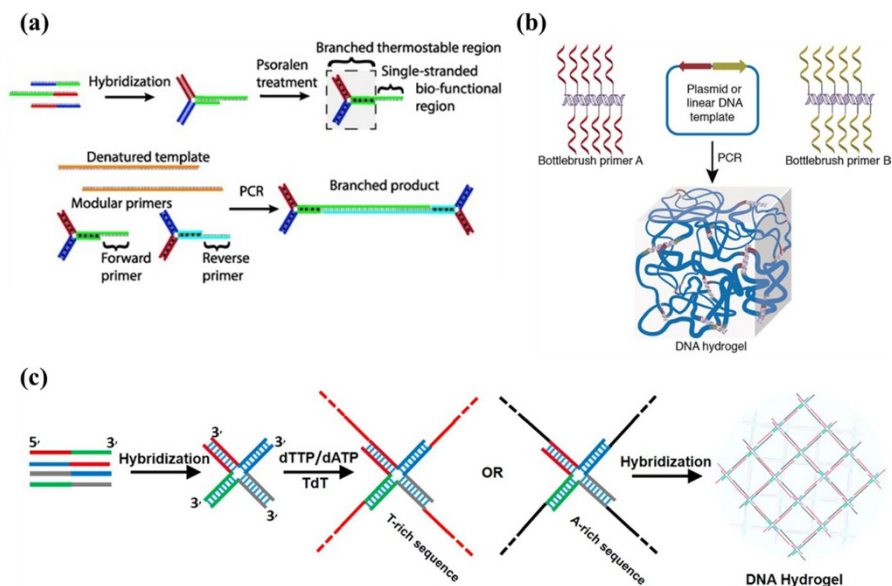


Fig. 8 DNA hydrogels formed with the assistance of polymerase. **a** Schematic of hydrogel formation using PCR with branched thermostable DNA primers. **b** Schematic of hydrogel formation via PCR using bottlebrush primers. **c** Schematic of hydrogel formation through the self-assembly of two kinds of X-shaped DNA motifs with poly-T and poly-A tails by terminal deoxynucleotidyl transferase (TdT). The tails were added to the X-shaped DNA motif in a previous step. Reproduced with permission from [78, 79, 81]

domains are configured as random coils due to electrostatic repulsion, leading to isolated Y-shaped DNA structures. Upon increasing the pH to 5.0, intermolecular i-motif structures form due to interactions of protonated cytosines with unprotonated cytosines. There were only the inter-Y-shaped i-motif structures because of the rational design. This DNA hydrogel was generated rapidly and exhibited high crosslinking density [17]. Liu and coworkers used an i-motif structure to prepare a hybrid DNA–single-walled carbon nanotube (SWNT) hydrogel in 2011 (Fig. 9b) [83]. Afterwards, Willner reported a pH-dependent dual-response DNA–pNIPAM hybrid hydrogel in which an i-motif was the pH-responsive unit (Fig. 9c). To construct this pH-triggered DNA–pNIPAM hybrid hydrogel, an acrylamide monomer modified with a cytosine-rich oligonucleotide was polymerized with *N*-isopropylacrylamide (NIPAM) monomer to obtain a hybrid copolymer with cytosine-rich sequences. When the pH was 5.2, the cytosine-rich sequences self-assembled into an i-motif structure that crosslinked the hybrid copolymer, leading to the formation of a hydrogel. When the pH was increased to 7.5, the i-motif structure and therefore the hydrogel disassembled. Due to the temperature sensitivity of pNIPAM, this hydrogel was found to respond to changes in both pH and temperature [84]. Because of their sensitivity to pH, i-motifs have been widely used in shape-memory hydrogels [85, 86]. In addition, in 2017, a hydrogel was generated using a linear DNA with half an i-motif sequence at both ends [87]. In a similar method, a single-stranded DNA with

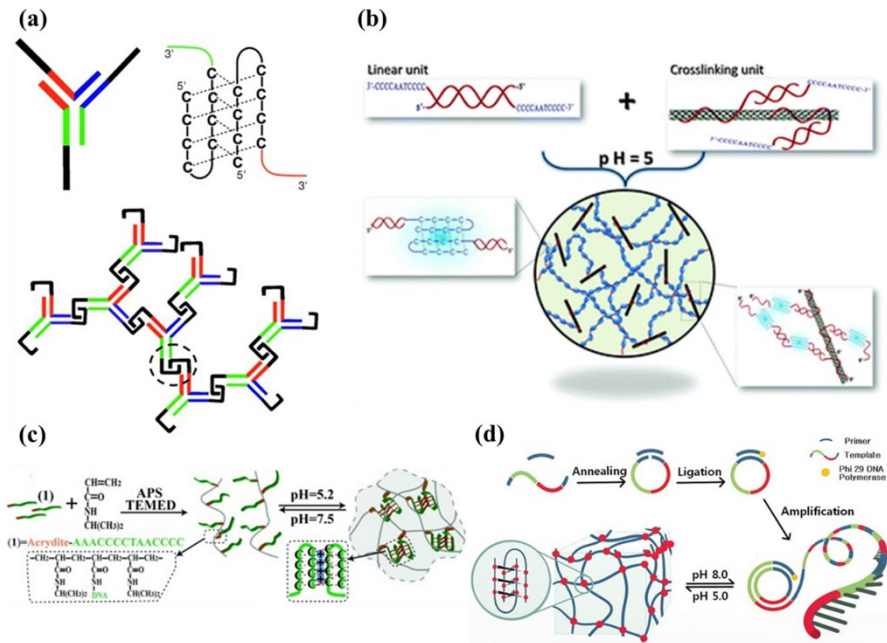


Fig. 9 DNA hydrogel formation based on i-motifs. **a** Schematic of DNA hydrogel formation based on an intramolecular i-motif. **b** Schematic of the formation of a DNA–SWNT hybrid hydrogel. **c** Schematic of the synthesis of a DNA–pNIPAM hybrid hydrogel that exhibits pH-controlled formation and dissociation. **d** Schematic of the self-assembly of RCA products with intermolecular i-motifs into a hydrogel. Reproduced with permission from [17, 83, 84, 89]

two self-complementary sequences and half an i-motif sequence was used to prepare a hydrogel [88]. Moreover, using appropriate design templates, RCA products containing intermolecular i-motifs were realized and used to form hydrogels under acidic conditions (Fig. 9d) [89].

Just like i-motifs, DNA triplexes are sensitive to pH. DNA triplexes are formed through Hoogsteen base pair interactions. Under acidic conditions, Hoogsteen base pair interactions mainly appear as CG·C⁺ domains, whereas, under neutral pH conditions, appear as TA·T parallel domains. In 2015, Willner was the first to use a triplex DNA structure as a crosslinker in the construction of a pH-responsive DNA hybrid hydrogel (Fig. 10a) [90]. DNA triplexes were then used by Willner's research group to prepare a shape-memory hydrogel (Fig. 10b, c) [91–93]. They have also been used to construct pH-activated pure DNA hydrogels (Fig. 10d) [94].

4.2 DNA Hydrogels Based on G-Quadruplexes

G-quadruplexes are the result of self-assembly by guanine (G)-rich nucleic acid sequences in the presence of ions (K⁺, Pb²⁺, or NH⁴⁺). Willner was the first to construct a DNA–polyacrylamide hybrid hydrogel via self-assembly of G-quadruplexes (Fig. 11a). That system included just one type of acrydite-modified,

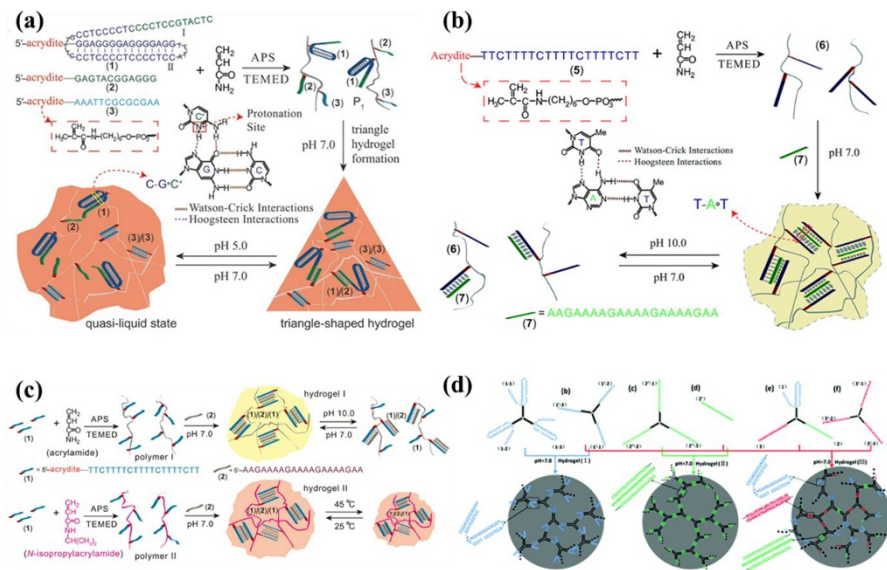


Fig. 10 DNA hydrogel formation using a DNA triple. **a** Schematic of a pH-responsive hydrogel based on C-G-C⁺ triple crosslinking. **b** Synthesis of a DNA hydrogel with T-A-T triple bridging. **c** Schematic of a DNA-pNIPAM hybrid hydrogel with T-A-T crosslinking. **d** Schematic of a pH-activated DNA triple for the preparation of a Y-shaped pure DNA hydrogel. Reproduced with permission from [90, 91, 93, 94]

G-containing oligonucleotide. Copolymerization of the acrydite-modified, G-containing oligonucleotide with acrylamide monomer resulted in G-containing copolymer chains. Upon the addition of K⁺, the G-containing oligonucleotides on the polyacrylamide chains self-assembled to form interchain G-quadruplexes that crosslinked the copolymer chains, thus inducing the formation of a hydrogel. Given that the crosslinking of the hydrogel depended on the presence of G-quadruplexes, when 18-crown-6 (a K⁺ ion chelator) was added to the system, the hydrogel dissociated because the 18-crown-6 abstracted K⁺ ions from the G-quadruplexes, causing them to fall apart. Furthermore, G-quadruplexes exhibit HRP-mimicking catalytic activity when they bind to hemin. The authors therefore found that adding hemin to the G-quadruplex-crosslinked acrylamide hydrogel resulted in a system with HRP-mimicking catalytic activity, and that this catalytic activity could be regulated through the addition of K⁺ ions or 18-crown-6 [95]. Utilizing the HRP-mimicking catalytic activity of this hydrogel, Willner was able to synthesize polyaniline (Fig. 11b), which was deposited on the hybrid hydrogel, increasing its conductivity [96]. G-quadruplexes were also used as crosslinkers in a DNA hybrid hydrogel with controllable network density (Fig. 11c). The strength of the hydrogel was decreased and its volume was therefore increased by deconstructing the G-quadruplex-based crosslinking; conversely, the strength of the hydrogel was increased and its volume was decreased by enhancing the G-quadruplex-based crosslinking (note that G-quadruplexes were not the only crosslinkers present in the hydrogel, so destroying the G-quadruplexes did not

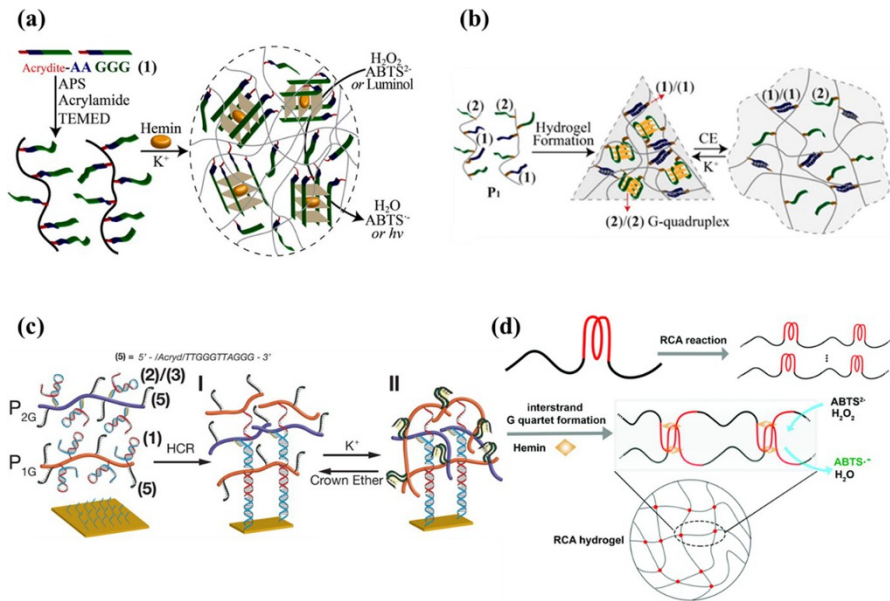


Fig. 11 DNA hydrogels based on G-quadruplexes. **a** Schematic of DNA hydrogel formation based on K^+ -stabilized G-quadruplex self-assembly. **b** Schematic of a shape-memory hydrogel with duplex/G-quadruplex double crosslinking. **c** Schematic of the construction of a G-quadruplex-based hydrogel with controllable network density on a gold-plated glass surface. **d** Schematic of the self-assembly of RCA products to form a hydrogel through G-quadruplex generation. Reproduced with permission from [28, 95, 97, 99]

cause the hydrogel to dissociate). Willner's research group has performed a series of studies based on this concept [28, 97, 98].

In another scheme, multi-repeat G-rich sequences were amplified from circular cytosine-rich DNA templates. Rational design of the template sequences permitted the generation of RCA products with the potential to form intermolecular G-quadruplexes under appropriate conditions, which in turn induced the formation of a hydrogel (Fig. 11d). When combined with hemin, this hydrogel presented HRP-like catalytic properties that could be applied in colorimetric bioanalysis [99, 100].

4.3 DNA Hydrogels Based on Metallo Base Pairs

Metallo base pairs such as $C-Ag^+-C$ and $T-Hg^{2+}-T$ can also be used to crosslink and therefore stabilize duplex DNA cooperatively, implying that they can be used to form DNA hydrogels [13]. In 2014, Willner used $C-Ag^+-C$ metallo base pairs to generate a hydrogel for the first time. Y-shaped DNA building blocks and DNA-functionalized acrylamide chains were crosslinked by $C-Ag^+-C$ metallo base pairs to prepare a pure DNA hydrogel and a DNA-polyacrylamide hybrid hydrogel, respectively (Fig. 12a, b). The authors designed a self-complementary DNA sequence with two $C-C$ mismatches, meaning that duplexes were unstable at room

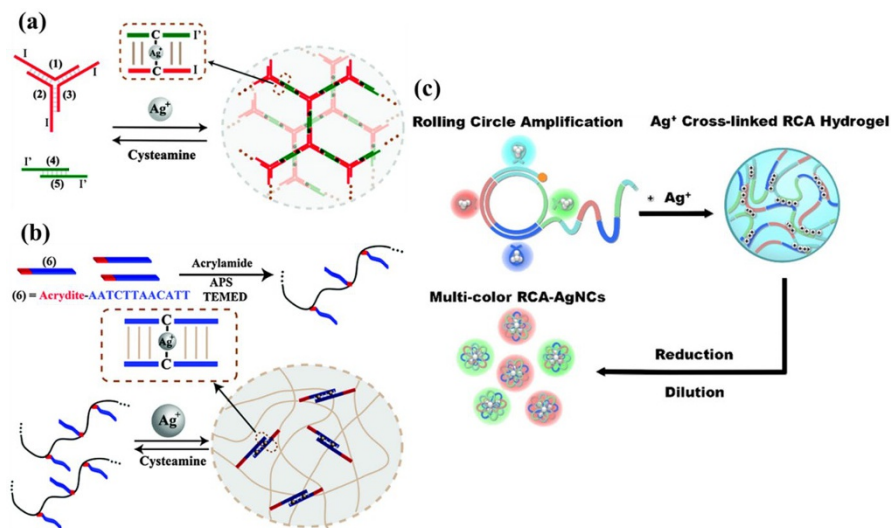


Fig. 12 DNA hydrogel formation based on cytosine– Ag^+ –cytosine bridges. **a** Schematic of the Ag^+ -induced crosslinking of Y-shaped DNA to form a hydrogel. **b** Schematic of the Ag^+ -stimulated formation of a DNA–polyacrylamide hybrid hydrogel. **c** Schematic of the preparation of a hydrogel through the Ag^+ -induced crosslinking of RCA products. Reproduced with permission from [101, 103]

temperature and failed to self-assemble into a hydrogel. However, when Ag^+ ions were added to the system, C– Ag^+ –C bridges were formed, stabilizing the duplexes and leading to the formation of a hydrogel in which the duplexes acted as crosslinkers [101]. A DNA–pNIPAM hybrid hydrogel was also obtained through the addition of Ag^+ ions [84]. This concept of a hydrogel that is cooperatively crosslinked using Ag^+ ions was also utilized to create a shape-memory hydrogel [102]. Just as above, RCA products with cytosine-rich sequences were produced, and then a DNA hydrogel containing silver nanoclusters was realized through DNA self-assembly based on C– Ag^+ –C interactions (Fig. 12c) [103]. Yang reported a different DNA hydrogel with silver nanoclusters that was generated through the physical entanglement of RCA products [104].

5 DNA Hydrogels Formed Using Novel Methods

5.1 Application of Aptamers and DNAzymes as DNA Crosslinkers

As well as the DNA hydrogels generated through traditional DNA interactions described above, a number of new concepts for DNA hydrogel formation have been reported recently. Interestingly, DNA aptamers and DNAzymes have been widely used in these schemes.

Aptamers are single-stranded oligonucleotides that can bind specifically to a target, enabling them to selectively recognize a variety of molecules ranging from macromolecules to small compounds [105]. Using DNA aptamers as crosslinkers

in hydrogels allows the creation of hydrogels that respond to a wide variety of targets. In the absence of the target, the aptamer acts just like a conventional DNA crosslinker, but when the target is present, the aptamer preferentially forms a complex with it, altering the structure of the hydrogel. Based on this principle, a series of hydrogels that respond to particular target molecules have been prepared for use in detection schemes.

In 2008, Tan reported an adenosine-responsive DNA–polyacrylamide hybrid hydrogel with a response mechanism based on aptamer–target interactions. This system was the first reported example of a DNA–polyacrylamide hybrid hydrogel that transitions from gel to solution upon the addition of adenosine (Fig. 13a). The method used to prepare the hydrogel was similar to that employed by Lin [19]. First, two acrydite-modified oligonucleotides named strand A and strand B were separately copolymerized with acrylamide, leading to two types of DNA-grafted polyacrylamide chains. These two DNA-grafted polyacrylamide chains were then mixed in solution at stoichiometric concentrations. Finally, the adenosine-responsive DNA–polyacrylamide hybrid hydrogel was generated by the addition of the linker DNA, which had an aptamer sequence for adenosine at the 3' end. Thus, when adenosine was added to the hydrogel, the aptamer sequence of the DNA linker formed a complex with the adenosine, leading to the dissociation of strand B from the linker. This triggered the dissociation of the crosslinking network in the

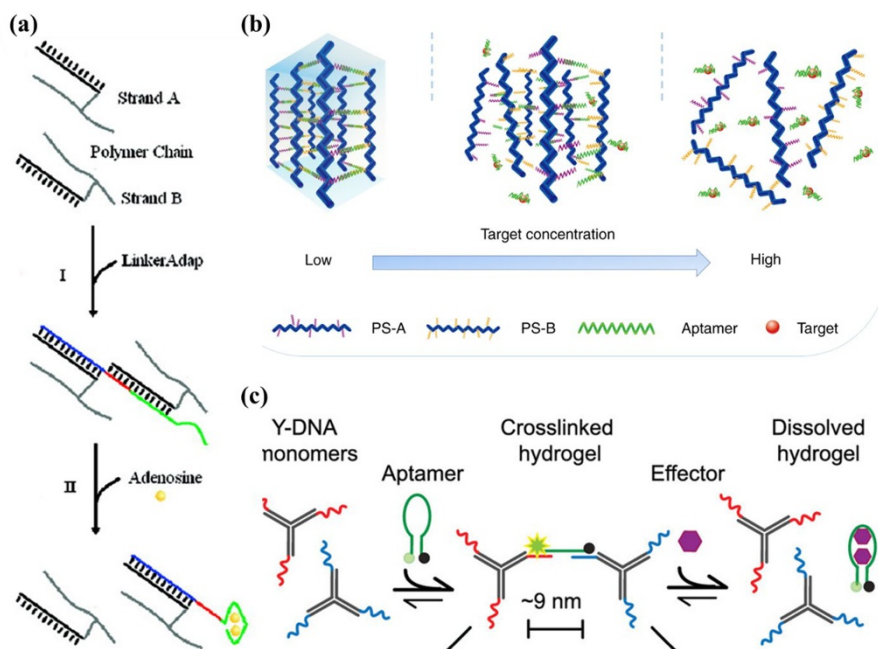


Fig. 13 Use of aptamers as crosslinkers in DNA hydrogel formation. **a** Schematic of an adenosine-responsive DNA hydrogel. **b** Schematic showing that the degree of hydrogel degradation was positively correlated with the concentration of the target. **c** Schematic of an adenosine-responsive DNA hydrogel based on the Y-DNA hydrogel model. Reproduced with permission from [106, 119, 123]

hydrogel; in other words, the hydrogel collapsed. A detection technique based on this concept of adenosine-induced hydrogel dissociation was also developed. First, gold nanoparticles used as indicators were mixed with solutions of the two DNA-grafted polyacrylamide chains before gelation. Upon adding the linker to form a hydrogel, gold nanoparticles were trapped in the hydrogel network. When adenosine was added, the hydrogel network collapsed and the gold nanoparticles were released into the solution, yielding obvious visual signals [106]. Since that report was published, aptamer-responsive hydrogels have been widely used for various biomedical applications, including sensing, diagnostics, and drug loading [107], and DNA linkers with aptamers for cocaine [108], ATP [109], AS1411 [107], ochratoxin A [110], aflatoxin B1 [111], and thrombin [112] (among others) have been developed for use in aptamer-responsive DNA hydrogels. In the context of applying aptamer-responsive hydrogels to biological detection and analysis, Yang's research group has constructed a series of detection devices and equipment based on this principle [110, 111, 113–119]. For example, a personal glucose meter that can be used to determine the concentrations of targets other than glucose was developed [113]. A volumetric bar-chart chip (V-Chip) device containing a target-responsive hydrogel was also devised as a means to detect specific targets [114]. Moreover, making use of the thermoreversible nature of DNA hydrogels and the principle of capillary action, a target-responsive hydrogel film in a capillary tube was created that permitted the quantitative detection of the target. It is worth mentioning that this sensor did not rely on hydrogel dissociation to detect the target: only a slight change in the internal structure of the hydrogel was required to quantitatively detect the concentration of the target in sample solutions. The only equipment required was a capillary tube (Fig. 13b) [119].

In contrast to using only one type of aptamer as the linker to construct an aptamer-responsive hydrogel, Tan and coworkers developed dual-responsive hydrogels that incorporated both ATP and cocaine aptamers, and then creating a logic gate system based on these dual-responsive hydrogels. The authors realized AND and OR logic gates by constructing two dual-aptamer linkers with different structures. For the AND gate, a DNA linker with a cocaine aptamer sequence was mixed with two types of DNA-grafted polyacrylamide chains, one of which contained an ATP aptamer sequence. These three kinds of single-stranded DNAs assembled into a hydrogel consisting of Y-shaped crosslinker units. The hydrogel was only dissociated when both ATP and cocaine were added because only then were the Y-shaped crosslinker units completely disintegrated. For the OR gate, the DNA linker contained both cocaine and ATP aptamer sequences located at opposite ends of the DNA strand. This DNA linker was added to DNA-grafted polyacrylamide chains to produce a hydrogel in which the DNA linker was the only component that was responsive to either ATP or cocaine; upon the addition of either ATP or cocaine to the hydrogel, the crosslinked network was destroyed and the hydrogel collapsed [120].

Aptamers can also be used as crosslinkers in pure DNA hydrogels. Lei and coworkers reported a pure DNA hydrogel that was constructed using a Y-shaped DNA and a thrombin aptamer linker through DNA self-assembly. Au nanoparticles (AuNPs) trapped in the hydrogel network were used as a signal indicator.

Upon adding thrombin, a complex of L-DNA aptamer with thrombin was generated, inducing the collapse and dissolution of the DNA hydrogel. This released the AuNPs, leading to a change in the color of the upper solution [121]. An aptamer for ochratoxin A was used as a DNA linker to construct a pure DNA hydrogel that was sensitive to ochratoxin A [122]. An adenine-responsive hydrogel was designed for use as a quantitative tool to measure the responsiveness and dissolution kinetics of this type of hydrogel (Fig. 13c) [123, 124]. Integrating an ATP aptamer into the DNA linker of a hydrogel also allowed the mechanical properties of the hydrogel to be tuned [125].

Other hydrogels that incorporate an aptamer do not use the aptamer as a crosslinker. For example, Chai and Yuan constructed a DNA hydrogel using a strategy similar to that employed for the second type of hydrogel (type II) created by Nagahara and Matsuda [15]. Three acrydite-modified DNA strands named S1, S2, and S3 were used, where S1 and S2 were complementary to each other. Two kinds of DNA-grafted polyacrylamide chains named P1 and P2 were employed; P1 was obtained by copolymerizing S1 with S3 and acrylamide monomer while P2 was obtained by copolymerizing S2 with S3 and acrylamide monomer. The DNA fragment on S1 in P1 was hybridized with a heparanase aptamer (HPA), which blocked hybridization with DNA fragments on S2 in P2. As a result, no hydrogel formation was possible until the addition of HPA. When HPA was added, the aptamer of HPA dissociated from P1, forming a HPA–aptamer complex. This meant that the DNA fragment on S1 could hybridize with the DNA fragment on S2, leading to crosslinking between P1 and P2 and the formation of a hydrogel. Based on this strategy, the authors developed a sensor for use in a heparinase (HPA) bioassay [126]. In addition, Du created a DNA hydrogel through the one-pot self-assembly of X-shaped DNA, a DNA linker, and an aptamer, but in this case the aptamer was only used as a functional unit for target protein capture, not to change the hydrogel network in the presence of the target [127]. Tan developed a DNA nanohydrogel that was efficiently taken up by cells due to the recognition of an aptamer in the nanohydrogel by the target cells. Although the nanohydrogel was eventually destroyed, this was induced not by the aptamer but by the disruption of disulfide linkages in the DNA strands [128].

DNAzymes can also be used as DNA crosslinkers. A DNAzyme is a single-stranded DNA that has a special sequence and secondary structure and presents a level of catalytic activity similar to that of normal enzymes [129, 130]. One DNAzyme is metal ion dependent; in the presence of certain metal ions, its ability to cleave nucleic acid molecules is activated, and the activated DNAzyme then irreversibly cleaves substrate nucleic acid molecules at the cleavage site [131]. This type of DNAzyme could be used in a DNA crosslinker to construct DNA hydrogels that are responsive to particular target metal ions.

In 2011, Yang provided the first report of a Cu^{2+} -responsive DNAzyme-crosslinked DNA–polyacrylamide hybrid hydrogel. To obtain this hydrogel, two kinds of single-stranded DNAs, DNAzyme, and substrate were incorporated into linear polyacrylamide, which yielded two kinds of DNA-grafted polyacrylamide chains, DNAzyme-grafted polyacrylamide chains, and substrate-grafted polyacrylamide chains. When the two kinds of DNA-grafted polyacrylamide chains were

mixed, the DNAzyme and the substrate on the polyacrylamide chains combined to form a DNAzyme–substrate complex, thus crosslinking the polyacrylamide chains and forming a hydrogel. The DNAzyme–substrate complex contained a domain that specifically recognized Cu^{2+} . When Cu^{2+} was added, the DNAzyme–substrate complex dissociated. Because the substrate was irreversibly cleaved by the DNAzyme, the hydrogel eventually dissolved. AuNPs were also introduced into the hydrogel as a colorimetric indicator in order to develop a Cu^{2+} sensor (Fig. 14a) [132]. Based on this strategy, various metal-ion-dependent DNAzymes have been used in the DNA crosslinkers of metal-ion-responsive hydrogels, including those that are sensitive to Pb^{2+} (Fig. 14b) [133, 134], UO^{2+} (Fig. 14c) [135], Mg^{2+} (Fig. 14d) [136], Zn^{2+} (Fig. 14d) [136], among others.

5.2 Control of DNA Hydrogel Formation Using Light

Light-responsive DNA has also been used to form gel networks. It is well known that the hybridization of DNA strands can be controlled by light. The most common strategy that utilizes this phenomenon involves the integration of azobenzene into single-stranded DNA. In 2011, Tan and colleagues integrated azobenzene into single-stranded DNA and used the resulting DNA as a crosslinker to

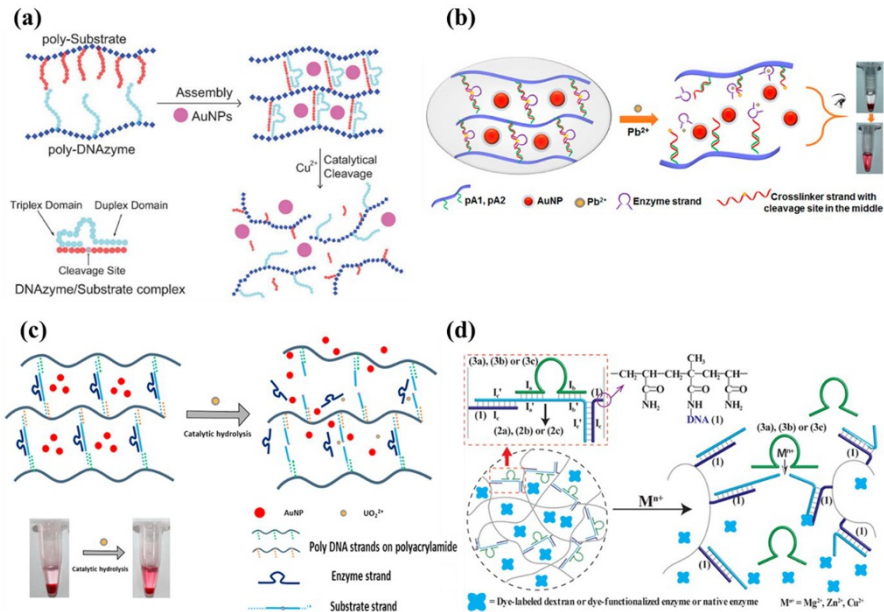


Fig. 14 DNAzymes used as crosslinkers in DNA hydrogel formation. **a** Schematic of a hydrogel which uses a DNAzyme crosslinker that is responsive to copper ion. **b** Schematic of a hydrogel which uses a DNAzyme crosslinker that is responsive to lead ion and is employed for visual detection. **c** Schematic of a hydrogel which uses a DNAzyme crosslinker that is responsive to uranyl ion and is employed in sensors. **d** Schematic of a detection platform based on the use of metal-ion-dependent DNAzyme/substrate sequences as crosslinkers. Reproduced with permission from [132, 133, 135, 136]

form a photoresponsive DNA hybrid hydrogel. This hydrogel exhibited reversible hydrogel to solution phase transitions that were controllable using light (Fig. 15a) due to the *trans/cis* photoisomerization of azobenzene, as the hybridization of the DNA linker with its complementary strand was dependent on the isomer of azobenzene present. Irradiation with 450-nm light led to *trans*-azobenzene, meaning that the linker DNA could hybridize with its complementary strand tethered to the polyacrylamide polymer chains, thus inducing hydrogel formation.

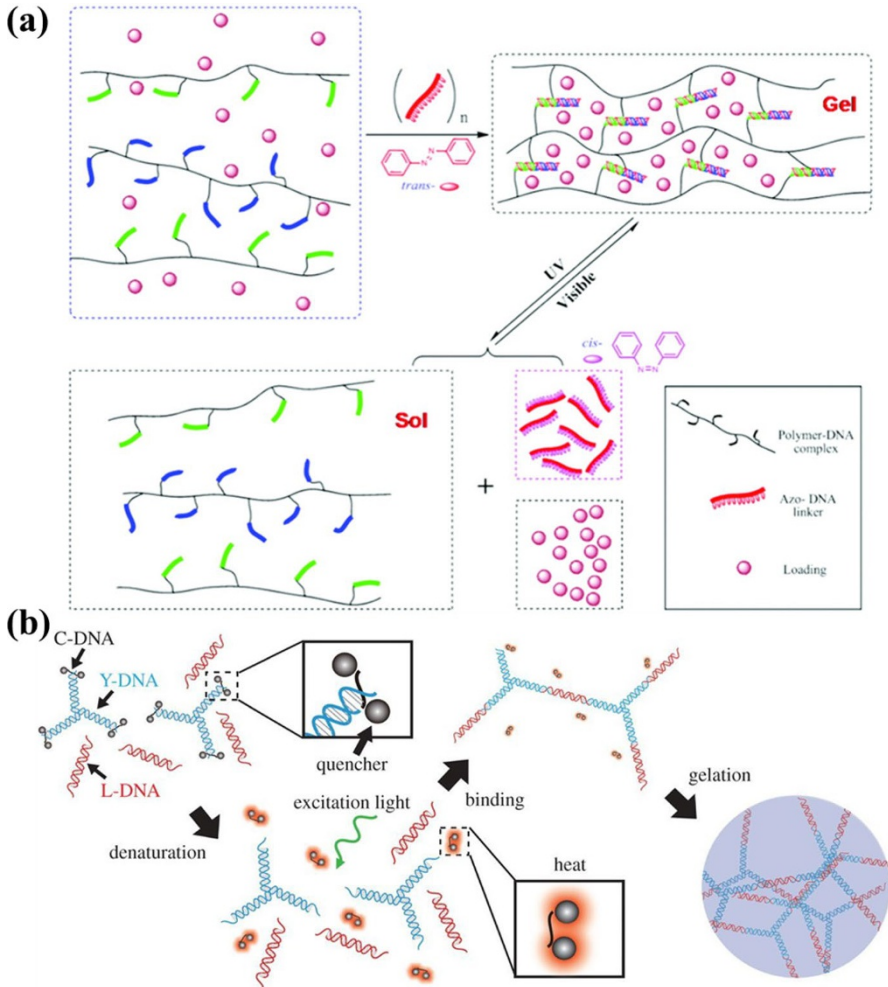


Fig. 15 Schematic of light-controllable DNA hydrogel formation. **a** Azo-incorporated DNA is used as a crosslinker to form the hydrogel, which enables the crosslinking process to be reversibly controlled by visible and UV light. **b** Schematic of photothermally induced DNA hydrogel formation. In this concept, thermal energy causes the Y-DNA to dissociate from the C-DNA and then link with L-DNA to create the DNA hydrogel. Reproduced with permission from [137, 138]

Irradiation with 350-nm light resulted in *cis*-azobenzene, which did not permit hybridization and caused the hydrogel to dissociate [137].

Light-controllable DNA hydrogels can also be achieved indirectly, using a photothermal approach. In 2018, Tanida and coworkers realized light-controllable DNA hydrogel formation based on a Y-scaffold and linker system. In this scheme, a ssDNA denoted Cap-DNA (C-DNA) was used that had quenchers at both ends and was complementary to the sticky ends of Y-DNA, meaning that the C-DNA prevented L-DNA from linking to the Y-DNA. Upon excitation with light, the quenchers became heat sources and the thermal energy they emitted caused the Y-DNA to dissociate from the C-DNA and link with the L-DNA, resulting in the creation of a DNA hydrogel (Fig. 15b). Furthermore, the shape of the hydrogel could be tailored by adjusting the irradiation pattern [138].

5.3 DNA Hydrogel Formation Based on Clamped HCR

Another novel mechanism that can be used to form gel networks is clamped HCR (C-HCR). Hybridization chain reaction (HCR), a type of toehold-mediated strand displacement (TMSD) reaction, was first developed and named by Dirks and Pierce in 2004 [139], and it has since attracted great interest due to its enzyme-free nature, isothermal conditions, simple protocols, and admirable amplification efficiency. In a typical linear HCR, a short ssDNA initiates the cross-opening of two DNA hairpins, yielding nicked double-helix DNA polymers [140]. Although there was a report of the use of HCR to form gel networks in 2015 [28], it was not used to prepare pure DNA hydrogels until clamped HCR was designed by Liu and coworkers [141]. Using clamped HCR, those authors prepared a 3D DNA hydrogel with favorable spatial and temporal control.

The process used to construct the DNA hydrogel using clamped HCR was as follows (Fig. 16a). Two kinds of hairpin strands were used, one of which (H1) was specifically designed for use in a clamped HCR system as it had palindromic sequences

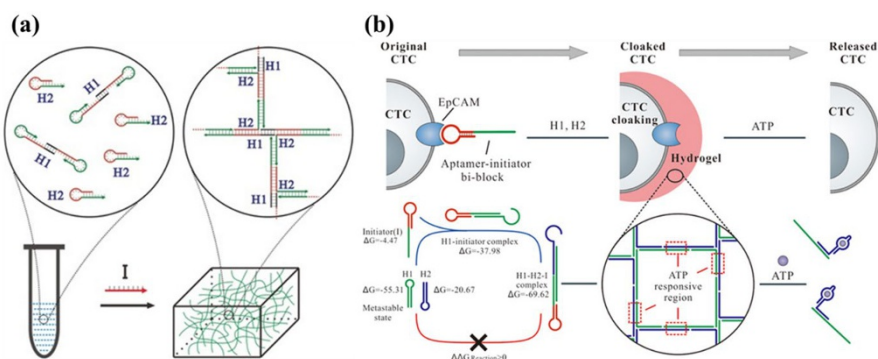


Fig. 16 Schematic of hydrogel formation based on clamped HCR. **a** Schematic of the utilization of clamped HCR for DNA hydrogel formation. **b** Schematic of an ATP-responsive DNA hydrogel cloaked on a cell surface; the aptamer-triggered hydrogel was obtained using clamped HCR. Reproduced with permission from [141, 142]

at its 5' end. The other hairpin strand was denoted H2. After annealing, an H1 dimer was formed due to hybridization of the palindromic sequences of H1. This H1 dimer and H2 coexisted in a metastable state until a small amount of initiator was added to the system. The introduction of the initiator triggered immediate HCR, which yielded HCR products. The H1 dimer had two branches, so it could form a three-arm junction (with one initiator and one H2 strand) or a four-arm junction (with two H2 strands) in divergent chain reactions during the C-HCR. The products of the clamped HCR were then crosslinked to form a DNA hydrogel [141].

Using a similar strategy, a method permitting the *in situ* formation of a DNA hydrogel on the surfaces of circulating tumor cells (CTCs) was developed (Fig. 16b). The authors first designed a specific aptamer initiator that specifically recognized epithelial cell adhesion molecule (EpCAM) on the CTC surface, as this specific aptamer initiator could then be anchored to the CTC surface. When the H1 dimer and H2 encountered the initiator on the CTC surface, a DNA hydrogel was formed via clamped HCR. An ATP aptamer was also incorporated into H2, causing the dissociation of the hydrogel in the presence of ATP and thus a phase transition from hydrogel to solution. The authors described the overall process as an aptamer-triggered clamped hybridization chain reaction (atcHCR) [142].

6 Conclusion and Outlook

In summary, DNA self-assembly has been found to be an effective approach to hydrogel creation. In this review, we divided DNA hydrogels into four categories according to the gelation mechanism: DNA hydrogels formed by conventional DNA hybridization, DNA hydrogels formed with the assistance of enzymes, DNA hydrogels based on the use of special DNA structures, and DNA hydrogels formed using novel methods. Various synthetic strategies and applications of DNA hydrogels have been detailed.

It is worth noting that among these hydrogels, stimuli-responsive and biologically compatible DNA hybrid hydrogels have received extensive attention [143]. A wide range of tailored DNAs can potentially be used as crosslinkers to achieve stimuli responsiveness, e.g., a DNA “toehold” can be used to achieve sensitivity to nucleic acid molecules [19], aptamers can be applied to enhance the response to the target [106], DNazymes can be used to improve the response to metal ions [132], and azobenzene-modified DNA can be employed to achieve light sensitivity [137]. Since these hydrogels have specific stimuli-responsive behaviors, they have been widely used as biosensors in the field of bioanalysis [144, 145]. In addition, pure DNA hydrogels have excellent biocompatibilities and biodegradabilities, which makes them superior carriers for drug delivery [146].

Due to the high cost of DNA, the large-scale use of DNA hybrid hydrogels and pure DNA hydrogels has been limited [147]. Although the amount of DNA used in DNA hybrid hydrogels is relatively small, it is usually necessary to chemically modify the DNA used [148–151], and the price of chemically modified DNA is very expensive [146, 147, 152–154]. Therefore, it is particularly important to develop

efficient and inexpensive DNA synthesis and modification methods to overcome this obstacle [155–158].

Moreover, nano/micro-DNA hydrogels may be an important research direction in the future, especially in the field of intracellular drug delivery, since nano/micro-DNA hydrogels have the advantages that they passively target tumor cells and they rapidly respond to stimuli [4].

Finally, the clamped HCR strategy that is sometimes used to construct DNA hydrogels permits high spatial and temporal control. It is worth mentioning that hydrogels are formed under physiological conditions using this method, and only a small amount of the initiator DNA is required. Hydrogels obtained through the rational design of DNA sequences could have specific biological functions [141, 142].

Acknowledgements The authors acknowledge financial support by the National Natural Science Foundation of China (21722310), the Youth Innovation Promotion Association of CAS (2012205, 2016236), the Fundamental Research Funds for the Central Universities, and the LU JIAXI International team program supported by the K.C. Wong Education Foundation and CAS.

Compliance with Ethical Standards

Conflict of interest On behalf of all the authors, the corresponding author states that there is no conflict of interest.

References

1. Peppas NA, Bures P, Leobandung W, Ichikawa H (2000) *Eur J Pharm Biopharm* 50:27. [https://doi.org/10.1016/s0939-6411\(00\)00090-4](https://doi.org/10.1016/s0939-6411(00)00090-4)
2. Drury JL, Mooney DJ (2003) *Biomaterials* 24:4337. [https://doi.org/10.1016/s0142-9612\(03\)00340-5](https://doi.org/10.1016/s0142-9612(03)00340-5)
3. Gaweł K, Barriet D, Sletmoen M, Stokke BT (2010) *Sensors* 10:4381. <https://doi.org/10.3390/s100504381>
4. Li J, Mooney DJ (2016) *Nat Rev Mater* 1:16071. <https://doi.org/10.1038/natrevmats.2016.71>
5. Peppas NA, Hilt JZ, Khademhosseini A, Langer R (2006) *Adv Mater* 18:1345. <https://doi.org/10.1002/adma.200501612>
6. Watson JD, Crick FH (1974) *Nature* 248:765. <https://doi.org/10.1038/248765a0>
7. Seeman NC (1982) *J Theor Biol* 99:237. [https://doi.org/10.1016/0022-5193\(82\)90002-9](https://doi.org/10.1016/0022-5193(82)90002-9)
8. Seeman NC (1998) *Annu Rev Biophys Biomol Struct* 27:225. <https://doi.org/10.1146/annurev.biophys.27.1.225>
9. Seeman NC (2003) *Nature* 421:427. <https://doi.org/10.1038/nature01406>
10. Wang ZG, Ding B (2013) *Adv Mater* 25:3905. <https://doi.org/10.1002/adma.201301450>
11. Jones MR, Seeman NC, Mirkin CA (2015) *Science* 347:1260901. <https://doi.org/10.1126/science.1260901>
12. Li F, Tang J, Geng J, Luo D, Yang D (2019) *Prog Polym Sci* 98:101163. <https://doi.org/10.1016/j.progpolymsci.2019.101163>
13. Kahn JS, Hu Y, Willner I (2017) *Acc Chem Res* 50:680. <https://doi.org/10.1021/acs.accounts.6b00542>
14. Amiya T, Tanaka T (1987) *Macromolecules* 20:1162. <https://doi.org/10.1021/ma00171a050>
15. Nagahara S, Matsuda T (1996) *Polym Gels Netw* 4:111. [https://doi.org/10.1016/0966-7822\(96\)00001-9](https://doi.org/10.1016/0966-7822(96)00001-9)
16. Um SH, Lee JB, Park N, Kwon SY, Umbach CC, Luo D (2006) *Nat Mater* 5:797. <https://doi.org/10.1038/nmat1741>

17. Cheng E, Xing Y, Chen P, Yang Y, Sun Y, Zhou D, Xu L, Fan Q, Liu D (2009) *Angew Chem Int Ed Engl* 48:7660. <https://doi.org/10.1002/anie.200902538>
18. Xing Y, Cheng E, Yang Y, Chen P, Zhang T, Sun Y, Yang Z, Liu D (2011) *Adv Mater* 23:1117. <https://doi.org/10.1002/adma.201003343>
19. Lin DC, Yurke B, Langrana NA (2004) *J Biomech Eng Trans ASME* 126:104. <https://doi.org/10.1115/1.1645529>
20. Lin DC, Yurke B, Langrana NA (2005) *J Mater Res* 20:1456. <https://doi.org/10.1557/jmr.2005.0186>
21. Liedl T, Dietz H, Yurke B, Simmel F (2007) *Small* 3:1688. <https://doi.org/10.1002/smll.200700366>
22. He Y, Yang X, Yuan R, Chai Y (2017) *Anal Chem* 89:8538. <https://doi.org/10.1021/acs.analchem.7b02321>
23. Liu S, Su W, Li Y, Zhang L, Ding X (2018) *Biosens Bioelectron* 103:1. <https://doi.org/10.1016/j.bios.2017.12.021>
24. Si Y, Li L, Wang N, Zheng J, Yang R, Li J (2019) *ACS Appl Mater Interfaces* 11:7792. <https://doi.org/10.1021/acsami.8b21727>
25. Cai W, Xie S, Zhang J, Tang D, Tang Y (2017) *Biosens Bioelectron* 98:466. <https://doi.org/10.1016/j.bios.2017.07.025>
26. Li C, Li H, Ge J, Jie G (2019) *Chem Commun* 55:3919. <https://doi.org/10.1039/c9cc00565j>
27. Lyu D, Chen S, Guo W (2018) *Small* 14:1704039. <https://doi.org/10.1002/smll.201704039>
28. Kahn JS, Trifonov A, Ceconello A, Guo W, Fan C, Willner I (2015) *Nano Lett* 15:7773. <https://doi.org/10.1021/acs.nanolett.5b04101>
29. Cangialosi A, Yoon C, Liu J, Huang Q, Guo J, Nguyen TD, Gracias DH, Schulman R (2017) *Science* 357:1126. <https://doi.org/10.1126/science.aan3925>
30. Fern J, Schulman R (2018) *Nat Commun* 9:3766. <https://doi.org/10.1038/s41467-018-06218-w>
31. English MA, Soenksen LR, Gayet RV, de Puig H, Angenent-Mari NM, Mao AS, Nguyen PQ, Collins JJ (2019) *Science* 365:780. <https://doi.org/10.1126/science.aaw5122>
32. Han D, Li J, Tan W (2019) *Science* 365:754. <https://doi.org/10.1126/science.aay4198>
33. Jin J, Xing Y, Xi Y, Liu X, Zhou T, Ma X, Yang Z, Wang S, Liu D (2013) *Adv Mater* 25:4714. <https://doi.org/10.1002/adma.201301175>
34. Chen P, Li C, Liu D, Li Z (2012) *Macromolecules* 45:9579. <https://doi.org/10.1021/ma302233m>
35. Li C, Faulkner-Jones A, Dun AR, Jin J, Chen P, Xing Y, Yang Z, Li Z, Shu W, Liu D, Duncan RR (2015) *Angew Chem Int Ed Engl* 54:3957. <https://doi.org/10.1002/anie.201411383>
36. Li C, Rowland MJ, Shao Y, Cao T, Chen C, Jia H, Zhou X, Yang Z, Scherman OA, Liu D (2015) *Adv Mater* 27:3298. <https://doi.org/10.1002/adma.201501102>
37. Zhou X, Li C, Shao Y, Chen C, Yang Z, Liu D (2016) *Chem Commun* 52:10668. <https://doi.org/10.1039/c6cc04724f>
38. Ma X, Yang Z, Wang Y, Zhang G, Shao Y, Jia H, Cao T, Wang R, Liu D (2017) *ACS Appl Mater Interfaces* 9:1995. <https://doi.org/10.1021/acsami.6b12327>
39. Wang Y, Shao Y, Ma X, Zhou B, Faulkner-Jones A, Shu W, Liu D (2017) *ACS Appl Mater Interfaces* 9:12311. <https://doi.org/10.1021/acsami.7b01604>
40. Li C, Zhou X, Shao Y, Chen P, Xing Y, Yang Z, Li Z, Liu D (2017) *Mater Chem Front* 1:654. <https://doi.org/10.1039/C6QM00176A>
41. Xing Z, Caciagli A, Cao T, Stoev I, Zupkauskas M, O'Neill T, Wenzel T, Lamboll R, Liu D, Eiser E (2018) *Proc Natl Acad Sci* 115:8137. <https://doi.org/10.1073/pnas.1722206115>
42. Li C, Chen P, Shao Y, Zhou X, Wu Y, Yang Z, Li Z, Weil T, Liu D (2015) *Small* 11:1138. <https://doi.org/10.1002/smll.201401906>
43. Gacanin J, Kovtun A, Fischer S, Schwager V, Quambusch J, Kuan SL, Liu W, Boldt F, Li C, Yang Z, Liu D, Wu Y, Weil T, Barth H, Ignatius A (2017) *Adv Healthc Mater* 6:1700392. <https://doi.org/10.1002/adhm.201700392>
44. Guo W, Orbach R, Mironi-Harpaz I, Seliktar D, Willner I (2013) *Small* 9:3748. <https://doi.org/10.1002/smll.201300055>
45. Van Nguyen K, Minteer SD (2015) *Chem Commun (Camb)* 51:13071. <https://doi.org/10.1039/c5cc04810a>
46. Van Khiem N, Holade Y, Minteer SD (2016) *Acs Catalysis* 6:2603. <https://doi.org/10.1021/acscatal.5b02699>
47. Shao Y, Sun Z-Y, Wang Y, Zhang B-D, Liu D, Li Y-M (2018) *ACS Appl Mater Interfaces* 10:9310. <https://doi.org/10.1021/acsami.8b00312>

48. Ren N, Sun R, Xia K, Zhang Q, Li W, Wang F, Zhang X, Ge Z, Wang L, Fan C, Zhu Y (2019) *ACS Appl Mater Interfaces* 11:26704. <https://doi.org/10.1021/acsami.9b08652>
49. Nishikawa M, Ogawa K, Umeki Y, Mohri K, Kawasaki Y, Watanabe H, Takahashi N, Kusuki E, Takahashi R, Takahashi Y, Takakura Y (2014) *J Control Release* 180:25. <https://doi.org/10.1016/j.jconrel.2014.02.001>
50. Nishida Y, Ohtsuki S, Araie Y, Umeki Y, Endo M, Emura T, Hidaka K, Sugiyama H, Takahashi Y, Takakura Y, Nishikawa M (2016) *Nanomed Nanotechnol Biol Med* 12:123. <https://doi.org/10.1016/j.nano.2015.08.004>
51. Ishii-Mizuno Y, Umeki Y, Onuki Y, Watanabe H, Takahashi Y, Takakura Y, Nishikawa M (2017) *Int J Pharm* 516:392. <https://doi.org/10.1016/j.ijpharm.2016.11.048>
52. Nomura D, Saito M, Takahashi Y, Takahashi Y, Takakura Y, Nishikawa M (2018) *Int J Pharm* 547:556. <https://doi.org/10.1016/j.ijpharm.2018.06.029>
53. Umeki Y, Saito M, Takahashi Y, Takakura Y, Nishikawa M (2017) *Adv Healthc Mater* 6:1700355. <https://doi.org/10.1002/adhm.201700355>
54. Yata T, Takahashi Y, Tan M, Nakatsuji H, Ohtsuki S, Murakami T, Imahori H, Umeki Y, Shiomi T, Takakura Y, Nishikawa M (2017) *Biomaterials* 146:136. <https://doi.org/10.1016/j.biomaterials.2017.09.014>
55. Bomboi F, Romano F, Leo M, Fernandez-Castanon J, Cerbino R, Bellini T, Bordini F, Filetici P, Sciorino F (2016) *Nat Commun* 7:13191. <https://doi.org/10.1038/ncomms13191>
56. Fernandez-Castanon J, Bianchi S, Saglimbeni F, Di Leonardo R, Sciorino F (2018) *Soft Matter* 14:6431. <https://doi.org/10.1039/c8sm00751a>
57. Nguyen DT, Saleh OA (2017) *Soft Matter* 13:5421. <https://doi.org/10.1039/c7sm00557a>
58. Zhang L, Jean SR, Ahmed S, Aldridge PM, Li X, Fan F, Sargent EH, Kelley SO (2017) *Nat Commun* 8:381. <https://doi.org/10.1038/s41467-017-00298-w>
59. Meng X, Zhang K, Dai W, Cao Y, Yang F, Dong H, Zhang X (2018) *Chem Sci* 9:7419. <https://doi.org/10.1039/c8sc02858c>
60. Guo B, Wen B, Cheng W, Zhou X, Duan X, Zhao M, Xia Q, Ding S (2018) *Biosens Bioelectron* 112:120. <https://doi.org/10.1016/j.bios.2018.04.027>
61. Noll T, Schonherr H, Wesner D, Schopferer M, Paululat T, Noll G (2014) *Angew Chem Int Ed Engl* 53:8328. <https://doi.org/10.1002/anie.201402497>
62. Noll T, Wenderhold-Reeb S, Bourdeaux F, Paululat T, Noll G (2018) *Chemistryselect* 3:10287. <https://doi.org/10.1002/slct.201802364>
63. Pan W, Wen H, Niu L, Su C, Liu C, Zhao J, Mao C, Liang D (2016) *Soft Matter* 12:5537. <https://doi.org/10.1039/c6sm00283h>
64. Oishi M, Nakatani K (2019) *Small* 15:1900490. <https://doi.org/10.1002/smll.201900490>
65. Jiang H, Pan V, Vivek S, Weeks ER, Ke Y (2016) *ChemBioChem* 17:1156. <https://doi.org/10.1002/cbic.201500686>
66. Park N, Kahn JS, Rice EJ, Hartman MR, Funabashi H, Xu J, Um SH, Luo D (2009) *Nat Protoc* 4:1759. <https://doi.org/10.1038/nprot.2009.174>
67. Ruiz RCH, Kiatwuthinon P, Kahn JS, Roh YH, Luo D (2012) *Ind Biotechnol* 8:372. <https://doi.org/10.1089/ind.2012.0024>
68. Shin SW, Park KS, Shin WJ, Um SH (2015) *Small* 11:5515. <https://doi.org/10.1002/smll.201501334>
69. Song J, Lee M, Kim T, Na J, Jung Y, Jung GY, Kim S, Park N (2018) *Nat Commun* 9:4331. <https://doi.org/10.1038/s41467-018-06864-0>
70. Nishikawa M, Mizuno Y, Mohri K, Matsuoaka N, Rattanakit S, Takahashi Y, Funabashi H, Luo D, Takakura Y (2011) *Biomaterials* 32:488. <https://doi.org/10.1016/j.biomaterials.2010.09.013>
71. Song J, Hwang S, Im K, Hur J, Nam J, Hwang S, Ahn GO, Kim S, Park N (2015) *J Mater Chem B* 3:1537. <https://doi.org/10.1039/c4tb01519c>
72. Song J, Im K, Hwang S, Hur J, Nam J, Ahn GO, Hwang S, Kim S, Park N (2015) *Nanoscale* 7:9433. <https://doi.org/10.1039/c5nr00858a>
73. Shin SW, Park KS, Jang MS, Song WC, Kim J, Cho S-W, Lee JY, Cho JH, Jung S, Um SH (2015) *Langmuir* 31:912. <https://doi.org/10.1021/la503754e>
74. Kim T, Park S, Lee M, Baek S, Lee JB, Park N (2016) *Biomicrofluidics* 10:034112. <https://doi.org/10.1063/1.4953046>
75. Hur J, Im K, Hwang S, Choi B, Kim S, Hwang S, Park N, Kim K (2013) *Sci Rep* 3:1282. <https://doi.org/10.1038/srep01282>

76. Hur J, Im K, Kim SW, Kim UJ, Lee J, Hwang S, Song J, Kim S, Hwang S, Park N (2013) *J Mater Chem A* 1:14460. <https://doi.org/10.1039/c3ta13382f>
77. Noll T, Wenderhold-Reeb S, Schonherr H, Noll G (2017) *Angew Chem Int Ed Engl* 56:12004. <https://doi.org/10.1002/anie.201705001>
78. Hartman MR, Yang D, Tran TN, Lee K, Kahn JS, Kiatwuthinon P, Yancey KG, Trotsenko O, Minko S, Luo D (2013) *Angew Chem Int Ed Engl* 52:8699. <https://doi.org/10.1002/anie.201302175>
79. Chen T, Romesberg FE (2017) *Angew Chem Int Ed Engl* 56:14046. <https://doi.org/10.1002/anie.201707367>
80. Deng S, Yan J, Wang F, Su Y, Zhang X, Li Q, Liu G, Fan C, Pei H, Wan Y (2019) *Biosens Bioelectron* 137:263. <https://doi.org/10.1016/j.bios.2019.04.053>
81. Xiang B, He K, Zhu R, Liu Z, Zeng S, Huang Y, Nie Z, Yao S (2016) *ACS Appl Mater Interfaces* 8:22801. <https://doi.org/10.1021/acsami.6b03572>
82. Hua X, Zhou X, Guo S, Zheng T, Yuan R, Xu W (2019) *Microchim Acta* 186:158. <https://doi.org/10.1007/s00604-019-3283-2>
83. Cheng E, Li Y, Yang Z, Deng Z, Liu D (2011) *Chem Commun (Camb)* 47:5545. <https://doi.org/10.1039/c1cc11028d>
84. Guo W, Lu C-H, Qi X-J, Orbach R, Fadeev M, Yang H-H, Willner I (2014) *Angew Chem Int Ed Engl* 53:10134. <https://doi.org/10.1002/anie.201405692>
85. Guo W, Lu CH, Orbach R, Wang F, Qi XJ, Ceconello A, Seliktar D, Willner I (2015) *Adv Mater* 27:73. <https://doi.org/10.1002/adma.201403702>
86. Wang CY, Li FY, Bi YH, Guo WW (2019) *Adv Mater Interfaces* 6:1900556. <https://doi.org/10.1002/admi.201900556>
87. Jia H, Shi J, Shao Y, Liu D (2017) *Chin J Polym Sci* 35:1307. <https://doi.org/10.1007/s10118-017-1978-6>
88. Shi J, Jia H, Liu D (2017) *Acta Polym Sin* 1:135. <https://doi.org/10.11777/j.issn1000-3304.2017.16278>
89. Xu W, Huang Y, Zhao H, Li P, Liu G, Li J, Zhu C, Tian L (2017) *Chemistry* 23:18276. <https://doi.org/10.1002/chem.201704390>
90. Ren J, Hu Y, Lu CH, Guo W, Aleman-Garcia MA, Ricci F, Willner I (2015) *Chem Sci* 6:4190. <https://doi.org/10.1039/c5sc00594a>
91. Hu Y, Lu C, Guo W, Aleman-Garcia MA, Ren J, Willner I (2015) *Adv Funct Mater* 25:6867. <https://doi.org/10.1002/adfm.201503134>
92. Hu Y, Guo W, Kahn JS, Aleman-Garcia MA, Willner I (2016) *Angew Chem Int Ed Engl* 55:4210. <https://doi.org/10.1002/anie.201511201>
93. Hu Y, Kahn JS, Guo W, Huang F, Fadeev M, Harries D, Willner I (2016) *J Am Chem Soc* 138:16112. <https://doi.org/10.1021/jacs.6b10458>
94. Lu S, Wang S, Zhao J, Sun J, Yang X (2018) *Chem Commun* 54:4621. <https://doi.org/10.1039/c8cc01603h>
95. Lu CH, Qi XJ, Orbach R, Yang HH, Mironi-Harpaz I, Seliktar D, Willner I (2013) *Nano Lett* 13:1298. <https://doi.org/10.1021/nl400078g>
96. Lu C, Guo W, Qi X, Neubauer A, Paltiel Y, Willner I (2015) *Chem Sci* 6:6659. <https://doi.org/10.1039/c5sc02203g>
97. Lu CH, Guo W, Hu Y, Qi XJ, Willner I (2015) *J Am Chem Soc* 137:15723. <https://doi.org/10.1021/jacs.5b06510>
98. Wu Y, Wang D, Willner I, Tian Y, Jiang L (2018) *Angew Chem Int Ed Engl* 57:7790. <https://doi.org/10.1002/anie.201803222>
99. Huang Y, Xu W, Liu G, Tian L (2017) *Chem Commun* 53:3038. <https://doi.org/10.1039/c7cc00636e>
100. Mao X, Pan S, Zhou D, He X, Zhang Y (2019) *Sens Actuators B Chem* 285:385. <https://doi.org/10.1016/j.snb.2019.01.076>
101. Guo W, Qi X, Orbach R, Lu C, Freage L, Mironi-Harpaz I, Seliktar D, Yang H-H, Willner I (2014) *Chem Commun* 50:4065. <https://doi.org/10.1039/C3CC49140D>
102. Yu X, Hu Y, Kahn JS, Ceconello A, Willner I (2016) *Chemistry* 22:14504. <https://doi.org/10.1002/chem.201603653>
103. Li J, Yu J, Huang Y, Zhao H, Tian L (2018) *ACS Appl Mater Interfaces* 10:26075. <https://doi.org/10.1021/acsami.8b09152>

104. Geng J, Yao C, Kou X, Tang J, Luo D, Yang D (2018) *Adv Healthc Mater* 7:1700998. <https://doi.org/10.1002/adhm.201700998>
105. Famulok M, Hartig JS, Mayer G (2007) *Chem Rev* 107:3715. <https://doi.org/10.1021/cr0306743>
106. Yang H, Liu H, Kang H, Tan W (2008) *J Am Chem Soc* 130:6320. <https://doi.org/10.1021/ja801339w>
107. Wang Z, Xia J, Cai F, Zhang F, Yang M, Bi S, Gui R, Li Y, Xia Y (2015) *Colloids Surf B Biointerfaces* 134:40. <https://doi.org/10.1016/j.colsurfb.2015.06.031>
108. Zhu Z, Wu C, Liu H, Zou Y, Zhang X, Kang H, Yang CJ, Tan W (2010) *Angew Chem Int Ed Engl* 49:1052. <https://doi.org/10.1002/anie.200905570>
109. Zhou L, Chen C, Ren J, Qu X (2014) *Chem Commun* 50:10255. <https://doi.org/10.1039/c4cc04791e>
110. Liu R, Huang Y, Ma Y, Jia S, Gao M, Li J, Zhang H, Xu D, Wu M, Chen Y, Zhu Z, Yang C (2015) *ACS Appl Mater Interfaces* 7:6982. <https://doi.org/10.1021/acsami.5b01120>
111. Ma Y, Mao Y, Huang D, He Z, Yan J, Tian T, Shi Y, Song Y, Li X, Zhu Z, Zhou L, Yang CJ (2016) *Lab Chip* 16:3097. <https://doi.org/10.1039/c6lc00474a>
112. Iwasaki Y, Kondo J, Kuzuya A, Moriyama R (2016) *Sci Technol Adv Mater* 17:285. <https://doi.org/10.1080/14686996.2016.1189798>
113. Yan L, Zhu Z, Zou Y, Huang Y, Liu D, Jia S, Xu D, Wu M, Zhou Y, Zhou S, Yang CJ (2013) *J Am Chem Soc* 135:3748. <https://doi.org/10.1021/ja3114714>
114. Zhu Z, Guan Z, Jia S, Lei Z, Lin S, Zhang H, Ma Y, Tian ZQ, Yang CJ (2014) *Angew Chem Int Ed Engl* 53:12503. <https://doi.org/10.1002/anie.201405995>
115. Wei X, Tian T, Jia S, Zhu Z, Ma Y, Sun J, Lin Z, Yang CJ (2015) *Anal Chem* 87:4275. <https://doi.org/10.1021/acs.analchem.5b00532>
116. Tian T, Wei X, Jia S, Zhang R, Li J, Zhu Z, Zhang H, Ma Y, Lin Z, Yang CJ (2016) *Biosens Bioelectron* 77:537. <https://doi.org/10.1016/j.bios.2015.09.049>
117. Liu D, Jia S, Zhang H, Ma Y, Guan Z, Li J, Zhu Z, Ji T, Yang CJ (2017) *ACS Appl Mater Interfaces* 9:22252. <https://doi.org/10.1021/acsami.7b05531>
118. Ma Y, Mao Y, An Y, Tian T, Zhang H, Yan J, Zhu Z, Yang CJ (2018) *Analyst* 143:1679. <https://doi.org/10.1039/c8an00010g>
119. Li Y, Ma Y, Jiao X, Li T, Lv Z, Yang CJ, Zhang X, Wen Y (2019) *Nat Commun* 10:1036. <https://doi.org/10.1038/s41467-019-08952-1>
120. Yin B, Ye B, Wang H, Zhu Z, Tan W (2012) *Chem Commun* 48:1248. <https://doi.org/10.1039/C1CC15639J>
121. Zhang L, Lei J, Liu L, Li C, Ju H (2013) *Anal Chem* 85:11077. <https://doi.org/10.1021/ac4027725>
122. Zhou L, Sun N, Xu L, Chen X, Cheng H, Wang J, Pei R (2016) *RSC Adv* 6:114500. <https://doi.org/10.1039/c6ra23462c>
123. Simon AJ, Walls-Smith LT, Freddi MJ, Fong FY, Gubala V, Plaxco KW (2017) *ACS Nano* 11:461. <https://doi.org/10.1021/acs.nano.6b06414>
124. Simon AJ, Walls-Smith LT, Plaxco KW (2018) *Analyst* 143:2531. <https://doi.org/10.1039/c8an00337h>
125. Liu H, Cao T, Xu Y, Dong Y, Liu D (2018) *Int J Mol Sci* 19:1633. <https://doi.org/10.3390/ijms19061633>
126. Yang Z, Zhuo Y, Yuan R, Chai Y (2017) *Nanoscale* 9:2556. <https://doi.org/10.1039/c6nr08353f>
127. Liu C, Han J, Pei Y, Du J (2018) *Appl Sci Basel* 8:1941. <https://doi.org/10.3390/app8101941>
128. Li J, Zheng C, Cansiz S, Wu C, Xu J, Cui C, Liu Y, Hou W, Wang Y, Zhang L, Teng I, Yang H, Tan W (2015) *J Am Chem Soc* 137:1412. <https://doi.org/10.1021/ja5122931>
129. Chen F, Bai M, Cao K, Zhao Y, Cao X, Wei J, Wu N, Li J, Wang L, Fan C, Zhao Y (2017) *ACS Nano* 11:11908. <https://doi.org/10.1021/acs.nano.7b06728>
130. Chen F, Bai M, Zhao Y, Cao K, Cao X, Zhao Y (2018) *Anal Chem* 90:2271. <https://doi.org/10.1021/acs.analchem.7b04634>
131. McGhee CE, Loh KY, Lu Y (2017) *Curr Opin Biotechnol* 45:191. <https://doi.org/10.1016/j.copbio.2017.03.002>
132. Lin H, Zou Y, Huang Y, Chen J, Zhang WY, Zhuang Z, Jenkins G, Yang CJ (2011) *Chem Commun (Camb)* 47:9312. <https://doi.org/10.1039/c1cc12290h>
133. Huang Y, Ma Y, Chen Y, Wu X, Fang L, Zhu Z, Yang CJ (2014) *Anal Chem* 86:11434. <https://doi.org/10.1021/ac503540q>
134. Mao Y, Li J, Yan J, Ma Y, Song Y, Tian T, Liu X, Zhu Z, Zhou L, Yang C (2017) *Chem Commun* 53:6375. <https://doi.org/10.1039/c7cc01360d>

135. Huang Y, Fang L, Zhu Z, Ma Y, Zhou L, Chen X, Xu D, Yang C (2016) *Biosens Bioelectron* 85:496. <https://doi.org/10.1016/j.bios.2016.05.008>
136. Lilienthal S, Shpilt Z, Wang F, Orbach R, Willner I (2015) *ACS Appl Mater Interfaces* 7:8923. <https://doi.org/10.1021/acsami.5b02156>
137. Kang H, Liu H, Zhang X, Yan J, Zhu Z, Peng L, Yang H, Kim Y, Tan W (2011) *Langmuir* 27:399. <https://doi.org/10.1021/la1037553>
138. Shimomura S, Nishimura T, Ogura Y, Tanida J (2018) *R Soc Open Sci* 5:171779. <https://doi.org/10.1098/rsos.171779>
139. Dirks RM, Pierce NA (2004) *Proc Natl Acad Sci* 101:15275. <https://doi.org/10.1073/pnas.0407024101>
140. Bi S, Yue SZ, Zhang SS (2017) *Chem Soc Rev* 46:4281. <https://doi.org/10.1039/c7cs00055c>
141. Wang J, Chao J, Liu H, Su S, Wang L, Huang W, Willner I, Fan C (2017) *Angew Chem Int Ed Engl* 56:2171. <https://doi.org/10.1002/anie.201610125>
142. Song P, Ye D, Zuo X, Li J, Wang J, Liu H, Hwang MT, Chao J, Su S, Wang L, Shi J, Wang L, Huang W, Lal R, Fan C (2017) *Nano Lett* 17:5193. <https://doi.org/10.1021/acs.nanolett.7b01006>
143. Li D, Song S, Fan C (2010) *Acc Chem Res* 43:631. <https://doi.org/10.1021/ar900245u>
144. Xue J, Chen F, Bai M, Yu X, Wei J, Huang P, Zhao Y (2017) *ChemNanoMat* 3:725. <https://doi.org/10.1002/cnma.201700177>
145. Zhao Y, Chen F, Qin J, Wei J, Wu W, Zhao Y (2018) *Chem Sci* 9:392. <https://doi.org/10.1039/C7SC03994H>
146. Li J, Fan C, Pei H, Shi J, Huang Q (2013) *Adv Mater* 25:4386. <https://doi.org/10.1002/adma.201300875>
147. Pei H, Zuo X, Zhu D, Huang Q, Fan C (2014) *Acc Chem Res* 47:550. <https://doi.org/10.1021/ar400195t>
148. Yang F, Zuo X, Fan C, Zhang X-E (2018) *Natl Sci Rev* 5:740. <https://doi.org/10.1093/nsr/nwx134>
149. Ye D, Zuo X, Fan C (2018) *Annu Rev Anal Chem* 11:171
150. Ge Z, Li Q, Fan C (2019) *Chem Res Chin Univ* 36:1. <https://doi.org/10.1007/s40242-019-9249-4>
151. Hu Q, Li H, Wang L, Gu H, Fan C (2019) *Chem Rev* 119:6459. <https://doi.org/10.1021/acs.chemrev.7b00663>
152. Song S, Qin Y, He Y, Huang Q, Fan C, Chen H (2010) *Chem Soc Rev* 39:4234. <https://doi.org/10.1039/c000682n>
153. Chen N, Li J, Song H, Chao J, Huang Q, Fan C (2014) *Acc Chem Res* 47:1720. <https://doi.org/10.1021/ar400324n>
154. Jia S, Chao J, Fan C, Liu H (2014) *Prog Chem* 26:695. <https://doi.org/10.7536/pc140130>
155. Liu X, Zhao Y, Liu P, Wang L, Lin J, Fan C (2019) *Angew Chem Int Ed Engl* 58:8996. <https://doi.org/10.1002/anie.201807779>
156. Wang F, Zhang X, Liu X, Fan C, Li Q (2019) *Small* 15:1900013. <https://doi.org/10.1002/smll.201900013>
157. Zhao Y, Dai X, Wang F, Zhang X, Fan C, Liu X (2019) *Nano Today* 26:123. <https://doi.org/10.1016/j.nantod.2019.03.004>
158. Wu N, Chen F, Zhao Y, Yu X, Wei J, Zhao Y (2018) *Langmuir* 34:14721. <https://doi.org/10.1021/acs.langmuir.8b01818>

Publisher's Note Springer Nature remains neutral with regard to jurisdictional claims in published maps and institutional affiliations.



DNA-Programmed Chemical Synthesis of Polymers and Inorganic Nanomaterials

Xuemei Xu¹ · Pia Winterwerber² · David Ng² · Yuzhou Wu^{1,2} 

Received: 30 October 2019 / Accepted: 17 February 2020 / Published online: 7 March 2020
© The Author(s) 2020

Abstract

DNA nanotechnology, based on sequence-specific DNA recognition, could allow programmed self-assembly of sophisticated nanostructures with molecular precision. Extension of this technique to the preparation of broader types of nanomaterials would significantly improve nanofabrication technique to lower nanometer scale and even achieve single molecule operation. Using such exquisite DNA nanostructures as templates, chemical synthesis of polymer and inorganic nanomaterials could also be programmed with unprecedented accuracy and flexibility. This review summarizes recent advances in the synthesis and assembly of polymer and inorganic nanomaterials using DNA nanostructures as templates, and discusses the current challenges and future outlook of DNA templated nanotechnology.

Keywords DNA origami · Polymer nanomaterial · Inorganic nanomaterial · Programmed synthesis · Bottom-up nanofabrication

1 Introduction

DNA, often known as the genetic code, exists in natural organisms. In 1953, the double helix structure of DNA was discovered, which revealed the mystery of life and enabled people to understand clearly the composition and transmission of genetic information [1]. Two reversely parallel complementary DNA single strands can recognize each other via Watson–Crick base pairing, forming a stable DNA

Chapter 3 was originally published as Xu, X., Winterwerber, P., Ng, D. & Wu, Y. Topics in Current Chemistry (2020) 378: 31. <https://doi.org/10.1007/s41061-020-0292-x>.

✉ Yuzhou Wu
wuyuzhou@hust.edu.cn

¹ Hubei Key Laboratory of Bioinorganic Chemistry and Materia Medica, School of Chemistry and Chemical Engineering, Huazhong University of Science and Technology, Luoyu Road 1037, Hongshan, Wuhan 430074, People's Republic of China

² Max Planck Institute for Polymer Research, Ackermannweg 10, 55128 Mainz, Germany

double helix with high accuracy from sequence to structure [2]. In the process of life activities, the double helix structure can be dissociated and hybridized dynamically during transcription, replication or repair, which provides a vital guarantee for the recording, transmission and translation of genetic information [3].

In recent decades, enthusiasm for DNA molecules has expanded from the initial biological and chemical arena to that of nanomaterials. Given the advantages of accuracy and design flexibility, advances in DNA self-assembly techniques [4] have made DNA structures a new type of “star” material in nanotechnology. DNA nanotechnology was pioneered by Seeman and co-workers in the 1980s [5–8], and has been revolutionized by Rothemund into a state-of-the-art technology, i.e., DNA origami [9]. This technology allows folding of DNA nanostructures by mixing and annealing a long single circular DNA scaffold with hundreds of short “staple” strands. In practice, this enables the construction of almost any kind of highly complex two-dimensional (2D) and three-dimensional (3D) nanostructure with the aid of computing software such as caDNAo [10–15]. To address the cost limitations of DNA material, Dietz has devised a biotechnological mass production method, which provides impetus for the practical application of DNA origami in the future [16].

Intriguingly, the glamour of life is that DNA is not only capable of storing genetic information, but can also precisely translate this information into another material—protein. The sequence-dependent hybridization mechanism ensures that DNA can stably store genetic information and its heredity. In its natural state, DNA provides limited structural features and functional diversity. Therefore, DNA does not directly serve as a functional material, but instead, its sequence-encoded information is transcribed and expanded into the sequence of protein, and, in this way, renders diversity in life. Such an elegant strategy has also inspired material chemists. If DNA nanotechnology could be expanded to prepare diverse materials, the programmable features of DNA nanostructures might endow them with exquisite and unlimited physical and chemical properties, thus bringing a potential revolution to nanomaterial science. Encouraged by this vision, the use of DNA nanostructures as templates to control the precise synthesis of organic and inorganic materials has attracted increasing attention in recent years. In this review, we discuss the latest progress in the field of DNA-programmed material science, with a focus on the synthesis of polymer and inorganic materials employing DNA nanostructures as templates in order to achieve unprecedented accuracy at the nano scale (Fig. 1).

2 DNA-Sequence-Encoded Polymer Synthesis

As the most important storage material of natural genetic information, DNA can encode the synthesis of proteins in natural organisms and, accordingly, determine all of life’s activities. The ability to synthesize protein macromolecules using nucleic acids as templates enables proteins to evolve into complex structures and functions with remarkable specificity and reliability. In contrast, traditional chemical polymerization reactions cannot precisely control the sequence of monomers, or their molecular weight distribution. Therefore, synthetic polymers typically could not display defined structures and functions as proteins [17–19]. Despite great progress

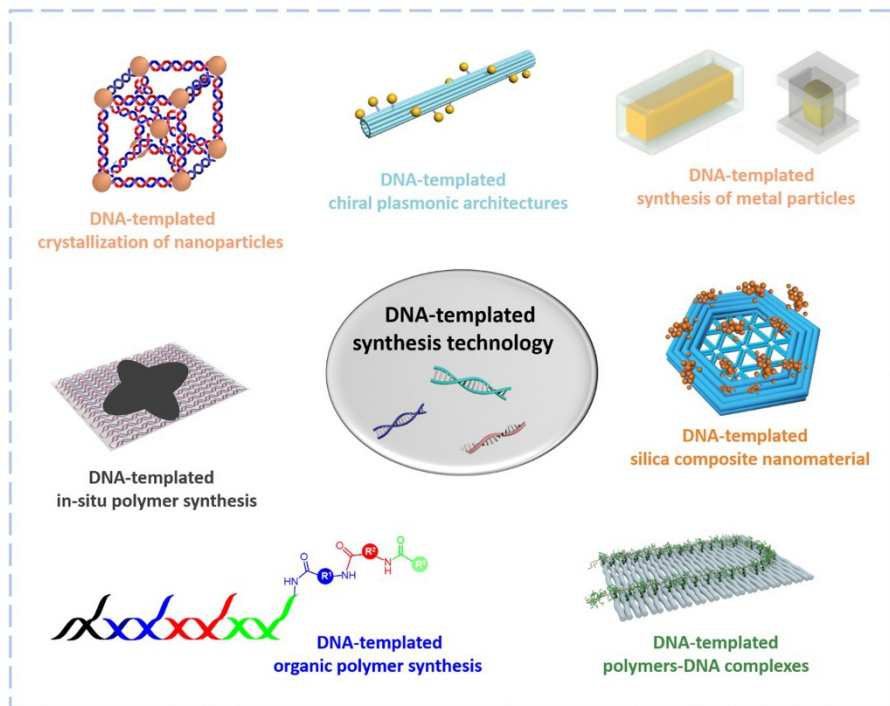


Fig. 1 DNA-templated synthetic technology

in controlling the structure [20, 21] and molecular weight distribution [22, 23] of synthetic polymers, it is still difficult to precisely control their sequence and length. However, it has been possible to achieve controlled polymer molecules by taking advantage of DNA sequences to guide the polymerization process. The technology of DNA-encoded polymer synthesis is devoted to more accurate design and preparation of polymer materials, and more precise control of their structure and function [24, 25].

Inspired by the DNA transcription process, Hollige et al. [26, 27] designed a DNA polymerase that allows enzymatic synthesis of nucleic acid analogs with non-natural polymer backbone and DNA hybridizing side chains, such as arabino nucleic acid (ANA) and 2'-fluoro-arabino-nucleic acid (FANA), locked nucleic acids (LNA), threose nucleic acid (TNA), hexonucleic acid (HNA), and cyclohexyl nucleic acid (CeNA) (Fig. 2). These DNA analogs are so-called XNAs. This study demonstrated for the first time that genetic information can be stored in, and recovered from, synthetic genetic polymers not found in nature. They have also shown that some XNAs could be replicated and folded into complex structures. In addition, Chaput and co-workers [28] obtained a thrombin-bound TNA adapter with high affinity and specificity from TNA libraries translated by enzyme-mediated primer extension, demonstrating that TNA has the ability to fold into tertiary structures with sophisticated chemical functions. The enzymatic DNA templating synthesis of synthetic polymer backbone showed therein suggest the potential to obtain synthetic

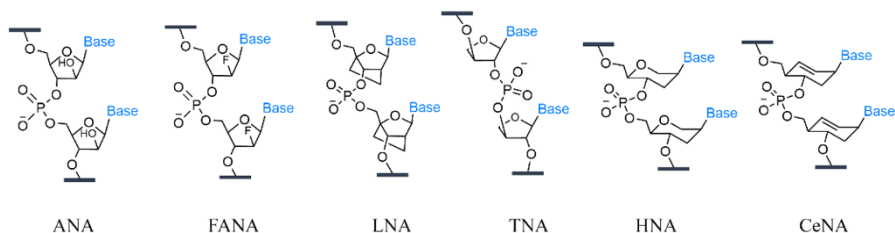


Fig. 2 DNA analogs with non-natural backbones that could be enzymatically synthesized based on DNA template

polymers also capable of storing sequence information. However, the type of polymer backbone is highly limited.

Liu and other researchers also attempted to mimic the principle of the natural gene translation process to achieve chemical synthesis of sequence-controlled polymers based on DNA templates [29–31]. They reported the efficient and sequence-specific polymerization of non-functional [32] and side-chain-functionalized peptide nucleic acid aldehydes [33] with DNA sequence templates, combined with an *in vitro* translation, functional screening and amplification system [34]. Although these studies showed the potential for chemically mimicking the gene translation process, they are still limited to nucleic acid analogs. Taking a step further, more flexible synthetic monomers could be sequence specifically aligned along the DNA template by conjugating the monomers with short DNA sequences. For instance, Schuster et al. [35] used cyclic and linear DNA structures as template and DNA conjugated 2,5-bis(2-thienyl)pyrrole as monomers to achieve controlled synthesis of highly defined conducting polymers. In addition, Liu's group devoted intensive effort to study sequentially multistep reactions in a single solution using DNA templates [29–31]. Their early strategy allow DNA-tagged synthetic monomers to sequentially hybridize on a predefined DNA single-strand template, thus initiating spontaneous proximity-driven cascade reactions to connect the monomers into sequence-specific oligomers [36]. Similarly, Turberfield's group [37] used short single-strand DNA adapters to hybridize two DNA-tagged monomers, thus controlling the reaction sequence, which can also allow orthogonal synthesis of several predefined oligomers in one vessel. Nevertheless, these designs depend highly on the close distance between the assembled monomers to initiate sequential reactions, thus limiting the choice of monomers to very small moieties and hindering reaction efficiency. Thereafter, they further devised an automatic DNA walker that allows programmable multistep organic reactions that better mimic the natural DNA-encoded protein synthesis process. Different monomers were encoded by specific DNA sequences so that they could be hybridized on DNA templates at predefined positions. The DNA walker could then sequentially create an amide bond between these monomers, just like a ribosome forming an ordered polypeptide chain (Fig. 3a) [38]. This strategy can potentially be applied to more diverse type of reactions, and significantly improve synthesis efficiency, particularly for longer sequences. Furthermore, these latter authors mimicked the process of transcription and translation

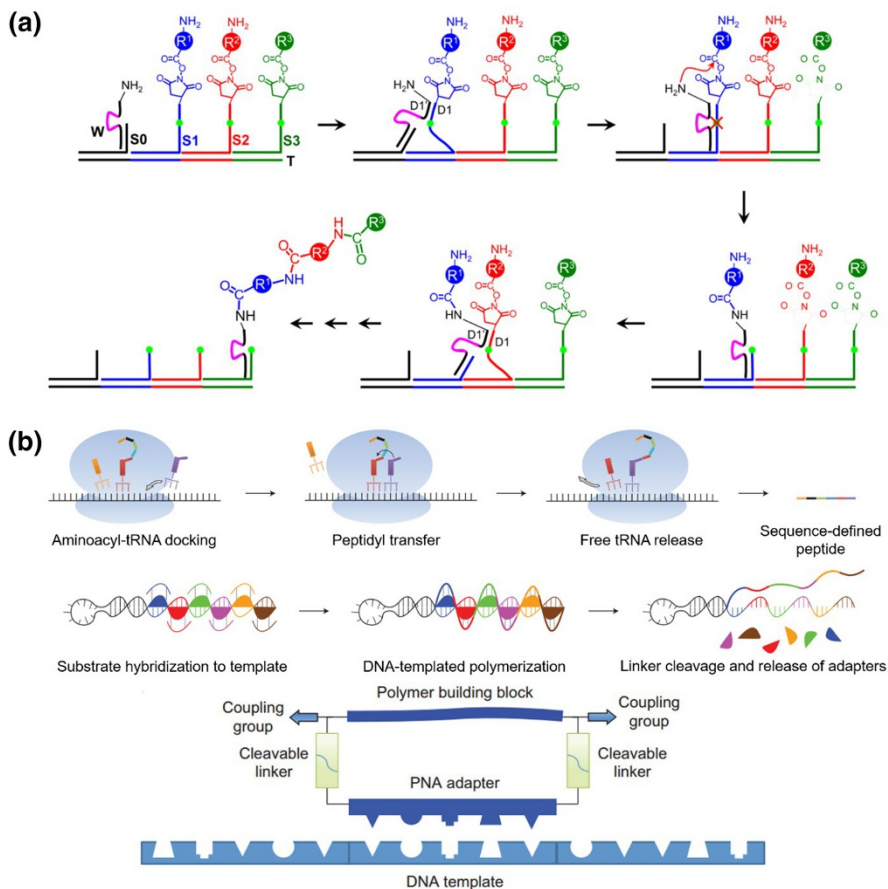


Fig. 3a,b Synthesis of polymers based on DNA templates. **a** DNAsome-mediated multistep synthesis of a triamide product. Reproduced with permission from Ref. [38]. Copyright 2010 Nature Publishing Group. **b** Synthesis of polymers with higher molecular weight arising from the process of translation from DNA into proteins. Reproduced with permission from Ref. [39]. Copyright 2013 Nature Publishing Group

of DNA into proteins in living systems, producing sequence-specific synthetic polymers with higher molecular weight; the structures of these polymers were independent of the DNA templates (Fig. 3b) [39]. These studies clearly exhibited the great potential of sequence-defined polymer synthesis using DNA templates. With this technique, polymers could be anticipated to possess more rationally designed functions and self-assembly behaviors, rather like biomacromolecules. The possibility of synthesizing sequence-defined polymers with diverse functional monomers might open up numerous new opportunities for polymer chemistry, such as precisely controlling dynamic macromolecular recognition, manipulation of sophisticated polymer assembly and creation of smart polymer nano-robots. However, as the aforementioned methods are somewhat tedious and expensive, they serve mainly as

a proof-of-concept studies with still limited applications. Therefore, more efficient and facile methods are still required to promote the practical application of DNA-templated polymer synthesis.

3 Synthesis of Polymer Nanomaterials Templated by DNA Nanostructures

As an extension of synthetic polymers encoded by simple DNA strands, in recent years, DNA nanostructures with 2D and 3D spatial conformation have also been used as templates for the synthesis of polymer nanomaterials. At present, there are two major objectives for these studies. On the one hand, researchers aim to improve the physical and chemical properties of DNA nanomaterials by polymer modification. Since DNA-folded “nano-robots” have been proposed as ideal intelligent drug carriers at the nanometer scale [40], there have been intensive studies to enhance the stability of DNA nano-robots under various practical application conditions, and to tune their physical and chemical properties by polymer modification. On the other hand, DNA nanostructures can also serve simply as templates to control polymer synthesis and assembly, providing more powerful nanofabrication techniques to achieve exquisite polymer nanostructures.

3.1 Polymer Modified DNA Nanomaterials

Various types of substances have been used to encapsulate DNA nanostructures to improve their physical and chemical stability. For instance, by immobilizing lipid-modified DNA on the nanostructure surface, liposome can be formed around the DNA nanostructure to enhance cell uptake efficiency (Fig. 4a) [41]. However, this method requires pre-modification of the DNA nanostructure, and it is tricky to avoid competitive micellar formation by amphiphilic DNA-lipid conjugates. Thereafter, Kostianen and co-workers studied a series of positively charged materials designed to wrap the negatively charged DNA nanostructures via simple electrostatic interactions. In this regard, the naturally positively charged cowpea chlorotic mottle virus capsid protein was first tested and found to be beneficial to increase the efficiency of DNA nanostructures entering cancer cells (Fig. 4b) [42]. In addition, they also designed synthetic polymer conjugates with a positively charged block to interact with DNA and an uncharged hydrophilic block to facilitate aqueous stability and biocompatibility. They showed that both the positively charged PDMAEMA-PEG copolymer and the dendron-conjugated bovine serum albumin (BSA) could provide the expected functions for encapsulating brick-shaped DNA nanostructures [43, 44]. The protected DNA nanostructures exhibited complete resistance to DNase degradation, and their cell uptake efficiency was significantly enhanced by more than 2.5 times [44]. These outcomes were consistent with reports from others. For instance, Schmidt and co-workers [45] showed that polyethylene glycol and polylysine copolymers (PEG-PLys) can protect the structure of DNA against DNase I degradation and improve stability in low ionic strength buffer. Shih's group also reported that

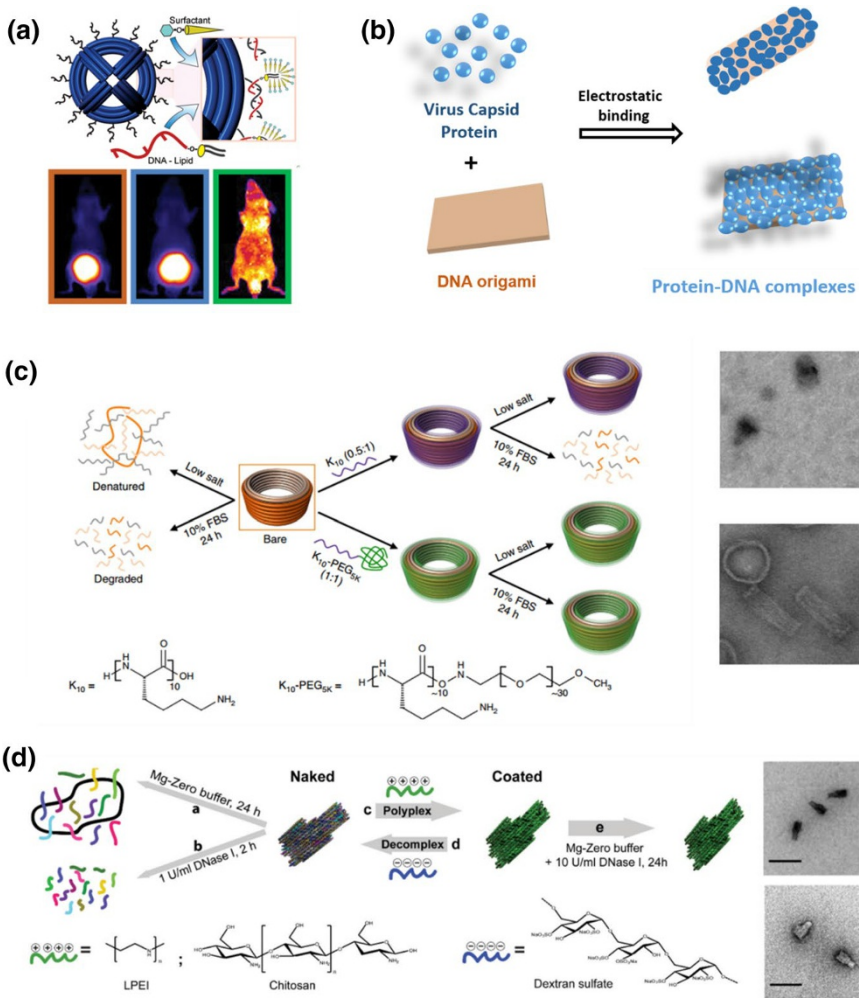


Fig. 4a–d Biopolymers interacting with DNA nanostructures. **a** Liposome membrane encapsulation of DNA nanostructures. Reproduced with permission from Ref. [41]. Copyright 2014 American Chemical Society. **b** Positively charged cowpea chlorotic mottle virus capsid protein encapsulated square DNA origami. Reproduced with permission from Ref. [42]. Copyright 2014 American Chemical Society. **c** Electrostatic adsorption between synthetic polymer and DNA nanostructure template. Reproduced with permission from Ref. [46]. Copyright 2017 Nature Publishing Group. **d** Reversible assembly of synthetic and natural cationic polymers with DNA nanostructures. Reproduced with permission from Ref. [47] Copyright 2018 Royal Society of Chemistry

PEG-PLys copolymers with different molecular weights have dissimilar impacts on the stability of DNA origami [46]. These conjugates confer >1000-fold increased stability against digestion by serum nucleases. Particularly, PEG-PLys copolymer-encapsulated DNA nanostructures can survive uptake into endosomal compartments and, in a mouse model, exhibit a modest increase in pharmacokinetic bioavailability (Fig. 4c). Similarly, Barišić and co-workers reported that the cationic polysaccharide

chitosan and synthetic linear polyethyleneimine (LPEI) can also protect the structural integrity of DNA origami (Fig. 4d) [47]. A similar effect was observed when using a chemically modified protein—cationic human serum albumin (HSA)—that is more biocompatible and easily available [48]. These investigations clearly demonstrated that decoration of DNA nanostructures with cationic polymers could be an efficient way to improve their physiological stability and modulate their *in vitro* and *in vivo* distribution. In this way, DNA nanostructures can better serve as smart drug delivery carriers for broader biomedical applications. However, it is noteworthy that some essential features of DNA nanostructures, such as their precisely positioned surface functionalities, DNA-sequence-dependent molecular recognition, and the intelligent mobility of specially design DNA robots, were lost during this encapsulation process. Therefore, future studies are expected to pay more attention to controlled polymer modification of DNA nanostructures at only specific positions to enhance their stability and biocompatibility while maintaining functionality. Some methods presented in the following section on [Bottom-up Fabrication of Polymer Materials](#) might provide such opportunity, but their potential in this aspect has not yet been fully explored.

3.2 Bottom-up Fabrication of Polymer Materials

Apart from their attractive properties and as yet not fully exploited potential as drug carriers, a role for DNA origami nanostructures as templates to control the growth of polymer nanomaterials has also been envisioned. Conventional synthetic polymerization reactions in liquid phase normally result in randomly entangled polymer chains. In contrast, by combining traditional polymer synthesis methods with DNA strands or nanostructures based on site-specific modification strategy, pre-designed polymer nanomaterials were successfully obtained. This could be achieved by *in situ* atom transfer radical polymerization (ATRP) polymerization on DNA chains—a technique established by Matyjaszewski and coworkers [49]. By modifying a DNA strand with a ATRP initiator, polymers can grow directly from the 5'-terminus of a DNA chain [49]. Based on this method, Weil and Wu and colleagues [50] achieved the synthesis of polymer nanomaterials with unique shape and patterns by pre-positioning of initiators on a rectangular DNA origami tile. In this regard, the DNA tile can be considered as a “screen” with around 200 sequence-encoded “pixels”. A single-strand sticky end was placed at the “pixel” that was desired to grow polymer later on. Thus, ATRP-initiator-modified DNA sequences could be hybridized on the sticky ends, thereby allowing an *in situ* polymerization reaction from the immobilized initiators (Fig. 5a). In this way, polymers with a designed nanopattern could be synthesized precisely. Moreover, polymer nanostructures could be released from the DNA template simply by heat-induced disassembly of the DNA tile. Compared with traditional lithography and self-assembly-based polymer nanomaterial preparation techniques, this method features high precision (up to a few nanometers) and efficiency (one-pot reaction in solution), and brings new opportunities in the synthesis of polymer nanomaterials. On the basis of this work, Weil and Wu and coworkers extended this *in situ* polymerization method from 2D DNA origami to its 3D

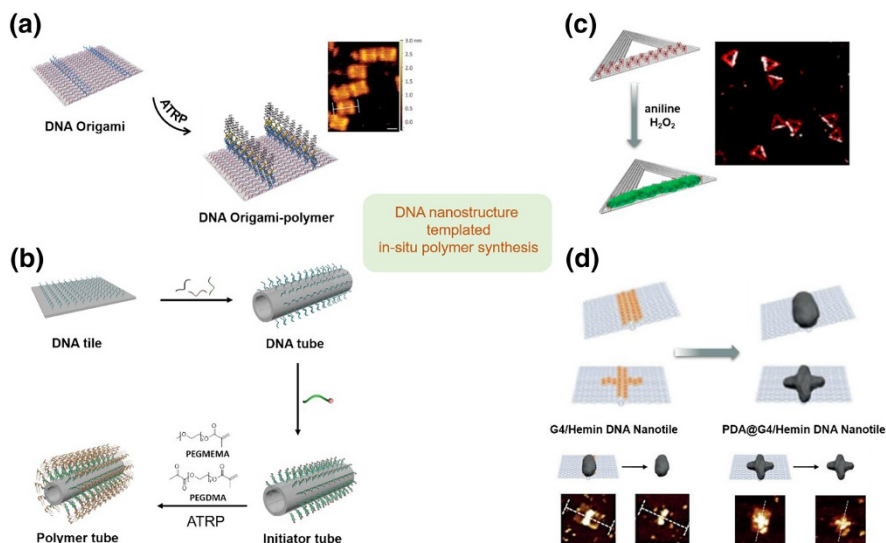


Fig. 5a–d In situ synthesis of DNA nanostructure templated polymers. **a** Bottom-up fabrication of polymers on DNA origami template by in situ atom transfer radical polymerization (ATRP). Reproduced with permission from Ref. [50]. Copyright 2016 Wiley-VCH. **b** Polymeric shell on DNA origami template for enhancing the stability of DNA materials. Reproduced with permission from Ref. [51]. Copyright 2018 Royal Society of Chemistry. **c** Shape-controlled conductive polyaniline on DNA templates. Reproduced with permission from Ref. [53]. Copyright 2014 American Chemical Society. **d** Shape-controlled nanofabrication of polydopamine on DNA templates. Reproduced with permission from Ref. [54, 55]. Copyright 2018 Wiley–VCH

counterpart [51]. The rectangular DNA origami was folded into a tube structure, and a controlled ATRP reaction was realized on the outer surface of the tube to construct a polymer-protecting shell. Meanwhile, the inner cavity of the tube is still available for further modification to accommodate other reactions (Fig. 5b). Notably, the defined polymer modification significantly enhanced the stability of DNA nanotubes, similar to that observed with the polymer encapsulation methods discussed above in the section on [Polymer modified DNA nanomaterials](#) [51]. Moreover, the functional positions (such as the inner cavity) on DNA nanostructures could remain unaffected, which could be further modified with guest molecules. Therefore, this method holds great potential for drug delivery, with more opportunities to tune the in vivo behaviors and design complex functionalities.

In addition to controlled radical polymerization, DNA template technology can also be applied to the synthesis of other patterned polymers. Ding's group reported the catalytic polymerization of aniline on DNA nanostructures [52, 53]. In the presence of hydrogen peroxide, conductive polyaniline could be synthesized at the desired position on double-stranded DNA [52] and on triangular DNA origami nanostructures via a pre-immobilized horseradish peroxidase- or hemin-catalyzed polymerization reaction (Fig. 5c) [53]. This method of preparing conductive polymers in a controllable manner on DNA origami provides a new strategy for the design of nanocircuits. Based on this localized catalysis concept, Weil and

co-workers reported shape-controllable in situ polydopamine synthesis on DNA nanostructures by positioning G-quadruplex groups as designed on a rectangular DNA tile and incorporating hemin as a cofactor [54, 55]. In the presence of hydrogen peroxide, the G-quadruplex/hemin DNAzymes mimic horseradish peroxidase activity and induce the oxidative polymerization of dopamine with predesigned patterns [54]. Alternatively, photoirradiation can also initiate the dopamine polymerization reaction in this system [55]. This methodology renders it possible to construct anisotropic polydopamine nanostructures such as nanorods and nano-crosses, which are difficult to achieve by conventional synthesis. These authors further demonstrated that the synthesized polydopamine nanostructure could be retained after removing the DNA template (Fig. 5d), therefore providing a new strategy for polydopamine nanofabrication.

In addition to DNA nanostructure-templated in situ polymer synthesis, Liu and colleagues have developed a series of methods to use DNA nanostructures as scaffolds to control the morphology of polymersomes and liposomes, which have been collectively named as the “frame guided assembly” technique. It is well known that spontaneously self-assembled vesicles of amphiphilic polymersomes and liposomes are usually spherical. However, Liu’s methods allowed construction of cubic shaped polymersomes and nanometer liposome sheets depending on the DNA template used. Hereby, they could even overcome the surface tension force in nature (Fig. 6a) [56, 57].

Other than controlling the shape and morphology of polymers, DNA templates allow the installation of functional handles on defined positions of polymer nanoparticles. Toward this end, Sleiman and colleagues reported a method of synthesizing DNA-imprinted polymer nanoparticles with monodispersity and prescribed DNA-strand patterns inside a DNA cage (Fig. 6b) [58]. They first immobilized DNA-polymer conjugates on predefined positions of the DNA cage, and then crosslinked the polymers inside the cage. In this way, once the DNA cage is decomposed, DNA handles pre-conjugated with polymer precursors are left on the crosslinked polymer cores with predesigned geometries. This is the first method to achieve nanoparticles with exact number and orientation of asymmetric modifications, which could significantly advance the area of polymer assembly. The works described above strongly indicate the unique advantages of DNA nanotechnology for controlling polymer morphology and function. The features achieved by these methods are almost impossible to achieve with conventional polymer synthesis, and are therefore particularly attractive for preparation of exquisite polymer materials for advance applications, such as intelligent polymer nanorobots, elaborate biosensors and intricate soft electronic devices.

3.3 Routing of Single Polymer Chain

In addition to controlling the morphology of polymer nanomaterials, DNA nanostructures can even be used to manipulate the molecular conformation of an individual polymer chain. Gothelf and colleagues prepared synthetic polymer wires containing short oligonucleotides that extend from each repeat [named

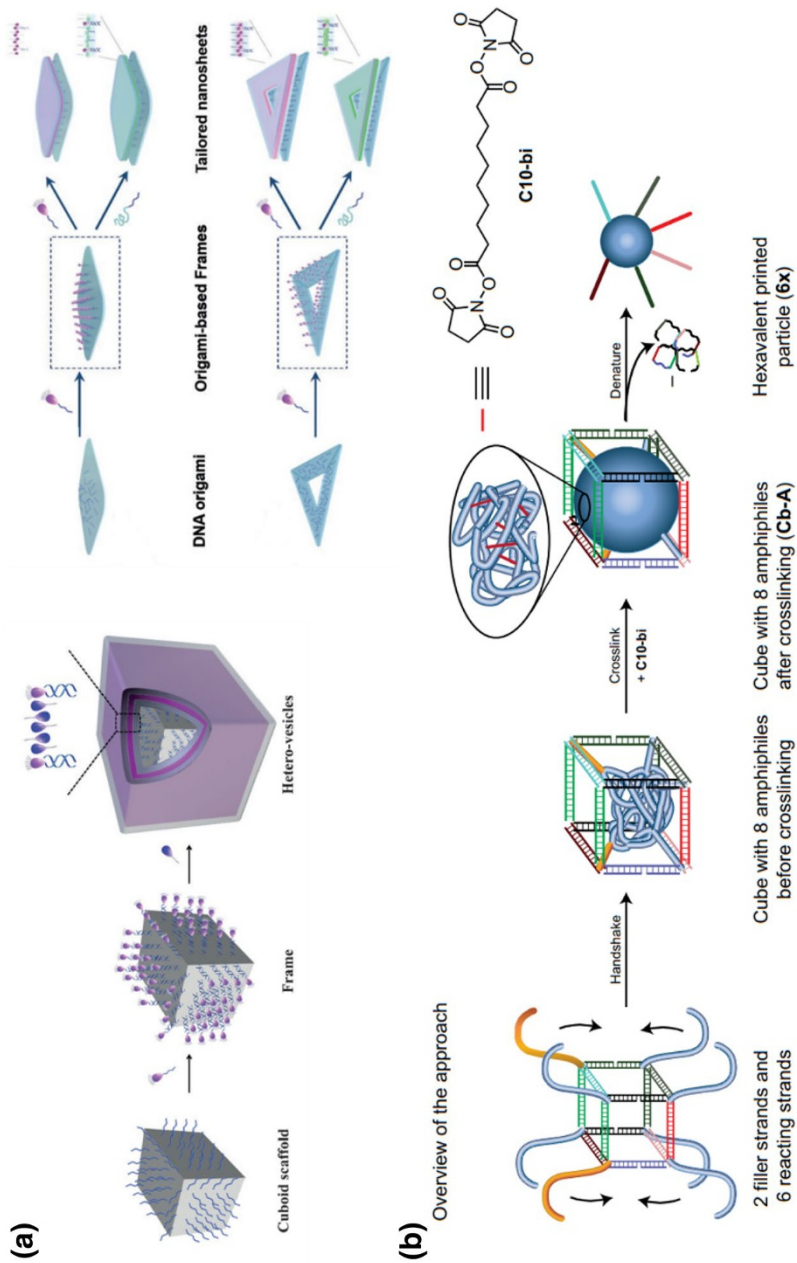


Fig. 6 Morphology control of polymersomes on DNA nanostructures as scaffolds. **a** DNA origami mediated "frame guided assembly". Reproduced with permission from Ref. [56, 57]. Copyright 2017 and 2016 Wiley-VCH. **b** Formation of hydrophobic polymer nanoparticle in DNA templates. Reproduced with permission from Ref. [58]. Copyright 2017 Nature Publishing Group

poly(APPV-DNA), see Fig. 7a]. The oligonucleotide side chains allow the polymer wire to assemble on the desired positions of DNA nanostructures where the complementary sticky sequences were pre-allocated. In this way, a single polymer chain could be picked up from the polymer solution and immobilized on a DNA template following a pre-designed route (Fig. 7a) [59]. Moreover, they can even achieve controlled conformational switching of a single polymer chain on the DNA nanotile based on toehold-mediated strand displacement (Fig. 7b) [60]. The controlled aggregation of poly(APPV-DNA) polymers in solution through varying the ionic environment and sequence-specific DNA interactions was demonstrated in their recent work [61].

On the basis of these works, the team developed a novel hybrid DNA–polyfluorene material, poly(F-DNA), wherein the backbone of polyfluorene was a conjugated polymer with special optical and electronic properties. The fluorescence emission of poly(F-DNA) could be quenched efficiently upon binding to very small amounts of complementary DNA carrying a small molecule quencher. Furthermore, they showed controlled energy transfer between poly(F-DNA) and poly(APPV-DNA) mediated by Watson–Crick base pairing (Fig. 7c) [62]. This concept opens up possibilities for studying the molecular interactions between polymers with different structures via intramolecular energy transfer. These studies clearly demonstrate that DNA nanotechnology provides unprecedented opportunities for handling individual synthetic polymer chains, thus revealing immense prospects for studying and utilizing the single-molecule properties of polymers. These designer organic polymer–DNA complexes are expected to be used as single molecular wires to support the design of high-precision nanocircuits in the future.

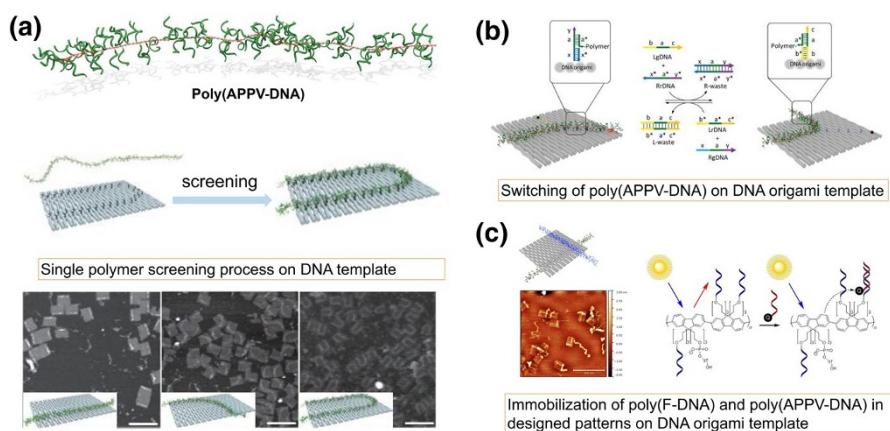


Fig. 7a–c DNA-nanostructure-templated synthesis of single synthetic polymers. **a** Single polymer screening process based on DNA origami templates. Reproduced with permission from Ref. [59]. Copyright 2015 Nature Publishing Group. **b** Programmed switching of single polymer conformation on DNA origami template. Reproduced with permission from Ref. [60]. Copyright 2016 American Chemical Society. **c** Single polymer manipulation and energy transfer investigation of poly(F-DNA) conjugated polymer. Reproduced with permission from Ref. [62]. Copyright 2016 Wiley-VCH

4 Assembly of Inorganic Nanoparticles Based on DNA Nanostructures

From the perspective of chemical structure, the DNA strand is an organic macromolecule composed of C, H, O, N, and P. Among the virtues of DNA molecules are their controllable structure, adjustable sequence and ease of modification. However, they lack the mechanical strength and quantum optical properties that are commonly available in inorganic nanomaterials. On the other hand, it remains challenging for conventional synthesis of inorganic nanoparticles to achieve arbitrary shapes and controllable assembly, which are highly important in achieving the desired optical and mechanical properties. Therefore, combining the benefits of both materials, DNA-assisted inorganic nanoparticle synthesis and assembly presents an attractive way to create rationally designed nanomaterials with unique features. In this context, modifying nanoparticles (Au, Ag, etc.) with oligonucleotides was found valuable to create nanoparticle crystals with the desired lattice form. DNA nanostructures could even serve as molds to control the morphology of inorganic nanoparticles during synthesis. Moreover, using DNA nanostructures as templates could even fabricate chiral plasmonic metamolecules. This section will summarize recent developments in this area.

4.1 DNA-Programmed Nanoparticle Super-Lattice Crystallization

In 1996, the groups of Mirkin and Schultz published two articles in *Nature* at the same time that revealed the possibility of using oligonucleotide-conjugated gold nanoparticles to guide the formation of nanoparticle assembly [63, 64]. DNA oligonucleotide chains with end-capped sulfhydryl groups were modified on gold nanoparticles (AuNPs) by Au–S bonds, while the reversible assembly of gold nanoparticles was controlled by adding designed DNA linkers with complementary sequences. When DNA duplexes with complementary sequences on both sides were added, the AuNPs formed aggregations with regular interspaces [63]. When the complementary oligonucleotides were positioned at the desired distances along the DNA duplex, defined AuNP dimers and trimers with controllable spacing could be achieved [64]. Since then, the self-assembly of inorganic nanoparticles templated by DNA oligonucleotide chains has advanced rapidly, and has found broad application in the construction of diagnostic tools for nucleic acid, protein and bacteria [65–69], as intracellular probes [70–73], and as selective detection biosensors [74–76] and gene regulators, etc. [77].

Despite the attractive applications of these small nanoparticle aggregates, preparation of perfect macroscopic nanoparticle crystals with super lattices was a long-standing challenge until 2008 when the groups of Gang and Mirkin independently reported DNA-guided gold nanoparticle crystals (Fig. 8a, b) [78, 79]. They demonstrated that the growth and assembly of gold nanocrystal structures could be controlled by changing the length of DNA strands between gold nanoparticles. Lattice structures could be accomplished through precisely designing the base sequences

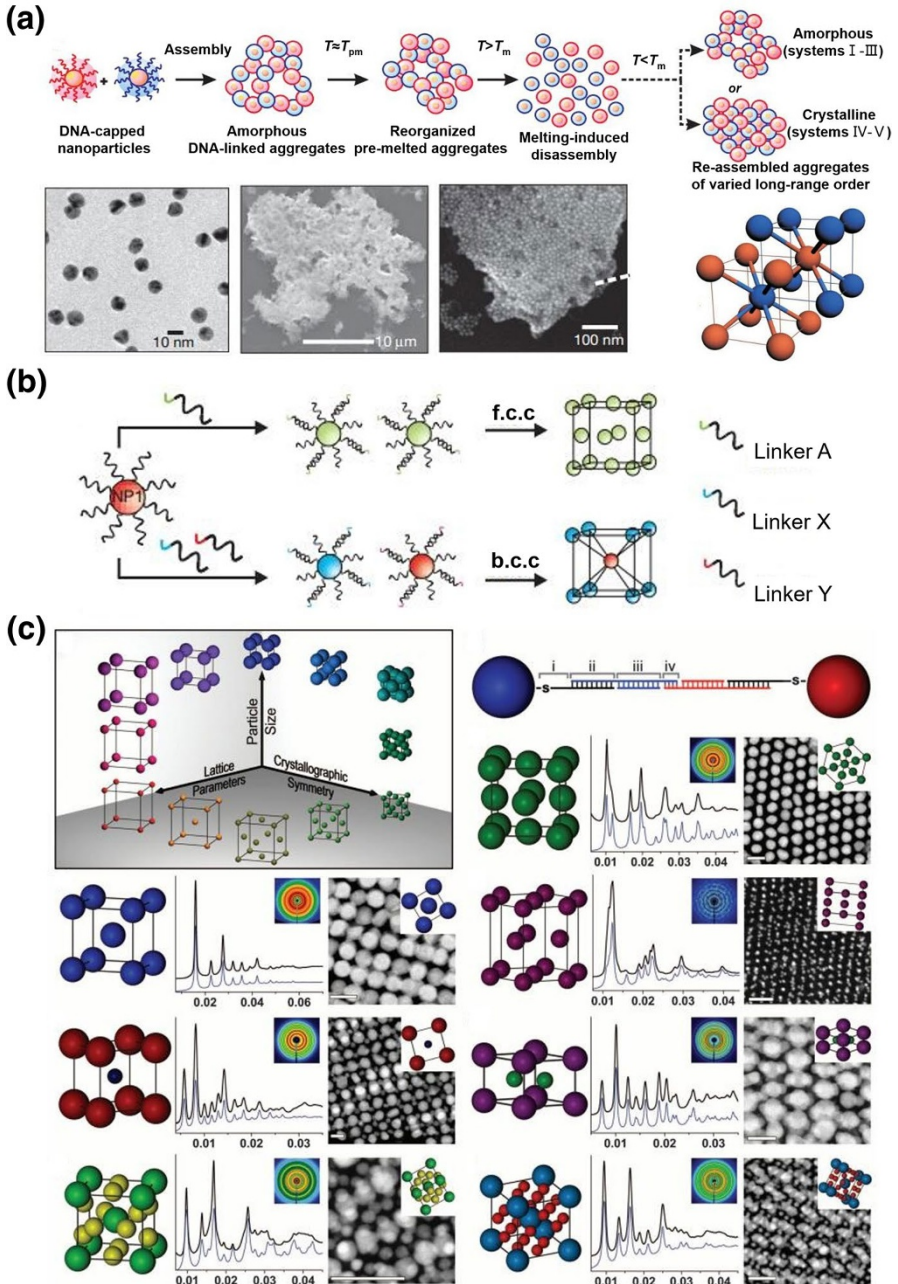


Fig. 8a–c DNA-strand-guided crystallization of inorganic nanoparticles. **a, b** The length of the DNA strand and the size of gold nanoparticles influence the crystal pattern. Reproduced with permission from Refs. [78] and [79]. Copyright 2008 Nature Publishing Group. **c** Various crystal lattice structures and their characterization based on DNA-guided assembly of gold nanoparticles. Reproduced with permission from Ref. [80] Copyright 2011 American Association for the Advancement of Science

and lengths of DNA strands. The Mirkin group subsequently engaged in the manipulation of gold nanoparticles using DNA chains to investigate more diverse crystal superlattices (Fig. 8c) [80]. Moreover, not only were various self-assembled structures from a single inorganic nanoparticle to a superlattice achieved [81–87], the properties of the assembled structures, such as temperature-dependent crystal topology [88], crystal surface energy [89], and dynamic DNA strand substitution [90], were also studied in detail. The mechanism of DNA-templated nanoparticle self-assembly was explained by the repulsive force between colloids [91] and the enthalpy change [92]. The dynamic properties of DNA-templated nanoparticle crystallization [93], in conjunction with previous works [94, 95], revealed that the number of DNA chains per nanoparticle and temperature were the main factors controlling the interaction strength between nanoparticle building blocks.

All the examples mentioned above require gold nanoparticles pre-modified with DNA linkers. Recently, Kostianin and colleagues reported that ordered 3D gold nanoparticle superlattices could be accessed through sole electrostatic interactions between positively charged gold nanoparticles and negatively charged DNA nanostructures [96]. This approach provided an easier alternative to create a nanoparticle crystal lattice when the accurate design of different types of lattice structure is not required.

These studies realized programmable synthesis of macroscopic materials from rationally designed microscopic nanoparticles, thus providing unprecedented control over the microstructures of bulk materials. Conventional material synthesis generally results in modest control over the placement of, the periodicity in, and the distance between, particles within the assembled material. DNA-assisted strategies allow nanoparticles to be assembled in a designed manner with high precision, which is essential for the design of metamaterials with superior properties in the future.

4.2 Inorganic Nanoparticle Growth with Controllable Dimensionality

In addition to guiding the assembly of pre-synthesized nanoparticles, DNA nanostructures could also serve as a mold to confine crystal growth during nanoparticle synthesis. In 2014, Yin and co-workers proposed the strategy of casting the growth of inorganic nanoparticles with controllable shapes inside DNA nanostructures cavities. Small gold nanoparticle seeds modified with DNA strands were hybridized onto sticky ends inside the origami cavity. Thereafter, gold nanoparticles were grown in the DNA cavities to completely fill the space. Various shapes of silver or gold nanoparticles can be obtained by designing DNA origami with the appropriate cavity structures. Moreover, composite inorganic nanoparticles were also accessible by introducing two quantum dots at both ends of the cavity (Fig. 9a) [97]. Analogously, Seidel and colleagues used the DNA origami cavity as a mold to control the growth of gold nanoparticles, and this process was successfully observed by TEM spectroscopy with stepwise addition of chloroauric acid [98, 99]. Inspired by these studies, Fan and Yan and their coworkers recently also presented a general method for creating biomimetic complex silica composite nanomaterials based on

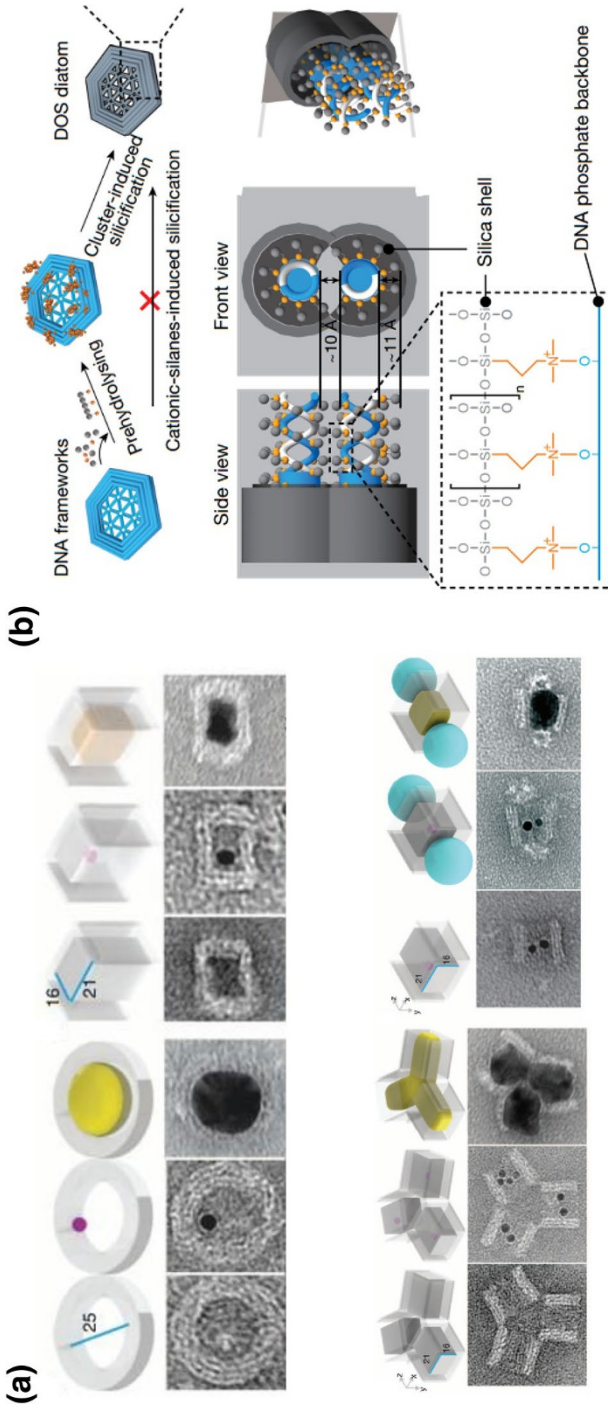


Fig. 9a,b DNA-nanostructure-templated casting growth of metal nanoparticles with controllable dimensionality. **a** Casting metal nanoparticles with pre-designed 3D shapes based on DNA nanostructure templates. Reproduced with permission from Ref. [97]. Copyright 2014 American Association for the Advancement of Science. **b** Complex silica composite nanomaterials templated by DNA origami. Reproduced with permission from Ref. [100]. Copyright 2018 Nature Publishing Group

1D, 2D, and 3D DNA nanostructures ranging in size from 10 to 1000 nm (Fig. 9b) [100]. Silicification was achieved through mixing DNA origami templates with pre-hydrolyzed TMAPS [*N*-trimethoxysilylpropyl-*N,N,N*-trimethylammonium chloride] and TEOS (tetraethyl orthosilicate), thus a silica shell was formed on DNA origami templates. This represents the first protocol to access highly sophisticated but flexibly designed silica oxide nanostructures that could not be realized by conventional silica nanofabrication techniques. The feasibility of this method was also demonstrated in a parallel study by Heuer-Jungemann [101], which collectively revealed the charm of DNA-templated synthesis to achieve various materials with ingenious nanostructures.

4.3 Chiral and Plasmonic Arrangement of Inorganic Nanoparticles

On the basis of controlling the crystallization and in situ growth of gold nanoparticles, DNA-templated synthesis and assembly techniques can also manipulate the assembly behavior of other diverse inorganic nanoparticles, and even change their inherent physical and chemical properties. It is known that when metal particles are placed in close proximity, their particle plasmons (collective oscillations of conduction electrons) become coupled and induce numerous interesting optical phenomena [102–104]. However, in practice, it is a challenge to ensure that the spacing between two nanoparticles can be arranged as closely as predesigned. As a fully addressable, easily functionalized platform, DNA nanostructures have been used recently to control the spatial organization of discrete nanoparticles with nanometer accuracy [105]. Nanoparticles can be arrayed in any nanometer distance and space on DNA nanostructures with defined patterns. For example, left-handed and right-handed arrangements of gold nanoparticles and nanorods on DNA nanostructures have been prepared to study chiral plasmonic properties at the nanoscale. Furthermore, a variety of chiral plasmonic metal–organic nanostructures [106–108] and chiral colloidal liquid crystals [109] are accessible via DNA-templated nanotechnology.

In this context, some pioneering work was carried out by Ding and co-workers, who prepared AuNPs arranged linearly on a rectangular DNA origami sheet with precisely controlled positions and particle spacing, and then assembled them into a 3D helical geometry with chiral plasmonic phenomenon by rational rolling of the DNA origami sheet. This study opened up the possibility of realizing programmable 3D plasmonic structures with desired optical properties [110]. Thereafter, Liedl and colleagues designed a 3D DNA origami nanostructure (a nanorod with around 100 nm in length) as nanotemplate to directly organize the helical arrangement of gold nanoparticles for the generation of chiral plasmonic nanostructures. The gold–DNA nanostructure exhibited defined circular dichroism and optical rotatory dispersion effects at visible wavelengths that originated from the collective plasmon–plasmon interactions of the nanoparticles positioned with an accuracy better than 2 nm (Fig. 10a) [111]. Moreover, Wang and co-workers constructed anisotropic gold nanorod (AuNR) helical superstructures with tailored chirality based on DNA origami nanostructure templates. The ‘X’ pattern of the DNA capturing strands was predesigned on both sides of a 2D DNA origami template, and several AuNRs

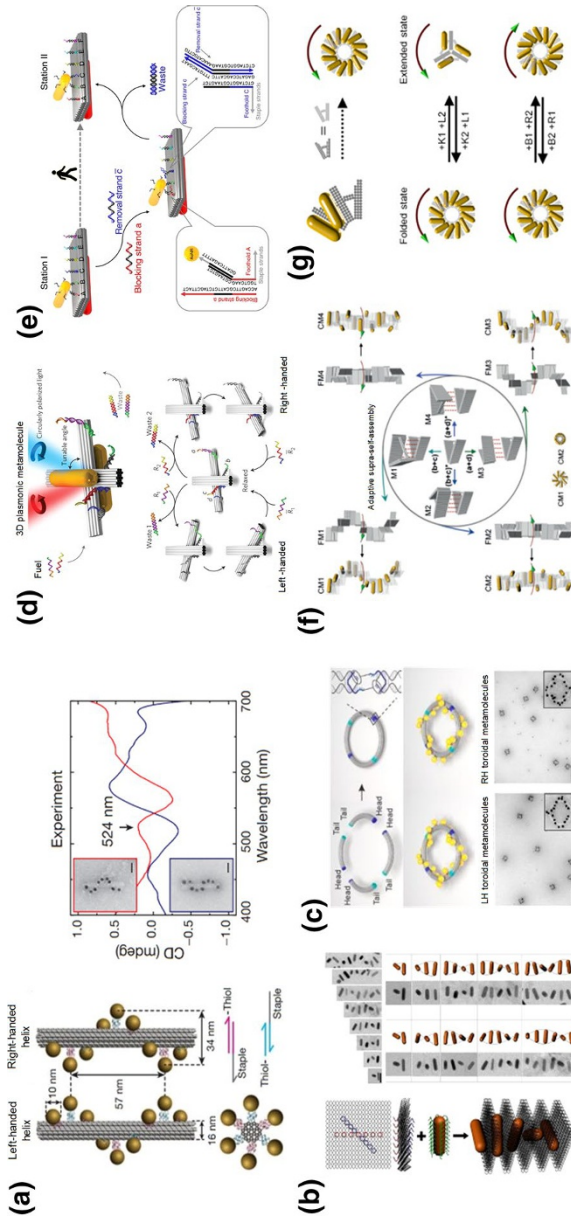


Fig. 10a–g DNA-nanostructure-templated arrangement of nanoparticles with chiral plasmonic properties. **a** Left- and right-handed arrangement and circular dichroism (CD) spectra of gold nanoparticles (AuNRs) on rod-like DNA origami template. Reproduced with permission from Ref. [111]. Copyright 2012 Nature Publishing Group. **b** Anisotropic gold nanorod (AuNR) helical superstructures based on DNA origami sheets. Reproduced with permission from Ref. [112]. Copyright 2015 American Chemical Society. **c** Plasmonic toroidal metamolecules assembled by a DNA origami template. Reproduced with permission from Ref. [113]. Copyright 2016 American Chemical Society. **d** Light-responsive and **e** pH-responsive dynamic plasmonic switching between a relaxed state or left-/right-handed version based on two DNA origami bundles templates. Reproduced with permission from refs. [114] and [116]. Copyright 2016 American Chemical Society and 2015 Nature Publishing Group. **f** Two and **g** three AuNRs plasmonic walking on DNA origami template. Reproduced with permission from Refs. [117] and [118]. Copyright 2017 Wiley-VCH and 2018 American Chemical Society

were modified on the origami template by base pairing, and assembled into AuNRs helices with the origami intercalated between neighboring AuNRs (Fig. 10b) [112]. Similarly, Liu's group presented chiral plasmonic Au NPs based on a 3D DNA origami ring template (Fig. 10c) [113]. These left-handed and right-handed helical metal–DNA nanostructures all show characteristic circular dichroism effects.

In addition to the above-mentioned static chiral plasmonic nanostructures, Liu et al. also developed dynamic chiral plasmonic nanostructures based on DNA origami templates. For example, light-responsive azobenzene-modified DNA strands (Fig. 10d) [114] and pH-responsive DNA triplexes [115] serve as construction materials to organize plasmonic nanoparticles in three dimensions while concurrently driving the metal–DNA molecules to distinct conformational states. The dynamic behavior of AuNRs towards light and H^+ stimuli was observed by CD signal changes. Similarly, strand displacement reactions were also applied to drive the plasmonic walking of AuNRs, which were recorded as dynamic CD signal changes (Fig. 10e) [116]. Recently, Lan et al. presented a new method for the tunable self-assembly of DNA chiral supramolecular architectures by creating a versatile DNA origami adapter (Fig. 10f) [117] and a reconfigurable chiral nanoparticle helix superstructure with fully switchable chirality (Fig. 10g) [118].

5 Summary and Perspectives

This review summarizes recent progress in nanomaterials synthesis based on DNA nanostructure templates. With computer-aided design, the use of DNA synthesizers, and the rapid development of DNA nanotechnology, we can construct a large variety of DNA nanomaterials. This technique provides valuable opportunities for more controllable preparation of organic and inorganic materials, polymer materials and other synthetic materials, indicating that its influence has distinctly penetrated all aspects of material science. Mimicking the central dogma, translating DNA sequence to other synthetic polymeric materials provides a valuable method of achieving sequence-controlled polymers. Based on larger DNA nanostructures, one can confine polymer synthesis to obtain more sophisticated polymer nanostructures or anisotropic polymer films, or even control the alignment of a single polymer chain to fabricate single molecular level electronic circuits. The self-assembly of inorganic nanoparticles based on DNA nanostructure templates can also be manipulated by DNA nanotechnology to achieve precise regulation at the nanoscale, including lattice regulation, chiral regulation and dynamic growth regulation. Moreover, in situ synthesis of inorganic nanomaterials inside a DNA model or outside a DNA template has also emerged as a powerful method to achieve inorganic nanostructures with intricate details.

The structural variability and the capability of precise customization make DNA nanostructures an extremely powerful tool for improving high precision and controllable preparation techniques for nanomaterials. Undoubtedly, DNA-encoded synthesis technology will also bring more innovations in the field of chemical materials preparation, especially given the advantages in high-precision control of nanomaterial assembly and highly complex nanomaterial processing. This has broad

application prospects in biomedicine, fine electronics, flexible materials and other fields. Despite their extraordinary prospects, several limitations have to be overcome before the widespread use of DNA nanostructures. Firstly, the cost of DNA materials has to be further reduced, which might be possible with advances in DNA synthesis techniques or the development of synthetic biology to allow direct production of DNA nanostructures in microorganisms; secondly, the yield and robustness of these methods have to be further proved. Since most of these methods require several steps of self-assembly and reactions, reliable scale up has been shown only rarely and further optimization is required. Thirdly, DNA nanotechnology has irreplaceable advantages in achieving elaborate nanostructures from several to hundreds of nanometers, but assembly of even larger structures is relatively inefficient. Therefore, the combination of DNA-based materials synthesis together with other nanofabrication techniques, such as lithography or 3D printing, would be essential to achieve desired materials with rational designed structure from micro- to macro-level.

Overall, the development of DNA-programmed material synthesis is just beginning, and extensive efforts are still required. However, along with increasing knowledge about structure–function relationships in materials, improving the precision of nanofabrication techniques for advanced material synthesis is apparently in highly demand. Therefore, one can envision that this field will develop rapidly in the next few years. The first application breakthroughs might be in medicinal and healthcare materials, considering their favorable biocompatibility and relatively high cost.

Acknowledgements Open access funding provided by Projekt DEAL. This work was funded by the National Natural Science Foundation of China, grant number 51703073 and the Fundamental Research Funds for the Central Universities of China (2017KFYXJJ167), the 1000 Young Talent Program of China.

Compliance with ethical standards

Conflict of interest On behalf of all authors, the corresponding author states that there is no conflict of interest.

Open Access This article is licensed under a Creative Commons Attribution 4.0 International License, which permits use, sharing, adaptation, distribution and reproduction in any medium or format, as long as you give appropriate credit to the original author(s) and the source, provide a link to the Creative Commons licence, and indicate if changes were made. The images or other third party material in this article are included in the article's Creative Commons licence, unless indicated otherwise in a credit line to the material. If material is not included in the article's Creative Commons licence and your intended use is not permitted by statutory regulation or exceeds the permitted use, you will need to obtain permission directly from the copyright holder. To view a copy of this licence, visit <http://creativecommons.org/licenses/by/4.0/>.

References

1. Watson JD, Crick FHC (1953) Molecular structure of nucleic acids: a structure for deoxyribose nucleic acid. *Nature* 171(4356):737–738

2. Watson JD, Crick FHC (1953) Genetical implications of the structure of deoxyribonucleic acid. *Nature* 171(4361):964–967
3. Crick FHC (1954) The complementary structure of DNA. *Proc Natl Acad Sci USA* 40(8):756–758
4. Shao Y, Jia H, Cao T, Lu D (2017) Supramolecular hydrogels based on DNA self-assembly. *Acc Chem Res* 50(4):659–668
5. Seeman NC (1982) Nucleic acid junctions and lattices. *J Theor Biol* 99(2):237–247
6. Seeman NC, Kallenbach NR (1983) Design of immobile nucleic acid junctions. *Biophys J* 44(2):201–209
7. Chen JH, Seeman NC (1991) Synthesis from DNA of a molecule with the connectivity of a cube. *Nature* 350(6319):631–633
8. Seeman NC (2003) DNA in a material world. *Nature* 421(6921):427–431
9. Rothmund PWK (2006) Folding DNA to create nanoscale shapes and patterns. *Nature* 440(7082):297–302
10. Douglas SM, Marblestone AH, Teerapittayanon S, Vazquez A, Church GM, Shih WM (2009) Rapid prototyping of 3D DNA-origami shapes with caDNA. *Nucleic Acids Res* 37(15):5001–5006
11. Douglas SM, Dietz H, Liedl T, Högberg BH, Graf F, Shih WM (2009) Self-assembly of DNA into nanoscale three-dimensional shapes. *Nature* 459(7245):414–418
12. Wei B, Dai M, Yin P (2012) Complex shapes self-assembled from single-stranded DNA tiles. *Nature* 485(7400):623–626
13. Benson E, Mohammed A, Gardell J, Masich S, Czeizler E, Orponen P, Högberg B (2015) DNA rendering of polyhedral meshes at the nanoscale. *Nature* 523(7561):441–444
14. Han D, Qi X, Myhrvold C, Wang B, Dai M, Jiang S, Bates M, Liu Y, An B, Zhang F, Yan H, Yin P (2017) Single-stranded DNA and RNA origami. *Science* 358(6369):eaao2648
15. Wagenbauer KF, Sig C, Dietz H (2017) Gigadalton-scale shape-programmable DNA assemblies. *Nature* 552(7683):78–83
16. Praetorius F, Kick B, Behler KL, Honemann MN, Weuster-Botz D, Dietz H (2017) Biotechnological mass production of DNA origami. *Nature* 552(7683):84–87
17. Badi N, Lutz J-F (2009) Sequence control in polymer synthesis. *Chem Soc Rev* 38(12):3383–3390
18. Schmidt BVKJ, Fechner N, Falkenhagen J, Lutz J-F (2011) Controlled folding of synthetic polymer chains through the formation of positionable covalent bridges. *Nat Chem* 3(3):234–238
19. Lutz J-F, Ouchi M, Liu DR, Sawamoto M (2013) Sequence-controlled polymers. *Science* 341(6146):1238149
20. Pfeifer S, Lutz J-F (2007) A facile procedure for controlling monomer sequence distribution in radical chain polymerizations. *J Am Chem Soc* 129(31):9542–9543
21. Nakatani K, Ogura Y, Koda Y, Terashima T, Sawamoto M (2012) Sequence-regulated copolymers via tandem catalysis of living radical polymerization and in situ transesterification. *J Am Chem Soc* 134(9):4373–4383
22. McHale R, Patterson JP, Zetterlund PB, O'Reilly RK (2012) Biomimetic radical polymerization via cooperative assembly of segregating templates. *Nat Chem* 4(6):491–497
23. Belowich ME, Valente C, Smaldone RA, Friedman DC, Thiel J, Cronin L, Stoddart JF (2012) Positive cooperativity in the template-directed synthesis of monodisperse macromolecules. *J Am Chem Soc* 134(11):5243–5261
24. Edwardson TGW, Carneiro KMM, Serpell CJ, Sleiman HF (2014) An efficient and modular route to sequence-defined polymers appended to DNA. *Angew Chem Int Ed* 53(18):4567–4571
25. de Rochambeau D, Sun Y, Barlog M, Bazzi HS, Sleiman HF (2018) Modular strategy to expand the chemical diversity of DNA and sequence-controlled polymers. *J Org Chem* 83(17):9774–9786
26. Pinheiro VB, Taylor AI, Cozens C, Abramov M, Renders M, Zhang S, Chaput JC, Wengel J, Peak-Chew S-Y, McLaughlin SH, Herdewijn P, Holliger P (2012) Synthetic genetic polymers capable of heredity and evolution. *Science* 336(6079):341–344
27. Pinheiro VB, Holliger P (2014) Toward XNA nanotechnology: new materials from synthetic genetic polymers. *Trends Biotechnol* 32(6):321–328
28. Yu H, Zhang S, Chaput JC (2012) Darwinian evolution of an alternative genetic system provides support for TNA as an RNA progenitor. *Nat Chem* 4(3):183–187
29. Usanov DL, Chan AI, Maianti JP, Liu DR (2018) Second-generation DNA-templated macrocycle libraries for the discovery of bioactive small molecules. *Nat Chem* 10(7):704–714
30. Chen Z, Lichter PA, Berliner AP, Chen JC, Liu DR (2018) Evolution of sequence-defined highly functionalized nucleic acid polymers. *Nat Chem* 10(4):420–427

31. Chan AI, McGregor LM, Liu DR (2015) Novel selection methods for DNA-encoded chemical libraries. *Curr Opin Chem Biol* 26:55–61
32. Rosenbaum DM, Liu DR (2003) Efficient and sequence-specific DNA-templated polymerization of peptide nucleic acid aldehydes. *J Am Chem Soc* 125(46):13924–13925
33. Kleiner RE, Brudno Y, Birnbaum ME, Liu DR (2008) DNA-templated polymerization of side-chain-functionalized peptide nucleic acid aldehydes. *J Am Chem Soc* 130(14):4646–4659
34. Brudno Y, Birnbaum ME, Kleiner RE, Liu DR (2010) An in vitro translation, selection and amplification system for peptide nucleic acids. *Nat Chem Biol* 6(2):148–155
35. Chen W, Schuster GB (2012) DNA-programmed modular assembly of cyclic and linear nanoarrays for the synthesis of two-dimensional conducting polymers. *J Am Chem Soc* 134(2):840–843
36. Snyder TM, Liu DR (2005) Ordered multistep synthesis in a single solution directed by DNA templates. *Angew Chem Int Ed* 44(45):7379–7382
37. Mckee ML, Milnes PJ, Bath J, Stulz E, O'Reilly RK, Turberfield AJ (2012) Programmable one-pot multistep organic synthesis using DNA junctions. *J Am Chem Soc* 134(3):1446–1449
38. He Y, Liu DR (2010) Autonomous multistep organic synthesis in a single isothermal solution mediated by a DNA walker. *Nat Nanotechnol* 5(11):778–782
39. Niu J, Hili R, Liu DR (2013) Enzyme-Free translation of DNA into sequence-defined synthetic polymers structurally unrelated to nucleic acids. *Nat Chem* 5(4):282–292
40. Jiang Q, Liu S, Liu J, Wang Z-G, Ding B (2018) Rationally designed DNA-origami nanomaterials for drug delivery in vivo. *Adv Mater* 4:e1804785
41. Perrault SD, Shih WM (2014) Virus-inspired membrane encapsulation of DNA nanostructures to achieve in vivo stability. *ACS Nano* 8(5):5132–5140
42. Mikkilä J, Eskelinen A-P, Niemelä EH, Linko V, Frilander MJ, Törmä P, Kostiaainen MA (2014) Virus-encapsulated DNA origami nanostructures for cellular delivery. *Nano Lett* 14(4):2196–2200
43. Kiviahio JK, Linko V, Ora A, Tiainen T, Järvihaavisto E, Mikkilä J, Tenhu H, Nonappa, Kostiaainen MA (2016) Cationic polymers for DNA origami coating-examining their binding efficiency and tuning the enzymatic reaction rates. *Nanoscale* 8(22):11674–11680
44. Auvinen H, Zhang H, Nonappa, Kopilow A, Niemelä EH, Nummelin S, Correia A, Santos HA, Linko V, Kostiaainen MA (2017) Protein coating of DNA nanostructures for enhanced stability and immunocompatibility. *Adv. Healthcare Mater.* 6(18):201700692
45. Agarwal NP, Matthies M, Gür FN, Osada K, Schmidt TL (2017) Block copolymer micellization as a protein strategy for DNA origami. *Angew Chem Int Ed* 56(20):5460–5464
46. Ponnuswamy N, Bastings MMC, Nathwani B, Ryu JH, Chou LYT, Vinther M, Li WA, Anastasacos FM, Mooney DJ, Shih WM (2017) Oligolysine-based coating protects DNA nanostructures from Low-salt denaturation and nuclease degradation. *Nat Commun* 8:15654
47. Ahmadi Y, Llano ED, Barišić I (2018) (poly)cation-induced protection of conventional and wire-frame DNA origami nanostructures. *Nanoscale* 10(16):7494–7504
48. Xu X, Fang S, Zhuang Y, Wu S, Pan Q, Li L, Wang X, Sun X, Liu B, Wu Y (2019) Cationic albumin encapsulated DNA origami for enhanced cellular transfection and stability. *Materials* 12(6):949
49. Averick SE, Dey SK, Grahacharya D, Matyjaszewski K, Das SR (2014) Solid-Phase incorporation of an ATRP initiator for polymer-DNA biohybrids. *Angew Chem Int Ed* 53(10):2739–2744
50. Tokura Y, Jiang Y, Welle A, Stenzel MH, Krzemien KM, Michaelis J, Berger R, Barner-Kowollik C, Wu Y, Weil T (2016) Bottom-up fabrication of nanopatterned polymers on DNA origami by in situ atom-transfer radical polymerization. *Angew Chem Int Ed* 55(19):5692–5697
51. Tokura Y, Harvey S, Xu X, Chen C, Morsbach S, Wunderlich K, Fytas G, Wu Y, Ng DYW, Weil T (2018) Polymer tube nanoreactors via DNA-origami templated synthesis. *Chem Commun* 54(22):2808–2811
52. Wang Z-G, Zhan P, Ding B (2013) Self-assembly catalytic DNA nanostructures for synthesis of para-directed polyaniline. *ACS Nano* 7(2):1591–1598
53. Wang Z-G, Liu Q, Ding B (2014) Shape-controlled nanofabrication of conducting polymer on planar DNA templates. *Chem Mater* 26(11):3364–3367
54. Tokura Y, Harvey S, Chen C, Wu Y, Ng DYW, Weil T (2018) Fabrication of defined polydopamine nanostructure by DNA origami-templated polymerization. *Angew Chem Int Ed* 57(6):1587–1591
55. Winterwerber P, Harvey S, Ng DYW, Weil T (2019) Photocontrolled dopamine polymerization on DNA origami with nanometer resolution. *Angew Chem Int Ed*. <https://doi.org/10.1002/anie.20191249>

56. Dong Y, Yang Y, Zhang Y, Wang D, Wei X, Banerjee S, Liu Y, Yang Z, Yan H, Liu D (2017) Cuboid vesicles formed by frame-guided assembly on DNA origami scaffolds. *Angew Chem Int Ed* 56(6):1586–1589
57. Zhou C, Zhang Y, Dong Y, Wu F, Wang D, Xin L, Liu D (2016) Precisely controlled 2D free-floating nanosheets of amphiphilic molecules through frame-guided assembly. *Adv Mater* 28(44):9819–9823
58. Trinh T, Liao C, Toader V, Barlóg M, Bazzi HS, Li J, Sleiman HF (2018) DNA-imprinted polymer nanoparticles with monodispersity and prescribed DNA-strand patterns. *Nat Chem* 10(2):184–192
59. Knudsen JB, Liu L, Kodal ALB, Madsen M, Li Q, Song J, Woehrstein JB, Wickham SFJ, Strauss MT, Schueder F, Vinther J, Krissanaprasit A, Gudnason D, Smith AAA, Ogaki R, Zelikin AN, Besenbacher F, Birkedal V, Yin P, Shih WM, Jungmann R, Dong M, Gothelf KV (2015) Routing of individual polymers in designed patterns. *Nat Nanotechnol* 10(10):892–898
60. Krissanaprasit A, Madsen M, Knudsen JB, Gudnason D, Surareungchai W, Birkedal V, Gothelf KV (2016) Programmed switching of single polymer conformation on DNA origami. *ACS Nano* 10(2):2243–2250
61. Gudnason D, Madsen M, Krissanaprasit A, Gothelf KV, Birkedal V (2018) Controlled aggregation of DNA functionalized poly(phenylene-vinylene). *Chem Commun* 54(44):5534–5537
62. Madsen M, Christensen RS, Krissanaprasit A, Bakke MR, Riber CF, Nielsen KS, Zelikin AN, Gothelf KV (2017) Preparation, single-molecule manipulation, and energy transfer investigation of a polyfluorene-graft-DNA polymer. *Chem Eur J* 23(44):10511–10515
63. Mirkin CA, Letsinger RL, Mucic RC, Storhoff JJ (1996) A DNA-based method for rationally assembling nanoparticles into macroscopic materials. *Nature* 382(6592):607–609
64. Alivisatos AP, Johnsson KP, Peng X, Wilson TE, Loweth CJ, Bruchez MP Jr, Schultz PG (1996) Organization of ‘nanocrystal molecules’ using DNA. *Nature* 382(6592):609–611
65. Rosi NL, Mirkin CA (2005) Nanostructures in biodiagnostics. *Chem Rev* 105(4):1547–1562
66. Seferos DS, Giljohann DA, Hill HD, Prigodich AE, Mirkin CA (2007) Nano-flares: probes for transfection and mRNA detection in living cells. *J Am Chem Soc* 129(50):15477–15479
67. Tram DTN, Wang H, Sugiarto S, Li T, Ang WH, Lee C, Pastorin G (2016) Advances in nanomaterials and their applications in point of care (POC) devices for the diagnosis of infectious diseases. *Biotechnol Adv* 34(8):1275–1288
68. Amini B, Kamali M, Salouti M, Yaghmaei P (2017) Fluorescence bio-barcode DNA assay based on gold and magnetic nanoparticles for detection of Exotoxin A gene sequence. *Biosens Bioelectron* 92:679–686
69. He F, Xiong Y, Liu J, Tong F, Yan D (2016) Construction of Au-IDE/CFP10-ESAT6 aptamer/DNA-AuNPs MSPQC for rapid detection of mycobacterium tuberculosis. *Biosens Bioelectron* 77:799–804
70. Wang G, Li Z, Luo X, Yue R, Shen Y, Ma N (2018) DNA-templated nanoparticle complexes for photothermal imaging and labeling of cancer cells. *Nanoscale* 10(35):16508–16520
71. Yang Y, Zhong S, Wang K, Huang J (2019) Gold nanoparticle based fluorescent oligonucleotide probes for imaging and therapy in living systems. *Analyst* 144(4):1052–1072
72. Dong B, Du S, Wang C, Fu H, Li Q, Xiao N, Yang J, Xue X, Cai W, Liu D (2019) Reversible self-assembly of nanoprobe in live cells for dynamic intracellular pH imaging. *ACS Nano* 13(2):1421–1432
73. Sun J, Pi F, Ji J, Lei H, Gao Z, Zhang Y, de Dieu Habimana J, Li Z, Sun X (2018) Ultrasensitive, “FRET-SEF” probe for sensing and imaging microRNAs in living cells based on gold nanoconjugates. *Anal Chem* 90(5):3099–3108
74. Nie W, Wang Q, Zou L, Zheng Y, Liu X, Yang X, Wang K (2018) Low-fouling surface plasmon resonance sensor for highly sensitive detection of microRNA in a complex matrix based on the DNA tetrahedron. *Anal Chem* 90(21):12584–12591
75. Li N, Xiang M, Liu J, Tang H, Jiang J (2018) DNA Polymer Nanoparticles programmed via super-sandwich hybridization for imaging and therapy of cancer cells. *Anal Chem* 90(21):12951–12958
76. Tavalalaie R, McCarroll J, Le Grand M, Ariotti N, Schuhmann W, Bakker E, Tilley RD, Hibbert DB, Kavallaris M, Gooding JJ (2018) Nucleic acid hybridization on an electrically reconfigurable network of gold-coated magnetic nanoparticles enables microRNA detection in blood. *Nat Nanotechnol* 13(11):1066–1071
77. Rosi NL, Giljohann DA, Thaxton CS, Lytton-Jean AKR, Han MS, Mirkin CA (2006) Oligonucleotide-modified gold nanoparticles for intracellular gene regulation. *Science* 312(5776):1027–1030

78. Nykypanchuk D, Maye MM, van der Lelie D, Gang O (2008) DNA-guided crystallization of colloidal nanoparticles. *Nature* 451(7178):549–552
79. Park SY, Lytton-Jean AKR, Lee B, Weigand S, Schatz GC, Mirkin CA (2008) DNA-programmable nanoparticle crystallization. *Nature* 451(7178):553–556
80. Macfarlane RJ, Lee B, Jones MR, Harris N, Schatz GC, Mirkin CA (2011) Nanoparticle superlattice engineering with DNA. *Science* 334(6053):204–208
81. Laramy CR, O'Brien MN, Mirkin CA (2019) Crystal engineering with DNA. *Nat Rev Mater* 4(3):201–224
82. Auyeung E, Cutler JI, Macfarlane RJ, Jones MR, Wu J, Liu G, Zhang K, Osberg KD, Mirkin CA (2012) Synthetically programmable nanoparticle superlattices using a hollow three-dimensional spacer approach. *Nat Nanotechnol* 7(1):24–28
83. Senesi AJ, Eichelsdoerfer DJ, Macfarlane RJ, Jones MR, Auyeung E, Lee B, Mirkin CA (2013) Stepwise evolution of DNA-programmable nanoparticle superlattices. *Angew Chem Int Ed* 52(26):6624–6628
84. Auyeung E, Li TI, Senesi AJ, Schmucker AL, Pals BC, de la Cruz MO, Mirkin CA (2014) DNA-mediated nanoparticle crystallization into Wulff polyhedra. *Nature* 505(7481):73–77
85. Sensi AJ, Eichelsdoerfer DJ, Brown KA, Lee B, Auyeung E, Choi CH, Macfarlane RJ, Young KL, Mirkin CA (2014) Oligonucleotide flexibility dictates crystal quality in DNA-programmable nanoparticle superlattices. *Adv Mater* 26(42):7235–7240
86. Zhang Y, Pal S, Srinivasan B, Vo T, Kumar S, Gang O (2015) Selective transformations between nanoparticle superlattices via the reprogramming of DNA-mediated interactions. *Nat Mater* 14(8):840–847
87. Lin Q, Mason JA, Li Z, Zhou W, O'Brien MN, Brown KA, Jones MR, Butun S, Lee B, Dravid VP, Aydin K, Mirkin CA (2018) Building superlattices from individual nanoparticles via template-confined DNA-mediated assembly. *Science* 359(6376):669–672
88. Macfarlane RJ, Jones MR, Lee B, Auyeung E, Mirkin CA (2013) Topotactic interconversion of nanoparticle superlattices. *Science* 341(615):1222–1225
89. Jones MR, Kohlstedt KL, O'Brien MN, Wu J, Schatz GC, Mirkin CA (2017) Deterministic symmetry breaking of plasmonic nanostructures enabled by DNA-programmable assembly. *Nano Lett* 17(9):5830–5835
90. Kim Y, Macfarlane RJ, Mirkin CA (2013) Dynamic interchangeable nanoparticle superlattices through the use of nucleic acid-based allosteric effectors. *J Am Chem Soc* 135(28):10342–10345
91. Seo SE, Li T, Sensi AJ, Mirkin CA, Lee B (2017) The role of repulsion in colloidal crystal engineering with DNA. *J Am Chem Soc* 139(46):16528–16535
92. Thaner RV, Kim Y, Li TI, Macfarlane RJ, Nguyen ST, de la Cruz MO, Mirkin CA (2015) Entropy-driven crystallization behavior in DNA-mediated nanoparticle assembly. *Nano Lett* 15(8):5545–5551
93. Yu Q, Zhang X, Hu Y, Zhang Z, Wang R (2016) Dynamic properties of DNA-programmable nanoparticle crystallization. *ACS Nano* 10(8):7485–7492
94. Knorowski C, Burleigh S, Travesset A (2011) Dynamics and statics of DNA-programmable nanoparticle self-assembly and crystallization. *Phys Rev Lett* 106(21):215501
95. Knorowski C, Travesset A (2012) Dynamic of DNA-programmable nanoparticle crystallization: gelation, nucleation and topological defects. *Soft Matter* 8(48):12053–12059
96. Julin S, Korpi A, Nonappa, Shen B, Liljeström V, Ikkala O, Keller A, Linko V, Kostiaainen MA (2019) DNA origami directed 3D nanoparticle superlattice via electrostatic assembly. *Nanoscale* 11(10):4546–4551
97. Sun W, Boulais E, Hakobyan Y, Wang WL, Guan A, Bathe M, Yin P (2014) Casting inorganic structures with DNA molds. *Science* 346(6210):1258361
98. Helmi S, Ziegler C, Kauert DJ, Seidel R (2014) Shape-controlled synthesis of gold nanostructures using DNA origami molds. *Nano Lett* 14(11):6693–6698
99. Ye J, Helmi S, Teske J, Seidel R (2019) Fabrication of metal nanostructures with programmable length and patterns using a modular DNA platform. *Nano Lett* 19(4):2707–2714
100. Liu X, Zhang F, Jing X, Pan M, Liu P, Li W, Zhu B, Li J, Chen H, Wang L, Lin J, Liu Y, Zhao D, Yan H, Fan C (2018) Complex silica composite nanomaterials templated with DNA origami. *Nature* 559(7715):593–598
101. Nguyen L, Döblinger M, Liedl T, Heuer-Jungemann A (2019) DNA origami templated silica growth by sol-gel chemistry. *Angew Chem Int Ed* 58(3):912–916


102. Sonnichsen C, Reinhard BM, Liphardt J, Alivisatos APA (2005) Molecular ruler based on plasmon coupling of single gold and silver nanoparticles. *Nat Biotechnol* 23(6):741–745
103. Hentschel M, Saliba M, Vogelgesang R, Giessen H, Alivisatos AP, Liu N (2010) Transition from isolated to collective modes in plasmonic oligomers. *Nano Lett* 10(7):2721–2726
104. Halas NJ, Lal S, Chang WS, Link S, Nordlander P (2011) Plasmons in strongly coupled metallic nanostructures. *Chem Rev* 111(6):3913–3961
105. Zhang J, Constantinou PE, Micheel C, Alivisatos AP, Kiehl RA, Seeman NC (2006) Two-dimensional nanoparticle arrays show the organizational power of robust DNA motifs. *Nano Lett* 6(7):1502–1504
106. Liu N, Liedl T (2018) DNA-assembled advanced plasmonic architectures. *Chem Rev* 118(6):3032–3053
107. Kuzyk A, Jungmann R, Acuna GP, Liu N (2018) DNA origami route for nanophotonics. *ACS Photonics* 5(4):1151–1163
108. Zhou C, Duan X, Liu N (2017) DNA-nanotechnology-enabled chiral plasmonics: from static to dynamic. *Acc Chem Res* 50(12):2906–2914
109. Siavashpouri M, Wachauf CH, Zakhary MJ, Praetorius F, Dietz H, Dogic Z (2017) Molecular engineering of chiral colloidal liquid crystals using DNA origami. *Nat Mater* 16(8):849–856
110. Shen X, Song C, Wang J, Shi D, Wang Z, Liu N, Ding B (2012) Rolling up gold nanoparticle-dressed DNA origami into three-dimensional plasmonic chiral nanostructures. *J Am Chem Soc* 134(1):146–149
111. Kuzyk A, Schreiber R, Fan Z, Pardatscher G, Roller E-M, Högele A, Simmel FC, Govorov AO, Liedl T (2012) DNA-based self-assembly of chiral plasmonic nanostructures with tailored optical response. *Nature* 483(7389):311–314
112. Lan X, Lu X, Shen C, Ke Y, Ni W, Wang Q (2015) Au nanorod helical superstructures with designed chirality. *J Am Chem Soc* 137(1):457–462
113. Urban MJ, Dutta PK, Wang P, Duan X, Shen X, Ding B, Ke Y, Liu N (2016) Plasmonic toroidal metamolecules assembled by DNA origami. *J Am Chem Soc* 138(17):5495–5498
114. Kuzyk A, Schreiber R, Zhang H, Govorov AO, Liedl T, Liu N (2014) Reconfigurable 3D plasmonic metamolecules. *Nat Mater* 13(9):862–866
115. Kuzyk A, Urban MJ, Idili A, Francesco R, Liu N (2017) Selective control of reconfigurable chiral plasmonic metamolecules. *Sci. Adv* 3(4):e1602803
116. Zhou C, Duan X, Liu N (2015) A plasmonic nanorod that walks on DNA origami. *Nat Commun* 6:8102
117. Lan X, Su Z, Zhou Y, Meyer T, Ke Y, Wang Q, Chiu W, Liu N, Zou S, Yan H, Liu Y (2017) Programmable supra-assembly of a DNA surface adapter for tunable chiral directional self-assembly of gold nanorods. *Angew Chem Int Ed* 56(46):14632–14636
118. Lan X, Liu T, Wang Z, Govorov AO, Yan H, Liu Y (2018) DNA-guided plasmonic helix with switchable chirality. *J Am Chem Soc* 140(37):11763–11770

Publisher's Note Springer Nature remains neutral with regard to jurisdictional claims in published maps and institutional affiliations.



REVIEW

Engineering Functional DNA–Protein Conjugates for Biosensing, Biomedical, and Nanoassembly Applications

Dan Zhao^{1,2} · Yuhan Kong^{1,2} · Sisi Zhao^{1,3} · Hang Xing^{1,2} 

Received: 15 December 2019 / Accepted: 5 May 2020 / Published online: 24 May 2020
© Springer Nature Switzerland AG 2020

Abstract

DNA and protein are the most important two classes of biomacromolecules forming the basis of life. The conjugation of the two using crosslinking chemistries enables a combination of molecular recognition, enzymatic catalysis, and Watson–Crick hybridization properties. The DNA–protein conjugate with combined properties enables a broad range of applications, such as sensitive and selective bioassays, therapeutic agents, and building blocks for programmable nanoassemblies. In this review, we survey the conjugates from the aspects of conjugation chemistries as well as applications in biomedical and nanotechnology fields. We highlight the functions of both biological moieties of a conjugate for target binding and signal transduction in bioassays. We also review the use of DNA–protein conjugates for the construction of a variety of functional and dynamic nanostructures, from isolated hybrid cages to three-dimensional (3D) protein crystalline lattices. Moreover, these conjugates have been used as carriers to deliver enzymes or functional nucleic acids for disease treatments and gene editing.

Keywords DNA–protein conjugates · Functional DNA · DNA nanotechnology · DNA origami · Diagnostics · Biosensors · Drug delivery

Chapter 4 was originally published as Zhao, D., Kong, Y., Zhao, S. & Xing, H. Topics in Current Chemistry (2020) 378: 41. <https://doi.org/10.1007/s41061-020-00305-7>.

✉ Hang Xing
hangxing@hnu.edu.cn

¹ Institute of Chemical Biology and Nanomedicine, State Key Laboratory for Chemo/Bio Sensing and Chemometrics, Hunan Provincial Key Laboratory of Biomacromolecular Chemical Biology, Hunan University, Changsha 410082, China

² College of Chemistry and Chemical Engineering, Hunan University, Changsha 410082, China

³ College of Biology, Hunan University, Changsha 410082, China

1 Introduction

In nature, nucleic acid–protein complexes play a central role in regulating genetic activity in all aspects within an organism. The first report of the nucleic acid–protein complexes dates back to the late 19th century, when scientists observed DNA–protein associations under optical microscope. Since then, enormous efforts have been made in studying the structures as well as the functions of natural nucleic acid–protein complexes. Many of these fascinating biological complexes are constructed through self-assembly of various protein and nucleic acid components to conduct complicated tasks in living systems [1]. Figure 1a presents the crystal structures of three iconic natural nucleic acid–protein complexes from the Protein Data Bank, including ribosomal RNA, transcription activator-like (TAL) effectors, and nucleosome complex. These nucleic acid–protein complexes together with many others enable critical biochemistry processes including transcription, translation, packaging, rearrangement, DNA replication, and repair in living systems. By examining the natural complexes forming between nucleic acids and proteins, scientists not only start to understand how these biochemistry processes take place but also learn to design and synthesize artificial complexes that outperform natural congeners and realize applications that cannot be achieved before. Figure 1b shows three representative examples of artificial DNA–protein complexes developed over the years, including aptamers–sandwiched thrombin, DNA origami cage loaded with multiple antibodies, and spherical nucleic acid structure with β -galactosidase core. These artificial complexes are able to represent delicate structures and functions of native complexes to some extent. More importantly, the integration of molecular recognition, catalytic activity, and Watson–Crick base pairing into one nanoscale biocompatible device has enabled a vast number of diagnostic, therapeutic, and nanoassembly applications, significantly expanding our knowledge of chemistry.

Over the past few decades, enormous efforts have been put into the research of artificial DNA–protein conjugates. Research interests are mainly focusing on the development of facile and reliable conjugation approaches as well as the exploration of their applications in various fields, including diagnostics, therapeutics, and programmable assembly. One of the first reports using the artificial complexes was described in the 1980s for diagnostic applications, where the DNA–enzyme conjugates were used to detect nucleic acid targets [2]. Two widely used immunoassays, Immuno-PCR and proximity ligation assay (PLA), which use an antibody as target recognition motif and DNA as amplified signal reporter, were developed in 1992 and 2002, respectively [3, 4]. These detection techniques have enabled the development of many different bioassays and have been successfully translated into commercial products. Lu and colleagues used DNA–invertase conjugates to allow versatile biotargets detection using portable glucose meter (PGM), which is a milestone towards point-of-care testing (POCT) applications. The conjugates have also been used to construct well-designed artificial biological assemblies. The structural organization of proteins on double-stranded DNA (dsDNA) scaffold was firstly reported in 1994 [5].

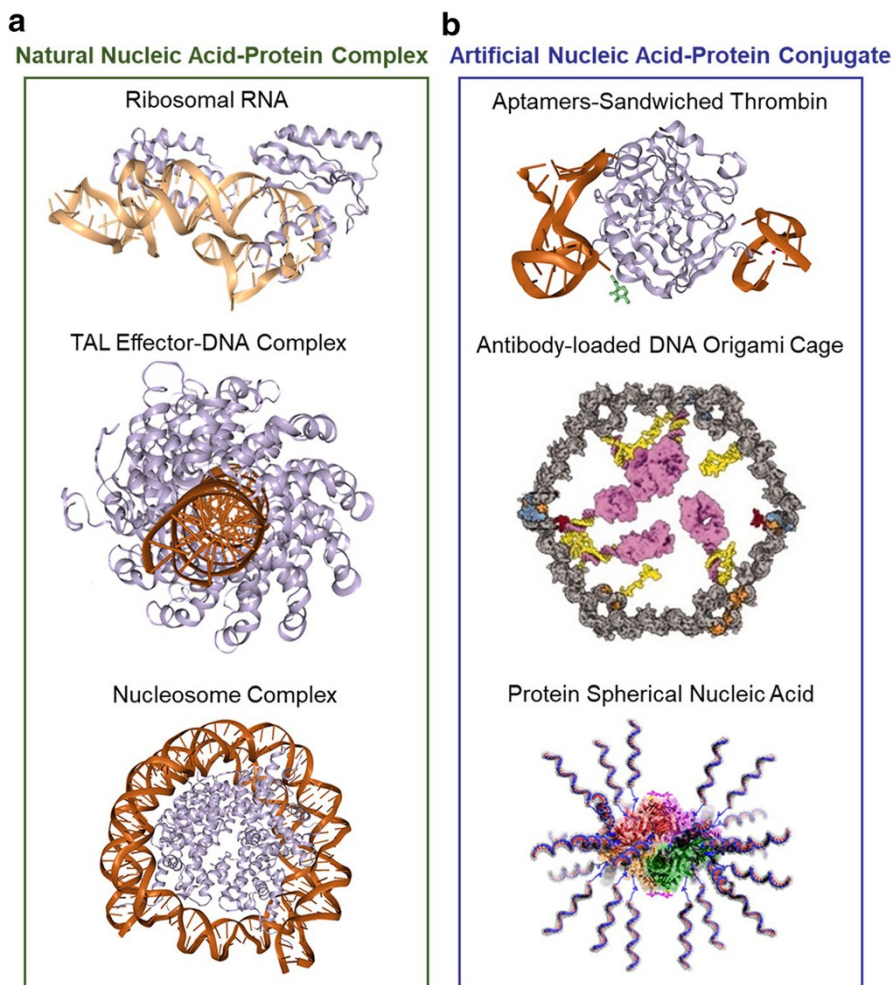


Fig. 1 Examples of natural and artificial nucleic acid–protein complexes. **a** Structures of three representative native nucleic acid–protein complexes from protein data bank. *From top to bottom*: ribosomal protein and RNA, TAL effector PthXo1 bound to its DNA target, and *Drosophila* nucleosome structure. **b** Structures and schemes of three representative artificial nucleic acid–protein complexes. *From top to bottom*: thrombin sandwiched between two DNA aptamers, antibody-loaded DNA origami cage, spherical nucleic acid structure with β -galactosidase core

Since the early 2000s, different structural DNA nanotechnology tools, such as DNA tile, DNA origami, and spherical nucleic acid, have been used to locate enzymes onto DNA network with precise spatial control. These studies have been summarized in several recent reviews [6–8]. In addition to diagnostic and structural applications, DNA–protein conjugates have recently been explored for biomedical applications, including the delivery of antibodies and enzymes, gene editing, and in vivo cancer therapy. Figure 2 provides a brief historical overview

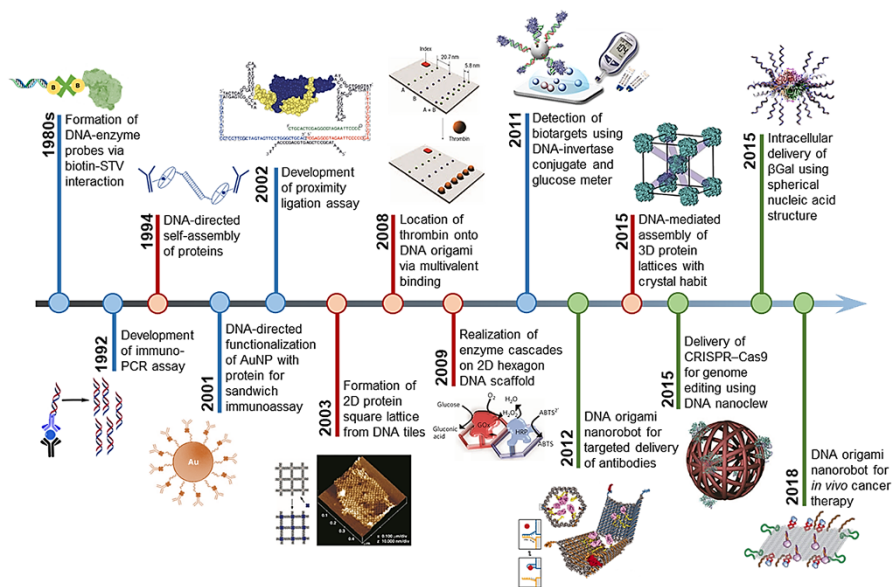


Fig. 2 A brief timeline of the development of artificial DNA–protein conjugates since their first report in 1980s. Three main application scenarios are highlighted in different colors (*blue*: diagnostics; *red*: nanoassembly; *green*: delivery and therapeutics)

of the research progress and milestone achievements in the field of DNA–protein conjugates. To date, remarkable progress has been made in the field of artificial DNA–protein conjugates for a broad range of applications.

Several recent reviews have discussed the use of DNA–protein complexes from one specific aspect of this field, such as antibody–nucleic acid conjugate or hybrid nanostructure [9, 10]. One comprehensive review on this topic by Christof M. Niemeyer was published 10 years ago in 2010 [11]. In this review, we aim to provide an overview of this field, ranging from conjugation chemistries to a wide range of applications (Fig. 3). We try to include the pioneering work published decades ago to provide the community a historical overview as well as to highlight some state-of-art reports published within the last 5 years. In this vein, we categorize the review of DNA–protein conjugates into four main sections. The first section covers the covalent and noncovalent chemistries to prepare DNA–protein conjugates. The second section discusses the use of DNA–protein conjugates for diagnostic applications. Two types of sensor modes of using DNA as reporter or using enzyme as reporter are reviewed, respectively. In the third section, we survey the design, synthesis, and application of DNA–protein nanoassemblies, specifically highlighting the recent process of using the hybrid structures for biomedical applications. Finally, we provide our perspectives on the major challenges in the field as well as the potential strategies for future development of optimized conjugates for clinical applications.

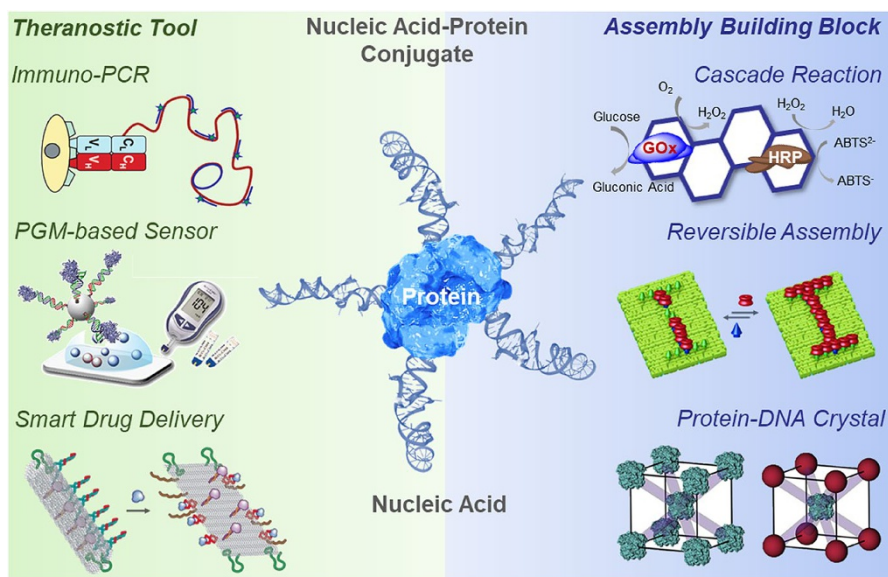


Fig. 3 Scientific scope of this review. We aim to provide an overview of using nucleic acid–protein conjugates as theranostic tools and assembly building blocks for many different applications

2 DNA–Protein Conjugation Approaches

The development of highly efficient, robust, and reliable DNA–protein conjugation chemistries is highly important for its applications. The design principle of an idea synthesis approach should possess the following features: (1) preservation of the native protein functions; (2) high yield, high efficiency, and low cost; (3) facile synthesis without complicated DNA modifications; and (4) robust and stable chemistries in physiological conditions. In this section, we review the widely used synthetic approaches, including non-covalent and covalent methods. Some state-of-art strategies, such as site-specific labeling and enzymatic ligation methods, are included as well.

2.1 Non-covalent Approaches

Non-covalent synthesis of DNA–protein conjugates uses weak interactions, including hydrogen bonding, hydrophobic effect, π – π stacking, electrostatic interaction, and van der Waals force, which does not require modification of both biomacromolecules. The synthesis process is generally rapid and easy-to-use with the protein activity well preserved.

2.1.1 Biotin–Avidin and Antibody–Antigen Interactions

One of the most widely used conjugation approaches is biotin–avidin interaction, which was used to immobilize DNAs onto protein substrates in the early 1980s [12].

The biotin–avidin interaction is recognized as one of the strongest non-covalent bindings, exhibiting high stability even under thermal and chemical denaturation conditions. The binding affinity between avidin and biotin is ca. 10^{-12} M, which can be improved by using streptavidin (STV) with K_a of ca. 10^{-14} M and neutravidin with K_a of ca. 10^{-16} M. In the synthesis process, the target protein is fused onto the hydrophobic epitope of the avidin and the target DNA strands are modified with biotin at the 3' or 5' end. Nowadays, since biotin-labeled oligonucleotides are commercially available and many STV proteins can be genetically engineered or chemically synthesized, the DNA–protein conjugates from biotin–(strept)avidin interactions are widely used in biosensing applications [13–16]. Recently, to incorporate reversibility into the biotin–avidin interactions, different types of the biotin analogues with relatively lower binding affinity are introduced to prepare DNA–protein conjugates, such as desthiobiotin (K_a of ca. 10^{-11} M) and iminobiotin (K_a of ca. 10^{-10} M). In 2013, Wong et al. demonstrated the reversible decoration of DNA origami tiles with streptavidin by using desthiobiotin and biotin of different binding affinities toward streptavidin [17].

Another widely used approach is antibody (Ab)–antigen interaction. Some haptens, such as digoxigenin, dinitrophenol, and FLAG tag, are commonly used to modify DNA terminals so as to further attach to corresponding antibodies [18]. One major advantage of using the Ab–antigen interaction to prepare DNA–protein conjugates is that the small molecule binding motif (hapten) can be easily adapted into the DNA solid-state synthesis process. Thus, it is convenient to incorporate multiple different types of end-function groups onto DNA strands for the use in multiplexed immunoassays [19].

2.1.2 Ni–NTA–His₆ Interaction

Coordination chemistry is also frequently used for conjugation of nucleic acids with proteins using Ni–nitrilotriacetic acid (NTA)–hexahistidine (His₆) interactions. The coordination compound formed by nickel(II) ion and NTA molecule with open binding sites, which can be coordinated by histidine molecules. Thus, the conjugation can be achieved by engineering protein with a His₆ tag and DNA with a terminal NTA group. Taking advantage of the fast reaction and stable binding between Ni–NTA and the His₆ tag, different DNA–protein conjugates have been created [20–22]. In 2009, Turberfield and colleagues demonstrated conjugation of His₆-tagged green fluorescent protein (GFP) to tris NTA-functionalized DNA strand [20]. Norton and colleagues also used the NTA and histidine-tag interaction to direct protein nanopatterning on DNA origami structures [23]. Moreover, one interesting property of Ni–NTA–His₆ binding is the reversibility under the treatment of a nickel chelator, such as dithiocarbamate (DTC), ethylenediaminetetraacetate (EDTA), chitosan, and imidazole, enabling protein purification applications.

2.1.3 Aptamers–Protein Interaction

Aptamer is one type of single-stranded oligonucleotide that can bind to target proteins with high specificity and binding affinity by folding into 3D binding pockets

for recognition [24], which can be generally considered as monoclonal Ab congener. Thus, DNA aptamer has also been used to prepare DNA–protein conjugate through specific interaction. When applying aptamer to conjugate protein, the DNA sequence is designed with two segments, in which the aptamer segment binds to protein of interest and the other segment serves as DNA hybridization functions. One widely used aptamer sequence is anti-thrombin aptamer, which has been widely used in diagnostic assays [25]. Though many advantages of using aptamers have been demonstrated, such as the enhanced chemical stability and easy of modification, the identification of new aptamers for protein of interests requires tedious in vitro selection process, limiting the availability of aptamers for desired targets. In addition, the average binding affinity between the aptamer and protein is ca. 10^{-7} – 10^{-8} M, which is relatively not stable enough for in vivo applications [26]. To address this issue, integrating multivalent binding with aptamer–protein interaction is a promising strategy for improving the binding affinity to generate more stable DNA–protein conjugates. For example, Yan and colleagues reported the incorporation of multiple-affinity ligands onto DNA origami tiles for systematical investigation of distance-dependent multivalent binding effects, illustrating the potential design strategy of multivalent aptamer [27].

2.2 Covalent Approaches

Differing from non-covalent conjugation, covalent coupling method creates much stronger chemical bonds than non-covalent interactions, resulting in more stable products suitable for use in physiological conditions. Up to now, various covalent coupling reactions have been developed through homo- and hetero-bifunctional crosslinkers, including dithiol coupling, maleimide-thiol addition, azide–alkyne cycloaddition, etc. Two highly effective approaches, site-specific labeling and enzyme ligation, have been demonstrated to generate conjugate products with better performance.

2.2.1 Labeling Natural Amino Acid on Protein

A straightforward route to conjugate DNA onto protein is to use the native functional groups on protein surface residues. Cysteine with thiol group (–SH) is one of the most used surface residues on protein. Disulfide coupling strategy is based on the formation of a disulfide bond between cysteine and alkylthiol-modified DNA, which was pioneered by Schultz and colleagues in 1987 using *Staphylococcus* nuclease with surface cysteines. After disulfide coupling with thiolated DNA, the enzymatic activity was observed to be enhanced [28]. Disulfide coupling is considered fast but reversible under reductive conditions, limiting its application in physiological environment.

Another widely used natural amino acid on protein for covalent conjugation is lysine with amine group (–NH₂). Using various terminal groups on DNA, different crosslinking reagents have been developed to couple DNA with the surface amine on proteins. For example, disuccinimidyl suberate, serving as a homo-bifunctional

reagent, was used to crosslink primary surface amine on alkaline phosphatase and terminal amine-modified DNA without affecting the enzyme activity [2]. In addition to homo-bifunctional coupling reaction, amine-thiol hetero-bifunctional coupling reaction is also widely used. The hetero-bifunctional reagents generally include two reactive groups with an amine-reacting group and a maleimide for thiol addition. For example, 6-maleimidohexanoic acid succinimido ester and *N,N'*-1,2-phenylenedimaleimide were used for coupling DNA thiol and protein amine, obtaining DNA-modified alkaline phosphatase and horseradish peroxidase, respectively [29]. In 2018, Ma et al. synthesized ortho-phthalaldehyde (OPA) modified DNA which can link to protein lysine residue rapidly and efficiently [30]. Compared with disulfide coupling reaction, hetero-bifunctional thiol-amine coupling chemistry using maleimide and active-ester is considered relatively more stable in reductive physiological conditions. Thus, some crosslinking reagents, such as succinimidyl 4-(*N*-maleimidomethyl)cyclohexane-1-carboxylate (SMCC) and water-soluble sulfo-SMCC that contain active ester and maleimide groups at opposite ends, are already commercially available and extensively used in research.

2.2.2 Site-Specific Labeling using Bioorthogonal Chemistry

The use of native amino acid on proteins for conjugation is straightforward, but sometimes inhibits enzyme activity due to the lack of selectivity. For example, some enzymes with catalytically active epitopes full of lysines or cysteine are sensitive to surface modifications. Once DNAs are randomly modified onto such native enzymes through coupling with native lysine or cysteine, the bioactivity would be largely imparted. In addition, it is difficult to control the valency and orientation of the DNA modifications on protein surface using native amino acids. To address these issues, site-specific labeling approach using bioorthogonal chemistry has been developed to control the position, orientation, and valency of conjugated DNAs via mutating and modifying specific residues on target proteins. Therefore, only target sites or genetic mutated sites on the protein of interest are labeled while other residues as well as other proteins are not affected.

Bioorthogonal chemistry was originally termed by Bertozzi and colleagues in 2003 and has been broadly applied to engineer polysaccharide and label proteins [31]. Staudinger ligation and copper(I)-catalyzed Huisgen 1,3-dipolar cycloaddition of azides and alkynes (CuAAC) are two of the most important bioorthogonal chemistries used in chemical biology. The bioorthogonal labeling process is normally user-friendly. For example, in the case of labeling polysaccharide in cell walls, glycan chains, which are metabolically labeled with azido sugars, are covalently coupled with desired modifications with phosphine or alkyne functional groups, forming irreversible covalent bonds [32]. Similarly, by genetic incorporation of azido groups onto glycoproteins or enzymes, covalent DNA–protein conjugates can be formed by coupling with the terminal alkyne-functionalized DNA strand [33]. A similar approach using copper-catalyzed azide-alkyne cycloaddition was reported by Guengerich and colleagues as a post-oligomerization strategy for synthesizing site-specific DNA–transferase crosslinking [34]. However, since the requirement of copper ions as catalyst limits the potential application in live organisms, copper-free approaches

are highly desired. One of the most widely used methods is strain-promoted alkyne–azide cycloaddition (SPAAC), which was developed in 2004 [35]. SPAAC was used to conjugate cysteine-bearing protein with azido-DNA using dibenzocyclooctyl (DBCO)-maleimide crosslinker [36].

Over the years, new chemical approaches have been exploited to achieve site-selective attachment of DNA to target proteins. Chemical reactions of high efficiency such as thiol-ene addition (alkene hydrothiolation), Diels–Alder (DA) reaction, and inverse-electron-demand Diels–Alder (ie-DA) reaction have also been used as biorthogonal chemistry to prepare DNA–protein conjugates [37–40]. For example, in 2019, Synakewicz et al. used bioorthogonal chemistries to enable site-specific attachment of DNA handles onto a target HEAT-repeat protein PR65 for single-molecule force spectroscopy measurements using a double-dumbbell optical tweezers set up. The full-length force-extension traces of different conjugations including SPAAC, ie-DA, and ybbR-tag methods were evaluated [41]. Other approaches, including the use of thiol-pyridine-activated protein [28], F-carboxyl-modified aptamers [42], and oxime ligation chemistry [43], were also reported to generate site-specific modifications. One commercially available product, Site-Click™ from Thermo Fisher, is intensively used to specifically label the Fc domain on an antibody [44]. Nowadays, biorthogonal chemistry and site-specific labeling have been used as a regular chemical biology tool in many different research fields.

2.2.3 Enzyme Ligation Method

To further improve the conjugation efficiency and to achieve even more stable DNA–protein conjugates, enzyme ligation method has been developed recently as an alternative to conventional chemical coupling. It is a unique strategy that forms the DNA–protein crosslinking through a DNA-binding enzyme-mediated covalent bond formation process.

In 2012, Kobatake and colleagues reported covalently linking ssDNA to a protein fused with Gene A* with no need of chemical modifications on ssDNA [45]. The DNA-binding enzyme Gene A* recognizes and cuts a specific oligonucleotide sequence, and further ligates to the rest of the strand through covalent binding. However, the relatively large size of Gene A* (MW = 38,700) limits the expression efficiency in *E. coli*. In 2019, a similar ligation method using a much smaller DNA-binding enzyme, porcine circovirus type 2 Rep (MW = ca. 13,400), was reported by the same group. They constructed DNA–luciferase conjugate via the catalytic domain of Rep, demonstrating a sandwich assay for thrombin [46]. Compared with other covalent methods, the enzyme ligation approach employs unmodified DNA strands, which is more facile and efficient. However, the current enzyme ligation method still suffers from low bioactivity of the conjugated enzyme, possibly due to the steric hindrance caused by fused DNA-binding protein [46]. One possible solution is to incorporate flexible peptide linkers to space the enzyme of interest and the DNA-binding protein, preserving the bioactivity of both biomacromolecules.

Taken together, we have reviewed here the most widely used conjugation methods to prepare DNA–protein conjugates. Table 1 and Fig. 4 summarize some of the representative chemistries we have discussed above. Nonetheless, ways to achieve

new conjugation methods with high reaction rate, high yield under mild conditions, and high selectivity are still sought after, which would enable DNA–protein conjugates for more challenging biological applications, including investigating living cells, imaging human organs, and treating disease *in vivo*.

3 DNA–Protein Conjugations for Diagnostic Applications

A general design of a typical biosensor consists of two motifs: target recognition motif and signal transduction motif. The target recognition motif such as antibody or aptamer recognizes biomolecules of interest with high selectivity and binding affinity, while the signal transduction motif transduces the binding process into detectable signals, followed by signal amplification process so as to achieve high sensitivity. Because of the versatile biofunctions of DNA and protein, they can both serve for either recognizing or transducing and amplifying signals (Fig. 5) in different usage scenarios. Therefore, biosensors for diagnostic applications using DNA–protein conjugates can be categorized into two groups based on the different roles of DNA and protein played. In this section, we survey these two types of biosensors: (1) protein as recognition motif and DNA as signaling motif, and (2) DNA as recognition motif and protein as signaling motif. Since the ways functional DNAs and antibodies recognize biotargets have already been comprehensively discussed in other reviews [49, 50], we herein focus on how DNAs and enzymes transduce and amplify signals in a typical biosensor design to provide low enough limit of detection.

3.1 DNA as Signal Reporter

Detection of antigens with antibodies is the basis of diagnostics in immunology. Enzyme-linked immunosorbent assay (ELISA) is the most commonly used method to detect target molecules [51]. The sensitivity of the assay can be improved by labeling antibodies with enzymes or isotopes to amplify signals, but the enzyme stability and isotope safety are long-lasting issues in application. Instead of using enzymes or isotopes, the use of exponential amplification of DNA provides an alternative approach to achieve satisfactory limit of detection. In this section, we survey two types of assays, immuno-polymerase chain reaction (immuno-PCR) assay and proximity ligation assay (PLA). The basic working principles of immune-PCR and PLA are illustrated in Fig. 6 and discussed later.

3.1.1 Immuno-PCR Assay

Immuno-PCR (IPCR) is an ultrasensitive diagnostic method that integrates the advantages of both ELISA and PCR. In a typical IPCR assay design, DNA sequence is attached to the Fc domain of an antibody forming the antibody–DNA conjugates. In the presence of the target antigens, antibody binds the target molecules through sandwich binding mode, immobilizing the whole conjugate onto the surface. DNA in the conjugate serves as an indicator molecule, which can be further amplified

Table 1 Summary of commonly used DNA–protein conjugation methods

Type	Modifications	Mechanism	Examples/reference
Antibody–antigen interaction	Hapten-modified DNA	Mainly hydrophobic force	DNA–STV dsDNA nanocircles [47]
Biotin–(strept) avidin interaction	Biotinylated DNA and (strept)avidin-modified protein	Hydrogen bonding, hydrophobic force, van der Waals forces, etc.	Biotinylated DNA–STV conjugates [15]
Ni–NTA–His ₆ interaction	Protein bearing a His ₆ tag and DNA-containing NTA groups	Coordination bond between nickel (II) ions–NTA and His ₆ tag	Attachment of proteins on DNA origami via Ni–NTA–His ₆ [23]
Aptamer	Aptamer sequences	Hydrogen bonding, π – π stacking, van der Waals forces, etc.	Anti-thrombin aptamers [48]
Disulfide coupling	Cysteine residues in proteins and thiolated DNA	Covalent coupling	Formation of a hybrid enzyme [28]
CuAAC, SPAAC	Azide and alkyne modifications	Covalent coupling	Glycoprotein–DNA conjugates [33]
Enzyme ligation	Gene A* fusion protein	Covalent coupling	A*–Zmab–DNA conjugate [45]

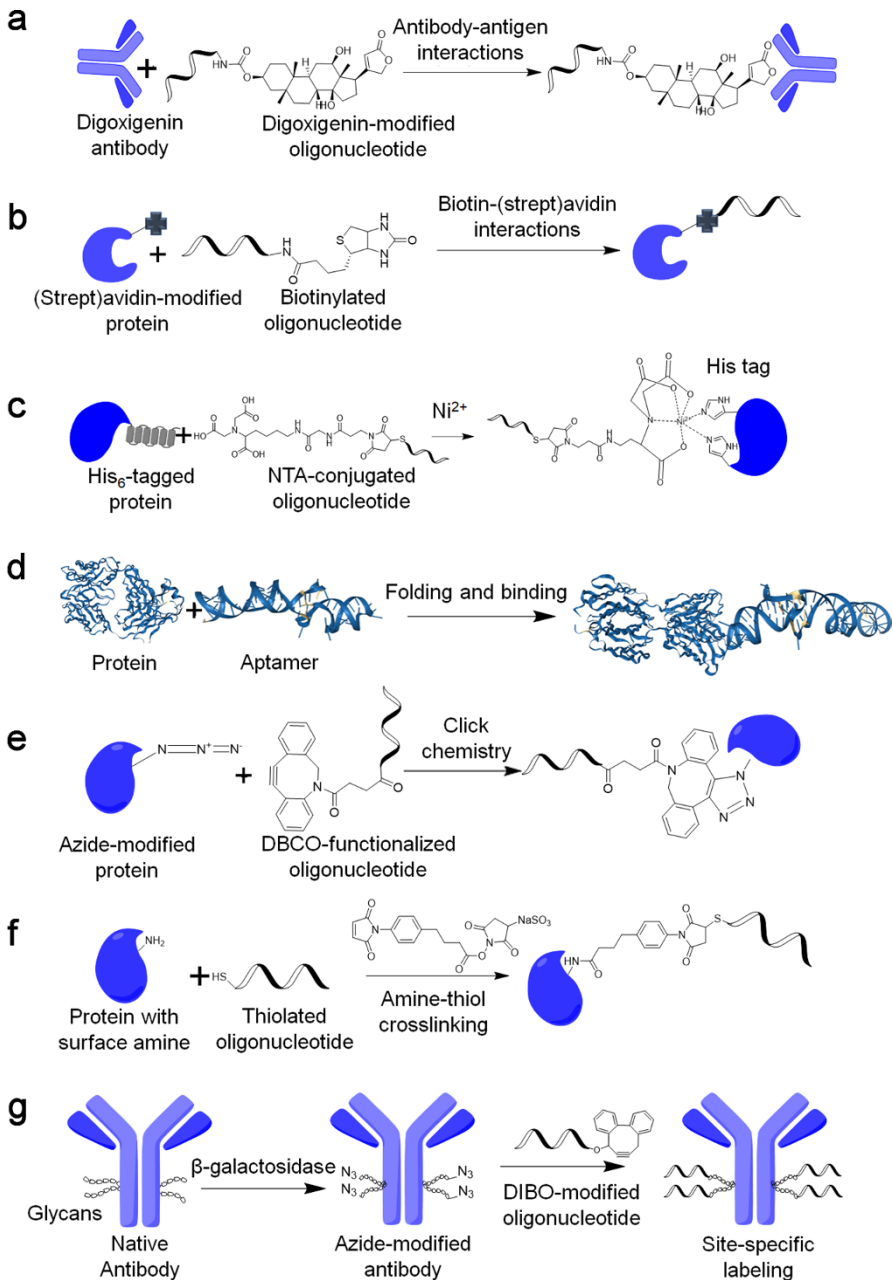


Fig. 4 Common strategies to conjugate DNA to a protein of interest. **a** Antibody–antigen interaction. **b** Strept(avidin)–biotin interaction. **c** Ni–NTA–His₆ interaction. **d** Aptamer–protein interaction. **e** Strain-promoted azide–alkyne cycloaddition. **f** Amine–thiol crosslinking. **g** Site-specific labeling of antibody with DNA using SiteClick™

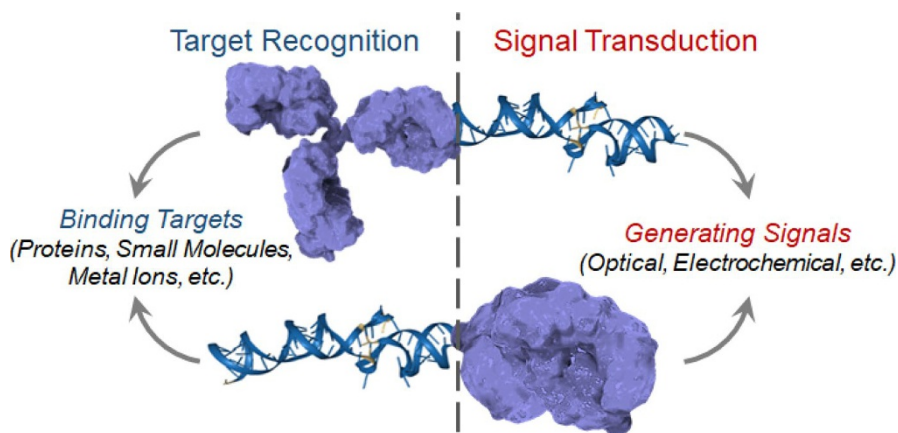


Fig. 5 Two designs of a typical biosensor using DNA–protein conjugates. *Top*: antibody as target recognition motif and DNA as signal transduction motif. *Bottom*: DNA aptamer as target recognition motif and protein enzyme as signal transduction motif

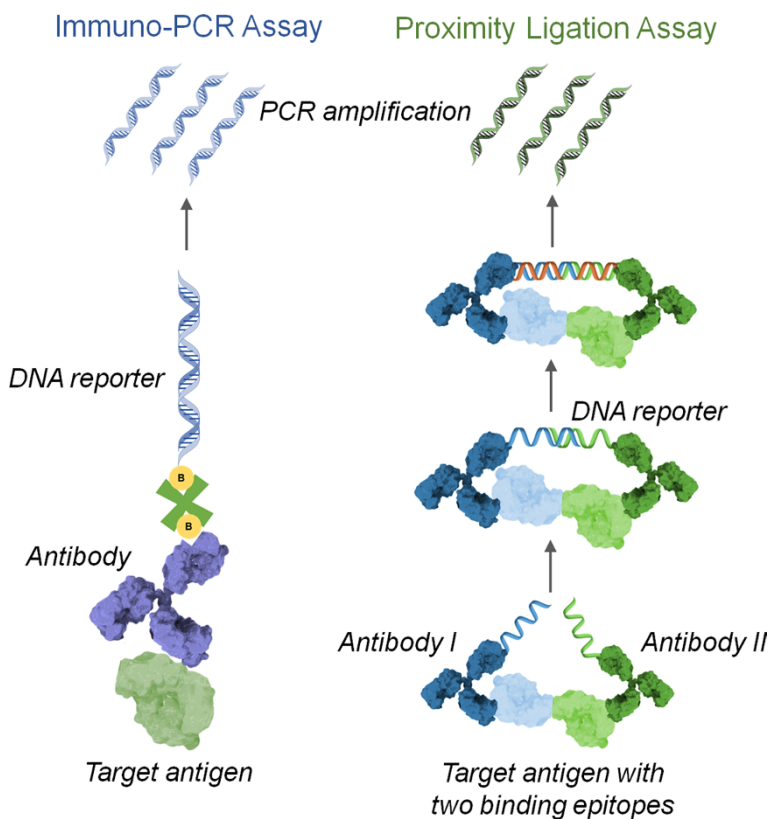


Fig. 6 Illustration of the working principles of (*left*) immuno-PCR assay and (*right*) proximity ligation assay (PLA). Both assays rely on the target binding using antibodies and signal amplification using DNA reporters

by DNA polymerase to detect antigens sensitively and quantitatively (Fig. 6). The original idea of IPCR was introduced by Sano et al. in 1992, when they attached biotinylated DNA to antibody for the detection of bovine serum albumin (BSA) [3]. They observed that the sensitivity of IPCR was more than 100 times higher than conventional ELISA for influenza virus antigen detection. Later work demonstrated that IPCR is particularly suitable for detecting extremely low levels of antigens, achieving approximately 100–10,000 times higher sensitivity than conventional ELISA [52–54].

Although IPCR is demonstrated to be highly sensitive with wide dynamic range, it still has drawbacks for improvements. First, IPCR possesses high background noise due to the generation of heterogeneous products. Second, chemical preparation process of DNA-antibody compounds is usually complicated and may affect the binding ability of antibodies. To overcome these problems, different approaches have been developed by increasing the number of linker molecules, introducing ready-to-use reagents, and using site-specific labeling methods [55]. For example, van Buggenum et al. used fast and convenient Diels–Alder reaction to synthesize a cleavable DNA–antibody complex [56]. The strategy was realized by coupling antibodies functionalized with tetrazine and DNA functionalized with *trans*-cyclooctene via a cleavable linker, which can efficiently release DNA strands for detection in the latter step. Schultz and colleagues exploited a site-specific conjugation method for IPCR to conjugate DNA onto an antibody containing a genetically encoded amino acid, significantly improving the sensitivity and specificity (Fig. 7a) [57].

Another potential route to improve the performance of IPCR is the optimization of DNA amplification and signal readout process. Gel electrophoresis as the most commonly used tool for analyzing quantitative PCR amplification in IPCR is considered time-consuming and tedious. Advanced PCR techniques such as real-time quantitative PCR (RT-qPCR) and droplet-based digital PCR have been integrated with IPCR to achieve better signal amplification and lower limit of detection [58, 59]. In addition, a variety of DNA amplification methods have been adopted in IPCR, such as rolling circle amplification (RCA) and hybridization chain reaction (HCR), which are based on isothermal amplification strategy, enabling exponential DNA amplification without the use of thermal cycles. Recently, Yin and colleagues

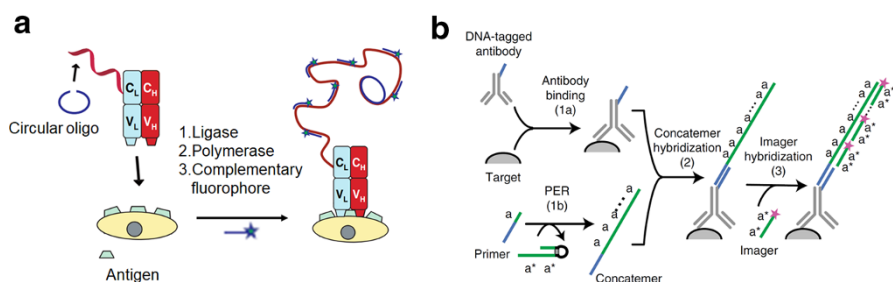


Fig. 7 **a** Immuno-PCR using site-specific DNA labeling and RCA improving the sensitivity and specificity [57]. **b** Illustration of the amplification process of immuno-SABER based on primer exchange amplification [60]

reported a protein mapping approach called immunostaining signal amplification by exchange reaction, termed as immuno-SABER (Fig. 7b) [60]. The signal amplification process of immuno-SABER is based on primer exchange reaction, which enables high-throughput programmable signal amplification via binding multiple fluorophore-bearing imager strands to barcoded-DNA in the absence of in situ enzymatic reactions. By integration with expansion microscopy, immuno-SABER realized rapid, multiplexed super-resolution imaging of proteins in tissues.

Nowadays, IPCR is used to detect a wide range of targets, including bacteria, viruses, and cell antibodies. For example, IPCR was successfully applied to detect bacterial pathogens *Streptococcus pyogenes* and *Staphylococcus aureus* [61, 62]. Cao et al. developed in situ immuno-PCR, in which marker DNA can be amplified in a complete cell or tissue section [63]. This technique was further applied to detect trace amounts of biomolecules in complete cells with high selectivity, showing great potential for detecting hepatitis B virus (HBV) expression [64]. Detection of H1N1 viruses using IPCR reached 2–3 orders of magnitude higher sensitivity compared to ELISA and RT-qPCR [65].

3.1.2 Proximity Ligation Assay (PLA)

Immuno-PCR relies on the ELISA detection using nucleic acids as readouts. The target-capture and binding process generally requires solid-phase support using microplates or antibody-modified microbeads, which involves multiple washing steps to remove unbound conjugates to lower the background. In addition, the mass transport at the liquid–solid interface of heterogenous assay may affect the performance. Therefore, a real-time and wash-free homogenous assay to detect proteins is in high demand [66]. In 2002, Landegren and colleagues developed a homogenous protein detection approach, termed as proximity ligation assay (PLA), which relies on the simultaneous identification of two epitopes of a protein using two different DNA aptamers (Fig. 8a) [4]. The key idea of PLA lies on the spatial constrain of a pair of DNA strands as signal output. When two DNA strands are located spatially confined with each other in the existence of the target protein, the hybridization reaction happens, leading to displacement of the reporter strand. Without a target protein, two detection strands cannot interact with each other to generate any signal, and thus no washing steps are needed. Compared with IPCR, PLA does not require multiple washing steps. The reported sensitivity of PLA is 1000-fold higher than conventional assay, enabling more efficient detection of target proteins.

However, the availability of DNA aptamers limits the application of aptamer-based PLAs. Antibody-based PLA was then developed based upon the simultaneous binding of two epitopes on the target protein by a pair of DNA-modified antibodies as the probe (Fig. 6). Landegren and colleagues reported the preparation of ligation probes by mixing streptavidin-DNA with biotinylated-antibodies [67]. To further improve the performance of PLA, the same group developed a method named triple-binder proximity ligation (3PLA), which outputs the specific DNA signal only when three DNA motifs are identified by the target protein at the same time [68] (Fig. 8b). The 3PLA technique was ca. 40,000 times more sensitive than traditional PLA assays. The specific binding to target proteins requires DNA-antibody probes

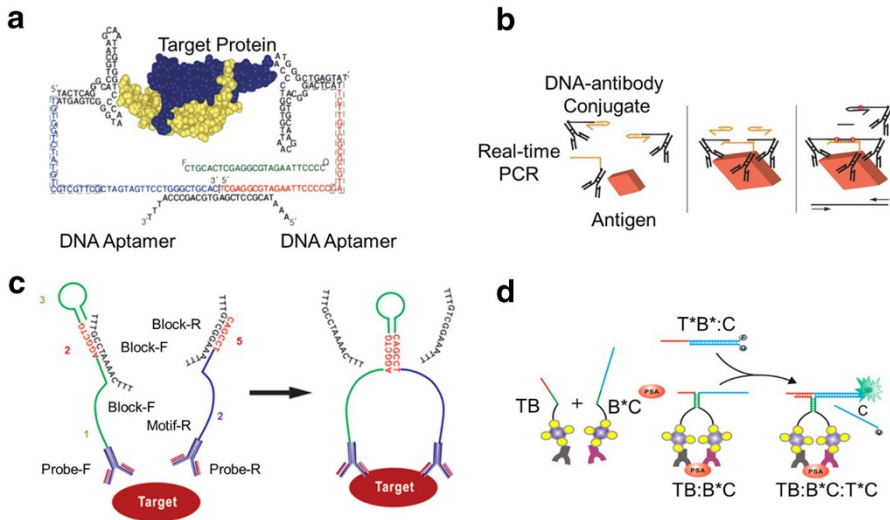


Fig. 8 Different proximity ligation-based assays. **a** The first reported PLA design through simultaneous identification of two epitopes of the target protein using two DNA aptamers [4]. **b** Triple-binder proximity ligation (3PLA) approach [68]. **c** Binding-induced DNA assembly (BINDA) approach. **d** Binding-induced formation of DNA three-way junction (TWJ) for direct fluorescence imaging [70]

to identify three single epitopes of target simultaneously, which can reduce the non-specific binding to unrelated proteins nearby. Koos et al. combined hybridization chain reactions (HCR) with PLAs to detect post-translational and protein–protein interactions in situ [69]. When the DNA–antibody probes were affiliated with proximity ligation, HCR occurred in the hairpin DNA structure of the probes, producing a long, gapped, double-stranded DNA as the signal output. Using this technique, it is possible to show the interactions between proteins in living cells. Up to now, PLA based on DNA–antibody conjugates is one of the most powerful tools for in situ detection of endogenous proteins. Several commercial PLA kits such as Duolink™ and Dovetail™ are available on the market.

Recent advances in PLA were reported by Le and colleagues, who developed a novel protein detection method called binding-induced DNA assembly (BINDA) based on two probes recognizing the target simultaneously (Fig. 8c) [70]. A pair of two DNA motifs is designed to have unstable hairpin structure with another complementary DNA sequence at the end. When two probes identify the target protein at the same time, the DNA motifs trigger binding-induced assembly, leading to a robust closed-loop structure and released ssDNAs for real-time PCR detection. The closed-loop structure increases the melting temperature by 30°, differentiating the assembled DNA from the unreacted one. BINDA assay can be easily operated in a test tube, decreasing the limit of detection for about 10^3 – 10^5 compared with conventional immunoassays. To further improve the BINDA performance, they further developed a DNA three-way junction (TWJ) strategy. After binding target molecule and forming DNA duplex, an additional fluorescent dsDNA is introduced to trigger the chain displacement reaction, resulting in a fluorescent three-way junction for

direct fluorescence imaging (Fig. 8d) [71]. TWJ design does not require enzymes and heat cycles needed in real-time PCR, which could be used for real-time imaging and protein analysis in live cells [72].

To sum up, PLA has been widely used to detect a variety of different biotargets, including platelet-derived growth factor (PDGF) [4], cytokines [67], individual exosomes [73], and active enzymes in a single cell [74]. The assay is also envisioned to have great potential in early stage cancer diagnosis by detecting multiplexed cancer biomarkers [75].

3.2 Using Protein as Signal Reporter

In addition to the use of DNA as signal reporter, many sensors employ functional DNAs as antibody analogues to recognize target molecules and use conjugated enzymes to generate detectable signals. DNA as one type of biomacromolecule can not only hybridize complementary strands through base pairing principles but can also selectively bind to various target molecules, known as functional DNA (fDNA). The fDNAs include aptamers, DNAzymes, and aptazymes, which can bind targets like antibodies or perform catalytic activity like enzymes. The identification of fDNAs through *in vitro* selection or systematic evolution of ligands by exponential enrichment (SELEX) has generated many fDNA molecules for diverse analytes, including metal ions, small molecules, proteins, cells, and intact viral particles [26, 49].

Protein enzymes are considered as one of the most sensitive reporters due to the extremely high enzymatic activity. Enzymes can convert biochemical substrates into different detectable signals, such as fluorescent, colorimetric, electrochemical, and thermal signals. For example, horseradish peroxidase (HRP) catalyzes oxidoreduction reactions, resulting in a colored or luminescent precipitate. Another example is alkaline phosphatase (ALP), which converts the phosphatase substrate 5-bromo-4-chloro-3-indolyl phosphate (BCIP) to purple precipitations with nitro blue tetrazolium (NBT).

In this section, we discuss the combination of functional DNAs with enzymes as biosensing platforms, in which DNA functions for recognition and enzyme function for signal output. This type of sensor design has been widely applied for detection of various biomolecules in different applications, such as environmental monitoring, industrial quality control, and clinical diagnostics. We categorize this section into three types of enzyme-mediated signal transduction processes: (1) generating optical and electrochemical signals; (2) producing glucose for PGM-based detection; and (3) coupling with nanoparticles to improve the signal outputs.

3.2.1 Optical and Electrochemical Signal Outputs

For the purpose of realizing a faster and safer detection of nucleic acids, DNA–enzyme conjugates appeared for the first time in the early 1980s [2], while at that time the most common method for nucleic acid detection was radioisotopes which is harmful. After hybridization between probe strands and target strands,

attached enzymes generated measurable outputs such as optical or electrochemical signals, providing a safer and more simplified detection process (Fig. 9a) [76–78].

Optical output, including colorimetric and fluorescent signals, is the most widely used output in a typical bioassay design. The colorimetric method allows naked-eye-based readout requiring no complicated instrument, while the fluorescent method requires a spectrophotometer for fluorescence quantification but with much higher sensitivity. One of the research interests for the development of bioassays is to integrate multiple optical outputs into one single assay by using DNA–enzyme conjugates. For example, Oh et al. reported a smart nanodevice for fast diagnosis of biotargets using DNA hybridization-mediated proximity assembly of biochemical reactions. With the addition of suitable enzyme-cofactor pairs, the detection of various biotarget can be realized through colorimetric or fluorescent outputs [79]. Another example is to use smart phones to capture optical signals generated by DNA–polymerase conjugates in a modular pathogen nucleic acids detection platform (Fig. 10a) [80]. In the absence of the nucleic acid targets, the DNA–polymerase complex was inactivated. Hybridization between the target nucleic acid and probe nucleic acid can activate polymerase, resulting in a self-priming signaling nanostructure followed by binding to HRP. The visual signals produced by HRP-catalyzed reaction can be captured and quantified by smart phones.

In addition to optical output, the electrical signal output is another widely used sensor readout, which is generally considered more sensitive and accurate. The electrical signal transduction process of a typical DNA–enzyme based sensor can be easily realized by triggering enzyme–catalyzed reaction on the interface of electronic transducers [81]. One early work was demonstrated by Fan and colleagues who demonstrated an electrochemical DNA sensor based on stem-loop DNA probe and digoxigenin–HRP interaction [82]. The presence of the target DNA triggers the conformational change of the stem-loop DNA probe with end digoxigenin, recruiting HRP to the surface of the electrodes. The electrochemical signal can be amplified through H_2O_2 reduction and TMB redox reaction, achieving femtomolar detection limit. Povedano et al. developed a biochip to rapidly monitor MGMT gene methylation states using 5-methylcytosine (anti-5-mC) monoclonal antibody

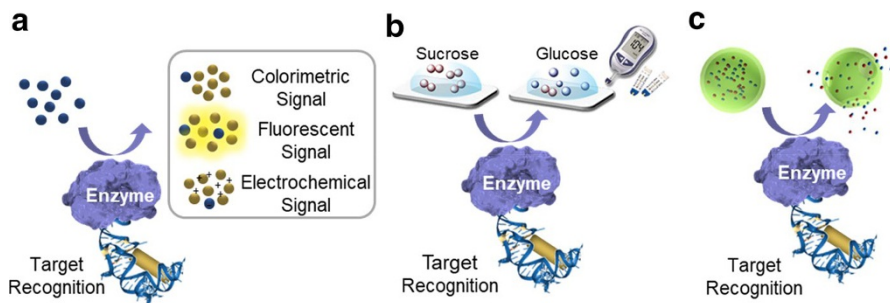


Fig. 9 Illustration of three types of enzyme-mediated signal transduction processes. **a** Generating optical and electrochemical signals. **b** Producing glucose for PGM-based detection. **c** Coupling with nanoparticles to improve the sensor performance

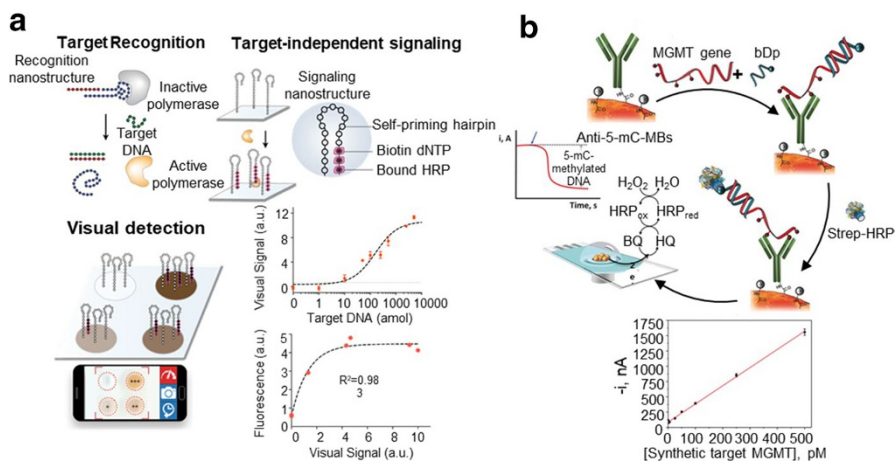


Fig. 10 Two recent examples of using enzyme-induced optical and electric signal outputs in DNA-enzyme based sensing platforms. **a** A pathogen detection platform using DNA polymerase for signal amplification for visual and fluorescent detection of pathogen nucleic acid [81]. **b** Fast assessment of MGMT gene methylation states using HRP-generated electrochemical signals [83]

(mAb)-modified magnetic beads. The methylated MGMT gene strand can be captured by anti-5-mC mAb onto beads surface, and then can be specifically labeled with biotinylated DNA. The subsequent binding of strep-HRP enabled the amperometric determination of gene methylation states in raw human serum, cancer cells, and tumor tissues (Fig. 10b) [83].

3.2.2 Portable Glucose Meter-Based Assay

Towards the realization of point-of-care testing (POCT) for clinically important targets, it is essential to develop compatible, portable, and affordable devices which can quantitatively monitor the concentrations of the biomarkers, such as metal ions, small molecules, and disease-related proteins [84]. The most successful and commonly used POCT device is a personal glucose meter (PGM). In order to apply PGM for detection of multifarious biomolecules, it is important to establish a direct relationship between generation of glucose and recognition of target molecules (Fig. 9b). Lu and colleagues designed a PGM-based assay for many different biotargets using DNA-conjugated invertase, which can efficiently catalyze disaccharide sucrose into reductive glucose, realizing PGM-based quantification of cocaine, adenosine, interferon- γ , and uranyl (Fig. 11a) [85]. The key setup of the assay is based on the magnetic beads immobilized with functional DNA-invertase conjugates. The presence of targets triggered the release of DNA-invertase into solution, subsequently converting sucrose into glucose for PGM detection. Thus, the direct correlation between the concentration of targets and the concentration of glucose can be established. This powerful method has been expanded to quantify a large number of biotargets using PGM, including nucleic acid disease markers [86], enzymes [87], melamine [88], and microRNA in serum matrix [89].

In the design of the first-generation PGM-based assay, it is crucial to fully remove the unreleased invertase on magnetic beads from solution in order to suppress the background signal. The magnetic separation of heterogeneous invertase largely affects the efficiency and usability of the assay. To improve the detection procedure, Lu et al. incorporated a lateral flow device (LFD) with the PGM to facilitate the

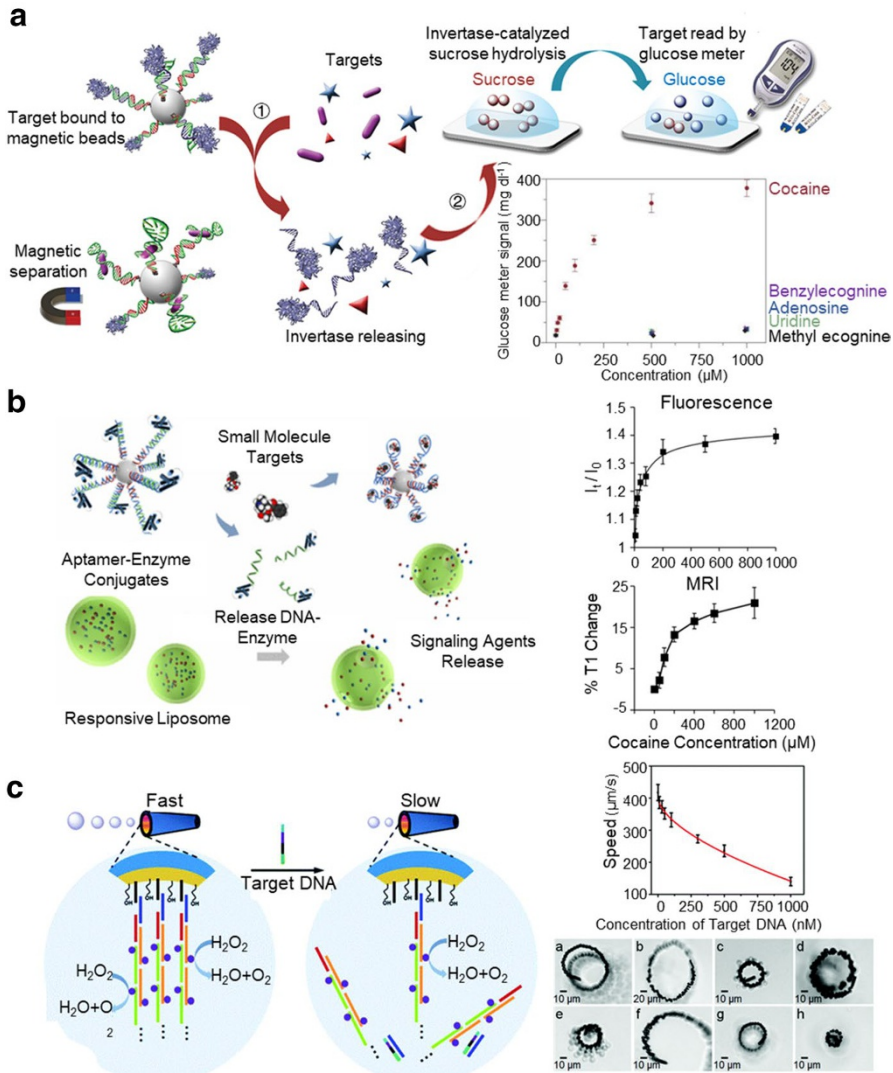


Fig. 11 Enzyme-induced signal outputs coupled with PGM readouts and responsive nanocarriers. **a** Design of PGM-based assay using DNA-conjugated invertase for the detection of various targets [85]. **b** Multimodal detection of small molecular targets using stimuli-responsive liposome as signal reporter carrier [92]. **c** Design of an enzyme-powered micromotor for the detection of target DNAs using the movement speed as the signal output [93]

purification and enrichment of invertase [90]. The sample matrix containing target molecules induces the release of DNA–invertase conjugates into the flow, enables the production of glucose in the reaction pad, and thus achieves the quantification of targets based on the converted concentration of glucose. They further demonstrated a logic gate system by coupling DNAzymes and protein enzymes to implement PGM response to a variety of biological substances in clinical samples [91].

3.2.3 Nanoparticle-Based Assay

In addition to optical, electrochemical, and PGM-based assays, current research interests have focused on incorporating nanoparticles with DNA–protein conjugates into diagnostic systems to further improve the sensor performance. Nanoparticles hold lots of unique physical and chemical properties that are not possessed by enzymes or nucleic acids. The incorporation of nanoparticles with DNA–protein conjugates would enable synergistic effects, such as enhanced activity and cascade reaction, which may further amplify signals or expand the application regimes of the sensor (Fig. 9c). In this section, we review the studies using nanomaterials integrated with DNA–protein conjugates to develop sensing systems, in which the target recognition can trigger the physiochemical response of nanomaterials, leading to generation of the signals.

One of the early studies reporting the integration of nanomaterials with DNA–protein conjugates is from Niemeyer et al. in 2001, who reported the DNA-directed immobilization of proteins onto colloidal gold nanoparticles (AuNP) using DNA–STV. The bio-hybrid AuNPs have specific recognition capabilities toward antigens [94]. In 2006, Hazarika et al. demonstrated the conjugation of fluorescent proteins with DNA–AuNP without impairing their biological activity. The hybrid conjugate provided a powerful tool to study distance-dependent fluorescence quenching effect by simply changing the lengths of DNA strands bridging fluorescent proteins and AuNPs [95]. In 2017, Breger et al. reported the assembly of semiconductor quantum dots (QDs) with phosphotriesterases via peptide–DNA linkers and observed the enhanced phosphotriesterases activity on QD surface [96]. Lu et al. used a DNA scaffold to construct a three-chromophore Förster resonance energy transfer (FRET) system containing luminescent QDs, enhanced green fluorescent proteins (EGFPs), and dye-modified oligonucleotides [97]. DNA scaffold precisely positioned EGFPs, QDs, and fluorophores with nanoscale accuracy, serving as a powerful tool to calibrate FRET process.

To improve the assay sensitivity, one route is to pack signal reporters such as enzymes into a nanocarrier with confined space so as to increase the reporter concentration. Tan and colleagues reported an enzyme-encapsulation strategy using aptamer-crosslinked hydrogel as responsive nanocarrier for enzyme reporters [98]. The presence of the targets can disassemble DNA hydrogels via target–aptamer interactions. The encapsulated enzymes can be released into solution and actuate the enzymatic reaction leading to matrix color change, which can be recognized by naked eyes. Another strategy was reported by Xing et al. who developed an enzyme-responsive liposomal nanocarrier for multimodal detection of small molecules [92]. As shown in Fig. 11b, DNA-phosphatidylcholine

2-acetylhydrolase (PLA₂) conjugates were immobilized onto the surface of magnetic beads together with aptamer strands. The presence of targets can trigger the release of DNA-PLA₂ into suspension containing responsive liposomes, breaking liposomal containers and releasing loaded signaling agents. By loading with different reporters, such as uranin and gadopentetic acid, the concentration of small molecule target cocaine can be determined through multimodal fluorescent and MRI detection. Furthermore, they applied the responsive liposome strategy to developed thermometer-based small molecule sensor by loading near-IR (NIR) photosensitizer into liposomes. The target-triggered release of photosensitizers resulted in an increase of temperature upon NIR irradiation, thus enabling the quantification of the target using thermometer [99]. Moreover, Ju et al. reported an enzyme-powered micromotor as a sensitive and simple DNA sensor [93]. In the micromotor design, multilayered DNA–catalase conjugates were immobilized on the inner surface of the microtubular structure. The existence of the target DNA sequence triggered the release of the DNA–catalase from the micromotor and decreased the rate of oxygen generation, resulting in the decrease of motion speed (Fig. 11c).

To sum up, enormous achievements have been made by using DNA–protein conjugates for diagnostic applications, while challenges still remain to be addressed. First, efficient coupling chemistries that can fully preserve both catalytic activity and binding affinity of the conjugates are highly desired. Second, the bench-to-bedside transition of developed bioassays needs to be accelerated. One possible route is to adapt commercially available devices such as PGM for the assay development. By addressing the above-mentioned two challenges, we can expect new clinical diagnostic tools with better performance based upon DNA–protein conjugates in the near future.

4 DNA–Protein Nanoassemblies

Introduced by Seeman in 1982, DNA has been recognized as one of the most promising structural materials which can programmably assemble into almost any shaped nanostructures with a single base pair spatial control, known later as the structural DNA nanotechnology [100]. In addition to the broad range of diagnostic applications enabled by DNA–protein conjugates, increasing research interests in this field have been attracted to use structural DNA nanotechnology to construct 3D protein structures. The synergistic incorporation of both DNA and protein molecules into a highly ordered nanostructure can generate advanced functional nanomaterials for biochemistry, bioimaging, and drug delivery applications. In this section, we firstly survey studies using versatile structural DNA nanotechnology tools to arrange proteins in 3D environments with sub-nanometer spatial resolution, including dsDNA scaffold, DNA tile structure, and DNA origami. Then, the studies of using DNA-tethered proteins to form 3D protein crystals or 2D protein polymers are reviewed. Lastly, we highlight some of the latest work using DNA–protein nanomaterials for *in vitro* and *in vivo* drug delivery applications.

4.1 Arrangement of Proteins on DNA Nanostructures

Taking advantage of structural DNA nanotechnology, proteins have been precisely arranged onto different DNA scaffolds with high spatial resolution. These attempts further lead to the study of protein–protein interactions with spatial proximity and the development of assembled nanostructures responsive to external stimuli.

4.1.1 Protein on dsDNA Scaffolds and DNA Tile Structures

One of the earliest attempts to position proteins on dsDNA-based scaffold was reported by Niemeyer et al. using biotin–STV interaction in 1994 [5]. DNA–STV hybrids served as connectors to conjugate biotinylated IgG or alkaline phosphatase on DNA backbone. Since STV molecules are tetravalent, the biotin-binding sites can be easily used for functionalization of different biotinylated components, such as enzymes and antibodies. This simple approach based on the interactions between STV and biotinylated ssDNA was widely used to form randomly assembled and stochastic DNA–protein networks in some early studies. In 1999, Niemeyer et al. used STV molecules to bridge adjacent DNA fragments to form linear nanostructures for competitive immunoassay, which is more sensitive than conventional methods [14]. Since then, different types of constructs based on DNA–protein conjugates have been reported, including linear chain, DNA–STV nanocircles, and ion-switchable structure, which can switch between branched and circular structures [101].

Nanostructures based on linear dsDNAs or branched DNA junctions are usually flexible, which are difficult to assemble into more complicated nanostructures. Inspired by the pioneering work from Seeman et al. in designing DNA tile structures in the 1980s, much effort has been made to programmably decorate proteins onto highly ordered DNA tile nanostructures. DNA tiles consist of two or multiple DNA duplexes with exchange strands, exhibiting enhanced rigidity and stability compared to that of linear DNAs. Thus, the use of DNA tile structures significantly extends the scope and addressability of DNA–protein assemblies. An early example was reported in 2003 by Yan et al., whereby they designed a 2D biotin-modified lattice from 4×4 DNA tiles (Fig. 12a). DNA-templated STV arrays were achieved by using biotin–STV interactions, which were further used as scaffold for producing highly conductive silver nanowire arrays [102]. DNA tile strategy was further applied to fabricate linear protein-nanoparticle hybrid arrays [103], “nanotape” with uniform wells for STV fixation [104], and symmetric finite grid with the size around 200 nm [105]. Using a three-way DNA junction design, single protein imaging was successfully demonstrated by Selmi et al. They showed that His₆ tag modified guanine nucleotide binding protein GRi1 formed densely packed protein arrays on Tris–NTA-functionalized DNA templates without protein aggregation, enabling analysis of GRi1 structure using cryo-EM [106]. In addition, Xu et al. reported a 3D tetrahedral cage consisting of a trivalent homotrimeric KDPG aldolase top and a triangular DNA nanostructure base with complementary handles [107].

To extend the functionality and application of DNA–protein nanoarrays, conjugation methods have been developed to incorporate different types of proteins onto one nanostructure. Lu and colleagues used DNA strands with

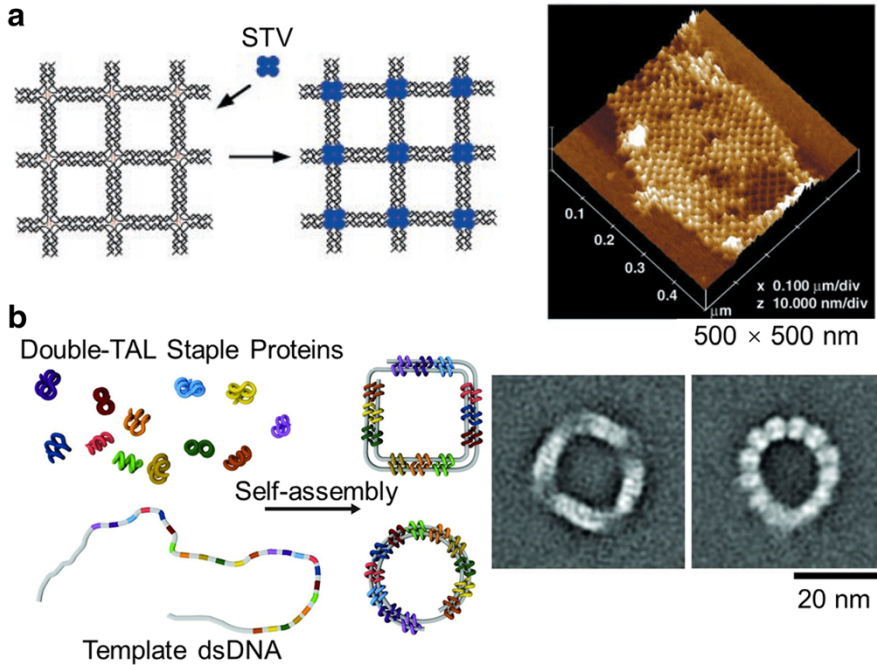


Fig. 12 Two examples of DNA–protein nanoassemblies via positioning protein on DNA tile structure or dsDNA scaffold. **a** Assembly of 2D STV lattices on top of DNA tile structure [102]. **b** Using TALs with DNA-recognizing repeat subunits as staple proteins to realize different dsDNA-based nanostructures [115]

phosphorothioate (PS)-modified backbone to achieve bioorthogonal positioning of STV and myoglobin on dsDNA backbone via biotin- and maleimide-containing bifunctional linkers [108]. A similar strategy was further used to decorate proteins onto the corners of a 3D DNA tetrahedron [109]. Meyer et al. extended the bioorthogonal conjugation to attach four different proteins onto a four-way junction X-tile motif using four different small-molecule tags [110]. In addition to small molecules, biomacromolecules such as aptamers and peptides, which can selectively capture target proteins, have also been used to recruit multiple different proteins onto DNA nanostructures. Using this approach, nanoarrays have been decorated with multiple different proteins, including antibody, thrombin, and platelet-derived growth factor. Furthermore, the ability to arrange enzymes onto DNA nanostructure in a controlled manner enables the study of enzyme cascade reactions. Since the diffusion rate of the substrate at the active center of an enzyme is a limiting step in a catalytic reaction, spatially ordered enzymes are demonstrated to have dramatically increased reaction rates. An enzyme cascade consisting of NAD(P)H-dependent FMN oxidoreductase (NFOR) and luciferase (LUC) on biotinylated dsDNA via biotin–STV interactions was developed in an early work [111]. Wilner and colleagues attached a pair of two enzymes, either glucose oxidase (GOx) and HRP pair or nicotinamide adenine dinucleotide (NAD⁺) cofactor and glucose dehydrogenase pair, onto a hexagon-like DNA

strip, showing that the enzyme cascade reaction or cofactor-mediated biocatalysis can proceed more effectively [112].

In addition to simply templating proteins onto DNA arrays, it is also possible to regulate the geometry of a pre-formed DNA nanostructure using DNA-binding proteins. For example, Seeman and colleagues constructed a DNA tile-based nano-mechanical device by using *E. coli* integration host factor (IHF) as the trigger. The binding of IHF changed the rectangular DNA tile structure to a bend shape [113]. Another DNA-binding protein used for regulating DNA nanostructure is RuvA, which binds to four-stranded DNA in the Holliday junction and unwinds the duplex DNA. Malo et al. demonstrated that both connectivity and symmetry of a 2D DNA–protein lattice can be changed by adding RuvA during the self-assembly process [114]. A recent example was reported by Dietz and colleagues who used transcription activator-like (TAL) effector, a protein that can bind to major grooves of dsDNA, to fold dsDNA into different shapes (Fig. 12b) [115]. They systematically designed a series of TALs with DNA-recognizing repeat subunits as staple proteins for dsDNA template. A variety of nanostructures, including square, triangle, double-ring circle, and multilayer nanostructures can be realized using a cell-free expression system.

4.1.2 Protein on DNA Origami Structures

In 2006, Paul Rothemund developed a computer-assisted DNA nanostructure design principle, coined as DNA origami, to assemble ssDNAs into any predefined nanostructures [116]. The structure design is based on a 7-kb M13mp18 single-stranded viral DNA as backbone and hundreds of well-designed short ssDNAs as staples. By designing the sequences of the staple strands, M13mp18 can be folded into almost any shape, including world map and the iconic smiling face. Compared with dsDNA scaffold and DNA tile structure, DNA origami structure is thermodynamically more stable and more programmable, thus enabling better control over the protein immobilization process. Due to the high programmability and addressability of DNA origami, significant efforts have been applied to organize proteins onto a variety of DNA origami patterns since 2008 [27]. Some well-practiced strategies previously used in the formation of protein arrays on dsDNA scaffold and DNA tile structure can be easily adapted to this new platform with improved spatial resolution. For example, His-tagged fluorescent proteins can be immobilized onto DNA origami modified with NTA groups, demonstrating the ability to arrange proteins in a site-specific manner [23]. Other examples used the purified cowpea chlorotic mottle virus capsid proteins (CCMV CPs) to decorate DNA origami surface through non-specific electrostatic interactions, improving the intracellular delivery efficiency of DNA origami-CCMV complex to HEK293 cell [117].

Similar to using DNA tile structures to study protein interactions, DNA origami–protein assemblies have also been applied to investigate the distance-dependent protein interactions and enzyme cascade reactions. Yan and colleagues pioneered early studies in this field. They designed and arranged a pair of enzymes, GOx and HRP, onto a 2D rectangular origami tile with controlled inter-enzyme distances ranging from 10 to 65 nm. They observed that the catalytic

efficiency was negatively correlated with the inter-enzyme distance and the overall reaction efficiency significantly increased by decreasing the distance [118]. They further used a similar design to study the diffusion kinetics of intermediary metabolic products in an artificial multi-enzyme system with three dehydrogenases in 2016 [119]. They incorporated glucose-6-phosphate dehydrogenase (G6pDH), malate dehydrogenase (MDH), lactate dehydrogenase (LDH), and a cofactor NAD⁺ onto a 2D origami tile (Fig. 13a). By controlling the position of the substrate, it is possible to regulate multi-enzyme pathways with fast response. In addition to aligning enzymes onto 1D or 2D origami tiles, confining enzymes within 3D DNA origami structures can also be achieved using the same principle. By decorating the inner surface of a 3D tubular structure with multiple protein-binding ligands, proteins can be encapsulated inside the hollow structure with controlled location and orientation [120]. Restricting diffusion of intermediates in an assembled DNA hollow chamber was also demonstrated to increase the GOx/HRP enzyme cascade efficiency [121].

Because of the ability to incorporate versatile coupling chemistries to DNA strands, dynamic and reversible modifications of proteins onto DNA origami are able to be achieved. Gothelf and colleagues used responsive linker with disulfide bond or 1,2-bis(alkylthio)ethene to pattern proteins onto specific locations in a 2D origami rectangle [122]. Since disulfide bond and 1,2-bis(alkylthio)ethene can be cleaved by dithiothreitol (DTT) and singlet oxygen generated by eosin, respectively, the introduction of DTT or eosin leads to release of proteins and change of the pattern. The bond cleavage and forming reactions can be investigated by AFM at the single-molecule level. Another reversible approach was demonstrated by Lu and colleagues [17]. They took advantage of the binding affinity differences between biotin and desthiobiotin toward STV, demonstrating a reversible STV decoration process on DNA origami structure. They successfully applied this approach to create an encrypted Morse code “NANO” on a single origami tile (Fig. 13b). The selectivity and reversibility of the dynamic chemistries demonstrated in these reports indicate their potential use in responsive nanomaterials.

In addition to responsive immobilization chemistries, DNA origami structures as protein templates have also been installed with dynamic and reversible motifs in order to activate and inactivate the activity of the enzyme in a controlled manner. An example of such a concept is the construction of tweezer-like DNA nanodevice. Liu et al. designed a DNA tweezer structure and attached a dehydrogenase and its NAD⁺ cofactor to different arms of the tweezer [125]. By adding a specific DNA sequence as the trigger, the switch of the DNA tweezer from an open state to a closed state decreased the enzyme-cofactor distance, thus resulting in the change the enzymatic kinetics. Grossi et al. designed a DNA origami “nanovault” to encapsulate a single endopeptidase alpha-Chymotrypsin inside [126]. The enzymatic activity can be turned on and off through reversible DNA hairpin “locks”. Despite all these achievements, the mechanism of how DNA scaffolds interact with enzyme activity is still under debate. Some hypotheses, including the proximity between catalysts and substrates, stabilizing effect of the negatively charged DNA strands, localized optimal pH environment, have been proposed and partially supported by some observations, calling for further investigations [127, 128]. Each of these studies

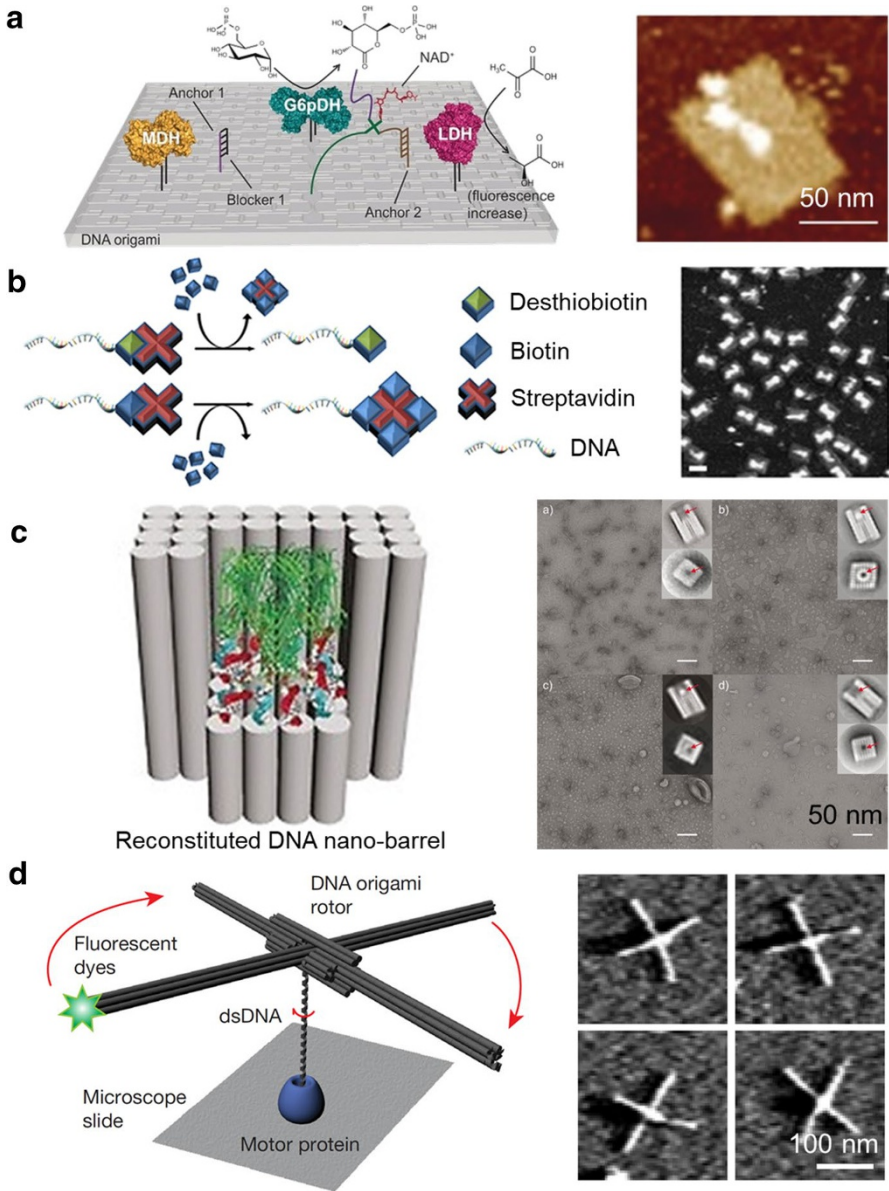


Fig. 13 Four examples of nanoassemblies based on proteins and DNA origami structures. **a** Assembly of G6pDH, MDH, and LDH on a 2D origami tile to study the enzyme cascade [119]. **b** Design of a reversible STV decoration process on DNA origami based on biotin and desthiobiotin modifications [17]. **c** Cryo-EM reconstruction of the membrane protein by trapping a single membrane protein within a DNA origami nanobarrel [123]. **d** Design of a DNA origami rotor with fluorescent dye to study the DNA unwinding process mediated by RecBCD helicase at the single-molecule level [124]

offers opportunities for investigating the distance-dependent substrate diffusion and mimicking the catalytic process of natural enzymes.

Furthermore, recent explorations of potential applications enabled by protein–DNA origami nanocomplexes have led to creative studies in single-molecule imaging. One of the examples is the use of DNA origami scaffolds to accurately image the cryogenic electron microscopy (cryo-EM) imaging of membrane protein, which is difficult to crystallize. A recent study reported the use of a hollow DNA origami cage to control the orientation of a dsDNA-binding protein p53, improving the identification of single protein particle and the alignment during cryo-EM imaging process [129]. The center of the hollow origami structure was designed to localize p53-binding sequence at different positions to align p53 in different tilt angles, thus benefiting the computer-assisted tomographic reconstruction. A similar strategy to trap a single membrane protein α -hemolysin within a lipid-modified DNA origami nanobarrel was reported by Dong et al. The hydrophobic interactions between α -hemolysin and lipids helped the alignment and cryo-EM reconstruction of the membrane protein (Fig. 13c) [123]. Zhuang and colleagues developed a DNA origami-rotor-based imaging and tracking (ORBIT) method to study the DNA unwinding process mediated by RecBCD helicase at the single-molecule level [124]. A DNA origami rotor with fluorophore labeling was attached to a RecBCD-binding dsDNA, enabling the DNA rotation measurement at a time resolution of milliseconds (Fig. 13d). Altogether, these studies indicate the potential of DNA origami as promising toolboxes for exploring important biological questions that are difficult to approach using conventional strategies.

4.2 Protein Superlattices and Protein Polymers Enabled by DNA

In the previous section, we surveyed DNA–protein nanoassemblies based on DNA nanostructures including dsDNA scaffold, DNA tile, and DNA origami. In these cases, DNA structures serve as the principal framework to template protein molecules, determining the final topology and organization of proteins. While DNA nanostructure offers precisely spatial control over protein position and orientation, generating extended protein nanoassemblies up to micrometer scale is still challenging. Unlike origami approach which decorates protein “cherries” onto a finite DNA nanostructure “cake”, Mirkin and other researchers utilize complementary DNA base pairing as the “glue” to program the protein–protein interface, forming well-defined protein polymers or 3D superlattices.

In nature, proteins bind to each other on specific epitopes through a combination of van der Waals forces, hydrophobic interactions, and salt bridges. Alternatively, native protein–protein interactions can be exchanged with programmable DNA–DNA hybridizations to direct the assembly of DNA-modified proteins. The concept of surface-driven DNA-mediated protein assembly was firstly reported in 2004, where Cowpea mosaic virus (CPMV) particles were crosslinked by 20-bp surface DNA strands into disordered aggregates [130]. By introducing short “sticky ends” of 4–10 bp to surface DNA strands on protein, an ordered NaTl lattice structure was reported to form from DNA-modified inorganic particles and Q β virus

capsid particles [131]. The introduction of short “sticky ends” enables reorganization of the lattice into a thermodynamically stable structure, thus leading to an ordered crystal. A more thorough work to investigate the design principles of DNA-mediated protein crystallization was reported by Bordin et al. in 2015 [132]. They chose a tetrameric catalase of D_2 symmetry as the model system and functionalized DNA strands onto protein through surface lysine residues (Fig. 14a). As lysine residues are relatively evenly distributed on catalase surface, DNA modifications can be considered as isotropic. By applying the DNA-mediated design rules Mirkin’s group established for inorganic systems [133], catalase can be deliberately constructed into six unique lattices consisting of either pure proteins or a combination of proteins and AuNPs. Importantly, catalase retained its catalytic activity after DNA modification. Some lattice structures even showed well-defined rhombic dodecahedral crystal habits.

So far, DNA-functionalized proteins are relatively isotropic, which normally generate cubic lattice like spherical building blocks behave. In 2017, Mirkin and colleagues used β -galactosidase (β Gal) to demonstrate a residue-specific DNA modification approach to decrease symmetry of surface chemistry [134]. β Gal presents ca. 32 lysine residues and eight cysteine residues at different positions on surface, which can be functionalized with DNA through different conjugation chemistries. β Gal with DNA modifications on evenly distributed lysine residues generated cubic CsCl lattice with complementary AuNPs, while β Gal with DNA modifications on cysteine residues resulted in low-symmetry AB_2 lattice because of the decreased binding sites (Fig. 14b). They further designed a protein–DNA Janus particle consisting of two GFP molecules modified with orthogonal DNA strands as asymmetric building block for crystal engineering [135]. The GFP molecule contains a single surface cysteine mutation and 18 native surface lysine residues and thus can be installed with two different DNA strands. Two GFP molecules can be dimerized into one Janus protein particle through the complementary DNA strands attached to cysteine, exposing orthogonal lysine strands on the opposite faces. The Janus protein–DNA particle of low symmetry can crystallize with two sets of AuNPs of different sizes, generating low-symmetry, hexagonal layered lattices. The ability to incorporate site-specific DNA modifications onto a protein surface to generate anisotropic building blocks significantly expands the scope of DNA-mediated colloidal crystal engineering.

In addition to 3D crystals, protein polymers engineered with DNA have also been explored recently. To design linear protein polymer structures from DNA–protein conjugates, it requires well-defined directional DNA modifications on the protein surface. Similar to the modification approach used in developing Janus protein–DNA particles, McMillan et al. introduced short DNAs at the desired sites on the surface of a β Gal through genetic mutation [136]. By designing the DNA modification sites closely positioned on β Gal, DNA- β Gal can assemble into segmented wire-like polymers via face-to-face cooperative hybridization (Fig. 14c). A similar strategy to form DNA-mediated 1D protein structure was demonstrated by Aida and colleagues using a heptamer GroEL protein with central cavity [137]. They modified two sets of GroELs with complementary DNA strands at their apical domains, forming 1D stable GroEL nanotubes. McMillan et al. further investigated two types of

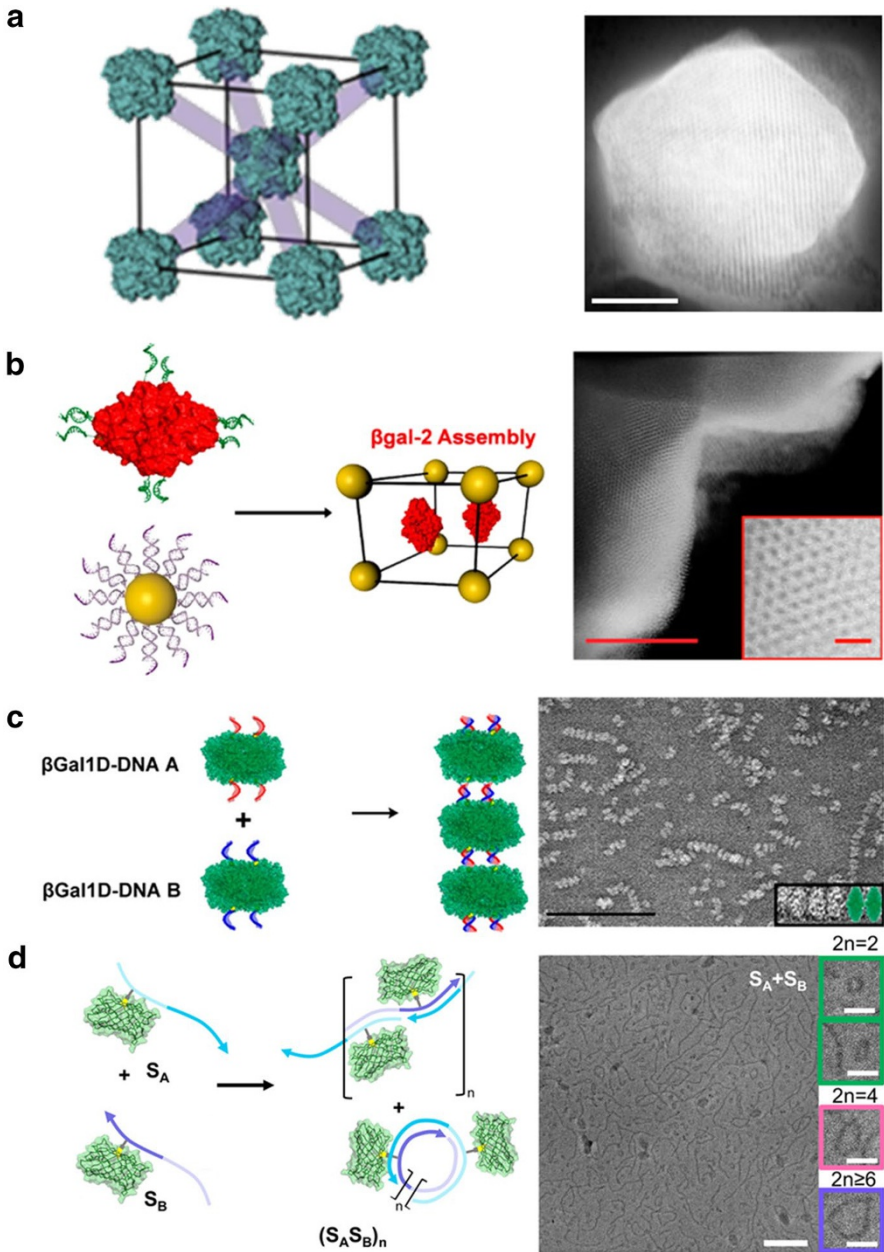


Fig. 14 Representative protein 3D superlattices or protein polymers. **a** Catalase evenly functionalized with DNA assembled into CsCl lattice [132]. **b** β Gal can be modified through either lysine or cysteine residues. Selective DNA modification on β Gal alters the crystallization of proteins with complementary AuNPs [134]. **c** Linear β Gal polymer chain from two sets of β Gal molecules modified with complementary DNA strands [136]. **d** Step-growth polymerization of mGFP–DNA monomers [138]

protein polymerization modes mediated by DNA [138]. They synthesized two sets of DNA-monofunctionalized mutant GFP (mGFP-DNA) as monomers for polymerization (Fig. 14d). By attaching ssDNA or hairpin DNA onto mGFP, it is possible to tune polymerization pathways of mGFP-DNA into step-growth or chain growth, respectively. As demonstrated by cryo-EM images, the step-growth process provided cyclic and linear polymer distributions, while the chain-growth pathway generated mostly 1D linear chains. The approach of using DNA to interface protein–protein interactions provides a potentially generalizable strategy to construct protein-based oligomers, polymers, and even 3D crystalline materials with exceptional control over their structures.

4.3 DNA–Protein Nanoassemblies for Biomedical Applications

So far, we have discussed the formation of different types of DNA–protein nanoassemblies. We have learned that proteins can be decorated onto DNA nanostructures with spatial control and DNA can also program protein–protein interactions forming polymers or crystals. Recently, emerging studies have focused on developing DNA–protein nanoassemblies for biomedical applications [139]. Though both DNA and proteins are important biomolecules for gene therapy and targeted medication, the efficient delivery of them *in vivo* is still challenging. DNA can be rapidly cleared by the kidneys through filtration because of the small size. Protein can be easily inactivated and degraded in blood vessels. Both of them also suffer from inefficient intracellular uptake issues. Therefore, a DNA–protein nanoassembly as a new type of delivery vehicle has been studied to overcome these challenges.

One strategy is to use spherical nucleic acid structures with a protein core, termed as ProSNA, to facilitate the intracellular delivery of both protein and DNA [140]. ProSNA with a highly oriented DNA shell exhibits some intriguing properties including low toxicity, minimum immune response, enhanced ability to penetrate biological barriers, and efficient delivery of nucleic acids and enzymes [141]. Brodin et al. used β gal as model enzyme and attached 25 DNA strands onto one protein to form a ProSNA structure [140]. The β gal ProSNA showed up to 280 times higher cellular uptake efficiency than the native β gal in several mammalian cell lines, possessing good stability to catalyze the hydrolysis of β -glycosidic linkages in live cells (Fig. 15a). Another promising approach is to use DNA origami structures loading with enzyme cargo for cellular delivery [142]. Ora et al. used tubular DNA origami to deliver Lucia luciferase into cells, facilitating the endocytosis process and protecting the enzyme activity during transportation process. In 2017, Nikolov et al. used DNA origami for the delivery of multiprotein complexes. In contrast to conventional nanomaterial endosome–lysosome uptake process, which may decrease protein activity and induce protein degradation, they used microfluidic “cell squeezing” to create transient holes on cell membrane, enabling multiprotein–origami complexes to directly enter cytoplasm [143]. Furthermore, Douglas et al. reported a unique aptamer-gated nanorobot loaded with combination of antibody fragments [144]. The aptamer locks can be opened by protein-induced displacement, activating the antibody within. The nanorobots were demonstrated to suppress Jun N-terminal

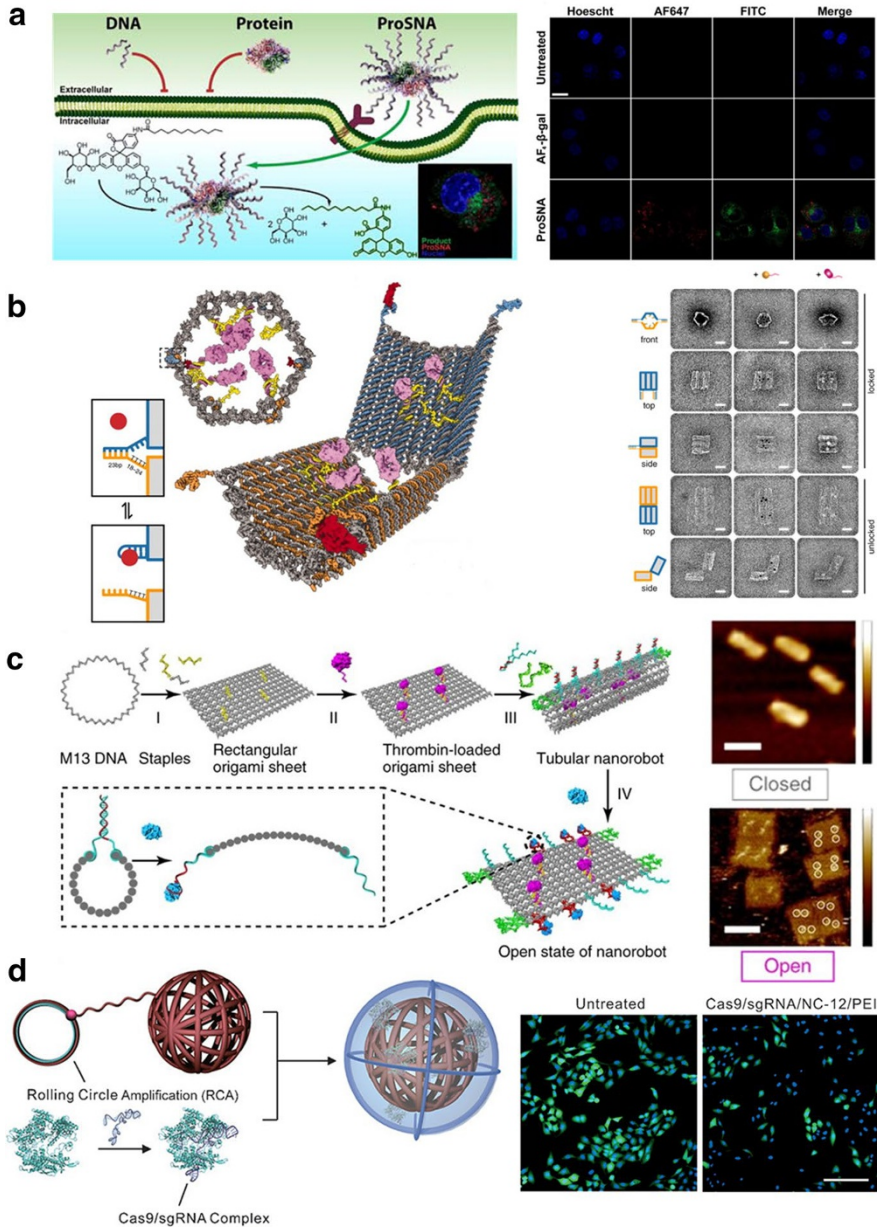


Fig. 15 Four examples of DNA–protein nanoassemblies for biomedical applications. **a** β gal ProSNA showed higher cellular uptake efficiency in several cell lines [140]. **b** An aptamer-gated nanorobot triggered by protein-induced displacement can be used to tune signaling pathway [144]. **c** A DNA origami-based nanorobot can release thrombin cargos at a specific site to inhibit tumor growth [145]. **d** Self-assembled DNA nanoclews can deliver CRISPR-Cas9 for gene editing [146]

kinase (JNK) and Akt (protein kinase B) cell-signaling in tissue culture (Fig. 15b). An example of using DNA origami structure loaded with enzymes for *in vivo* antitumor therapy has been reported by Li et al. [145]. They constructed a nanorobot consisting of thrombin-loaded origami structure and AS1411 DNA aptamer “lock” that binds nucleolin. At the initial state, nanorobot was in a closed conformation with loaded thrombin protected. When approaching the tumor site *in vivo*, overexpressed nucleolin bound to AS1411 and opened the aptamer “lock”, exposing the loaded thrombin molecules (Fig. 15c). The exposed thrombin induced the coagulation at the tumor site, resulting in intravascular thrombosis and inhibition of tumor growth.

Furthermore, DNA–protein nanoassemblies have been applied to deliver the CRISPR–Cas9 system, which is a revolutionary gene editing tool. One of the major barriers restricting its further clinical translation is the lack of safe and effective delivery vectors. Recently, DNA nanostructures have emerged as a promising delivery platform to deliver CRISPR–Cas9 for gene editing *in vivo*. Gu et al. constructed self-assembled DNA nanoclews through rolling-circle amplification [146]. Cas9/sgRNA is then loaded onto the surface of nanoclew through partial base-pair hybridization between sgRNA and DNA on nanoclew (Fig. 15d). Further compression of Cas9/sgRNA-loaded DNA nanoclew with polyethyleneimine facilitated its endosomal escape, improving gene editing efficiency. A Cas9–AuNP delivery system was reported by Murthy et al. [147]. Cas9/sgRNA complex was hybridized onto DNA-modified AuNP together with donor DNA. The system can simultaneously deliver Cas9/sgRNA and donor DNA to the target tissue through local administration, thereby achieving homology-mediated directional repair of dsDNA. They demonstrated the correction of the DNA mutation causing Duchenne muscular dystrophy in a mice model with minimal off-target effects.

In summary, the nanostructures reviewed here not only protect protein and DNA cargos from denaturation but also enhance the cellular uptake efficiency and *in vivo* efficacy. It is foreseeable that DNA–protein nanostructures of superior programmability and biocompatibility are promising drug delivery platforms with broad biomedical application prospects.

5 Conclusions and Perspectives

We have reviewed the research progress of synthetic DNA–protein conjugates over the past decades. Synthetic methods to efficiently conjugate nucleic acid with protein are summarized, including covalent coupling chemistries and non-covalent interactions. DNAs as well as proteins can both function in target recognition and signal transduction process, enabling a vast number of biosensor designs. We have surveyed the use of DNA–protein conjugate as an analytical tool for the detection of biomarkers, which are important for early diagnosis of diseases. The achievements in exploring DNA–protein conjugates for building functional nanostructures as well as developing novel therapeutic agents are also summarized. Specific properties of DNA–protein conjugates that have been leveraged to enable these applications are (1) the diverse conjugation chemistries which are stable in physiological conditions and applicable to different types of proteins without impact much on the biological

activities; (2) the combination of with both target recognition and signal amplification properties into one construct, enabling a variety of biosensors of high sensitivity; and (3) the ability of Watson–Crick hybridization that can organize proteins in 3D space with single-base spatial resolution.

Despite all the achievements, challenges still remain in developing and using DNA–protein conjugates. For example, non-covalent methods to construct DNA–protein conjugates do not have high binding affinity, while the covalent methods require cumbersome reaction procedures. Thus, a highly robust and facile synthetic approach compatible with native nucleic acids and proteins is still sought after. In addition, although DNA–protein conjugates have been used for in vitro clinical diagnosis, their applications for therapy and in vivo detection are still at early state. Possible reasons could be the batch-to-batch variations in preparing the samples and the difficulty in controlling the bioactivity in living systems. To develop optimized DNA–protein conjugates suitable for an even broader range of applications, we envision here three potential research strategies that may significantly improve the preparation process, the functionality, and the application of the conjugates. The first strategy is to employ enzymatic ligation to improve the synthesis process of DNA–protein conjugates. The second strategy is to incorporate stimuli-responsive motifs into the conjugate to dynamically control the biofunctions. Finally, novel synthetic biology and chemical biology tools that may facilitate the development of DNA–protein conjugate are needed.

A promising approach to speed up the preparation of DNA–protein conjugates is the use of enzymatic ligation method. Conventional conjugation methods based on coupling chemistry require the terminal-modified DNA sequences, leading to tedious synthesis and purification procedure. The bioactivity may also be largely affected. To solve the problems, DNA-binding enzymes in the replication initiator protein (Rep) family, such as porcine circovirus type 2 Rep (pRep) and Gene A*, can be genetically fused with the protein of interests, serving as binding sites for ssDNA [45]. Using this method, the engineered proteins can be covalently linked to ssDNA through sequence-dependent cleavage and ligation. The enzymatic ligation process is facile and efficient. It does not need any chemical modifications on DNAs and the reaction time is normally within 30 min. The enzymatic ligation method can be envisioned to be applied to many different types of proteins, revolutionizing the preparing of DNA–protein conjugates.

Up to now, using DNA–protein conjugates for sensing and biomedical applications in living system is still at a very early stage and only a few examples have been reported. The lack of spatial and temporal control over bioactivity may result in unexpected turn-on of the fluoresce and increased background signal during the delivery process, affecting the results obtained in vivo. To address this issue, stimuli-responsive strategies, which can enable spatial–temporal controlled activation of biofunctions, have been introduced to design DNA–protein conjugates. In particular, the DNA nanostructures can adapt photolabile or other stimuli-responsive motifs, serving as regulators to tune the activity of the associated proteins. One of the early works using photoactivation strategy was reported by Tan et al. [148]. They introduced azobenzene molecules into DNA duplex base pairs. By switching between UV and visible light, the *cis–trans* transitions of

azobenzene lead to duplex structure switching, thus changing the catalytic activities of GOx and HRP attached to the DNAs. In addition to photo control, some emerging studies have also been focusing on using biochemical stimuli to regulate the activity of the enzymes. For example, when β -lactamase was attached to four λ phage DNA branches, the enzymatic activity can be tuned up or down through unfolding or folding of the DNA branches [149]. The activity turn-on and turn-off can also be triggered by adding biomolecules such as specific DNA strands as “key” to open and close a 3D dynamic DNA origami nanocontainer [144]. Nonetheless, strategies to achieve high spatiotemporal control of the activity are highly required for advanced bioimaging and biosensing in live species.

Furthermore, ways to accelerate the development process of DNA–protein conjugates are in high demand. One potential direction is to adapt state-of-art chemical biology and synthetic biology tools to genetically express and assemble DNA–protein conjugate as a whole product in vivo. One method to genetically encode ssDNA in living bacteria is the use of reverse transcriptase [150]. Genetically encoded DNA–protein nanostructures have been reported recently using a cell-free transcription and translation mixture system [115]. If one can efficiently incorporate protein expression together with ssDNA expression in vivo, it is possible to achieve one-step biosynthesis of versatile DNA–protein conjugates using well-established yeast or *E. coli* systems. In this vein, large-scale, low-cost manufacturing of many different types of DNA–protein conjugates can be possibly realized without further purification, which potentially lowers development costs and facilitates development cycles. Further high-throughput screening technologies towards structure and activity optimization can then be developed to identify the best formulation for clinical applications.

To sum up, we foresee a bright future for the use of DNA–protein conjugate as a dual functional biomaterial that has great potential for diagnostic, therapeutic, and nanoassembly applications. We believe that further improvements in enzymatic ligation methods, stimuli-responsive structures, and advanced synthetic biology tools will facilitate the research and development cycles for DNA–protein conjugates. Multifunctional and robust biomaterials could then be achieved by integration of the protein libraries and the DNA nanostructures. The improved DNA–protein hybrid nanomaterials will afford a broader range of diagnostic applications from field tests to in situ single cell analysis. At the same time, the ability to create structure–function controlled DNA–protein nanostructures will help not only the understanding of biological processes but also the development of personalized medications.

Acknowledgements We thank Prof. Yi Lu (e-mail: yi-lu@illinois.edu) from the Department of Chemistry at the University of Illinois at Urbana-Champaign for valuable advice and discussion. We thank National Natural Science Foundation of China (No. 21877032), Hunan Province Talented Young Scientist Program (2019RS2021, 2019RS2023), and Fundamental Research Funds for the Central Universities from Hunan University for financial support.

Compliance with Ethical Standards

Conflict of interest The authors declare no competing financial interests.

References

1. Luscombe NM, Austin SE, Berman HM, Thornton JM (2000) An overview of the structures of protein–DNA complexes. *Genome Biol* 1(1):REVIEWS001
2. Jablonski E, Moomaw EW, Tullis RH, Ruth JL (1986) Preparation of oligodeoxynucleotide-alkaline phosphatase conjugates and their use as hybridization probes. *Nucleic Acids Res* 14(15):6115–6128
3. Sano T, Smith CL, Cantor CR (1992) Immuno-PCR: very sensitive antigen detection by means of specific antibody–DNA conjugates. *Science* 258(5079):120–122
4. Fredriksson S, Gullberg M, Jarvius J, Olsson C, Pietras K, Gustafsdottir SM, Ostman A, Landegren U (2002) Protein detection using proximity-dependent DNA ligation assays. *Nat Biotechnol* 20(5):473–477
5. Niemeyer CM, Sano T, Smith CL, Cantor CR (1994) Oligonucleotide-directed self-assembly of proteins: semisynthetic DNA–streptavidin hybrid molecules as connectors for the generation of macroscopic arrays and the construction of supramolecular bioconjugates. *Nucleic Acids Res* 22(25):5530–5539
6. Dong YC, Mao YD (2019) DNA origami as scaffolds for self-assembly of lipids and proteins. *ChemBioChem* 20(19):2422–2431
7. Bujold KE, Lacroix A, Sleiman HF (2018) DNA nanostructures at the interface with biology. *Chem* 4(3):495–521
8. McMillan JR, Hayes OG, Winegar PH, Mirkin CA (2019) Protein materials engineering with DNA. *Acc Chem Res* 52(7):1939–1948
9. Trads JB, Topping T, Gothelf KV (2017) Site-selective conjugation of native proteins with DNA. *Acc Chem Res* 50(6):1367–1374
10. Grossi G, Jaekel A, Andersen ES, Sacca B (2017) Enzyme-functionalized DNA nanostructures as tools for organizing and controlling enzymatic reactions. *Mrs Bull* 42(12):920–924
11. Niemeyer CM (2010) Semisynthetic DNA–protein conjugates for biosensing and nanofabrication. *Angew Chem Int Ed* 49(7):1200–1216
12. Leary JJ, Brigati DJ, Ward DC (1983) Rapid and sensitive colorimetric method for visualizing biotin-labeled DNA probes hybridized to DNA or RNA immobilized on nitrocellulose: bioblots. *Proc Natl Acad Sci USA* 80(13):4045–4049
13. Zhang Z, Hejlesen C, Kjelstrup MB, Birkedal V, Gothelf KV (2014) A DNA-mediated homogeneous binding assay for proteins and small molecules. *J Am Chem Soc* 136(31):11115–11120
14. Niemeyer CM, Adler M, Pignataro B, Lenhart S, Gao S, Chi L, Fuchs H, Blohm D (1999) Self-assembly of DNA–streptavidin nanostructures and their use as reagents in immuno-PCR. *Nucleic Acids Res* 27(23):4553–4561
15. Choi JW, Jo BG, deMello AJ, Choo J, Kim HY (2016) Streptavidin-triggered signal amplified fluorescence polarization for analysis of DNA–protein interactions. *Analyst* 141(24):6499–6502
16. Zhou Z, Xiang Y, Tong A, Lu Y (2014) Simple and efficient method to purify DNA–protein conjugates and its sensing applications. *Anal Chem* 86(8):3869–3875
17. Wong NY, Xing H, Tan LH, Lu Y (2013) Nano-encrypted Morse code: a versatile approach to programmable and reversible nanoscale assembly and disassembly. *J Am Chem Soc* 135(8):2931–2934
18. Hage DS (1999) Immunoassays. *Anal Chem* 71(12):294–304
19. He Y, Tian Y, Ribbe AE, Mao C (2006) Antibody nanoarrays with a pitch of approximately 20 nanometers. *J Am Chem Soc* 128(39):12664–12665
20. Goodman RP, Erben CM, Malo J, Ho WM, McKee ML, Kapanidis AN, Turberfield AJ (2009) A facile method for reversibly linking a recombinant protein to DNA. *ChemBioChem* 10(9):1551–1557
21. Uchinomiya SH, Nonaka H, Fujishima SH, Tsukiji S, Ojida A, Hamachi I (2009) Site-specific covalent labeling of His-tag fused proteins with a reactive Ni(II)-NTA probe. *Chem Commun* 39:5880–5882
22. Kapanidis AN, Ebricht YW, Ebricht RH (2001) Site-specific incorporation of fluorescent probes into protein: hexahistidine-tag-mediated fluorescent labeling with Ni(2+):nitrilotriacetic acid (n)-fluorochrome conjugates. *J Am Chem Soc* 123(48):12123–12125
23. Shen W, Zhong H, Neff D, Norton ML (2009) NTA directed protein nanopatterning on DNA origami nanoconstructs. *J Am Chem Soc* 131(19):6660–6661

24. Nimjee SM, White RR, Becker RC, Sullenger BA (2017) Aptamers as therapeutics. *Annu Rev Pharmacol Toxicol* 57:61–79
25. Lin C, Katilius E, Liu Y, Zhang J, Yan H (2006) Self-assembled signaling aptamer DNA arrays for protein detection. *Angew Chem Int Ed* 45(32):5296–5301
26. Lu Y, Liu J (2006) Functional DNA nanotechnology: emerging applications of DNazymes and aptamers. *Curr Opin Biotechnol* 17(6):580–588
27. Rinker S, Ke YG, Liu Y, Chhabra R, Yan H (2008) Self-assembled DNA nanostructures for distance-dependent multivalent ligand-protein binding. *Nature Nanotechnol* 3(7):418–422
28. Corey DR, Schultz PG (1987) Generation of a hybrid sequence-specific single-stranded deoxyribonuclease. *Science* 238(4832):1401
29. Ghosh SS, Kao PM, McCue AW, Chappelle HL (1990) Use of maleimide-thiol coupling chemistry for efficient syntheses of oligonucleotide-enzyme conjugate hybridization probes. *Bioconjug Chem* 1(1):71–76
30. Ma Y, Lv Z, Li T, Tian T, Lu L, Liu W, Zhu Z, Yang C (2018) Design and synthesis of orthophthalaldehyde phosphoramidite for single-step, rapid, efficient and chemoselective coupling of DNA with proteins under physiological conditions. *Chem Commun* 54(68):9434–9437
31. Ramil CP, Lin Q (2013) Bioorthogonal chemistry: strategies and recent developments. *Chem Commun (Camb)* 49(94):11007–11022
32. Laughlin ST, Bertozzi CR (2007) Metabolic labeling of glycans with azido sugars and subsequent glycan-profiling and visualization via Staudinger ligation. *Nat Protoc* 2(11):2930–2944
33. Spiccarich DR, Nolley R, Maund SL, Purcell SC, Herschel J, Iavarone AT, Peehl DM, Bertozzi CR (2017) Bioorthogonal labeling of human prostate cancer tissue slice cultures for glycoproteomics. *Angew Chem Int Ed* 56(31):8992–8997
34. Ghodke PP, Albertolle ME, Johnson KM, Guengerich FP (2019) Synthesis and characterization of site-specific O(6)-alkylguanine DNA-alkyl transferase-oligonucleotide crosslinks. *Curr Protoc Nucleic Acid Chem* 20:e74
35. Agard NJ, Prescher JA, Bertozzi CR (2005) A strain-promoted [3+2] azide-alkyne cycloaddition for covalent modification of biomolecules in living systems. *J Am Chem Soc* 127(31):11196–11196
36. Mukhortava A, Schlierf M (2016) Efficient formation of site-specific protein–DNA hybrids using copper-free click chemistry. *Bioconjug Chem* 27(7):1559–1563
37. Li J, Jia S, Chen PR (2014) Diels–Alder reaction-triggered bioorthogonal protein decaging in living cells. *Nat Chem Biol* 10(12):1003–1004
38. Wu HX, Devaraj NK (2016) Inverse electron-demand Diels–Alder bioorthogonal reactions. *Top Curr Chem* 374:3
39. Oliveira BL, Guo Z, Bernardes GJL (2017) Inverse electron demand Diels–Alder reactions in chemical biology. *Chem Soc Rev* 46(16):4895–4950
40. Ravasco JMM, Coelho JAS (2020) Predictive multivariate models for bioorthogonal inverse-electron demand Diels–Alder reactions. *J Am Chem Soc* 142(9):4235–4241
41. Synakewicz M, Bauer D, Rief M, Itzhaki LS (2019) Bioorthogonal protein–DNA conjugation methods for force spectroscopy. *Sci Rep-Uk* 20:9
42. Wang R, Lu D, Bai H, Jin C, Yan G, Ye M, Qiu L, Chang R, Cui C, Liang H, Tan W (2016) Using modified aptamers for site specific protein–aptamer conjugations. *Chem Sci* 7(3):2157–2161
43. Pujari SS, Zhang Y, Ji S, Distefano MD, Tretyakova NY (2018) Site-specific cross-linking of proteins to DNA via a new bioorthogonal approach employing oxime ligation. *Chem Commun* 54(49):6296–6299
44. Boeggeman E, Ramakrishnan B, Pasek M, Manzoni M, Puri A, Loomis KH, Waybright TJ, Qasba PK (2009) Site specific conjugation of fluoroprobes to the remodeled Fc *N*-glycans of monoclonal antibodies using mutant glycosyltransferases: application for cell surface antigen detection. *Bioconjug Chem* 20(6):1228–1236
45. Akter F, Mie M, Grimm S, Nygren P-Å, Kobatake E (2012) Detection of antigens using a protein–DNA chimera developed by enzymatic covalent bonding with phiX Gene A*. *Anal Chem* 84(11):5040–5046
46. Mie M, Niimi T, Mashimo Y, Kobatake E (2019) Construction of DNA-NanoLuc luciferase conjugates for DNA aptamer-based sandwich assay using Rep protein. *Biotechnol Lett* 41(3):357–362
47. Niemeyer CM, Wacker R, Adler M (2001) Hapten-Functionalized DNA-streptavidin nanocircles as supramolecular reagents in a competitive immuno-PCR assay. *Angew Chem Int Ed* 40(17):3169–3172

48. Yigit MV, Mazumdar D, Lu Y (2008) MRI detection of thrombin with aptamer functionalized superparamagnetic iron oxide nanoparticles. *Bioconjug Chem* 19(2):412–417
49. Liu J, Cao Z, Lu Y (2009) Functional nucleic acid sensors. *Chem Rev* 109(5):1948–1998
50. Sharma S, Byrne H, O’Kennedy RJ (2016) Antibodies and antibody-derived analytical biosensors. *Essays Biochem* 60(1):9–18
51. Lequin RM (2005) Enzyme immunoassay (EIA)/enzyme-linked immunosorbent assay (ELISA). *Clin Chem* 51(12):2415–2418
52. Niemeyer CM, Adler M, Wacker R (2005) Immuno-PCR: high sensitivity detection of proteins by nucleic acid amplification. *Trends Biotechnol* 23(4):208–216
53. Niemeyer CM, Adler M, Wacker R (2007) Detecting antigens by quantitative immuno-PCR. *Nat Protoc* 2(8):1918–1930
54. Barletta J, Bartolome A, Constantine NT (2009) Immunomagnetic quantitative immuno-PCR for detection of less than one HIV-1 virion. *J Virol Methods* 157(2):122–132
55. Malou N, Raoult D (2011) Immuno-PCR: a promising ultrasensitive diagnostic method to detect antigens and antibodies. *Trends Microbiol* 19(6):295–302
56. van Buggenum JA, Gerlach JP, Eising S, Schoonen L, van Eijl RA, Tanis SE, Hogeweg M, Hubner NC, van Hest JC, Bongers KM, Mulder KW (2016) A covalent and cleavable antibody–DNA conjugation strategy for sensitive protein detection via immuno-PCR. *Sci Rep* 6:22675
57. Kazane SA, Sok D, Cho EH, Uson ML, Kuhn P, Schultz PG, Smider VV (2012) Site-specific DNA-antibody conjugates for specific and sensitive immuno-PCR. *Proc Natl Acad Sci USA* 109(10):3731–3736
58. Heid CA, Stevens J, Livak KJ, Williams PM (1996) Real time quantitative PCR. *Genome Res* 6(10):986–994
59. Hindson BJ, Ness KD, Masquelier DA, Belgrader P, Heredia NJ, Makarewicz AJ, Bright IJ, Lucero MY, Hiddessen AL, Legler TC, Kitano TK, Hodel MR, Petersen JF, Wyatt PW, Steenblock ER, Shah PH, Bousse LJ, Troup CB, Mellen JC, Wittmann DK, Erndt NG, Cauley TH, Koehler RT, So AP, Dube S, Rose KA, Montesclaros L, Wang S, Stumbo DP, Hodges SP, Romine S, Milanovich FP, White HE, Regan JF, Karlin-Neumann GA, Hindson CM, Saxonov S, Colston BW (2011) High-throughput droplet digital PCR system for absolute quantitation of DNA copy number. *Anal Chem* 83(22):8604–8610
60. Saka SK, Wang Y, Kishi JY, Zhu A, Zeng YT, Xie WX, Kirli K, Yapp C, Cicconet M, Beliveau BJ, Lapan SW, Yin SY, Lin M, Boyden ES, Kaeser PS, Pihan G, Church GM, Yin P (2019) Immuno-SABER enables highly multiplexed and amplified protein imaging in tissues. *Nature Biotechnol* 37(9):1080
61. Liang H, Cordova SE, Kieft TL, Rogelj S (2003) A highly sensitive immuno-PCR assay for detecting Group A Streptococcus. *J Immunol Methods* 279(1–2):101–110
62. Huang SH, Chang TC (2004) Detection of *Staphylococcus aureus* by a sensitive immuno-PCR assay. *Clin Chem* 50(9):1673–1674
63. Cao Y, Kopplov K, Liu GY (2000) In-situ immuno-PCR to detect antigens. *Lancet* 356(9234):1002–1003
64. Guo YC, Zhou YF, Zhang XE, Zhang ZP, Qiao YM, Bi LJ, Wen JK, Liang MF, Zhang JB (2006) Phage display mediated immuno-PCR. *Nucleic Acids Res* 34(8):e62
65. Deng MJ, Xiao XZ, Zhang YM, Wu XH, Zhu LH, Xin XQ, Wu DL (2011) A highly sensitive immuno-PCR assay for detection of H5N1 avian influenza virus. *Mol Biol Rep* 38(3):1941–1948
66. Spengler M, Adler M, Niemeyer CM (2015) Highly sensitive ligand-binding assays in pre-clinical and clinical applications: immuno-PCR and other emerging techniques. *Analyst* 140(18):6175–6194
67. Gullberg M, Gustafsdottir SM, Schallmeiner E, Jarvius J, Bjarnegard M, Betsholtz C, Landegren U, Fredriksson S (2004) Cytokine detection by antibody-based proximity ligation. *Proc Natl Acad Sci USA* 101(22):8420–8424
68. Schallmeiner E, Oksanen E, Ericsson O, Spangberg L, Eriksson S, Stenman UH, Pettersson K, Landegren U (2007) Sensitive protein detection via triple-binder proximity ligation assays. *Nat Methods* 4(2):135–137
69. Koos B, Cane G, Grannas K, Lof L, Arngarden L, Heldin J, Clausson CM, Klaesson A, Hirvonen MK, de Oliveira FM, Talibov VO, Pham NT, Auer M, Danielson UH, Haybaeck J, Kamali-Moghaddam M, Soderberg O (2015) Proximity-dependent initiation of hybridization chain reaction. *Nat Commun* 6:7294

70. Zhang H, Li X-F, Le XC (2012) Binding-induced DNA assembly and its application to yoctomole detection of proteins. *Anal Chem* 84(2):877–884
71. Li F, Lin Y, Le XC (2013) Binding-induced formation of DNA three-way junctions and its application to protein detection and DNA strand displacement. *Anal Chem* 85(22):10835–10841
72. Tang Y, Wang Z, Yang X, Chen J, Liu L, Zhao W, Le XC, Li F (2015) Constructing real-time, wash-free, and reiterative sensors for cell surface proteins using binding-induced dynamic DNA assembly. *Chem Sci* 6(10):5729–5733
73. Wu D, Yan J, Shen X, Sun Y, Thulin M, Cai Y, Wik L, Shen Q, Oelrich J, Qian X, Dubois KL, Ronquist KG, Nilsson M, Landegren U, Kamali-Moghaddam M (2019) Profiling surface proteins on individual exosomes using a proximity barcoding assay. *Nat Commun* 10:3854
74. Li G, Montgomery JE, Eckert MA, Chang JW, Tienda SM, Lengyel E, Moellering RE (2017) An activity-dependent proximity ligation platform for spatially resolved quantification of active enzymes in single cells. *Nat Commun* 8:1775
75. Fredriksson S, Dixon W, Ji H, Koong AC, Mindrinos M, Davis RW (2007) Multiplexed protein detection by proximity ligation for cancer biomarker validation. *Nat Methods* 4(4):327–329
76. Li P, Medon PP, Skingle DC, Lanser JA, Symons RH (1987) Enzyme-linked synthetic oligonucleotide probes: non-radioactive detection of enterotoxigenic *Escherichia coli* in faecal specimens. *Nucleic Acids Res* 15(13):5275–5287
77. Urdea MS, Warner BD, Running JA, Stempien M, Clyne J, Horn T (1988) A comparison of non-radioisotopic hybridization assay methods using fluorescent, chemiluminescent and enzyme labeled synthetic oligodeoxyribonucleotide probes. *Nucleic Acids Res* 16(11):4937–4956
78. Li Y, Sun L, Zhao Q (2019) Aptamer-structure switch coupled with horseradish peroxidase labeling on a microplate for the sensitive detection of small molecules. *Anal Chem* 91(4):2615–2619
79. Oh SW, Pereira A, Zhang T, Li T, Lane A, Fu J (2018) DNA-mediated proximity-based assembly circuit for actuation of biochemical reactions. *Angew Chem Int Ed* 57(40):13086–13090
80. Ho NRY, Lim GS, Sundah NR, Lim D, Loh TP, Shao H (2018) Visual and modular detection of pathogen nucleic acids with enzyme–DNA molecular complexes. *Nat Commun* 9:3238
81. Yang H (2012) Enzyme-based ultrasensitive electrochemical biosensors. *Curr Opin Chem Biol* 16(3):422–428
82. Liu G, Wan Y, Gau V, Zhang J, Wang L, Song S, Fan C (2008) An enzyme-based E-DNA sensor for sequence-specific detection of femtomolar DNA targets. *J Am Chem Soc* 130(21):6820–6825
83. Povedano E, Valverde A, Montiel VR-V, Pedrero M, Yáñez-Sedeño P, Barderas R, San Segundo-Acosta P, Peláez-García A, Mendiola M, Hardisson D, Campuzano S, Pingarrón JM (2018) Rapid electrochemical assessment of tumor suppressor gene methylations in raw human serum and tumor cells and tissues using immunomagnetic beads and selective DNA hybridization. *Angew Chem Int Ed* 57(27):8194–8198
84. Quesada-González D, Merkoçi A (2018) Nanomaterial-based devices for point-of-care diagnostic applications. *Chem Soc Rev* 47(13):4697–4709
85. Xiang Y, Lu Y (2011) Using personal glucose meters and functional DNA sensors to quantify a variety of analytical targets. *Nat Chem* 3:697
86. Xiang Y, Lu Y (2012) Using commercially available personal glucose meters for portable quantification of DNA. *Anal Chem* 84(4):1975–1980
87. Zhang J, Xiang Y, Novak DE, Hoganson GE, Zhu J, Lu Y (2015) Using a personal glucose meter and alkaline phosphatase for point-of-care quantification of galactose-1-phosphate uridylyltransferase in clinical galactosemia diagnosis. *Chem Asian J* 10(10):2221–2227
88. Gu C, Lan T, Shi H, Lu Y (2015) Portable detection of melamine in milk using a personal glucose meter based on an in vitro selected structure-switching aptamer. *Anal Chem* 87(15):7676–7682
89. Gu Y, Zhang T-T, Huang Z-F, Hu S-W, Zhao W, Xu J-J, Chen H-Y (2018) An exploration of nucleic acid liquid biopsy using a glucose meter. *Chem Sci* 9(14):3517–3522
90. Zhang J, Shen Z, Xiang Y, Lu Y (2016) Integration of solution-based assays onto lateral flow device for one-step quantitative point-of-care diagnostics using personal glucose meter. *ACS Sens* 1(9):1091–1096
91. Zhang J, Lu Y (2018) Biocomputing for portable, resettable, and quantitative point-of-care diagnostics: making the glucose meter a logic-gate responsive device for measuring many clinically relevant targets. *Angew Chem Int Ed* 57(31):9702–9706
92. Xing H, Zhang CL, Ruan G, Zhang J, Hwang K, Lu Y (2016) Multimodal detection of a small molecule target using stimuli-responsive liposome triggered by aptamer–enzyme conjugate. *Anal Chem* 88(3):1506–1510

93. Fu SZ, Zhang XQ, Xie YZ, Wu J, Ju HX (2017) An efficient enzyme-powered micromotor device fabricated by cyclic alternate hybridization assembly for DNA detection. *Nanoscale* 9(26):9026–9033
94. Niemeyer CM, Ceyhan B (2001) DNA-directed functionalization of colloidal gold with proteins. *Angew Chem Int Ed* 40(19):3685–3688
95. Hazarika P, Kukulka F, Niemeyer CM (2006) Reversible binding of fluorescent proteins at DNA–gold nanoparticles. *Angew Chem Int Ed* 45(41):6827–6830
96. Breger JC, Buckhout-White S, Walper SA, Oh E, Susumu K, Ancona MG, Medintz IL (2017) Assembling high activity phosphotriesterase composites using hybrid nanoparticle peptide–DNA scaffolded architectures. *Nano Futures* 1(1):011002
97. Lu H, Schöps O, Woggon U, Niemeyer CM (2008) Self-assembled donor comprising quantum dots and fluorescent proteins for long-range fluorescence resonance energy transfer. *J Am Chem Soc* 130(14):4815–4827
98. Zhu Z, Wu C, Liu H, Zou Y, Zhang X, Kang H, Yang CJ, Tan W (2010) An aptamer cross-linked hydrogel as a colorimetric platform for visual detection. *Angew Chem Int Ed* 49(6):1052–1056
99. Zhang J, Xing H, Lu Y (2018) Translating molecular detections into a simple temperature test using a target-responsive smart thermometer. *Chem Sci* 9(16):3906–3910
100. Seeman NC (1982) Nucleic acid junctions and lattices. *J Theor Biol* 99(2):237–247
101. Niemeyer CM (2002) The developments of semisynthetic DNA–protein conjugates. *Trends Biotechnol* 20(9):395–401
102. Yan H, Park SH, Finkelstein G, Reif JH, LaBean TH (2003) DNA-templated self-assembly of protein arrays and highly conductive nanowires. *Science* 301(5641):1882–1884
103. Li HY, Park SH, Reif JH, LaBean TH, Yan H (2004) DNA-templated self-assembly of protein and nanoparticle linear arrays. *J Am Chem Soc* 126(2):418–419
104. Kuzuya A, Numajiri K, Komiyama M (2008) Accommodation of a single protein guest in nanometer-scale wells embedded in a "DNA Nanotape". *Angew Chem Int Ed* 47(18):3400–3402
105. Liu Y, Ke Y, Yan H (2005) Self-assembly of symmetric finite-size DNA nanoarrays. *J Am Chem Soc* 127(49):17140–17141
106. Selmi DN, Adamson RJ, Attrill H, Goddard AD, Gilbert RJ, Watts A, Turberfield AJ (2011) DNA-templated protein arrays for single-molecule imaging. *Nano Lett* 11(2):657–660
107. Xu Y, Jiang S, Simmons CR, Narayanan RP, Zhang F, Aziz AM, Yan H, Stephanopoulos N (2019) Tunable nanoscale cages from self-assembling DNA and protein building blocks. *ACS Nano*
108. Lee JH, Wong NY, Tan LH, Wang Z, Lu Y (2010) Controlled alignment of multiple proteins and nanoparticles with nanometer resolution via backbone-modified phosphorothioate DNA and bifunctional linkers. *J Am Chem Soc* 132(26):8906–8908
109. Wong NY, Zhang C, Tan LH, Lu Y (2011) Site-specific attachment of proteins onto a 3D DNA tetrahedron through backbone-modified phosphorothioate DNA. *Small* 7(10):1427–1430
110. Meyer R, Niemeyer CM (2011) Orthogonal protein decoration of DNA nanostructures. *Small* 7(22):3211–3218
111. Niemeyer CM, Koehler J, Wuerdemann C (2002) DNA-directed assembly of bienzymic complexes from in vivo biotinylated NAD(P)H:FMN oxidoreductase and luciferase. *ChemBioChem* 3(2–3):242–245
112. Wilner OI, Weizmann Y, Gill R, Lioubashevski O, Freeman R, Willner I (2009) Enzyme cascades activated on topologically programmed DNA scaffolds. *Nature Nanotechnol* 4(4):249–254
113. Shen WQ, Bruist MF, Goodman SD, Seeman NC (2004) A protein-driven DNA device that measures the excess binding energy of proteins that distort DNA. *Angew Chem Int Ed* 43(36):4750–4752
114. Malo J, Mitchell JC, Vénien-Bryan C, Harris JR, Wille H, Sherratt DJ, Turberfield AJ (2005) Engineering a 2D protein–DNA crystal. *Angew Chem Int Ed* 44(20):3057–3061
115. Praetorius F, Dietz H (2017) Self-assembly of genetically encoded DNA–protein hybrid nanoscale shapes. *Science* 355:6331
116. Rothmund PWK (2006) Folding DNA to create nanoscale shapes and patterns. *Nature* 440(7082):297–302
117. Mikkilä J, Eskelinen AP, Niemela EH, Linko V, Frilander MJ, Torma P, Kostiaainen MA (2014) Virus-encapsulated DNA origami nanostructures for cellular delivery. *Nano Lett* 14(4):2196–2200
118. Fu J, Liu M, Liu Y, Woodbury NW, Yan H (2012) Interenzyme substrate diffusion for an enzyme cascade organized on spatially addressable DNA nanostructures. *J Am Chem Soc* 134(12):5516–5519

119. Ke G, Liu M, Jiang S, Qi X, Yang YR, Wootten S, Zhang F, Zhu Z, Liu Y, Yang CJ, Yan H (2016) Directional regulation of enzyme pathways through the control of substrate channeling on a DNA origami scaffold. *Angew Chem Int Ed* 55(26):7483–7486
120. Sprengel A, Lill P, Stegemann P, Bravo-Rodriguez K, Schoneweiss EC, Merdanovic M, Gudnason D, Aznauryan M, Gamrad L, Barcikowski S, Sanchez-Garcia E, Birkedal V, Gatsogiannis C, Ehrmann M, Sacca B (2017) Tailored protein encapsulation into a DNA host using geometrically organized supramolecular interactions. *Nat Commun* 8:14472
121. Linko V, Eerikainen M, Kostiaainen MA (2015) A modular DNA origami-based enzyme cascade nanoreactor. *Chem Commun* 51(25):5351–5354
122. Voigt NV, Topping T, Rotaru A, Jacobsen MF, Ravnsbaek JB, Subramani R, Mamdouh W, Kjems J, Mokhir A, Besenbacher F, Gothelf KV (2010) Single-molecule chemical reactions on DNA origami. *Nat Nanotechnol* 5(3):200–203
123. Dong Y, Chen S, Zhang S, Sodroski J, Yang Z, Liu D, Mao Y (2018) Folding DNA into a lipid-conjugated nanobarrel for controlled reconstitution of membrane proteins. *Angew Chem Int Ed* 57(8):2072–2076
124. Kosuri P, Altheimer BD, Dai MJ, Yin P, Zhuang XW (2019) Rotation tracking of genome-processing enzymes using DNA origami rotors. *Nature* 572(7767):136
125. Liu MH, Fu JL, Hejesen C, Yang YH, Woodbury NW, Gothelf K, Liu Y, Yan H (2013) A DNA tweezer-actuated enzyme nanoreactor. *Nat Commun* 4:2127
126. Grossi G, Jepsen MDE, Kjems J, Andersen ES (2017) Control of enzyme reactions by a reconfigurable DNA nanovault. *Nat Commun* 8:992
127. Zhao Z, Fu J, Dhakal S, Johnson-Buck A, Liu M, Zhang T, Woodbury NW, Liu Y, Walter NG, Yan H (2016) Nanocaged enzymes with enhanced catalytic activity and increased stability against protease digestion. *Nat Commun* 7:10619
128. Gao YN, Roberts CC, Zhu J, Lin JL, Chang CEA, Wheeldon I (2015) Tuning enzyme kinetics through designed intermolecular interactions far from the active site. *ACS Catal* 5(4):2149–2153
129. Martin TG, Bharat TAM, Joerger AC, Bai XC, Praetorius F, Fersht AR, Dietz H, Scheres SHW (2016) Design of a molecular support for cryo-EM structure determination. *Proc Natl Acad Sci USA* 113(47):E7456–E7463
130. Strable E, Johnson JE, Finn MG (2004) Natural nanochemical building blocks: icosahedral virus particles organized by attached oligonucleotides. *Nano Lett* 4(8):1385–1389
131. Cigler P, Lytton-Jean AKR, Anderson DG, Finn MG, Park SY (2010) DNA-controlled assembly of a NaTl lattice structure from gold nanoparticles and protein nanoparticles. *Nat Mater* 9(11):918–922
132. Brodin JD, Auyeung E, Mirkin CA (2015) DNA-mediated engineering of multicomponent enzyme crystals. *Proc Natl Acad Sci USA* 112(15):4564
133. Macfarlane RJ, Lee B, Jones MR, Harris N, Schatz GC, Mirkin CA (2011) Nanoparticle superlattice engineering with DNA. *Science* 334(6053):204–208
134. McMillan JR, Brodin JD, Millan JA, Lee B, Olvera de la Cruz M, Mirkin CA (2017) Modulating nanoparticle superlattice structure using proteins with tunable bond distributions. *J Am Chem Soc* 139(5):1754–1757
135. Hayes OG, McMillan JR, Lee B, Mirkin CA (2018) DNA-encoded protein Janus nanoparticles. *J Am Chem Soc* 140(29):9269–9274
136. McMillan JR, Mirkin CA (2018) DNA-functionalized, bivalent proteins. *J Am Chem Soc* 140(22):6776–6779
137. Kashiwagi D, Sim S, Niwa T, Taguchi H, Aida T (2018) Protein nanotube selectively cleavable with DNA: supramolecular polymerization of “DNA-appended molecular chaperones”. *J Am Chem Soc* 140(1):26–29
138. McMillan JR, Hayes OG, Remis JP, Mirkin CA (2018) Programming protein polymerization with DNA. *J Am Chem Soc* 140(46):15950–15956
139. Teller C, Willner I (2010) Organizing protein–DNA hybrids as nanostructures with programmed functionalities. *Trends Biotechnol* 28(12):619–628
140. Brodin JD, Sprangers AJ, McMillan JR, Mirkin CA (2015) DNA-mediated cellular delivery of functional enzymes. *J Am Chem Soc* 137(47):14838–14841
141. Choi CH, Hao L, Narayan SP, Auyeung E, Mirkin CA (2013) Mechanism for the endocytosis of spherical nucleic acid nanoparticle conjugates. *Proc Natl Acad Sci USA* 110(19):7625–7630
142. Ora A, Järvihaavisto E, Zhang H, Auvinen H, Santos HA, Kostiaainen MA, Linko V (2016) Cellular delivery of enzyme-loaded DNA origami. *Chem Commun* 52(98):14161–14164

143. Nikolov PM, Kossmann KJ, Schilling A, Angelin A, Brglez J, Klein A, Tampe R, Rabe KS, Niemeyer CM (2017) Cytosolic delivery of large supramolecular protein complexes arranged on DNA nanopegboards. *bioRxiv* 20:236729
144. Douglas SM, Bachelet I, Church GM (2012) A logic-gated nanorobot for targeted transport of molecular payloads. *Science (New York, NY)* 335(6070):831
145. Li S, Jiang Q, Liu S, Zhang Y, Tian Y, Song C, Wang J, Zou Y, Anderson GJ, Han J-Y, Chang Y, Liu Y, Zhang C, Chen L, Zhou G, Nie G, Yan H, Ding B, Zhao Y (2018) A DNA nanorobot functions as a cancer therapeutic in response to a molecular trigger in vivo. *Nature Biotechnol* 36:258
146. Sun WJ, Ji WY, Hall JM, Hu QY, Wang C, Beisel CL, Gu Z (2015) Self-assembled DNA nanoclews for the efficient delivery of CRISPR-Cas9 for genome editing. *Angew Chem Int Ed* 54(41):12029–12033
147. Lee K, Conboy M, Park HM, Jiang F, Kim HJ, Dewitt MA, Mackley VA, Chang K, Rao A, Skinner C, Shobha T, Mehdipour M, Liu H, Huang WC, Lan F, Bray NL, Li S, Corn JE, Kataoka K, Doudna JA, Conboy I, Murthy N (2017) Nanoparticle delivery of Cas9 ribonucleoprotein and donor DNA in vivo induces homology-directed DNA repair. *Nat Biomed Eng* 1:889–901
148. You M, Wang R-W, Zhang X, Chen Y, Wang K, Peng L, Tan W (2011) Photon-regulated DNA-enzymatic nanostructures by molecular assembly. *ACS Nano* 5(12):10090–10095
149. Rudiuk S, Venancio-Marques A, Baigl D (2012) Enhancement and modulation of enzymatic activity through higher-order structural changes of giant DNA–protein multibranch conjugates. *Angew Chem Int Ed* 51(51):12694–12698
150. Elbaz J, Yin P, Voigt CA (2016) Genetic encoding of DNA nanostructures and their self-assembly in living bacteria. *Nat Commun* 7:11179

Publisher's Note Springer Nature remains neutral with regard to jurisdictional claims in published maps and institutional affiliations.



DNA-Scaffolded Proximity Assembly and Confinement of Multienzyme Reactions

Jinglin Fu^{1,2} · Zhicheng Wang^{1,2} · Xiao Hua Liang¹ · Sung Won Oh² · Ezry St. Iago-McRae² · Ting Zhang¹

Received: 21 October 2019 / Accepted: 7 March 2020 / Published online: 4 April 2020
© Springer Nature Switzerland AG 2020

Abstract

Cellular functions rely on a series of organized and regulated multienzyme cascade reactions. The catalytic efficiencies of these cascades depend on the precise spatial organization of the constituent enzymes, which is optimized to facilitate substrate transport and regulate activities. Mimicry of this organization in a non-living, artificial system would be very useful in a broad range of applications—with impacts on both the scientific community and society at large. Self-assembled DNA nanostructures are promising applications to organize biomolecular components into prescribed, multidimensional patterns. In this review, we focus on recent progress in the field of DNA-scaffolded assembly and confinement of multienzyme reactions. DNA self-assembly is exploited to build spatially organized multienzyme cascades with control over their relative distance, substrate diffusion paths, compartmentalization and activity actuation. The combination of addressable DNA assembly and multienzyme cascades can deliver breakthroughs toward the engineering of novel synthetic and biomimetic reactors.

Keywords Biomimetic systems · DNA nanotechnology · DNA scaffolded assembly · Enzyme encapsulation · Enzyme immobilization · Enzyme regulation · Multienzyme cascade · Synthetic reactors

Abbreviations

BG Benzylguanine
BQ Benzoquinone

Chapter 5 was originally published as Fu, J., Wang, Z., Liang, X. H., Oh, S. W., St. Iago-McRae, E. & Zhang, T. Topics in Current Chemistry (2020) 378: 38. <https://doi.org/10.1007/s41061-020-0299-3>.

✉ Jinglin Fu
jinglin.fu@rutgers.edu

¹ Department of Chemistry, Rutgers University–Camden, Camden, NJ 08102, USA

² Center for Computational and Integrative Biology, Rutgers University–Camden, Camden, NJ 08102, USA

CH	Chlorohexane
DSS	Disuccinimidyl suberate
DTPC	DNA-templated protein conjugation
DX	Double-crossover DNA tile
G6PDH	Glucose-6-phosphate dehydrogenase
GOx	Glucose oxidase
HRP	Horseradish peroxidase
IDE	Inhibitor–DNA–enzyme
LDH	Lactate dehydrogenase
MDH	Malic dehydrogenase
MTG	Microbial transglutaminase
NHS	<i>N</i> -hydroxysuccinimide
NiR	Nitrite reductase
ORBIT	Origami-rotor-based imaging and tracking
Paz	Pseudoazurin
Pg	Plasminogen
PLP	Pyridoxal 5'-phosphate
SK	Streptokinase
SMCC	Succinimidyl-4-(<i>N</i> -maleimidomethyl) cyclohexane-1-carboxylate
SPDP	Succinimidyl 3-(2-pyridyldithio) propionate
STVs	Streptavidins
TAL	Transcription activator-like

1 Introduction

Multistep enzyme pathways play critical roles in cellular metabolism that produces biomolecules and harvests energy for sustaining and propagating living systems. As of 2019, 7727 different enzymes have been recorded in the BRENDA database, a comprehensive enzyme information system, including enzymes found in human cells and bacteria. These enzymes catalyze more than 5000 different biochemical reactions in the human body [1]. Enzyme cascades are highly sophisticated systems that control and regulate thousands of chemical reactions in cells. Peter Roach described chaos reactions with a set of spatio-temporally disorganized enzymes as a symphony without a conductor [2] (Fig. 1a). Enzyme cascades, therefore, can behave as a conductor of a symphony, controlling and guiding biochemical reactions into productive and coordinated pathways. The functions of many pathways critically depend on the relative position, orientation and number of participating enzymes [3, 4]. Living things have evolved several strategies to organize and confine multienzyme reactions. One such strategy is a protein scaffold, such as the long, glycoprotein “scaffold” used by cellulosomes to selectively integrate various cellulases and xylanases into a proximity complex for the efficient binding and degradation of cellulose [5] (Fig. 1b). Another example is substrate channeling; as shown in Fig. 1c, an indole tunnel observed in a tryptophan synthase $\alpha_2\beta_2$ complex passes indole intermediates between active sites of the alpha subunit and beta subunit at a very rapid rate of 1000 s^{-1} or faster [6]. A third biological strategy,

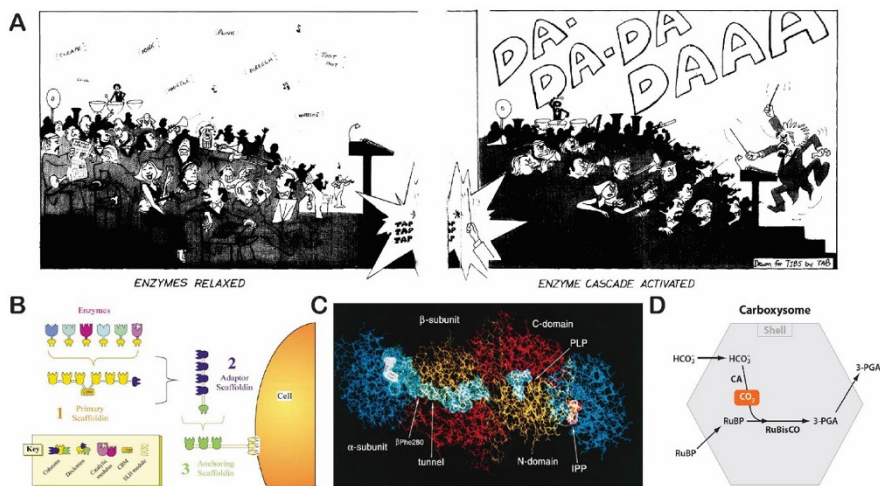


Fig. 1 Cellular multienzyme cascade pathways. **a** A cartoon of symphony performance to describe the integrated and regulatory function of enzyme cascades. Reproduced from Roach [2], with permission, copyright 1977, *Trends in Biochemical Sciences*. **b** The proximity assembly of enzymes on a protein scaffold in a cellulosome. Reproduced from Bayor et al. [5], with permission, copyright 2004, *Annual Review of Microbiology*. **c** Substrate channeling in tryptophan synthase. Reproduced from Miles et al. [6], with permission, copyright 1999, American Society for Biochemistry and Molecular Biology. **d** Confined carbon dioxide (CO_2) fixation in a carboxysome. Reproduced from Yeates et al. [7], with permission, copyright 2010, *Annual Review of Biophysics*

compartmentalization, shown in Fig. 1d, is used by bacterial carboxysomes to carry out carbon dioxide (CO_2) fixation [7].

The ability to exert control over these biochemical pathways on the nanoscale will not only increase our understanding of cellular metabolism, but also provide innovative tools to mimic and translate cellular mechanisms into non-living artificial systems for novel applications. Recent decades have seen the development of various approaches to create artificial multienzyme complexes, including genetic fusion [8], chemical crosslinking [9], surface co-immobilization [10], polymer vesicles [11–13] and virus-like particles [14, 15]. However, several obstacles remain in terms of their broader applications, such as limited control over the spatial arrangement (sizes and shapes), low encapsulation yield of large proteins due to steric hindrance, insufficient access of substrates to enzyme assemblies and aggregation of vesicle shells. It also remains challenging to engineer biomimetic functions on nanoreactors, such as artificial nanopores that govern the transmembrane diffusion of molecules and the feedback regulation of enzyme functions.

Double-stranded DNA (dsDNA) is a self-assembling biopolymer that is directed by Watson–Crick base pairing. Ned Seeman first proposed and demonstrated that artificially branched DNA tiles could be assembled by rationally designed single-stranded DNA (ssDNA) [16]. Such structures can have complex shapes beyond those attained by biological evolution and can be designed using “simple” elements, such as the “Holliday” junction (Fig. 2a) and double-crossover (DX) tiles (Fig. 2b) [16–19]. Two key breakthroughs in structural DNA nanotechnology are

Fig. 2 Overview of structural DNA nanotechnology. **a** A four-way “Holliday” junction. Reproduced from Seeman [19], with permission, copyright 2003, Springer Nature. **b** DNA double-crossover (left) and triple-crossover (right) tiles. Reproduced from Zadegan and Norton [18], with permission, copyright 2012, MDPI. **c** DNA origami assembly. Reproduced from Rothemund [20], with permission, copyright 2006, Springer Nature. **d** Assembly of single-stranded DNA tiles. Reproduced from Wei et al. [21], with permission, copyright 2012, Springer Nature. **e** DNA scaffold-directed assembly of biomolecular complexes. Reproduced from Fu et al. [36], with permission, copyright 2019, John Wiley and Sons

scaffolded DNA origami, invented by Paul Rothemund in 2006 (Fig. 2b) [20], and ssDNA tiles (SST), reported by Peng Yin in 2012 (Fig. 2c) [21, 22]. These methods have empowered the design and fabrication of complex and multidimensional nanostructures, including one-dimensional (1D) nanotubes, two-dimensional (2D) rectangular or triangular shapes [20], curved containers [23, 24], nanoscale polyhedrons [25], polyhedral meshes [26, 27] and periodic DNA crystals [28, 29]. Recent progress has been made to scale up DNA assemblies in terms of size and quantity [30] and to fold nanostructures with single-stranded nucleic acids [31]. To facilitate the design of DNA nanostructures, several computational tools, including TIAMAT [32], NUPACK [33], caDNAo [34] and CanDo [35], have been developed that benefit researchers worldwide.

DNA nanostructures are promising assembly scaffolds for positioning other elements into diverse patterns at the nanoscale [36, 37]. As shown in Fig. 2d, DNA scaffold-directed assembly has the advantages of programmable and prescribed geometry, sequence-addressable assembly and adaptability to various bioconjugations [36]. Utilizing these unique features, Researchers have used DNA nanostructures to assemble complex biomolecular systems, such as multienzyme complexes, protein confinement and biomimetic channeling [37, 38]. They have also been used to guide the assembly of synthetic vesicles, including membrane confinement [39, 40] and transmembrane nanopores [41, 42].

In this review, we summarize and discuss the recent progress in the field of DNA scaffold-directed assembly of multienzyme reactions, including proximity assembly, confinement, biomimetic substrate channeling and regulation circuits, as well as bioconjugation techniques of hybrid DNA–protein structures.

2 Protein–DNA Bioconjugation

A variety of chemical methods have been developed to attach proteins to DNA nanostructures [37, 43]. Most DNA–protein conjugations can fall into one of three categories: covalent crosslinking, noncovalent binding and fusion tags (summarized in Table 1). Covalent crosslinking usually involves conjugation of an existing amino acid group (e.g. primary amine or thiol) on the protein surface to a chemically modified oligonucleotide. For example, succinimidyl-4-(*N*-maleimidomethyl) cyclohexane-1-carboxylate (SMCC) and succinimidyl 3-(2-pyridyldithio) propionate (SPDP) are two widely used crosslinkers that conjugate a primary amine from a lysine residue on an enzyme surface to a thiol-modified oligonucleotide [44, 45]. The difference between the two crosslinkers is that the disulfide linkage of SPDP is

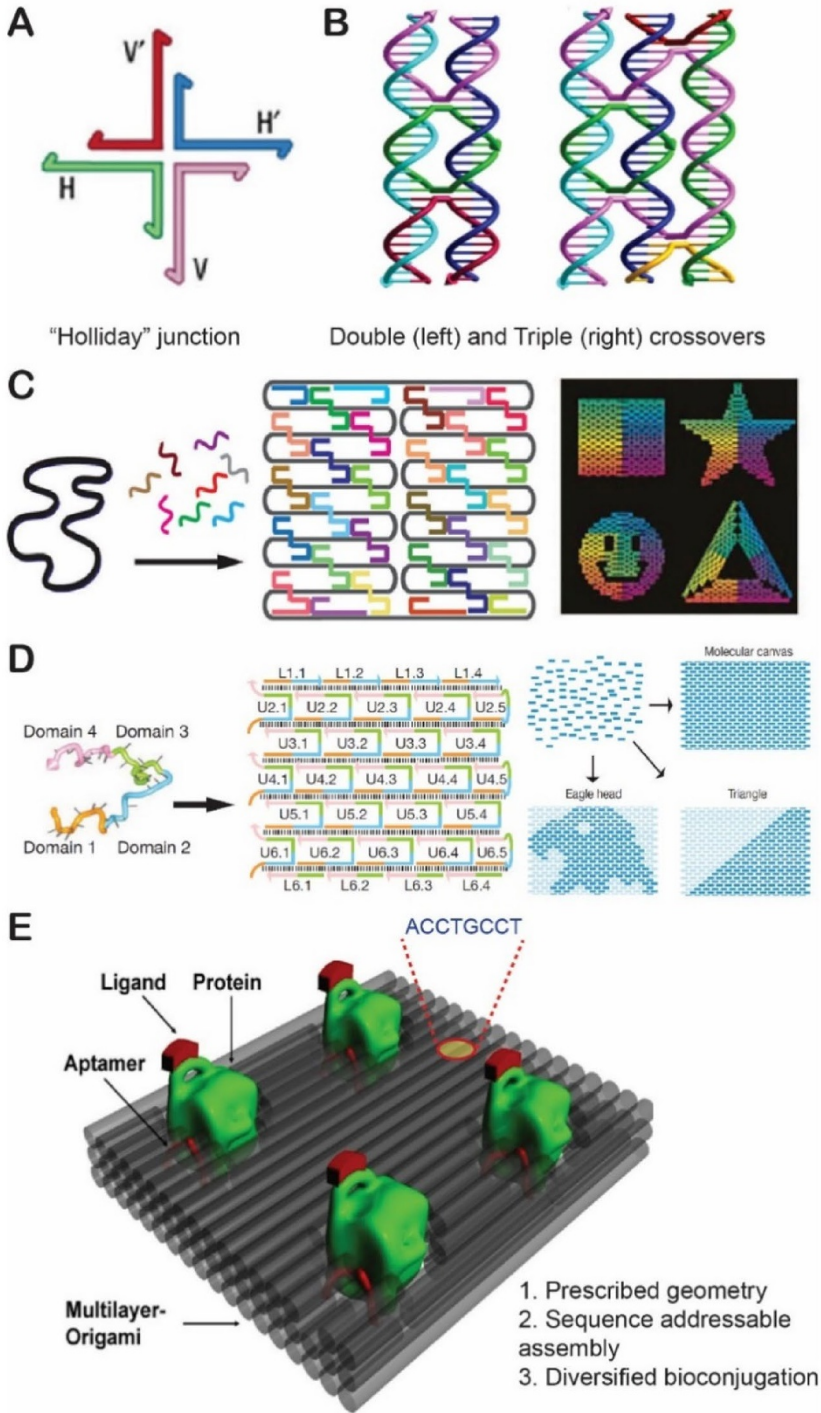


Table 1 Summary of protein–DNA conjugation chemistry

Chemistry	Reagent ^a	Reactive groups	Site-specific
Covalent crosslinking	SMCC [44]	Primary amine and thiol	No
	SPDP [45]	Primary amine and thiol (cleavable)	No
	DSS [38]	Amine	No
	Click chemistry [50] N-terminus conjugation [52]	Alkene and azide Pyridoxal phosphate (PLP)-mediated transamination	Depends on labeling position N-terminus amino acid
Chemistry	DNA-templated protein conjugation [55]	Primary amine on lysine	Approximate position
Noncovalent binding	Ligand	Binding affinity	Site-specific
	Biotin–streptavidin [58]	$K_d \sim 10^{-12} - 10^{-15}$ M	Depends on labeling position
	Aptamer–protein [62]	nM to μ M K_d	Yes
	Cofactor–apozyme [66]	pM to μ M K_d	Yes
Chemistry	Tag/fusion	Ligand	Site-specific
Peptide tag/protein fusion	His-Tag [67]	Ni-NTA	N- or C-terminus
	Intein [68]	N-terminal cysteine	N-terminus
	DegP [72]	DPMFKLV	N-terminus
	Halo [69]	Chlorohexane (CH)	Preferred C-terminus
	SNAP [69]	Benzylguanidine (BG)	N- or C-terminus
	MTG [70]	Carbobenzyl/oxyl glutaminy] glycine (Z-QG)	N-terminus
	CLIP [54]	Benzylcytosine (BC)	N- or C-terminus
	HUH [71]	Endonuclease	N- or C-terminus
	DNA-binding protein	TAL effector [73]	N- or C-terminus

 K_d , Dissociation constant

^aSee Abbreviation list

cleavable upon the addition of a reducing reagent, such as T-CEP or mercaptoethanol, while the linkage of SMCC is not cleavable. SMCC and SPDP crosslinkers are generally not site-specific in their reaction with lysines due to the presence of multiple lysine residues on the protein surface. The product of such non-specific conjugation is a heterogeneous mixture of DNA-tagged proteins. In some studies, SMCC or SPDP was used to conjugate a cysteine residue of a protein with an amine-modified DNA strand. This could be site-specific if there were only one cysteine displayed on the protein surface, such as cytochrome *c* [46]. Another commonly used crosslinker is disuccinimidyl suberate (DSS) in which the double succinimide ends can react with two primary amines to link them together [47]. DSS is especially useful for conjugating amine-modified ssDNA with organic cofactors, such as NAD or ATP [47–49].

Considerable progress has been made over the past two decades to improve the site-specificity of DNA–protein crosslinking. Click reactions (such as copper-catalyzed, azide-alkyne cycloaddition) combined with non-natural amino acid incorporation can produce easily purified conjugates with high site-specificity and yield [50]. To reduce the toxic damage of copper ions, Khatwani et al. used a copper-free click reaction (e.g. strain-promoted [3+2] azide-alkyne cycloaddition) to produce protein–DNA conjugates [51]. Francis and coworkers reported a protein bioconjugation at an N-terminal amino acid via a pyridoxal 5′-phosphate (PLP)-mediated transamination reaction [52], and Takeda et al. reported the development of a method to chemically modify an oligonucleotide to a N-terminal cysteine of a protein [53]. Proximity ligation has also been applied to site-specific labeling of an oligonucleotide on a protein by affinity binding-mediated conjugation [54]. Rosen et al. developed a DNA-templated protein conjugation (DTPC) technique to create site-selective DNA–protein conjugation [55]. In the DTPC technique, a guiding DNA strand first co-locates with a metal-binding site of a protein, followed by the introduction of a second DNA strand that conjugates to the lysine residues in the vicinity of the metal-binding site. For a more detailed discussion of site-selective conjugation of native proteins with DNA, the reader is referred to a recent review by Trads et al. [56].

Noncovalent binding may also be used to link DNA with proteins. The classic example is that of the strong binding of biotin to streptavidin [dissociation constant (K_d) < 10^{-12} M] to attach a biotinylated DNA to a streptavidin [57] or streptavidin-tagged enzymes [58]. With the development of oligonucleotide aptamers, aptamer-directed assembly has been adapted to immobilize proteins onto DNA nanostructures by site-specifically incorporating aptamer sequences into DNA nanostructures. This approach has been demonstrated to effectively anchor multiple protein targets onto rationally-designed DNA nanoscaffolds, including thrombin [59], platelet-derived growth factor [60] and cell–cell interactions [61]. More importantly, DNA nanostructures can be used to organize multivalent aptamers with optimized spacing distances to enhance their binding affinity [62]. These spatially optimized multivalent aptamers bind to a protein with low nanomolar—or even picomolar— K_d , whereas a single aptamer–protein binding is much weaker with several hundred-fold higher K_d [62, 63]. Similarly, short polypeptide ligands can also be positioned onto the surface of DNA nanostructures for protein binding (e.g. antibody, tumor necrosis

factor- α and transferrin) [64, 65]. In addition to aptamers, reconstituted apoenzymes are used to tightly bind to an organic cofactor-modified oligonucleotide [66].

Genetically modified proteins with a short peptide tag or a fusion tag offer more control over the site-specificity of any DNA–protein conjugation. Poly(histidine)₆ is one widely used peptide tag that can be incorporated into either the N- or C-terminus of a protein by binding to a nitrilotriacetic acid (NTA)-modified oligonucleotide in the presence of nickel ions [67]. In the last 20 years many techniques have been developed for constructing recombinant (terminus fused) proteins that can bind with ligand-modified nucleic acids. For example, intein-fused proteins can ligate with an N-terminal cysteine-tagged oligonucleotide via the formation of a peptide bond linkage [68]. The research group of Niemeyer and coworkers used “Halo-tag”- and “SNAP-tag”-modified proteins to conjugate with chlorohexane (CH) or benzylguanine (BG)-modified oligonucleotides, respectively [69]. Similar examples of fusion-mediated DNA–protein conjugation include a microbial transglutaminase (MTG) fusion [70], a CLIP tagging [54], a HUH tagging [71] and a DegP (serine protease) fusion [72]. Additionally, Dietz and coworkers recently used transcription activator-like (TAL) effector proteins to recognize and bind to specific DNA sequences for creating DNA–protein hybrid nanostructures [73]. These TAL effectors can be genetically introduced into the sequence of other enzymes for anchoring them onto DNA nanostructures.

Following conjugation, the purification of DNA-conjugated proteins is especially important to produce a high-quality sample. The presence of unconjugated DNA or free proteins decreases the assembly yield of proteins onto DNA nanostructures. The most common purification methods include molecular-weight cutoff filtration, gel electrophoresis and chromatography. Due to the negative charge of the DNA phosphate backbone, ion-exchange chromatography is the preferred method to purify DNA-conjugated proteins while separating proteins labeled with different numbers of DNA sidechains. Detailed procedures for purifying DNA-conjugated proteins have been summarized in a recently published protocol [38].

3 Spatial Organization of Multienzyme Assemblies on DNA Nanostructures

In cellular metabolism, the function of multienzyme cascades largely depends on their spatial organization, such as the relative distance, orientation, stoichiometry and confinements of the individual protein components [3]. Self-assembled DNA nanostructures are promising scaffolds on which to organize macromolecules because of the spatial addressability of DNA nanostructures [36]. Through various conjugations linking proteins with nucleic acids, DNA nanostructures are capable of controlling multienzyme assemblies in 1D, 2D, and three-dimensional (3D) geometric patterns that can be used to boost catalytic efficiency, improve reaction selectivity and investigate mechanistic kinetics of multienzyme reactions.

Early efforts in this field started with CM Niemeyer’s work of aligning enzymes on linear dsDNA scaffolds [58]. As shown in Fig. 3a, a bienzymatic NAD(P)H:FMN oxidoreductase (flavin reductase) and luciferase cascade were assembled together

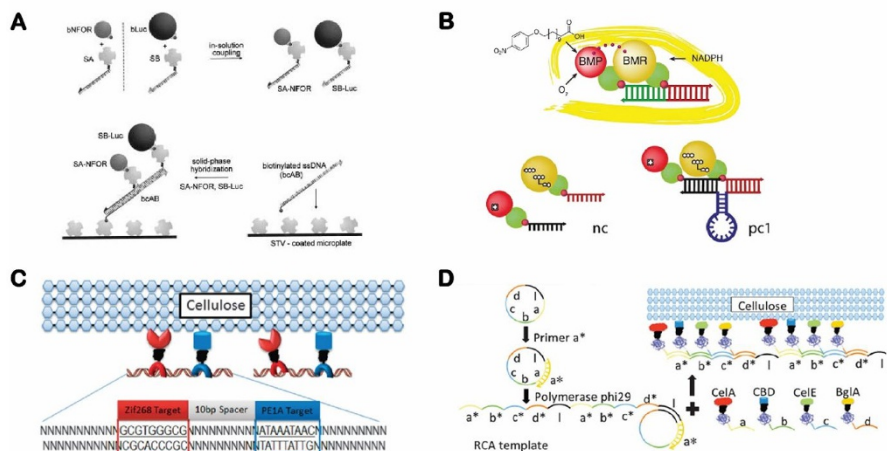


Fig. 3 Assembly of enzyme cascades on linear double-stranded DNA scaffolds. **a** NAD(P)H:FMN oxidoreductase and luciferase cascade. Reproduced from Niemeyer et al. [58], with permission, copyright 2002, John Wiley and Sons. **b** Engineered cytochrome P450 BM3 complex varying the distance between the BMR reductase domain and the BMP porphyrin domain. Reproduced from Erkelenz et al. [74], with permission, copyright 2011, American Chemical Society. **c** Zinc finger protein (ZFP)-appended proteins for cellulose degradation. Reproduced from Sun et al. [76], with permission, copyright 2013, Royal Society of Chemistry. **d** Rolling circle amplification (RCA) assembly of multienzyme nanowires to promote cellulose degradation. Reproduced from Sun and Chen [77], with permission, copyright 2016, Royal Society of Chemistry

onto a dsDNA scaffold via the strong binding of biotinylated enzymes with DNA-streptavidins [58]. A similar strategy was later used to assemble a cytochrome P450 BM3 enzyme on an adjustable dsDNA scaffold that could vary the distance between the two chimeras of the BMR reductase domain and the BMP porphyrin domain (Fig. 3b) [74]. Linear dsDNA scaffolds have also been used to guide the assembly of artificial cellulosomes composed of multiple cellulases [75–78]. As shown in Fig. 3c, the research group of Chen and coworkers used zinc-finger protein (ZFP) fusion to guide the assembly of two ZFP-appended proteins (an endoglucanase Cela and a cellulose-binding module CBM) into a bifunctional cellulosome structure for enhanced cellulose hydrolysis [76]. Rolling circle amplification (RCA) can produce long ssDNA scaffolds using a circular vector, a primer and a polymerase [77, 79]. As shown in Fig. 3d, these long ssDNA scaffolds produced by RCA can be used to anchor multiple copies of enzyme cascades via specific hybridizations between the section of DNA templates and the anchor DNA on the enzymes [77].

2D and 3D DNA nanostructures offer the ability to design more complex geometric patterns of multienzyme systems. As shown in Fig. 4a, the Wilner research group reported the self-assembly of a two-enzyme cascade array on 2D hexagonal DNA tiles with a controlled distance between enzymes [44]. The assembled glucose oxidase (GOx)–horseradish peroxidase (HRP) cascade showed a more than tenfold activity enhancement compared with unassembled enzymes. To precisely control the spacing distance between enzymes, Fu et al. organized a GOx–HRP pair on a

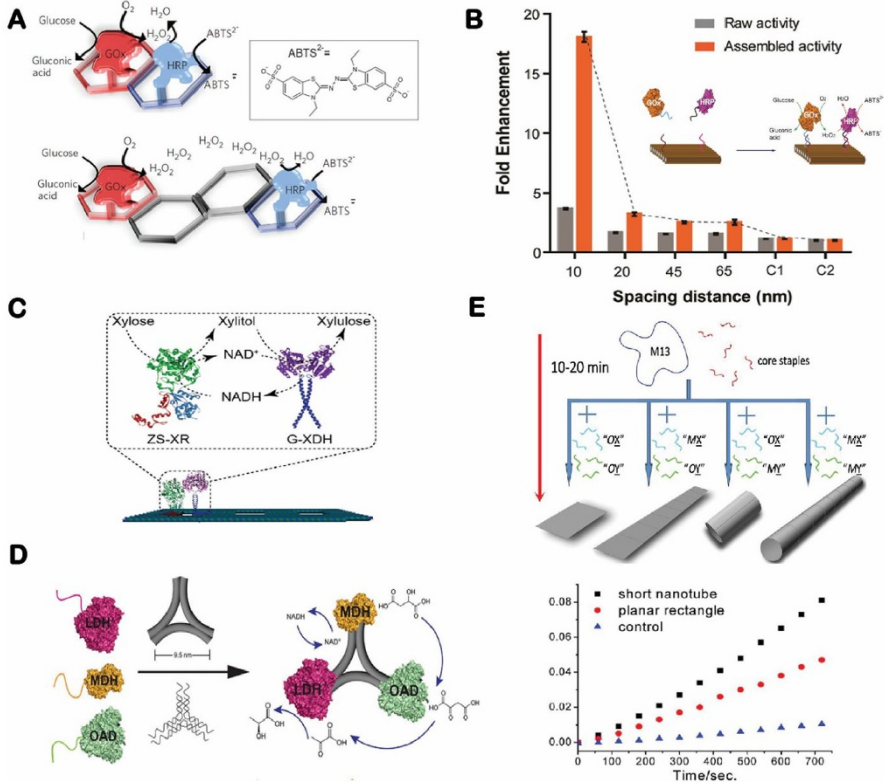


Fig. 4 Enzyme cascades organized on two-dimensional DNA nanostructures. **a** A glucose oxidase–horseradish peroxidase (GOx/HRP) cascade array on two-dimensional (2D) hexagonal DNA strips. Reproduced from Wilner et al. [44], with permission, copyright 2009, Springer Nature. **b** Organization of a GOx/HRP cascade on DNA origami tiles with controlled spacing. Reproduced from Fu et al. [45], with permission, copyright 2012, American Chemical Society. **c** Assembly of an NAD cofactor-coupled enzyme cascade (*XR* xylose reductase, *XDH* xylitol dehydrogenase). Reproduced from Ngo et al. [81], with permission, copyright 2016, American Chemical Society. **d** A three-enzyme (*MDH* malic dehydrogenase, *OAD* oxaloacetate decarboxylase, *LDH* lactate dehydrogenase) cascade organized on a triangular DNA origami structure. Reproduced from Liu et al. [83], with permission, copyright 2016, John Wiley and Sons. **e** A rectangular DNA origami rolling into a DNA nanotube for assembly of an enzyme cascade. Reproduced from Fu et al. [80], with permission, copyright 2013, American Chemical Society

rectangular DNA nanostructure with controlled distances between enzymes that varied from 10 to 65 nm (Fig. 4b). This spatially organized assembly was used to probe the distance-dependent activity of enzyme cascade reactions and to enhance the mass transport of the H_2O_2 intermediate [45]. Similarly, Morii and coworkers reported the assembly of an NAD^+ cofactor-coupled enzyme cascade of xylose reductase and xylitol dehydrogenase on a 2D DNA origami for carrying out the conversion of xylose into xylulose (Fig. 4c) [81]. The close proximity of two enzymes was found to facilitate the recycling of NAD^+ to NADH, thereby increasing the xylulose production rate. A subsequent study by the same group extended the assembly

of a three-enzyme cascade converting xylose to xylulose 5-phosphate with coupled NAD^+ and ATP cofactors [82]. As shown in Fig. 4d, the research group of Yan and coworkers demonstrated a three-enzyme pathway involving malic dehydrogenase, oxaloacetate decarboxylase and lactate dehydrogenase on a triangular DNA origami [83]. The geometric patterns of these assembled enzyme complexes were found to affect the overall pathway activities by promoting the recycling rate of cofactors in the coupled reactions. Regarding 3D structures, the Fan research group developed a one-pot assembly of DNA nanostructures by rolling a rectangular DNA origami into a DNA nanotube (Fig. 4e) [80]. Using this strategy, enzyme cascade pairs were first anchored onto a rectangular origami, followed by structural rolling to confine enzymes to the exterior of a DNA nanotube, enhancing the cascade's activity.

In addition to DNA, RNA molecules can also be engineered into discrete and multidimensional nanostructures [31, 84]. Because RNA structures can be expressed inside cells, they offer the capability to organize metabolic pathways for in vivo applications. Delebecque et al. designed and assembled multiple shapes of discrete 1D and 2D RNA nanostructures that were formed inside cells (Fig. 5a) [85]. Using these RNA assemblies, they demonstrated an organized [FeFe]-hydrogenase and ferredoxin reaction network which enhanced the biological hydrogen production up to 48-fold. A continuous study from the research group of Silver and coworkers showed that RNA scaffolds could be used to co-localize proteins and to increase the

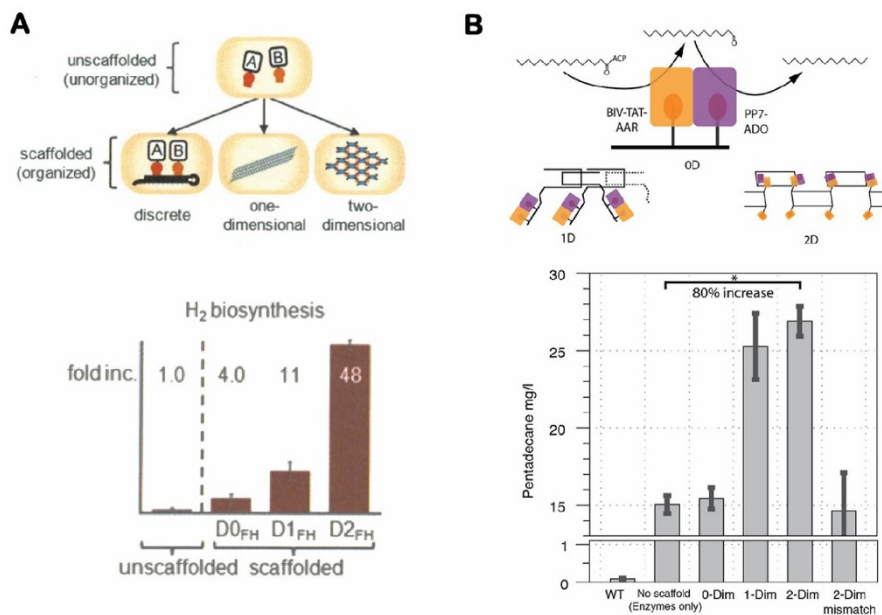


Fig. 5 In vivo assembly of enzyme cascades on RNA nanostructures. **a** Organization of [FeFe]-hydrogenase and ferredoxin on one-dimensional (1D) and 2D RNA nanostructures (top) with enhanced hydrogen production in vivo (bottom). Reproduced from Delebecque et al. [85], with permission, copyright 2011, The American Association for the Advancement of Science. **b** Assembly of a two-enzyme pentadecane production pathway on RNA scaffolds (top) with enhanced pentadecane output in vivo (bottom). Reproduced from Sachdeva et al. [86], with permission, copyright 2014, Oxford University Press

metabolic output of a two-enzyme pentadecane production pathway in *Escherichia coli* (Fig. 5b) [86]. Nevertheless, potential applications of RNA scaffolds face challenges in terms of in vivo stability, survival of engineered cells, and loss of RNA information during cell division.

DNA nanostructure-organized systems offer an opportunity for investigating the detailed kinetics of enzyme cascade reactions. One conception of the past several decades is that the proximity of enzymes promotes the mass transport of intermediate substrates between enzymes, which in turn boosts the overall activity of enzyme cascade reactions [6, 87, 88]. This theory/hypothesis seems to be supported by some recent studies of assembled enzyme cascades on DNA scaffolds [44, 45, 80, 81, 85] and metabolon engineering [8, 89], in which multienzyme complexes reacted with proximity assembly more actively than did unassembled and freely diffused enzymes. However, this hypothesis is problematic if we consider the fact that many small-molecule substrates diffuse quite quickly in solution, with diffusion coefficients ranging from 100 to 1000 $\mu\text{m}^2/\text{s}$. To interpret the diffusion, Fu et al. described the concentration profile of a H_2O_2 intermediate in a coupled GOx–HRP reaction by Brownian motion (Fig. 6a), which was simulated based on Eq. (1): [45]

$$n(r, t) = \sum_{i=0}^{t/\tau-1} \frac{1}{(4\pi D(t - i \times \tau))^{3/2}} \times \exp\left(-\frac{r^2}{4D(t - i \times \tau)}\right), \quad (1)$$

where $n(r, t)$ is the number of molecules at a distance r from the initial produced position of production, D is the diffusion coefficient and t is the time given for diffusion. When the Brownian motion of H_2O_2 is considered in a GOx–HRP reaction in the given t , τ is the average time between GOx turnovers ($\tau = 1/k$, where k is the

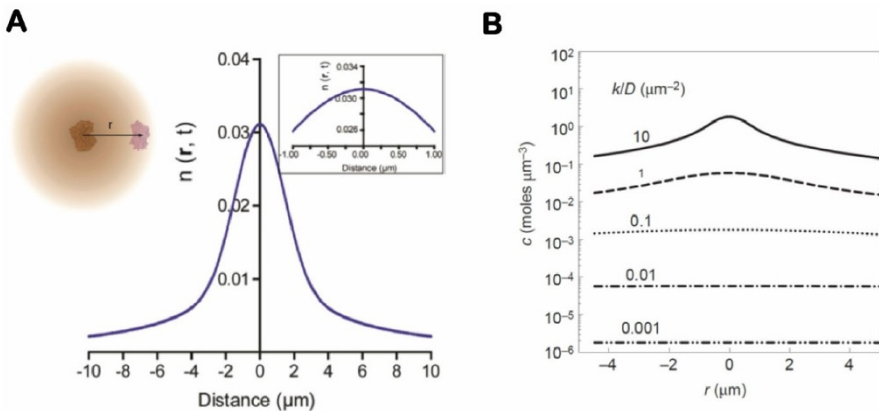


Fig. 6 Theoretical modeling of distance-dependent enzyme cascade reactions. **a** Brownian diffusion of H_2O_2 in a GOx/HRP reaction depending on distance [$n(r, t)$ Number of molecules at a distance r from the initial produced position of production]. Reproduced from Fu et al. [45], with permission, copyright 2012, American Chemical Society. **b** Concentration profiles of the reaction product as a function of radial distance (r) from an active site under different ratios of turnover frequency to diffusion coefficient (k/D). Reproduced from Wheeldon et al. [90], with permission, copyright 2016, Springer Nature

turnover rate). The simulation of the diffusion profile showed that H_2O_2 concentrations varied slightly (<5%) within a few hundred nanometers of GOx due to the fast diffusion of H_2O_2 ($D \sim 1000 \mu\text{m}^2/\text{s}$). This simulation result suggests that the proximity between enzymes has little benefits on the diffusion of H_2O_2 from GOx to HRP. As shown in Fig. 6b, Wheeldon et al. applied Eq. (1) to simulating the concentrations of product molecules at discrete distances from the active site of an enzyme as a function of k/D [90]. For most enzymes, the diffusion coefficients (generally ~ 100 to $1000 \mu\text{m}^2/\text{s}$) of the small-molecule products were much larger than the turnover rates (generally ~ 1 – 100 s^{-1}), resulting in a small value of k/D ($0 < k/D < 1$). Thus, product concentration profiles are spanned quite uniformly over a few micrometers distance, a result which also indicates the minimal effect of spatial proximity on the concentration of intermediates in a cascade reaction. Hess and coworkers mathematically modeled the reaction–diffusion kinetics of a GOx–HRP cascade reaction [91, 92]. The simulation of cascade kinetics showed that proximity did not contribute to the activity enhancement of the assembled GOx–HRP pairs. Other more recent reaction–diffusion modelings suggested that a close proximity between enzymes could only enhance the rate of a cascade reaction under crowding conditions where the diffusion of enzymes and substrates was significantly slowed down [93]. Similar modeling techniques have also been applied to in vivo metabolic pathways, which likewise showed that diffusion was not a rate-limiting factor for many enzyme systems and, therefore, proximity or substrate channeling would not significantly increase the overall rate of the cascade reaction at steady state [88, 93]. Thus, substrate channeling is more likely used to regulate metabolite flux, improve pathway selectivity and protect metabolites from degradation or competing side reactions [88, 93].

Since proximity-enhanced mass-transport effect may not contribute to the activity enhancement of enzyme assemblies directed by DNA/RNA scaffolds or protein scaffolds, some recent studies have focused on the effects of assembly scaffolds themselves on altering enzyme kinetics, with the aim to provide unique microenvironments that favor stronger activity [88, 94, 95]. Such effects include modifying the local pH [96], including a hydration layer [94] and exerting an inhibitory effect [97]. Scaffolded microenvironments will be discussed in more detail in next section [Enzyme Compartmentalization by DNA Nanocages](#). For non-freely diffused systems (e.g. constrained diffusion on a surface or within a compartment), the appropriate organization of multienzyme systems is still essential to maximize the efficiency of the system [47]. Some recent modeling studies have provided novel perspectives on enzyme assemblies on surfaces [98, 99] or within compartments [100, 101].

4 Enzyme Compartmentalization by DNA Nanocages

Many metabolic pathways are organized by confinement within membrane-delimited or membrane-free compartments, such as mitochondria, lysosomes, peroxisomes, carboxysomes and metabolosomes [102]. Compartmentalization affects biochemical reactions in many ways: by increasing local concentrations, facilitating mass transport of reaction intermediates, reducing toxicity of intermediates and

protecting encapsulated contents from competing pathways [103]. Compartmentalization also plays a functional role in the chaperone-assisted folding of tertiary and quaternary protein structures and by preventing proteins from aggregating under cellular stress conditions [104]. Results from recent studies show that nucleoli could promote structure maintenance of nuclear proteins by compartmentalization in the presence of stressors [105].

The assembly of a DNA nanocube was first reported by the research group of Seeman and coworkers in 1991 (Fig. 7a) [106]. However, the constructed cage was not tested for the encapsulation of proteins or other large biomolecules. In 2006, Turberfield and coworkers designed a DNA tetrahedron with each edge comprising a 20-bp double helix (~ 7 nm) (Fig. 7b) [107]. This tetrahedron was shown to encapsulate a small protein [cytochrome *c* (inner diameter ~ 3.5 nm)]. The research group of Fan and coworkers very recently reported that the electroactivity of cytochrome *c* is enhanced on tetrahedral DNA frameworks [108]. As shown in Fig. 7c, DNA polyhedra have been used to organize streptavidin proteins into various 3D patterns [109]. To encapsulate larger proteins, DNA origami nanocages have been designed with larger inner cavities that range from 10 to 50 nm [110]. Zhao et al. developed a general approach to encapsulate enzymes within a fully closed DNA nanocage (Fig. 7d) [94]. In their method, enzymes are first anchored onto open, half cages at a very high yield ($> 90\%$), following which two half cages are combined into a closed cage by adding bridge strands [94]. Sprengel et al. reported the selective encapsulation of a protein guest into a DNA origami hollow cage by decorating multiple ligands

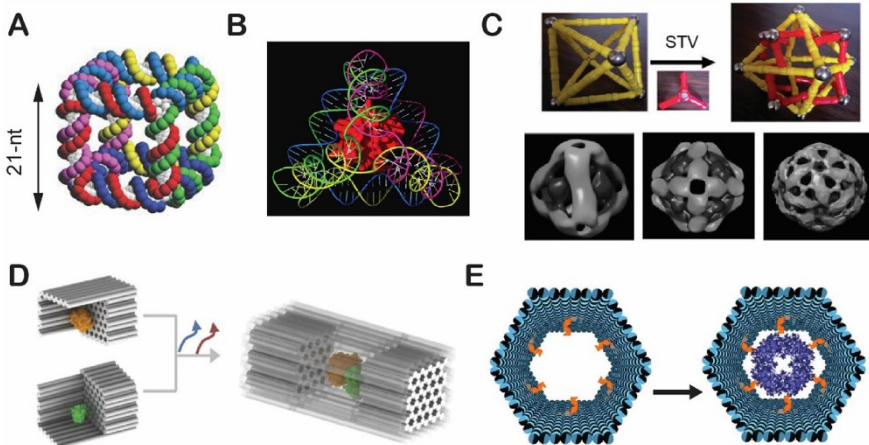


Fig. 7 Development of DNA nanocages for enzyme encapsulation. **a** The first 3D DNA cube. Reproduced from Seeman [19], with permission, copyright 2003, Springer Nature. **b** A DNA tetrahedron for encapsulating a protein. Reproduced from Erben et al. [107], with permission, copyright 2006, John Wiley and Sons. **c** DNA polyhedrons for organizing proteins (STV streptavidin). Reproduced from Zhang et al. [109], with permission, copyright 2019, John Wiley and Sons. **d** The combination of half DNA nanocages for enclosing enzymes. Reproduced from Zhao et al. [94], with permission, copyright 2016, Springer Nature. **e** Protein encapsulation into a DNA host using noncovalent protein–ligand interactions. Reproduced from Sprengel et al. [72] under the terms and conditions of the Creative Commons Attribution 4.0 International License, copyright 2017, Springer Nature

on the inner surface of the cage to guide supramolecular interactions (Fig. 7e) [72]. This noncovalent protein–ligand binding enabled the capture of very large protein complexes (up to DegP₂₄, ~1 million Da) into a well-defined DNA host.

Regarding smart nanoreactors, switchable DNA nanocages have been designed to regulate the encapsulation and release of protein payloads. As shown in Fig. 8a, Fan and coworkers developed a single-step wrap-over of a planar DNA origami sheet into nanoribbons and nanotubes which they used to encapsulate enzyme cascades [80]. The research group of Knudsen and coworkers designed a temperature-sensitive DNA nanocage which exhibited a closed conformation at 4 °C and an open conformation at 37 °C (Fig. 8b) [111]. This switchable nanocage was used to encapsulate and release HRP in response to temperature. Kohman et al. reported a light-triggered release of bioactive cargoes of proteins and small molecules from a DNA nanocage through the incorporation of a photolabile crosslinker (Fig. 8c) [112]. An *o*-nitrobenzyl motif was photocleavable upon ultraviolet (UV) radiation at 240–400 nm to release a linked cargo of protein or small molecules. Kim et al. designed a pH-switchable DNA tetrahedron for regulating protein stability against protease digestion, protein–antibody binding and enzyme activity (Fig. 8d) [113]. Andersen and coworkers designed a DNA nanovault to control the access of substrate molecules to encapsulated enzymes by the reversible opening (accessible to substrate) and closing (inaccessible) of the cage (Fig. 8e) [114].

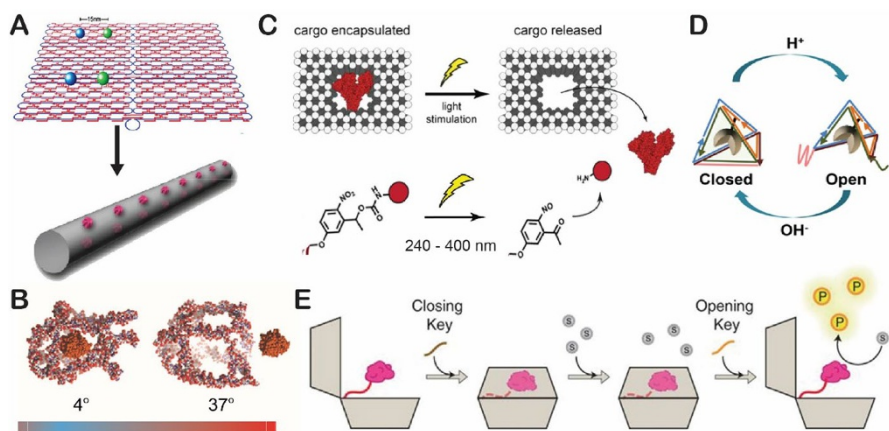


Fig. 8 DNA nanocage-regulated encapsulation and release of protein cargoes. **a** Single-step folding of DNA nanotubes for enzyme encapsulation. Reproduced from Fu et al. [80], with permission, copyright 2013, American Chemical Society. **b** A temperature-sensitive DNA nanocage for encapsulating and releasing an enzyme. Reproduced from Juul et al. [111], with permission, copyright 2013, American Chemical Society. **c** A light-triggered release of bioactive cargoes from a DNA nanocage. Reproduced from Kohman et al. [112], with permission, copyright 2016, American Chemical Society. **d** A pH-switchable DNA tetrahedron for regulating protein stability and activity. Reproduced from Kim et al. [113], with permission, copyright 2017, American Chemical Society. **e** A DNA nanovault with reversible opening and closing to regulate enzyme–substrate accessibility. Reproduced from Grossi et al. [114] under the terms and conditions of the Creative Commons Attribution 4.0 International License, copyright 2017, Springer Nature

More interestingly, DNA nanoscaffolds have been found to affect the activities of the enzymes that were attached onto them. Figure 9 summarizes some of the DNA structures that have been reported to enhance enzyme activities [115], including a long dsDNA molecule (e.g. λ DNA, ~ 1 – 2 fold improved activity) [116], a DNA structure binding to enzyme substrates (~ 1 – 2 fold) [117], a 2D rectangular DNA origami (~ 1 – 3 fold) [45], DNA nanocaged enzymes (~ 3 – 6 fold) [94, 118] and DNA-crowded enzyme particles (~ 2 – 3 fold) [95]. To better understand these effects, several mechanisms have been proposed to interpret DNA scaffolds-enhanced enzyme activities, including locally decreased pH on the DNA scaffolds [115], the presence of a stabilized hydration layer by DNA phosphate backbones [94], nanoconfinement of water [119], enrichment of substrate molecules on DNA scaffolds [117] and substrate channeling [45, 47]. However, many questions still remain on just how DNA confinements modify the local chemical and physical environment and affect enzyme functions. Experiments combining experimental data with molecular modeling may shed light on the chaperone-like function of DNA nanocages.

5 Biomimetic Assembly of Macromolecular Complexes

Biomimetic systems represent one of the most exciting research frontiers in the twenty-first century. Life on earth has been diversifying for nearly four billion years, evolving into complex and diverse species. All living organisms have developed the appropriate functions and solutions to address the challenges of Earth's environment. Living systems have inspired humanity and provided the principles to solve problems and explore questions both in and out of the laboratory. Biomimetic materials have shown exciting potential in applications ranging from catalysis and energy transformation to smart materials, diagnostic tools and therapeutics [120]. Equally, structural DNA nanotechnology has been applied to engineering artificial systems mimicking cellular structures and biological functions. In the following paragraphs we list several examples of DNA-scaffolded biomimetic assemblies.

The swinging arm, or the covalently attached prosthetic group, is a key functional structure in substrate channeling in multistep catalytic transformations within metabolic pathways [121]. For example, a lipoyl-lysine arm is found in the pyruvate

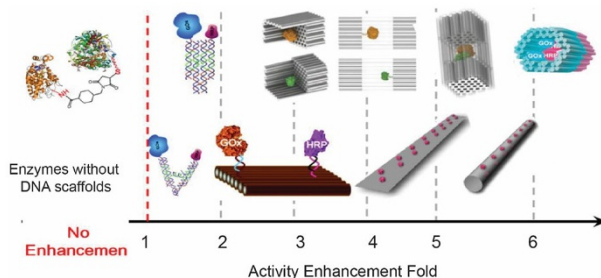


Fig. 9 Enhancement of enzyme activity by DNA nanostructures. Reproduced from Zhang and Hess [115], with permission, copyright 2017, American Chemical Society

dehydrogenase complex (Fig. 10a); this arm transfers acetyl CoA and carries out oxidation and reduction between three enzymes [122]. To mimic this, Fu et al. designed an NAD^+ -modified DNA arm that facilitated the hydride transfer between two dehydrogenases [47]. As shown in Fig. 10b, a two-enzyme cascade consisting of a glucose-6-phosphate dehydrogenase (G6PDH) and a malate dehydrogenase (MDH) was displayed on a DX tile. An NAD^+ -modified poly(T)₂₀ was placed halfway between G6PDH and MDH. The activity of the cascade was enhanced by approximately 90-fold by substrate channeling of one NAD^+ arm (Fig. 10c). Adjusting the number of swinging arms produced even more activity enhancement. As shown in Fig. 10d, the reaction specificity of the G6PDH–MDH cascade was also increased in the presence of a competing enzyme of lactate dehydrogenase (LDH). NAD^+ -modified DNA arms have also been successfully used to regulate the pathway direction between G6PDH–MDH and G6PDH–LDH [123], with the directional regulation of enzyme pathways controlled by DNA strand displacement [123] or the photo-responsive reaction (Fig. 11a) [124]. Additionally, swinging arms have been used to organize NAD^+ transfer in a 2D enzyme array of G6PDH and LDH (Fig. 11b) [125].

DNA-based swinging arms can also facilitate electron transfer in bioelectroactive systems. The research group of Wilner and coworkers used a DNA scaffold to organize the spatial interaction of a GOx enzyme with an electrode surface to generate an

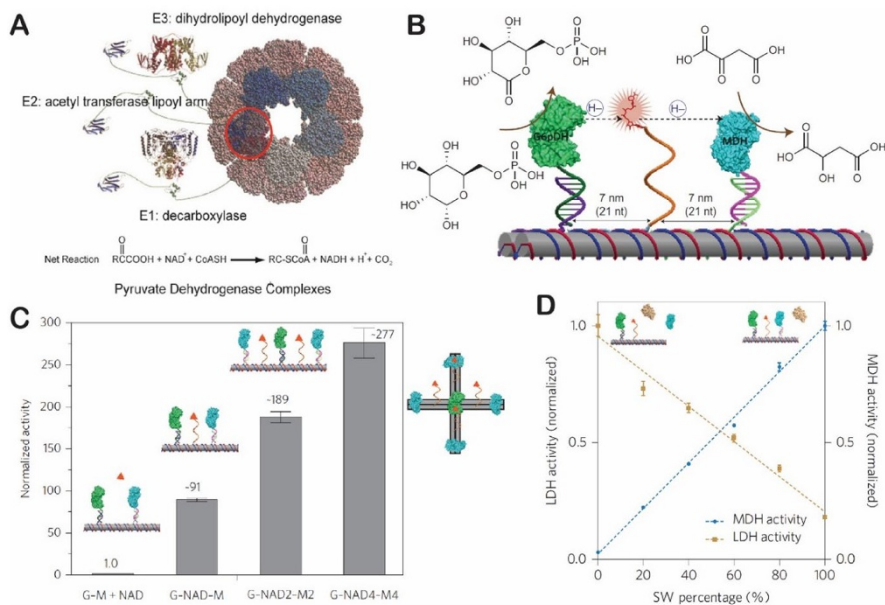


Fig. 10 Biomimetic assembly of swinging arms. **a** Swinging domains in pyruvate dehydrogenase complex. Reproduced from Perham [121], with permission, copyright 2000, *Annual Review of Biochemistry*. **b** An artificial swinging arm to transfer NAD^+ cofactor between two dehydrogenases (G6PDH glucose-6-phosphate dehydrogenase and MDH) on DNA nanoscaffolds. **c** Enhanced enzyme cascade activity by swinging arms. **d** Improved reaction selectivity by swinging arms. Reproduced from Fu et al. [47], with permission, copyright 2014, Springer Nature

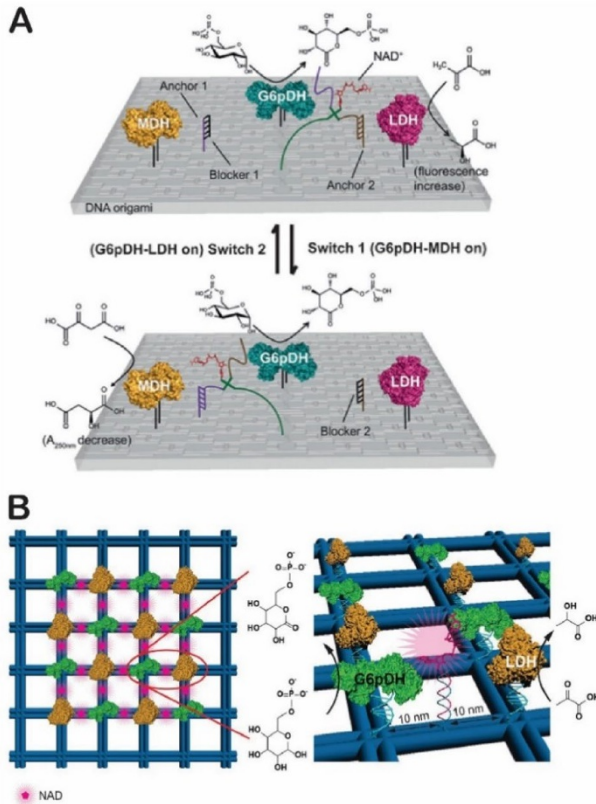


Fig. 11 Large biomolecular nanostructures organized by artificial swinging arms. **a** NAD^+ arms for regulating pathway activity between the G6PDH–MDH cascade and the G6PDH–LDH cascade. Reproduced from Ke et al. [123], with permission, copyright 2016, John Wiley and Sons. **b** 2D enzyme arrays of the G6PDH–MDH reaction with NAD^+ swinging arms. Reproduced from Yang et al. [125], with permission, copyright 2018, John Wiley and Sons

anodic electrocatalytic current (Fig. 12a) [126]. In this organized system, a ferrocene-modified ssDNA served as a relay to transfer electrons between the enzyme redox center and the electrode surface. As shown in Fig. 12b, Armand Tepper used DNA scaffolds to organize the electrochemical contact of redox enzymes and the electrode surface by immobilizing the copper enzyme of nitrite reductase (NiR) and its natural electron-exchange partner, pseudoazurin (Paz), onto a gold electrode by DNA scaffold-directed assembly [127]. Electron-transfer patches were realized by conjugating enzymes to specific ssDNA tags that allowed them to swing and perform nitrite reduction by accepting electrons from the gold electrode. As shown in Fig. 12c, Cha and coworkers used DNA scaffolds as a structure-directing template to organize TiO_2 and CdS nanocrystals [128]. Enhanced hydrogen production was achieved when a benzoquinone (BQ)-modified ssDNA was used to transfer electrons between a TiO_2 and a CdS.

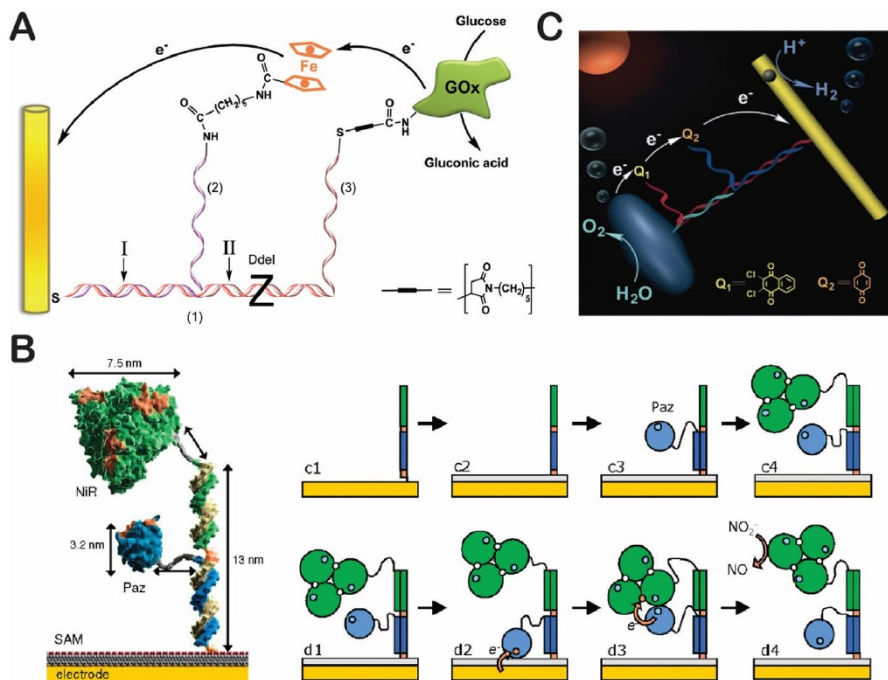


Fig. 12 DNA swinging arms for facilitating bioelectroactive reactions. **a** A GOx–ferrocene–electrode contact. Reproduced from Piperberg et al. [126], with permission, copyright 2009, American Chemical Society. **b** A nitrite reductase–pseudourin (*NiR-Paz*) system (*SAM* self-assembled monolayer). Reproduced from Tepper [127], with permission, copyright 2010, American Chemical Society. **c** A TiO_2 –CdS complex for H_2 production. Reproduced from Ma et al. [128], with permission, copyright 2015, John Wiley and Sons

DNA-based molecular arms have also been useful in engineering nanorobotic systems and assembly lines. The research group of Simmel and coworkers studied the diffusive transport of DNA cargo strands that were bound to a DNA origami surface (Fig. 13a) [129]. These authors concluded that a more rigid DNA arm transferred cargo more efficiently than a more flexible, hinged arm. Based on this result, they developed a nanoscale robotic arm on a rectangular DNA origami tile, the rotation of which was driven and controlled by an electrical field (Fig. 13b) [130]. As shown in Fig. 13c, two research groups, namely those of Zhuang and coworkers and Yin and coworkers, collaborated to develop a DNA origami rotor that was driven by the unwinding function of a helicase (RecBCD complex) during the transcription process [131]. These authors introduced a method of origami-rotor-based imaging and tracking (ORBIT) to track DNA rotation at the single-molecule level with a time resolution of milliseconds.

In addition to swinging arms, DNA nanostructures can also be used to engineer artificial membrane transporters to facilitate the diffusion of ions and small molecules across lipid membranes [36]. Ohmann and co-workers recently designed a

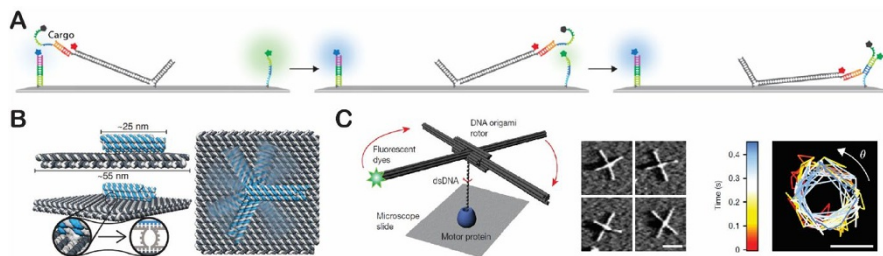


Fig. 13 DNA arm-based nanorobotic system. **a** Double-stranded DNA (*dsDNA*) arms for fluorescent cargo transport. Reproduced from Kopperger et al. [129], with permission, copyright 2015, American Chemical Society. **b** A nanoscale robotic arm driven by an electric field. Reproduced from Kopperger et al. [130], with permission, copyright 2018, The American Association for the Advancement of Science. **c** DNA origami rotor driven by a motor protein (left), atomic force microscopy images of a DNA rotor (middle) and origami-rotor-based imaging and tracking (ORBIT) for tracking DNA rotation (right). Reproduced from Kosuri et al. [131], with permission, copyright 2019, Springer Nature

synthetic scramblase built from DNA nanostructures [132]. As shown in Fig. 14a, the lipid-scrambling DNA nanostructure was made by the self-assembly of eight ssDNA with two cholesterol prosthetic groups to stabilize the inserted DNA structure in the lipid bilayer. Figure 14b shows molecular dynamic simulations of the lipid scrambling process catalyzed by DNA nanostructures; this DNA-based scramblase could flip 10^7 lipids per second, which is much faster than a natural enzyme ($\sim 3 \times 10^4$ lipids per second).

DNA scaffolding has also shown its value in more complex synthetic systems. Photosynthesis, for example, is an essential process that provides energy and oxygen for most living organisms on earth. The development of artificial photosynthetic systems, therefore, would present great opportunities in such areas as food and fuel production, energy transformation and catalysis, with broad social and economic impact. DNA nanostructures have been applied to engineering these artificial photosynthetic systems, particularly light-harvesting complexes. As shown in Fig. 15a,

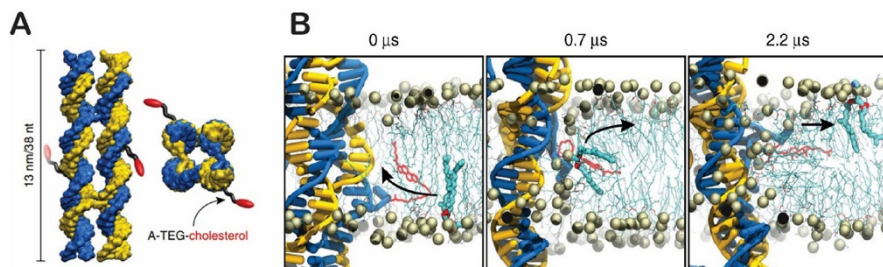


Fig. 14 Synthetic scramblase built from DNA. **a** The structure of a DNA-based scramblase with two cholesterol prosthetic groups. **b** Molecular dynamic simulation of the lipid scrambling process. Reproduced from Ohmann et al. [132] under the terms and conditions of the Creative Commons Attribution 4.0 International License, copyright 2018, Springer Nature

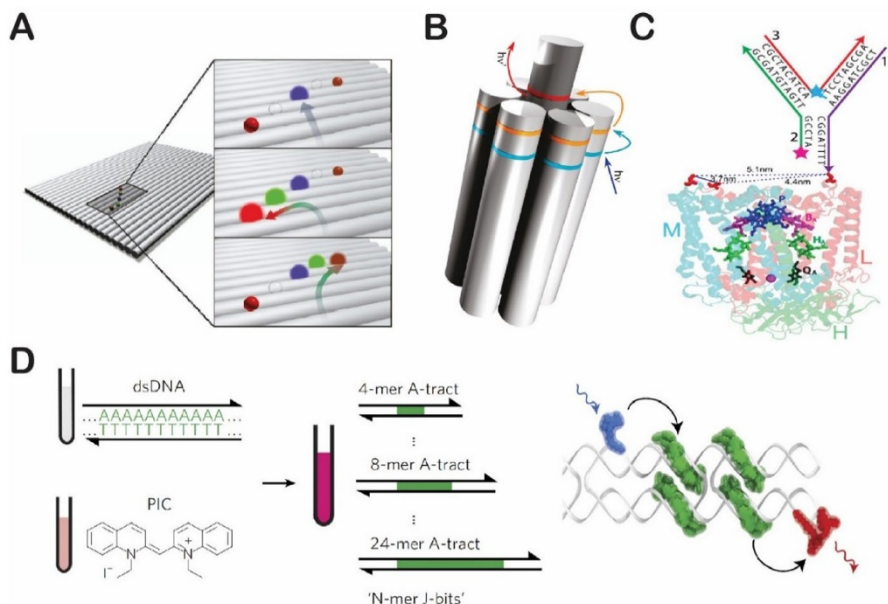


Fig. 15 Artificial photosynthetic systems organized by DNA nanoscaffolds. **a** Multicolor fluorophore array for photo-energy transfer. Reproduced from Stein et al. [133], with permission, copyright 2011, American Chemical Society. **b** Artificial light-harvesting network. Reproduced from Dutta et al. [134], with permission, copyright 2011, American Chemical Society. **c** A DNA-directed light-harvesting/reaction center. Reproduced from Dutta et al. [135], with permission, copyright 2014, American Chemical Society. **d** A synthetic DNA-based excitonic circuit based on J-aggregates (PIC pseudoisocyanine). Reproduced from Boulais et al. [136], with permission, copyright 2017, Springer Nature

Tinnefeld and coworkers were the first to report a multi-fluorophore array on a DNA origami tile; these researchers controlled the spacing distance and the position of each fluorophore to direct the energy transfer [133]. Yan and coworkers constructed an artificial light-harvesting antenna by assembling multiple donor/acceptor pairs on a seven-helix DNA bundle (Fig. 15b) [134]. In this system, stepwise funneling of the excitation energy was directed from the primary donor array (pyrylium [Py] dye) to the acceptor core (Alexa Fluor® [AF] dye) through the intermediate donor (cyanine [Cy3] dye). In a collaboration with the research group of Woodbury and coworkers, Yan and coworkers also assembled a tunable artificial light-harvesting system which used a three-arm DNA nanostructure instead of a the seven-helix bundle (Fig. 15c). This structure was conjugated to a photosynthetic center protein and served as an antenna to transfer energy to the reaction center [135]. Recently, the research groups of Bathe and coworkers and Yan and coworkers worked together to develop a strategy to organize Cy3 dye aggregates on rigid dsDNA scaffolds. These dye/DNA aggregates showed a tunable absorption spectrum and strongly coupled exciton dynamics similar to that of natural light-harvesting systems (Fig. 15d) [136]. These DNA-templated dye aggregates can be used to engineer long-range, directional photo-energy transfer and harvest [137].

6 Regulation of Proximity Interactions in Biochemical Reactions

DNA nanostructures can be used to mediate the proximity assembly of enzymes and catalytic cofactors in order to regulate their reaction activities. Ghadiri and coworkers engineered an artificial allosteric enzyme by tethering a metalloprotease with an inhibitor-conjugated ssDNA, which they called an inhibitor-DNA-enzyme (IDE) construct (Fig. 16a) [138]. Due to the flexible ssDNA linker, the inhibitor was able to bind to the active site of an enzyme. The activation of this IDE was triggered by hybridizing the ssDNA linker with a complementary ssDNA to form a dsDNA segment. The relatively rigid dsDNA blocked the inhibitor from binding to the active site, thus permitting the enzyme to function. This IDE structure was subsequently used to engineer molecular logic circuits by programmable DNA hybridizations [139]. As shown in Fig. 16b, the IDE was used to regulate the fibrinolytic activity that resulted from the binding of a streptokinase (SK) to the plasma proenzyme plasminogen (Pg) [140], with the result being a DNA-linked protease inhibitor bound with a SK–Pg complex that inhibited fibrinolytic activity. Specific DNA inputs disrupted the inhibited binding complex, releasing an active SK–Pg complex. The research group of Merx and coworkers used DNA-mediated assembly and disassembly to regulate enzyme–inhibitor binding to reversibly switching enzyme activity on and off (Fig. 16c) [141]. As shown in Fig. 16d, Tan and coworkers used a *cis*–*trans* photoisomerization of an azobenzene prosthetic group to regulate the binding of a thrombin with its aptamer [142]. In the *cis*-form of azobenzene, a

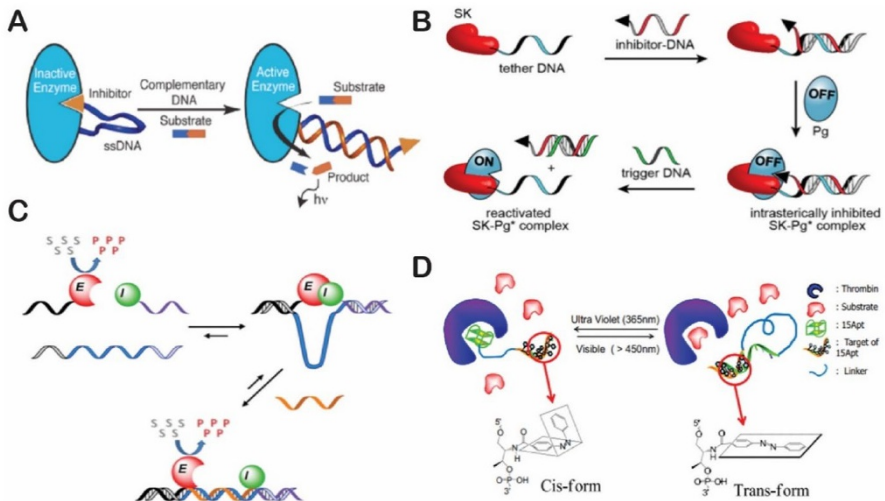


Fig. 16 DNA hybridization-regulated enzyme activity. **a** An enzyme–inhibitor interaction (ssDNA Single-stranded DNA). Reproduced from Saghatelian et al. [138], with permission, copyright 2003, American Chemical Society. **b** Streptokinase–plasminogen (SK–Pg) complex for regulating fibrinolytic activity. Reproduced from Mukherjee et al. [140], with permission, copyright 2018, American Chemical Society. **c** Enzyme actuation (*E* enzyme, *I* inhibitor). Reproduced from Janssen [141], with permission, copyright 2015, American Chemical Society. **d** Photo-regulated thrombin-aptamer complex. Reproduced from Kim et al. [142], with permission, copyright 2009, National Academy of Sciences

thrombin was bound to an DNA aptamer which inhibited thrombin-mediated coagulation. Upon UV irradiation, azobenzene switched the from *cis*-form to the *trans*-form, exposing a regulatory domain that disrupted the thrombin–aptamer complex, allowing the unbound thrombin to induce blood coagulation [142].

To engineer more complicated regulatory systems, DNA-based nanomachines were developed to regulate the spatial interactions between components of biochemical reactions. Liu and coworkers designed DNA nanotweezers to regulate the spacing distance between a G6PDH and a NAD⁺ cofactor that were anchored on the two arms of DNA tweezers (Fig. 17a) [48]. By switching the DNA tweezers from the open to closed state, the activity of the enzyme and its cofactor was turned on. As shown in Fig. 17b, Liu and coworkers used similar DNA tweezers to regulate the spacing distance between a GOx and HRP with tunable activities [143], while Wilner and coworkers reported DNA nanomachines that could perform “ON/OFF” switchable activation and deactivation of a three-component biocatalytic cascade (Fig. 17c) [144]. When the tweezers were closed, the cascade reaction was activated by the formation of a hemin/G-quadruplex-bridged structure, but when the tweezers

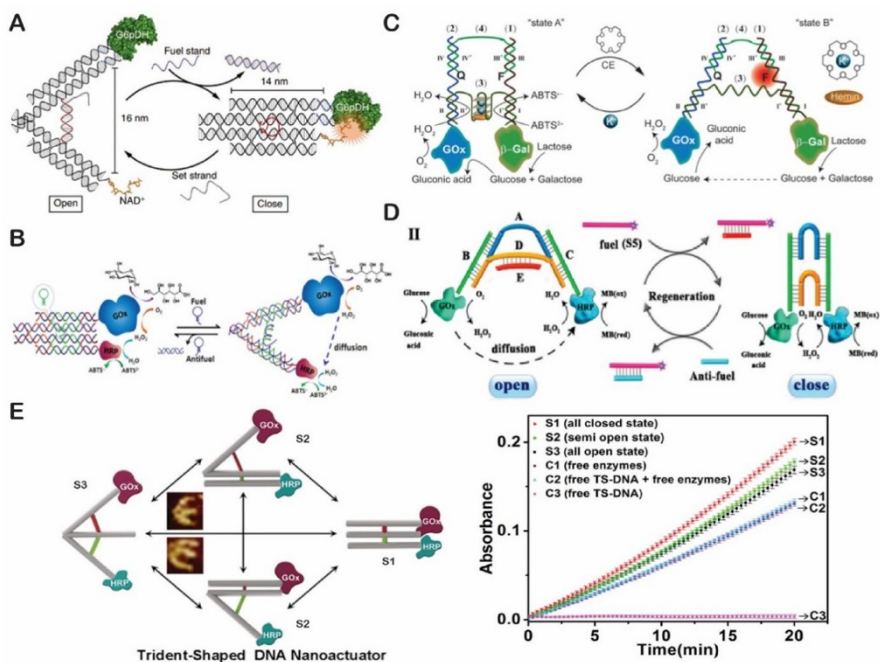


Fig. 17 DNA nanotweezers-regulated enzyme reaction. **a** A G6PDH/NAD⁺ pair. Reproduced from Liu et al. [48], with permission. Copyright 2013, Springer Nature. **b** A GOx/HRP cascade. Reproduced from Xin et al. [143], with permission, copyright 2013, John Wiley and Sons. **c** A three-component biocatalytic cascade of β -Gal/GOx/hemin. Reproduced from Hu et al. [144], with permission, copyright 2014, John Wiley and Sons. **d** Distance regulation of a GOx/HRP pair. Reproduced from Kou et al. [145], with permission, copyright 2018, American Chemical Society. **e** A trident-shaped DNA nanomachine with several conformational states for regulating an enzyme cascade. Reproduced from Xing et al. [146], with permission, copyright 2018, American Chemical Society

were opened, the hemin/G-quadruplex was disrupted. DNA nanotweezers were also used by Kou et al. [145] to regulate the electrochemical response of a GOx/HRP cascade reaction (Fig. 17d). Yang and coworkers constructed a trident-shaped DNA nanoactuator that could switch between four distinct structural conformations [146]. As shown in Fig. 17e, different GOx/HRP activities could be achieved with each conformation of the trident-shaped DNA nanomachine. However, because many enzyme cascade reactions (e.g. GOx/HRP cascade) are not sensitive to enzyme proximity, as discussed previously [92], only small differences of enzyme cascade activities were observed for these four conformations of DNA tweezers. In contrast, DNA nanomachines were more efficient in regulating enzyme/cofactor pairs (which do rely on proximity interaction), with enhanced activities ranging from a few fold up to 100-fold or more [48, 49].

Using a simpler approach, Fu and coworkers reported a method of using a DNA hairpin structure to mediate the proximity assembly of biochemical reactions (Fig. 18a) [49]. The self-folded DNA hairpin carried a cofactor that was not able to interact with its partner enzyme, resulting in very low catalytic activity. A triggered opening of the DNA hairpin was subsequently assembled with an enzyme to bring together the enzyme/cofactor pair for actuating the reaction with a 100-fold more activity. Based on this result, a biochemical sensing circuit was designed which combined a sensing module (made of DNA structural switches) with a triggered proximity assembly of an enzyme/cofactor pair. When the sensing module was activated by a target molecule, the enzyme could bind to the cofactor and catalyze a reaction to produce a detectable signal (Fig. 18b). This DNA-based sensing circuit could be used either for detecting microRNA (via strand displacement) or small-molecule metabolites, such as adenosine (using an aptamer) (Fig. 18c). DNA nanostructure-regulated enzyme assemblies provide a new approach to programming enzyme

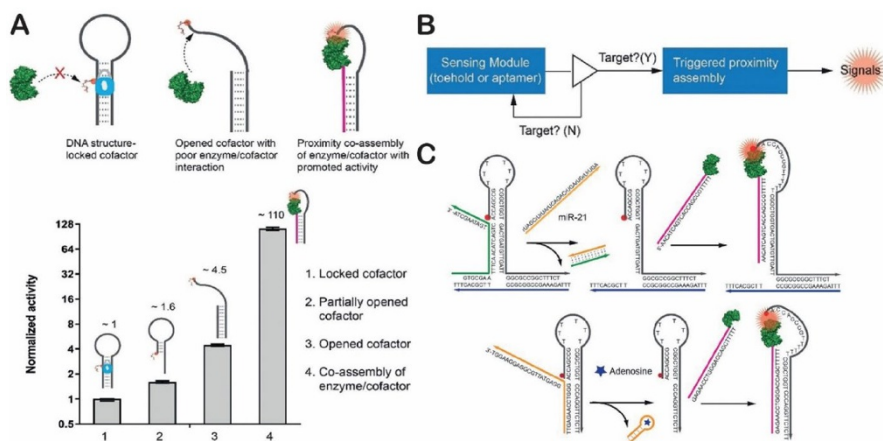


Fig. 18 DNA hairpin-mediated proximity assembly of an enzyme and a cofactor. **a** Enzyme activities for a hairpin-locked cofactor, opened cofactor and co-assembled enzyme/cofactor pair. **b** A design chart of a biochemical sensing circuit. **c** Detection of microRNA and adenosine. Reproduced from Oh et al. [49], with permission, copyright 2018, John Wiley and Sons

activities. This may lead to the development of a new generation of enzyme-based diagnostic tools and therapeutics. They may also be used as a basis for developing protein feedback loops or allosteric regulation as an alternative or complementary technology to protein engineering.

7 Conclusions and Future Perspectives

Structural DNA nanotechnology has enabled the design and fabrication of various nano-objects with prescribed geometry and regulated spatial interaction. The combination of DNA nanostructures with enzyme–DNA conjugation provides an efficient approach for engineering artificial biomolecule complexes with finely controlled spatial arrangement and confinement. Considering these advantages together, it can be concluded that DNA nanostructures have the potential to deliver breakthroughs toward the engineering of more sophisticated biomimetic systems, such as synthetic cells, artificial subcellular components and photosynthetic and energy-harvesting structures. For example, DNA scaffolds can be used to organize multilevel assemblies for the construction of a synthetic reactor, including membrane confinement, artificial transmembrane nanopores and encapsulated biochemical reaction pathways [36]. Another potential use of DNA nanotechnology is the design and construction of dynamic and regulated structures with conformational switches triggered by external inputs. Dynamic nanostructures may find utility in the development of feedback-regulated biochemical systems. Some early examples have already demonstrated the feasibility of using DNA nanostructures to regulate enzyme activities, including inhibitor–DNA–enzyme structures, DNA tweezers and DNA swinging arms. It is possible to design substrate cooperativity or product feedback inhibition by incorporating aptamer switches into enzyme inhibition and activation complexes. Finally, diagnostic applications provide great challenges and opportunities to design DNA-based molecular circuits for sensing various molecular targets *in vitro* or *in vivo*. Smart DNA circuits can be adapted to various point-of-care diagnosis platforms, such as paper strips and color-change-based assays. This will fit the growing need for fast, sensitive and easy detection of infectious diseases, such as the recent outbreaks of coronavirus, Ebola and Zika virus that resulted in Public Health Emergencies of International Concern as announced by the World Health Organization. Overall, DNA-scaffolded enzyme assemblies will have a bright future and be useful in various applications of biocatalysis, functional biomaterials and novel theranostic medicine.

Acknowledgements This work was supported by a PECASE award to J.F. (W911NF1910240) and a DoD DURIP (W911NF-16-1-0220). J.F. is also supported by the Start-up Fund, Provost's Fund for Research and Research Council Grant from Rutgers University-Camden. X.L. is sponsored by MARC internship at Rutgers-Camden. The authors are also grateful to the Equipment Leasing Funds from the State of New Jersey.

Author Contributions The manuscript was written through contributions of all authors. All authors have given approval to the final version of the manuscript.

Compliance with Ethical Standards

Conflict of interest The authors declare no competing financial interest.

References

- Schomburg I, Chang A, Placzek S, Söhngen C, Rother M, Lang M, Munaretto C, Ulas S, Stelzer M, Grote A, Scheer M, Schomburg D (2013) BRENDA in 2013: integrated reactions, kinetic data, enzyme function data, improved disease classification: new options and contents in BRENDA. *Nucleic Acids Res* 41:D764–D772
- Roach PJ (1977) Functional significance of enzyme cascade systems. *Trends Biochem Sci* 2:87–90
- Savage DF, Afonso B, Chen AH, Silver PA (2010) Spatially ordered dynamics of the bacterial carbon fixation machinery. *Science* 327:1258–1261
- Srere PA, Mosbach K (1974) Metabolic compartmentation: symbiotic, organellar, multienzymic, and microenvironmental. *Annu Rev Microbiol* 28:61–84
- Bayer EA, Belaich JP, Shoham Y, Lamed R (2004) The cellulosomes: multienzyme machines for degradation of plant cell wall polysaccharides. *Annu Rev Microbiol* 58:521–554
- Miles EW, Rhee S, Davies DR (1999) The molecular basis of substrate channeling. *J Biol Chem* 274:12193–12196
- Yeates TO, Crowley CS, Tanaka S (2010) Bacterial microcompartment organelles: protein shell structure and evolution. *Annu Rev Biophys* 39:185–205
- Dueber JE, Wu GC, Malmirchegini GR, Moon TS, Petzold CJ, Ullal AV, Prather KLJ, Keasling JD (2009) Synthetic protein scaffolds provide modular control over metabolic flux. *Nat Biotechnol* 27:753–759
- Sheldon RA (2007) Cross-linked enzyme aggregates (CLEAs): stable and recyclable biocatalysts. *Biochem Soc Trans* 35:1583–1587
- Sheldon RA (2007) Enzyme immobilization: the quest for optimum performance. *Adv Synth Catal* 349:1289–1307
- Vriezema DM, Garcia PML, Sancho ON, Hatzakis NS, Kuiper SM, Nolte RJM, Rowan AE, van Hest JCMA (2007) Positional assembly of enzymes in polymersome nanoreactors for cascade reactions. *Angew Chem Int Ed Engl* 46:7378–7382
- van Dongen SFM, Nallani M, Cornelissen JJLM, Nolte RJM, van Hest JCMA (2009) Three-enzyme cascade reaction through positional assembly of enzymes in a polymersome nanoreactor. *Chem Eur J* 15:1107–1114
- Kim KT, Meeuwissen SA, Nolte RJM, van Hest JCM (2010) Smart nanocontainers and nanoreactors. *Nanoscale* 2:844–858
- Fiedler JD, Brown SD, Lau JL, Finn MG (2010) RNA-directed packaging of enzymes within virus-like particles. *Angew Chem Int Ed Engl* 49:9648–9651
- Comellas-Aragones M, Engelkamp H, Claessen VI, Sommerdijk NAJM, Rowan AE, Christianen PCM, Maan JC, Verduin BJM, Cornelissen JJLM, Nolte RJM (2007) A virus-based single-enzyme nanoreactor. *Nat Nanotechnol* 2:635–639
- Seeman NC (1982) Nucleic acid junctions and lattices. *J Theor Biol* 99:237–247
- Fu TJ, Seeman NC (1993) DNA double-crossover molecules. *Biochemistry* 32:3211–3220
- Zadegan RM, Norton ML (2012) Structural DNA nanotechnology: from design to applications. *Int J Mol Sci* 13:7149–7162
- Seeman NC (2003) DNA in a material world. *Nature* 421:427–431
- Rothemund PWK (2006) Folding DNA to create nanoscale shapes and patterns. *Nature* 440:297–302
- Wei B, Dai M, Yin P (2012) Complex shapes self-assembled from single-stranded DNA tiles. *Nature* 485:623–626
- Ke Y, Ong LL, Shih WM, Yin P (2012) Three-dimensional structures self-assembled from DNA bricks. *Science* 338:1177–1183
- Dietz H, Douglas SM, Shih WM (2009) Folding DNA into twisted and curved nanoscale shapes. *Science* 325:725–730

24. Han D, Pal S, Nangreave J, Deng Z, Liu Y, Yan H (2011) DNA origami with complex curvatures in three-dimensional space. *Science* 332:342–346
25. Veneziano R, Ratanalert S, Zhang K, Zhang F, Yan H, Chiu W, Bathe M (2016) Designer nanoscale DNA assemblies programmed from the top down. *Science* 352:1534
26. Benson E, Mohammed A, Gardell J, Masich S, Czeizler E, Orponen P, Hogberg B (2015) DNA rendering of polyhedral meshes at the nanoscale. *Nature* 523:441–444
27. Zhang F, Jiang S, Wu S, Li Y, Mao C, Liu Y, Yan H (2015) Complex wireframe DNA origami nanostructures with multi-arm junction vertices. *Nat Nanotechnol* 10:779–784
28. Ke Y, Ong LL, Sun W, Song J, Dong M, Shih WM, Yin P (2014) DNA brick crystals with prescribed depths. *Nat Chem* 6:994–1002
29. Zheng J, Birktoft JJ, Chen Y, Wang T, Sha R, Constantinou PE, Ginell SL, Mao C, Seeman NC (2009) From molecular to macroscopic via the rational design of a self-assembled 3D DNA crystal. *Nature* 461:74–77
30. Zhang F, Yan H (2017) DNA self-assembly scaled up. *Nature* 552:34–35
31. Han D, Qi X, Myhrvold C, Wang B, Dai M, Jiang S, Bates M, Liu Y, An B, Zhang F, Yan H, Yin P (2017) Single-stranded DNA and RNA origami. *Science* 358(6369):eaao2648. <https://doi.org/10.1126/science.aao2648>
32. Williams S, Lund K, Lin C, Wonka P, Lindsay S, Yan H (2008) Tiamat: a three-dimensional editing tool for complex DNA structures. *Lect Notes Comput Sci* 5347:99–101
33. Zadeh JN, Steenberg CD, Bois JS, Wolfe BR, Pierce MB, Khan AR, Dirks RM, Pierce NA (2011) NUPACK: analysis and design of nucleic acid systems. *J Comput Chem* 32:170–173
34. Douglas SM, Marblestone AH, Teerapittayanon S, Vazquez A, Church GM, Shih WM (2009) Rapid prototyping of 3D DNA-origami shapes with caDNAno. *Nucleic Acids Res* 37:5001–5006
35. Castro CE, Kilchherr F, Kim DN, Shiao EL, Wauer T, Wortmann P, Bathe M, Dietz H (2011) A primer to scaffolded DNA origami. *Nat Methods* 8:221–229
36. Fu J, Oh SW, Monckton K, Arbuckle-Keil G, Ke Y, Zhang T (2019) Biomimetic compartments scaffolded by nucleic acid nanostructures. *Small*. <https://doi.org/10.1002/sml.201900256>
37. Fu J, Liu M, Liu Y, Yan H (2012) Spatially-interactive biomolecular networks organized by nucleic acid nanostructures. *Acc Chem Res* 45:1215–1226
38. Fu J, Yang YR, Dhakal S, Zhao Z, Liu M, Zhang T, Walter NG, Yan H (2016) Assembly of multi-enzyme complexes on DNA nanostructures. *Nat Protoc* 11:2243–2273
39. Yang Y, Wang J, Shigematsu H, Xu W, Shih WM, Rothman JE, Lin C (2016) Self-assembly of size-controlled liposomes on DNA nanotemplates. *Nat Chem* 8:476–483
40. Zhang Z, Yang Y, Pincet F, Llaguno M, Lin C (2017) Placing and shaping liposomes with reconfigurable DNA nanocages. *Nat Chem* 9:653–659
41. Burns JR, Seifert A, Fertig N, Howorka S (2016) A biomimetic DNA-based channel for the ligand-controlled transport of charged molecular cargo across a biological membrane. *Nat Nanotechnol* 11:152–156
42. Langecker M, Arnaut V, Martin TG, List J, Renner S, Mayer M, Dietz H, Simmel FC (2012) Synthetic lipid membrane channels formed by designed DNA nanostructures. *Science* 338:932–936
43. Niemeyer CM (2010) Semisynthetic DNA-protein conjugates for biosensing and nanofabrication. *Angew Chem Int Ed Engl* 49:1200–1216
44. Wilner OI, Weizmann Y, Gill R, Lioubashevski O, Freeman R, Willner I (2009) Enzyme cascades activated on topologically programmed DNA scaffolds. *Nat Nanotechnol* 4:249–254
45. Fu J, Liu M, Liu Y, Woodbury NW, Yan H (2012) Interenzyme substrate diffusion for an enzyme cascade organized on spatially addressable DNA nanostructures. *J Am Chem Soc* 134:5516–5519
46. Lu N, Pei H, Ge Z, Simmons CR, Yan H, Fan C (2012) Charge transport within a three-dimensional DNA nanostructure framework. *J Am Chem Soc* 134:13148–13151
47. Fu J, Yang YR, Johnson-Buck A, Liu M, Liu Y, Walter NG, Woodbury NW, Yan H (2014) Multi-enzyme complexes on DNA scaffolds capable of substrate channelling with an artificial swinging arm. *Nat Nanotechnol* 9:531–536
48. Liu M, Fu J, Hejesen C, Yang Y, Woodbury NW, Gothelf K, Liu Y, Yan H (2013) A DNA tweezer-actuated enzyme nanoreactor. *Nat Commun*. <https://doi.org/10.1038/ncomms3127>
49. Oh SW, Pereira A, Zhang T, Li T, Lane A, Fu J (2018) DNA-mediated proximity-based assembly circuit for actuation of biochemical reactions. *Angew Chem Int Ed Engl* 57:13086–13090
50. El-Sagheer AH, Brown T (2012) Click nucleic acid ligation: applications in biology and nanotechnology. *Acc Chem Res* 45:1258–1267

51. Khatwani SL, Kang JS, Mullen DG, Hast MA, Beese LS, Distefano MD, Taton TA (2012) Covalent protein–oligonucleotide conjugates by copper-free click reaction. *Bioorg Med Chem* 20:4532–4539
52. Witus LS, Francis M (2010) Site-specific protein bioconjugation via a pyridoxal 5'-phosphate-mediated N-terminal transamination reaction. *Curr Protoc Chem Biol* 2:125–134
53. Takeda S, Tsukiji S, Ueda H, Nagamune T (2008) Covalent split protein fragment–DNA hybrids generated through N-terminus-specific modification of proteins by oligonucleotides. *Org Biomol Chem* 6:2187–2194
54. Gu GJ, Friedman M, Jost C, Johnsson K, Kamali-Moghaddam M, Plückthun A, Landegren U, Söderberg O (2013) Protein tag-mediated conjugation of oligonucleotides to recombinant affinity binders for proximity ligation. *New Biotechnol* 30:144–152
55. Rosen CB, Kodal ALB, Nielsen JS, Schaffert DH, Scavenius C, Okholm AH, Voigt NV, Enghild JJ, Kjems J, Tørring T, Gothelf KV (2014) Template-directed covalent conjugation of DNA to native antibodies, transferrin and other metal-binding proteins. *Nat Chem* 6:804–809
56. Trads JB, Tørring T, Gothelf KV (2017) Site-selective conjugation of native proteins with DNA. *Acc Chem Res* 50:1367–1374
57. Yan H, Park SH, Finkelstein G, Reif JH, LaBean TH (2003) DNA-templated self-assembly of protein arrays and highly conductive nanowires. *Science* 301:1882–1884
58. Niemeyer CM, Koehler J, Wuerdemann C (2002) DNA-directed assembly of bienzymic complexes from in vivo biotinylated NAD(P)H:FMN oxidoreductase and luciferase. *ChemBioChem* 3:242–245
59. Liu Y, Lin C, Li H, Yan H (2005) Aptamer-directed self-assembly of protein arrays on a DNA nanostructure. *Angew Chem Int Ed Engl* 44:4333–4338
60. Chhabra R, Sharma J, Ke Y, Liu Y, Rinker S, Lindsay S, Yan H (2007) Spatially addressable multiprotein nanoarrays templated by aptamer-tagged DNA nanoarchitectures. *J Am Chem Soc* 129:10304–10305
61. Liu X, Yan H, Liu Y, Chang Y (2011) Targeted cell–cell interactions by DNA nanoscaffold-templated multivalent bispecific aptamers. *Small* 7:1673–1682
62. Rinker S, Ke Y, Liu Y, Chhabra R, Yan H (2008) Self-assembled DNA nanostructures for distance-dependent multivalent ligand–protein binding. *Nat Nanotechnol* 3:418–422
63. Zhou Y, Qi X, Liu Y, Zhang F, Yan H (2019) DNA nanoscaffold-assisted selection of femtomolar bivalent aptamers for human α -thrombin with potent anticoagulant activity. *Chembiochem* 20(19):2494–2503
64. Williams BAR, Lund K, Liu Y, Yan H, Chaput JC (2007) Self-assembled peptide nanoarrays: an approach to studying protein–protein interactions. *Angew Chem Int Ed Engl* 46:3051–3054
65. Williams BAR, Diehnelt CW, Belcher P, Greving M, Woodbury NW, Johnston SA, Chaput JC (2009) Creating protein affinity reagents by combining peptide ligands on synthetic DNA scaffolds. *J Am Chem Soc* 131:17233–17241
66. Fruk L, Kuo C-H, Torres E (2009) Apoenzyme reconstitution as a chemical tool for structural enzymology and biotechnology. *Angew Chem Int Ed Engl* 48:1550–1574
67. Shen W, Zhong H, Neff D, Norton ML (2009) NTA directed protein nanopatterning on DNA origami nanoconstructs. *J Am Chem Soc* 131:6660–6661
68. Lovrinovic M, Spengler M, Deutsch C, Niemeyer CM (2005) Synthesis of covalent DNA–protein conjugates by expressed protein ligation. *Mol Biosyst* 1:64–69
69. Saccà B, Meyer R, Erkelenz M, Kiko K, Arndt A, Schroeder H, Rabe KS, Niemeyer CM (2010) Orthogonal protein decoration of DNA origami. *Angew Chem Int Ed Engl* 49:9378–9383
70. Tominaga J, Kemori Y, Tanaka Y, Maruyama T, Kamiya N, Goto M (2007) An enzymatic method for site-specific labeling of recombinant proteins with oligonucleotides. *Chem Commun* 43:401–403
71. Lovendahl KN, Hayward AN, Gordon WR (2017) Sequence-directed covalent protein–DNA linkages in a single step using HUH-Tags. *J Am Chem Soc* 139:7030–7035
72. Sprengel A, Lill P, Stegemann P, Bravo-Rodriguez K, Schöneweiß E-C, Merdanovic M, Gudnason D, Aznauryan M, Gamrad L, Barcikowski S, Sanchez-Garcia E, Birkedal V, Gatsogiannis C, Ehrmann M, Saccà B (2017) Tailored protein encapsulation into a DNA host using geometrically organized supramolecular interactions. *Nat Commun* 8:14472
73. Praetorius F, Dietz H (2017) Self-assembly of genetically encoded DNA-protein hybrid nanoscale shapes. *Science* 355(6331):eaam5488. <https://doi.org/10.1126/science.aam5488>

74. Erkelenz M, Kuo CH, Niemeyer CM (2011) DNA-mediated assembly of cytochrome P450 BM3 subdomains. *J Am Chem Soc* 133:16111–16118
75. Mori Y, Ozasa S, Kitaoka M, Noda S, Tanaka T, Ichinose H, Kamiya N (2013) Aligning an endoglucanase Cel5A from *Thermobifida fusca* on a DNA scaffold: potent design of an artificial cellulosome. *Chem Commun* 49:6971–6973
76. Sun Q, Madan B, Tsai S-L, DeLisa MP, Chen W (2014) Creation of artificial cellulosomes on DNA scaffolds by zinc finger protein-guided assembly for efficient cellulose hydrolysis. *Chem Commun* 50:1423–1425
77. Sun Q, Chen W (2016) HaloTag mediated artificial cellulosome assembly on a rolling circle amplification DNA template for efficient cellulose hydrolysis. *Chem Commun* 52:6701–6704
78. Chen Q, Yu S, Myung N, Chen W (2017) DNA-guided assembly of a five-component enzyme cascade for enhanced conversion of cellulose to gluconic acid and H₂O₂. *J Biotechnol* 263:30–35
79. Wilner OI, Shimron S, Weizmann Y, Wang Z-G, Willner I (2009) Self-assembly of enzymes on DNA scaffolds: en route to biocatalytic cascades and the synthesis of metallic nanowires. *Nano Lett* 9:2040–2043
80. Fu Y, Zeng D, Chao J, Jin Y, Zhang Z, Liu H, Li D, Ma H, Huang Q, Gothelf KV, Fan C (2013) Single-step rapid assembly of DNA origami nanostructures for addressable nanoscale bioreactors. *J Am Chem Soc* 135:696–702
81. Ngo TA, Nakata E, Saimura M, Morii T (2016) Spatially organized enzymes drive cofactor-coupled cascade reactions. *J Am Chem Soc* 138:3012–3021
82. Nguyen TM, Nakata E, Saimura M, Dinh H, Morii T (2017) Design of modular protein tags for orthogonal covalent bond formation at specific DNA sequences. *J Am Chem Soc* 139:8487–8496
83. Liu M, Fu J, Qi X, Wootten S, Woodbury NW, Liu Y, Yan H (2016) A three-enzyme pathway with an optimised geometric arrangement to facilitate substrate transfer. *Chembiochem* 17:1097–1101
84. Afonin KA, Bindewald E, Yaghoobian AJ, Voss N, Jacovetty E, Shapiro BA, Jaeger L (2010) In vitro assembly of cubic RNA-based scaffolds designed in silico. *Nat Nanotechnol* 5:676–682
85. Delebecque CJ, Lindner AB, Silver PA, Aldaye FA (2011) Organization of intracellular reactions with rationally designed RNA assemblies. *Science* 333:470–474
86. Sachdeva G, Garg A, Godding D, Way JC, Silver PA (2014) In vivo co-localization of enzymes on RNA scaffolds increases metabolic production in a geometrically dependent manner. *Nucleic Acids Res* 42:9493–9503
87. Bauler P, Huber G, Leyh T, McCammon JA (2010) Channeling by proximity: the catalytic advantages of active site colocalization using brownian dynamics. *J Phys Chem Lett* 1:1332–1335
88. Sweetlove LJ, Fernie AR (2018) The role of dynamic enzyme assemblies and substrate channelling in metabolic regulation. *Nat Commun* 9:2136
89. You C, Myung S, Zhang YHP (2012) Facilitated substrate channeling in a self-assembled trifunctional enzyme complex. *Angew Chem Int Ed Engl* 51:8787–8790
90. Wheeldon I, Minteer SD, Banta S, Barton SC, Atanassov P, Sigman M (2016) Substrate channeling as an approach to cascade reactions. *Nat Chem* 8:299–309
91. Idan O, Hess H (2012) Diffusive transport phenomena in artificial enzyme cascades on scaffolds. *Nat Nanotechnol* 7:769–770
92. Zhang Y, Tsitkov S, Hess H (2016) Proximity does not contribute to activity enhancement in the glucose oxidase–horseradish peroxidase cascade. *Nat Commun* 7:13982. <https://doi.org/10.1038/ncomms13982>
93. Kuzmak A, Carmali S, von Lieres E, Russell AJ, Kondrat S (2019) Can enzyme proximity accelerate cascade reactions? *Sci Rep* 9:455. <https://doi.org/10.1038/s41598-018-37034-3>
94. Zhao Z, Fu J, Dhakal S, Johnson-Buck A, Liu M, Zhang T, Woodbury NW, Liu Y, Walter NG, Yan H (2016) Nanocaged enzymes with enhanced catalytic activity and increased stability against protease digestion. *Nat Commun* 7:10619. <https://doi.org/10.1038/ncomms10619>
95. Collins J, Zhang T, Oh SW, Maloney R, Fu J (2017) DNA-crowded enzyme complexes with enhanced activities and stabilities. *Chem Commun* 53:13059–13062
96. Zhang Y, Wang Q, Hess H (2017) Increasing enzyme cascade throughput by pH-engineering the microenvironment of individual enzymes. *ACS Catal* 7:2047–2051
97. Jørgensen K, Rasmussen AV, Morant M, Nielsen AH, Bjarnholt N, Zagrobelny M, Bak S, Møller BL (2005) Metabolite formation and metabolic channeling in the biosynthesis of plant natural products. *Curr Opin Plant Biol* 8:280–291
98. Roberts CC, Chang CA (2015) Modeling of enhanced catalysis in multi-enzyme nanostructures: effect of molecular scaffolds, spatial organization, and concentration. *J Chem Theory Comput* 11:286–292

99. Chado GR, Stoykovich MP, Kaar JL (2016) Role of dimension and spatial arrangement on the activity of biocatalytic cascade reactions on scaffolds. *ACS Catal* 6:5161–5169
100. Tsitkov S, Hess H (2019) Design principles for a compartmentalized enzyme cascade reaction. *ACS Catal* 9:2432–2439
101. Tsitkov S, Pesenti T, Palacci H, Blanchet J, Hess H (2018) Queuing theory-based perspective of the kinetics of “channeled” enzyme cascade reactions. *ACS Catal* 8:10721–10731
102. Kerfeld CA, Heinhorst S, Cannon GC (2010) Bacterial microcompartments. *Annu Rev Microbiol* 64:391–408
103. Chen AH, Silver PA (2012) Designing biological compartmentalization. *Trends Cell Biol* 22:662–670
104. Hartl FU (1996) Molecular chaperones in cellular protein folding. *Nature* 381:571–580
105. Frotin F, Schueder F, Tiwary S, Gupta R, Körner R, Schlichthaerle T, Cox J, Jungmann R, Hartl FU, Hipp MS (2019) The nucleolus functions as a phase-separated protein quality control compartment. *Science* 365:342–347
106. Chen J, Seeman NC (1991) Synthesis from DNA of a molecule with the connectivity of a cube. *Nature* 350:631–633
107. Erben CM, Goodman RP, Turberfield AJ (2006) Single-molecule protein encapsulation in a rigid DNA cage. *Angew Chem Int Ed Engl* 45:7414–7417
108. Ge Z, Su Z, Simmons CR, Li J, Jiang S, Li W, Yang Y, Liu Y, Chiu W, Fan C, Yan H (2019) Redox engineering of cytochrome *c* using DNA nanostructure-based charged encapsulation and spatial control. *ACS Appl Mater Interfaces* 11:13874–13880
109. Zhang C, Tian C, Guo F, Liu Z, Jiang W, Mao C (2012) DNA-directed three-dimensional protein organization. *Angew Chem Int Ed Engl* 51:3382–3385
110. Zhao Z, Jaconetty EL, Liu Y, Yan H (2011) Encapsulation of gold nanoparticles in a DNA origami cage. *Angew Chem Int Ed Engl* 50:2041–2044
111. Juul S, Iacovelli F, Falconi M, Kragh SL, Christensen B, Fröhlich R, Franch O, Kristoffersen EL, Stougaard M, Leong KW, Ho Y-P, Sørensen ES, Birkedal V, Desideri A, Knudsen BR (2013) Temperature-controlled encapsulation and release of an active enzyme in the cavity of a self-assembled DNA nanocage. *ACS Nano* 7:9724–9734
112. Kohman RE, Cha SS, Man H-Y, Han X (2016) Light-triggered release of bioactive molecules from DNA nanostructures. *Nano Lett* 16:2781–2785
113. Kim SH, Kim K-R, Ahn D-R, Lee JE, Yang EG, Kim SY (2017) Reversible regulation of enzyme activity by pH-responsive encapsulation in DNA nanocages. *ACS Nano* 11:9352–9359
114. Grossi G, Dalgaard Ebbesen Jepsen M, Kjems J, Andersen ES (2017) Control of enzyme reactions by a reconfigurable DNA nanovault. *Nat Commun*. <https://doi.org/10.1038/s41467-017-01072-8>
115. Zhang Y, Hess H (2017) Toward rational design of high-efficiency enzyme cascades. *ACS Catal* 7:6018–6027
116. Rudiuk S, Venancio-Marques A, Baigl D (2012) Enhancement and modulation of enzymatic activity through higher-order structural changes of giant DNA–protein multibranch conjugates. *Angew Chem Int Ed Engl* 124:12866–12870
117. Lin J-L, Wheeldon I (2013) Kinetic enhancements in DNA–enzyme nanostructures mimic the sabatier principle. *ACS Catal* 3:560–564
118. Linko V, Eerikainen M, Kostianen MA (2015) A modular DNA origami-based enzyme cascade nano-reactor. *Chem Commun* 51:5351–5354
119. Jonchhe S, Pandey S, Emura T, Hidaka K, Hossain MA, Shrestha P, Sugiyama H, Endo M, Mao H (2018) Decreased water activity in nanoconfinement contributes to the folding of G-quadruplex and i-motif structures. *Proc Natl Acad Sci USA* 115:9539–9544
120. Yaraghi NA, Kisailus D (2018) Biomimetic structural materials: inspiration from design and assembly. *Annu Rev Phys Chem* 69:23–57
121. Perham RN (2000) Swinging arms and swinging domains in multifunctional enzymes: catalytic machines for multistep reactions. *Annu Rev Biochem* 69:961–1004
122. Jones DD, Stott KM, Howard MJ, Perham RN (2000) Restricted motion of the lipoyl-lysine swinging arm in the pyruvate dehydrogenase complex of *Escherichia coli*. *Biochemistry* 39:8448–8459
123. Ke G, Liu M, Jiang S, Qi X, Yang YR, Wooten S, Zhang F, Zhu Z, Liu Y, Yang CJ, Yan H (2016) Directional regulation of enzyme pathways through the control of substrate channeling on a DNA origami scaffold. *Angew Chem Int Ed Engl* 55:7483–7486
124. Chen Y, Ke G, Ma Y, Zhu Z, Liu M, Liu Y, Yan H, Yang CJ (2018) A synthetic light-driven substrate channeling system for precise regulation of enzyme cascade activity based on DNA origami. *J Am Chem Soc* 140:8990–8996

125. Yang YR, Fu J, Wootten S, Qi X, Liu M, Yan H, Liu Y (2018) 2D enzyme cascade network with efficient substrate channeling by swinging arms. *ChemBiochem* 19:212–216
126. Piperberg G, Wilner OI, Yehezkeili O, Tel-Vered R, Willner I (2009) Control of bioelectrocatalytic transformations on DNA scaffolds. *J Am Chem Soc* 131:8724–8725
127. Tepper AWJW (2010) Electrical contacting of an assembly of pseudoazurin and nitrite reductase using DNA-directed immobilization. *J Am Chem Soc* 132:6550–6557
128. Ma K, Yehezkeili O, Domaille DW, Funke HH, Cha JN (2015) Enhanced hydrogen production from DNA-assembled Z-scheme TiO₂-CdS photocatalyst systems. *Angew Chem Int Ed Engl* 54:11490–11494
129. Kopperger E, Pirzer T, Simmel FC (2015) Diffusive transport of molecular cargo tethered to a DNA origami platform. *Nano Lett* 15:2693–2699
130. Kopperger E, List J, Madhira S, Rothfischer F, Lamb DC, Simmel FC (2018) A self-assembled nanoscale robotic arm controlled by electric fields. *Science* 359:296–301
131. Kosuri P, Altheimer BD, Dai M, Yin P, Zhuang X (2019) Rotation tracking of genome-processing enzymes using DNA origami rotors. *Nature* 572:136–140
132. Ohmann A, Li C-Y, Maffeo C, Al Nahas K, Baumann KN, Göpfrich K, Yoo J, Keyser UF, Aksimentiev A (2018) A synthetic enzyme built from DNA flips 107 lipids per second in biological membranes. *Nat Commun* 9:2426. <https://doi.org/10.1038/s41467-018-04821-5>
133. Stein IH, Steinhauer C, Tinnefeld P (2011) Single-molecule four-color FRET visualizes energy-transfer paths on DNA origami. *J Am Chem Soc* 133:4193–4195
134. Dutta PK, Varghese R, Nangreave J, Lin S, Yan H, Liu Y (2011) DNA-directed artificial light-harvesting antenna. *J Am Chem Soc* 133:11985–11993
135. Dutta PK, Levenberg S, Loskutov A, Jun D, Saer R, Beatty JT, Lin S, Liu Y, Woodbury NW, Yan H (2014) A DNA-directed light-harvesting/reaction center system. *J Am Chem Soc* 136:16618–16625
136. Boulais É, Sawaya NPD, Veneziano R, Andreoni A, Banal JL, Kondo T, Mandal S, Lin S, Schlau-Cohen GS, Woodbury NW, Yan H, Aspuru-Guzik A, Bathe M (2017) Programmed coherent coupling in a synthetic DNA-based excitonic circuit. *Nat Mater* 17:159–166
137. Zhou X, Mandal S, Jiang S, Lin S, Yang J, Liu Y, Whitten DG, Woodbury NW, Yan H (2019) Efficient long-range, directional energy transfer through DNA-templated dye aggregates. *J Am Chem Soc* 141:8473–8481
138. Saghatelian A, Guckian KM, Thayer DA, Ghadiri MR (2003) DNA detection and signal amplification via an engineered allosteric enzyme. *J Am Chem Soc* 125:344–345
139. Gianneschi NC, Ghadiri MR (2007) Design of molecular logic devices based on a programmable DNA-regulated semisynthetic enzyme. *Angew Chem Int Ed Engl* 46:3955–3958
140. Mukherjee P, Leman LJ, Griffin JH, Ghadiri MR (2018) Design of a DNA-programmed plasminogen activator. *J Am Chem Soc* 140:15516–15524
141. Janssen BMG, Engelen W, Merckx M (2015) DNA-directed control of enzyme–inhibitor complex formation: a modular approach to reversibly switch enzyme activity. *ACS Synth Biol* 4:547–553
142. Kim Y, Phillips JA, Liu H, Kang H, Tan W (2009) Using photons to manipulate enzyme inhibition by an azobenzene-modified nucleic acid probe. *Proc Natl Acad Sci USA* 106:6489–6494
143. Xin L, Zhou C, Yang Z, Liu D (2013) Regulation of an enzyme cascade reaction by a DNA machine. *Small* 9:3088–3091
144. Hu Y, Wang F, Lu C-H, Girsh J, Golub E, Willner I (2014) Switchable enzyme/DNAzyme cascades by the reconfiguration of DNA nanostructures. *Chem Eur J* 20:16203–16209
145. Kou B, Chai Y, Yuan Y, Yuan R (2018) Dynamical regulation of enzyme cascade amplification by a regenerated DNA nanotweezer for ultrasensitive electrochemical DNA detection. *Anal Chem* 90:10701–10706
146. Xing C, Huang Y, Dai J, Zhong L, Wang H, Lin Y, Li J, Lu C-H, Yang H-H (2018) Spatial regulation of biomolecular interactions with a switchable trident-shaped DNA nanoactuator. *ACS Appl Mater Interfaces* 10:32579–32587

Publisher's Note Springer Nature remains neutral with regard to jurisdictional claims in published maps and institutional affiliations.



Directional Assembly of Nanoparticles by DNA Shapes: Towards Designed Architectures and Functionality

Ningning Ma^{1,2} · Brian Minevich³ · Jiliang Liu⁴ · Min Ji^{1,2} · Ye Tian^{1,2,5} · Oleg Gang^{3,6,7}

Received: 18 November 2019 / Accepted: 11 March 2020 / Published online: 27 March 2020
© Springer Nature Switzerland AG 2020

Abstract

In bottom–up self-assembly, DNA nanotechnology plays a vital role in the development of novel materials and promises to revolutionize nanoscale manufacturing technologies. DNA shapes exhibit many versatile characteristics, such as their addressability and programmability, which can be used for determining the organization of nanoparticles. Furthermore, the precise design of DNA tiles and origami provides a promising technique to synthesize various complex desired architectures. These nanoparticle-based structures with targeted organizations open the possibility to specific applications in sensing, optics, catalysis, among others. Here we review progress in the development and design of DNA shapes for the self-assembly of nanoparticles and discuss the broad range of applications for these architectures.

Keywords DNA shapes · DNA tiles · DNA origami · Nanoparticles · Self-assembly · Nanomaterials

1 Introduction

In the early 1980s, Seeman first proposed the use of DNA as a molecular building material for constructing well-defined architectures on the nanoscale [1]. Approximately two decades earlier, Holliday had suggested that a branched DNA structure can naturally occur as a key intermediate of the chromosome synapses and recombination [2]. As opposed to the traditional linear conformation of DNA, Seeman realized an opportunity for using these branched DNA architectures, or

Chapter 6 was originally published as Ma, N., Minevich, B., Liu, J., Ji, M., Tian, Y. & Gang, O. Topics in Current Chemistry (2020) 378: 36. <https://doi.org/10.1007/s41061-020-0301-0>.

✉ Ye Tian
ytian@nju.edu.cn

✉ Oleg Gang
og2226@columbia.edu

Extended author information available on the last page of the article

Holliday junctions, as the basis for crystallizing proteins using the designed periodic DNA structures [1]. These structures are formed through the assembly of two-dimensional (2D) and three-dimensional (3D) networks of oligomeric nucleic acids. He hypothesized that there is a significant potential for creating non-traditional nucleic acid architectures that possess a high degree of spatial orientation and addressability. The initial vision of self-assembled DNA shapes came with three over-arching goals: (1) development of individual DNA constructs with designed architecture, (2) establishing methods for creating large-scale organized assemblies from DNA, and (3) using DNA-based assembly approaches for guiding the organization of nano-objects into finite and periodic structures.

As a direct result of this vision, the field of DNA nanotechnology has emerged as an active field of research. While the challenges outlined in the original vision are not yet fully resolved, the current state of the field and its fast progress show the feasibility of using DNA nanotechnology methods for solving them, as well as for addressing many other scientifically and technologically important problems across a wide range of disciplines, from material science to sensing, and from nanomedicine to information storage. Efforts over the last few decades have been accompanied by the development of various methods for the design and synthesis of complex DNA shapes ranging from DNA tiles, designed using branched junctions [3], double-crossover molecules [4], and triple crossover molecules [5], to three-dimensional DNA shapes, including cubes [6], an octahedron [7], and many others, using a technique known as DNA origami [8]. The ability to generate complex DNA shapes has been used as the basis of various DNA architectures and nano-structuring platforms. Concurrently, efforts were made to integrate inorganic nanoparticles with DNA through the use of chemically modified DNA sequences that are grafted to nanoparticle (NP) surfaces, as was first demonstrated in 1996 by Mirkin and Alivisatos [9, 10]. The ability to form DNA shells of spherical or other morphologies through grafting to NPs directly led to strategies for the self-assembly of NP superlattices, as was demonstrated by the research groups of Gang and Mirkin, respectively, and coworkers in their pioneering 2008 studies [11–13] and expanded upon in later NP-based systems [14–17]. On the other hand, there has been tremendous progress on combining various strategies for guiding DNA-functionalized NPs into one-dimensional (1D), 2D, and 3D assemblies using DNA-based objects. Recent demonstrations of the integration of complex designed 3D DNA constructs with NPs with the aim to produce designed 3D NP organizations [18–20] merged NPs with DNA shaped direction and opens up enormous possibilities for creating designed 3D NP-based materials.

In this review we begin with a detailed discussion of the design of DNA shapes, and the origin and development of DNA tiles for guiding NP organization through scaffolding. We then summarize the development of DNA origami and its application for the programmable organization of NPs, followed by a detailed discussion of 3D polyhedral DNA frames for the assembly of periodic 3D NP organizations [19]. The latter strategy utilizes 3D polyhedral origami, rather than 2D DNA origami motifs, commonly either rectangular [8] or triangular [21], and allows for the guiding of NPs into 3D periodic structures. We conclude the review with a discussion

of applications of these assemblies of NPs based on DNA shapes and the overall impact of these shapes on structural DNA nanotechnology.

2 DNA Tiles

2.1 DNA Tiles: Fundamental Design and Development

The Holliday junction, a branched conformation of DNA, was used as the basis for synthesizing the first generation of DNA structures, known as DNA tiles. This led to the leveraging of more sophisticated designs of DNA tiles, with the realization of larger and more complex DNA architectures [22–25]. Advancements in the design of DNA tiles stemmed from the introduction of so-called “sticky ends,” which are unbound regions of single-stranded DNA (ssDNA) used at the site of linking to induce the binding of DNA shapes and structures, as shown in Fig. 1. Due to the accuracy of connection and the programmability of the location of the sticky ends, this became a crucial strategy for the construction of complex architectures from various DNA constructs. The initial immobile junction used was a tetrameric junction formed with oligonucleotides by combining sequence symmetry constraints with equilibrium calculations (Fig. 2a) [3], and the three-arm junction was designed in the same manner (Fig. 2b) [26]. With the development of branched DNA junctions, a set of 3D assemblies were designed, such as a cube [6] (Fig. 2e) and a truncated octahedron (Fig. 2f) [7]. Building upon these design principles, junctions with a higher degree of branching were developed [22], as shown in Fig. 2c. Researchers noted that increasing the degree of branching would reduce the structural stability of the structure and proposed increasing the number of nucleotide base pairings in each arm to mitigate this resultant structural instability. Leveraging this strategy of DNA branched junctions with a greater number of arms, it was possible to design

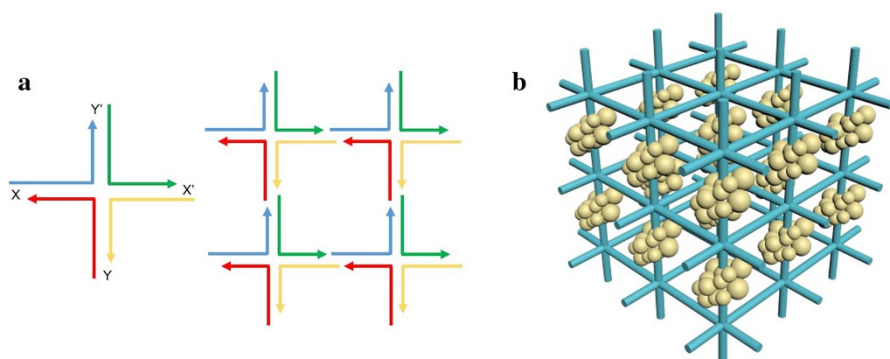


Fig. 1 The core concept of DNA nanotechnology. **a** An immobile Holliday junction and its combination. The junction structure (left) consists of four different single-stranded DNA sequences distinguished by the four colors, and it was designed with four sticky ends: X, Y, and their complements X' and Y'. Through hybridization, the junction structure can be extended into a two-dimensional (2D) array. **b** Schematic diagram of a three-dimensional (3D) DNA crystal for protein crystallization

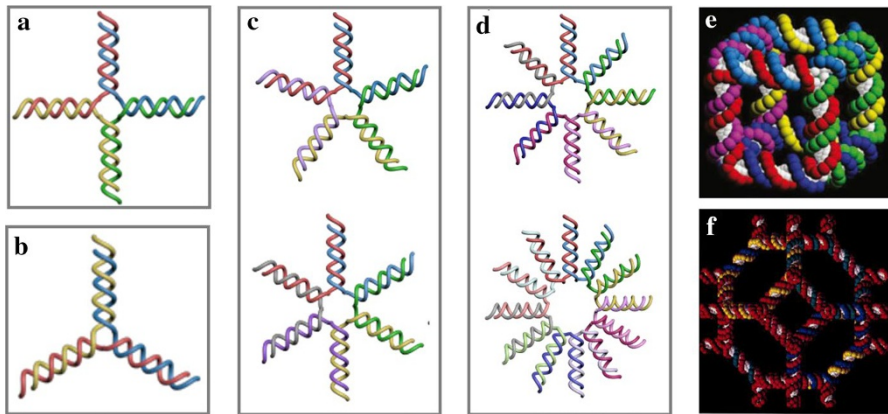


Fig. 2 Library of branched DNA junction structures and their typical assemblies. **a–d** Branched junction structures: **a** Four-arm branched junction, **b** three-arm branched junction, **c** five- and six-arm branched junction, **d** 8- and 12-arm branched junction. **e, f** Typical assemblies. **e** Molecule with the connectivity of a cube. Reproduced with permission from Seeman et al. [134], copyright 2017, Materials Research Society. **f** Molecule with the connectivity of a truncated octahedron. Reproduced with permission from Seeman et al. [134], copyright 2017, Materials Research Society

a wide range of 3D polygons, including those from more than ten space-filling networks with 432 symmetries, through the selection and control of the sticky end design [22]. Continued efforts related to these highly branched junctions resulted in the development of 8- and 12-arm junctions without any branch migration [27] (Fig. 2d). However, it remained vital to stabilize the structure by tuning the number of nucleotide pairs per arm. The 8- and 12-arm connected networks could be used to achieve an N-connected network, which represents highly complex 3D organizations, such as a series of connected cuboctahedra [27]. The development of branched DNA structures enriched the library of elements that could be used for the assembly of DNA architectures and for guiding nano-objects.

Seeman later proposed the use of an alternative DNA shape or motif, named a DNA double-crossover (DX) molecule [4], which could be used as the basis of structural design using DNA (Fig. 3a). In order to assemble crystalline structures or guide the organization of NPs, the fundamental units of the DNA structure require definable intermolecular interactions and sufficient rigidity to ensure the formation of the desired architecture. In the DX motif, two DNA strands follow an approximately continuous helical trajectory, while two additional strands form a crossover to bind the two original sequences together. This strategy results in increased mechanical stability, where the stiffness is twofold higher than that of a conventional linear duplex [double-stranded DNA (dsDNA)]. The DX motif was used to design five structurally unique arrangements, all of which were used as building blocks to assemble 2D structures; this method was then used to produce 2D crystals with specified patterning. A DNA hairpin was incorporated into the design of a DX molecule as a topographic label (Fig. 3a), the periodic spacing of which could be controlled and used to tether nanomaterials of interest [23]. A different motif, a 4×4 branched tile, was later used to generate 2D crystals with a programmable

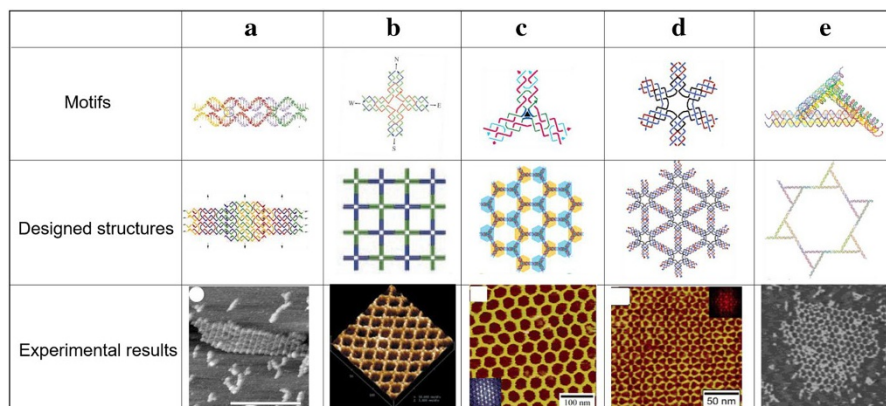


Fig. 3 Library of motifs basing on the double-crossover (DX) structure and their assemblies. **a** DX structure. Reproduced from Winfree et al. [23], with permission, copyright 1998, Nature Publishing Group. **b** 4×4 branched tile. Reproduced from Yan et al. [28], with permission, copyright 2003, *Science*. **c** Three-point-star. Reproduced from He et al. [29], with permission, copyright 2005, American Chemical Society. **d** Six-point-star. Reproduced from He et al. [24], with permission, copyright 2006, American Chemical Society. **e** DX triangle. Reproduced from Ding et al. [31], with permission, copyright 2004, American Chemical Society

designation for proteins and was metallized to demonstrate the assembled structure's functionality as a nanowire [28]. A high-order 2D array that was assembled with the proper designation of sticky ends is shown in Fig. 3b [28]. Additional structures were generated on the basis of these branched units, such as the three-arm branched junction analogue named the three-point-star [29] that can assemble 2D hexagonal arrays (Fig. 3c). The balance of flexibility and stress in the design of DNA motifs, particularly for the three-point-star, was investigated, and it was shown that this balance is critical to the assembly of well-ordered 2D arrays [29, 30]. Based on the same strategy, other DNA shapes were designed for the assembly of 2D crystalline organizations. These included a DNA six-point-star that assembled highly connective 2D arrays, as shown in Fig. 3d [24] and, as shown in Fig. 3e, a new motif that can generate trigonal arrays using the DX triangle whose stiffness had been significantly improved by the geometry of the design [31]. However, there was still a need to develop a platform or design that would allow for assembly in 3D space. It was with this in mind that Zheng et al. introduced key concepts for the synthesis of 3D architectures using DNA shapes [25]. The three simple principles that these researchers introduced to produce precisely designed 3D macroscopic objects were: (1) a robust motif with 3D structure, (2) introduction of affinity interactions to the interior of the motif, and (3) the use of predictable structures that can be assembled based on these interactions. The proposed design was a tensegrity triangle consisting of three helices not in the same plane with six exposed sticky ends. The interactions of these prescribed sticky ends was the basis for the assembly of a 3D periodic lattice [25]. There was an introduction of additional motifs, including the triple-crossover (TX) [5], the DNA parallelogram [32], and layered crossovers (LX) [33], all of which became vital elements for self-assembly in future studies. Meanwhile, efforts

continued on the development of strategies to access additional architectures. One of these efforts consisted of the assembly of DNA nanotubes with half-tube components. Two half-tube species were designed using two different bent TX (BTX) molecules and a single arched four-helix [4-helix bundle (4HB)] component to assemble a 6HB nanotube and an 8HB nanotube array, respectively. This work included an investigation of the influence of the external environment on the self-assembly of these objects into 1D arrays and reported the assemblies of DNA nanotubes with lengths of up to 500 nm [34].

The two important concepts in structural DNA nanotechnology, namely, branched DNA structures and the DNA crossover design, were then combined to self-assemble a 1.7-kb nucleotide sequence into a 3D octahedron, as shown in Fig. 4a. In the presence of five 40-mer synthetic oligodeoxynucleotides, the long ssDNA molecule can be folded into the octahedron structure using a denaturation–renaturation procedure. The programmability of this 3D object, which is related to the design of the oligodeoxynucleotides, can also be utilized to position the NPs with precision [35]. It was later proposed that the assembly of many distinct DNA strands could become quite difficult to achieve due to the increased number of DNA strands needed for the assembly of large, complex structures. It can also become quite difficult to design large numbers of unique DNA sequences, which is done in an effort to minimize any parasitic crosstalk and unintentional interactions between the DNA sequences used in a particular design. These difficulties result in a reduction in the overall addressability of the design and can affect the assembly and fidelity of the structure. To simplify the overall design, He et al. used symmetric three-point-star motif as the building block [29]. In subsequent studies, researchers investigated several factors to promote polyhedron formation, and through adjusting the length of

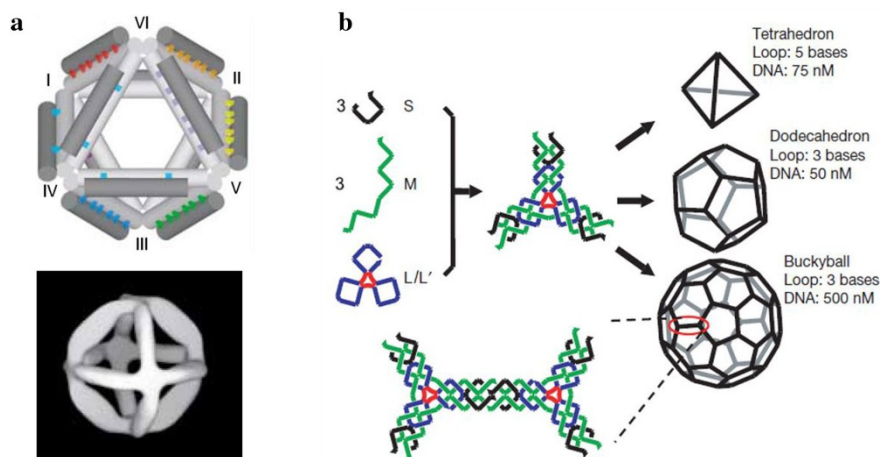


Fig. 4 **a** An octahedron structure folded by a 1669-nucleotide single-stranded DNA and its cryo-electron micrograph. Reproduced from Shih et al. [35], with permission, copyright 2004, Nature Publishing Group. **b** Diagram showing the formation of the symmetric three-point-star motif (left) and the DNA polyhedron (right). Top to bottom: tetrahedron, dodecahedron, and buckyball, respectively. Reproduced from He et al. [36], with permission, copyright 2008, Nature Publishing Group

loops and DNA concentration they were able to synthesize three distinct polyhedral objects (Fig. 4b), a tetrahedron, a dodecahedron, and a buckyball [36]. It was then shown that a modification of this star motif in which there is an increase in the number of points can serve as a building block to assemble an icosahedra [37]. Subsequent comprehensive exploration has resulted in the construction of a wide variety of architectures through the assembly of branched DNA building units becoming a robust strategy for the formation of complex structures. In 2012, Ke et al. proposed a different method to construct 3D architectures. These researchers designed and fabricated a series of short synthetic DNA strands, which were termed “DNA bricks.” In a procedure that is analogous to building a structure out of Lego bricks, they fabricated diverse discretionary architectures by using DNA bricks as the building block. With precise design of the functional DNA sticky ends, Ke et al. realized the guidance of NP assembly, which further expanded on structural fabrication and the guiding of nano-objects [38–40].

2.2 Organization of NPs with DNA Tiles

Since the emergence of the research field referred to as DNA nanotechnology, the development of DNA-based approaches for creating ordered materials has been very rapid. These complex structures, composed entirely of DNA, can be leveraged for the organization of nanomaterials into either clusters or crystalline architectures. By applying the methodology proposed for the hierarchical self-assembly of polyhedra from the three-point-star DNA tile motif [36], it was therefore possible to successfully synthesize a wide-range of DNA polyhedrons and utilize these as nanoscale cages for the programmable encapsulation of NPs. The inherent addressability of the design allowed for controlled variation in the number of DNA-functionalized gold NPs (AuNPs) and encapsulation of these AuNPs into correlated DNA cages via hybridization, as shown in Fig. 5a. The reversibility of this system was also demonstrated, whereby the AuNPs could be released from the DNA cages [41]. In another study, DNA polyhedrons were utilized to interrupt the symmetry of spherical NPs and coordinate these with defined valences [42]. The resultant valency of the object would dictate directional bonds for further architectural assembly. These programmable clusters of AuNPs were viewed as atomic and molecular analogs, with a defined valence and bonding direction. Researchers were able to demonstrate various geometries using distinct DNA cages, including a tetrahedron, an octahedron, a trigonal prism, and a D_3 symmetry structure. In the case of the tetrahedral cage, a NP was encapsulated and fixed at the center of the cage and it could only interact with complementary NPs, based on the complementarity of the DNA shells that were grafted onto the surfaces of the respective particles through the faces of the polyhedral cage. These interparticle interactions would organize the NPs into their desired positions. Thus, the five-NP structure can be seen as a molecular analog of methane (CH_4). Additional work with this strategy showed the viability of this structure to generate a sulfur hexafluoride (SF_6)-like structure, hexamethyltungsten [$\text{W}(\text{CH}_3)_6$]-like structure, and even ethane (C_2H_6)-like structures with two cores (Fig. 5b) [42].

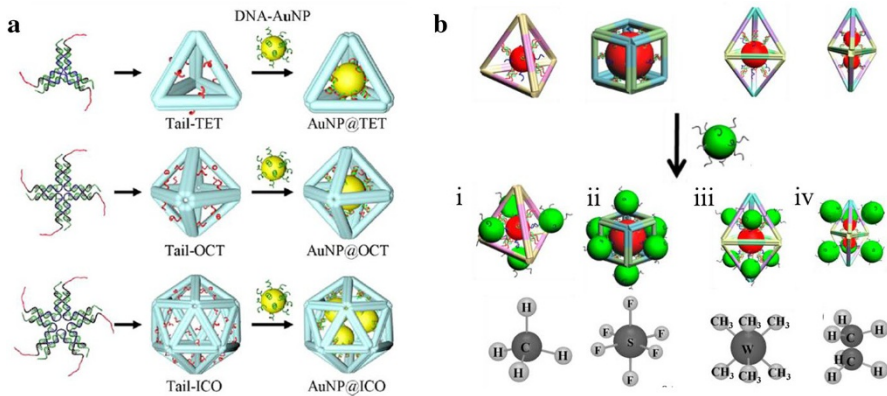


Fig. 5 **a** Schematic diagram of gold nanoparticle–DNA conjugate ($AuNP@DNA$) cage structures fabricated through DNA polyhedrons used to encapsulate AuNPs. Three different DNA polyhedrons are shown: a tetrahedron (*TET*) (top), an octahedron (*OCT*) (middle), and an icosahedron (*ICO*) (bottom). The size of the icosahedron is sufficiently large for encapsulating three AuNPs (bottom), while the other two can only accommodate one AuNP (top and middle). Reproduced from Zhang et al. [41], with permission, copyright 2014, American Chemical Society. **b** Diagram showing the self-assembly of molecule-like NPs directed by DNA polyhedron nanocages. With different polyhedrons, a set of molecule-like nanoparticles are assembled, including methane (CH_4)-like (i), sulfur hexafluoride (SF_6)-like (ii), hexamethyltungsten [$W(CH_3)_6$]-like (iii), and ethane (C_2H_6)-like (iv) structures. Reproduced from Li et al. [42], with permission, copyright 2015, American Chemical Society

The successful fabrication of DNA tiles and subsequent assembly into periodic structures opened up the possibility to organize NPs beyond finite size structures and clusters and enable the organization of low-dimensional arrays. For example, the TX structure was used as a template for guiding NPs into linear arrays, whereby the tiles were modified with two DNA stem loops located at the upper and lower sections of the helices, respectively. The modification of one or both of the two stem loops for the association of the streptavidin molecule resulted in linear arrays of streptavidin, including single- and double-layer designs, as shown in Fig. 6a [43]. Additional efforts made to guide the organization of other nanomaterials via DNA tile assemblies. A 2D array was assembled using the DX molecule design and was used to align AuNPs. Four different DX molecules were integrated and investigated as the scaffold for the 2D crystal. Small AuNPs (diameter 1.4 nm) were arranged into 2D arrays through covalent attachment with controllable interparticle spacings of 4 and 64 nm (Fig. 6b) [44]. As an extension of this work, AuNPs were organized onto arrays of DNA tiles via hybridization rather than covalent bonding. Using DNA hybridization as the method of attachment to the 2D array, the crystal growth conditions and the component synthesis could be independently optimized. Efforts were also made to guide more than one kind of nanomaterial onto a single surface and then to subsequently assemble that unit into periodic 2D arrays. By designing distinct binding sequences, the research group of Kiehl and coworkers successfully guided the positioning of two sizes of AuNPs (diameters 5 and 10 nm) onto a 2D multi-nanocomponent array (Fig. 6c) [45, 46]. In another study, the previously

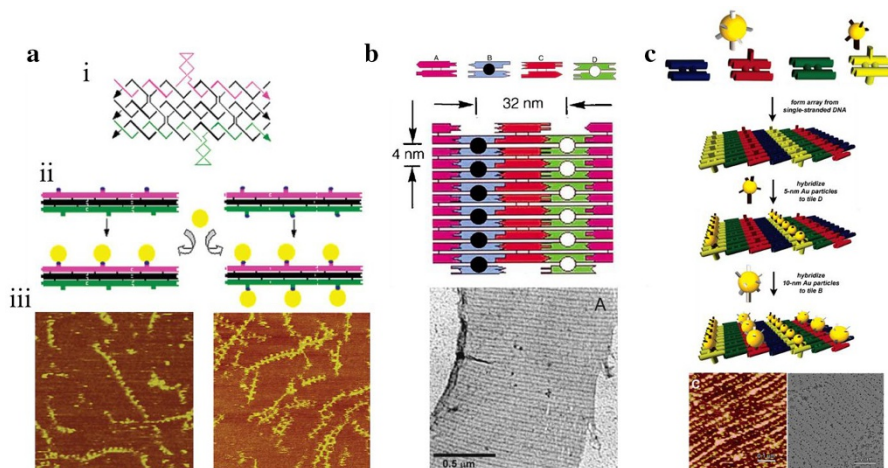


Fig. 6 One-dimensional (1D) and 2D NP arrays assembled by DNA structures. **a** Streptavidin linear arrays fabricated with TX DNA template. i–iii Structure diagram of the TX molecule (i), design and formation of the linear array (ii), and atomic force microscopy (AFM) images of the single-layer and double-layer arrays (iii). Reproduced from Li et al. [43], with permission, copyright 2004, American Chemical Society. **b** Schematic diagram and transmission electron microscopy (TEM) image of 1.4 nm-AuNP 2D array assembled with DX DNA template. Reproduced from Xiao et al. [44], with permission, copyright 2002, Nature Publishing Group. **c** Process of two different size AuNPs arranging into a common 2D array, with the AFM and TEM images shown at the bottom left and bottom right, respectively. Reproduced from Le et al. [45], with permission, copyright 2004, American Chemical Society

mentioned four-arm tiles were used to assemble 2D arrays with precise AuNP positioning whereby the distance between neighboring particles was designed to be ~ 38 nm [47]. The factors influencing the formation of these 2D arrays were also being studied, including the number of sticky ends, the symmetry and size of the DNA tile, and the programmable distances between the AuNPs relative to the size of the DNA tiles and 2D arrays. Various tiles were mixed together to diversify the types of 2D assemblies that could be obtained, and this mixing resulted in the generation of three different 2D arrays (Fig. 7a) [48]. At approximately the same time, a research group also demonstrated that multiple 2D arrays of NPs could be obtained by using more than one triangular DNA motif in the same design. In particular, the two triangular motifs, based on stiff DX molecules, used could each capture a particle independent of the other tile and then assemble into 2D arrays of ordered NPs (Fig. 7b) [49].

Efforts continued on constructing 3D assemblies based on methods developed for ordering NPs via DNA tiles organized in well-ordered 2D arrays. As such, the 2D assembly method was modified to develop a strategy for the generation of 3D architectures. This strategy consisted of the programmable rolling of a 2D sheet into a variety of 3D tube conformations. Four variants of DX tiles were designed to assemble 2D arrays, including one that had a site ready to associate AuNPs (denoted as “A”) and another that had a DNA stem loop located on the opposite side (denoted as “B”). When the arrays were assembled, 5-nm AuNPs were aligned in parallel lines. However, the chosen tiles were packed side by side

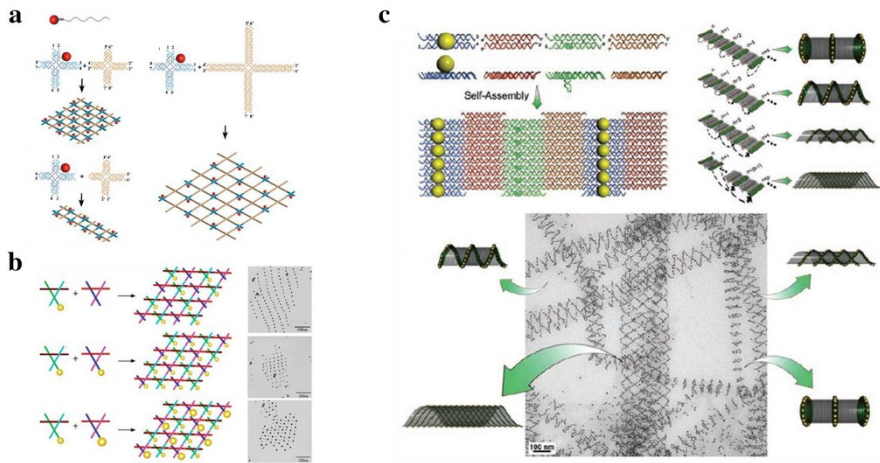


Fig. 7 Schematic representations of 2D AuNP arrays assembled with 4×4 tiles and tensegrity triangles. **a** Diagram showing three different assembly of periodical AuNP nanoarrays. The different forms of the three lattices depends on the design of the tile structure, including size and sticky ends. Reproduced from Sharma et al. [48], with permission, copyright 2006, Wiley-VCH Verlag GmbH and Co. KGaA. **b** Diagram showing the schematic and TEM images of three different AuNP arrays with varying number and size of AuNPs. Reproduced from Zheng et al. [49], with permission, copyright 2006, American Chemical Society. **c** Diagram of 3D DNA nanostructures fabricated with DX tiles showing the design of the DX tiles for AuNPs arranging (top left), two of which are specifically designed, including one that carries a 5-nm AuNP pointing upwards (shown in blue) and one that carries a DNA stem loop pointing downwards (shown in green). Four different 3D tubular structures were assembled through adjustment of the interval of the corresponding edge tiles that associate (top right). The bottom image is the TEM image of the tubular nanoscale architectures. Reproduced from Sharma et al. [50], with permission, copyright 2009, *Science*

at distances of < 5 nm and, consequently, the 2D arrays began to curl due to the strong electrostatic and steric repulsions between the neighboring AuNPs. This design was deemed useful for tuning the 2D NP organization with either neighboring or alternating NP positions. It was noted that when the 2D sheet is rolled into a tube, a variety of 3D NPs can be designed, including stacked rings, single spirals, double spirals, and nested spiral tubes, as shown in Fig. 7c. A follow-up study revealed that the ultimate dominant tube conformation is related to the size of the AuNPs and the design of the DX tiles. In that study, three different sizes of AuNPs were used, and it was discovered that with increasing AuNP size, from 5 to 15 nm, the stacked-ring conformation dominated. For example, in the system with 10-nm AuNPs, 92% of the formed tubes were stacked rings [50]. Significant efforts have since have been made to use DNA tiles for the organization of NPs into complex 2D architectures. However, reliable methods to assemble 3D assemblies of NPs using DNA tiles remain very limited.

3 Shaping DNA strands with NPs

DNA can be shaped not only through the formation of constructs as discussed above, but also by organizing DNA strands on NP surfaces, a construct referred to as a DNA shell. Concurrent with the efforts expended to design DNA tiles, significant work was directed towards diversifying the assemblies of NPs through the tailoring of DNA shells grafted onto a NP's surface. After the first reports of successfully grafting synthetic DNA to a AuNP [9, 10], it took over a decade to discover the design principles needed to dictate the crystallization of DNA-functionalized NPs [11–13]. It has been shown that NPs whose respective surfaces are functionalized with DNA can assemble into NP lattices when the designs of the DNA shells are favorable for an interaction potential that can stabilize a 3D ordered phase. Moreover, a specific pathway to crystallization is required for proper hybridization of the grafted DNA and for particles repositioning into ordered phases. Two common strategies for directing these interparticle interactions have been direct hybridization [11] and linker-mediated hybridization [12, 14]. Many parameters associated with the DNA shell and its morphology, including composition of the shell [51–53] and length [17] and design of the DNA motifs, with sequence design referring to both a Watson–Crick interacting portion or an entropic spacer [11], optimize interactions favorable for the formation of ordered phases [54, 55]. It is also possible to diversify the structure of the assembled phase of isotropic NPs by varying the number of hybridizing DNA sequences and the hydrodynamic radius [56, 57]. The tuning of two key parameters, namely, DNA linker length and the number of linkers per particle, can dictate the transformations between different ordered and disordered phases [14], as shown in Fig. 8a, b.

The conformation of the DNA shell can also be tuned by grafting DNA to anisotropic NPs. It has been shown computationally that solid polyhedral objects can assemble into a variety of structures [58]. Researchers have demonstrated the 3D assembly of anisotropic NPs grafted with DNA [16] typically favor phases that maximize interparticle hybridizations. However, a range of interesting and unexpected effects can occur in the multi-strand shell. For example, the spontaneous breaking of DNA shell symmetry was observed for nanorods due to the collective hybridization and flexibility of the DNA chains [15], which results in the formation of a ladder-like linear organization rather than smectic or nematic types of organization. These DNA shells have complex morphologies, and Lu et al. discovered for nanocubes that the polymeric effects of DNAs on shaped NPs can result in the anisotropic distribution of sequences on particle surfaces and effective complex shapes [59]. This phenomenon can drastically affect the resultant assembly. These researchers noticed that for a specific range of linker lengths, DNA functionalized nanocubes packed in a peculiar zigzag arrangement [59], which is a breakdown of the orientational symmetry of the underlying nanoscale object (Fig. 8c, d). The shape of DNA shells of anisotropic particles plays a key role in the self-assembly process, particularly for interactions between dissimilarly shaped particles. In one case, functionalized anisotropic particles were used

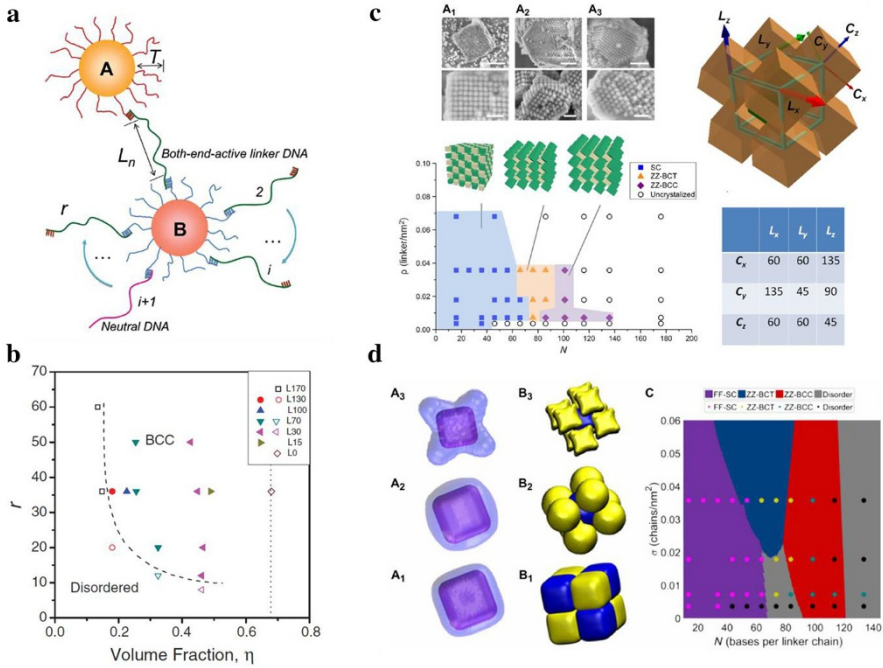


Fig. 8 Design and assembly of spherical and cubic NPs with DNA shells. **a, b** Schematic representation of DNA-grafted particles connected by r DNA linkers with length L_n (**a**) and experimental phase diagram showing the transition from the ordered to disordered state as a function of the nominal linker/NP ratio and NP volume fraction (**b**). Dashed line in **b** represents the boundary between dis-ordered and ordered phases. **a, b** Reproduced from Xiong et al. [14], with permission, copyright 2009, American Physical Society. **c** Scanning electronic microscopy (SEM) images of nanocube lattices with varying distributions of DNA grafted to the particle surface, and phase diagram of assemblies through variations in grafting density and DNA sequence length. **d** Simulations of DNA corona morphologies as a function of grafting chain length. A combined computational and experimental phase diagram reveals simple cubic, body-centred cubic (*BCC*) or body-centred tetragonal (*BCT*) phases and a novel, so-called ZZ packing arrangement. **c, d** Reproduced from Lu et al. [59], with permission, copyright 2019, American Association for the Advancement of Science

to coordinate isotropic particles. The inherent symmetry of the anisotropic particles and its respective shell will dictate the organization of the spherical nanoparticles [60]. In this study, Lu et al. showed that cubic NPs can coordinate spherical particles through local arrangements in the designed DNA shell that cannot be realized for spheres, giving rise to the formation of the unique 3D lattice of alternating cubes and spheres. The particle shape complementarity can be also used to promote a formation of 3D lattices [61]. In this respect, the nature of the DNA shell can be seen as a tunable DNA shape that can leverage a large diversity of existing NP shapes for the prescribed organization of functional nanomaterials.

At the same time, there is a plethora of new nanoscale effects in this regime that remain to be discovered and well understood.

4 DNA Origami

4.1 DNA Origami: Folding by Design

The DNA tile has been demonstrated to be a highly programmable scaffold for guiding NPs into complex architectures. However, The DNA tile has a certain lack of design flexibility that limits the number and complexity of possible NP architectures. In 2006, Rothemund proposed a new method to build DNA structures, which is known as “DNA origami” [8]. Similar to traditional paper origami, DNA origami involves the folding of a long ssDNA sequence, known as the scaffold sequence, through prescribed hybridizations with many shorter sequences, known as staple sequences. The DNA origami technique uses a scaffold sequence, M13mp18, derived from the M13 bacteriophage. The specific interactions between the staple sequences and the scaffold result in the self-assembly of the designed shape, as shown in Fig. 9a. As a direct result of this development, many researchers in various fields were able to utilize this technique for the development of a number of symmetric shapes, such as a square, rectangle, smile face, star, or triangle (Fig. 9b), and even highly asymmetric shapes, such as a dolphin [62] or a Chinese map [63]. Douglas et al. demonstrated the use of DNA origami for the design of a 6HB [64, 65] that was developed to facilitate nuclear magnetic resonance studies of membrane proteins in solution, and this strategy was later extended to realize a 24-helix bundle (24HB) for guiding NPs [66]. This type of tubular structure was also utilized to assemble NPs in a 3D chiral architecture [67].

The cornerstone of DNA nanotechnology is the ability to reliably design and generate target 2D and 3D structures with the prescribed nanoscale features. The

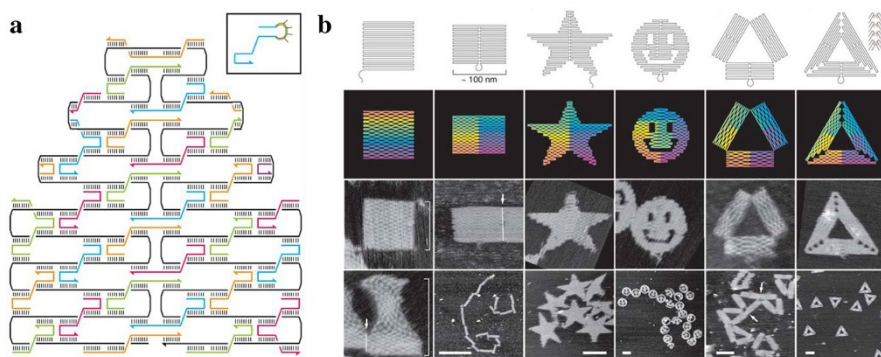


Fig. 9 **a** Schematic representation of the design of DNA origami, **b** 2D patterns designed by the DNA origami technique. **a**, **b** Reproduced from Rothemund [8], with permission, copyright 2006, Nature Publishing Group

introduction of the DNA origami technique enabled research related to a variety of fields and applications as it was a simpler platform to utilize. One example is the work carried out to design a 2D DNA origami sheet subsequently folded into a DNA tetrahedron that could be used as a molecular container [68]. A similar strategy was reported with the development of a nanoscale DNA box with a programmable lid that can open based on a specific DNA input signal [69]. The research group of Shih and coworkers conducted comprehensive studies on the formation of 3D DNA origami that resulted in the successful design and assembly of complex shapes using a honeycomb lattice as the basis of the designs [70–72], as shown in Fig. 10a. These origami shapes included the monolith, square nut, railed bridge, genie bottle, stacked cross, and slotted cross, with precisely controlled dimensions ranging from 10 to 100 nm. To make the design of DNA origami more accessible, a software package, named caDNAno, was developed to aid with scaffold sequence routing and staple sequence design [71, 72]. Ke et al. subsequently reported assembled 3D objects whereby the origami design consisted of double helices with the four nearest neighbors separated by 8 bp and the staple strand positioned to cross over one of its four neighbors, as shown in Fig. 10b. Using this design, the helices were arranged as a square lattice, forming overall a cuboid structure from the successful stacking of two to eight repeating layers [73]. Efforts were also made to design origami and multilayered structures based on hexagonal and hybrid arrangements of helices (Fig. 10c), resulting in four different origami structures. This strategy took full advantage of the three different arrangements of DNA helices within the designed objects, including the honeycomb, square, and the hexagonal lattice of helices, to build a hybrid-lattice origami [74].

The development of additional design strategies and thorough investigation of the origami technique contributed to the increasing number of possible DNA structures, such as a nanotube, a helix bundle, and even more complex 3D structures, each of which could serve as the basis of guiding complex organizations of NPs. An

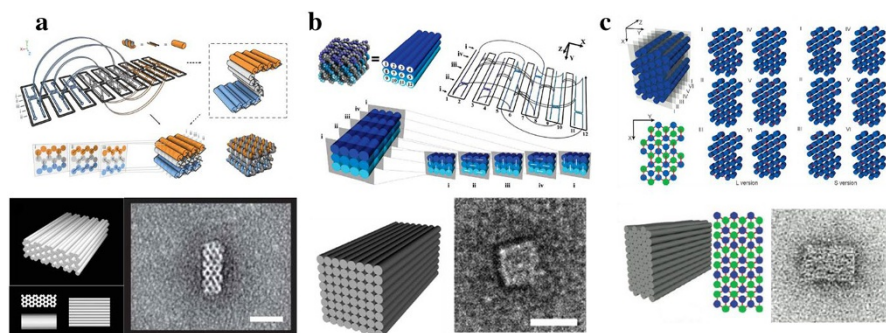


Fig. 10 Three different designs of 3D helices in lattice arrangements within DNA origami and the typical products. **a** Honeycomb lattice. Reproduced from Douglas et al. [72], under the terms of the Creative Commons Attribution Non-Commercial License, copyright 2009, the Authors, published by *Nucleic Acids Research*. **b** Square lattice. Reproduced from Ke et al. [73], with permission, copyright 2009, American Chemical Society. **c** Hexagonal lattice. Reproduced from Ke et al. [74], with permission, copyright 2012, American Chemical Society

example of such a complex DNA origami design is the DNA-origami ball, reported by Han et al. [75], which can be used as a vessel for drug delivery. Building upon this work, the same research group went on to design square, triangle, and 24HB structures of larger sizes but only after incorporating more than one scaffold into the design [76]. Additional efforts have been made to improve the folding efficiency or experimental yield of DNA origami, as this is necessary for DNA origami to become a viable platform for application purposes or use in large-scale manufacturing. Recent studies have shown that DNA can be efficiently folded at constant temperature, which is preferable to the long and complex annealing protocols traditionally performed to achieve DNA origami folding [77, 78].

Using the caDNA software, Tian et al. successfully synthesized an octahedron frame [79] (Fig. 11a), similar to the nanoscale octahedron assembled from the 1.7-kb scaffold [35], except that each strut of the octahedron of this design was a 6HB. Compared to the previous strategy used to form an octahedron, the DNA origami technique enabled a much more straightforward design of a nanoscale octahedron with high yield. This octahedron frame comprised twelve 6HBs and was assembled from a single scaffold sequence and 144 staple sequences. The overall design is highly programmable, whereby sticky ends can be positioned virtually anywhere along the struts of the octahedron. In this case, researchers constructed the octahedron with sticky ends at the vertices of the frame, as well as sticky ends that could be placed facing towards the interior of the frame for the programmable capture of a nanomaterial. This modification in the design of the origami facilitated the assembly of this object and AuNPs into a 3D superlattice. Meanwhile, several other kinds of 3D frames were designed with different symmetries, as shown in Fig. 11b, including a cube, a prism, a triangular bipyramid, and an extended octahedron [19]. The programmability of the DNA origami technique allowed these frames to be incorporated into a library of building blocks for crystal assembly and NP guiding, which

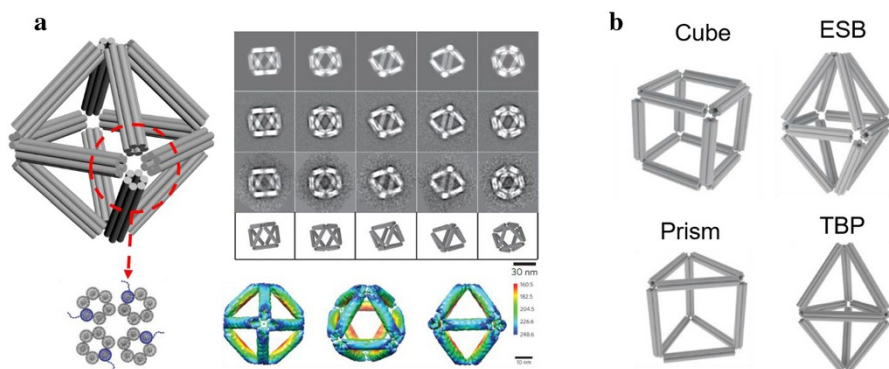


Fig. 11 DNA origami frame structures. **a** Diagram of the octahedron frame (left top) and a detailed view of the design of the vertexes (left bottom). To the right are cryo-electron microscopy images and the reconstructed structures. Reproduced from Tian et al. [79], with permission, copyright 2015, Nature Publishing Group. Additional designs of DNA frames, including the cube, elongated square bipyramid (*ESB*), prism, and triangular bipyramid (*TBP*). Reproduced from Tian et al. [19], with permission, copyright 2016, Nature Publishing Group

was a significant development in the field of structural DNA nanotechnology [19, 79]. The research groups of Bathe and coworkers and Yan and coworkers together developed sophisticated software packages for the design of complex DNA structures [80]. The accuracy of this method will enable the expansion of the overall library of DNA shapes and make many desired shapes easily accessible. Simultaneously, there has been rapid progress in mineralizing DNA structures [81, 82] and expanding the structure size [38, 76], which will enable DNA-based material to be transferred into a broad range of environments and applications.

4.2 Organization of NPs with DNA Origami

As a straightforward strategy for the fabrication of complex architectures, the DNA origami technique has been used to develop a variety of building blocks for assemblies, templating, and bio-applications. Researchers worked on combining two maturing subsets of DNA nanotechnology, namely, the tailoring of the DNA shell grafted to NPs and the use of DNA origami to assemble structures in one, two, and three dimensions to achieve well-ordered NP architectures. The high degree of programmability and addressability of DNA origami allowed access to many desired structures. One example of a programmable DNA origami motif was the “nanoflower” [83], a DNA origami that could host a NP at its center and had tunable interactions at its exterior surface to direct the assembly of either 1D or 2D structures depending on the angles of the prescribed sites of the inter-frame interactions or sticky ends (Fig. 13b). It is also possible to achieve the same complex structures assembled with DNA tiles using DNA origami. The DNA origami

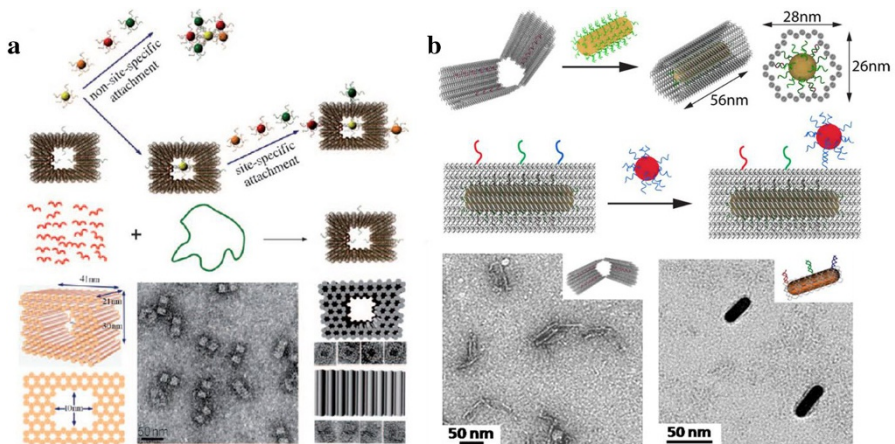


Fig. 12 **a** Design of the DNA nanocage for interrupting the symmetry of AuNPs, and schematic diagram of the site-specific AuNP attachment. TEM images of the DNA nanocages are shown at bottom. Reproduced from Zhao et al. [84], with permission, copyright 2011, Wiley-VCH Verlag GmbH and Co. KGaA. **b** Diagram showing the function of a gold nanorod (AuNR) and the arrangement of AuNPs. TEM images at bottom show the actual state of the nanocage and the functioned AuNR. Reproduced from Shen et al. [85], with permission, copyright 2016, American Chemical Society

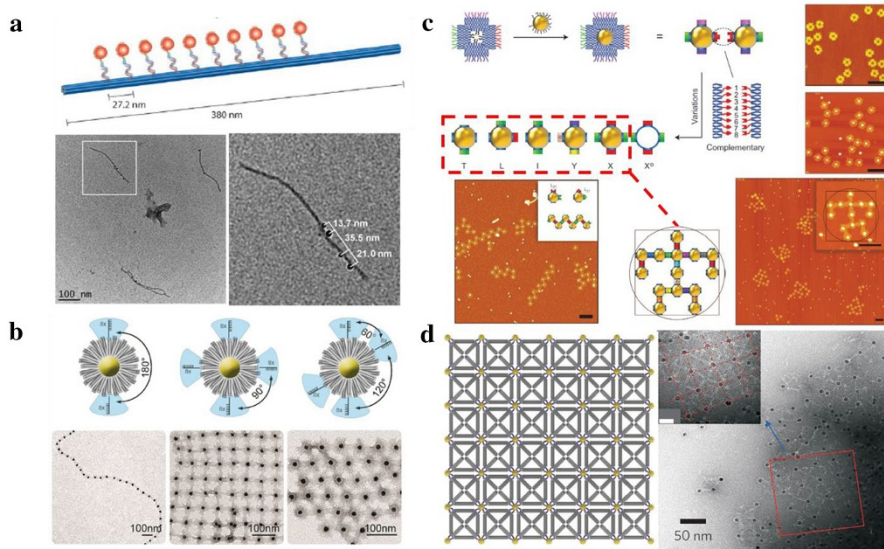


Fig. 13 One-dimensional (1D) and 2D NP arrays fabricated with DNA origami. **a** Schematic diagram and TEM image of linear array of AuNPs arranged with a 380-nm six-helix bundle (6HB). Reproduced from Stearns et al. [86], with permission, copyright 2009, Wiley-VCH Verlag GmbH and Co. KGaA. **b** Diagram showing the design of the “nanoflower” origami motif. With different ssDNA exposed, various AuNP arrays could be fabricated. Reproduced from Schreiber et al. [83], with permission, copyright 2016, American Chemical Society. **c** Fabrication of the DNA-framed NPs and corresponding AFM images. A nanoscale analog of Leonardo da Vinci’s Vitruvian Man was assembled with various types of DNA-framed NPs. Reproduced from Liu et al. [92], with permission, copyright 2016, Nature Publishing Group. **d** 2D AuNP arrays fabricated with octahedron frames. Reproduced from Tian et al. [79], with permission, copyright 2015, Nature Publishing Group

technique can be used to design structures for the purpose of breaking the symmetry of spherical NPs and to guide the arrangement of NPs with defined orientation and interparticle distances, one of which was a hollow rectangular prism based on the honeycomb lattice [84], as shown in Fig. 12a. The targeted attachment of distinct particles showed the ability to position particles both inside and outside of the origami cage with designed symmetry. Similar work was done utilizing a hollow, rod-like DNA origami (Fig. 12b) [85]. The realization of DNA nanotubes and N-helix bundles served as additional templates for the high-ordered organization of NPs. Before the introduction of DNA origami in 2006, DNA AuNPs were extensively organized into complex structures with DNA tiles. DNA origami was used by Stearns et al. [86] to direct the in situ nucleation and growth of AuNPs. These researchers designed and synthesized a 380-nm 6HB and chose an A3 peptide as the means to guide the positioning of the generated NPs; following the addition of soluble gold ions, the AuNPs grew 5–10 nm at the designated growth sites (Fig. 13a) [86]. In an effort to expand the number of available materials that can be organized via DNA origami, semiconductor nanocrystals or quantum dots (QDs) were organized into 1D arrays utilizing DNA origami [87]. More complex

assemblies were achieved, as evidenced by the helical assembly of AuNPs onto a DNA origami template [66]. Similarly, helical assemblies of AuNPs were made by first organizing 15-nm AuNPs onto the surface of a rectangular sheet and then rolling the sheet, which resulted in a helical assembly of particles [67].

Based on nanoarrays assembled using DNA tiles, which were used as a means to organize 2D arrays of proteins, a rectangular-shaped DNA origami was shown to exhibit a high degree of flexibility and programmability. This design was no longer bound by the conventional sticky end designation specific to DNA tiles, and the origami could be modified to designate the location of an aptamer at any location on the origami surface. The programmable nature of the origami was used to position proteins in an “S” shape, and these protein arrays could be assembled with high efficiency. Aptamers were used to retain their specific functionality, even after the assembly of complex structures [88]. Supplementary to these efforts, work was done to investigate alternative methods to bind AuNPs to these assembled structures. The use of AuNPs monofunctionalized with lipoic acid-modified DNA sequences was shown to increase functionality and binding efficiency, which rose from 45 to 91% with reduced errors in NP positioning [89]. Work continued on the organization of nanomaterials other than gold. A triangular DNA origami motif was designed to organize silver nanoparticles (AgNPs) at specified positions. Three variations of dimeric AgNP structures were designed, each with specified interparticle spacings, as well as an asymmetric trimetric AgNP structure and a heterodimer of a AuNP and AgNP [21]. Complex clusters from metallic NPs were assembled using rigid linear DNA origami linkers that were used to define large interparticle distances [90]. Recently, Lin et al. demonstrated the use of a site-specific covalent binding, instead of base-pairing, enables the fabrication of supra-architectures from shaped origami and NPs [91].

The research group of Gang and coworkers explored the possibility of using different types of building blocks that could be co-assembled into a complex yet designed cluster and with periodic planar architectures. These researchers realized this aim by using the so-called polychromatic 2D origami frames [92], which possess multiple types of distinguishable bonds arranged in defined anisotropic configuration, resulting in “colored” valence of these building blocks. Different types of these polychromatic frames exhibit differently colored valence, which allows for the building of complex architectures through the selection of a specific set of the polychromatic building blocks. These researchers developed a planar DNA origami structure that had a fourfold valency with respect to its programmable binding interactions, and an empty square window in the interior of the origami was used to hold a DNA-functionalized AuNP, as shown in Fig. 13c [92]. Each of the four exterior faces were decorated with distinct binding interactions, labeled with different colors, resulting in the various species of polychromatic 2D frames. Through the selection of polychromatic building blocks and their valence, it was possible to achieve programmable connectivity of the blocks. By controlling the types of different blocks and their ratio in the multi-component assembly, different periodic and non-periodic structures can be rationally formed, including clusters of different shapes, 1D linear structures, the zig-zag chain, and 2D arrays. This strategy was used to assemble a nanoscale analogue of Leonardo da Vinci’s Vitruvian Man [92].

In an effort to achieve designed 3D NP clusters with controlled placement of particles, Tian et al. used polyhedral DNA origami, as discussed in detail in an earlier publication [79]. In this design, the six distinct vertices of the octahedron were used to encode the binding locations for particles of varying size. Using this method, these researchers assembled an octahedral cluster, a square-shape cluster, and non-chiral and chiral hetero-clusters, all based on three types of NPs. Furthermore, 1D and 2D arrays of AuNPs (Fig. 13d) were assembled with the octahedral frames and NPs serving as connectors between the frames [79].

In order to gain further control over NP organization in three dimensions, the research group of Gang and coworkers proposed a strategy in which designed DNA constructs of different shapes could serve as programmable topological linkers between NPs [18, 19, 93, 94]. The overall strategy is powerful since it permits the building of different lattice types for the same type of particles; thus, it addresses a major problem in nanotechnology—that of creating different materials from the same type of functional nanoblocks. For example, the octahedron frame was used to assemble 3D superlattices of AuNPs, and this technique was expanded to include a variety of lattice symmetries using multiple polyhedral frames [19], inspiring the development of a set of 3D nanoscale molecular frames and their use in this

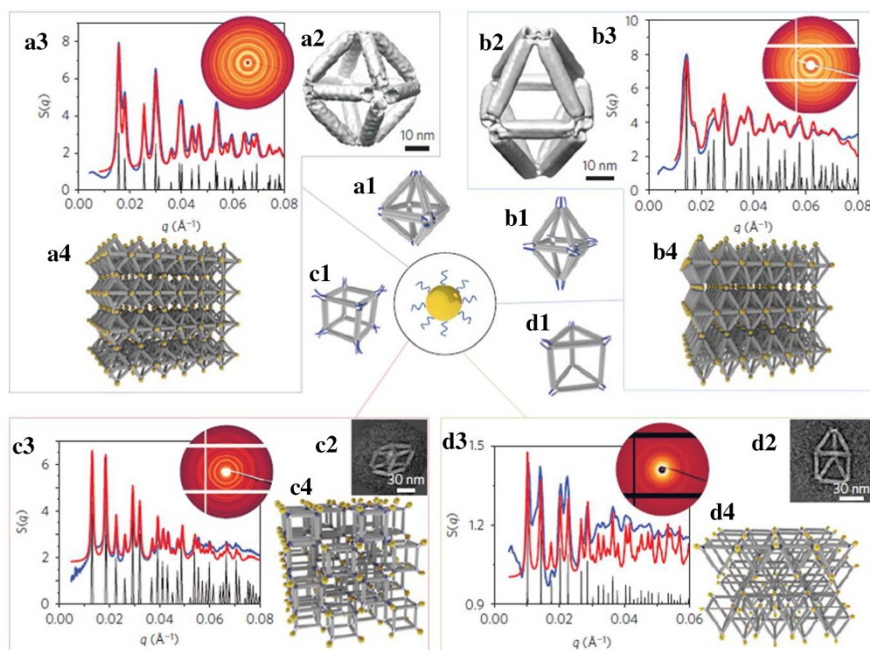


Fig. 14 Schematic diagram of four different DNA origami frames guiding NPs into the ordered 3D lattice. Models of DNA origami shape are shown. **a1–d1** Octahedron (**a1**), elongated square bipyramid (**b1**), cube (**c1**), and prism (**d1**). **a2–d2** Reconstruction of DNA origami frames from cryo-electron microscopy. **a3–d3** X-ray scattering (SAXS) results of different architectures. **a4–d4** Models of ordered 3D lattices. Reproduced from Tian et al. [19] with permission, copyright 2016, Nature Publishing Group

self-assembly approach. The structure of these assemblies was investigated using small angle X-ray scattering (SAXS) and shown to have a long-range order with structural characteristics matching their respective designs, as shown in Fig. 14 [19]. This strategy was combined with encapsulation of the NP inside frames to assemble a series of NP superlattices from the cubic diamond family [18], which had up to that point been a considerable challenge in the field of colloidal self-assembly. In this case, tetrahedral DNA origami frames were used to coordinate DNA-functionalized AuNPs (Fig. 15a). Moreover, several design requirements with respect to the particles and origami frames were revealed [95]. The resultant structure could also be tuned by adjusting the size of the NPs, resulting in a zinc blende structure or a “wandering” zinc blende structure [18]. In addition to 3D nanoscale frames, there are a few other viable strategies for the assembly of complex 3D structures. For crystalline assemblies and NP organization, the prerequisites of high rigidity and sufficient

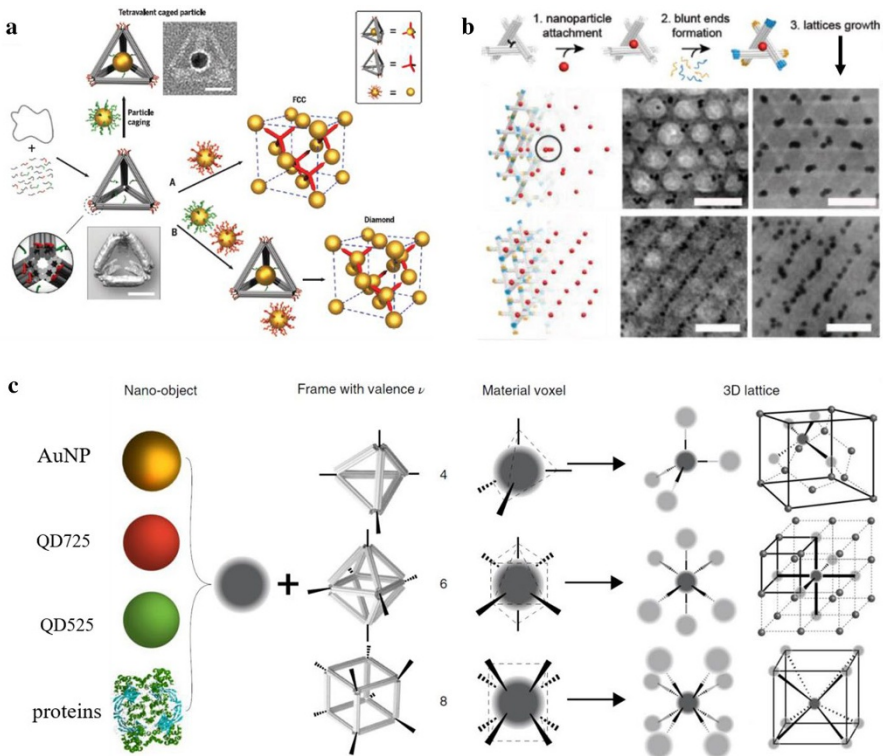


Fig. 15 Three-dimensional (3D) AuNP lattice assembled with 3D DNA origami frames. **a** Schematic diagram of FCC lattice and diamond lattice of AuNP fabricated with tetrahedron DNA origami. Reproduced from Liu et al. [18], with permission, copyright 2016, American Association for the Advancement of Science. **b** Rhombohedral lattices fabricated with the DNA origami tetravalent triangle structure. Reproduced from Zhang et al. [20], with permission, copyright 2018 Wiley-VCH Verlag GmbH and Co. KGaA. **c** Schematic of the broadly applicable platform for 3D lattice assembly from material voxels, showing 3D origami frames of different shapes (tetrahedron, octahedron, cube) that can be integrated with NPs and proteins as desired. Reproduced from Tian et al. [94], with permission, copyright 2020, Nature Publishing Group

open guest space are essential for the design of the building blocks. However, with increasing size, DNA structures become more flexible and lose their ability to precisely control distances at the nanoscale. Recently, a DNA–origami-based tensegrity with a triangle structure was synthesized by the research group of Liedl and coworkers for the purpose of assembling a 3D architecture entirely from DNA [20]. This design yielded a rhombohedral lattice that was constructed using this tensegrity triangle motif that had both sufficient rigidity and available space (Fig. 15b). In this work, these researchers show that this motif can host NPs with a diameter of 20 nm, thereby greatly expanding the application of DNA nanotechnology.

A broadly applicable platform for the assembly of 3D nanomaterials from so-called material voxels, which are 3D origami frames of different shapes that can be integrated with NPs, proteins and enzymes, was recently demonstrated by Tian et al. [94]. This strategy decouples the assembly process, governed by DNA programmable bonds between origami, from nano-object details, as shown in Fig. 15c. This decoupling allows for the assembly of 3D designed, functional arrays from NPs, proteins and enzymes using the same assembly approach. Novel optical and chemical properties were shown in this study for QDs and enzymatic arrays, respectively.

5 Applications of DNA Architectures for Nanomaterials

Despite the field of DNA nanotechnology emerging from the concept of specifically crystallizing proteins into ordered 3D structures, there have been tremendous efforts to utilize numerous functional nanomaterials in a variety of real-life applications. A significant portion of this review has been dedicated to the organization of metallic NPs through the use of DNA tiles and origami, and these studies are of particular interest because the optical properties of plasmonic NPs can be controlled based on their structure. Researchers used dsDNA to fabricate chiral nanostructures in which the DNA was folded into a pyramid so that the vertices of the pyramid designated a particle binding site [96]. Additional study was directed towards investigating this design while incorporating various materials into the structure [97]. This strategy proved to be highly effective for the generation of single- or multi-component chiral isomers with strong R/S optical activity. The incorporation of gold nanorods (AuNRs) with DNA origami assembly strategies has also been a popular strategy in the research field of plasmonic properties. Pal et al. used a triangular DNA origami motif to immobilize anisotropic AuNRs onto the origami surface and demonstrate the control of NR orientation in dimer structures (Fig. 16a) and in AuNP–AuNR heterodimers [98]. A 2D DNA origami can have two programmable surfaces, and both can be utilized to immobilize AuNRs to fabricate chiral structures (Fig. 16b) [99, 100]. This dual-faced functionalization of the 2D origami was also used to assemble the AuNR helix structure shown in Fig. 16c [101]. The strategy of using planar origami plates to assemble complex supra-NP linear architectures from AuNPs and QDs was recently demonstrated by Tian et al. [102]. This approach allowed these researchers to investigate plasmonic effects in linear meso-structures [102]. Recently, the research group of Gang and coworkers demonstrated single QD polarized emitters that were assembled by 3D origami from plasmonic and

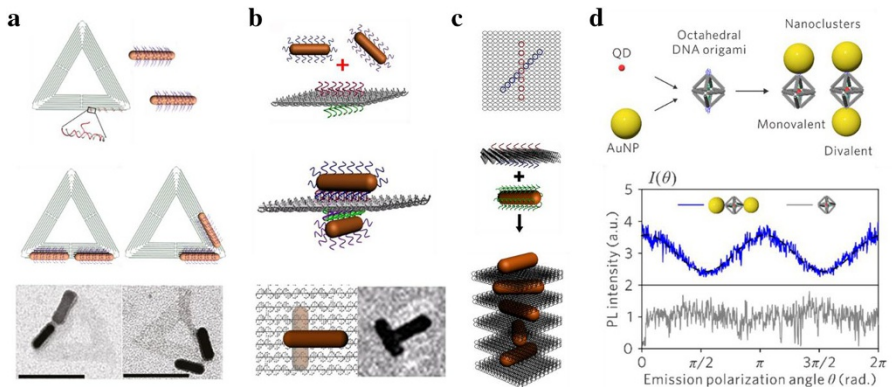


Fig. 16 Plasmonic structures assembled with 2D DNA origami. **a** AuNR dimer structures with different angles (180° and 60°) between AuNPs based on a triangular origami. Reproduced from Pal et al. [98], with permission, copyright 2011, American Chemical Society. **b** AuNR dimer structures with various relative positions were fabricated with a bifacial DNA origami. Reproduced from Lan et al. [99], with permission, copyright 2013, American Chemical Society. **c** The AuNR helix was assembled with bifacial DNA origami as template. Reproduced from Lan et al. [101], with permission, copyright 2015, American Chemical Society. **d** Light-emitting (PL photoluminescence) clusters with polarized emission were assembled from 3D octahedral origami, AuNPs and quantum dots (QDs). Reproduced from Zhang et al. [103], with permission, copyright 2019, American Chemical Society

light-emitting NPs (Fig. 16d) [103]. This integration permitted the control of active optical elements at the nanoscale, thereby providing opportunities for the manipulation of emitted light.

Assemblies of AuNRs organized by DNA origami motifs have been developed to have dynamic properties. Based on the same AuNR–DNA origami design, one of the AuNRs was stationary (“stator”) while the AuNR bound to the opposite side of the DNA origami could move across the origami in one direction in programmable intervals (“walker”) based on DNA strand displacement reactions. This type of AuNR walking was also achieved using a DNA origami design with a more complex topology (Fig. 17a) [104]. This research was built upon to include multiple walkers relative to a single stator, where the walkers could walk either independently or together (Fig. 17b) [105]. The orientations of the AuNRs could also be programmed through the use of a pair of 14HB origami. The relative angle of the rods was controlled by two DNA locks, and these locks could be reconfigured to tune this angle based on strand displacement reactions (Fig. 17c) [106]. This lock design was modified to be tuned by UV-light when azobenzene-modified DNA oligonucleotides [107] were used or by changes in pH based on Hoogsteen interactions whereby a duplex and ssDNA could hybridize into triplets [108]. This design has recently been utilized as a platform to detect viral RNA at picomolar concentrations [109].

DNA origami has also been leveraged in multiple ways for the chiral assembly of spherical gold NPs (Fig. 18). To achieve this goal, various DNA origami templates have been used, such as 14HB [66], DNA origami sheet subsequently rolled up into a tube [67], tubular DNA origami for prescribed AuNR and AuNP helices [110], a DNA origami toroid [111], or a bifacial DNA origami [112].

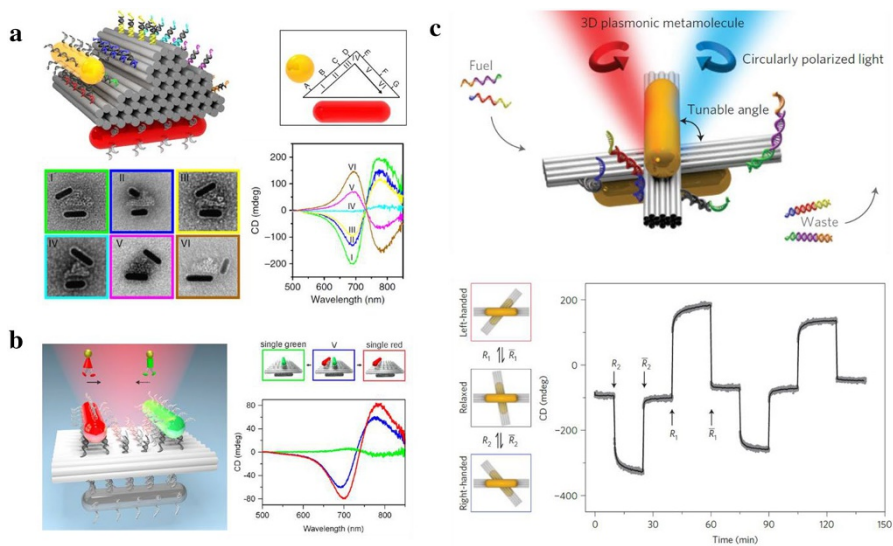


Fig. 17 Dynamic chiral plasmonic devices assembled by DNA origami. **a** A plasmonic AuNR can walk on a triangular prism origami using DNA strand displacement reactions. The TEM images and the circular dichroism (CD) spectra show the movement of the AuNR (Movement of AuNRs shown from I–VI positions). Reproduced from Zhou et al. [104] under a Creative Commons Attribution 4.0 International License, copyright 2015, Nature Publishing Group. **b** Diagram showing that two AuNRs could walk stepwise on DNA origami separately or together. Movements are shown by the CD spectra. Reproduced from Urban et al. [105], with permission, copyright 2015, American Chemical Society. **c** 3D plasmonic metamolecule could tune the angle of two bundles and switch between the left-handed and right-handed states through the strand displacement reaction. The change in angle is shown by CD spectra. Reproduced from Kuzyk et al. [106], with permission, copyright 2014, Nature Publishing Group

Subsequent work with the 14HB template design resulted in a dynamic two-state plasmonic material in which the optical response of the system is switchable [113]. DNA origami was also used to construct plasmonic nano-antennas to enhance the fluorescence intensity in a plasmonic hotspot [114]. Similar efforts were made to probe surface-enhanced Raman spectroscopy and future sensing applications [115–117]. The nanometer precision of DNA origami was utilized to prescribe the relative positions of QDs and AuNPs in various geometries to control the average photon count rate and lifetime of the QD [118]. A triangular DNA origami was used to study long-range quenching of QDs based on its distance to a AuNP [119].

The stability and rigidity of DNA origami allowed these structures to be used as molds with desired cavity morphologies. A branched DNA origami structure was metallized in a two-step process that was a significant development towards DNA-templated nanocircuits [120]. Origami templates were also used to synthesize gold structures with arbitrary shapes, including rings, pairs of parallel bars, H shapes, gold nanocuboids and nanodonuts (Fig. 19a) [121, 122]. The same strategy was employed to adjust the size of AuNPs for further application, such as optoelectronics [66, 90]. A new concept was introduced to seed AuNPs inside of 3D DNA origami nanostructures to nucleate the growth of gold structures into

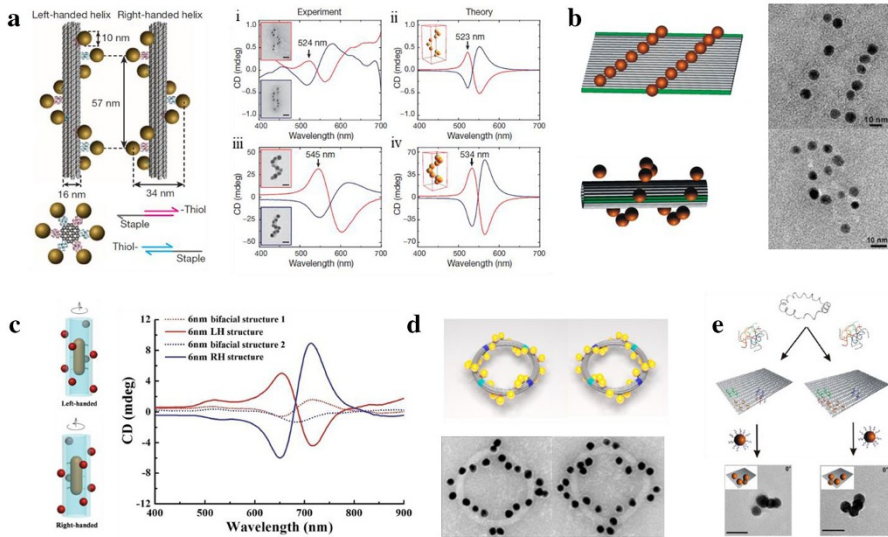


Fig. 18 Anisotropic chiral plasmonic structures assembled by DNA origami. **a** Diagram showing a chiral AuNP helix assembled with a 24HB. In designing different sites, right-handed and left-handed structures are obtained. Various sizes of AuNPs are assembled, and a peak shift is captured by CD spectra (i–iv). Reproduced from Kuzyk et al. [66], with permission, copyright 2012, Nature Publishing Group. **b** An AuNP helix structure assembled through rolling up a rectangular origami. Reproduced from Shen et al. [67], with permission, copyright 2012, American Chemical Society. **c** Schematic diagram of the AuNP@AuNR structure and its CD spectra (*RH* right-handed, *LH* left-handed). Reproduced from Shen et al. [110], with permission, copyright 2017, Wiley-VCH Verlag GmbH and Co. KGaA. **d** Diagram of toroidal super-chiral plasmonic structure assembled with DNA origami and its TEM images. Reproduced from Urban et al. [111], with permission, copyright 2016, American Chemical Society. **e** Four AuNPs arranged into RH and LH structures with bifacial DNA origami. Reproduced from Shen et al. [112], with permission, copyright 2013, American Chemical Society

shapes whose resultant structure would be determined by the DNA origami mold (for example, see Fig. 19b) [123]. In another study, a series of shape-controlled inorganic nanostructures were reported, including gold and silver nanostructures, using DNA origami structures with different cavities; examples of the shape of these cavities are cuboid, triangle, sphere and Y-shape. Silver and QDs were also combined to fabricate a novel structure (Fig. 19c). To meet the demand of the casting highly stiff DNA origami molds were created [124]. Recently, there have been reports of the mineralization of DNA origami shapes and structures through a sol–gel chemistry that results in biomimetic silica nanostructures that are more robust. Compared to their precursor DNA nanostructure, these DNA–silica hybrid materials possess greater stability against a variety of factors, including temperature, pressure, salt concentration, and other buffer conditions [81, 82].

DNA shapes have also shown potential for utilization in biomedical applications as chemical nanoreactors and for drug delivery. One study reported a hexagonal barrel made using DNA origami capable of carrying nanoscale cargo, with a lock and key mechanism whereby the lock consisted of a DNA aptamer and

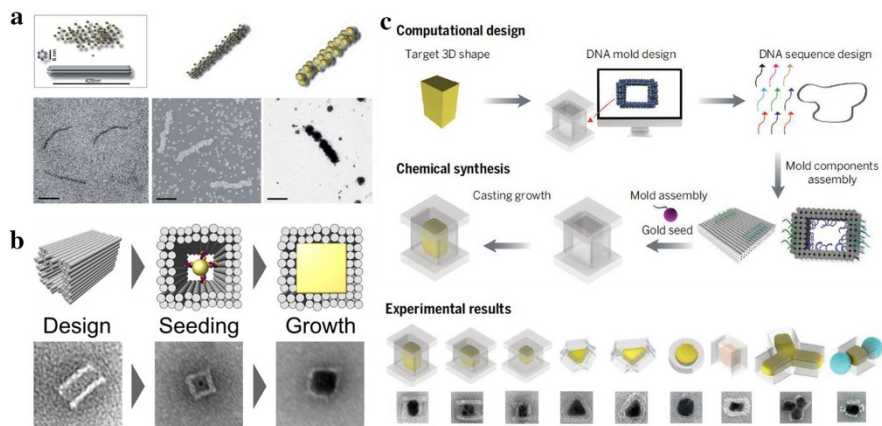


Fig. 19 Shaped-controlled growth of inorganic nanostructures. **a** Schematic diagram of a AuNP cluster assembled by DNA origami and growth of NPs. The TEM images (bottom) show the structures in different states. Reproduced from Schreiber et al. [121], with permission, copyright 2011, Wiley-VCH Verlag GmbH and Co. KGaA. **b** Cuboid gold nanostructure is synthesized using DNA origami with a rectangular cavity. The diagram shows the process and the TEM images of each step (bottom). Reproduced from Helmi et al. [123], with permission, copyright 2014, American Chemical Society. **c** Schematic diagram showing the design of the DNA origami and various shape-controlled growth of inorganic nanostructures. Reproduced from Sun et al. [124], with permission, copyright 2014, American Association for the Advancement of Science

complementary strand and the key was the corresponding antigen [125]. DNA tiles were used to design a tweezer-like structure that is used to actuate the activity of an enzyme–cofactor pair [126]. 3D DNA origami structures were developed as nanoscale reactor vessels; in one case a hexagonal cylinder origami was used as a nanoreactor to confine a cascading enzymatic reaction between glucose oxidase and horseradish peroxidase [127]. DNA origami was also used in efforts to compartmentalize enzyme to enhance their catalytic activity and stability [128] and was also studied as a molecular delivery system for targeted therapeutics [129].

DNA nanotechnology is considered to be a powerful method for the development of nanoelectronics. However, during the past decade, the guiding and fabricating reactions of NPs have always occurred in the liquid phase, and the organization or aggregation is formless and difficult to predict. Kershner et al. proposed a strategy to construct controllable and predictable DNA architectures [130]. These researchers designed a template involving the self-assembly of DNA origami and a top–down microfabrication technique known as lithography to pattern a substrate. After the triangular origami was arranged on the templated-substrate, the desired architecture was obtained, as shown in Fig. 20. The final positions of the AuNPs could be determined and were found to be quite accurate according to the design. This methodology can be applied to a wide range of applications in the fabrication of functional devices [131].

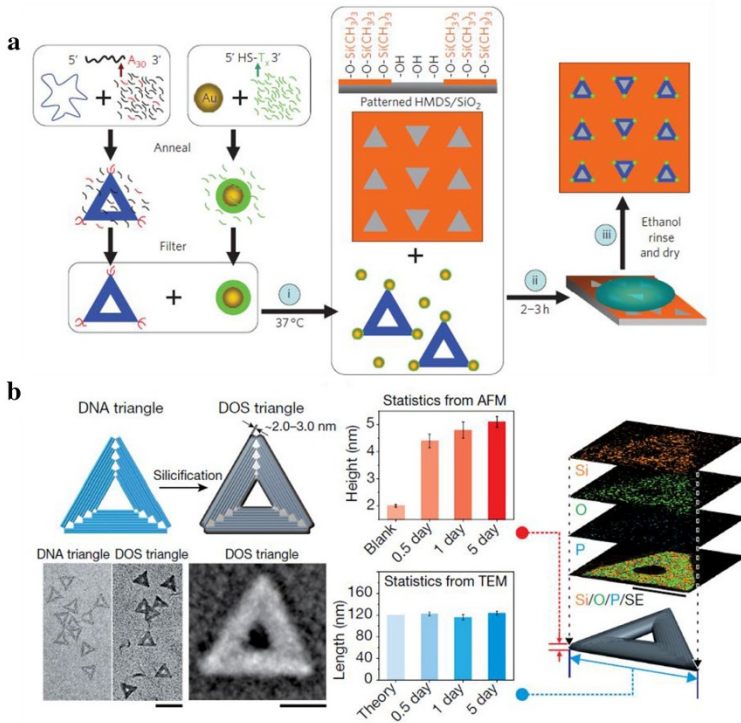


Fig. 20 **a** Diagram shows that results from combining the lithography technique and DNA origami with NPs attached could be predictable arranged. Reproduced from Hung et al. [131], with permission, copyright 2010, Nature Publishing Group. **b** Method for creating silica nanostructures from DNA templates by a sol-gel chemistry shown for triangular origami with height mapping and corresponding energy-dispersive X-ray spectroscopy (EDS) spectra [81]. Reproduced with permission. Copyright 2018, Nature Publishing Group

6 Summary and Outlook

DNA nanotechnology was originally proposed to address a problem in protein crystallography, but in only a few decades it has become a powerful methodology for building at nanoscale. DNA nanotechnology has become a rapidly maturing field that extends to many new conventional and nonconventional applications in material science, chemistry, biotechnology, and nanomedicine. The development of DNA tiles [4, 6, 32, 65] and DNA origami [33, 62, 71–73, 130] enabled the realization of complex architectures, from low-dimension arrays [18, 46, 48, 79, 98] to complex structures [18–20, 50, 92, 132, 133], and from static structures [98–101] to dynamic architectures [104–108]. The programmability of DNA shapes provided a new nanotechnology toolbox for establishing platform approaches for the designed NP organizations [18, 19, 134, 135], particularly in three dimensions, where conventional nanofabrication methods are limited. These advances in DNA nanotechnology have been applied to the development of materials with specific function. Even with

complex programmable characteristics, DNA structures might retain their stability in the bio-environment, which is an attractive feature for emerging biomedical applications [125–128].

The discovery and design of functional nanomaterials for a diverse application require the design and synthesis of specifically designed DNA structures, the ability to integrate them with nanoscale building blocks, and the ability to assemble them into the desired structures.

Acknowledgements The work was supported by National Natural Science Foundation of China (Grant nos. 21971109 and 21834004), Jiangsu Youth Fund (Grant no. BK20180337), the Fundamental Research Funds for the Central Universities (Grant no. 14380151), and the US Department of Energy, Office of Basic Energy Sciences (Grant DE-SC0008772). The research carried out at the Center for Functional Nanomaterials, Brookhaven National Laboratory was supported by US Department of Energy, Office of Science Facility, under Contract No. DE-SC0012704. This work was also supported by the Program for Innovative Talents and Entrepreneur in Jiangsu (No. 133181), Shenzhen International Cooperation Research Project (No. GJHZ20180930090602235) and Nanjing Science and Technology Innovation Project for Oversea Scholars' Merit Funding (No. 133170).

References

1. Seeman NC (1982) Nucleic acid junctions and lattices. *J Theor Biol* 99(2):237–247. [https://doi.org/10.1016/0022-5193\(82\)90002-9](https://doi.org/10.1016/0022-5193(82)90002-9)
2. Holliday R (1964) A mechanism for gene conversion in fungi. *Genet Res.* <https://doi.org/10.1017/s0016672300001233>
3. Kallenbach NR, Ma RI, Seeman NC (1983) An immobile nucleic-acid junction constructed from oligonucleotides. *Nature* 305(5937):829–831. <https://doi.org/10.1038/305829a0>
4. Fu TJ, Seeman NC (1993) DNA double-crossover molecules. *Biochemistry* 32(13):3211–3220. <https://doi.org/10.1021/bi00064a003>
5. LaBean TH, Yan H, Kopatsch J, Liu FR, Winfree E, Reif JH, Seeman NC (2000) Construction, analysis, ligation, and self-assembly of DNA triple crossover complexes. *J Am Chem Soc* 122(9):1848–1860. <https://doi.org/10.1021/ja993393e>
6. Chen JH, Seeman NC (1991) Synthesis from DNA of a molecule with the connectivity of a cube. *Nature* 350(6319):631–633. <https://doi.org/10.1038/350631a0>
7. Zhang YW, Seeman NC (1994) Construction of a DNA-truncated octahedron. *J Am Chem Soc* 116(5):1661–1669. <https://doi.org/10.1021/ja00084a006>
8. Rothmund PWK (2006) Folding DNA to create nanoscale shapes and patterns. *Nature* 440(7082):297–302. <https://doi.org/10.1038/nature04586>
9. Alivisatos AP, Johnsson KP, Peng X, Wilson TE, Loweth CJ, Bruchez MP, Schultz PG (1996) Organization of 'nanocrystal molecules' using DNA. *Nature* 382(6592):609–611. <https://doi.org/10.1038/382609a0>
10. Mirkin CA, Letsinger RL, Mucic RC, Storhoff JJ (1996) A DNA-based method for rationally assembling nanoparticles into macroscopic materials. *Nature* 382(6592):607–609. <https://doi.org/10.1038/382607a0>
11. Nykpanchuk D, Maye MM, van der Lelie D, Gang O (2008) DNA-guided crystallization of colloidal nanoparticles. *Nature* 451(7178):549–552. <https://doi.org/10.1038/nature06560>
12. Park SY, Lytton-Jean AKR, Lee B, Weigand S, Schatz GC, Mirkin CA (2008) DNA-programmable nanoparticle crystallization. *Nature* 451(7178):553–556. <https://doi.org/10.1038/nature06508>
13. Xiong HM, van der Lelie D, Gang O (2008) DNA linker-mediated crystallization of nanocolloids. *J Am Chem Soc* 130(8):2442–2443. <https://doi.org/10.1021/ja710710j>
14. Xiong H, van der Lelie D, Gang O (2009) Phase behavior of nanoparticles assembled by DNA linkers. *Phys Rev Lett* 102(1):015504. <https://doi.org/10.1103/PhysRevLett.102.015504>

15. Vial S, Nykypanchuk D, Yager KG, Tkachenko AV, Gang O (2013) Linear mesostructures in DNA–nanorod self-assembly. *ACS Nano* 7(6):5437–5445. <https://doi.org/10.1021/nn401413b>
16. Jones MR, Macfarlane RJ, Lee B, Zhang J, Young KL, Senesi AJ, Mirkin CA (2010) DNA–nanoparticle superlattices formed from anisotropic building blocks. *Nat Mater* 9(11):913–917. <https://doi.org/10.1038/nmat2870>
17. Macfarlane RJ, Lee B, Jones MR, Harris N, Schatz GC, Mirkin CA (2011) Nanoparticle superlattice engineering with DNA. *Science* 334(6053):204–208. <https://doi.org/10.1126/science.1210493>
18. Liu W, Tagawa M, Xin HL, Wang T, Emamy H, Li H, Yager KG, Starr FW, Tkachenko AV, Gang O (2016) Diamond family of nanoparticle superlattices. *Science* 351(6273):582–586. <https://doi.org/10.1126/science.aad2080>
19. Tian Y, Zhang Y, Wang T, Xin HL, Li H, Gang O (2016) Lattice engineering through nanoparticle–DNA frameworks. *Nat Mater* 15(6):654–661. <https://doi.org/10.1038/nmat4571>
20. Zhang T, Hartl C, Frank K, Heuer-Jungemann A, Fischer S, Nickels PC, Nickel B, Liedl T (2018) 3D DNA origami crystals. *Adv Mater* 30(28):e1800273. <https://doi.org/10.1002/adma.201800273>
21. Pal S, Deng Z, Ding B, Yan H, Liu Y (2010) DNA-origami-directed self-assembly of discrete silver-nanoparticle architectures. *Angew Chem Int Ed Engl* 49(15):2700–2704. <https://doi.org/10.1002/anie.201000330>
22. Wang YL, Mueller JE, Kemper B, Seeman NC (1991) Assembly and characterization of 5-arm and 6-arm DNA branched junctions. *Biochemistry* 30(23):5667–5674. <https://doi.org/10.1021/bi00237a005>
23. Winfree E, Liu FR, Wenzler LA, Seeman NC (1998) Design and self-assembly of two-dimensional DNA crystals. *Nature* 394(6693):539–544. <https://doi.org/10.1038/28998>
24. He Y, Tian Y, Ribbe AE, Mao C (2006) Highly connected two-dimensional crystals of DNA six-point-stars. *J Am Chem Soc* 128(50):15978–15979. <https://doi.org/10.1021/ja0665141>
25. Zheng J, Birktoft JJ, Chen Y, Wang T, Sha R, Constantinou PE, Ginell SL, Mao C, Seeman NC (2009) From molecular to macroscopic via the rational design of a self-assembled 3D DNA crystal. *Nature* 461(7260):74–77. <https://doi.org/10.1038/nature08274>
26. Ma RI, Kallenbach NR, Sheardy RD, Petrillo ML, Seeman NC (1986) 3-Arm nucleic-acid junctions are flexible. *Nucleic Acids Res* 14(24):9745–9753. <https://doi.org/10.1093/nar/14.24.9745>
27. Wang X, Seeman NC (2007) Assembly and characterization of 8-arm and 12-arm DNA branched junctions. *J Am Chem Soc* 129(26):8169–8176. <https://doi.org/10.1021/ja0693441>
28. Yan H, Park SH, Finkelstein G, Reif JH, LaBean TH (2003) DNA-templated self-assembly of protein arrays and highly conductive nanowires. *Science* 301(5641):1882–1884. <https://doi.org/10.1126/science.1089389>
29. He Y, Chen Y, Liu HP, Ribbe AE, Mao CD (2005) Self-assembly of hexagonal DNA two-dimensional (2D) arrays. *J Am Chem Soc* 127(35):12202–12203. <https://doi.org/10.1021/ja0541938>
30. He Y, Mao C (2006) Balancing flexibility and stress in DNA nanostructures. *Chem Commun (Camb)* 9:968–969. <https://doi.org/10.1039/b513962g>
31. Ding BQ, Sha RJ, Seeman NC (2004) Pseudo-hexagonal 2D DNA crystals from double crossover cohesion. *J Am Chem Soc* 126(33):10230–10231. <https://doi.org/10.1021/ja047486u>
32. Mao CD, Sun WQ, Seeman NC (1999) Designed two-dimensional DNA Holliday junction arrays visualized by atomic force microscopy. *J Am Chem Soc* 121(23):5437–5443. <https://doi.org/10.1021/ja9900398>
33. Hong F, Jiang S, Wang T, Liu Y, Yan H (2016) 3D framework DNA origami with layered crossovers. *Angew Chem Int Ed* 55(41):12832–12835. <https://doi.org/10.1002/anie.201607050>
34. Kuzuya A, Wang R, Sha R, Seeman NC (2007) Six-helix and eight-helix DNA nanotubes assembled from half-tubes. *Nano Lett* 7(6):1757–1763. <https://doi.org/10.1021/nl070828k>
35. Shih WM, Quispe JD, Joyce GF (2004) A 1.7-kilobase single-stranded DNA that folds into a nanoscale octahedron. *Nature* 427(6975):618–621. <https://doi.org/10.1038/nature02307>
36. He Y, Ye T, Su M, Zhang C, Ribbe AE, Jiang W, Mao C (2008) Hierarchical self-assembly of DNA into symmetric supramolecular polyhedra. *Nature* 452(7184):198–U141. <https://doi.org/10.1038/nature06597>
37. Zhang C, Su M, He Y, Zhao X, Fang P-A, Ribbe AE, Jiang W, Mao C (2008) Conformational flexibility facilitates self-assembly of complex DNA nanostructures. *Proc Natl Acad Sci USA* 105(31):10665–10669. <https://doi.org/10.1073/pnas.0803841105>
38. Ong LL, Hanikel N, Yaghi OK, Grun C, Strauss MT, Bron P, Lai-Kee-Him J, Schueder F, Wang B, Wang P, Kishi JY, Myhrvold C, Zhu A, Jungmann R, Bellot G, Ke Y, Yin P (2017)

- Programmable self-assembly of three-dimensional nanostructures from 10,000 unique components. *Nature* 552(7683):72–77. <https://doi.org/10.1038/nature24648>
39. Ke Y, Ong LL, Sun W, Song J, Dong M, Shih WM, Yin P (2014) DNA brick crystals with prescribed depths. *Nat Chem* 6(11):994–1002. <https://doi.org/10.1038/nchem.2083>
 40. Ke Y, Ong LL, Shih WM, Yin P (2012) Three-dimensional structures self-assembled from DNA bricks. *Science* 338(6111):1177–1183. <https://doi.org/10.1126/science.1227268>
 41. Zhang C, Li X, Tian C, Yu G, Li Y, Jiang W, Mao C (2014) DNA nanocages swallow gold nanoparticles (AuNPs) to form AuNP@DNA cage core-shell structures. *ACS Nano* 8(2):1130–1135. <https://doi.org/10.1021/nn406039p>
 42. Li Y, Liu Z, Yu G, Jiang W, Mao C (2015) Self-assembly of molecule-like nanoparticle clusters directed by DNA nanocages. *J Am Chem Soc* 137(13):4320–4323. <https://doi.org/10.1021/jacs.5b01196>
 43. Li HY, Park SH, Reif JH, LaBean TH, Yan H (2004) DNA-templated self-assembly of protein and nanoparticle linear arrays. *J Am Chem Soc* 126(2):418–419. <https://doi.org/10.1021/ja0383367>
 44. Xiao SJ, Liu FR, Rosen AE, Hainfeld JF, Seeman NC, Musier-Forsyth K, Kiehl RA (2002) Self assembly of metallic nanoparticle arrays by DNA scaffolding. *J Nanopart Res* 4(4):313–317. <https://doi.org/10.1023/a:1021145208328>
 45. Le JD, Pinto Y, Seeman NC, Musier-Forsyth K, Taton TA, Kiehl RA (2004) DNA-templated self-assembly of metallic nanocomponent arrays on a surface. *Nano Lett* 4(12):2343–2347. <https://doi.org/10.1021/nl048635+>
 46. Pinto YY, Le JD, Seeman NC, Musier-Forsyth K, Taton TA, Kiehl RA (2005) Sequence-encoded self-assembly of multiple-nanocomponent arrays by 2D DNA scaffolding. *Nano Lett* 5(12):2399–2402. <https://doi.org/10.1021/nl0515495>
 47. Zhang JP, Liu Y, Ke YG, Yan H (2006) Periodic square-like gold nanoparticle arrays templated by self-assembled 2D DNA nanogrids on a surface. *Nano Lett* 6(2):248–251. <https://doi.org/10.1021/nl052210l>
 48. Sharma J, Chhabra R, Liu Y, Ke YG, Yan H (2006) DNA-templated self-assembly of two-dimensional and periodical gold nanoparticle arrays. *Angew Chem Int Ed* 45(5):730–735. <https://doi.org/10.1002/anie.200503208>
 49. Zheng J, Constantinou PE, Micheel C, Alivisatos AP, Kiehl RA, Seeman NC (2006) Two-dimensional nanoparticle arrays show the organizational power of robust DNA motifs. *Nano Lett* 6(7):1502–1504. <https://doi.org/10.1021/nl060994c>
 50. Sharma J, Chhabra R, Cheng A, Brownell J, Liu Y, Yan H (2009) Control of self-assembly of DNA tubules through integration of gold nanoparticles. *Science* 323(5910):112–116. <https://doi.org/10.1126/science.1165831>
 51. Maye MM, Nykypanchuk D, van der Lelie D, Gang O (2007) DNA-regulated micro- and nanoparticle assembly. *Small* 3(10):1678–1682. <https://doi.org/10.1002/sml.200700357>
 52. Maye MM, Nykypanchuk D, Cuisinier M, van der Lelie D, Gang O (2009) Stepwise surface encoding for high-throughput assembly of nanoclusters. *Nat Mater* 8(5):388–391. <https://doi.org/10.1038/nmat2421>
 53. Song M, Ding Y, Zerze H, Snyder MA, Mittal J (2018) Binary superlattice design by controlling DNA-mediated interactions. *Langmuir* 34(3):991–998. <https://doi.org/10.1021/acs.langmuir.7b02835>
 54. Zhang YG, Lu F, Yager KG, van der Lelie D, Gang O (2013) A general strategy for the DNA-mediated self-assembly of functional nanoparticles into heterogeneous systems. *Nat Nanotechnol* 8(11):865–872. <https://doi.org/10.1038/nnano.2013.209>
 55. Zhang YG, Pal S, Srinivasan B, Vo T, Kumar S, Gang O (2015) Selective transformations between nanoparticle superlattices via the reprogramming of DNA-mediated interactions. *Nat Mater* 14(8):840–847. <https://doi.org/10.1038/Nmat4296>
 56. Srinivasan B, Vo T, Zhang Y, Gang O, Kumar S, Venkatasubramanian V (2013) Designing DNA-grafted particles that self-assemble into desired crystalline structures using the genetic algorithm. *Proc Natl Acad Sci USA* 110(46):18431. <https://doi.org/10.1073/pnas.1316533110>
 57. Vo T, Venkatasubramanian V, Kumar S, Srinivasan B, Pal S, Zhang Y, Gang O (2015) Stoichiometric control of DNA-grafted colloid self-assembly. *Proc Natl Acad Sci USA* 112(16):4982–4987. <https://doi.org/10.1073/pnas.1420907112>
 58. Damasceno PF, Engel M, Glotzer SC (2012) Predictive self-assembly of polyhedra into complex structures. *Science* 337(6093):453–457. <https://doi.org/10.1126/science.1220869>

59. Lu F, Vo T, Zhang Y, Frenkel A, Yager KG, Kumar S, Gang O (2019) Unusual packing of soft-shelled nanocubes. *Sci Adv* 5(5):eaaw2399. <https://doi.org/10.1126/sciadv.aaw2399>
60. Lu F, Yager KG, Zhang Y, Xin H, Gang O (2015) Superlattices assembled through shape-induced directional binding. *Nat Commun* 6(1):6912. <https://doi.org/10.1038/ncomms7912>
61. O'Brien MN, Jones MR, Lee B, Mirkin CA (2015) Anisotropic nanoparticle complementarity in DNA-mediated co-crystallization. *Nat Mater* 14:833. <https://doi.org/10.1038/nmat4293>
62. Andersen ES, Dong M, Nielsen MM, Jahn K, Lind-Thomsen A, Mamdough W, Gothelf KV, Besenbacher F, Kjems J (2008) DNA origami design of dolphin-shaped structures with flexible tails. *ACS Nano* 2(6):1213–1218. <https://doi.org/10.1021/nn800215j>
63. Qian L, Wang Y, Zhang Z, Zhao J, Pan D, Zhang Y, Liu Q, Fan C, Hu J, He L (2006) Analogic China map constructed by DNA. *Chin Sci Bull* 51(24):2973–2976. <https://doi.org/10.1007/s11434-006-2223-9>
64. Douglas SM, Chou JJ, Shih WM (2007) DNA-nanotube-induced alignment of membrane proteins for NMR structure determination. *Proc Natl Acad Sci USA* 104(16):6644–6648. <https://doi.org/10.1073/pnas.0700930104>
65. Mathieu F, Liao SP, Kopatsch J, Wang T, Mao CD, Seeman NC (2005) Six-helix bundles designed from DNA. *Nano Lett* 5(4):661–665. <https://doi.org/10.1021/nl050084f>
66. Kuzyk A, Schreiber R, Fan Z, Pardatscher G, Roller EM, Hogege A, Simmel FC, Govorov AO, Liedl T (2012) DNA-based self-assembly of chiral plasmonic nanostructures with tailored optical response. *Nature* 483(7389):311–314. <https://doi.org/10.1038/nature10889>
67. Shen X, Song C, Wang J, Shi D, Wang Z, Liu N, Ding B (2012) Rolling up gold nanoparticle-dressed DNA origami into three-dimensional plasmonic chiral nanostructures. *J Am Chem Soc* 134(1):146–149. <https://doi.org/10.1021/ja209861x>
68. Ke Y, Sharma J, Liu M, Jahn K, Liu Y, Yan H (2009) Scaffolded DNA origami of a DNA tetrahedron molecular container. *Nano Lett* 9(6):2445–2447. <https://doi.org/10.1021/nl901165f>
69. Andersen ES, Dong M, Nielsen MM, Jahn K, Subramani R, Mamdough W, Golas MM, Sander B, Stark H, Oliveira CLP, Pedersen JS, Birkedal V, Besenbacher F, Gothelf KV, Kjems J (2009) Self-assembly of a nanoscale DNA box with a controllable lid. *Nature* 459(7243):73–U75. <https://doi.org/10.1038/nature07971>
70. Dietz H, Douglas SM, Shih WM (2009) Folding DNA into twisted and curved nanoscale shapes. *Science* 325:725–730. <https://doi.org/10.1126/science.1174251>
71. Douglas SM, Dietz H, Liedl T, Hoegberg B, Graf F, Shih WM (2009) Self-assembly of DNA into nanoscale three-dimensional shapes. *Nature* 459(7245):414–418. <https://doi.org/10.1038/nature08016>
72. Douglas SM, Marblestone AH, Teerapittayanon S, Vazquez A, Church GM, Shih WM (2009) Rapid prototyping of 3D DNA-origami shapes with caDNAno. *Nucleic Acids Res* 37(15):5001–5006. <https://doi.org/10.1093/nar/gkp436>
73. Ke Y, Douglas SM, Liu M, Sharma J, Cheng A, Leung A, Liu Y, Shih WM, Yan H (2009) Multilayer DNA origami packed on a square lattice. *J Am Chem Soc* 131(43):15903–15908. <https://doi.org/10.1021/ja906381y>
74. Ke Y, Voigt NV, Gothelf KV, Shih WM (2012) Multilayer DNA origami packed on hexagonal and hybrid lattices. *J Am Chem Soc* 134(3):1770–1774. <https://doi.org/10.1021/ja209719k>
75. Han D, Pal S, Nangreave J, Deng Z, Liu Y, Yan H (2011) DNA origami with complex curvatures in three-dimensional space. *Science* 332(6027):342–346. <https://doi.org/10.1126/science.1202998>
76. Yang Y, Han D, Nangreave J, Liu Y, Yan H (2012) DNA origami with double-stranded DNA as a unified scaffold. *ACS Nano* 6(9):8209–8215. <https://doi.org/10.1021/nn302896c>
77. Sobczak J-PJ, Martin TG, Gerling T, Dietz H (2012) Rapid folding of DNA into nanoscale shapes at constant temperature. *Science* 338(6113):1458–1461. <https://doi.org/10.1126/science.1229919>
78. Iinuma R, Ke Y, Jungmann R, Schlichthaerle T, Woehrstein JB, Yin P (2014) Polyhedra self-assembled from DNA tripods and characterized with 3D DNA-PAINT. *Science* 344(6179):65–69. <https://doi.org/10.1126/science.1250944>
79. Tian Y, Wang T, Liu W, Xin HL, Li H, Ke Y, Shih WM, Gang O (2015) Prescribed nanoparticle cluster architectures and low-dimensional arrays built using octahedral DNA origami frames. *Nat Nanotechnol* 10(7):637–644. <https://doi.org/10.1038/nnano.2015.105>

80. Veneziano R, Ratanalert S, Zhang K, Zhang F, Yan H, Chiu W, Bathe M (2016) Designer nanoscale DNA assemblies programmed from the top down. *Science* 352(6293):1534. <https://doi.org/10.1126/science.aaf4388>
81. Liu X, Zhang F, Jing X, Pan M, Liu P, Li W, Zhu B, Li J, Chen H, Wang L, Lin J, Liu Y, Zhao D, Yan H, Fan C (2018) Complex silica composite nanomaterials templated with DNA origami. *Nature* 559(7715):593–598. <https://doi.org/10.1038/s41586-018-0332-7>
82. Linh N, Doeblinger M, Liedl T, Heuer-Jungemann A (2019) DNA-origami-templated silica growth by sol–gel chemistry. *Angew Chem Int Ed* 58(3):912–916. <https://doi.org/10.1002/anie.201811323>
83. Schreiber R, Santiago I, Ardavan A, Turberfield AJ (2016) Ordering gold nanoparticles with DNA origami nanoflowers. *ACS Nano* 10(8):7303–7306. <https://doi.org/10.1021/acsnano.6b03076>
84. Zhao Z, Jacovetty EL, Liu Y, Yan H (2011) Encapsulation of gold nanoparticles in a DNA origami cage. *Angew Chem Int Ed Engl* 50(9):2041–2044. <https://doi.org/10.1002/anie.201006818>
85. Shen C, Lan X, Lu X, Meyer TA, Ni W, Ke Y, Wang Q (2016) Site-specific surface functionalization of gold nanorods using DNA origami clamps. *J Am Chem Soc* 138(6):1764–1767. <https://doi.org/10.1021/jacs.5b11566>
86. Stearns LA, Chhabra R, Sharma J, Liu Y, Petuskey WT, Yan H, Chaput JC (2009) Template-directed nucleation and growth of inorganic nanoparticles on DNA scaffolds. *Angew Chem Int Ed Engl* 48(45):8494–8496. <https://doi.org/10.1002/anie.200903319>
87. Bui H, Onodera C, Kidwell C, Tan Y, Graunard E, Kuang W, Lee J, Knowlton WB, Yurke B, Hughes WL (2010) Programmable periodicity of quantum dot arrays with DNA origami nanotubes. *Nano Lett* 10(9):3367–3372. <https://doi.org/10.1021/nl101079u>
88. Chhabra R, Sharma J, Ke Y, Liu Y, Rinker S, Lindsay S, Yan H (2007) Spatially addressable multiprotein nanoarrays templated by aptamer-tagged DNA nanoarchitectures. *J Am Chem Soc* 129(34):10304–10305. <https://doi.org/10.1021/ja072410u>
89. Sharma J, Chhabra R, Andersen CS, Gothelf KV, Yan H, Liu Y (2008) Toward reliable gold nanoparticle patterning on self-assembled DNA nanoscaffold. *J Am Chem Soc* 130(25):7820–7821. <https://doi.org/10.1021/ja802853r>
90. Schreiber R, Do J, Roller EM, Zhang T, Schuller VJ, Nickels PC, Feldmann J, Liedl T (2014) Hierarchical assembly of metal nanoparticles, quantum dots and organic dyes using DNA origami scaffolds. *Nat Nanotechnol* 9(1):74–78. <https://doi.org/10.1038/nnano.2013.253>
91. Lin ZW, Xiong Y, Xiang ST, Gang O (2019) Controllable covalent-bound nanoarchitectures from DNA frames. *J Am Chem Soc* 141(17):6797–6801. <https://doi.org/10.1021/jacs.9b01510>
92. Liu W, Halverson J, Tian Y, Tkachenko AV, Gang O (2016) Self-organized architectures from assorted DNA-framed nanoparticles. *Nat Chem* 8(9):867–873. <https://doi.org/10.1038/nchem.2540>
93. Liu WY, Mahynski NA, Gang O, Panagiotopoulos AZ, Kumar SK (2017) Directionally interacting spheres and rods form ordered phases. *ACS Nano* 11(5):4950–4959. <https://doi.org/10.1021/acsnano.7b01592>
94. Tian Y, Lhermitte JR, Bai L, Vo T, Xin HL, Li H, Li R, Fukuto M, Yager KG, Kahn JS, Xiong Y, Minevich B, Kumar SK, Gang O (2020) Ordered three-dimensional nanomaterials using DNA-prescribed and valence-controlled material voxels. *Nat Mater*. <https://doi.org/10.1038/s41563-019-0550-x>
95. Emamy H, Gang O, Starr FW (2019) The stability of a nanoparticle diamond lattice linked by DNA. *Nanomaterials* (Basel) 9(5):661. <https://doi.org/10.3390/nano9050661>
96. Mastroianni AJ, Claridge SA, Alivisatos AP (2009) Pyramidal and chiral groupings of gold nanocrystals assembled using DNA scaffolds. *J Am Chem Soc* 131(24):8455–8459. <https://doi.org/10.1021/ja808570g>
97. Yan W, Xu L, Xu C, Ma W, Kuang H, Wang L, Kotov NA (2012) Self-assembly of chiral nanoparticle pyramids with strong R/S optical activity. *J Am Chem Soc* 134(36):15114–15121. <https://doi.org/10.1021/ja3066336>
98. Pal S, Deng Z, Wang H, Zou S, Liu Y, Yan H (2011) DNA directed self-assembly of anisotropic plasmonic nanostructures. *J Am Chem Soc* 133(44):17606–17609. <https://doi.org/10.1021/ja207898r>
99. Lan X, Chen Z, Dai G, Lu X, Ni W, Wang Q (2013) Bifacial DNA origami-directed discrete, three-dimensional, anisotropic plasmonic nanoarchitectures with tailored optical chirality. *J Am Chem Soc* 135(31):11441–11444. <https://doi.org/10.1021/ja404354c>
100. Shen X, Zhan P, Kuzyk A, Liu Q, Asenjo-Garcia A, Zhang H, de Abajo FJ, Govorov A, Ding B, Liu N (2014) 3D plasmonic chiral colloids. *Nanoscale* 6(4):2077–2081. <https://doi.org/10.1039/c3nr06006c>

101. Lan X, Lu X, Shen C, Ke Y, Ni W, Wang Q (2015) Au nanorod helical superstructures with designed chirality. *J Am Chem Soc* 137(1):457–462. <https://doi.org/10.1021/ja511333q>
102. Tian C, Cordeiro MAL, Lhermitte J, Xin HLL, Shani L, Liu MZ, Ma CL, Yeshurun Y, DiMarzio D, Gang O (2017) Supra-nanoparticle functional assemblies through programmable stacking. *ACS Nano* 11(7):7036–7048. <https://doi.org/10.1021/acsnano.7b02671>
103. Zhang H, Li M, Wang K, Tian Y, Chen J-S, Fountaine KT, DiMarzio D, Liu M, Cotlet M, Gang O (2020) Polarized single-particle quantum dot emitters through programmable cluster assembly. *ACS Nano* 14(2):1369–1378. <https://doi.org/10.1021/acsnano.9b06919>
104. Zhou C, Duan X, Liu N (2015) A plasmonic nanorod that walks on DNA origami. *Nat Commun* 6:8102. <https://doi.org/10.1038/ncomms9102>
105. Urban MJ, Zhou C, Duan X, Liu N (2015) Optically resolving the dynamic walking of a plasmonic walker couple. *Nano Lett* 15(12):8392–8396. <https://doi.org/10.1021/acs.nanolett.5b04270>
106. Kuzyk A, Schreiber R, Zhang H, Govorov AO, Liedl T, Liu N (2014) Reconfigurable 3D plasmonic metamolecules. *Nat Mater* 13(9):862–866. <https://doi.org/10.1038/nmat4031>
107. Kuzyk A, Yang Y, Duan X, Stoll S, Govorov AO, Sugiyama H, Endo M, Liu N (2016) A light-driven three-dimensional plasmonic nanosystem that translates molecular motion into reversible chiroptical function. *Nat Commun* 7:10591. <https://doi.org/10.1038/ncomms10591>
108. Kuzyk A, Urban MJ, Idili A, Ricci F, Liu N (2017) Selective control of reconfigurable chiral plasmonic metamolecules. *Sci Adv*. <https://doi.org/10.1126/sciadv.1602803>
109. Funck T, Nicoli F, Kuzyk A, Liedl T (2018) Sensing picomolar concentrations of RNA using switchable plasmonic chirality. *Angew Chem Int Ed* 57(41):13495–13498. <https://doi.org/10.1002/anie.201807029>
110. Shen C, Lan X, Zhu C, Zhang W, Wang L, Wang Q (2017) Spiral patterning of Au nanoparticles on Au nanorod surface to form chiral AuNR@AuNP helical superstructures templated by DNA origami. *Adv Mater*. <https://doi.org/10.1002/adma.201606533>
111. Urban MJ, Dutta PK, Wang P, Duan X, Shen X, Ding B, Ke Y, Liu N (2016) Plasmonic toroidal metamolecules assembled by DNA origami. *J Am Chem Soc* 138(17):5495–5498. <https://doi.org/10.1021/jacs.6b00958>
112. Shen X, Asenjo-García A, Liu Q, Jiang Q, García de Abajo FJ, Liu N, Ding B (2013) Three-dimensional plasmonic chiral tetramers assembled by DNA origami. *Nano Lett* 13(5):2128–2133. <https://doi.org/10.1021/nl400538y>
113. Schreiber R, Luong N, Fan Z, Kuzyk A, Nickels PC, Zhang T, Smith DM, Yurke B, Kuang W, Govorov AO, Liedl T (2013) Chiral plasmonic DNA nanostructures with switchable circular dichroism. *Nat Commun* 4(1):2948. <https://doi.org/10.1038/ncomms3948>
114. Acuna GP, Möller FM, Holzmeister P, Beater S, Lalkens B, Tinnefeld P (2012) Fluorescence enhancement at docking sites of DNA-directed self-assembled nanoantennas. *Science* 338(6106):506. <https://doi.org/10.1126/science.1228638>
115. Thacker VV, Herrmann LO, Sigle DO, Zhang T, Liedl T, Baumberg JJ, Keyser UF (2014) DNA origami based assembly of gold nanoparticle dimers for surface-enhanced Raman scattering. *Nat Commun* 5:3448. <https://doi.org/10.1038/ncomms4448>
116. Kuhler P, Roller EM, Schreiber R, Liedl T, Lohmuller T, Feldmann J (2014) Plasmonic DNA-origami nanoantennas for surface-enhanced Raman spectroscopy. *Nano Lett* 14(5):2914–2919. <https://doi.org/10.1021/nl5009635>
117. Simoncelli S, Roller EM, Urban P, Schreiber R, Turberfield AJ, Liedl T, Lohmuller T (2016) Quantitative single-molecule surface-enhanced raman scattering by optothermal tuning of DNA origami-assembled plasmonic nanoantennas. *ACS Nano* 10(11):9809–9815. <https://doi.org/10.1021/acsnano.6b05276>
118. Ko SH, Du K, Liddle JA (2013) Quantum-dot fluorescence lifetime engineering with DNA origami constructs. *Angew Chem Int Ed* 52(4):1193–1197. <https://doi.org/10.1002/anie.201206253>
119. Samanta A, Zhou Y, Zou S, Yan H, Liu Y (2014) Fluorescence quenching of quantum dots by gold nanoparticles: a potential long range spectroscopic ruler. *Nano Lett* 14(9):5052–5057. <https://doi.org/10.1021/nl501709s>
120. Liu J, Geng Y, Pound E, Gyawali S, Ashton JR, Hickey J, Woolley AT, Harb JN (2011) Metallization of branched DNA origami for nanoelectronic circuit fabrication. *ACS Nano* 5(3):2240–2247. <https://doi.org/10.1021/nn1035075>
121. Schreiber R, Kempter S, Holler S, Schuller V, Schiffels D, Simmel SS, Nickels PC, Liedl T (2011) DNA origami-templated growth of arbitrarily shaped metal nanoparticles. *Small* 7(13):1795–1799. <https://doi.org/10.1002/sml.201100465>

122. Pilo-Pais M, Goldberg S, Samano E, Labean TH, Finkelstein G (2011) Connecting the nanodots: programmable nanofabrication of fused metal shapes on DNA templates. *Nano Lett* 11(8):3489–3492. <https://doi.org/10.1021/nl202066c>
123. Helmi S, Ziegler C, Kauert DJ, Seidel R (2014) Shape-controlled synthesis of gold nanostructures using DNA origami molds. *Nano Lett* 14(11):6693–6698. <https://doi.org/10.1021/nl503441v>
124. Sun W, Boulais E, Hakobyan Y, Wang WL, Guan A, Bathe M, Yin P (2014) Casting inorganic structures with DNA molds. *Science* 346(6210):1258361. <https://doi.org/10.1126/science.1258361>
125. Douglas SM, Bachelet I, Church GM (2012) A logic-gated nanorobot for targeted transport of molecular payloads. *Science* 335(6070):831–834. <https://doi.org/10.1126/science.1214081>
126. Liu M, Fu J, Hejesen C, Yang Y, Woodbury NW, Gothelf K, Liu Y, Yan H (2013) A DNA tweezer-actuated enzyme nanoreactor. *Nat Commun* 4:2127. <https://doi.org/10.1038/ncomms3127>
127. Linko V, Eerikainen M, Kostianen MA (2015) A modular DNA origami-based enzyme cascade nanoreactor. *Chem Commun (Camb)* 51(25):5351–5354. <https://doi.org/10.1039/c4cc08472a>
128. Zhao Z, Fu J, Dhakal S, Johnson-Buck A, Liu M, Zhang T, Woodbury NW, Liu Y, Walter NG, Yan H (2016) Nanocaged enzymes with enhanced catalytic activity and increased stability against protease digestion. *Nat Commun* 7:10619. <https://doi.org/10.1038/ncomms10619>
129. Wang P, Rahman MA, Zhao Z, Weiss K, Zhang C, Chen Z, Hurwitz SJ, Chen ZG, Shin DM, Ke Y (2018) Visualization of the cellular uptake and trafficking of DNA origami nanostructures in cancer cells. *J Am Chem Soc* 140(7):2478–2484. <https://doi.org/10.1021/jacs.7b09024>
130. Kershner RJ, Bozano LD, Micheel CM, Hung AM, Fornof AR, Cha JN, Rettner CT, Bersani M, Frommer J, Rothmund PW, Wallraff GM (2009) Placement and orientation of individual DNA shapes on lithographically patterned surfaces. *Nat Nanotechnol* 4(9):557–561. <https://doi.org/10.1038/nnano.2009.220>
131. Hung AM, Micheel CM, Bozano LD, Osterbur LW, Wallraff GM, Cha JN (2010) Large-area spatially ordered arrays of gold nanoparticles directed by lithographically confined DNA origami. *Nat Nanotechnol* 5(2):121–126. <https://doi.org/10.1038/nnano.2009.450>
132. Chao J, Wang JB, Wang F, Ouyang XY, Kopperger E, Liu HJ, Li Q, Shi JY, Wang LH, Hu J, Wang LH, Huang W, Simmel FC, Fan CH (2019) Solving mazes with single-molecule DNA navigators. *Nat Mater* 18(3):273–279. <https://doi.org/10.1038/s41563-018-0205-3>
133. Kwon PS, Ren S, Kwon S-J, Kizer ME, Kuo L, Zhou F, Zhang F, Kim D, Fraser K, Kramer LD, Seeman NC, Dordick JS, Linhardt RJ, Chao J, Wang X (2020) Designer DNA architecture offers precise and multivalent spatial pattern-recognition for viral sensing and inhibition. *Nat Chem* 12(1):26–35. <https://doi.org/10.1101/608380>
134. Seeman NC, Gang O (2017) Three-dimensional molecular and nanoparticle crystallization by DNA nanotechnology. *MRS Bull* 42(12):904–912. <https://doi.org/10.1557/mrs.2017.280>
135. Zhang YN, Chao J, Liu HJ, Wang F, Su S, Liu B, Zhang L, Shi JY, Wang LH, Huang W, Wang LH, Fan CH (2016) Transfer of two-dimensional oligonucleotide patterns onto stereocontrolled plasmonic nanostructures through DNA-origami-based nanoimprinting lithography. *Angew Chem Int Ed* 55(28):8036–8040. <https://doi.org/10.1002/anie.201512022>

Publisher's Note Springer Nature remains neutral with regard to jurisdictional claims in published maps and institutional affiliations.

Affiliations

Ningning Ma^{1,2} · Brian Minevich³ · Jiliang Liu⁴ · Min Ji^{1,2} · Ye Tian^{1,2,5} · Oleg Gang^{3,6,7}

¹ College of Engineering and Applied Sciences, National Laboratory of Solid State Microstructures, Collaborative Innovation Center of Advanced Microstructures, Jiangsu Key Laboratory of Artificial Functional Materials, Nanjing University, Nanjing 210093, China

² Chemistry and Biomedicine Innovation Center, Nanjing University, Nanjing 210023, China

³ Department of Chemical Engineering, Columbia University, New York, NY 10027, USA

- ⁴ National Synchrotron Light Source II, Brookhaven National Laboratory, Upton, NY 11973, USA
- ⁵ Shenzhen Research Institute of Nanjing University, Shenzhen 518000, China
- ⁶ Center for Functional Nanomaterials, Brookhaven National Laboratory, Upton, NY 11973, USA
- ⁷ Department of Applied Physics and Applied Mathematics, Columbia University, New York, NY 10027, USA



Oligonucleotide–Polymer Conjugates: From Molecular Basics to Practical Application

Fan Xiao^{1,2} · Zixiang Wei¹ · Maggie Wang³ · Alexandra Hoff³ · Ying Bao³ · Leilei Tian¹

Received: 9 October 2019 / Accepted: 21 January 2020 / Published online: 17 February 2020
© Springer Nature Switzerland AG 2020

Abstract

DNA exhibits many attractive properties, such as programmability, precise self-assembly, sequence-coded biomedical functions, and good biocompatibility; therefore, DNA has been used extensively as a building block to construct novel nanomaterials. Recently, studies on oligonucleotide–polymer conjugates (OPCs) have attracted increasing attention. As hybrid molecules, OPCs exhibit novel properties, e.g., sophisticated self-assembly behaviors, which are distinct from the simple combination of the functions of DNA and polymer, making OPCs interesting and useful. The synthesis and applications of OPCs are highly dependent on the choice of the polymer block, but a systematic summary of OPCs based on their molecular structures is still lacking. In order to design OPCs for further applications, it is necessary to thoroughly understand the structure–function relationship of OPCs. In this review, we carefully categorize recently developed OPCs by the structures of the polymer blocks, and discuss the synthesis, purification, and applications for each category. Finally, we will comment on future prospects for OPCs.

Keywords Oligonucleotide–polymer conjugates · DNA block copolymers · Functional nucleic acid · Self-assembly · Drug delivery

Chapter 7 was originally published as Xiao, F., Wei, Z., Wang, M., Hoff, A., Bao, Y. & Tian, L. Topics in Current Chemistry (2020) 378: 24. <https://doi.org/10.1007/s41061-020-0286-8>.

✉ Ying Bao
baoy@wwu.edu

✉ Leilei Tian
tianll@sustech.edu.cn

¹ Department of Materials Science and Engineering, Southern University of Science and Technology, 1088 Xueyuan Blvd, Nanshan District, Shenzhen 518055, Guangdong, People's Republic of China

² School of Materials Science and Engineering, Harbin Institute of Technology, Nangang District, Harbin 150001, People's Republic of China

³ Department of Chemistry, Western Washington University, 516 High Street, Bellingham, WA 98225-9150, USA

Abbreviations

DNA	Deoxyribonucleic acid
ODN	Oligonucleotide
OPC	Oligonucleotide–polymer conjugate
DX	Double-crossover
siRNA	Small interference RNA
RISC	RNA-induced silencing complex
PLA	Poly(lactic acid)
PGA	Poly(glycolic acid)
PLGA	Poly (lactic-co-glycolic acid)
PCL	Polycaprolactone
PASP	Polyaspartic acid
PNIPAM	Poly[<i>N</i> -isopropylacrylamide]
PEG	Poly(ethylene glycol)
DMSO	Dimethyl sulfoxide
DMF	Dimethylformamide
PS	Polystyrene
CPG	Controlled pore glass
PPE	Poly-(phenylene–ethynylene)
HE	Dodecanediol phosphoramidite
ATRP	Atom transfer radical polymerization
RAFT	Reversible addition-fragmentation chain transfer polymerization
CPADB	4-Cyano-4-(phenylcarbonothioylthio) pentanoic acid
BTPA	2-(Butylthiocarbonothioyl) propionic acid
EY	Eosin Y
AscA	Ascorbic acid
APS	Ammonium persulfate
TEMED	Tetramethylethylenediamine
PAGE	Polyacrylamide gel electrophoresis
FDA	Food and Drug Administration
PEI	Polyethyleneimine
SNA	Spherical nucleic acid
shRNA	Short hairpin RNAs
RCT	Rolling circle transcription
MDR1	Multidrug resistance protein 1
DOX	Doxorubicin
PPT-g-PEG	Peptide-grafted poly (ethylene glycol)
Fc	Ferrocene
MNP	Magnetic nanoparticle
PNB	Polynorbornene
PPO	Polypropylene oxide
LCST	Low critical solution temperature
VPTT	Volume phase transition temperature
DMT	Dimethoxytrityl
HPLC	High performance liquid chromatography
PPE	Poly (phenyleneethynylene)

HEX	Hexachlorofluorescein
FRET	Fluorescence Resonance Energy Transfer
SWNT	Single-walled carbon nanotube
PFO	Polyfluorene
PT	Polythiophene
PFP	Poly [fluorine-co-phenylene fluorene]
ACQ	Aggregation caused quenching
APPV	(2,5-Dialkoxy) paraphenylene vinylene
PAM	Polyacrylamide
ROMP	Ring-opening metathesis polymerization
pRNA	Passenger-stranded RNA

1 Introduction

Nucleic acids are bio-macromolecules that encode genetic information for living organisms. As solid-phase nucleic acid synthesis techniques are now well developed, their unique molecular structure and conformation make nucleic acids interesting molecules in the field of materials science. Due to specific Watson–Crick base pair interactions, nucleic acids not only specifically recognize complementary sequences, but can also conduct precise self-assembly and organize other molecules or nanomaterials in a well-defined manner at the nanoscale [1–4]. Therefore, nucleic acid-based nanotechnology has attracted significant attention in recent years (Fig. 1) [5, 6]. For instance, as a kind of DNA self-support nanostructure, DNA origami shows unparalleled advantages in precise controlling size and position at the nanoscale. However, DNA origami depends on a complicated and costly fabrication technique, which also exhibits susceptible stability (most structures require an environment with a high concentration of Mg^{2+}). Moreover, a large number of drugs and contrast agents with low-solubility in water need to be incorporated into nanostructures with hydrophobic domains—a feature lacking in DNA origami. Therefore, the application of DNA origami in certain directions will be limited.

Oligodeoxynucleotide (ODN) is a general term for a class of short-chain nucleic acids. Plenty of functional ODNs have been screened and well investigated, and show sequence-dependent functions, such as CpG islands (DNA sequences containing a large amount of “-C-phosphate-G-”) for immune activation [7], aptamers for targeted recognition [8], DNAszymes for catalysis [9], antisense ODNs and small interference RNAs (siRNA) for gene silencing (Fig. 2a, b) [10, 11]. Additionally, certain sequences can undergo conformational changes in reaction to external stimuli, including the quadruplex folding of cytosine-rich sequences at low pH [12] and G-quadruplex formation in the presence of monocations (Fig. 2c) [13]. More importantly, ODNs can be modified easily by well-developed chemical methods to increase their functionality and intelligence. These excellent properties of ODNs make them attractive in the fields of controllable self-assembly, diagnostics, and therapeutics. However, as for free functional nucleic acids, they display some inherent disadvantages for biomedical applications, including poor biological stability, non-specific immunogenicity, and unsatisfactory cellular uptake.

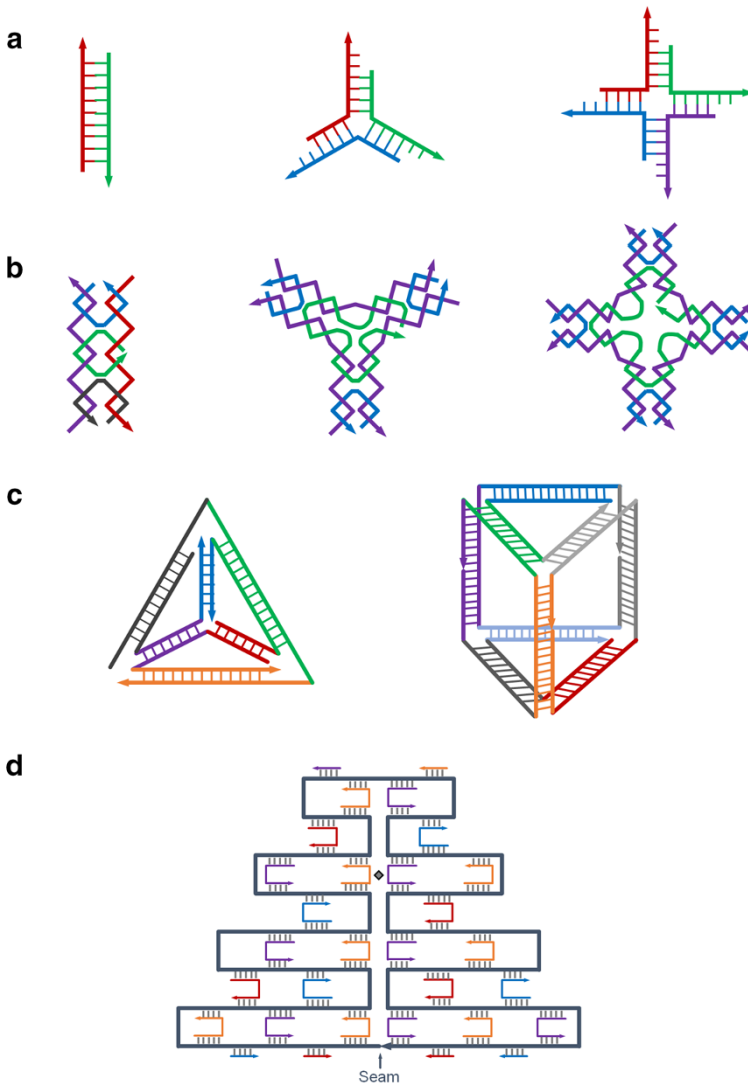


Fig. 1 Nucleic acid-based nanotechnology [5]. **a** The schematic diagram from left to right represents: linear, Y-shaped, X-shaped nucleic acid tiles. Nucleic acid tiles with single-stranded ends (“sticky ends”) can self-assemble into complex structures. **b** The schematic diagram from left to right represents rectangular double-crossover (DX) tiles, a Y-shaped DX tile, and an X-shaped DX tile. Unlike the structures in **a**, these double-crossover nucleic acid tiles have enhanced rigidity and highly planar structures that can assemble into a higher-order structure. **c** Three-dimensional nucleic acid structures. Left A nucleic acid tetrahedron constructed from four single strands. Right Nucleic acid cube constructed from five single strands. **d** Schematic representation of DNA origami. Long genomic DNA is folded with the help of small staple strands to give the desired, computationally designed, structure

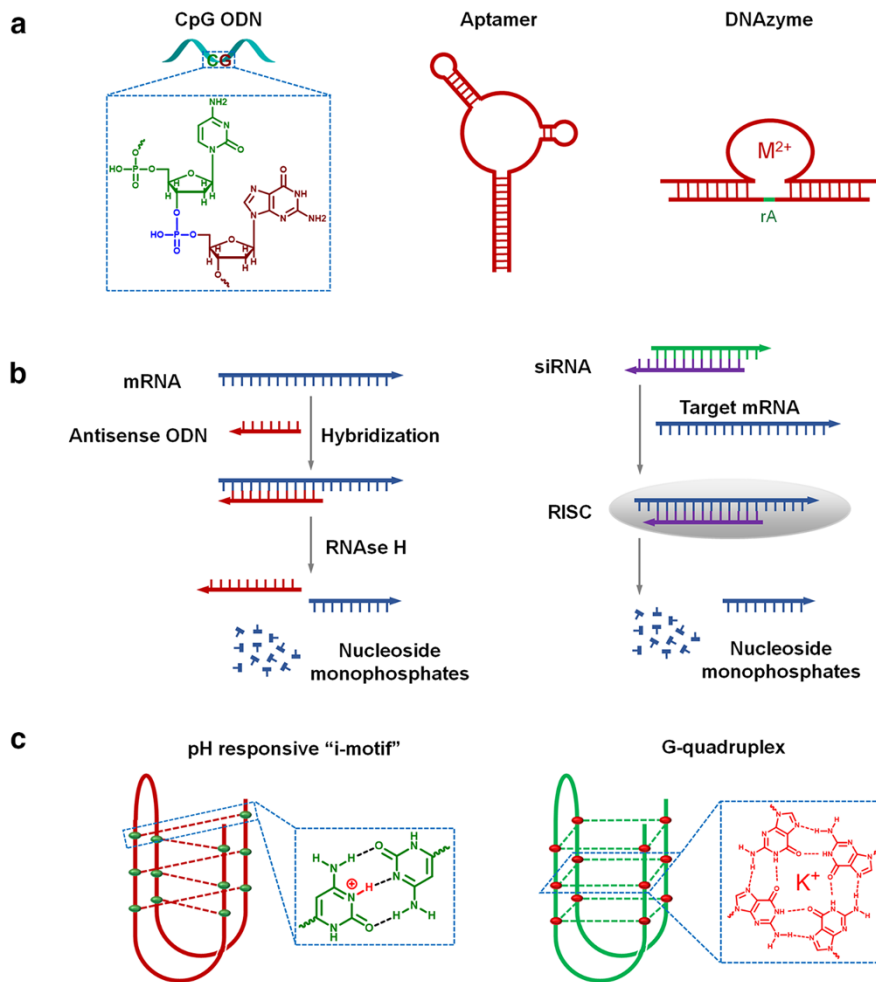


Fig. 2 Functional nucleic acids. **a** A CpG oligodeoxynucleotide (ODN) containing a “C–G” sequence can elicit an immune response in a mammal through the TLR9 signaling pathway, thereby enhancing immunotherapy as an immunological adjuvant [7]. The nucleic acid aptamer is referred to as a “chemical antibody” that can specifically bind to a target substance for targeted delivery and therapeutic purposes [8]. With the aid of metal ions, specific nucleic acid sequences have a catalytic effect [9]. **b** Both the antisense ODN and the small interfering RNA (siRNA) can regulate gene expression in a target cell [10, 11]. The most common mechanism of action is that RNase H or RISC (RNA-induced silencing complex) complexes inhibit expression of target genes. **c** Some specific sequences can form stable quadruplex structures under acidic conditions or under metal ion-mediated conditions [12, 13]

Synthetic polymers are attractive to researchers because of their enriched chemical structure and tunable properties. To avoid confusion, in this review, “polymers” are defined as chemically synthesized macromolecules, while “DNA” is a naturally occurring biomacromolecule; although DNA can be chemically synthesized nowadays, it originally exists in nature, whereas synthetic “polymers” do not. Polymers,

including biodegradable polymers, amphiphilic block copolymers, graft copolymers, and π -conjugated conductive polymers, have been well developed in recent years. Research into these polymers is changing rapidly in the fields of macromolecular self-assembly [14], drug delivery [15], biosensing [16], bioimaging [17], phototherapy [18], and polymer solar cells (Fig. 3) [19]. However, conventional synthetic polymers are used mainly as passive matrix materials to deliver hydrophobic drugs and contrast agents, which generally lack biological functions, such as targeting and stimuli-responsiveness to biomolecules.

Because of the attractive properties of both nucleic acids and polymers, the idea of integrating the two naturally came into being. Compared with pure DNA nanostructures or polymer self-assemblies, oligonucleotide–polymer conjugates (OPCs) can combine the advantages of both and result in more capable nanomaterials due to the synergetic effects: (1) in addition to providing programmability, the DNA block

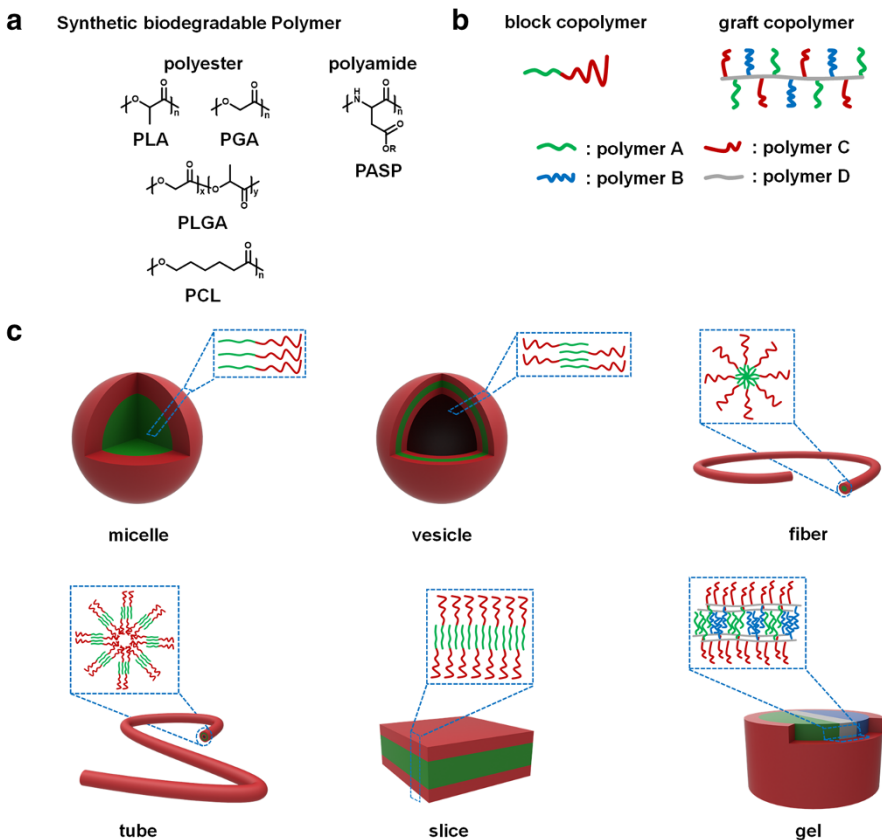


Fig. 3 Synthetic polymers and their self-assembly. **a** Chemical structure of biodegradable polymers. There are two main types: polyester and polyamine. *PLA* Polylactic acid, *PGA* polyglycolic acid, *PLGA* poly (lactic-co-glycolic acid), *PCL* polycaprolactone, *PASP* polyaspartic acid. **b** Structure of two common copolymers: block copolymers and graft copolymers. **c** Some interesting macromolecular self-assemblies

also renders many distinctive biological functionalities to OPCs, such as gene regulation, targeting, and stimuli-responsiveness. (2) The polymer block provides diverse interactions, including, but not limited to, hydrophobic interactions, π - π stacking, and host-guest interactions, which will bring many other organic functional materials into OPCs. (3) In particular, amphiphilic OPCs will self-assemble into stable nanostructures through hierarchical supramolecular interactions. On the one hand, the self-assembly structure will drive DNA blocks to be closely packed together, which will make DNA more resistant to nuclease degradation and enhance the cellular penetration capability. On the other hand, the self-assembly structures may show more intelligent stimuli-responsive properties; for instance, both the conformational changes of DNA blocks (e.g., pH-sensitive DNA i-motifs) and phase-transition of the synthetic polymer blocks (e.g., temperature-sensitive polyNIPAM) will change the amphiphilicity of OPCs, and result in morphological or functional variations. Therefore, OPCs will surely set off a revolutionary wave in the fields of supramolecular chemistry and biomedicine. In recent years, plenty of excellent related work has been reported. Although several reviews have reported on OPC research [20–26], this comprehensive review will first classify OPCs through the coupled polymer block, and then systematically summarize the synthesis and purification methods of various OPCs. A perspective for the future development of OPCs is also provided.

2 Synthesis of OPCs

2.1 Direct Coupling of Polymer and ODN

Obviously, the most straightforward method to synthesize OPCs is through direct coupling reactions between functionalized ODNs and polymers. Various ODNs with reactive functional groups (“X” in Fig. 4) can be synthesized on a DNA synthesizer via phosphoramidite chemistry; polymers with reactive functional groups (“Y” in Fig. 4) can be synthesized by certain chemical methods. The two kinds of functional groups (X and Y) can react with each other to form the desired OPCs (“X–Y” in Fig. 4).

To date, a number of coupling reactions have been applied to the synthesis of OPCs (Fig. 4). Each coupling reaction has its own characteristics: (1) for the amidation reaction between the amine group and the carboxyl group, the two functional groups are easy to introduce to ODN and the polymer, and the coupling condition is mild [27, 28]; however, the resultant amide bond is unstable and easily hydrolyzed. (2) The OPCs prepared by disulfide bonds are responsive to the reducing environment, and this characteristic can be used to realize stimuli-responsiveness in tumor environments [29, 30]. (3) The chemical bonds formed by other reactions, including Michael addition [31, 32] and copper-catalyzed [33] (or copper-free [34, 35]) cycloaddition reactions, are relatively stable. Overall, a proper coupling reaction can be selected according to different research priorities and purposes.

The coupling reaction in Fig. 4 can be broadly classified into two types: (1) reactions in solution; (2) reactions on solid supports.

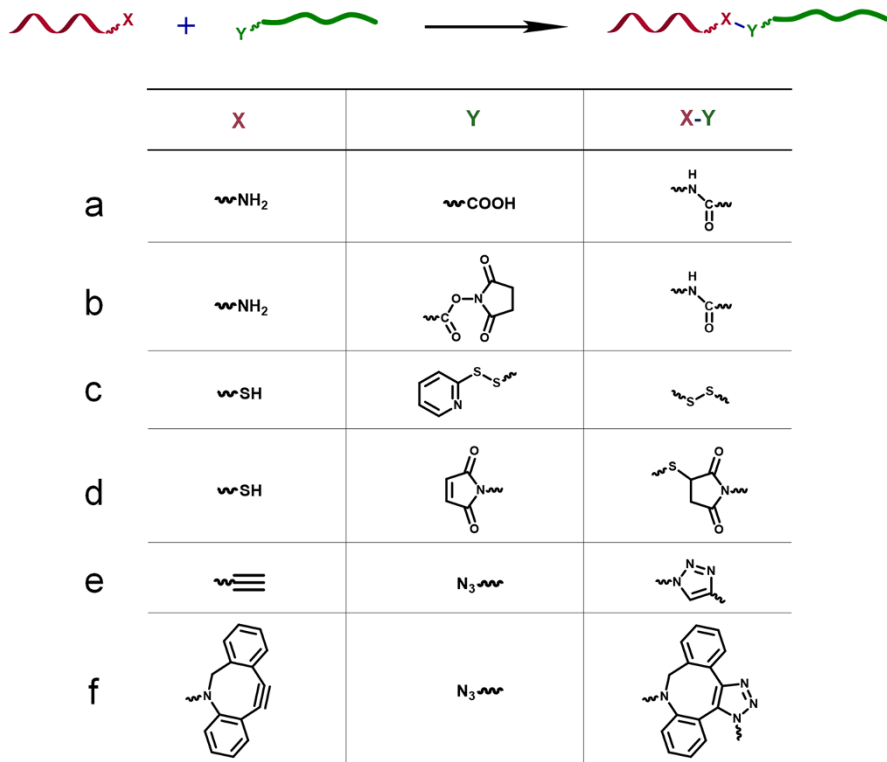


Fig. 4 Various synthetic methods for direct coupling of ODNs and polymers. **a** Amidation of amine and carboxyl groups [27, 28]. **b** Direct coupling of amine and NHS (*N*-hydroxysuccinimide) ester-activated polymers [67]. **c** 2-Pyridyldithiol and sulfhydryl groups can form cleavable disulfide bonds [29, 30]. **d** Michael addition reaction of mercapto and maleimide [31, 32, 125]. **e** Copper-catalyzed cycloaddition reaction of alkyne and azide [33]. **f** Copper-free “click” reaction of cyclooctyne and azide [34]

2.1.1 Reactions in Solution

A high coupling efficiency generally results from the reaction in a homogeneous system. DNA is a fully hydrophilic molecule, which readily couples with hydrophilic polymers, such as polypeptide chains [36, 37], polyethylene glycol (PEG) [38], and polyacrylamide [39], resulting in fully hydrophilic OPCs.

Due to the heterogeneity of the reaction, coupling hydrophobic polymer to hydrophilic ODN becomes more difficult. Herrmann’s group has attempted to introduce surfactants to transfer ODN into the organic phase to promote the coupling reactions with hydrophobic polymers [40]; however, additional steps are needed to remove the organic surfactant, which may induce biosafety risks. Another attempt was to synthesize OPCs in a mixed solvent that can dissolve both ODNs and organic polymers. Generally, ODN has the highest solubility in water, high solubility in DMSO (dimethyl sulfoxide), and moderate solubility in DMF (dimethylformamide). Some hydrophobic polymers, such as PCL, PLA, or PS (polystyrene), have good solubility

in DMSO or DMF. Therefore, mixed solvents, such as DMSO/water [34], DMSO/DMF mixed solvents [41], and even pure DMF solvents [33], were used in the synthesis of amphiphilic OPCs with satisfactory yields.

2.1.2 Reactions on Solid Support

The solid phase support, controlled pore glass (CPG), is a carrier for synthesizing ODN on a DNA synthesizer. After synthesizing the ODN with a reactive functional group, the polymer to be coupled can be conjugated to the ODN on the CPG. Compared with the solution-phase reaction, the solid-phase reaction shows advantages in wider solvent choice and more convenience in the subsequent purification.

The most classic solid-phase reaction is based on phosphoramidite chemistry [42–44], as shown in Fig. 5a, b, which is highly efficient with no need for any catalysts. However, such reactions are sensitive to water; the incorporation of a small amount of water will greatly reduce the efficiency of the reaction. Therefore, phosphoramidite synthesis is generally performed “on-line” on a DNA synthesizer that can provide a highly anhydrous environment [45, 46]. “Click” (Fig. 5c) [47, 48] and amidation reactions (Fig. 5d) [49, 50] are also widely used solid-phase synthesis methods. However, as solid-phase synthesis involves an aminolysis step to cut ODNs from CPG supports, reaction products with chemical bonds that are sensitive to the alkaline conditions, are not suitable for solid-phase methods.

2.2 In Situ Polymerization from the End of ODN

According to the collision theory of reaction kinetics, conjugation reactions from the single end of a polymer will be less efficient. In order to improve conjugation yields, new polymerization strategies have been developed to prepare OPCs, one of which is to perform polymerization in situ from the end of the ODN/polymer with a functionalized group.

Yang et al. [51] carried out the direct polymerization of poly-(phenylene–ethynylene) (PPE) derivatives from the end of the ODN (Fig. 6a), which was capped with a 5I-dU functional group to initiate PPE polymerization and finally obtain ODN–PPE conjugates. It is worth mentioning that the reaction was carried out on a CPG solid support, which has convenient advantages in product synthesis and purification.

Also to take advantage of the solid-phase phosphoramidite chemistry, Sleiman’s group developed a method for the synthesis of sequence-defined polymers appended to ODNs (Fig. 6b) [52, 53]. They used a commercially available DMT-protected dodecanediol phosphoramidite (HE), which is sequentially coupled to the 5’ terminus of an ODN strand. The resulting OPCs consisted of ODN portions conjugated with 1–12 HE units punctuated by phosphate moieties, showing distinct amphiphilic properties.

Matyjaszewski’s group [54–56] utilized atom transfer radical polymerization (ATRP) reactions to polymerize polymer from the end of an ODN. In their method, an ATRP initiator was bonded to an ODN during solid-phase synthesis, from

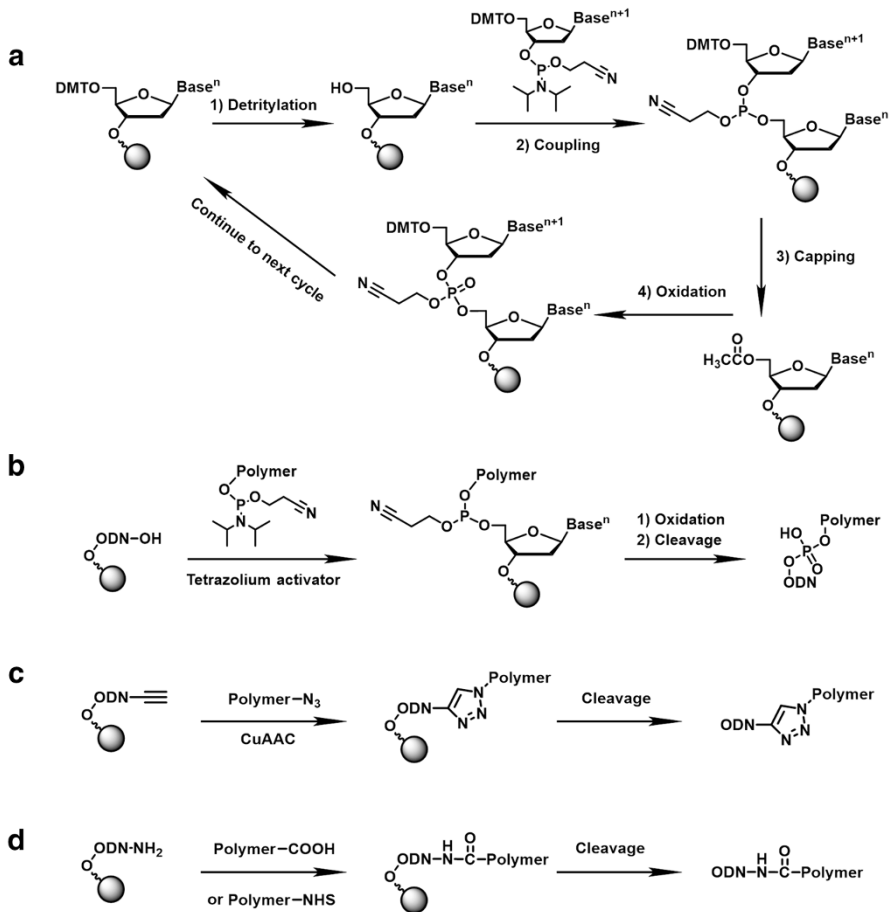


Fig. 5 **a** Schematic diagram of the synthesis of ODN by a DNA synthesizer. **b** The polymer with a hydroxyl group may be modified with a phosphoramidite; further, OPCs are chemically synthesized by phosphoramidite chemistry. **c** A copper-catalyzed cycloaddition reaction carried out on solid support [47, 48]. **d** Amidation reaction carried out on solid support [49, 50]

which a polymer chain was grown to produce OPCs (Fig. 6c). The authors claimed that ATRP polymerization can be carried out in solution after the ODN-initiator sequence is cut from the solid support, or directly on the solid support. Therefore, it is a versatile and high-yield method of preparing OPCs, wherein both fully hydrophilic polymers and amphiphilic polymers can be applied.

Reversible addition-fragmentation chain transfer polymerization (RAFT) is another kind of controlled radical polymerization method, which provides similar flexibility in monomer scope and end-group functionalization. Moreover, unlike ATRP methods that rely on toxic transition metal catalysts, the RAFT approach typically does not require metal catalysts and can be photo-initiated, which can offer a biocompatible polymerization platform for the synthesis of OPCs. Weil and

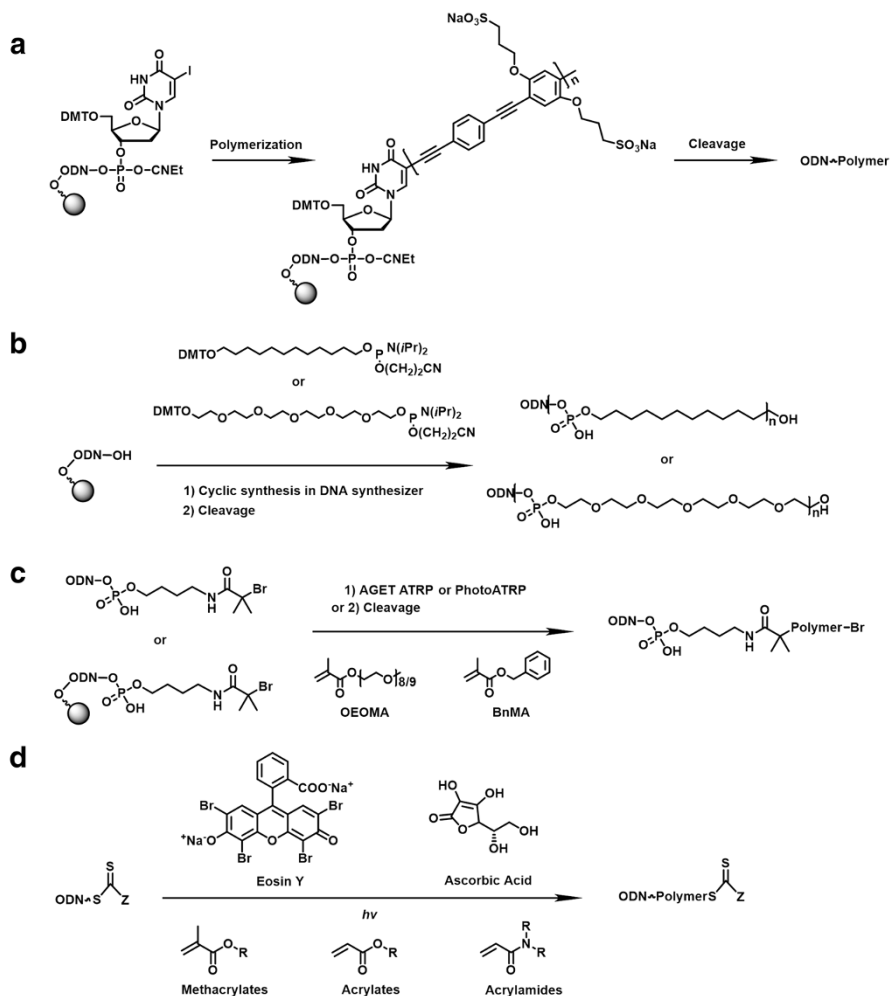


Fig. 6 Polymers were polymerized directly at the end of the ODN to prepare OPCs. **a** Polymerization of water-soluble PPE on controlled pore glass (CPG) solid support [51]. **b** Sequence synthesis of well-defined OPCs on a DNA synthesizer [52, 53]. **c** The atom transfer radical polymerization (ATRP) reaction was directly carried out at the end of the ODN to synthesize OPCs [54–56]. **d** In the solution, the ODN containing the reversible addition-fragmentation chain transfer polymerization (RAFT) initiator was subjected to RAFT polymerization to prepare OPCs [57]

colleagues [57] developed a new “graft-from” approach based on photo-induced RAFT polymerization, by which OPCs can be prepared in solution (Fig. 6d). First, ODNs were functionalized by the established RAFT agents 4-cyano-4-(phenylcarbonothioylthio) pentanoic acid (CPADB) and 2-(butylthiocarbonothioyl) propionic acid (BTPA), and then subjected to light-induced RAFT polymerization. It should be noted that: (1) RAFT reagents are unstable in alkaline media and cannot be synthesized directly on CPG solid support. (2) The deoxygenation of this

ultra-small-volume reaction system is a challenge. The use of Eosin Y (EY) and ascorbic acid (AscA) as reducing agents can replace the deoxygenation step in the polymerization process [57].

2.3 Acrydite-Functionalized ODN for Free-Radical Polymerization

In order to efficiently obtain ODN-graft polymer conjugates, one approach is to prepare polymerizable macromonomers containing ODNs and then copolymerize the macromonomers with other functional monomers (Fig. 7). Acrydite-functionalized ODN is the macromonomer used most widely to prepare OPCs such as ODN-g-PNIPAM (poly[*N*-isopropylacrylamide]) [58], and ODN-g-polyacrylamide [39, 59, 60]. These OPCs are used widely for preparing stimuli-responsive DNA hydrogels.

3 Separation and Purification of OPCs

Whether used in therapeutic, diagnostic, or self-assembly research, the purity of OPCs is critical. The unreacted hydrophobic polymer in the crude product can be removed by centrifugation due to its low solubility in aqueous solution. Another impurity is the unreacted ODNs. Briefly, there are several methods that can be used to remove free ODNs (Fig. 8): (1) dialysis [41, 61]; (2) ultrafiltration [27, 62]; (3) electrophoresis-cutting [48]; (4) reversed-phase column chromatography [34, 53]; (5) size exclusion chromatography [63–66]; and (6) anion exchange chromatography [46].

Most of the free ODN can be removed by selecting a dialysis bag or ultrafiltration tube with a suitable molecular weight cutoff. However, inevitably, there

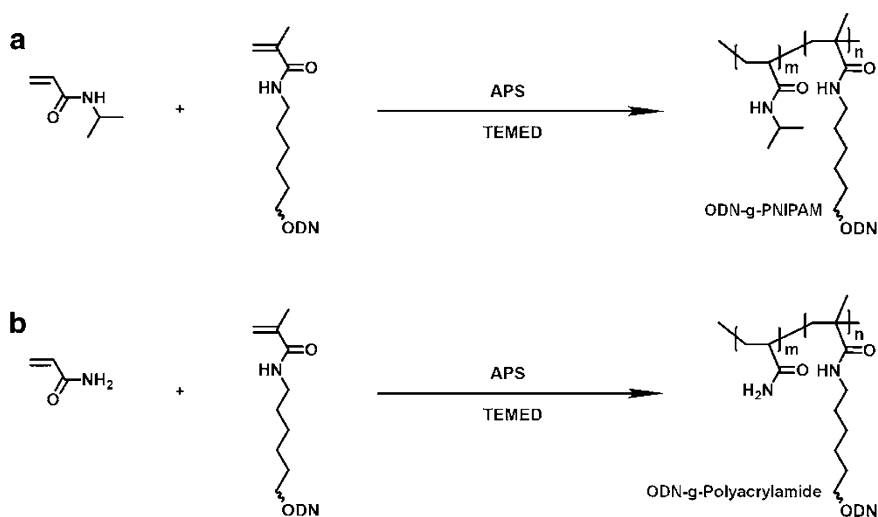


Fig. 7 Synthetic route of two representative ODN-graft polymer conjugates. **a** ODN-g-PNIPAM [58]. **b** ODN-g-Polyacrylamide [39, 59, 60]. APS Ammonium persulfate, TEMED tetramethylethylenediamine

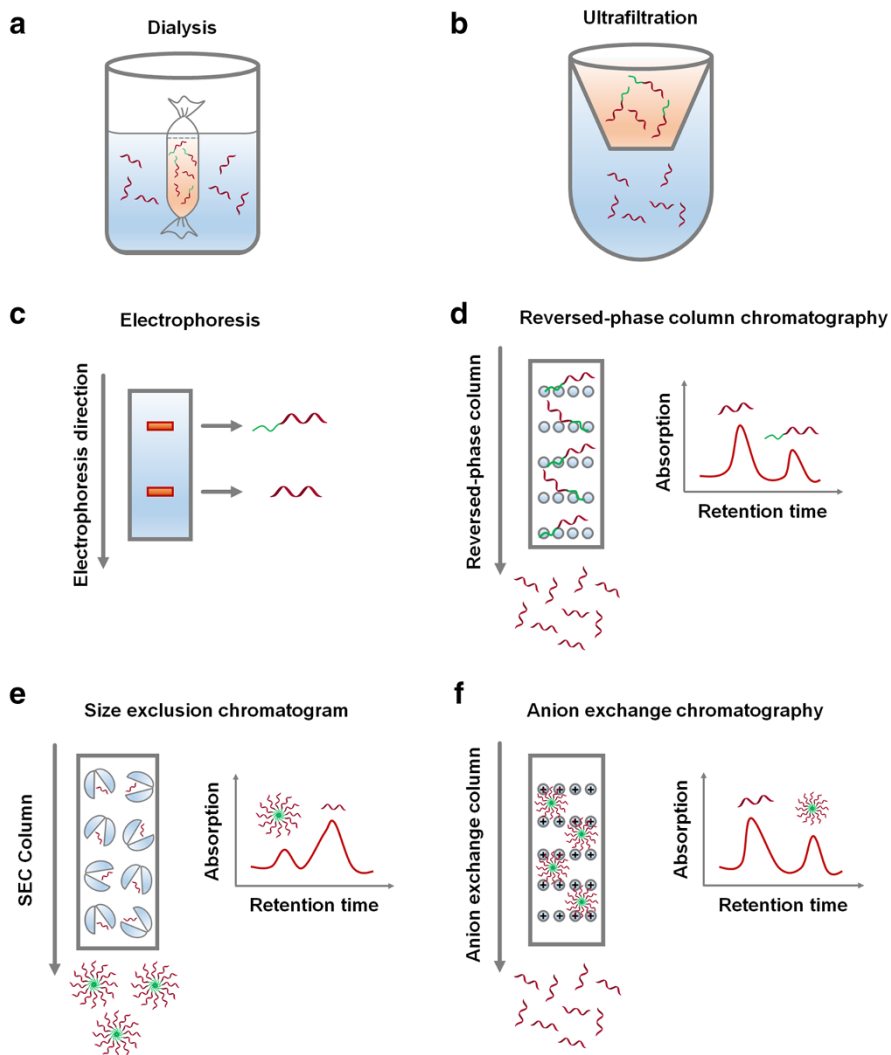


Fig. 8 Separation and purification of OPCs. **a** Dialysis. ODNs with small molecular weights will pass through the dialysis bag, while OPCs with large molecular weights will be trapped in the dialysis bag [41, 61]. **b** Ultrafiltration. Its separation principle is similar to dialysis, but the processing time is shorter compared with dialysis [27, 62]. **c** Electrophoresis-cutting purification. Separation by polyacrylamide gel electrophoresis (PAGE) or agarose gel electrophoresis, then cutting the target bands to obtain the purified OPCs [48]. **d** Purification by reversed-phase column chromatography. Separation and purification via differences in hydrophilicity [34, 53]. **e** Size exclusion chromatography purification: separation and purification by the difference in size [63–66]. **f** Anion exchange chromatography purification: separation and purification by the difference in charge density [46]

will still be a portion of the residual ODN in the sample of OPCs. These residual ODNs can potentially affect the properties of OPCs in subsequent studies.

Gel electrophoresis is the most common method for nucleic acid purification, and can separate products with very small differences in molecular weight. However, it requires the use of nucleic acid dyes to trace nucleic acids, which introduces new impurities to the OPCs.

Purification of OPCs by column chromatography is the most ideal separation method. For reversed-phase column chromatography, OPCs consisting of a hydrophobic-polymer-block will show longer retention time compared with the hydrophilic ODNs. Using this principle, we can get relatively pure OPCs. Notably, when separating OPCs using such methods, the hydrophobicity of the coupled polymer should not be too strong, otherwise the OPCs will not be eluted in the reversed-phase chromatographic column.

Another type of column chromatography that can be used for OPC purification is size exclusion chromatography. The principle of this method is that the substance with a larger size is eluted first, and the small-size one is eluted later. For highly hydrophobic polymers, the corresponding OPCs are likely to form large assembled structures due to the hydrophobic interactions, which will have larger sizes than the free ODNs. Using this principle, OPCs can be purified thoroughly.

The principle of anion exchange chromatography is to use the differences in charge densities of the substances to be separated. Amphiphilic OPCs containing hydrophobic moieties will form aggregates in aqueous solution. These aggregates have higher charge densities than free ODNs. Thus, free ODNs show shorter retention time in the anion exchange column compared to OPCs.

4 Classification of OPCs

Many types of OPCs have been reported. In the past, most review articles classify OPCs by their application directions. Here, we summarized various OPCs according to their coupled polymers. So far, the coupled polymers can be divided roughly into the following categories: biodegradable polymers, strong hydrophobic polymers, polymers with weak hydrophobicity, π -conjugated polymers, and other polymers. These polymers with different structures show very different properties; therefore, the research priorities and applications of the corresponding OPCs will be very different.

4.1 Biodegradable Polymer-Based OPCs

When applying OPCs to therapeutics, there is no doubt that biodegradable polymers are preferred. Currently, biodegradable polymers coupled with ODNs include mainly PLGA, PCL, and PLA.

4.1.1 ODN–PLGA Conjugates

PLGA is approved for clinical use by the Food and Drug Administration (FDA) of many countries due to its good biocompatibility and tunable degradation rate. PLGA contains two repeating units: lactic acid and glycolic acid. The degradation rate of PLGA can be regulated by adjusting the molecular weight of PLGA or the ratio between the lactic acid and glycolic acid units. Compared to PLA and PCL, PLGA has a faster degradation rate due to its good hydrophilicity. These excellent properties make PLGA a promising material in the biomedical field.

Antisense ODN can block the expression of specific proteins to treat a particular disease, but its most serious problem is its low cell permeability. In 2001, Park's group reported the coupling of antisense ODN and PLGA (Fig. 9a) [67]. The amphiphilic ODN-b-PLGA block copolymers could self-assemble into stable micelles in aqueous solution. More importantly, these ODN-b-PLGA micelles can enter cells via endocytosis without the need for a cationic transfection agent. In addition, the controlled degradation of PLGA allows the sustainable release of antisense DNA to efficiently inhibit the expression of certain genes [67].

siRNA can target mRNA and mediate the degradation of the target mRNA to realize gene silencing. Likewise, intracellular delivery of siRNA also requires the utilization of toxic cationic polymeric carriers. In order to realize self-delivery, siRNA was chemically conjugated to PLGA via a cleavable disulfide bond [29, 30] to form siRNA–PLGA conjugates, which would subsequently self-assemble into micelles in aqueous solution with a high density of siRNAs at the surface (Fig. 9a,

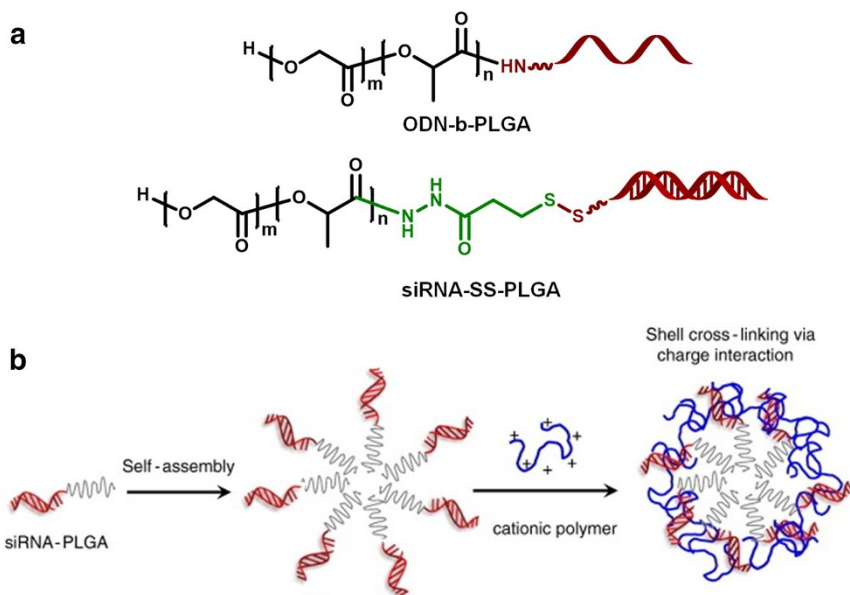


Fig. 9 **a** Structural formula of two common ODN–PLGA conjugates. **b** Self-assembled siRNA–PLGA conjugates for intracellular delivery of siRNA (adapted with permission from [30])

b). Compared to the free siRNA, siRNA-b-PLGA was more readily complexed by linear-low-molecular-weight PEI (polyethyleneimine), which shows comparatively lower cytotoxicity. In addition, the siRNA-b-PLGA/PEI complex exhibited improved cell permeability and gene silencing efficiency than the siRNA/PEI complex [30].

4.1.2 ODN–PCL Conjugates

PCL is also a biodegradable polymer that is approved by the FDA for biomedical applications. PCL can be prepared by the ring-opening polymerization of ϵ -caprolactone monomers catalyzed by a metal anion complex. By optimizing the polymerization conditions, PCL of different molecular weights can be synthesized. Compared to PLGA and PLA, modifications of PCL are more readily performed.

According to the theory of spherical nucleic acids (SNAs) [68, 69], densely packed and highly oriented nucleic acids in a spherical geometry show properties that differ markedly from their linear cousins. SNAs can enter cells more efficiently to induce gene regulation or detect biological targets in live cells. Generally, SNAs are constructed on spherical nanoparticle cores, to the surfaces of which ODNs were covalently attached; in addition to this, the self-assembled OPCs can also build SNA structures. In 2015, Zhang et al. [61] reported two ODN–PCL conjugates: linear ODN-b-PCL and ODN-g-PCL conjugates (Fig. 10a, b). They believe that the nucleic acid micelles formed by ODN-g-PCL conjugates have a higher surface density of ODNs than the micelles formed by linear ODN-b-PCL. Compared with ODN-b-PCL, ODN-g-PCL showed more negative surface charge, higher melting temperatures, higher cell uptake efficiency, and more efficient gene suppression efficiency [61].

In a follow-up work, Zhang's group developed a method of using siRNA as a cross-linker to mediate further self-assembly of the ODN-g-PCL conjugates, forming spherical and nanosized hydrogels. The siRNAs were fully embedded in the nanogel, which showed good bio-stability during the systemic delivery. This size-adjustable cross-linked siRNA@DNA-g-PCL nanogel could deliver siRNAs efficiently to different cells without the need for any transfection agents, and achieved efficient gene silencing both in vitro and in vivo. Through this, significant inhibition of tumor growth was realized in the anticancer treatment (Fig. 10a, c) [41].

4.1.3 ODN–PLA Conjugates

PLA is also an FDA-approved biodegradable material that degrades at a slower rate than PLGA. PLA can be synthesized by the controlled ring-opening polymerization of lactide. To synthesize ODN–PLA conjugates, a “Click” reaction can be performed using azide-terminated PLA and alkynyl-terminated ODN [33]. Similarly, ODN–PLA conjugates could self-assemble into spherical micelles in aqueous solution. Chen's group used in situ rolling circle transcription (RCT) to prepare short hairpin RNAs (shRNA) from the amphiphilic ODN–PLA micelles, using the peripheral ODNs as primers. The shRNAs were applied to inhibit the expression of multidrug resistance protein 1 (MDR1) in breast cancer. In addition, the hydrophobic

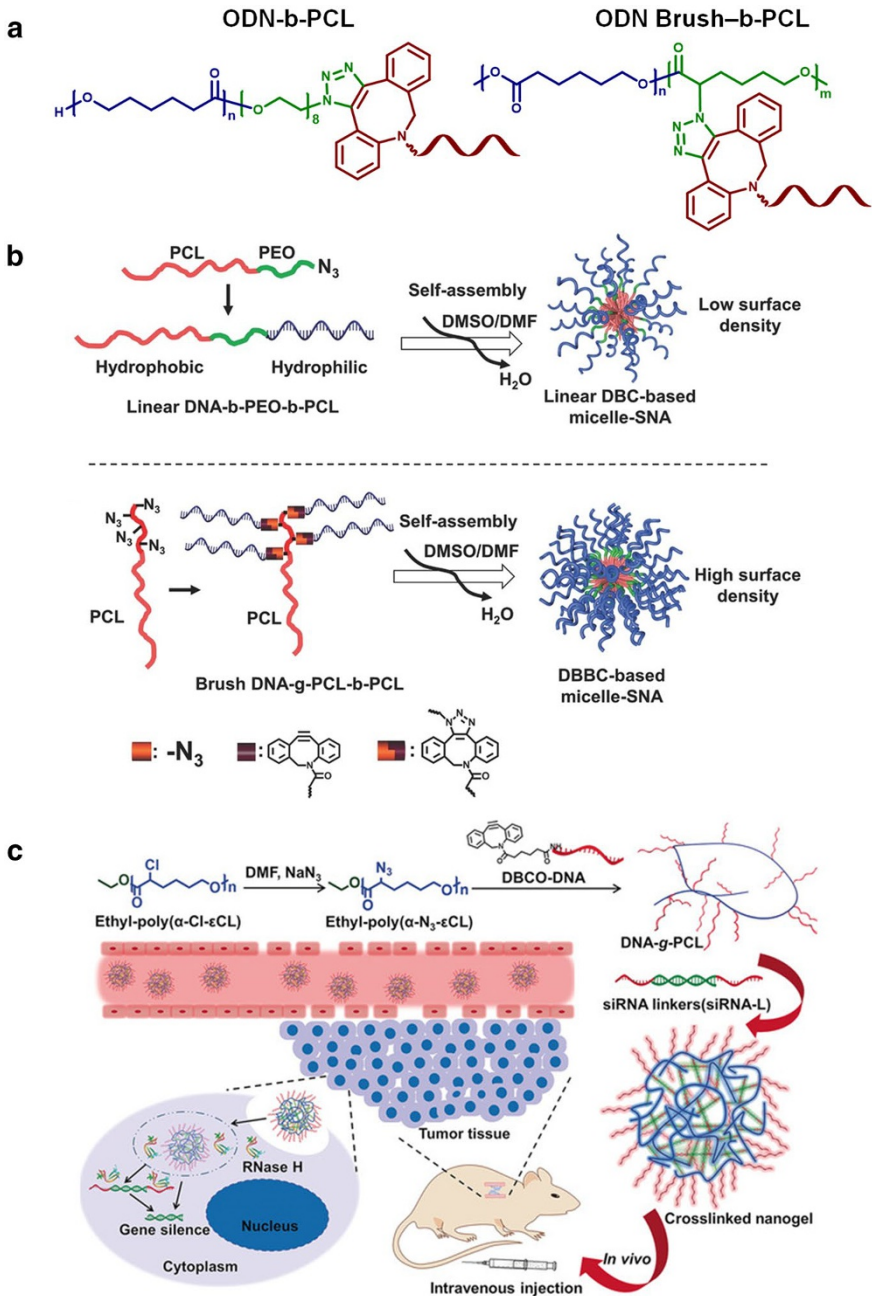


Fig. 10 Assembly and application of ODN–PCL conjugates. **a** The chemical structures of two typical ODN–PCL conjugates [61]. **b** Two ODN–PCL micelles with different surface nucleic acid densities are used for intracellular gene silencing (reproduced with permission from [61]). **c** siRNA@ODN-g-PCL nanogel prepared using siRNA as a crosslinker for siRNA delivery and anti-tumor therapy (reproduced with permission from [41])

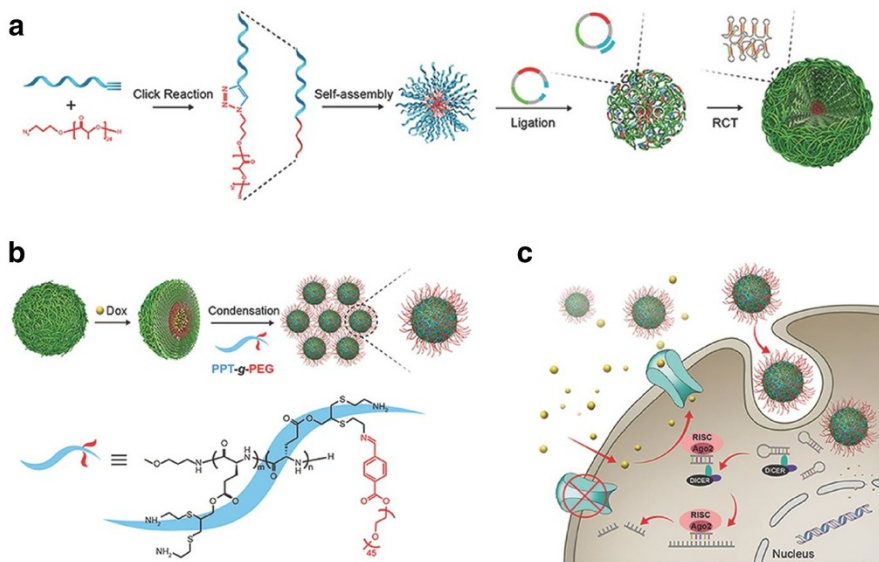


Fig. 11 Assembly and application of ODN-PLA conjugates (reproduced with permission from [33]). **a** Self-assembly of ODN-b-PLA synthesized by a copper-catalyzed “click” reaction to form spherical micelles. Rolling circle transcription (RCT) was then performed in situ on the micelles to prepare a large amount of shRNA. **b** shRNA@ODN-PLA encapsulates hydrophobic doxorubicin (DOX) and is further condensed by PPT-g-PEG to obtain nanoparticles for the synergistic treatment of multidrug-resistant breast cancer (**c**)

PLA core can carry hydrophobic drugs, such as doxorubicin (DOX). The product of shRNA@ODN-PLA was then condensed by positively charged peptide-grafted poly(ethylene glycol) (PPT-g-PEG) into nanoparticles. This multifunctional composite nanoparticle could be efficiently delivered to cancer cells and accumulate in xenograft tumors, enabling multi-modal therapy for MDR breast cancer (Fig. 11) [33].

4.2 DNA-Strong Hydrophobic Polymer Conjugates

Generally, polymers bearing hydrocarbon chains ($-\text{CH}_2$) and aromatic units (benzene, etc.) show strong hydrophobic properties. Examples of this include polystyrene and polynorbornene. When these highly hydrophobic polymers are coupled to hydrophilic ODNs, the resulting amphiphilic OPCs typically form compact and small micelles with “solid” cores. This type of micelle is more suitable for encapsulating substances that we do not want to leak from the micelles, such as toxic contrast agents and organic dyes.

4.2.1 ODN-Polystyrene Conjugates

The strong hydrophobicity of polystyrene (PS) makes the synthesis of ODN-PS conjugates difficult. Several approaches that have been applied to the synthesis of

ODN-PS conjugates include phosphoramidite chemistry [70, 71], amidation reactions [72, 73], Michael addition reactions [32], and copper-catalyzed Click reactions [48].

Due to the strong hydrophobicity of PS, ODN-PS conjugates are able to self-assemble into very stable micelles, which can be used to encapsulate hydrophobic dyes and drugs with high efficiency and stability. Park's group co-assembled magnetic nanoparticles (MNP) and ODN-PS conjugates into hybrid nanostructures, which show potential applications in magnetic separation and handling of DNA molecules, magnetic resonance imaging, local drug delivery, and treatment of diseases by magnetic hyperthermia therapy. The surfaces of such nanostructure consist of high-density ODN chains, resulting in SNAs-like properties. Therefore, these hybrid nanostructures display excellent DNA hybridization properties including a

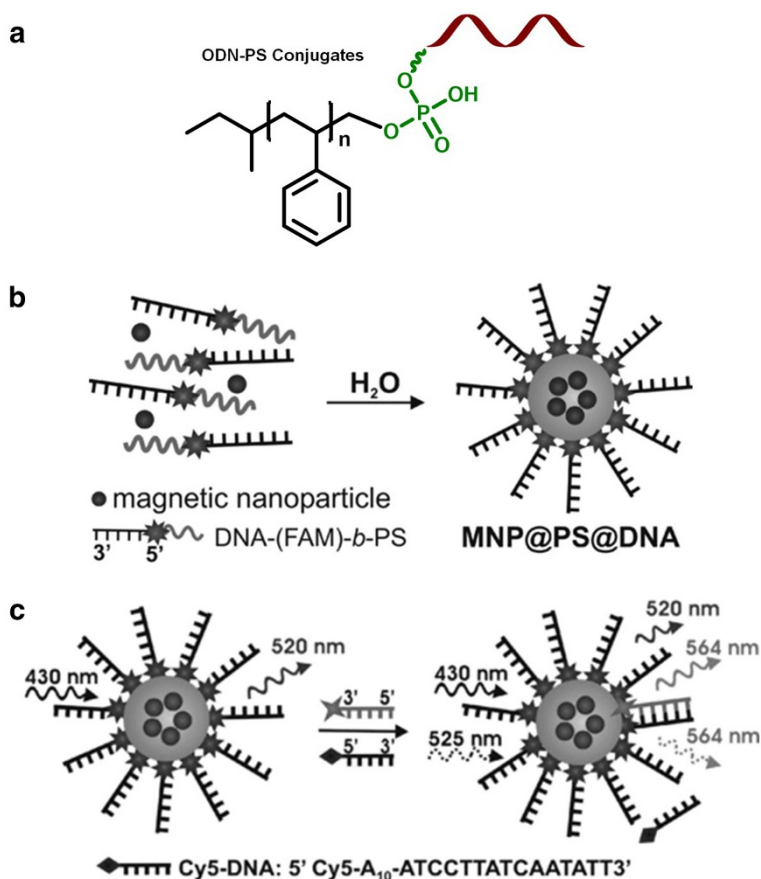


Fig. 12 Assembly and application study of ODN-PS conjugates (reproduced with permission from [71]). **a** Chemical structure of ODN-PS conjugates prepared by phosphoramidite chemistry. **b** Preparation of ODN-PS assembly with magnetic nanoparticles. **c** Cy3-labeled target DNA preferentially binds to MNP@ODN-PS in the presence of Cy5-labeled competing ODN (i.e., the free ODN having the same sequence as that on MNP@PS-DNA)

high DNA binding constant for DNA detection and delivery applications (Fig. 12) [71].

In addition, Herrmann's group [32] incorporated ferrocene (Fc) into micelles formed by ODN-PS conjugates. They found that the introduction of Fc molecules into the hydrophobic core would not affect the micellar morphology. Moreover, Fc encapsulation significantly changes the electrical properties of the micelles, which are expected to be applied to nanoelectronics or biosensing [32].

4.2.2 ODN-Hydrophobic PNB Conjugates

In order to build a polymer micellar SNA to improve the biostability of ODN for intracellular and in vivo applications, Gianneschi's group conjugated a carboxylic

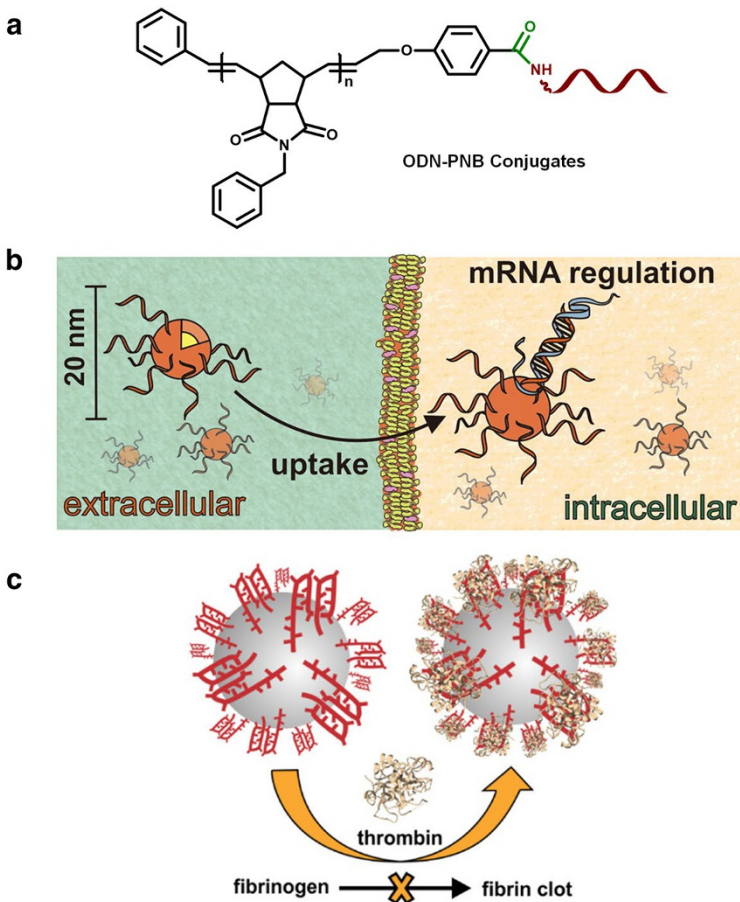


Fig. 13 **a** Chemical structure of ODN-PNB conjugates. **b** Amphiphilic ODN-PNB conjugates self-assemble into micellar nanoparticles for intracellular gene regulation (reproduced with permission from [65]). **c** Micellar thrombin-binding aptamers for anticoagulation (reproduced with permission from [64])

acid terminated polynorbornene (PNB) with an amine-modified ODN through solid-phase coupling reaction (Fig. 13a). Due to the strong hydrophobicity of PNB, ODN–PNB conjugates self-assembled into solid micelles [63–66]. Initially, they grafted long ODNs to the side chain of PNB to form an amphiphilic brush copolymer. When the long ODN strand is cleaved by the DNAzyme, the assembly of the amphiphilic copolymer is converted from a spherical to a cylindrical structure. This cylindrical structure could reconvert into a spherical structure by adding a long complementary strand, which was a reversible process by strand competition [49]. The same group also explored a variety of applications for these kinds of ODN–PNB based SNAs including gene regulation (Fig. 13a, b) [63, 65] and micellar thrombin-binding aptamers (Fig. 13c) [64].

4.3 ODN–Dynamic Polymer Conjugates

Polymers show tunable hydrophobicity upon response to environmental changes, and are thus defined as “dynamic polymers”. These polymers generally have low glass transition temperatures; therefore, the corresponding OPCs could form micelles showing properties different from “solid” micelles, which could go through dynamic changes under different conditions. Therefore, smart micelles fabricated from this kind of OPCs show interesting application potentials in the biomedical field, and are able to respond to pH, enzymes, and temperature.

4.3.1 ODN–PPO Conjugates

Polypropylene oxide (PPO) shows a glass transition temperature ($T_g = -70\text{ }^\circ\text{C}$) much lower than that of PLGA and PS. PPO is a polymer that shows temperature-dependent properties: it is hydrophilic at low temperatures (below $20\text{ }^\circ\text{C}$) and changes to hydrophobic at room temperature. Therefore, OPC micelles with PPO as the hydrophobic core show “dynamic” characteristics. Moreover, the synthesis of ODN–PPO conjugates is very accessible, as PPO polymers with hydroxyl end groups can be readily coupled with ODN through the phosphoramidite chemistry on a DNA synthesizer (Fig. 14a).

The amphiphilic block copolymer ODN-b-PPO can self-assemble in aqueous solution to form dynamic spherical micelles. Thus, these micelles, which display a recognition function at the ODN shell and an encapsulation function at the PPO core, were applied to DNA-templated organic synthesis [45], targeted drug delivery (Fig. 14b) [74, 75], and virus loading [76]. In addition, ODN-b-PPO could be inserted into the lipid vesicle layer [77], or co-assembled with other amphiphilic micelles [78] to prepare hybrid materials. Making use of the hydrophilicity of PPO at low temperatures, ODN-b-PPO was inserted into the network of a DNA hydrogel to study the process of molecular self-collapse (due to the phase transition of PPO) [79]. In another work, the authors claimed that the dynamic micelles of ODN-b-PPO could switch from spherical to rod-shaped structures via hybridization with cDNA (Fig. 14c) [80]. In addition, the use of a stimuli-responsive ODN sequence could also induce the dynamic change of ODN-b-PPO micelles. For example, the

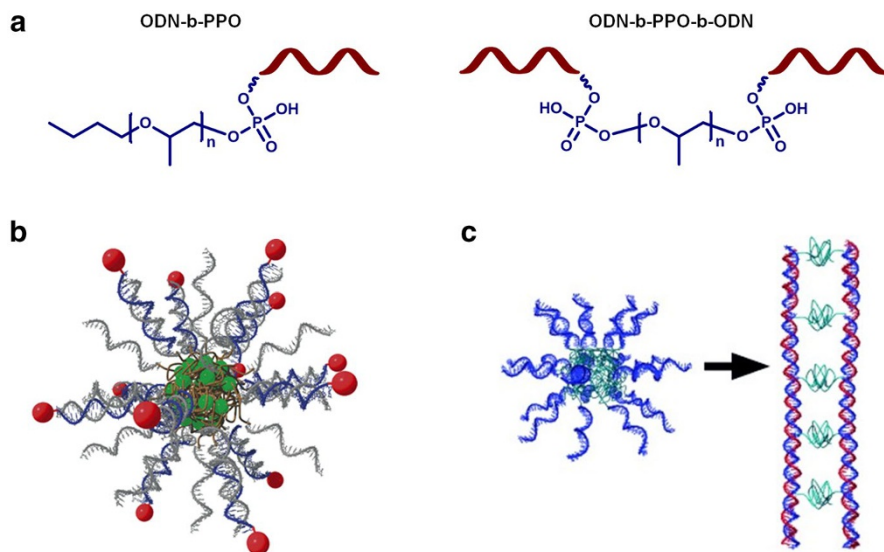


Fig. 14 **a** Structures of ODN-b-PPO [74] and ODN-b-PPO-ODN [79]. **b** Micelles formed by the self-assembly of ODN-b-PPO amphiphilic block copolymer are used for the treatment of cancer (reproduced with permission from [74]). (Green ball hydrophobic drug, red ball targeting group.) **c** Morphological changes of ODN-b-PPO with thermodynamic equilibrium induced by long-chain DNA hybridization (reproduced with permission from [80])

pH-responsive “i-motif” sequence will fold at acidic pH conditions, which would drive the morphology change of the self-assembly from spherical micelles to long fibers [81]. The biological methods, such as enzymatic polymerization or ligation [82–84], can also be used to change the properties of ODNs and subsequently control the morphology changes of the OPC self-assemblies.

4.3.2 ODN–PNIPAM Conjugates

Poly(*N*-isopropylacrylamide) (PNIPAM) is a widely studied temperature-sensitive polymer. At room temperature, linear PNIPAM dissolves well in aqueous solution, but when the temperature reaches a certain temperature, PNIPAM will undergo a transition from hydrophilic to hydrophobic in nature. The critical temperature for hydrophilic–hydrophobic transition is called low critical solution temperature (LCST). Accordingly, a PNIPAM-based microgel exhibits a high degree of swelling (hydration state) at room temperature, and, when the temperature is raised to about 32 °C, the PNIPAM microgel will convert into a dehydrated state, resulting in significant shrinkage. The transition temperature of PNIPAM microgel is defined by the volume phase transition temperature (VPTT). The fast-response and temperature-sensitive properties of PNIPAM make it suitable for biomedical applications such as controlled drug delivery and biosensing.

Based on the reversible phase-transition properties of PNIPAM, ODN–PNIPAM conjugates are expected to show new and interesting properties (Fig. 15a).

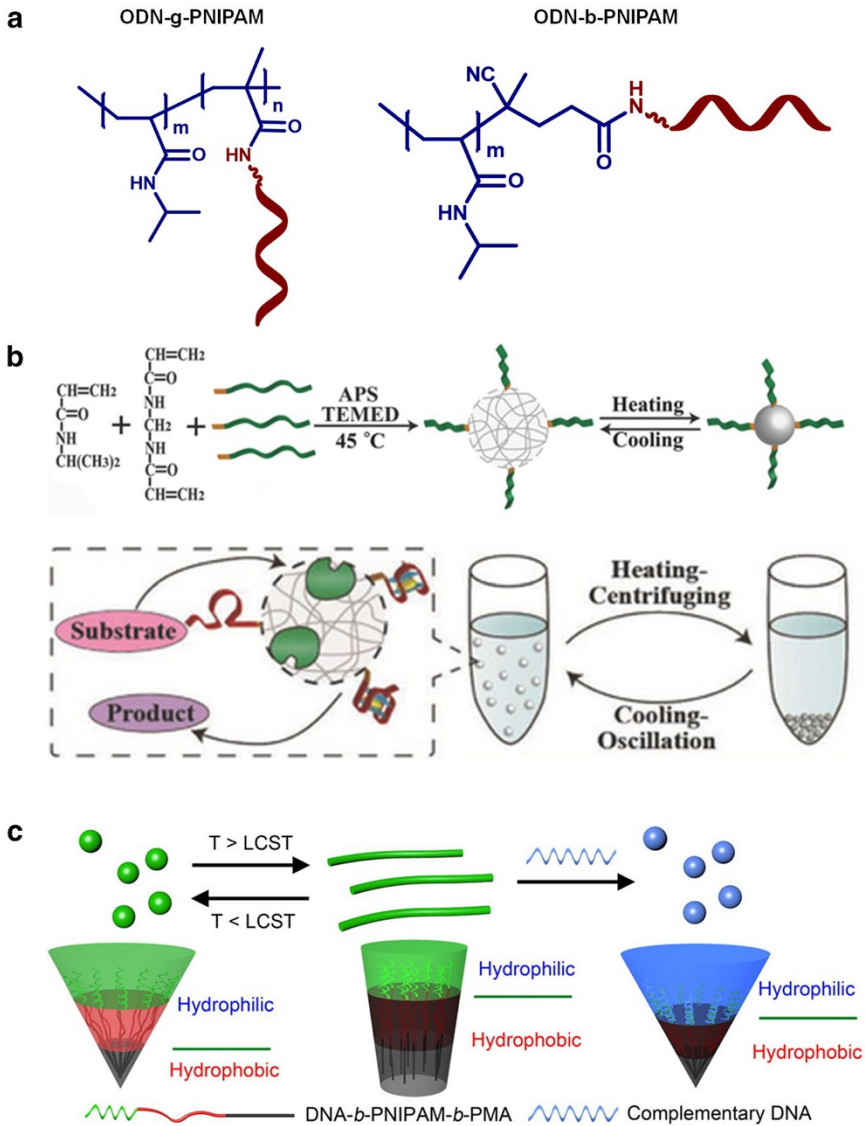


Fig. 15 Application and assembly behavior of ODN–PNIPAM conjugates. **a** Structures of ODN-*g*-PNIPAM [86] and ODN-*b*-PNIPAM [91]. **b** A multifunctional poly-*N*-isopropylacrylamide/DNAzyme microgel as a highly efficient and recyclable catalyst for biosensing (reproduced with permission from [58]). **c** Multimodal shape transformation of a dual responsive ODN block copolymer (reproduced with permission from [91])

For example, the charge of ODN would affect the phase transition behavior of ODN–PNIPAM conjugates [85], and the molecular recognition capability, stimuli-responsiveness, and therapeutic functions of ODNs would greatly broaden the properties of PNIPAM. Various materials (such as hydrogels [86]) have been developed

based on ODN–PNIPAM conjugates, which have been applied in the separation of nucleic acids [87, 88] and proteins [89], as well as recyclable biocatalysts [58] (Fig. 15b). ODN–PNIPAM conjugates also showed more versatile self-assembly properties. For example, the molecular hybridization capability of ODN allows PNIPAM to form layer-by-layer assemblies [90] or aggregate by non-covalent crosslinking [31]; Some switchable self-assemblies can also be prepared by using the phase-transition properties of PNIPAM (Fig. 15c) [91]. In addition, PNIPAM can be combined with classical DNA nanostructures (such as DNA tetrahedral [92]) to produce smart nano-materials.

4.3.3 ODN–HE_n Conjugates

The structure and properties of DNA can be well-defined by its sequence. Inspired by this, synthesized organic molecules can be coupled sequentially to the ODN strand on the solid support using a DNA synthesizer. Sleiman's group [53] used commercially available dimethoxytrityl (DMT)-protected dodecanediol phosphoramidite, which corresponds to the hexamer portion of polyethylene (HE) for the synthesis of sequence-controlled OPCs. Due to highly efficient phosphoramidite chemistry reactions, the degree of polymerization can be fully controlled (up to 72 units). Upon purification by reverse-phase high-performance liquid chromatography (HPLC), monodispersed ODN–HE_n conjugates can be obtained (Fig. 16a) [53]. The presence of the phosphate moiety in the polymer backbone does not affect the hydrophobic nature of the HE moiety. Moreover, the hydrophobicity of the OPCs increased as the degree of polymerization increased. When the number of HE units reached six, ODN–HE₆ conjugates formed spherical micelles in the presence of magnesium ions (Mg²⁺). The more HE units incorporated, the more stable the resultant micelles became, with a higher loading capability for hydrophobic guest molecules. It should be noted that all ODN–HE_n conjugates retained hybridization capability to cDNAs. Taking advantage of the controlled self-assembled properties of ODN–HE_n conjugates, as well as the precise hybridization of ODNs, a large number of newly assembled structures or materials were prepared [93]. Examples include the superstructure formed by DNA nanocages (Fig. 16b) [94] and DNA cage-based ring structures formed through hydrophobic interactions (Fig. 16c) [95]. With regard to the application, the micelles of ODN–HE_n conjugates were used as nano-reactors to improve the efficiency of the coupling reaction between hydrophobic molecules and ODNs [96]. Similar to other OPCs, ODN–HE_n conjugates were also applied to drug delivery [97, 98] and gene regulation [99, 100].

4.4 ODN–Conjugated Polymer Conjugates

The π -conjugated polymer is one of the most important organic functional materials, which shows extended π -conjugation along the molecular backbone with delocalized π -electrons. Due to their excellent light-harvesting and light-amplifying properties, π -conjugated polymers have been used widely in the biomedical and biosensing fields [101]. In addition, π -conjugated polymer-based OPCs show strong π – π and

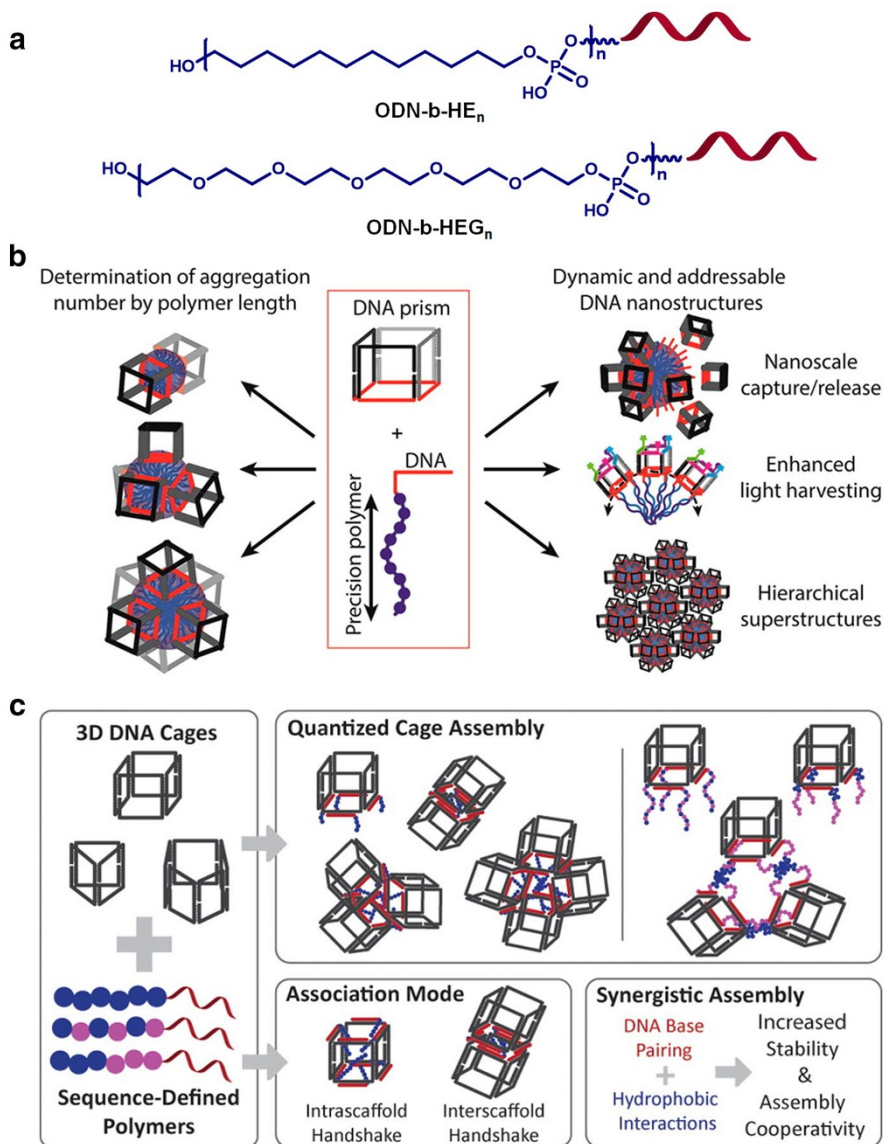


Fig. 16 Self-assembly of sequence-defined ODN-HE_n conjugates. **a** Chemical structure of ODN-HE_n and ODN-HEG_n conjugates [53]. **b** Precision assembly of ODN-HE_n conjugates with 3D DNA cages into DNA cage-micelles or hierarchical superstructures (reproduced with permission from [94]), as well as the ring structure of DNA cages (c) (reproduced with permission from [95])

hydrophobic interactions, which would result in unique self-assembly behaviors and interesting optical and electronic properties [102].

4.4.1 ODN–PPE Conjugates

Water-soluble poly(phenyleneethynylene) (PPE) is easy to synthesize and has a high fluorescence quantum yield in aqueous solution, so it has been applied widely to fluorescence biosensing. Yang et al. [51] developed a molecular beacon system using PPE polymer as the fluorescence reporter. Due to the super-quenching property of their π -conjugated polymer, the fluorescence of PPE was completely quenched when the molecular beacon was folded to a hairpin structure. When hybridized with the target DNA, the hairpin structure was opened to generate fluorescence signal. This molecular beacon based on a π -conjugated polymer shows a high sensitivity for nucleic acid detection [51], due to the good light-harvesting capability and efficient energy transfer along the molecular backbone of PPE. A DNA molecular beacon modified with PPE as the energy donor and the HEX (hexachlorofluorescein) dye as the energy acceptor has also been developed, which would detect nucleic acids through FRET (fluorescence resonance energy transfer) signals, resulting in a more specific and quantitative detection capability (Fig. 17) [27].

4.4.2 ODN–PFO Conjugates

The single-walled carbon nanotube (SWNT) is one of the most important carbon nanomaterials, exhibiting excellent mechanical, electrical, thermal and optical properties. SWNTs intrinsically tend to bundle together due to van der Waals interactions. Surface functionalization with amphiphilic dispersant provides an efficient method to disperse and purify SWNTs with minimal introduction of defects. It is interesting to note that polyfluorene (PFO) can selectively dissolve semiconducting SWNTs rather than the conductive counterpart with a narrow size distribution.

Herrmann's group [46] coupled PFO and ODN to synthesize ODN–PFO conjugates (Fig. 18), which could effectively and selectively disperse SWNTs as well as provide a platform for precise operation. Using the ODN–PFO conjugates, electronic devices can be fabricated by the bottom-up method on an extended surface, resulting in high yields. Electrostatic repulsion between ODNs and the strong interaction between PFO and the sidewalls of the SWNTs make ODN–PFO a good dispersion agent for SWNTs. In addition, ODN-modified gold nanoparticles could be readily functionalized to the surface of the nanodevice through hybridization with ODN–PFO dispersed SWNTs [46].

4.4.3 ODN–PT Conjugates

Due to the liquid crystal properties of rigid–rod type polymers, rod–coil type block copolymers show higher structural diversity than conventional coil–coil type polymers. Conjugates of ODN and rigid–rod polymers were thus predicted to have unusual assembly behaviors; they could be either rod–coil type block copolymers (single-stranded ODN with a flexible structure) or rod–rod type

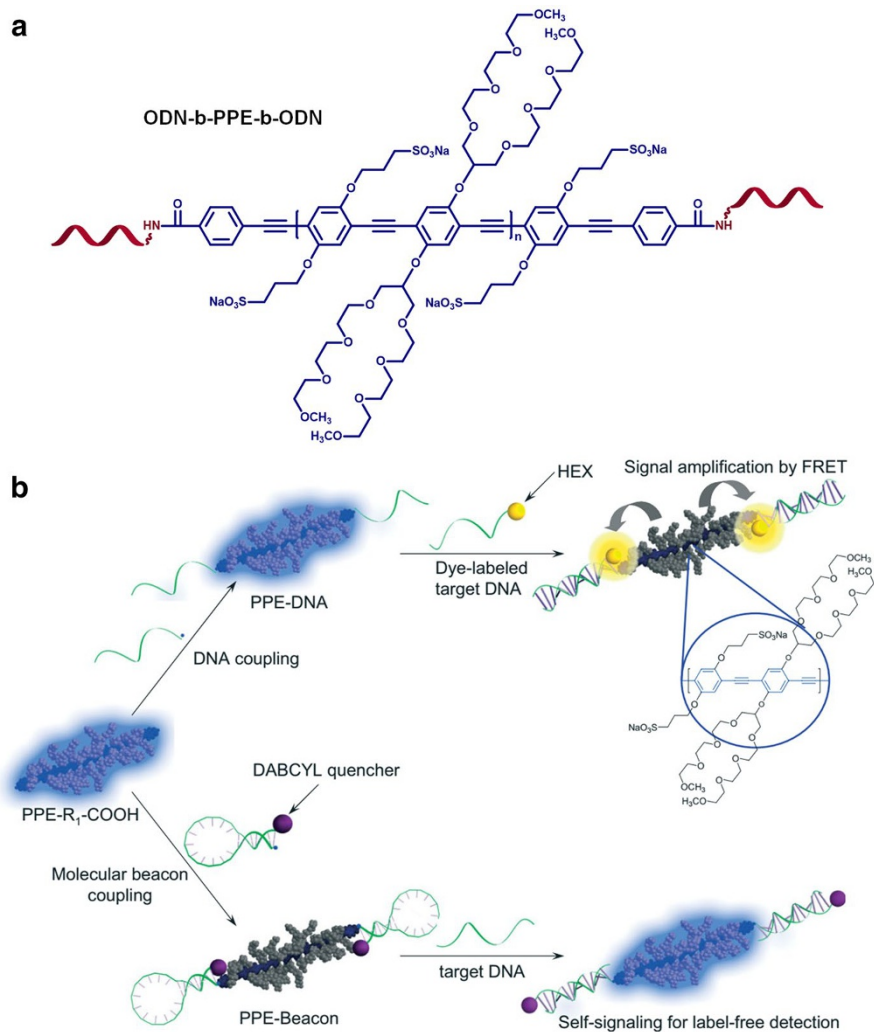


Fig. 17 a Chemical structure of water-soluble poly(phenyleneethynylene) (PPE)–ODN conjugates. **b** Molecular beacons and signal amplification systems based on conjugated polymers (reproduced with permission from [27])

block copolymers (duplex nucleic acid with a relatively rigid structure). Park's group coupled the rigid–rod polymer PT (polythiophene) with ODN to synthesize ODN-b-PT conjugates (Fig. 19). In general, ODN amphiphilic block copolymers tend to form simple spherical micelles. However, due to the rigid structure of PT and its strong π – π interaction, ODN-b-PT conjugates formed a hollow vesicle structure. It should be noted that, due to the dense stacking of PTs, the vesicles formed by ODN-b-PT show very weak fluorescent signals in water. The size of the vesicles formed by self-assembly is regulated by adjusting the concentration

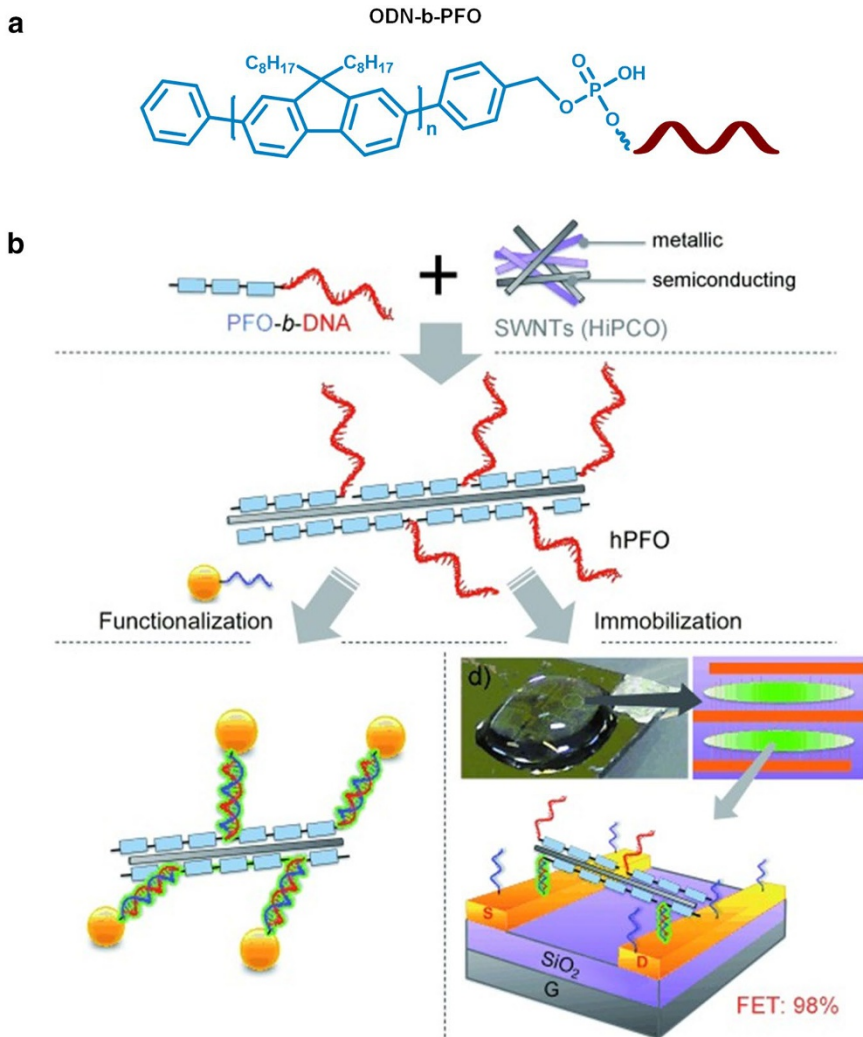


Fig. 18 **a** Chemical structure of ODN–PFO conjugates. **b** Co-assembly of ODN–PFO conjugates and single-walled carbon nanotubes (SWNTs) and their application in nanoelectronics (reproduced with permission from [46])

of ODN-b-PT in aqueous solution. In addition, increasing the salt concentration in solution converted ODN-b-PT from a vesicular morphology to a sheet structure; this change was reversible. Interestingly, the researchers incorporated ODN-b-PT into a one-dimensional nanoribbon assembled from PEG-b-PT to functionalize the nanoribbon with AuNPs. The ODN-conjugated polymer prepared by coupling ODN with a rigid conjugated polymer show interesting morphologies due to the strong π – π interactions, and new properties due to the optoelectronic properties of conjugated polymers [103].

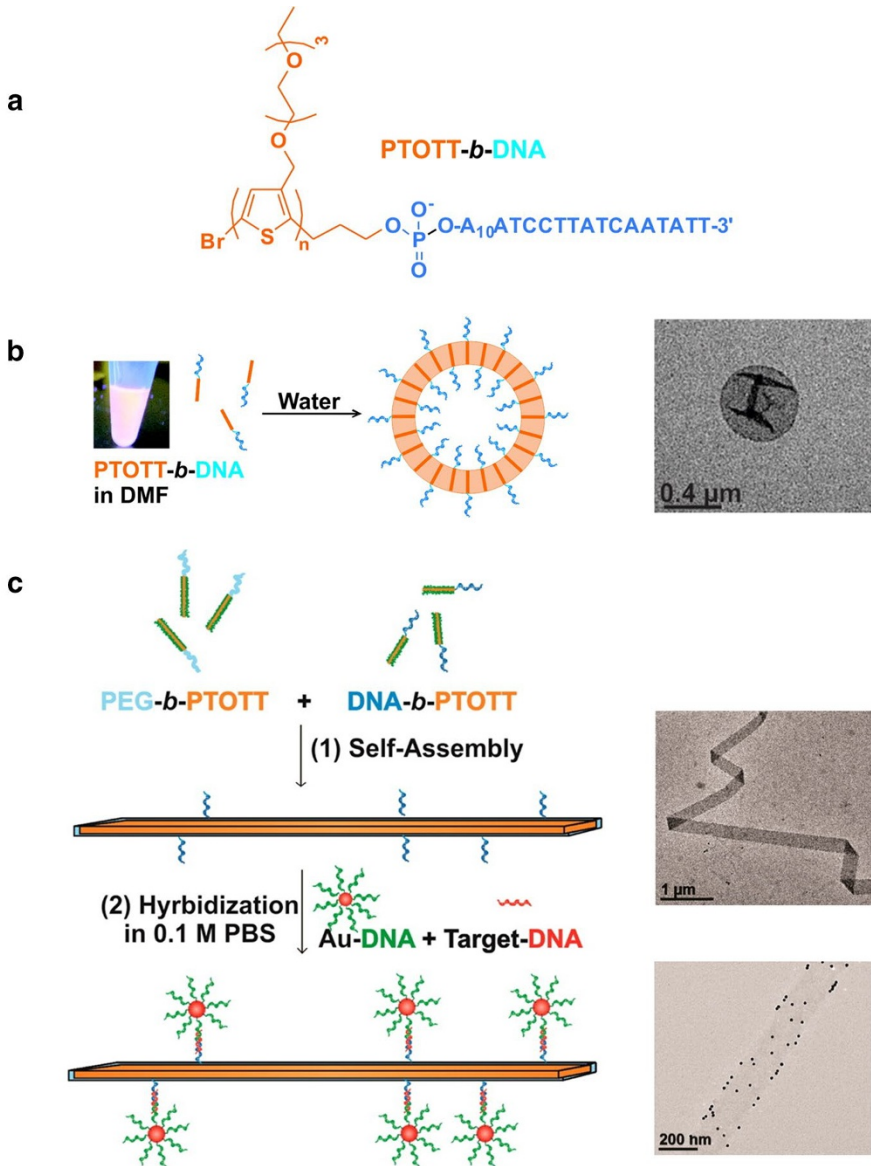


Fig. 19 **a** Chemical structure of ODN–PT conjugates. **b** ODN–PT conjugates self-assemble into vesicles in water; transmission electron microscopy (TEM) images of vesicles at the right. **c** ODN-*b*-PT conjugates can be co-assembled with PEG-*b*-PT to achieve the functionalization of the nanoribbons. TEM images at the right. Insets **b**, **c** are adapted with permission from [103]

4.4.4 ODN–PFP Conjugates

PFP (poly[fluorine-co-phenylene fluorene]) is a typical fluorescent polymer that displays an effect called “aggregation caused quenching” (ACQ). Xia’s group [28] prepared ODN-b-PFP conjugates by coupling ODN and PFP via amidation reactions. Due to the hydrophobicity of the benzene ring on the PFP backbone and the hydrophilicity of the ODN phosphate backbone, ODN-b-PFP formed a micellar structure in aqueous solution. In the presence of Hg^{2+} ions, the formation of T- Hg^{2+} -T complex leads to the further aggregation of the micelles, which would quench the fluorescence of the PFP due to the ACQ effect. After addition of the chloride anion, the formation of HgCl_2 reduced the concentration of Hg^{2+} in solution, which could efficiently recover the ODN-b-PFP conjugates. In another study, a strand of ODN that could be recognized by telomerase was used, and the resultant ODN-b-PFP tightly self-assembled into micelles showing quenched fluorescence. In the presence of telomerase, the length of ODN increased via the addition of GGGTTA repeats, which increased the hydrophilicity of the ODN-b-PFP conjugates. Due to this, the aggregation state of the micelles became unstable and loose, and the PFP fluorescence was increased. These interesting ODN–PFP conjugates can be applied in bioassays and environmental analysis (Fig. 20) [28].

4.4.5 ODN–APPV Conjugates

Molecular conformation is crucial to the performance of nanodevices based on single polymers; however, this needs precise control at the molecular scale and is still very challenging for recent techniques. Gothelf et al. [104] prepared hydroxyl-group-modified (2,5-dialkoxy) paraphenylene vinylene (APPV) conjugated polymers. ODNs were directly synthesized on the side chains of APPV by automated solid-phase synthesis to obtain ODN-grafted APPV (ODN-g-APPV; Fig. 21a). DNA origami technology can produce unique two- or three-dimensional nanostructures with very precise addressable capability. Anchor DNA chains with a specific shape were predesigned on the DNA origami template, and then the conformation of the individual APPV was controlled at the nanoscale by DNA hybridization manipulation. By virtue of this method, an individual APPV can be assembled into arbitrary shapes in 2D or 3D geometry (Fig. 21b). Therefore, this method was the first to use a DNA origami technique to control the geometry of a π -conjugated polymer at the molecular scale, which may generate interesting electric or optical properties.

4.5 ODN–Other Polymer Conjugates

4.5.1 ODN–PAM Conjugates

Polyacrylamide (PAM) was initially used in electrophoresis. More recently, due to its low cost and availability, PAM has been used widely in enzyme immobilization, drug delivery, and other biomedical applications. Acrylamide can

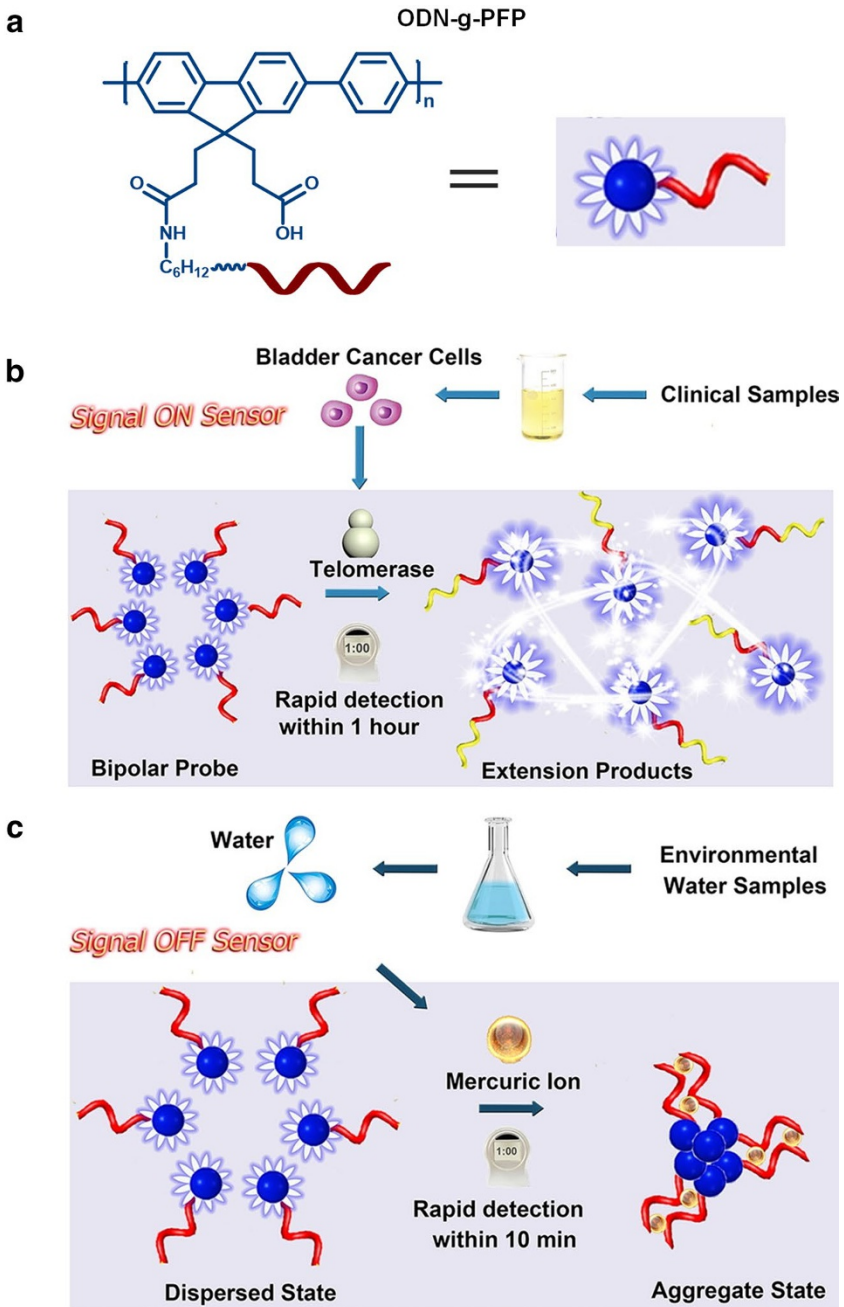


Fig. 20 **a** Chemical structure of ODN–PFP conjugates. **b** Detection of telomerase by prolonging the ODN chain to release the fluorescence of PFP. **c** Decreased fluorescence due to increased aggregation by the addition of Hg^{2+} (adapted with permission from [28])

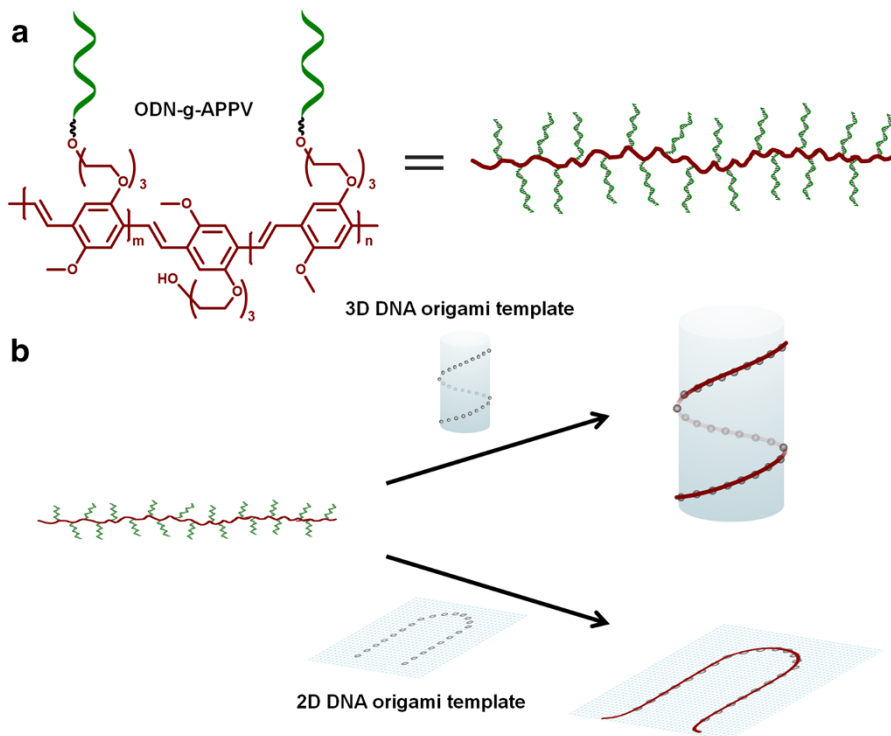


Fig. 21 **a** Chemical structure of ODN-g-(2,5-dialkoxy) paraphenylene vinylene (APPV). **b** Illustration of the organization of an individual ODN-g-APPV by DNA origami template

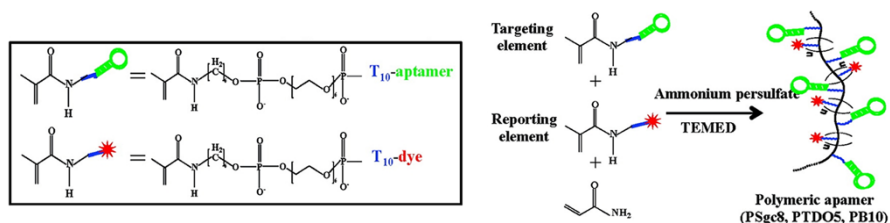


Fig. 22 Synthesis of polymeric aptamers via ODN-PAM conjugates (reproduced with permission from [39])

polymerize into linear polyacrylamide, and can also copolymerize with many bi-functional crosslinking agents (the most commonly used is diacrylamide) to give gelation. Gel polymerization is usually initiated by ammonium persulfate (APS), and the reaction rate can be accelerated by adding catalysts such as *N,N,N',N'*-tetramethylethylenediamine (TEMED) [105]. Since PAM can be prepared easily, among many OPCs, ODN-PAM conjugates were readily synthesized and processed.

Based on the stability and biocompatibility of PAM, Tan's group [39] incorporated acrydite-modified ODN into the PAM backbone by copolymerization (Fig. 22). The three components are copolymerized into ODN–PAM conjugates by a one-step process: 5'-acrydite-T₁₀-dye was used for tracking cell internalization; multiple targeting aptamers on the polymer chain can promote intracellular delivery through multivalent effects [39].

ODN–PAM conjugates also show unparalleled potential for the preparation of smart hydrogels. ODN–PAM hydrogels are more economical and adaptable than expensive full-DNA hydrogels [106]. In addition, by regulating the diversity of ODN, pH-responsive [107, 108], specific DNA sequence-responsive [109], or shape-memory hydrogels [59, 110, 111] were prepared. As for hydrogel swelling, the conformational change of the DNA chain can cause ODN–PAM hydrogels to swell by 10–15% of their original size, which is usually insufficient to alter the shape of the macroscopic gel system; thus Schulman's group prepared a DNA-triggered, deformable hydrogel with a significant degree of swelling, in which multiple DNA strands were inserted into the duplex. Moreover, a “terminator hairpin” can be created by modifying the sequence of the polymerizing hairpins. By adjusting the relative concentrations of polymerizing hairpins and terminator hairpins, the hydrogel swell could be well controlled to a certain degree [60].

4.5.2 Brush PNB-Based OPCs

Ring-opening metathesis polymerization (ROMP) is a living polymerization reaction, in which a carbon–carbon double bond in a cyclic olefin is broken to form a new chemical bond in the presence of a metal catalyst. Norbornene and its derivatives are the monomers most studied and widely used for ROMP because of their high reactivity, abundant sources, and low price [112]. Moreover, many functional molecules can be coupled easily to the norbornene monomer, such as hydrophilic PEG [113], hydrophobic drugs [114], or charged ferrocene [115, 116], etc., to explore different possibilities for research.

Zhang's group designed and synthesized a new brush polymer/ODN conjugate [117–120]. The dense PEG side chain protects the ODN from protein degradation but allows accessibility of DNA hybridization. This ODN conjugate, protected by the dense PEG side chain, exhibits better biopharmaceutical properties compared to naked ODN, including better gene silencing efficiency and better physiological stability (Fig. 23a) [117].

More stable and controllable drug delivery effect can be obtained by chemically conjugating hydrophobic drug molecules to the micelles instead of physically encapsulation. Therefore, Zhang's group chemically conjugated paclitaxel to polynorbornene to form amphiphiles with hydrophilic ODN, which formed stable micelle nanoparticles enabling simultaneous intracellular delivery of drug molecules and therapeutic ODNs (Fig. 23b) [114].

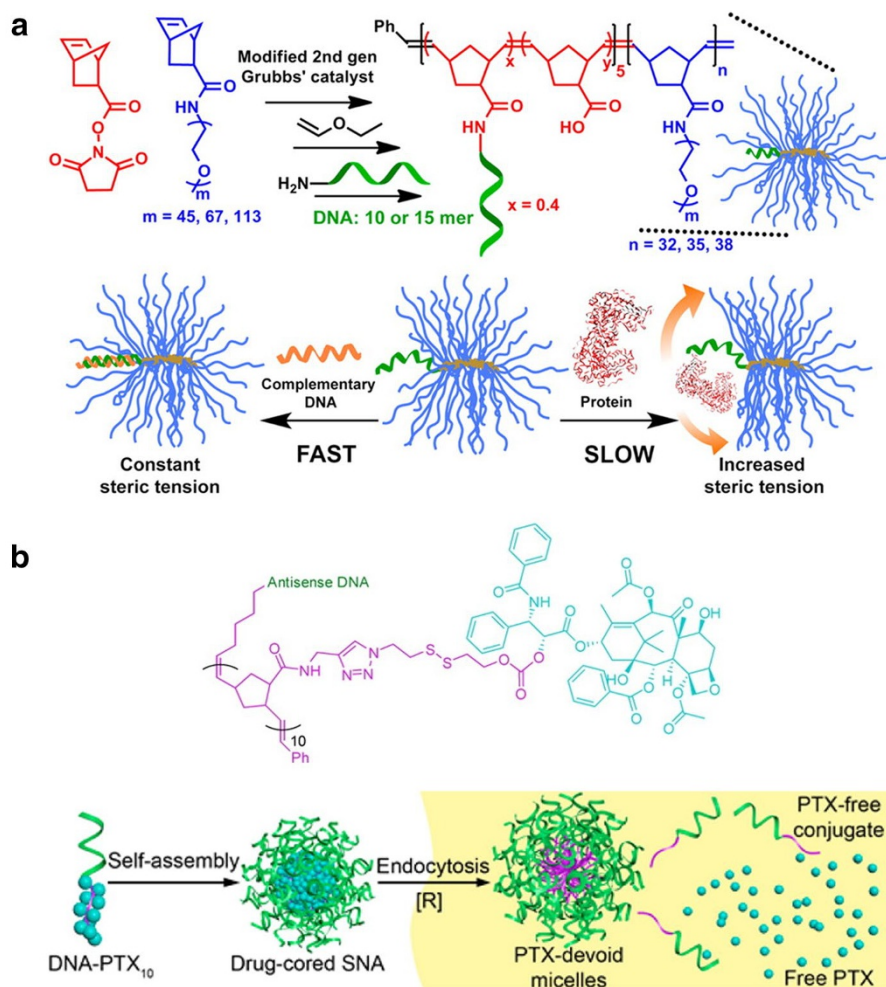


Fig. 23 **a** Compact brush-polymers provide steric selectivity to the ODN (reproduced with permission from [117]). **b** Chemical conjugation of paclitaxel to the polynorbornene side chain for stable and controlled intracellular delivery (adapted with permission from [114])

4.5.3 ODN-ATRPolymer Conjugates

ATRP has been applied successfully to the preparation of various materials with controlled structures [121]. Using ATRP, it is possible to synthesize a variety of well-defined, multi-component polymers, such as block copolymers, graft copolymers, and hyper-branched polymers. In addition, the polymers synthesized by ATRP can be further functionalized by three synthetic strategies: (1) using functional ATRP initiators; (2) direct polymerization of functional monomers; (3) coupling chemistry utilizing end groups. Due to the attractive

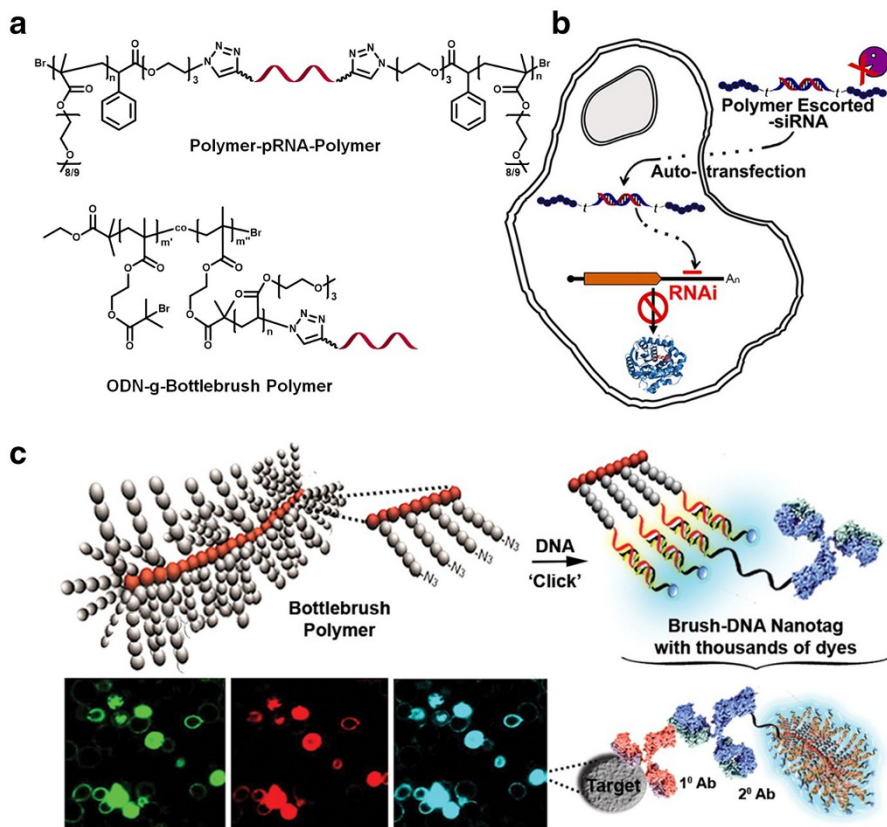


Fig. 24 **a** The chemical structure of ODN brush/bottlebrush polymer conjugates. **b** Self-transfection of siRNA escorted by polymers (reproduced with permission from [122]). **c** ODN brush/bottlebrush polymer conjugates as a scaffold for functionality organization [123]

nature of ATRPolymers, the combination of ATRPolymers with ODN makes it easy to prepare special polymers with interesting structures or for some unusual applications.

In 2013, Das's group [122] used activators generated by electron ATRP to prepare a series of well-defined azide-terminated polymers for chemical conjugation with di-alkyne-functionalized passenger-stranded RNA (pRNA). This polymer-pRNA-polymer can escort the sense strand into the cell to realize RNA interference, and the polymer-pRNA-polymer structure could efficiently resist nuclease degradation (Fig. 24a, b) [122]. In 2015, the same group synthesized a bottlebrush polymer using ATRP, and then chemically conjugated the ODN to the bottlebrush polymer. These ODN-bottlebrush polymer conjugates can hold thousands of dye molecules, and, thanks to the array of ODN brushes, dye self-quenching could be efficiently avoided, resulting in a bright fluorescent signal (Fig. 24c) [123]. In addition, the ODN on this bottlebrush polymer, with a high local concentration, still retained its accessibility to endonucleases and kept chain displacement capability [124].

Table 1 Various oligonucleotide-polymer conjugates (OPCs) and their applications in different research fields

OPCs	Research field
ODN-biodegradable polymer	Micelles for ODN delivery [67], siRNA delivery [29, 30] ODN delivery [34, 61], Nanogel for siRNA delivery [41] Gene therapy and drug delivery [33]
ODN-highly hydrophobic polymer	Loading inorganic nanoparticles [71] or organic molecules [32] Gene regulation [63, 65], micellar aptamers [64]
ODN-dynamic polymer	Template-based synthesis [45], drug delivery [74, 75], virus loading [77, 78, 80, 81], hydrogels [79] Separation of nucleic acid [87, 88] and protein [89], self-assembly [31, 90–92], hydrogel [86], biocatalytic carrier [58] Self-assembly [93–95], drug delivery [97, 98], gene regulation [99, 100], nanoreactors [96]
ODN-conjugated polymer	Self-assembly [47], nucleic acid detection [27, 51] Nanoelectronics [46] Self-assembly [103] Detection of ion and enzyme [28] Routing of individual polymers [104]
ODN-other polymer	Drug delivery [39], hydrogel [59, 110, 111] Drug delivery [114], self-assembly [113], ODN delivery [117–120], electrochemistry [115, 116] Self-assembly [126], siRNA delivery [122], fluorescence labeling [123]

5 Conclusion and Outlook

After nearly a century of development, a wide range of synthetic polymers with tunable physical, chemical, and biological properties are available for various applications. Since research on nucleic acids has extended from the biological applications to the material fields since 1980s, a wide variety of OPCs have been synthesized and used in supramolecular self-assembly, drug delivery, and bio-sensing. Table 1 summarizes the application of different types of OPCs in different fields.

Although many synthetic methods to produce OPCs have been developed, compared with conventional polymers, the synthesis of OPCs still needs special conditions or machines (solid-phase DNA synthesizer) and generally exhibits low efficiency due to the high heterogeneity between DNA and synthetic polymers. Thus, simple and efficient synthesis strategies that can be commonly applied to all kinds of OPCs are still urgently required. In particular, as for amphiphilic OPCs block copolymer, how to control and tune their self-assembly behavior by adjusting the ratio between hydrophobic and hydrophilic blocks has not been thoroughly investigated. In addition, compared with other blocks that are used to construct amphiphilic polymers, DNA shows many unique properties, including well-defined molecular weights and conformations, molecular recognition properties, stimuli-responsiveness, and therapeutic capability. All of these interesting properties make OPCs a promising branch of amphiphilic polymers. However, the application scope of OPCs is still relatively narrow, and it is necessary to continually explore more OPCs for new application purposes. As for *in vivo* application, many critical properties of OPCs, such as bio-stability, biocompatibility, immunogenicity, and intracellular penetration capability, need more in-depth characterization and further improvement. Last, but most importantly, the integration of DNA functions and polymer characteristics will be the future development direction of OPCs. For example, the programmability and molecular recognition of DNA can be used to regulate the aggregation state of polymers at the nanoscale; hydrophobic polymers can contain some functional molecules and their properties can be tuned through DNA hybridization; π -conjugated polymers with strong light-harvesting and energy transfer capabilities can enrich the application of DNA-based biomaterials in the field of optoelectronics. Therefore, we believe that there are still many opportunities for investigation of OPCs in future research, and that we require further efforts in this direction.

Acknowledgements The authors acknowledge financial support by Grants from Shenzhen Fundamental Research Programs (no. JCYJ20160226193029593, JCYJ20170817105645935), Guangdong Innovative and Entrepreneurial Research Team Program (no. 2016ZT06G587), and the National Natural Science Foundation of China (no. 51503096).

Compliance with Ethical Standards

Conflict of interest On behalf of all authors, Ying Bao and Leilei Tian state that there is no conflict of interest.

References

1. Fang WN, Jia SS, Chao J, Wang LQ, Duan XY, Liu HJ, Li Q, Zuo XL, Wang LH, Wang LH, Liu N, Fan CH (2019) Quantizing single-molecule surface-enhanced Raman scattering with DNA origami metamolecules. *Sci Adv* 5:eau4506
2. Chen P, Zhang T, Zhou T, Liu D (2016) Number-controlled spatial arrangement of gold nanoparticles with DNA dendrimers. *RSC Adv* 6:70553–70556
3. Ponnuswamy N, Bastings MMC, Nathwani B, Ryu JH, Chou LYT, Vinther M, Li WA, Anastasacacos FM, Mooney DJ, Shih WM (2017) Oligolysine-based coating protects DNA nanostructures from low-salt denaturation and nuclease degradation. *Nat Commun* 8:15654
4. Zhang H, Wang Y, Zhang H, Liu X, Lee A, Huang Q, Wang F, Chao J, Liu H, Li J, Shi J, Zuo X, Wang L, Wang L, Cao X, Bustamante C, Tian Z, Fan C (2019) Programming chain-growth copolymerization of DNA hairpin tiles for in vitro hierarchical supramolecular organization. *Nat Commun* 10:1006
5. Seeman NC, Sleiman HF (2017) DNA nanotechnology. *Nat Rev Mater* 3:17068
6. Chidchob P, Sleiman HF (2018) Recent advances in DNA nanotechnology. *Curr Opin Chem Biol* 46:63–70
7. Ohto U, Shibata T, Tanji H, Ishida H, Krayukhina E, Uchiyama S, Miyake K, Shimizu T (2015) Structural basis of CpG and inhibitory DNA recognition by Toll-like receptor 9. *Nature* 520:702–705
8. Zhou JH, Rossi J (2017) Aptamers as targeted therapeutics: current potential and challenges. *Nat Rev Drug Discov* 16:181–202
9. Guo YH, Chen JL, Cheng MP, Monchard D, Zhou J, Ju HX (2017) A thermophilic tetramolecular G-quadruplex/hemin DNAzyme. *Angew Chem Int Edit* 56:16636–16640
10. Wittrup A, Lieberman J (2015) Knocking down disease: a progress report on siRNA therapeutics. *Nat Rev Genet* 16:543–552
11. Wang YH, Miao L, Satterlee A, Huang L (2015) Delivery of oligonucleotides with lipid nanoparticles. *Adv Drug Deliver Rev* 87:68–80
12. Guo WW, Lu CH, Orbach R, Wang FA, Qi XJ, Ceconello A, Seliktar D, Willner I (2015) pH-stimulated DNA hydrogels exhibiting shape-memory properties. *Adv Mater* 27:73–78
13. Ma DL, Zhang ZH, Wang MD, Lu LH, Zhong HJ, Leung CH (2015) Recent developments in G-quadruplex probes. *Chem Biol* 22:812–828
14. Zhang S, Zou J, Elsabahy M, Karwa A, Li A, Moore DA, Dorshow RB, Wooley KL (2013) Poly(ethylene oxide)-block-polyphosphester-based paclitaxel conjugates as a platform for ultra-high paclitaxel-loaded multifunctional nanoparticles. *Chem Sci* 4:2122–2126
15. Tao D, Feng C, Cui Y, Yang X, Manners I, Winnik MA, Huang X (2017) Monodisperse fiber-like micelles of controlled length and composition with an oligo(*p*-phenylenevinylene) core via “living” crystallization-driven self-assembly. *J Am Chem Soc* 139:7136–7139
16. Lee K, Povlich LK, Kim J (2010) Recent advances in fluorescent and colorimetric conjugated polymer-based biosensors. *Analyst* 135:2179–2189
17. Li K, Liu B (2012) Polymer encapsulated conjugated polymer nanoparticles for fluorescence bioimaging. *J Mater Chem A* 22:1257–1264
18. Meng Z, Hou W, Zhou H, Zhou L, Chen H, Wu C (2018) Therapeutic considerations and conjugated polymer-based photosensitizers for photodynamic therapy. *Macromol Rapid Commun* 39:1700614
19. Liu LZ, Chen H, Chen W, He F (2019) From binary to quaternary: high-tolerance of multi-acceptors enables development of efficient polymer solar cells. *J Mater Chem A* 7:7815–7822
20. Alemdaroglu FE, Herrmann A (2007) DNA meets synthetic polymers—highly versatile hybrid materials. *Org Biomol Chem* 5:1311–1320
21. Kwak M, Herrmann A (2010) Nucleic acid/organic polymer hybrid materials: synthesis, superstructures, and applications. *Angew Chem Int Edit* 49:8574–8587
22. Kwak M, Herrmann A (2011) Nucleic acid amphiphiles: synthesis and self-assembled nanostructures. *Chem Soc Rev* 40:5745–5755
23. Schnitzler T, Herrmann A (2012) DNA block copolymers: functional materials for nanoscience and biomedicine. *Accounts Chem Res* 45:1419–1430

24. Peterson AM, Heemstra JM (2015) Controlling self-assembly of DNA-polymer conjugates for applications in imaging and drug delivery. *Wiley Interdiscip Rev Nanomed Nanobiotechnol* 7:282–297
25. Pan G, Jin X, Mou Q, Zhang C (2017) Recent progress on DNA block copolymer. *Chinese Chem Lett* 28:1822–1828
26. Zhao Z, Du T, Liang F, Liu S (2018) Amphiphilic DNA organic hybrids: functional materials in nanoscience and potential application in biomedicine. *Int J Mol Sci* 19:2283
27. Lee K, Povlich LK, Kim J (2007) Label-free and self-signal amplifying molecular DNA sensors based on bioconjugated polyelectrolytes. *Adv Funct Mater* 17:2580–2587
28. Jia Y, Zuo X, Lou X, Miao M, Cheng Y, Min X, Li X, Xia F (2015) Rational designed bipolar, conjugated polymer-DNA composite beacon for the sensitive detection of proteins and ions. *Anal Chem* 87:3890–3894
29. Zhao Y, Zheng C, Zhang L, Chen Y, Ye Y, Zhao M (2015) Knockdown of STAT3 expression in SKOV3 cells by biodegradable siRNA-PLGA/CSO conjugate micelles. *Colloids Surf B Biointerfaces* 127:155–163
30. Lee SH, Mok H, Lee Y, Park TG (2011) Self-assembled siRNA-PLGA conjugate micelles for gene silencing. *J Control Release* 152:152–158
31. Isoda K, Kanayama N, Fujita M, Takarada T, Maeda M (2013) DNA terminal mismatch-induced stabilization of polymer micelles from RAFT-generated poly(*N*-isopropylacrylamide)-DNA block copolymers. *Chem-Asian J* 8:3079–3084
32. Sowwan M, Faroun M, Mentovich E, Ibrahim I, Haboush S, Alemдарoglu FE, Kwak M, Richter S, Herrmann A (2010) Polarizability of DNA block copolymer nanoparticles observed by electrostatic force microscopy. *Macromol Rapid Commun* 31:1242–1246
33. Ni Q, Zhang F, Zhang Y, Zhu G, Wang Z, Teng Z, Wang C, Yung BC, Niu G, Lu G, Zhang L, Chen X (2018) In situ shRNA synthesis on DNA-poly(lactide) nanoparticles to treat multidrug resistant breast cancer. *Adv Mater* 30:1705737
34. Wang D, Lu X, Jia F, Tan X, Sun X, Cao X, Wai F, Zhang C, Zhang K (2017) Precision tuning of DNA- and poly(ethylene glycol)-based nanoparticles via coassembly for effective antisense gene regulation. *Chem Mater* 29:9882–9886
35. Li S, Schroeder CM (2018) Synthesis and direct observation of thermoresponsive DNA copolymers. *ACS Macro Lett* 7:281–286
36. Kubo T, Rumiana B, Ohba H, Fujii M (2003) Antisense effects of DNA-peptide conjugates. *Nucleic acids symposium series, vol 1*. Oxford University Press, Oxford, pp 179–180
37. Li C, Faulkner-Jones A, Dun AR, Jin J, Chen P, Xing Y, Yang Z, Li Z, Shu W, Liu D, Duncan RR (2015) Rapid formation of a supramolecular polypeptide-DNA hydrogel for in situ three-dimensional multilayer bioprinting. *Angew Chem Int Edit* 54:3957–3961
38. Jeong J (2003) A new antisense oligonucleotide delivery system based on self-assembled ODN-PEG hybrid conjugate micelles. *J Control Release* 93:183–191
39. Yang L, Meng L, Zhang X, Chen Y, Zhu G, Liu H, Xiong X, Sefah K, Tan W (2011) Engineering polymeric aptamers for selective cytotoxicity. *J Am Chem Soc* 133:13380–13386
40. Liu K, Zheng LF, Liu Q, de Vries JW, Gerasimov JY, Herrmann A (2014) Nucleic acid chemistry in the organic phase: from functionalized oligonucleotides to DNA side chain polymers. *J Am Chem Soc* 136:14255–14262
41. Ding F, Mou Q, Ma Y, Pan G, Guo Y, Tong G, Choi CHJ, Zhu X, Zhang C (2018) A crosslinked nucleic acid nanogel for effective siRNA delivery and antitumor therapy. *Angew Chem Int Edit* 57:3064–3068
42. Talom RM, Fuks G, Kaps L, Oberdisse J, Cerclier C, Gaillard C, Mingotaud C, Gauffre F (2011) DNA-polymer micelles as nanoparticles with recognition ability. *Chem-Eur J* 17:13495–13501
43. Mentovich ED, Livanov K, Prusty DK, Sowwan M, Richter S (2012) DNA-nanoparticle assemblies go organic: macroscopic polymeric materials with nanosized features. *J Nanobiotechnol* 10:21
44. Sun Y, Ji Y, Wang D, Wang J, Liu D (2018) Stabilization of an intermolecular i-motif by lipid modification of cytosine-oligodeoxynucleotides. *Org Biomol Chem* 16:4857–4863
45. Alemдарoglu FE, Ding K, Berger R, Herrmann A (2006) DNA-templated synthesis in three dimensions: introducing a micellar scaffold for organic reactions. *Angew Chem Int Edit* 45:4206–4210
46. Kwak M, Gao J, Prusty DK, Musser AJ, Markov VA, Tombros N, Stuart MC, Browne WR, Boekema EJ, ten Brinke G, Jonkman HT, van Wees BJ, Loi MA, Herrmann A (2011) DNA block

- copolymer doing it all: from selection to self-assembly of semiconducting carbon nanotubes. *Angew Chem Int Edit* 50:3206–3210
47. Albert SK, Thelu HV, Golla M, Krishnan N, Chaudhary S, Varghese R (2014) Self-assembly of DNA-oligo(*p*-phenylene–ethynylene) hybrid amphiphiles into surface-engineered vesicles with enhanced emission. *Angew Chem Int Edit* 53:8352–8357
 48. Jia F, Lu X, Tan X, Zhang K (2015) Facile synthesis of nucleic acid-polymer amphiphiles and their self-assembly. *Chem Commun* 51:7843–7846
 49. Chien MP, Rush AM, Thompson MP, Gianneschi NC (2010) Programmable shape-shifting micelles. *Angew Chem Int Edit* 49:5076–5080
 50. Luo Q, Shi Z, Zhang Y, Chen XJ, Han SY, Baumgart T, Chenoweth DM, Park SJ (2016) DNA island formation on binary block copolymer vesicles. *J Am Chem Soc* 138:10157–10162
 51. Yang CJ, Pinto M, Schanze K, Tan W (2005) Direct synthesis of an oligonucleotide-poly(phenylene ethynylene) conjugate with a precise one-to-one molecular ratio. *Angew Chem Int Edit* 44:2572–2576
 52. Bousmail D, Chidchob P, Sleiman HF (2018) Cyanine-mediated DNA nanofiber growth with controlled dimensionality. *J Am Chem Soc* 140:9518–9530
 53. Edwardson TGW, Carneiro KMM, Serpell CJ, Sleiman HF (2014) An efficient and modular route to sequence-defined polymers appended to DNA. *Angew Chem Int Edit* 53:4567–4571
 54. Averick SE, Dey SK, Grahacharya D, Matyjaszewski K, Das SR (2014) Solid-phase incorporation of an ATRP initiator for polymer-DNA biohybrids. *Angew Chem Int Edit* 53:2739–2744
 55. Pan X, Lathwal S, Mack S, Yan J, Das SR, Matyjaszewski K (2017) Automated synthesis of well-defined polymers and biohybrids by atom transfer radical polymerization using a DNA synthesizer. *Angew Chem Int Edit* 56:2740–2743
 56. Fu L, Wang Z, Lathwal S, Enciso AE, Simakova A, Das SR, Russell AJ, Matyjaszewski K (2018) Synthesis of polymer bioconjugates via photoinduced atom transfer radical polymerization under blue light irradiation. *ACS Macro Lett* 7:1248–1253
 57. Lueckerath T, Strauch T, Koynov K, Barner-Kowollik C, Ng DYW, Weil T (2019) DNA-polymer conjugates by photoinduced RAFT polymerization. *Biomacromol* 20:212–221
 58. Li F, Wang C, Guo W (2018) Multifunctional poly-*N*-isopropylacrylamide/DNAzyme microgels as highly efficient and recyclable catalysts for biosensing. *Adv Funct Mater* 28:1705876
 59. Hu Y, Guo W, Kahn JS, Aleman-Garcia MA, Willner I (2016) A shape-memory DNA-based hydrogel exhibiting two internal memories. *Angew Chem Int Edit* 55:4210–4214
 60. Cangialosi A, Yoon C, Liu J, Huang Q, Guo J, Nguyen TD, Gracias DH, Schulman RJS (2017) DNA sequence-directed shape change of photopatterned hydrogels via high-degree swelling. *Science* 357:1126–1130
 61. Zhang C, Hao L, Calabrese CM, Zhou Y, Choi CH, Xing H, Mirkin CA (2015) Biodegradable DNA-brush block copolymer spherical nucleic acids enable transfection agent-free intracellular gene regulation. *Small* 11:5360–5368
 62. Levenson EA, Kiick KL (2014) DNA-polymer conjugates for immune stimulation through Toll-like receptor 9 mediated pathways. *Acta Biomater* 10:1134–1145
 63. Roloff A, Nelles DA, Thompson MP, Yeo GW, Gianneschi NC (2018) Self-transfecting micellar RNA: modulating nanoparticle cell interactions via high density display of small molecule ligands on micelle coronas. *Bioconjug Chem* 29:126–135
 64. Roloff A, Carlini AS, Callmann CE, Gianneschi NC (2017) Micellar thrombin-binding aptamers: reversible nanoscale anticoagulants. *J Am Chem Soc* 139:16442–16445
 65. Rush AM, Nelles DA, Blum AP, Barnhill SA, Tatro ET, Yeo GW, Gianneschi NC (2014) Intracellular mRNA regulation with self-assembled locked nucleic acid polymer nanoparticles. *J Am Chem Soc* 136:7615–7618
 66. Rush AM, Thompson MP, Tatro ET, Gianneschi NC (2013) Nuclease-resistant DNA via high-density packing in polymeric micellar nanoparticle coronas. *ACS Nano* 7:1379–1387
 67. Jeong JH, Park TG (2001) Novel polymer–DNA hybrid polymeric micelles composed of hydrophobic poly(*D*, *l*-lactic-co-glycolic acid) and hydrophilic oligonucleotides. *Bioconjug Chem* 12:917–923
 68. Cutler JJ, Auyeung E, Mirkin CA (2012) Spherical nucleic acids. *J Am Chem Soc* 134:1376–1391
 69. Li H, Zhang BH, Lu XG, Tan XY, Jia F, Xiao Y, Cheng ZH, Li Y, Silva DO, Schrekker HS, Zhang K, Mirkin CA (2018) Molecular spherical nucleic acids. *Proc Natl Acad Sci USA* 115:4340–4344
 70. Li Z, Zhang Y, Fullhart P, Mirkin CA (2004) Reversible and chemically programmable micelle assembly with DNA block-copolymer amphiphiles. *Nano Lett* 4:1055–1058

71. Chen XJ, Sanchez-Gaytan BL, Hayik SE, Fryd M, Wayland BB, Park SJ (2010) Self-assembled hybrid structures of DNA block-copolymers and nanoparticles with enhanced DNA binding properties. *Small* 6:2256–2260
72. Kim CJ, Jeong EH, Lee H, Park SJ (2019) A dynamic DNA nanostructure with switchable and size-selective molecular recognition properties. *Nanoscale* 11:2501–2509
73. Carneiro KMM, Hamblin GD, Hanni KD, Fakhoury J, Nayak MK, Rizis G, McLaughlin CK, Bazzi HS, Sleiman HF (2012) Stimuli-responsive organization of block copolymers on DNA nanotubes. *Chem Sci* 3:1980–1986
74. Alemdaroglu FE, Alemdaroglu NC, Langguth P, Herrmann A (2008) DNA block copolymer micelles—a combinatorial tool for cancer nanotechnology. *Adv Mater* 20:899–902
75. Alemdaroglu FE, Alemdaroglu NC, Langguth P, Herrmann A (2008) Cellular uptake of DNA block copolymer micelles with different shapes. *Macromol Rapid Commun* 29:326–329
76. Kwak M, Minten IJ, Anaya D-M, Musser AJ, Brasch M, Nolte RJM, Müllen K, Cornelissen JJLM, Herrmann A (2010) Virus-like particles templated by DNA Micelles: a general method for loading virus nanocarriers. *J Am Chem Soc* 132:7834–7835
77. Rodriguez-Pulido A, Kondrachuk AI, Prusty DK, Gao J, Loi MA, Herrmann A (2013) Light-triggered sequence-specific cargo release from DNA block copolymer-lipid vesicles. *Angew Chem Int Edit* 52:1008–1012
78. Kwak M, Musser AJ, Lee J, Herrmann A (2010) DNA-functionalised blend micelles: mix and fix polymeric hybrid nanostructures. *Chem Commun* 46:4935–4937
79. Wu F, Zhao Z, Chen C, Cao T, Li C, Shao Y, Zhang Y, Qiu D, Shi Q, Fan QH, Liu D (2018) Self-collapsing of single molecular poly-propylene oxide (PPO) in a 3D DNA network. *Small* 14:1703426
80. Ding K, Alemdaroglu FE, Borsch M, Berger R, Herrmann A (2007) Engineering the structural properties of DNA block copolymer micelles by molecular recognition. *Angew Chem Int Edit* 46:1172–1175
81. Zhao Z, Wang L, Liu Y, Yang Z, He YM, Li Z, Fan QH, Liu D (2012) pH-induced morphology-shifting of DNA-b-poly(propylene oxide) assemblies. *Chem Commun* 48:9753–9755
82. Safak M, Alemdaroglu FE, Li Y, Ergen E, Herrmann A (2007) Polymerase chain reaction as an efficient tool for the preparation of block copolymers. *Adv Mater* 19:1499–1505
83. Alemdaroglu FE, Wang J, Borsch M, Berger R, Herrmann A (2008) Enzymatic control of the size of DNA block copolymer nanoparticles. *Angew Chem Int Edit* 47:974–976
84. Ayaz MS, Kwak M, Alemdaroglu FE, Wang J, Berger R, Herrmann A (2011) Synthesis of DNA block copolymers with extended nucleic acid segments by enzymatic ligation: cut and paste large hybrid architectures. *Chem Commun* 47:2243–2245
85. Sugawara Y, Tamaki T, Ohashi H, Yamaguchi T (2013) Control of the poly(*N*-isopropylacrylamide) phase transition via a single strand-double strand transformation of conjugated DNA. *Soft Matter* 9:3331–3340
86. Guo W, Lu CH, Qi XJ, Orbach R, Fadeev M, Yang HH, Willner I (2014) Switchable bifunctional stimuli-triggered poly-*N*-isopropylacrylamide/DNA hydrogels. *Angew Chem Int Edit* 53:10134–10138
87. Umeno D, Mori T, Maeda M (1998) Single stranded DNA-poly(*N*-isopropylacrylamide) conjugate for affinity precipitation separation of oligonucleotides. *Chem Commun* 20:1433–1434
88. Mori T, Umeno D, Maeda M (2001) Sequence-specific affinity precipitation of oligonucleotide using poly(*N*-isopropylacrylamide)-oligonucleotide conjugate. *Biotechnol Bioeng* 72:261–268
89. Umeno D, Kawasaki M, Maeda M (1998) Water-soluble conjugate of double-stranded DNA and poly(*N*-isopropylacrylamide) for one-pot affinity precipitation separation of DNA-binding proteins. *Bioconjug Chem* 9:719–724
90. Cavalieri F, Postma A, Lee L, Caruso F (2009) Assembly and functionalization of DNA–polymer microcapsules. *ACS Nano* 3:234–240
91. Kim CJ, Hu X, Park SJ (2016) Multimodal shape transformation of dual-responsive DNA block copolymers. *J Am Chem Soc* 138:14941–14947
92. Wilks TR, Bath J, de Vries JW, Raymond JE, Herrmann A, Turberfield AJ, O’Reilly RK (2013) “Giant surfactants” created by the fast and efficient functionalization of a DNA tetrahedron with a temperature-responsive polymer. *ACS Nano* 7:8561–8572
93. Trinh T, Liao C, Toader V, Barlog M, Bazzi HS, Li J, Sleiman HF (2018) DNA-imprinted polymer nanoparticles with monodispersity and prescribed DNA-strand patterns. *Nat Chem* 10:184–192

94. Serpell CJ, Edwardson TG, Chidchob P, Carneiro KM, Sleiman HF (2014) Precision polymers and 3D DNA nanostructures: emergent assemblies from new parameter space. *J Am Chem Soc* 136:15767–15774
95. Chidchob P, Edwardson TG, Serpell CJ, Sleiman HF (2016) Synergy of two assembly languages in DNA nanostructures: self-assembly of sequence-defined polymers on DNA cages. *J Am Chem Soc* 138:4416–4425
96. Trinh T, Chidchob P, Bazzi HS, Sleiman HF (2016) DNA micelles as nanoreactors: efficient DNA functionalization with hydrophobic organic molecules. *Chem Commun* 52:10914–10917
97. Bousmail D, Amrein L, Fakhoury JJ, Fakhoury HH, Hsu JCC, Panasci L, Sleiman HF (2017) Precision spherical nucleic acids for delivery of anticancer drugs. *Chem Sci* 8:6218–6229
98. Rahbani JF, Vengut-Climent E, Chidchob P, Gidi Y, Trinh T, Cosa G, Sleiman HF (2018) DNA nanotubes with hydrophobic environments: toward new platforms for guest encapsulation and cellular delivery. *Adv Healthc Mater* 7:1701049
99. Fakhoury JJ, Edwardson TG, Conway JW, Trinh T, Khan F, Barlóg M, Bazzi HS, Sleiman HF (2015) Antisense precision polymer micelles require less poly(ethylenimine) for efficient gene knockdown. *Nanoscale* 7:20625–20634
100. Dore MD, Fakhoury JJ, Lacroix A, Sleiman HF (2018) Templated synthesis of spherical RNA nanoparticles with gene silencing activity. *Chem Commun* 54:11296–11299
101. Wu WB, Bazan GC, Liu B (2017) Conjugated-polymer-amplified sensing, imaging, and therapy. *Chem-Us* 2:760–790
102. Han L, Wang M, Jia X, Chen W, Qian H, He F (2018) Uniform two-dimensional square assemblies from conjugated block copolymers driven by π - π interactions with controllable sizes. *Nat Commun* 9:865
103. Kamps AC, Cativo MHM, Chen X-J, Park S-J (2014) Self-Assembly of DNA-coupled semiconducting block copolymers. *Macromolecules* 47:3720–3726
104. Knudsen JB, Liu L, Bank Kodal AL, Madsen M, Li Q, Song J, Woehrstein JB, Wickham SF, Strauss MT, Schueder F, Vinther J, Krissanaprasit A, Gudnason D, Smith AA, Ogaki R, Zelikin AN, Besenbacher F, Birkedal V, Yin P, Shih WM, Jungmann R, Dong M, Gothelf KV (2015) Routing of individual polymers in designed patterns. *Nat Nanotechnol* 10:892–898
105. Yang T-HJRPoMS (2008) Recent applications of polyacrylamide as biomaterials. *Recent Patents Mater Sci* 1:29–40
106. Kang HZ, Trondoli AC, Zhu GZ, Chen Y, Chang YJ, Liu HP, Huang YF, Zhang XL, Tan WH (2011) Near-infrared light-responsive core-shell nanogels for targeted drug delivery. *ACS Nano* 5:5094–5099
107. Ren J, Hu Y, Lu C-H, Guo W, Aleman-Garcia MA, Ricci F, Willner I (2015) pH-responsive and switchable triplex-based DNA hydrogels. *Chem Sci* 6:4190–4195
108. Liao WC, Lilienthal S, Kahn JS, Riutin M, Sohn YS, Nechushtai R, Willner I (2017) pH- and ligand-induced release of loads from DNA-acrylamide hydrogel microcapsules. *Chem Sci* 8:3362–3373
109. Sicilia G, Grainger-Boulby C, Francini N, Magnusson JP, Saeed AO, Fernández-Trillo F, Spain SG, Alexander C (2014) Programmable polymer–DNA hydrogels with dual input and multi-scale responses. *Biomater Sci* 2:203–211
110. Lu CH, Guo W, Hu Y, Qi XJ, Willner I (2015) Multitriggered shape-memory acrylamide–DNA hydrogels. *J Am Chem Soc* 137:15723–15731
111. Hu Y, Lu C-H, Guo W, Aleman-Garcia MA, Ren J, Willner I (2015) A shape memory acrylamide/DNA hydrogel exhibiting switchable dual pH-responsiveness. *Adv Funct Mater* 25:6867–6874
112. Sutthasupa S, Shiotsuki M, Sanda F (2010) Recent advances in ring-opening metathesis polymerization and application to synthesis of functional materials. *Polym J* 42:905–915
113. Lu X, Watts E, Jia F, Tan X, Zhang K (2014) Polycondensation of polymer brushes via DNA hybridization. *J Am Chem Soc* 136:10214–10217
114. Tan X, Lu X, Jia F, Liu X, Sun Y, Logan JK, Zhang K (2016) Blurring the role of oligonucleotides: spherical nucleic acids as a drug delivery vehicle. *J Am Chem Soc* 138:10834–10837
115. Gibbs JM, Park S-J, Anderson DR, Watson KJ, Mirkin CA, Nguyen ST (2005) Polymer–DNA hybrids as electrochemical probes for the detection of DNA. *J Am Chem Soc* 127:1170–1178
116. Watson KJ, Park SJ, Im JH, Nguyen ST, Mirkin CA (2001) DNA-block copolymer conjugates. *J Am Chem Soc* 123:5592–5593

117. Lu X, Tran TH, Jia F, Tan X, Davis S, Krishnan S, Amiji MM, Zhang K (2015) Providing oligonucleotides with steric selectivity by brush-polymer-assisted compaction. *J Am Chem Soc* 137:12466–12469
118. Jia F, Lu X, Wang D, Cao X, Tan X, Lu H, Zhang K (2017) Depth-profiling the nuclease stability and the gene silencing efficacy of brush-architected poly(ethylene glycol)-DNA conjugates. *J Am Chem Soc* 139:10605–10608
119. Jia F, Lu X, Tan X, Wang D, Cao X, Zhang K (2017) Effect of PEG architecture on the hybridization thermodynamics and protein accessibility of PEGylated oligonucleotides. *Angew Chem Int Edit* 56:1239–1243
120. Lu X, Jia F, Tan X, Wang D, Cao X, Zheng J, Zhang K (2016) Effective antisense gene regulation via noncationic, polyethylene glycol brushes. *J Am Chem Soc* 138:9097–9100
121. Matyjaszewski K (2018) Advanced materials by atom transfer radical polymerization. *Adv Mater* 30:1706441
122. Averick SE, Paredes E, Dey SK, Snyder KM, Tapinos N, Matyjaszewski K, Das SR (2013) Autotransfecting short interfering RNA through facile covalent polymer escorts. *J Am Chem Soc* 135:12508–12511
123. Fouz MF, Mukumoto K, Averick S, Molinar O, McCartney BM, Matyjaszewski K, Armitage BA, Das SR (2015) Bright fluorescent nanotags from bottlebrush polymers with DNA-tipped bristles. *ACS Cent Sci* 1:431–438
124. Fouz MF, Dey SK, Mukumoto K, Matyjaszewski K, Armitage BA, Das SR (2018) Accessibility of densely localized DNA on soft polymer nanoparticles. *Langmuir* 34:14731–14737
125. Dong YC, Chen SB, Zhang SJ, Sodroski J, Yang ZQ, Liu DS, Mao YD (2018) Folding DNA into a lipid-conjugated nanobarrel for controlled reconstitution of membrane proteins. *Angew Chem Int Edit* 57:2072–2076
126. Averick S, Paredes E, Li W, Matyjaszewski K, Das SR (2011) Direct DNA conjugation to star polymers for controlled reversible assemblies. *Bioconjug Chem* 22:2030–2037

Publisher's Note Springer Nature remains neutral with regard to jurisdictional claims in published maps and institutional affiliations.



Biotechnological and Therapeutic Applications of Natural Nucleic Acid Structural Motifs

Jinwei Duan^{1,2,3} · Xing Wang^{2,3,4} · Megan E. Kizer^{5,6}

Received: 31 October 2019 / Accepted: 11 February 2020 / Published online: 18 February 2020
© Springer Nature Switzerland AG 2020

Abstract

Genetic information and the blueprint of life are stored in the form of nucleic acids. The primary sequence of DNA, read from the canonical double helix, provides the code for RNA and protein synthesis. Yet these already-information-rich molecules have higher-order structures which play critical roles in transcription and translation. Uncovering the sequences, parameters, and conditions which govern the formation of these structural motifs has allowed researchers to study them and to utilize them in biotechnological and therapeutic applications *in vitro* and *in vivo*. This review covers both DNA and RNA structural motifs found naturally in biological systems including catalytic nucleic acids, non-coding RNA, aptamers, G-quadruplexes, i-motifs, and Holliday junctions. For each category, an overview of the structural characteristics, biological prevalence, and function will be discussed. The biotechnological and therapeutic applications of these structural motifs are highlighted. Future perspectives focus on the addition of proteins and unnatural modifications to enhance structural stability for greater applicability.

Keywords Nucleic acids · Structural motifs · G-quadruplex · i-Motif · Ribozymes · Holliday junction · Therapeutics · Nanotechnology

Chapter 8 was originally published as Duan, J., Wang, X. & Kizer, M. E. Topics in Current Chemistry (2020) 378: 26. <https://doi.org/10.1007/s41061-020-0290-z>.

✉ Jinwei Duan
duanjw@chd.edu.cn

✉ Xing Wang
xingw@illinois.edu

✉ Megan E. Kizer
mkizer@mit.edu

Extended author information available on the last page of the article

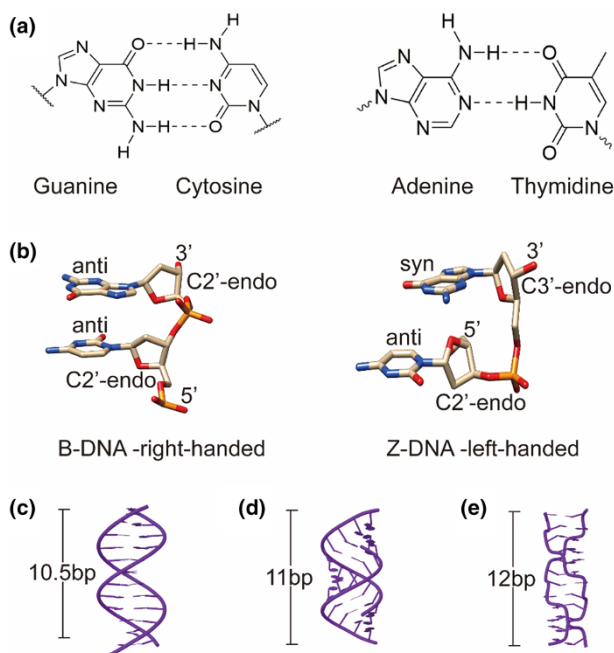


Fig. 1 Structure of DNA. **a** Watson–Crick base pairs. **b** *Anti*- and *syn*-conformations which differentiate Z- and B-DNA. Structural representation of B-DNA (**c**), A-DNA (**d**) and Z-DNA (**e**), with respective helical pitches

1 Introduction: Hierarchy of Interactions and Major Structural Motifs

The discovery of DNA structure in 1953 [1] has quickly evolved from the simplistic, Watson–Crick base-paired double helix to a more complex view. Soon, unique base–base or base–backbone interactions and higher-order nucleic acid structural states began to be uncovered [2–4]. Though initial structural knowledge provided an understanding of the basics of information storage from nucleic acid biomolecules, scientists soon realized there was much more at play than just sequence. It is now generally known that both sequence and structure of DNA and RNA are implicated in transcription, translation, and nuclear organization. This article highlights predominant nucleic acid structural motifs found in natural systems, their role in cellular function, and how they may be leveraged in therapeutic and biotechnological applications. To understand these higher-order structures, we must first understand the simplest forms of nucleic acids.

Nucleic acid structure can be broken down into three major hierarchical levels: primary, secondary, and tertiary. The primary form of DNA in nature is double stranded, while that of RNA is single stranded. Double stranded DNA (dsDNA) is formed through hybridization of bases, A–T and G–C (Fig. 1a), which promote an antiparallel arrangement of strands. DNA double helices can be found in one of three forms: B-DNA, A-DNA, and Z-DNA; they are structurally unique and their

characteristics are summarized in Table 1. B-DNA, being the predominant form physiologically, is a right-handed double helix with a major groove of 2.2 nm, a minor groove of 1.2 nm, and a helical pitch of 10.5 base pairs (bp) (Fig. 1c) [5]. DNA sequences are read from this structural form in the major groove, where a distinct pattern of hydrogen bonding accessible from the major groove is formed from each base pair. It is therefore this structural form which allows proteins to identify sequences for binding, transcription, and gene regulation. A-DNA is the double-stranded helix which forms under low humidity conditions. Its characteristics include a narrower and deeper major groove, a broader and shallower minor groove, and a helical pitch of 11 bp (Fig. 1d) [5]. This duplex form is still found in natural systems predominantly during DNA–protein complex interactions; it is also the form RNA adopts during hybridization (RNA–RNA). Interestingly, an RNA–DNA hybrid exhibits an intermediate of both B- and A-form helices in solution [6].

Much more distinct from the other two double-stranded forms is the left-handed Z-DNA. The purine and pyrimidine bases are usually in the *anti* position in right-handed DNA, but in left-handed DNA, the purine flips to the *syn* position (Fig. 1b) [5]. This rotation results in a puckering of the ribose sugar and generates a zig-zag pattern along the backbone, the basis for the name “Z-DNA”. Structurally this form of DNA is more elongated, with a helical pitch of 12 bases per turn (Fig. 1e) [7]. Functionally, its exact role has not been unambiguously identified, though it has been implicated in regulating transcription events, following a moving polymerase. It is thought that the high energy conformer is able to form as a result of the negatively superhelical stress produced immediately after transcription and the Z-DNA that trails a polymerase can therefore block other polymerases from transcribing the same region. In other words, the Z-DNA provides control over the kinetics of transcription [5, 8]. Many proteins have been identified to bind Z-DNA with high affinity and specificity, further suggesting that they play important roles in transcriptional regulation, and therefore growth and development. The negatively superhelical stress also relieves topological strain from intertwining during recombination; chromosomal breakpoints in human tumors could arise from potential Z-DNA sequences. The secondary structures of DNA are only observed under specific conditions relevant for controlling biological processes and will be discussed in further detail in proceeding sections.

While DNA forms duplexes in its primary form, it is unusual that RNA forms long stretches of dsRNA. Instead, RNA retains single-stranded nature or folds back on itself for short, local dsRNA regions. When in duplex form, RNA resembles the

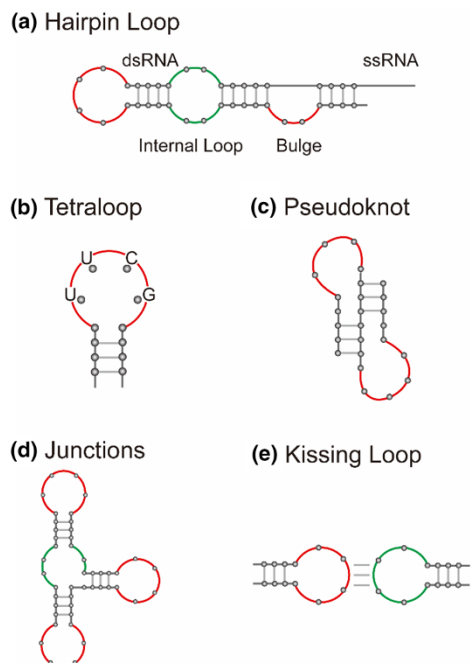
Table 1 Feature comparison of the different forms of biologically relevant duplex DNA

Duplex form	Handedness	Helical pitch (bp)	Diameter (Å)
B-DNA	Right	10.5	20
A-DNA	Right	11	23
Z-DNA	Left	12	18

A-DNA helix structural characteristics. The local dsRNA regions are considered secondary structural elements and include structures such as loops, hairpins, bulges, and pseudoknots (Fig. 2). Loops are flexible regions that connect two regions of secondary structure; they provide flexibility of the overall RNA molecule as well as flexibility in local and long-range base pairing [9]. Often, these structures confer specialized stability locally and globally. Hairpins are self-complementary sequences, connected by a loop which is usually at least four nucleotides (nt) long. The loop sequence UUCG shows special base-stacking interactions that promote stability of hairpin secondary structures. The hairpin structure has been heavily utilized in the biotechnological space in strand displacement-based methods of detection. Bulges provide local flexibility as well as enthalpic control over base pairing. A bulge in a region of dsRNA promotes melting to a greater extent than a fully duplexed strand; this is advantageous in hairpins and strand displacement events. When free distant ends of RNA fold over one another and hybridize with distant complementary sequences a pseudoknot structure is formed. Finally, pseudoknots result when one strand of RNA containing two stem-loops with one half of one stem intercalated between the two. This secondary structure is highly important for tertiary structure formation in vivo [10]. Formation of RNA knots in vivo has recently been accomplished to further understanding of RNA topology and development of RNA-based structural technologies [11].

DNA and RNA also form tertiary structures, though the greater flexibility imparted by the ribose sugar of RNA promotes a greater prevalence of non-Watson–Crick interactions which underscore these tertiary structures [12, 13].

Fig. 2 Structural motifs of RNA. **a** Loops and bulges are intermittently observed along an RNA oligonucleotide, with single-stranded and double-stranded regions. **b** Certain nucleotide sequences in a loop confer special stability, such as the UUCG tetraloop. The **c** pseudoknot, **d** junctions, and **e** loop:loop secondary structures are prominent in tertiary RNA structures



Interactions such as G–U base pairs, base triples, and base–backbone interactions provide a much more diverse landscape of structural possibilities for RNA over DNA [13]. These tertiary structures are a result of multiple secondary structures which interact to fold the RNA into a highly compact and stable form [12]. Though not often mentioned, RNA can form quaternary structures by the assistance of proteins (e.g., ribosome). With this fundamental knowledge of nucleic acid structure, we are poised to fully understand higher-order natural structural motifs implicated in biological function and disease therapeutics.

2 RNA-Based Structural Technologies

2.1 Therapeutic Noncoding RNAs

RNA is well known for its crucial role in protein translation. But RNA plays equally important roles in many other biological processes. It, commonly called “noncoding RNA”, protects and maintains the genome, processes RNA transcripts, is used as a defense mechanism against foreign DNA, exhibits enzymatic functions, and acts as structural elements which organize nuclear chromatin for gene expression [14, 15]. These diverse roles are linked by the primary, secondary, and tertiary structural elements which underscore proper RNA function. Biotechnological tools have leveraged the knowledge of sequence and structure information to control gene expression. The biochemical and structural background of dominant biotechnological tools is discussed in this section.

The well-characterized role of RNA in protein biosynthesis has been a long-standing target for controlling gene expression. Eukaryotes have a mechanism which allows for degradation of RNA (Fig. 3a). During transcription, a sense messenger RNA (mRNA) and antisense RNA (asRNA) strand are produced [14]. This asRNA hybridizes to the sense mRNA and the resulting dsRNA serves as a nucleation point for RNases, facilitating degradation. Specifically, an RNase called DICER degrades these transcripts into 20–25-nt-long dsRNAs containing a 2–3-base overhang at their 3' end [16]. These are considered small interfering RNA (siRNA), where they are recognized by an RNAi-induced silencing complex (RISC) [17]. Current asRNA-based therapies rely on primary structure (or ssRNA) for effective control over biological processes. Introducing mRNA-targeted asRNA blocks the translation of the protein of interest, decreasing the diseased state cellular viability. In some cases, this interference does not directly block translation but rather blocks secondary RNA transcripts necessary for protein production. This mechanism is also imperative in the degradation of foreign RNA transcripts, resulting in RNA interference (RNAi) [18].

The use of primary structure is also observed in other RNA species, which have the potential to be targeted in a similar manner as to mRNA. These include small RNAs such as piwi-interacting RNA (piRNA) [19], small nuclear RNA (snRNA) [20], small nucleolar RNA (snoRNA) [21, 22], and micro RNA (miRNA) [23, 24]. For example, the *lin-4* RNA from *Caenorhabditis elegans* forms a dsRNA with multiple bulges; after processing into its mature form, the miRNA sequences exhibit

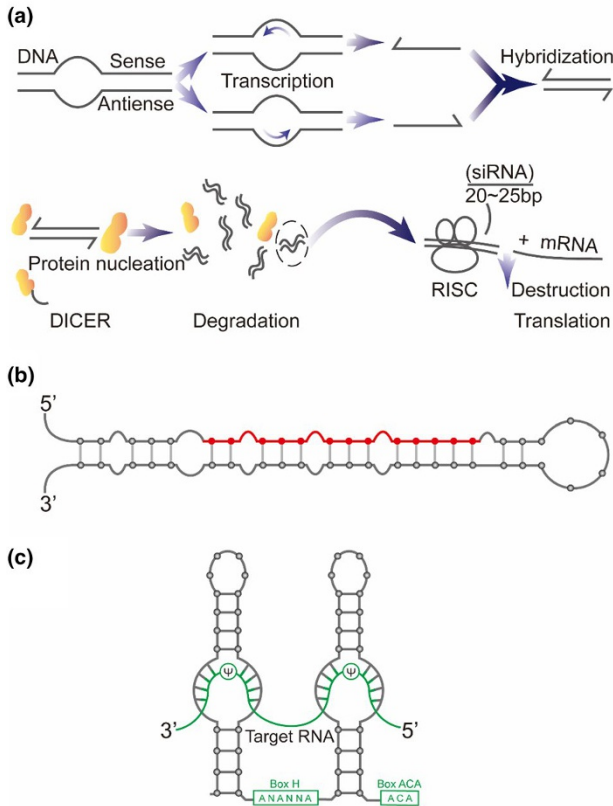


Fig. 3 Mechanism and structures of noncoding RNAs. **a** Antisense RNA binds mRNA and signals degradation. **b** The precursor structure of the miRNA *lin-4*. Mature *lin-4* miRNA is highlighted in red; regions of *lin-4* exhibit dsRNA with bulge regions to many portions of the *lin-14* target RNA, which degrades upon *lin-4* binding. **c** The structure of a snoRNA hybridized to its target rRNA. The H and ACA boxes are conserved sequences brought into proximity by two stem-loops. Base pairing within the stem bulge allows for rRNA specificity during pseudouridylation (Ψ)

complementarity to a cell fate determining protein, *lin-14*, exhibiting the ability to downregulate protein expression through RNAi mechanisms (Fig. 3b) [25]. SnoRNAs contain conserved sequence elements required for the conversion of specific ribosomal RNA (rRNA) uridines into pseudouridine [26]. These conserved sequences are always brought into close proximity to one another through the formation of two stem-loops. The secondary structure of two stem-loops containing bulges is necessary to allow for binding the rRNA substrate, where the modified pseudouridine base resides in the unpaired region of the bulge (Fig. 3c) [26]. These exemplify how an understanding of secondary structural elements in RNAi-related species can lead to the development of targeted nucleic acid therapies. Several RNAi-based therapies are in clinical trials and, most notably, one developed by Alnylam Pharmaceuticals to treat hereditary transthyretin-mediated (hATTR)

amyloidosis in adults was recently approved by the US Food and Drug and Administration (FDA) [27–29]. Furthermore, longer RNAs such as long noncoding RNAs (lncRNA) have just recently been implicated in ability to control gene expression and may represent a novel class of RNA as therapeutic targets [15, 30].

Prokaryotes exhibit similar protective strategies. The CRISPR system recognizes and removes foreign DNA, and since its discovery has burgeoned into a major therapeutic and biotechnology tool [31]. The strategic design of CRISPR RNA (crRNA), guide RNA (gRNA), and the combined single guide RNA (sgRNA) incorporates both primary sequence and secondary structure [32]. Recognition by the CRISPR-associated proteins involves specific secondary structures such as stem–loops, and targeting gene expression requires specific base pairing for each CRISPR system (PAM and NGG). The stem–loop secondary structure of the RNA makes key contacts with the Cas9 protein, allowing for highly efficient cleavage of the target DNA [33, 34]. This has been utilized in various genome editing contexts [35, 36].

2.2 Structural RNA Nanotechnology

Beyond its therapeutic applications of targeting gene expression, RNA has garnered great traction in the biotechnology space as a controllable nanomaterial for probes and tools [37]. Employing the naturally known interactions of RNA bases into higher-order structures, researchers have been able to develop large nanoscale RNA structures to perform specific tasks [11, 38]. This is executed in the same manner as DNA nanostructures (discussed in further detail in Sect. 5), where knowledge of the interactions between RNA sequences allows for the programmable formation of structures [39].

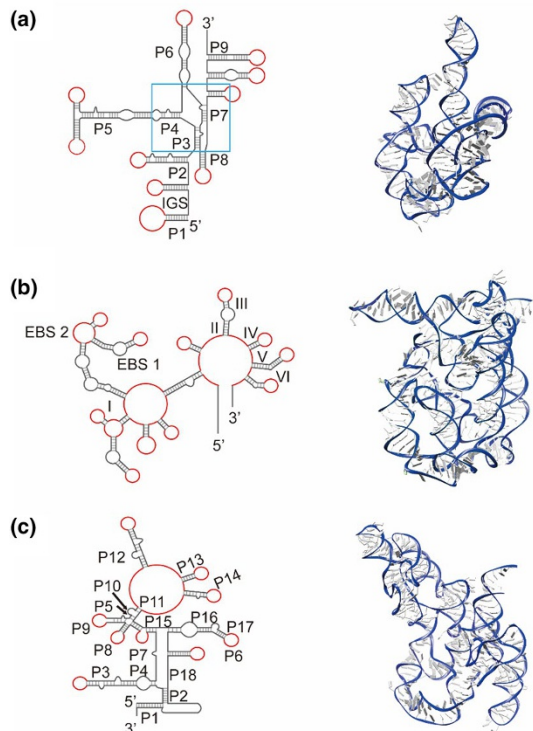
2.3 Catalytic Nucleic Acids: Ribozymes and DNAzymes

While primary structure underscores RNAi methods, RNA tertiary structure is utilized in quite a different mechanism for gene regulation and disease therapy. Certain RNAs in their tertiary form have been shown to catalyze reactions. These RNA-based enzymes, or ribozymes, are the only molecule known to catalyze their own cleavage and have revolutionized the way in which we view the primordial beginnings of the universe [40]. Discovered in the early 1980s, ribozymes have since become a heavily studied area of research, even developing novel ones [41]. Natural ribozymes are found in plants, bacteria, viruses, and lower eukaryotes, and mainly catalyze phosphate backbone cleavage (aside from RNase P which is discussed later). They exhibit the principal features of a protein enzyme, containing an active site, substrate, and cofactor binding site, yet they are 10^3 -fold slower than proteins [42]. The chemical nature of RNA as an enzyme allows for substrate recognition through base pairing, conferring specificity for the ribonucleotide sequence to be removed.

They are categorized into two classes based on size and reaction mechanism. The large ribozymes include RNase P, group I and group II introns, while the small ribozymes include the hammerhead, hairpin, hepatitis delta virus (HDV),

and *Neurospora* Varkud satellite (VS) RNA [43]. Though they differ by reaction mechanism, they all require the presence of the divalent cation magnesium to facilitate tertiary structure formation and catalysis [44]. Group I and II introns catalyze a transesterification reaction to splice out introns from an RNA transcript. Group I introns range from a few hundred nt to around 3000; they have little sequence similarity across organisms, yet their secondary structures are highly conserved in four short regions which comprise a catalytic junction (boxed in Fig. 4a) [43]. In these regions, individual segments partially base pair with one another to confer the necessary structural requirements for strand cleavage. A total of ten paired segments form in these phylogenetically conserved secondary structures and retain catalytic active site function. Beyond secondary sequence, the group I introns contain large open reading frames (ORFs) and an internal guide sequence (IGS) which allows for the positioning of the target transcript and confers control over substrate specificity. The full secondary structural representation of the *Tetrahymena* ribozyme intron is shown in Fig. 4a. Group II introns, ranging only from several hundred to 2500 nt, are generally more elusive than group I introns since they are less widely distributed among organisms, and are rarely self-splicing *in vitro* because of extreme reaction condition requirements. Their secondary structure, generally across organisms, contains six helical domains (helices I–VI, Fig. 4b) where only helices I and V are indispensable. Specific intron binding sequences (IBS) and exon binding sequences (EBS) align the intron such that the 5' and 3' splice sites are in their proper locations.

Fig. 4 Secondary and tertiary structures of the large class ribozymes: **a** *Tetrahymena* ribozyme, PDB file: 1GRZ; **b** Group IIC intron, PDB file: 3EOH; **c** RNase P, PDB file: 3Q1R



Any modification to these secondary structural motifs leads to diminished activity, revealing a common theme that conserved structural elements are highly important for proper tertiary structure formation, and therefore proper substrate binding and catalytic activity of ribozymes.

RNase P in all organisms processes the 5' termini of transfer RNA (tRNA) precursors; it is unusual in that it is the only ribozyme that acts in a *trans*-active manner on multiple substrates, making it the only true naturally occurring RNA enzyme. It is also a unique ribozyme in that it is a ribonucleoprotein complex, where protein subunits are essential for proper formation of the full catalytic center. In eubacteria, the catalytic core is entirely made up of RNA, meanwhile in eukaryotes the protein content is much higher and RNA does not play the catalytic role. The general, common core structure of the catalytic RNase P RNA consists of 18 paired helices (Fig. 4c); different species contain extra stems and stem-loop structures to facilitate stability, and lower ionic strength requirements for catalysis. The 3' half of the acceptor stem is thought to function as an external guide sequence (EGS) to position the substrate through tertiary structural features.

Small catalytic RNA species also include the hammerhead ribozyme, hairpin ribozyme, and VS ribozyme (Fig. 5). Similar to group I, the smaller ribozymes have conserved secondary structural motifs which enable function. The hammerhead ribozyme recognizes and cleaves an NUH sequence. The catalytic RNA contains three stem regions (Fig. 5a), of which sequences are conserved in stems I and III. Hammerhead ribozymes also contain single-stranded regions with highly conserved nucleotides, as well as three variable helical regions to effect self-cleavage. Mutational studies were performed to determine which nucleotides and structural motifs were requisite for catalysis. The hammerhead ribozyme is well characterized and utilized in many biotechnological applications. One major use is in the production of in vitro transcribed RNAs prepared for NMR studies; self-cleavage by the hammerhead ribozyme releases the desired transcript in high purity. They are also making strides in a therapeutic space, where a *trans*-cleaving hammerhead has been approved for phase II clinical trials against HIV-1 [45, 46]. The hairpin ribozyme, found in pathogenic plant satellite viruses, also requires conserved secondary structures for proper tertiary folding and catalysis. This ribozyme consists of four stem regions which comprise two major domains. The secondary structures of domain A (stem I-loop A-stem 2) and domain B (stem 3-loop B-stem 4), when lined up, resemble a hairpin (Fig. 5b) [47]. It recognizes the substrate of sequence RYN*CUG, where cleavage occurs at the *. Hairpin ribozymes from the tobacco ringspot virus, the arabis mosaic virus, and the chicory yellow mottle virus exhibit subtle nucleotide differences within helical regions that maintain the overall structure. Nucleotides are primarily conserved in the single-stranded regions, as well as the bulged motif between helices III and IV (Fig. 5b). The hairpin ribozyme has been modified to recognize and cleave mRNA of diseases including HIV-1, hepatitis B, and the Sindbis virus [46, 48]. The VS ribozyme mediates rolling-circle replication of plasmids from the *Neurospora* mitochondrion through formation of a multimeric, self-cleaving RNA [49]. During transcription of the VS plasmid, a dimeric RNA species is formed with each monomer containing one substrate domain and five catalytic domains (Fig. 5c). The substrate domain (helix 1) exhibits a stem-loop

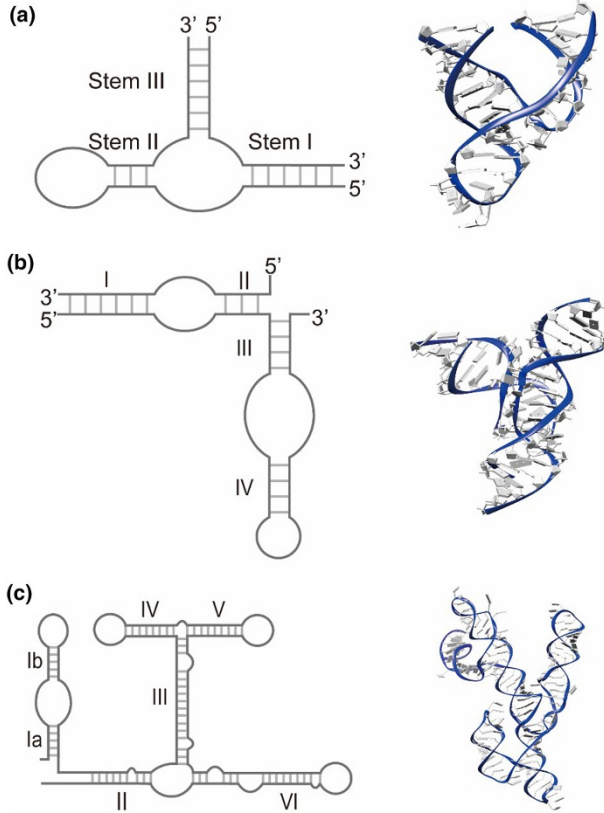


Fig. 5 Secondary and tertiary structures of the small class ribozymes: **a** the hammerhead ribozyme, PDB file: 299D; **b** hairpin ribozyme, PDB file: 1ZFV; and **c** the VS ribozyme (monomeric secondary and dimeric tertiary structures), PDB file: 4R4P

structure while the catalytic domains (helices 2–6) also exhibit stem–loop structures in addition to multiple tertiary contacts. These include three-way junctions and loop–loop kissing interactions to stabilize the catalytic domain. Globally, the catalytic helices come together in a tertiary structure such that the scissile phosphates are proximal to the catalytic nucleotides on the opposing monomer. The trend of secondary structure conservation for hairpin ribozyme catalysis emphasizes the fact that structural motifs, rather than individual nucleotides, are responsible for the function of catalytic RNAs. These RNA structures with known catalytic functionality can be leveraged to act as antivirals, therapeutics, and biotechnological agents.

Though there are a set number of ribozymes known to nature, researchers have developed methods to generate novel ribozymes to catalyze a variety of different reactions. This relies on the SELEX method [50, 51], where a random oligonucleotide pool is evolved in vitro to perform a specific task such as catalysis or binding (also called aptamers; see next section). Some groups have even developed a

strategy where certain secondary elements are retained, while other regions are evolved through mutagenesis. This has resulted in ribozymes which are able to catalyze reactions which recognize a specific sequence, perform nucleophilic attacks on various chemical centers, add metal ions to complexes, and isomerize ring structures. Catalytic DNA species, or DNAzymes, are not known to be found in natural systems and have been evolved from the SELEX method as well [52, 53]. Initially evolved DNAzymes were developed to recreate their natural RNA counterparts, cleaving and ligating RNA species [52]. Since the initial discovery of the capability of DNA to perform similar reactions, other DNAzymes processing RNA or DNA have been developed including those that catalyze RNA cleavage, DNA cleavage, DNA depurination, RNA ligation, DNA phosphorylation, and thymine dimer cleavage [14]. Scientists have investigated these DNA-based enzymes not only for their greater stability but also in an effort to understand the beginnings and evolution of information storage and catalytic species.

Ribozymes have been heavily utilized in molecular biology, but have seen limited translation to the clinical setting. Most predominantly used is the hammerhead ribozyme since it is small, easy to incorporate, and well characterized. Of notable examples are hammerhead ribozymes which have been developed to inhibit HIV. Ribozymes are often incorporated into RNAi systems, so that the hammerhead will perform catalytic cleavage to release the therapeutic siRNA. Though the discussed RNA systems have great therapeutic potential, they suffer major limitations including efficient and targeted cell delivery, target transcript specificity, and RNA stability [46]. Research directives are focused on overcoming these limitations; some, such as nucleic acid modification, are discussed in Sect. 6.

3 G-Quadruplex

3.1 Sequence, Structure, and Topology

Guanine (G)-rich sequences of DNA and RNA can associate into G-quartets, stabilized by Hoogsteen base pairing; stacks of two or more of these G-quartets lead to a higher-order nucleic acid structural motif called a G-quadruplex (G4) (Fig. 6) [54]. These higher-order structures are highly prevalent in the genomic context and are generally understood to play diverse roles in DNA replication, transcription, and translation, as well as controlling gene expression and genome stability. They are abundant in cancer genomes, making them potential therapeutic targets. Additionally, their stable structure is prevalent in aptamers, making them a major structural force in DNA/RNA-based biotechnological ligands.

The sequence requirement for G4 formation is $G_3 N_{1-7} G_3 N_{1-7} G_3 N_{1-7} G_3$, but is driven by environmental factors such as monovalent cations and molecular crowding. Monovalent cations are crucial for this structure to form; preferentially, K^+ ions occupy the interior of the G-quartet to mitigate ion interactions by the bases. Na^+ has also been shown to occupy this ion space, but may alter the overall structure. The general trend of cations which promote G4 formation follows $K^+ > Na^+ > NH_4^+ > Li^+$. It was also revealed that the loop region length affects G4

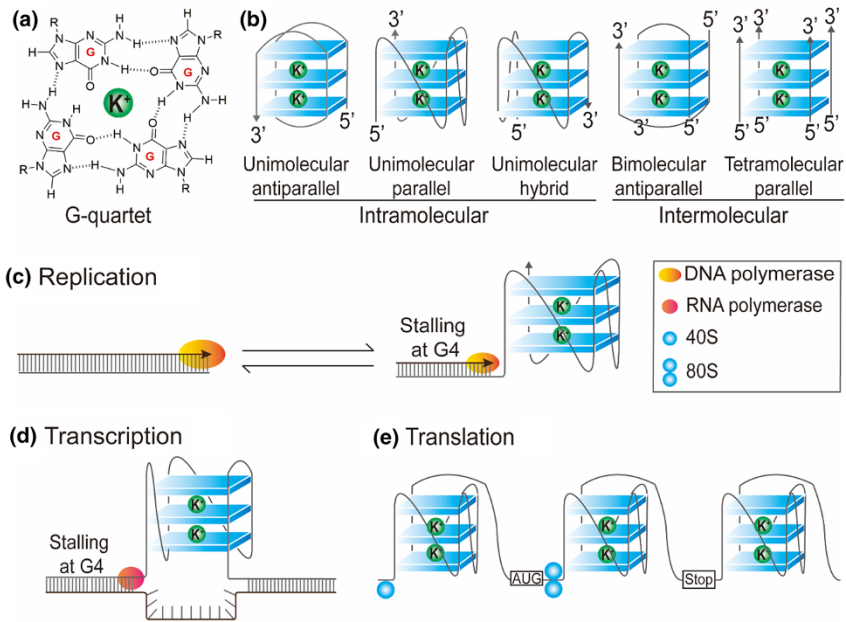


Fig. 6 G-Quadruplex structure and biological function. **a** Four guanine bases interact with a central K^+ ion to make one G-quartet. **b** Stacking of G-quartets forms G-quadruplexes (G4). The number of strands and their directionality dictate G4 topology. The presence of G4 structures in the genomic context regulates replication (c), transcription (d), and translation (e)

stability, and that G4 structures may also deviate from the general sequence requirements through incorporation of bulges. Structurally, the G4 is composed of four strands which can be unimolecular, bimolecular, or tetramolecular, and can have varying topologies governed by the parallel or antiparallel arrangements of the individual strands [54]. The different strand arrangements, schematically illustrated in Fig. 6, generate different topological features. G4 topology can crudely be determined through experimental methods such as monitoring of positive or negative changes in circular dichroism (CD) spectra at specific wavelengths. Complete structure determination is obtained through NMR studies. Many G4 structures have been confirmed *in vitro*, but fewer have been confirmed *in vivo*.

3.2 Biological Relevance

G4s are known to form at a variety of different regions in the cellular context including telomeres in eukaryotes, promoter regions, between introns and exons, 5' untranslated regions (5'-UTR), and at DNA breakpoints. Stable G4 structures impede the progression of DNA polymerase and lead to replication stalling, DNA damage, and genomic instability. Still, the entire picture of G4 biological relevance is not complete. To clarify the elusive relevance of G4s, G-rich regions have been predicted from a number of algorithms, and G4-specific sequencing techniques and

detection probes have been developed to monitor said sequences. Over 300,000 sequences have been identified as potential G-quadruplex forming sequences (pG4s) [55]. And a more recent study identifies over 700,000 pG4s. Their prevalence is certainly great, but the spatiotemporal formation of pG4s and their relevance *in vivo* is a greater and more complex matter. Therefore, the pG4s must be unambiguously detected *in vivo* to validate these predictions.

G4 sequencing *in vitro* utilizes G4-induced DNA polymerase stalling followed by next-generation sequencing [56]. The sequencing is first performed under non-G4-promoting conditions then under G4-promoting conditions (presence of K^+). This type of sequencing has identified G4s in gene regulatory regions including 5'-UTR and splicing sites, and in cancer-related genes and in regions of somatic copy number alteration (SCNA) in cancer genomes.

Direct detection of G4 structures is mainly executed with small molecules or proteins which specifically bind G4s. G4-interacting molecules including pyridostatin (PDS) and its fluorescent analog PDS- α , as well as telomestatin have been utilized for imaging and therapeutics. Their interaction with G4s also traps the structure in the G4 formation, allowing a snapshot into the G4 but preventing the investigation of dynamics and regulation of G4 formation. A more spatiotemporal method of G4 mapping can be done with proteins which bind to naturally forming G4 as opposed to promoting G4 formation under specific conditions. The first antibody against G4s, a scFv antibody Sty49, was used to show that G4s form at telomeres [55]. Later two structure-specific antibodies were developed, BG4 and 1H6, which allowed for pull-down sequencing and immunofluorescence imaging of G4 location in eukaryotic cells. These proteins are paramount for G4 ChIP sequencing, where the G4-specific antibodies are used as probes. G4 ChIP-seq has identified double-stranded break sites induced by PDS, identification of protein interactions that promote formation of other G4 and other DNA structures, that G4s predominantly lie in regulatory, nucleosome-depleted chromatin regions that are highly transcribed.

Other dye- and protein-based probes have been developed to monitor G4 formation *in vitro* and *in vivo*. These include TSQ1, CyT, and anthrathiophenedione dyes, a G4-triggered fluorogenic hybridization probe, the zinc-finger protein GQ1, and ankyrin repeat binding proteins (DARPin)s [55]. Helicases which resolve G4s have also been mapped to bind G4s, implicating that their biological functions are linked to G4 structures or genomic regions enriched in G4. One group developed a fluorophore-conjugated RHAU helicase peptide as a probe for G4 formation.

Overall, these methods have confirmed that G4s are prevalent in a genomic context and their formation is dynamic and regulated. This reasons that the expression of G4 structural motifs will vary depending on cell type and cell cycle progression. Yet there is much more work to be done to specifically determine their biological roles in various contexts.

3.3 Therapeutic and Biotechnological Applications

The G4 structure, as was just discussed, is heavily implicated in biological processes and predominantly prevalent in cancer genomics and is therefore a prime therapeutic

target. Telomeres are a particularly major target for G4 binding molecules since their abnormal processing in cancers ubiquitously confers cell immortality. Additionally, many oncogenes have pG4s or confirmed G4 structures in their promoter regions. Targeting these G4 structures with small molecules promotes the downregulation of expression of these genes, thereby reducing tumor viability. Since the G4s found in telomeres and oncogene promoter regions are so similar, it is imperative to obtain a selective binding G4 ligand for the particular target. Though small molecules have been developed which target G4s, selectivity of the particular oncogenic G4s still proves a challenging, yet crucial task.

Many ligands have been identified which bind to G4s in a therapeutic context. For telomeric G4s, these are chiefly 2,6-diaminoanthraquinone derivatives and telomestatin. Telomeric G4s may exist as dimers or multimers and some ligands have even been identified to selectively bind to multimeric G4s over monomeric G4s. These include a dinickel salophen dimer, berberine dimer, and telomestatin derivative tetramer which bind to dimeric G4s and m-TMPipEOPP which preferentially binds multimeric G4s. Interestingly, the junctions between the monomers in multimeric G4s have also been specifically recognized by ligands [57].

Oncogenic G4s are similarly targeted for therapeutic applications. Generally, rational and high-throughput screens have been employed to develop various molecular ligands to oncogenic-specific G4 structures. To enhance specificity for a particular oncogene, pyrrole-imidazole polyamide (PIP) molecules bind in a sequence-selective manner to duplex DNA and can be hybridized to G4-targeting ligands to enhance the overall selectivity. This was shown in the development of cyclic imidazole/lysine polyamide conjugated PIP (cIKP-PIP) [58]. Some specific oncogenes of interest include the promoter region G4 of *c-Myc*, which is specifically targeted by GQC-05 [59], crescent-shaped thiazole peptide (TH3) [60], four-leaf-clover-like molecule (IZCZ-3) [61], and others identified by a microarray screen of 20,000 small molecule binders. VEGF G4s are targeted by perylene monoimide derivative (PM2) [62], and a quinoline derivative (SYUIQ-FM05) [63]; these have encouraged studies of small molecule VEGF-G4-preferred ligands obtained through a low-volume screening approach [57]. BCL2 G4 structures are preferentially targeted through furo[2,3-*d*]pyridazin-4(5*H*)-one derivatives [64], as well as the fluorescent dye carbazole TO [65]. G4s in the promoter region of *c-Kit* oncogene (also known as mast/stem cell growth factor receptor Kit) are targeted by derivatives of isoalloxazine (*N,N*-dimethyl amine and *N,N*-dimethyl amine/2-fluorine substitutions) [66], naphthalene diimide [67], benzo[*a*]phenoxazine (BPO) [68], and carbazole derivatives [69]. Human telomerase reverse transcriptase (hTERT) is overexpressed in cancers and contains G4 tracts in the promoter region which form higher-order G4 structures; a dual-motif targeting small molecule, GTC365, binds to the G4 and mismatched duplex stem-loop structures [70]. *KRAS* G4 structures have recently been selectively targeted with triple-cation derivatives of indolo[3,2-*c*]quinolines (IQc) [71]. The *KRAS* oncogene is also downregulated through a unique decoy system where pyrene-modified oligonucleotides which form a more stable G4 attract essential transcription factors, preventing transcription from actually happening [72]. Topotecan was developed to selectively target *c-myb* G4 structures [73]. Beyond these recent examples, many other oncogenes have been identified to contain G-rich

promoter regions, suggesting that there may be selective small molecule inhibitors to genes such as *PDGFRB*, *PDGFA*, *STAT3*, and *FGFR2*.

In addition to being a therapeutic target, G4s are also highly prevalent in biotechnological applications such as biosensors and diagnostics. Aptamers, predominant therapeutic and diagnostic agents to a variety of substrates, exhibit G4s as a crucial structural feature [55]. G4 structures in an aptamer are highly advantageous as they provide thermodynamic and chemical stability, resist serum nucleases, reduce immunogenicity, and increase cellular uptake. Aptamers evolved to target a variety of different ligands using the SELEX method from G4s previous to or upon ligand binding. Some notable examples of G4-containing aptamers include the well-characterized thrombin-binding aptamer (TBA) which forms G4 upon interaction with thrombin [74]. Another catalytic aptamer that forms G4 upon ligand binding is PS2.M, which binds heme to form a G-quadruplex–hemin complex [75]. This unique aptamer requires G4 sequence for function and can be used to mimic the activity of horseradish peroxidase, providing a visual output for detection of various molecules. The spinach aptamer, which recognizes 3,5-difluoro-4-hydroxybenzylidene imidazolinone, contains a G4 motif [76]; since development of the spinach aptamer, derivatives which act as fluorescent binders to other molecules also contain G4 motifs. This provides insight into the structural requirements for fluorescent aptamer ligands.

One unique application of G4s involves the modulation of G4 formation to detect lead ions (Pb^{2+}) in solution [77]. A G4 tethered to a carbon nanotube electrode is linear in its native form. In the presence Pb^{2+} ions, a G4 structure is induced, resulting in a greater emission by intercalating agent ethyl green. Another creative diagnostic application includes G4 motifs that were utilized to detect low-abundance nucleic acid molecules such as pathogenic DNA [78, 79]. This employs a technique called quadruplex priming amplification (QPA) where the dissociation of dsDNA and formation of G4 occurs upon primer extension [79]. The G4 structure that forms during QPA is detected by incorporation of 2-aminopurine (2-AP) bases; 2-AP is quenched by neighboring bases in the linear form, but regains emissive properties in the G4 form. It is clear from the current research landscape that G4 structures are (1) highly abundant in the human genome, suggesting their role in biology and therapeutics; (2) predominant in various aptamer structures, suggesting that they play vital stabilizing roles; and (3) emerging in biosensor and diagnostic applications, signifying their potential in other disciplines.

4 i-Motif

4.1 Sequence, Structure, and Topology

The cytosine (C) complement to G-quadruplexes also forms unique higher-order structures. Initially discovered by Gehring et al. [80], C-rich oligonucleotides form an intercalated quadruple-helical tetramolecular structure, called intercalated or i-motifs. Similar to G-quadruplexes, the C-rich region preferentially forms under acidic conditions, but recently it has been shown that these sequences can form

i-motifs at neutral pH depending on the sequence and environmental conditions [81, 82]. The i-motif structure consists of two parallel-stranded duplexes intercalated in an antiparallel orientation (Fig. 7), generally composed of cytosine–cytosine base pair regions and loop regions [83]. The interacting C bases allow for the intercalated structure through a hemi-protonated C:C⁺ base pair with three hydrogen bonds which confers significant stability [82]. The fundamental factor contributing to i-motif stability is the number of C:C⁺ base pairs. A central positive charge and some π stacking further stabilize the interaction of the bases. Loop regions also add a special stability, such as the case of the G:T:G:T tetrad loop [82]. The loop regions define the two classes of i-motifs, where class I and II are characteristic of shorter and longer loops, respectively [84]. Longer loops, contrary to G4 motifs, are more stable than the shorter loops.

i-Motif structures also have topological features associated with their unique secondary structure. As a result of the spatial arrangement of the C:C⁺ base pair, two

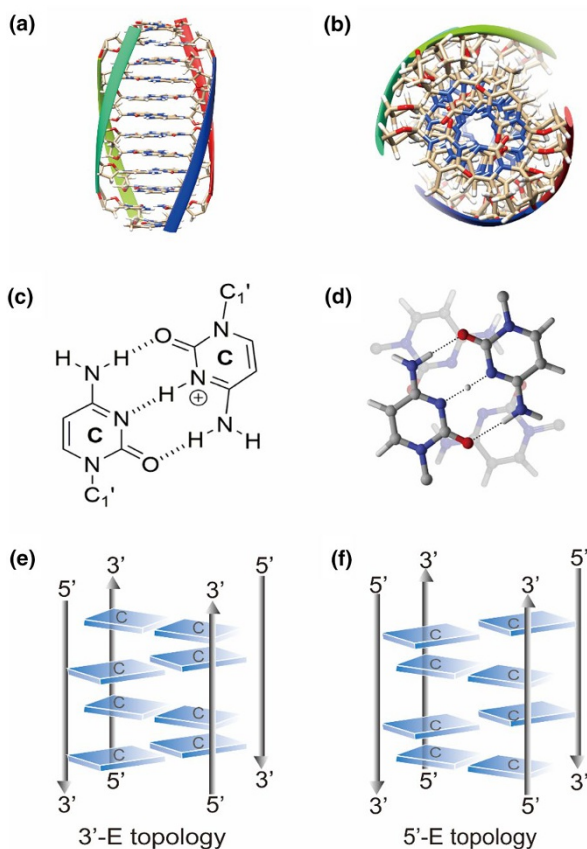


Fig. 7 i-Motif structure. **a** Side and **b** top view of the d(TC₅) intermolecular i-motif. PDB file: 225D. **c** Chemical and **d** ball-and-stick representation of the C:C⁺ base pair. i-Motifs exhibit either 3' (**e**) or 5' (**f**) topology depending on where the outmost C:C⁺ base pair resides

topologies arise, 3E' and 5E' [83]. 3E' forms when the outmost C:C⁺ base pair is at the 3' end of the base, and 5E' forms when the terminal C:C⁺ base pair is at the 5' end. As a result of extended sugar–sugar contacts along the narrow grooves, the 3E' topology imparts greater stability to the structure [82, 85].

4.2 Biological Relevance

It has been established that i-motifs can form *in vivo*; furthermore, that they are dependent on the cell cycle and the pH [81, 82, 86]. The environmental conditions which allow for this at physiological pH include salt concentration, negative superhelicity, and molecular crowding. Increasing NaCl concentration to 100 mM destabilizes the i-motif, but further increasing to 300 mM has no more destabilizing effect [85]. Negative superhelicity arises during unwinding of dsDNA during transcription events, and this also promotes i-motif formation. Finally, molecular crowding promotes i-motif formation by preventing Watson–Crick duplex formation and is likely the major factor which allows i-motifs to form *in vivo*. Uracil bases (U) from spontaneous deamination of cytosine significantly reduce the thermal stability of i-motifs; however, ribonucleic acid i-motif structures, with and without U, have been identified *in vitro* [87].

Understanding the conditions which promote formation at physiological conditions gives insight into the biological role i-motifs may play. Since G canonically base pairs with C, it is presumed that i-motifs form at the same genomic loci as G4s and therefore that they perform opposite gene regulatory functions. Also like G-rich regions, C-rich regions are found enriched at promoter regions, telomeres, and centromeres. However, not all C-rich regions form i-motifs as formation is dependent on the environmental conditions discussed. Promoter regions shown to form i-motifs include *c-Myc*, *BCL2*, and human acetyl-CoA carboxylase (*ACCI*). Whether or not the *c-Myc* expression is turned on is dependent on the extent of transcriptionally induced negative superhelicity which promotes i-motif formation. Regulation of *Bcl2* by stabilizing molecules identified in a screen shows that presence of the i-motif structure upregulates *Bcl2* expression while a hairpin structure represses transcription [85, 88]. *AACI* i-motif formation under molecular crowding conditions upregulates expression. i-Motif foci are more prominent during the G1/S phase, further supporting the notion that i-motif structures play an opposing role to G4 structures in cell biology; G4 suppresses transcription while i-motif activates transcription [82].

Uncovering other i-motif-forming genomic loci requires specific ligands which can recognize these structural motifs. Unlike G4s, there are much fewer i-motif-specific peptide and small molecule ligands ideal for studying i-motifs. This makes it more difficult to identify the spatiotemporal expression of these C-rich higher-order structures in a cellular context. Though some notable ligands have been developed to further this understanding, they each have their disadvantages. A porphyrin ligand, TMPyP4, initially utilized to study G4 interactions showed independent binding to i-motif structures to induce an inhibitory effect on the NM23-H2 involved in transcriptional activation of the *c-Myc* gene [82, 89]. Molecules such as crystal

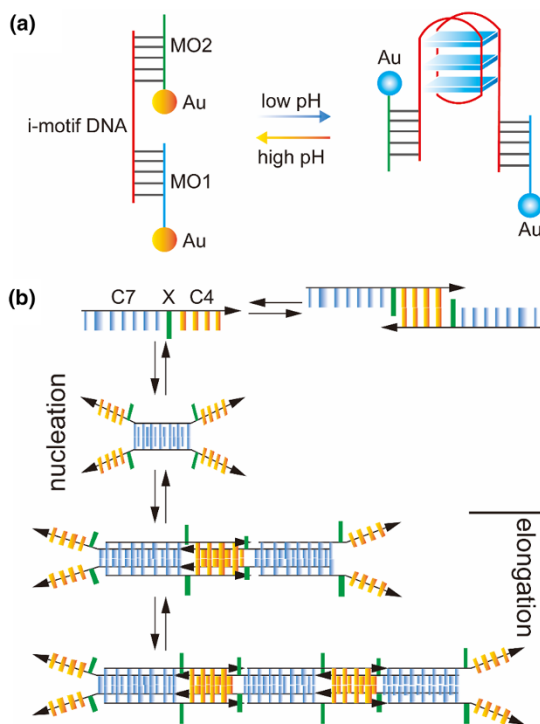
violet, bisacridine (BisA), and phenanthroline derivatives have exhibited binding to i-motifs; some were stabilizing probes, but were not selective [88, 90]. Metal-centered ligands such as the ruthenium complex $[\text{Ru}(\text{bpy})_2(\text{dppx})]^{2+}$ and the terbium aminoacid complex $[\text{Tb}_2(\text{DLHVal})_4(\text{H}_2\text{O})_8]\text{Cl}_6$ bind i-motifs and cause slight structural perturbations. Nanomaterials like carboxyl-modified single-walled carbon nanotubes (C-SWNTs) and graphene quantum dots (GQDs) have shown stabilization of i-motifs through respectively binding the end of the major groove and the internal TAA loop [91, 92]. Two small molecule ligands, IMC-48 and IMC-76, were identified to bind to the i-motif and hairpin conformation of C-rich regions, respectively. These two ligands were utilized to shift the equilibrium of the structures and as a result control expression of *BCL2* mRNA. Many proteins have been identified as poly C binding proteins (PCBP) and include heterogeneous nuclear riboprotein K (hnRNPK), a 39-kDa polypeptide from *Trypanosoma brucei*, and the BmlLF protein of *Bombyx mori*. Finally, one antibody exists against the i-motif, iMab. This antibody binds to C-rich, i-motif-forming DNA sequences over other DNA species (dsDNA, hairpins, and G4s) [86].

4.3 Therapeutic and Biotechnological Applications

In stark contrast to G4s as therapeutic targets, i-motifs are significantly lacking. Not many i-motifs have emerged as promising candidates for therapeutics since there are limited selective i-motif ligands, yet creative approaches are being pursued to incorporate i-motifs in therapeutics. The small molecule IMC-76 in concert with ellipticine (GQC-05) simultaneously targets the *BCL2* and *c-Myc* oncogene promoters. GQC-05 stabilizes the *c-Myc* G4 structure and turns off gene expression, while IMC-76 stabilizes the hairpin structure of *BCL2* and decreases mRNA levels [93]. The combinatorial approach to nucleic acid structure-targeted therapeutics resulted in high sensitivity of lymphoma cells to the chemotherapeutic drug cyclophosphamide. Further development and refinement of i-motif-specific ligands is paramount to their efficacy as cancer therapeutics.

The i-motif sees a much greater role in the biotechnology space; it is central in the design of nanotechnological systems for analytical and biomedical purposes, relying on the structural transition of i-motif sequences as a result of pH changes. The ease of changing structure is leveraged to provide desired outputs. Some notable examples of the i-motif switch (I-switch) in nanotechnology include monitoring pH, controlling DNA nanostructure assemblies, drug release platforms, and biosensors [83]. The first I-switch, developed by the Krishnan group, was designed to sense and report pH changes along endosomal maturation in living cells in culture and in vivo [94]. The addition of gold nanoparticles (AuNPs) to these switches enhances their ability to detect pH changes by a visible readout of aggregated AuNPs (Fig. 8a) [95]. Leveraging i-motif structural changes, their incorporation into DNA-based assemblies can provide sensitive readouts and key functionalities for various biotechnological applications [96]. Aside from detecting pH, i-switches can act as a controllable release mechanism, e.g., capping mesoporous silica nanoparticles that can open and close their pores to release cargo by changing pH [97]. Anchoring a

Fig. 8 i-Motif biotechnological applications. **a** Structural transition of a linear \leftrightarrow i-motif assembly under different pH results in aggregation of attached AuNPs and change in color. This i-motif molecular switch produces a visible color change to detect pH. **b** Association of i-motif-containing oligonucleotides into a 1D supramolecular “wire”



dense monolayer of i-motifs with polyA connectors to a flat gold surface also generates a nanocarrier; the i-motifs effectively cap the interior polyA, creating a lid over encapsulated ions or small molecules. i-Motifs have also been utilized in the controlled formation of DNA-based nanomaterials [96]. A 1D “wire” of i-motif-containing oligonucleotides was initially developed by Ghodke et al., where the designed DNA strands were annealed at low pH to allow for growth to persist in one direction (Fig. 8b) [98]. In a similar design, i-motifs were central to the formation of DNA pillars [99]. Allowing i-motif oligos to propagate in three dimensions generates a pH-responsive DNA hydrogel [100].

5 Nucleic Acid Junctions and Nanostructures

5.1 Biological Relevance and Structure

Helical junctions, or points where two nucleic acid helices cross over one another, are important in biological processes. For RNA, as discussed in Sect. 1, three-way junctions mainly serve an architectural and stabilizing role. Meanwhile for DNA, four-way junctions are key intermediates of homologous recombination events during meiosis; they are observed in various DNA repair events to maintain genomic integrity. The biological relevance of this junction was initially proposed by Robin Holliday in 1964 to describe the mechanism of DNA strand

exchange which results in genetic diversity. As such, these DNA-based four-way helical junctions are also known as Holliday junctions (HJ). In biology, HJs exhibit the ability to migrate along the DNA axis based on homologous sequence and are resolved by the action of enzymes which recognize the specific topological features of the crossover. Though most prominently studied in DNA, crossover events have also been observed in RNA of the Brome mosaic virus (BMV) [101]. Since HJ structures exhibit homology, they are mobile along the DNA strand, a phenomenon called branch migration (Fig. 9a). This initially rendered it difficult to characterize them *in vitro*, but the generation of “immobilized” junctions [102, 103] allowed for the characterization of the DNA crossover structures [104–106].

The two DNA helices can align parallel or antiparallel to one another, resulting in two different mechanisms of strand exchange: crossed and un-crossed (or “square”) (Fig. 9b). But how these strands exchange in three-dimensional space was first determined through biochemical assays performed by Lilley [107]; the crossovers adopt a global X shape, where the two helical arms stack over one another. Lilley also showed that these crossovers require divalent cations such as Mg^{2+} to remain stable. In 1994, the first crystal structure of a Holliday junction complexed with a resolving enzyme was obtained [108]. We now have many

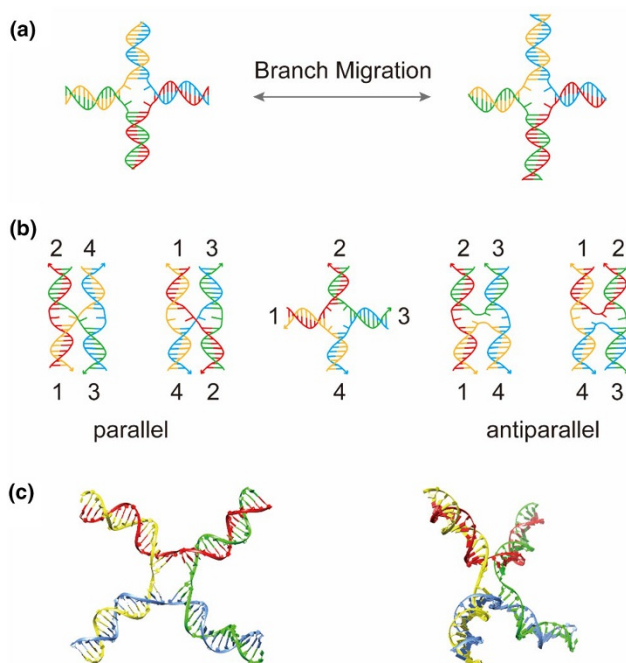


Fig. 9 Structure of a 4-way DNA junction (Holliday junction). **a** Homologous sequences of DNA can come together via reciprocal strand exchange to generate a 4-way junction. The junction is mobile along the DNA allowing for branch migration. **b** Strand exchange can occur from different helical alignments (parallel and antiparallel) as well as different strand arrangements (crossed or square). **c** Crystal structure of a Holliday junction [109] (PDB 2CRX) revealing an X-type tertiary structure

crystal structures of HJ-resolvases, providing a clear picture of these crossovers (Fig. 9c).

5.2 Therapeutic and Biotechnological Applications

The most prominent use of DNA junctions in biotechnology and therapeutics has been in the construction of DNA nanostructures. This significant discipline of the structural DNA nanotechnology field emerged from the ability to generate immobile (those which do not undergo branch migration) four-way helical junctions [102, 110]. Ned Seeman utilized these immobile junctions in the construction of repeating and periodic DNA branched junctions, resulting in DNA lattices and other higher-order DNA structures [102]. Some systems rely on structural motifs such as branched junctions [111] and stem-loops [112] to generate DNA-based hydrogels. The judicious incorporation of these elements and the base-pairing design allows for hybridization chain reactions to propagate and generate a long, complex, and entangled mesh of DNA, or hydrogel. Such hydrogels have broad biomedical applications for controlling cell growth or development as well as controllable drug release [113, 114].

In another design approach, the alignment of multiple, parallel HJ motifs along two DNA duplexes generates paranemic crossover (PX) structures [115]; these have been used in nanostructure formation, computation, and nanomachines [116]. The expansion of HJ motifs into an *in vitro* assembly of multiple repeating units pioneered the DNA nanostructure field and gave rise to the use of DNA as a spatially addressable material [102]. Later, others began developing different types of DNA nanostructures based on the same concept. Paul Rothemund utilized multiple branched junctions as structural motifs to fold single-stranded bacteriophage DNA, M13mp18, creating the DNA origami technique (Fig. 10a) [117, 118]. Peng Yin developed the self-assembly of DNA tiles and bricks to further expand the rapidly growing number of structures that can be made using short DNA oligonucleotides (Fig. 10b, c) [119–121].

Strategic base pairing and formation of crossover junctions underscores the DNA nanotechnology field, allowing researchers to develop specific and precise shapes on the nanometer scale. The ever-growing chemical modifications available to DNA and the inherent specificity of DNA allows for the precise placement of various ligands [121]. Incorporation of stimuli-responsive species imparts control to DNA nanostructures, promoting mechanical motions, specific outputs, or timed-release. These exquisite properties and characteristics make DNA nanostructures advantageous tools for a variety of biotechnological and therapeutic applications, the major categories being molecular tools, biosensors, and cell delivery agents [127].

The precise placement of ligands has enabled development of “molecular pegboards” as tools to study individual molecular interactions, distance requirements, and enzymatic cascades. Recent efforts have utilized DNA origami and other DNA-based structures to understand physical determinants for energy transfer [128–130]. Investigation and utilization of enzymatic cascades have also benefitted greatly from the properties of templated DNA nanostructures (Fig. 10d) [122, 131, 132]. One

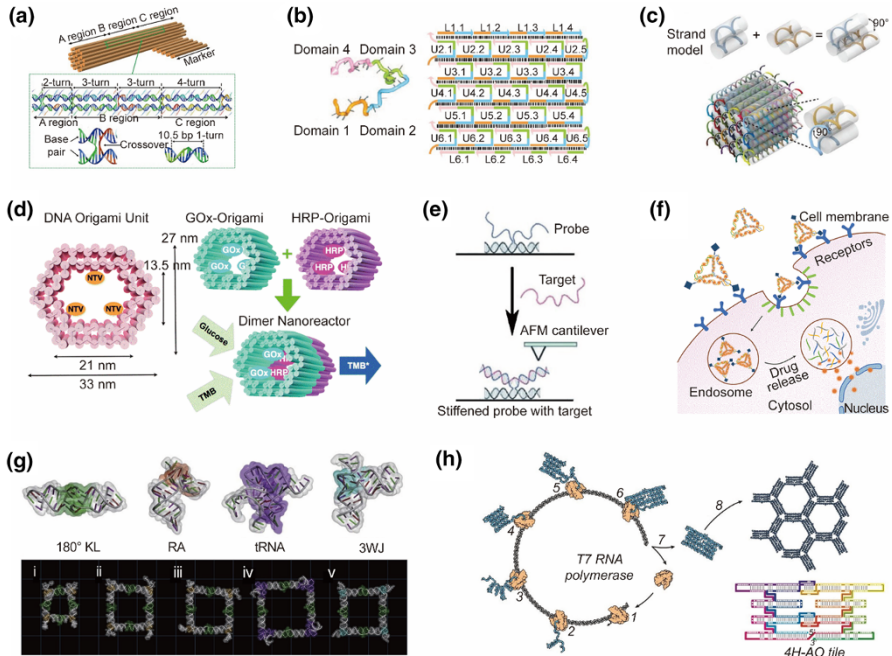


Fig. 10 DNA and RNA nanostructures and their applications. **a** The DNA origami technique judiciously places crossover junctions to fold ssDNA into nanoscale objects. Adapted with permission from Ref. [118]. Copyright 2017, The Japan Society of Applied Physics. **b** Single-stranded oligonucleotides containing four variable domains repeatedly assemble by crossovers, leading to the design of DNA tiles which generate various shapes and patterns. Adapted with permission from Ref. [120]. Copyright 2012, Springer Nature. **c** DNA bricks form a “LEGO-like” interaction of two DNA strands with complementary head/tail regions. The perpendicular arrangement of complementary DNA strands generates three parallel helices for each pair of bricks, allowing the structure to be built into controlled, three-dimensional shapes. Adapted with permission from Ref. [119]. Copyright 2012, American Association for the Advancement of Science. **d** Enzymatic reactions are studied using DNA origami. A DNA origami unit containing NeutrAvidin (NTV) sites was designed to encapsulate biotinylated glucose oxidase (GOx) or horseradish peroxidase (HRP) enzymes. The nanoreactors dimerize through base pair interactions and their close proximity allows for the enzymatic cascade to ensue, producing TMB*. Adapted with permission from Ref. [122]. Copyright 2015, Royal Society of Chemistry. **e** DNA origami enables single-molecule analysis. A single-stranded probe placed on the origami surface is indistinguishable by atomic force microscopy (AFM). Upon hybridization with a single target RNA strand, a V-shaped junction is formed and is easily visible by AFM. Adapted with permission from Ref. [123]. Copyright 2012, Wiley-VCH Verlag GmbH and Co. **f** DNA nanostructures act as drug delivery systems. Drug-loaded DNA nanostructures can be appended with cell-targeting ligands. The nanostructures enter the cells via receptor-mediated endocytosis where they are then degraded to release the drug cargo. Adapted with permission from Ref. [124]. Copyright 2018, American Chemical Society. **g** RNA structural motifs are utilized to controllably build polygons. The top row shows the 3D structures of representative structural motifs, PDB codes from left to right: 180° KL (1JJM), RA (1JJ2), tRNA (4TNA), and 3WJ (4V4Q). The bottom row shows various polygonal shapes made with the representative structural motifs. The colors in the polygons correspond to the regions colored in the top row. Adapted with permission from Ref. [125]. Copyright, 2018 Elsevier. **h** RNA origami can be folded co-transcriptionally to produce RNA tiles. As the RNA is transcribed from the DNA template, the programmed 180° and 120° KL motifs form to produce 11 helical subdomains. Adapted with permission from Ref. [126]. Copyright 2014, American Association for the Advancement of Science

particular system incorporates a four-way junction and two crossover motifs to strategically place glucose oxidase (GOx) and horseradish peroxidase (HRP) enzymes which are controlled by a strand displacement mechanism [133]. Origami surfaces are also an advantageous platform for single-molecule analysis (Fig. 10e) [123], and the development of a DNA origami “frame” allowed for the investigation of various nucleic acid interactions [127]. At the same time, origami structures can be designed to mimic more intractable biological structures, such as transmembrane pores, to understand the key determinants for molecular transport [134, 135]. In a unique approach, a DNA-based copy-print system confers two-dimensional information from a DNA origami sheet to the surface of AuNPs [136]. DNA origami-based nanoimprinting lithography (DONIL) [136] shows great promise for self-assembly of nanostructures to be applied in biomedical applications for precisely tailored optical and electronic properties. Together, the variety of applications of DNA origami as molecular tools provides a wealth of opportunities for the translation of these structures in diverse disciplines related to biomedical research.

Aside from providing a platform for fundamental understanding of biological phenomena as just described, these controllable origami structures are incredibly advantageous for therapeutic applications such as biosensing and drug delivery. The addition of i-motifs, fluorophores, AuNPs, and other responsive modules and outputs are all major players in the development of DNA origami biosensors [137, 138]. Recently, we have constructed a star-shaped DNA architecture, called “DNA star” that contains five 4-arm junctions at each of the inner pentagon vertices. At these junctions, 10 dengue envelope protein domain III (ED3)-binding aptamers are placed in a precise 2D pattern which mirror the spatial arrangement of ED3 clusters on the dengue viral surface. The resulting polyvalent, spatial pattern-matching interactions provide high dengue-binding avidity, which leads to potent viral inhibition. Hybridization of fluorescent output pairs renders the DNA star into a sensitive dengue biosensor [139]. In another recent work, a supramolecular DNA origami precisely immobilized AuNPs to localize single dye molecules for the generation of surface-enhanced Raman scattering (SERS) [140]. This provides a new approach to single-molecule studies using the well-characterized DNA origami as a platform, showing the breadth of disciplines where DNA origami-based advances are still being uncovered. Finally, DNA-based materials have been intercalated with anticancer drugs such as doxorubicin, and directly conjugated with disease-targeting ligands for specific, efficient, and controllable drug delivery (Fig. 10f) [124].

As a more conformationally dynamic and complex nucleic acid species, RNA has also been employed for the generation of nanostructures [125]. The rise of RNA as a nanostructure scaffold has emerged from the assembly of packaging RNA (pRNA) into dimers, trimers, and hexamers, and the observation that kissing loops promote RNA structural formation [141]. Since these formative discoveries, great efforts were made to generate more complex and chemically defined RNA nanostructures. Precise programming of secondary and tertiary interactions including kissing loops, hand-in-hand, foot-to-foot, crossovers, and junctions leads to the engineering of higher-order RNA structures such as nanoparticles, tiles, lattices, polyhedra, and origami [141, 142]. Specific structural motifs have been utilized to build various polygonal nanostructures (Fig. 10g), and are fully summarized with in a recent review by

Ohno et al. [125]. Exemplar advancements in RNA as structural tools involve the design of single-stranded RNA to fold back over on itself without the formation of knots [143], and the unique design of an RNA which concomitant with transcription folds back on itself to form structural elements requisite for tile formation (Fig. 10h) [126]. RNA nanoparticles are utilized to contain other therapeutically active RNA species such as siRNA, ribozymes, and aptamers [37]; meanwhile, other structural RNAs are utilized as molecular scaffolds to enhance bacterial metabolic activity, control mammalian cell surface interactions, and cell fate signals through localization and aggregation of distinct molecular targets [125].

6 Conclusions and Future Outlooks

6.1 Proteins Join the Game

Proteins existing naturally in biological systems specifically bind DNA on the basis of sequence. These include transcription activator-like (TAL) effector proteins and the CRISPR-associated proteins. TAL proteins produced by plant pathogenic bacteria recognize sequence-specific promoter regions of host cells; meanwhile, the protein recognition region allows for protein engineering to develop those which bind user-defined sequences. These proteins have been cleverly applied to fold DNA species into DNA–protein hybrid shapes, similar to the DNA origami method [144]. Bringing proteins into the fold of megadalton, multilayer DNA structures promotes structural rigidity for more robust applications. This natural, sequence-specific DNA–protein interaction can also be leveraged by the CRISPR-associated proteins and can lead to greater nucleic acid-based tools for biotechnological applications.

RNA nanostructures have also been constructed through a combination of RNA–protein (RNP) interactions. Various proteins are known to interact with specific RNA structural motifs, e.g., the L7 protein binds a specific target called “box C/D”. Tailoring the RNA sequence and judicious choice of RNA-binding protein result in formation of complex which can generate triangular and square RNP structures [125].

6.2 Unnatural Modifications for Stability and Applicability

Extensive reports of unnatural modifications in the nucleic acid structural motifs discussed above have revealed our ability to chemically manipulate these naturally found structures for prolonged stability or to promote a particular equilibrium/structure formation *in vivo*. G4 and i-motif both have the ability to incorporate nucleic acid modifications to increase stability. While most sugar modifications destabilize i-motifs, modification of the phosphates promotes i-motif formation [82]. Phosphorothioate allows formation at neutral pH and Rp-chirality exhibits greater stabilization of the i-motif [82]. Peptide nucleic acids (PNA) and locked nucleic acids (LNA) have been investigated to form these higher-order structures [54]. While they have been shown to form G4 and i-motifs, PNA tends to do so at narrower pH ranges.

Though RNA has greater conformational flexibility which confers a greater molecular design space, it is also more susceptible to degradation, a tremendous disadvantage for applicability. Yet the increasing number and incorporation of nucleic acid modifications have enabled the use of RNA as a molecular scaffold amenable to applications in vivo [141].

Funding Xing Wang was funded by HT Materials Corporation. Jinwei Duan was funded by Natural Science Foundation of Shaanxi Province (Nos. 2017JQ2035, 2018JQ2023) and Fundamental Research Funds for the Central Universities (No. 300102129101).

Compliance with Ethical Standards

Conflict of interest On behalf of all authors, the corresponding authors state that there is no conflict of interest.

References

1. Watson JD, Crick FHC (1953) Molecular structure of nucleic acids: a structure for deoxyribose nucleic acid. *Nature* 171(4356):737–738. <https://doi.org/10.1038/171737a0>
2. Das J, Mukherjee S, Mitra A, Bhattacharyya D (2006) Non-canonical base pairs and higher order structures in nucleic acids: crystal structure database analysis. *J Biomol Struct Dyn* 24(2):149–161. <https://doi.org/10.1080/07391102.2006.10507108>
3. Lipps HJ, Gruissem W, Prescott DM (1982) Higher order DNA structure in macronuclear chromatin of the hypotrichous ciliate *Oxytricha nova*. *Proc Natl Acad Sci* 79(8):2495. <https://doi.org/10.1073/pnas.79.8.2495>
4. Guéron M, Leroy J-L (2000) The i-motif in nucleic acids. *Curr Opin Struct Biol* 10(3):326–331. [https://doi.org/10.1016/S0959-440X\(00\)00091-9](https://doi.org/10.1016/S0959-440X(00)00091-9)
5. Watson J, Baker TA, Bell SP, Gann A, Levine M, Losick R (2014) The structures of DNA and RNA. In: *Molecular biology of the gene*. Pearson, London
6. Salazar M, Fedoroff OY, Miller JM, Ribeiro NS, Reid BR (1993) The DNA strand in DNA–RNA hybrid duplexes is neither B-form nor A-form in solution. *Biochemistry* 32(16):4207–4215. <https://doi.org/10.1021/bi00067a007>
7. Rich A, Nordheim A, Wang AHJ (1984) The chemistry and biology of left-handed Z-DNA. *Annu Rev Biochem* 53(1):791–846. <https://doi.org/10.1146/annurev.bi.53.070184.004043>
8. Herbert A, Rich A (1998) Left-handed Z-DNA: structure and function. In: Bradbury EM, Pongor S (eds) *Structural biology and functional genomics*, vol 71. Kluwer, Dordrecht. https://doi.org/10.1007/978-94-011-4631-9_3
9. Conn GL, Draper DE (1998) RNA structure. *Curr Opin Struct Biol* 8(3):278–285. [https://doi.org/10.1016/S0959-440X\(98\)80059-6](https://doi.org/10.1016/S0959-440X(98)80059-6)
10. Staple DW, Butcher SE (2005) Pseudoknots: RNA structures with diverse functions. *PLoS Biol* 3(6):e213–e213. <https://doi.org/10.1371/journal.pbio.0030213>
11. Qi X, Zhang F, Su Z, Jiang S, Han D, Ding B, Liu Y, Chiu W, Yin P, Yan H (2018) Programming molecular topologies from single-stranded nucleic acids. *Nat Commun* 9(1):4579. <https://doi.org/10.1038/s41467-018-07039-7>
12. Batey RT, Rambo RP, Doudna JA (1999) Tertiary motifs in RNA structure and folding. *Angew Chem Int Ed* 38(16):2326–2343. [https://doi.org/10.1002/\(SICI\)1521-3773\(19990816\)38:16%3c2326::AID-ANIE2326%3e3.0.CO;2-3](https://doi.org/10.1002/(SICI)1521-3773(19990816)38:16%3c2326::AID-ANIE2326%3e3.0.CO;2-3)
13. Butcher SE, Pyle AM (2011) The molecular interactions that stabilize RNA tertiary structure: RNA motifs, patterns, and networks. *Acc Chem Res* 44(12):1302–1311. <https://doi.org/10.1021/ar200098t>

14. Clark DP, Pazdernik NJ (2016) RNA-based technologies, chapter 5. In: Clark DP, Pazdernik NJ (eds) *Biotechnology*, 2nd edn. Academic Cell, Boston, pp 131–179. <https://doi.org/10.1016/B978-0-12-385015-7.00005-3>
15. Mercer TR, Mattick JS (2013) Structure and function of long noncoding RNAs in epigenetic regulation. *Nat Struct Mol Biol* 20:300. <https://doi.org/10.1038/nsmb.2480>
16. Jaskiewicz L, Filipowicz W (2008) Role of dicer in posttranscriptional RNA silencing. In: Paddison PJ, Vogt PK (eds) *RNA interference*. Springer, Berlin, pp 77–97. https://doi.org/10.1007/978-3-540-75157-1_4
17. Houseley J, Tollervey D (2009) The many pathways of RNA degradation. *Cell* 136(4):763–776. <https://doi.org/10.1016/j.cell.2009.01.019>
18. Tuschl T (2001) RNA interference and small interfering RNAs. *ChemBioChem* 2(4):239–245. [https://doi.org/10.1002/1439-7633\(20010401\)2:4%3c239:AID-CBIC239%3e3.0.CO;2-R](https://doi.org/10.1002/1439-7633(20010401)2:4%3c239:AID-CBIC239%3e3.0.CO;2-R)
19. Ozata DM, Gainetdinov I, Zoch A, O'Carroll D, Zamore PD (2019) PIWI-interacting RNAs: small RNAs with big functions. *Nat Rev Genet* 20(2):89–108. <https://doi.org/10.1038/s41576-018-0073-3>
20. Paul CP, Good PD, Winer I, Engelke DR (2002) Effective expression of small interfering RNA in human cells. *Nat Biotechnol* 20(5):505–508. <https://doi.org/10.1038/nbt0502-505>
21. Aftab MN, He H, Skogerbø G, Chen R (2008) Microarray analysis of ncRNA expression patterns in *Caenorhabditis elegans* after RNAi against snoRNA associated proteins. *BMC Genom* 9(1):278. <https://doi.org/10.1186/1471-2164-9-278>
22. Kiss T (2002) Small nucleolar RNAs: an abundant group of noncoding RNAs with diverse cellular functions. *Cell* 109(2):145–148. [https://doi.org/10.1016/S0092-8674\(02\)00718-3](https://doi.org/10.1016/S0092-8674(02)00718-3)
23. Fang W, Bartel DP (2015) The menu of features that define primary microRNAs and enable de novo design of microRNA genes. *Mol Cell* 60(1):131–145. <https://doi.org/10.1016/j.molcel.2015.08.015>
24. Hammond SM (2006) RNAi, microRNAs, and human disease. *Cancer Chemother Pharmacol* 58(1):63–68. <https://doi.org/10.1007/s00280-006-0318-2>
25. Lee RC, Feinbaum RL, Ambros V (1993) The *C. elegans* heterochronic gene *lin-4* encodes small RNAs with antisense complementarity to *lin-14*. *Cell* 75(5):843–854. [https://doi.org/10.1016/0092-8674\(93\)90529-Y](https://doi.org/10.1016/0092-8674(93)90529-Y)
26. Ganot P, Bortolin M-L, Kiss T (1997) Site-specific pseudouridine formation in preribosomal RNA is guided by small nucleolar RNAs. *Cell* 89(5):799–809. [https://doi.org/10.1016/S0092-8674\(00\)80263-9](https://doi.org/10.1016/S0092-8674(00)80263-9)
27. Kim D, Rossi J (2008) RNAi mechanisms and applications. *Biotechniques* 44(5):613–616. <https://doi.org/10.2144/000112792>
28. Setten RL, Rossi JJ, Han S-p (2019) The current state and future directions of RNAi-based therapeutics. *Nat Rev Drug Discov* 18(6):421–446. <https://doi.org/10.1038/s41573-019-0017-4>
29. Weng Y, Xiao H, Zhang J, Liang X-J, Huang Y (2019) RNAi therapeutic and its innovative biotechnological evolution. *Biotechnol Adv* 37(5):801–825. <https://doi.org/10.1016/j.biotechadv.2019.04.012>
30. Fernandes JCR, Acuña SM, Aoki JI, Floeter-Winter LM, Muxel SM (2019) Long non-coding RNAs in the regulation of gene expression: physiology and disease. *Noncoding RNA* 5(1):17. <https://doi.org/10.3390/nrna5010017>
31. Hsu Patrick D, Lander Eric S, Zhang F (2014) Development and applications of CRISPR-Cas9 for genome engineering. *Cell* 157(6):1262–1278. <https://doi.org/10.1016/j.cell.2014.05.010>
32. Jinek M, Chylinski K, Fonfara I, Hauer M, Doudna JA, Charpentier E (2012) A programmable dual-RNA-guided DNA endonuclease in adaptive bacterial immunity. *Science* 337(6096):816. <https://doi.org/10.1126/science.1225829>
33. Jiang F, Taylor DW, Chen JS, Kornfeld JE, Zhou K, Thompson AJ, Nogales E, Doudna JA (2016) Structures of a CRISPR-Cas9 R-loop complex primed for DNA cleavage. *Science* 351(6275):867. <https://doi.org/10.1126/science.aad8282>
34. Nishimasu H, Ran FA, Hsu Patrick D, Konermann S, Shehata Soraya I, Dohmae N, Ishitani R, Zhang F, Nureki O (2014) Crystal structure of Cas9 in complex with guide RNA and target DNA. *Cell* 156(5):935–949. <https://doi.org/10.1016/j.cell.2014.02.001>
35. Dominguez AA, Lim WA, Qi LS (2015) Beyond editing: repurposing CRISPR-Cas9 for precision genome regulation and interrogation. *Nat Rev Mol Cell Biol* 17:5. <https://doi.org/10.1038/nrm.2015.2>

36. Donohoue PD, Barrangou R, May AP (2018) Advances in industrial biotechnology using CRISPR-Cas systems. *Trends Biotechnol* 36(2):134–146. <https://doi.org/10.1016/j.tibtech.2017.07.007>
37. Guo P (2010) The emerging field of RNA nanotechnology. *Nat Nanotechnol* 5:833. <https://doi.org/10.1038/nnano.2010.231>
38. Li M, Zheng M, Wu S, Tian C, Liu D, Weizmann Y, Jiang W, Wang G, Mao C (2018) In vivo production of RNA nanostructures via programmed folding of single-stranded RNAs. *Nat Commun* 9(1):2196. <https://doi.org/10.1038/s41467-018-04652-4>
39. Grabow WW, Jaeger L (2014) RNA self-assembly and RNA nanotechnology. *Acc Chem Res* 47(6):1871–1880. <https://doi.org/10.1021/ar500076k>
40. Cech TR (2002) Ribozymes, the first 20 years. *Biochem Soc Trans* 30(6):1162. <https://doi.org/10.1042/bst0301162>
41. Cech TR (1990) Self-splicing and enzymatic activity of an intervening sequence RNA from *Tetrahymena*. *Biosci Rep* 10(3):239. <https://doi.org/10.1007/BF01117241>
42. Doudna JA, Lorsch JR (2005) Ribozyme catalysis: not different, just worse. *Nat Struct Mol Biol* 12(5):395–402. <https://doi.org/10.1038/nsmb932>
43. Tanner NK (1999) Ribozymes: the characteristics and properties of catalytic RNAs. *FEMS Microbiol Rev* 23(3):257–275. <https://doi.org/10.1111/j.1574-6976.1999.tb00399.x>
44. Walter NG, Engelke DR (2002) Ribozymes: catalytic RNAs that cut things, make things, and do odd and useful jobs. *Biologist (London)* 49(5):199–203
45. Fedoruk-Wyszomirska A, Szymański M, Głodowicz P, Gabryelska M, Wyszko E, Estrin William J, Barciszewski J (2015) Inhibition of HIV-1 gp41 expression with hammerhead ribozymes. *Biochem J* 471(1):53. <https://doi.org/10.1042/BJ20150398>
46. James HA, Gibson I (1998) The therapeutic potential of ribozymes. *Blood* 91(2):371
47. Fedor MJ (2000) Structure and function of the hairpin ribozyme. *J Mol Biol* 297(2):269–291. <https://doi.org/10.1006/jmbi.2000.3560>
48. Famulok M, Hartig JS, Mayer G (2007) Functional aptamers and aptazymes in biotechnology, diagnostics, and therapy. *Chem Rev* 107(9):3715–3743. <https://doi.org/10.1021/cr0306743>
49. Suslov NB, DasGupta S, Huang H, Fuller JR, Lilley DMJ, Rice PA, Piccirilli JA (2015) Crystal structure of the Varkud satellite ribozyme. *Nat Chem Biol* 11:840. <https://doi.org/10.1038/nchembio.1929>. <https://www.nature.com/articles/nchembio.1929#supplementary-information>
50. Tuerk C, Gold L (1990) Systematic evolution of ligands by exponential enrichment: RNA ligands to bacteriophage T4 DNA polymerase. *Science* 249(4968):505. <https://doi.org/10.1126/science.2200121>
51. Ellington AD, Szostak JW (1990) In vitro selection of RNA molecules that bind specific ligands. *Nature* 346(6287):818–822. <https://doi.org/10.1038/346818a0>
52. Breaker RR, Joyce GF (1994) A DNA enzyme that cleaves RNA. *Chem Biol* 1(4):223–229. [https://doi.org/10.1016/1074-5521\(94\)90014-0](https://doi.org/10.1016/1074-5521(94)90014-0)
53. Cuenoud B, Szostak JW (1995) A DNA metalloenzyme with DNA ligase activity. *Nature* 375(6532):611–614. <https://doi.org/10.1038/375611a0>
54. Burge S, Parkinson GN, Hazel P, Todd AK, Neidle S (2006) Quadruplex DNA: sequence, topology and structure. *Nucleic Acids Res* 34(19):5402–5415. <https://doi.org/10.1093/nar/gkl655>
55. Kwok CK, Merrick CJ (2017) G-Quadruplexes: prediction, characterization, and biological application. *Trends Biotechnol* 35(10):997–1013. <https://doi.org/10.1016/j.tibtech.2017.06.012>
56. Lam EYN, Beraldi D, Tannahill D, Balasubramanian S (2013) G-quadruplex structures are stable and detectable in human genomic DNA. *Nat Commun* 4:1796. <https://doi.org/10.1038/ncomms2792>. <https://www.nature.com/articles/ncomms2792#supplementary-information>
57. Asamitsu S, Obata S, Yu Z, Bando T, Sugiyama H (2019) Recent progress of targeted G-quadruplex-preferred ligands toward cancer therapy. *Molecules* 24(3):429. <https://doi.org/10.3390/molecules24030429>
58. Asamitsu S, Li Y, Bando T, Sugiyama H (2016) Ligand-mediated G-quadruplex induction in a double-stranded DNA context by cyclic imidazole/lysine polyamide. *ChemBioChem* 17(14):1317–1322. <https://doi.org/10.1002/cbic.201600198>
59. Brown RV, Danford FL, Gokhale V, Hurley LH, Brooks TA (2011) Demonstration that drug-targeted down-regulation of MYC in non-Hodgkins lymphoma is directly mediated through the promoter G-quadruplex. *J Biol Chem* 286(47):41018–41027. <https://doi.org/10.1074/jbc.M111.274720>

60. Dutta D, Debnath M, Müller D, Paul R, Das T, Bessi I, Schwalbe H, Dash J (2018) Cell penetrating thiazole peptides inhibit c-MYC expression via site-specific targeting of c-MYC G-quadruplex. *Nucleic Acids Res* 46(11):5355–5365. <https://doi.org/10.1093/nar/gky385>
61. Hu M-H, Wang Y-Q, Yu Z-Y, Hu L-N, Ou T-M, Chen S-B, Huang Z-S, Tan J-H (2018) Discovery of a new four-leaf clover-like ligand as a potent c-MYC transcription inhibitor specifically targeting the promoter G-quadruplex. *J Med Chem* 61(6):2447–2459. <https://doi.org/10.1021/acs.jmedchem.7b01697>
62. Taka T, Joonlasak K, Huang L, Randall Lee T, Chang S-WT, Tuntiwechapikul W (2012) Down-regulation of the human VEGF gene expression by perylene monoimide derivatives. *Bioorg Med Chem Lett* 22(1):518–522. <https://doi.org/10.1016/j.bmcl.2011.10.089>
63. Wu Y, Zan L-P, Wang X-D, Lu Y-J, Ou T-M, Lin J, Huang Z-S, Gu L-Q (2014) Stabilization of VEGF G-quadruplex and inhibition of angiogenesis by quindoline derivatives. *Biochim Biophys Acta* 9:2970–2977. <https://doi.org/10.1016/j.bbagen.2014.06.002>
64. Amato J, Pagano A, Capasso D, Di Gaetano S, Giustiniano M, Novellino E, Randazzo A, Pagano B (2018) Targeting the BCL2 gene promoter G-quadruplex with a new class of furo-pyridazinone-based molecules. *ChemMedChem* 13(5):406–410. <https://doi.org/10.1002/cmdc.201700749>
65. Gu Y, Lin D, Tang Y, Fei X, Wang C, Zhang B, Zhou J (2018) A light-up probe targeting for Bcl-2 2345 G-quadruplex DNA with carbazole TO. *Spectrochim Acta Part A Mol Biomol Spectrosc* 191:180–188. <https://doi.org/10.1016/j.saa.2017.10.012>
66. Bejugam M, Sewitz S, Shirude PS, Rodriguez R, Shahid R, Balasubramanian S (2007) Trisubstituted isoalloxazines as a new class of G-quadruplex binding ligands: small molecule regulation of c-kit oncogene expression. *J Am Chem Soc* 129(43):12926–12927. <https://doi.org/10.1021/ja075881p>
67. Gunaratnam M, Collie GW, Reszka AP, Todd AK, Parkinson GN, Neidle S (2018) A naphthalene diimide G-quadruplex ligand inhibits cell growth and down-regulates BCL-2 expression in an imatinib-resistant gastrointestinal cancer cell line. *Bioorg Med Chem* 26(11):2958–2964. <https://doi.org/10.1016/j.bmc.2018.04.050>
68. McLuckie KIE, Waller ZAE, Sanders DA, Alves D, Rodriguez R, Dash J, McKenzie GJ, Venkitaraman AR, Balasubramanian S (2011) G-quadruplex-binding benzo[a]phenoxazines down-regulate c-KIT expression in human gastric carcinoma cells. *J Am Chem Soc* 133(8):2658–2663. <https://doi.org/10.1021/ja109474c>
69. Głuszyńska A, Juskowiak B, Kuta-Siejkowska M, Hoffmann M, Haider S (2018) Carbazole derivatives' binding to c-KIT G-quadruplex DNA. *Molecules* 23(5):1134. <https://doi.org/10.3390/molecules23051134>
70. Kang H-J, Cui Y, Yin H, Scheid A, Hendricks WPD, Schmidt J, Sekulic A, Kong D, Trent JM, Gokhale V, Mao H, Hurley LH (2016) A pharmacological chaperone molecule induces cancer cell death by restoring tertiary DNA structures in mutant hTERT promoters. *J Am Chem Soc* 138(41):13673–13692. <https://doi.org/10.1021/jacs.6b07598>
71. Lavrado J, Brito H, Borralho PM, Ohnmacht SA, Kim N-S, Leitão C, Pisco S, Gunaratnam M, Rodrigues CMP, Moreira R, Neidle S, Paulo A (2015) KRAS oncogene repression in colon cancer cell lines by G-quadruplex binding indolo[3,2-c]quinolines. *Sci Rep* 5:9696. <https://doi.org/10.1038/srep09696>
72. Cogoi S, Paramasivam M, Filichev V, Géci I, Pedersen EB, Xodo LE (2009) Identification of a new G-quadruplex motif in the KRAS promoter and design of pyrene-modified G4-decoys with antiproliferative activity in pancreatic cancer cells. *J Med Chem* 52(2):564–568. <https://doi.org/10.1021/jm800874t>
73. Li F, Zhou J, Xu M, Yuan G (2018) Exploration of G-quadruplex function in c-Myb gene and its transcriptional regulation by topotecan. *Int J Biol Macromol* 107:1474–1479. <https://doi.org/10.1016/j.ijbiomac.2017.10.010>
74. Schultze P, Macaya RF, Feigon J (1994) Three-dimensional solution structure of the thrombin-binding DNA aptamer d(GTTTGGTGTGGTTGG). *J Mol Biol* 235(5):1532–1547. <https://doi.org/10.1006/jmbi.1994.1105>
75. Travascio P, Li Y, Sen D (1998) DNA-enhanced peroxidase activity of a DNA aptamer–hemin complex. *Chem Biol* 5(9):505–517. [https://doi.org/10.1016/S1074-5521\(98\)90006-0](https://doi.org/10.1016/S1074-5521(98)90006-0)
76. Paige JS, Wu KY, Jaffrey SR (2011) RNA mimics of green fluorescent protein. *Science* 333(6042):642. <https://doi.org/10.1126/science.1207339>

77. Ebrahimi M, Raouf JB, Ojani R (2017) Design of a novel electrochemical biosensor based on intra-molecular G-quadruplex DNA for selective determination of lead(II) ions. *Anal Bioanal Chem* 409(20):4729–4739. <https://doi.org/10.1007/s00216-017-0416-5>
78. Gogichaishvili S, Lomidze L, Kankia B (2014) Quadruplex priming amplification combined with nicking enzyme for diagnostics. *Anal Biochem* 466:44–48. <https://doi.org/10.1016/j.ab.2014.08.025>
79. Taylor A, Joseph A, Okyere R, Gogichaishvili S, Musier-Forsyth K, Kankia B (2013) Isothermal quadruplex priming amplification for DNA-based diagnostics. *Biophys Chem* 171:1–8. <https://doi.org/10.1016/j.bpc.2012.11.001>
80. Gehring K, Leroy JL, Guéron M (1993) A tetrameric DNA structure with protonated cytosine–cytosine base pairs. *Nature* 363(6429):561–565. <https://doi.org/10.1038/363561a0>
81. Wright EP, Huppert JL, Zoë ZAE (2017) Identification of multiple genomic DNA sequences which form i-motif structures at neutral pH. *Nucleic Acids Res*. <https://doi.org/10.1093/nar/gkx090>
82. Abou Assi H, Garavís M, González C, Damha MJ (2018) i-Motif DNA: structural features and significance to cell biology. *Nucleic Acids Res* 46(16):8038–8056. <https://doi.org/10.1093/nar/gky735>
83. Benabou S, Aviñó A, Eritja R, González C, Gargallo R (2014) Fundamental aspects of the nucleic acid i-motif structures. *RSC Adv* 4(51):26956–26980. <https://doi.org/10.1039/c4ra02129k>
84. Gurung SP, Schwarz C, Hall JP, Cardin CJ, Brazier JA (2015) The importance of loop length on the stability of i-motif structures. *Chem Commun* 51(26):5630–5632. <https://doi.org/10.1039/c4cc07279k>
85. Day HA, Pavlou P, Waller ZAE (2014) i-Motif DNA: structure, stability and targeting with ligands. *Bioorg Med Chem* 22(16):4407–4418. <https://doi.org/10.1016/j.bmc.2014.05.047>
86. Zeraati M, Langley DB, Schofield P, Moye AL, Rouet R, Hughes WE, Bryan TM, Dinger ME, Christ D (2018) I-motif DNA structures are formed in the nuclei of human cells. *Nat Chem* 10(6):631–637. <https://doi.org/10.1038/s41557-018-0046-3>
87. Snoussi K, Nonin-Lecomte S, Leroy JL (2001) The RNA i-motif. *J Mol Biol* 309(1):139–153. <https://doi.org/10.1006/jmbi.2001.4618>
88. Sedghi Masoud S, Nagasawa K (2018) i-Motif-binding ligands and their effects on the structure and biological functions of i-motif. *Chem Pharm Bull* 66(12):1091–1103. <https://doi.org/10.1248/cpb.c18-00720>
89. Dexheimer TS, Carey SS, Zuohe S, Gokhale VM, Hu X, Murata LB, Maes EM, Weichsel A, Sun D, Meuillet EJ, Montfort WR, Hurley LH (2009) NM23-H2 may play an indirect role in transcriptional activation of c-myc gene expression but does not cleave the nucleosome hypersensitive element III(1). *Mol Cancer Ther* 8(5):1363–1377. <https://doi.org/10.1158/1535-7163.MCT-08-1093>
90. Zhang XY, Luo HQ, Li NB (2014) Crystal violet as an i-motif structure probe for reversible and label-free pH-driven electrochemical switch. *Anal Biochem* 455:55–59. <https://doi.org/10.1016/j.ab.2014.03.015>
91. Li X, Peng Y, Ren J, Qu X (2006) Carboxyl-modified single-walled carbon nanotubes selectively induce human telomeric i-motif formation. *Proc Natl Acad Sci* 103(52):19658. <https://doi.org/10.1073/pnas.0607245103>
92. Chen X, Zhou X, Han T, Wu J, Zhang J, Guo S (2013) Stabilization and induction of oligonucleotide i-motif structure via graphene quantum dots. *ACS Nano* 7(1):531–537. <https://doi.org/10.1021/nm304673a>
93. Kendrick S, Muranyi A, Gokhale V, Hurley LH, Rimsza LM (2017) Simultaneous drug targeting of the promoter MYC G-quadruplex and BCL2 i-motif in diffuse large B-cell lymphoma delays tumor growth. *J Med Chem* 60(15):6587–6597. <https://doi.org/10.1021/acs.jmedchem.7b00298>
94. Modi S, Swetha MG, Goswami D, Gupta GD, Mayor S, Krishnan Y (2009) A DNA nanomachine that maps spatial and temporal pH changes inside living cells. *Nat Nanotechnol* 4(5):325–330. <https://doi.org/10.1038/nnano.2009.83>
95. Zhao Y, Cao L, Ouyang J, Wang M, Wang K, Xia X-H (2013) Reversible plasmonic probe sensitive for pH in micro/nanospaces based on i-motif-modulated morpholino-gold nanoparticle assembly. *Anal Chem* 85(2):1053–1057. <https://doi.org/10.1021/ac302915a>
96. Dong Y, Yang Z, Liu D (2014) DNA nanotechnology based on i-motif structures. *Acc Chem Res* 47(6):1853–1860. <https://doi.org/10.1021/ar500073a>
97. Chen C, Pu F, Huang Z, Liu Z, Ren J, Qu X (2010) Stimuli-responsive controlled-release system using quadruplex DNA-capped silica nanocontainers. *Nucleic Acids Res* 39(4):1638–1644. <https://doi.org/10.1093/nar/gkq893>

98. Ghodke HB, Krishnan R, Vignesh K, Kumar GVP, Narayana C, Krishnan Y (2007) The I-tetraplex building block: rational design and controlled fabrication of robust 1D DNA scaffolds through non-Watson–Crick interactions. *Angew Chem Int Ed* 46(15):2646–2649. <https://doi.org/10.1002/anie.200604461>
99. Yang Y, Zhou C, Zhang T, Cheng E, Yang Z, Liu D (2012) DNA pillars constructed from an i-motif stem and duplex branches. *Small* 8(4):552–556. <https://doi.org/10.1002/sml.201102061>
100. Cheng E, Xing Y, Chen P, Yang Y, Sun Y, Zhou D, Xu L, Fan Q, Liu D (2009) A pH-triggered, fast-responding DNA hydrogel. *Angew Chem Int Ed* 48(41):7660–7663. <https://doi.org/10.1002/anie.200902538>
101. Bruyere A, Wantroba M, Flasincki S, Dzianott A, Bujarski JJ (2000) Frequent homologous recombination events between molecules of one RNA component in a multipartite RNA virus. *J Virol* 74(9):4214–4219. <https://doi.org/10.1128/jvi.74.9.4214-4219.2000>
102. Seeman NC (1982) Nucleic acid junctions and lattices. *J Theor Biol* 99(2):237–247. [https://doi.org/10.1016/0022-5193\(82\)90002-9](https://doi.org/10.1016/0022-5193(82)90002-9)
103. Kallenbach NR, Ma R-I, Seeman NC (1983) An immobile nucleic acid junction constructed from oligonucleotides. *Nature* 305(5937):829–831. <https://doi.org/10.1038/305829a0>
104. Ma R-I, Kallenbach NR, Sheardy RD, Petrillo ML, Seeman NC (1986) Three-arm nucleic acid junctions are flexible. *Nucleic Acids Res* 14(24):9745–9753. <https://doi.org/10.1093/nar/14.24.9745>
105. Wang X, Seeman NC (2007) Assembly and characterization of 8-arm and 12-arm DNA branched junctions. *J Am Chem Soc* 129(26):8169–8176. <https://doi.org/10.1021/ja0693441>
106. Wang Y, Mueller JE, Kemper B, Seeman NC (1991) Assembly and characterization of five-arm and six-arm DNA branched junctions. *Biochemistry* 30(23):5667–5674. <https://doi.org/10.1021/bi00237a005>
107. Lilley DMJ (2000) Structures of helical junctions in nucleic acids. *Q Rev Biophys* 33(2):109–159. <https://doi.org/10.1017/s0033583500003590>
108. Ariyoshi M, Vassilyev DG, Iwasaki H, Nakamura H, Shinagawa H, Morikawa K (1994) Atomic structure of the RuvC resolvase: a Holliday junction-specific endonuclease from *E. coli*. *Cell* 78(6):1063–1072. [https://doi.org/10.1016/0092-8674\(94\)90280-1](https://doi.org/10.1016/0092-8674(94)90280-1)
109. Gopaul DN, Guo F, Van Duyne GD (1998) Structure of the Holliday junction intermediate in Cre–loxP site-specific recombination. *EMBO J* 17(14):4175–4187. <https://doi.org/10.1093/emboj/17.14.4175>
110. Seeman NC (2010) Nanomaterials based on DNA. *Annu Rev Biochem* 79:65–87. <https://doi.org/10.1146/annurev-biochem-060308-102244>
111. Um SH, Lee JB, Park N, Kwon SY, Umbach CC, Luo D (2006) Enzyme-catalysed assembly of DNA hydrogel. *Nat Mater* 5(10):797–801. <https://doi.org/10.1038/nmat1741>
112. Wang J, Chao J, Liu H, Su S, Wang L, Huang W, Willner I, Fan C (2017) Clamped hybridization chain reactions for the self-assembly of patterned DNA hydrogels. *Angew Chem Int Ed* 56(8):2171–2175. <https://doi.org/10.1002/anie.201610125>
113. Gačanin J, Synatschke CV, Weil T (2019) Biomedical applications of DNA-based hydrogels. *Adv Funct Mater*. <https://doi.org/10.1002/adfm.201906253>
114. Wang D, Hu Y, Liu P, Luo D (2017) Bioresponsive DNA hydrogels: beyond the conventional stimuli responsiveness. *Acc Chem Res* 50(4):733–739. <https://doi.org/10.1021/acs.accounts.6b00581>
115. Shen Z, Yan H, Wang T, Seeman NC (2004) Paranemic crossover DNA: a generalized Holliday structure with applications in nanotechnology. *J Am Chem Soc* 126(6):1666–1674. <https://doi.org/10.1021/ja038381e>
116. Wang X, Chandrasekaran AR, Shen Z, Ohayon YP, Wang T, Kizer ME, Sha R, Mao C, Yan H, Zhang X, Liao S, Ding B, Chakraborty B, Jonoska N, Niu D, Gu H, Chao J, Gao X, Li Y, Ciengshin T, Seeman NC (2019) Paranemic crossover DNA: there and back again. *Chem Rev* 119(10):6273–6289. <https://doi.org/10.1021/acs.chemrev.8b00207>
117. Rothmund PWK (2006) Folding DNA to create nanoscale shapes and patterns. *Nature* 440(7082):297–302. <https://doi.org/10.1038/nature04586>
118. Ma Z, Kawai K, Hirai Y, Tsuchiya T, Tabata O (2017) Tuning porosity and radial mechanical properties of DNA origami nanotubes via crossover design. *Jpn J Appl Phys* 56(6S1):06GJ02. <https://doi.org/10.7567/jjap.56.06gj02>
119. Ke Y, Ong LL, Shih WM, Yin P (2012) Three-dimensional structures self-assembled from DNA bricks. *Science* 338(6111):1177. <https://doi.org/10.1126/science.1227268>

120. Wei B, Dai M, Yin P (2012) Complex shapes self-assembled from single-stranded DNA tiles. *Nature* 485(7400):623–626. <https://doi.org/10.1038/nature11075>
121. Wang P, Meyer TA, Pan V, Dutta PK, Ke Y (2017) The beauty and utility of DNA origami. *Chem* 2(3):359–382. <https://doi.org/10.1016/j.chempr.2017.02.009>
122. Linko V, Erikäinen M, Kostianinen MA (2015) A modular DNA origami-based enzyme cascade nanoreactor. *Chem Commun* 51(25):5351–5354. <https://doi.org/10.1039/C4CC08472A>
123. Rajendran A, Endo M, Sugiyama H (2012) Single-molecule analysis using DNA origami. *Angew Chem Int Ed* 51(4):874–890. <https://doi.org/10.1002/anie.201102113>
124. Hu Q, Li H, Wang L, Gu H, Fan C (2019) DNA nanotechnology-enabled drug delivery systems. *Chem Rev* 119(10):6459–6506. <https://doi.org/10.1021/acs.chemrev.7b00663>
125. Ohno H, Akamine S, Saito H (2019) RNA nanostructures and scaffolds for biotechnology applications. *Curr Opin Biotechnol* 58:53–61. <https://doi.org/10.1016/j.copbio.2018.11.006>
126. Geary C, Rothmund PWK, Andersen ES (2014) A single-stranded architecture for cotranscriptional folding of RNA nanostructures. *Science* 345(6198):799. <https://doi.org/10.1126/science.1253920>
127. Chandrasekaran AR, Anderson N, Kizer M, Halvorsen K, Wang X (2016) Beyond the fold: emerging biological applications of DNA origami. *ChemBioChem* 17(12):1081–1089. <https://doi.org/10.1002/cbic.201600038>
128. Albinsson B, Hannestad JK, Börjesson K (2012) Functionalized DNA nanostructures for light harvesting and charge separation. *Coord Chem Rev* 256(21):2399–2413. <https://doi.org/10.1016/j.ccr.2012.02.024>
129. Anderson NT, Dinolfo PH, Wang X (2018) Synthesis and characterization of porphyrin–DNA constructs for the self-assembly of modular energy transfer arrays. *J Mater Chem C* 6(10):2452–2459. <https://doi.org/10.1039/C7TC05272C>
130. Anderson NT, Ren S, Chao J, Dinolfo PH, Wang X (2019) Exploiting plasmon-mediated energy transfer to enhance end-to-end efficiency in a DNA origami energy transfer array. *ACS Appl Nano Mater* 2(9):5563–5572. <https://doi.org/10.1021/acsanm.9b01137>
131. Grossi G, Jaekel A, Andersen ES, Saccà B (2017) Enzyme-functionalized DNA nanostructures as tools for organizing and controlling enzymatic reactions. *MRS Bull* 42(12):920–924. <https://doi.org/10.1557/mrs.2017.269>
132. Fu J, Li T (2017) Spatial organization of enzyme cascade on a DNA origami nanostructure. In: Ke Y, Wang P (eds) *3D DNA nanostructure: methods and protocols*. Springer, New York, pp 153–164. https://doi.org/10.1007/978-1-4939-6454-3_11
133. Xin L, Zhou C, Yang Z, Liu D (2013) Regulation of an enzyme cascade reaction by a DNA machine. *Small* 9(18):3088–3091. <https://doi.org/10.1002/smll.201300019>
134. Krishnan S, Ziegler D, Arnaut V, Martin TG, Kapsner K, Henneberg K, Bausch AR, Dietz H, Simmel FC (2016) Molecular transport through large-diameter DNA nanopores. *Nat Commun* 7(1):12787. <https://doi.org/10.1038/ncomms12787>
135. Wang D, Zhang Y, Wang M, Dong Y, Zhou C, Isbell MA, Yang Z, Liu H, Liu D (2016) A switchable DNA origami nanochannel for regulating molecular transport at the nanometer scale. *Nanoscale* 8(7):3944–3948. <https://doi.org/10.1039/C5NR08206D>
136. Zhang Y, Chao J, Liu H, Wang F, Su S, Liu B, Zhang L, Shi J, Wang L, Huang W, Wang L, Fan C (2016) Transfer of two-dimensional oligonucleotide patterns onto stereocontrolled plasmonic nanostructures through DNA-origami-based nanoimprinting lithography. *Angew Chem Int Ed* 55(28):8036–8040. <https://doi.org/10.1002/anie.201512022>
137. Selnihhin D, Sparvath SM, Preus S, Birkedal V, Andersen ES (2018) Multifluorophore DNA origami beacon as a biosensing platform. *ACS Nano* 12(6):5699–5708. <https://doi.org/10.1021/acsnano.8b01510>
138. Tinnefeld P, Acuna GP, Wei Q, Ozcan A, Vietz C, Lalkens B, Trofymchuk K, Close CM, Inan H, Ochmann S, Grabenhorst L, Glembockyte V (2019) DNA origami nanotools for single-molecule biosensing and superresolution microscopy. In: *Biophotonics congress: optics in the life sciences congress 2019 (BODA,BRAIN,NTM,OMA,OMP)*, Tucson, 2019/04/15. OSA Technical Digest. Optical Society of America, p AW5E.5. <https://doi.org/10.1364/oma.2019.aw5e.5>
139. Kwon PS, Ren S, Kwon S-J, Kizer ME, Kuo L, Xie M, Zhu D, Zhou F, Zhang F, Kim D, Fraser K, Kramer LD, Seeman NC, Dordick JS, Linhardt RJ, Chao J, Wang X (2020) Designer DNA architecture offers precise and multivalent spatial pattern-recognition for viral sensing and inhibition. *Nat Chem* 12(1):26–35. <https://doi.org/10.1038/s41557-019-0369-8>

140. Fang W, Jia S, Chao J, Wang L, Duan X, Liu H, Li Q, Zuo X, Wang L, Wang L, Liu N, Fan C (2019) Quantizing single-molecule surface-enhanced Raman scattering with DNA origami meta-molecules. *Sci Adv* 5(9):eaau4506. <https://doi.org/10.1126/sciadv.aau4506>
141. Jasinski D, Haque F, Binzel DW, Guo P (2017) Advancement of the emerging field of RNA nano-technology. *ACS Nano* 11(2):1142–1164. <https://doi.org/10.1021/acs.nano.6b05737>
142. Leontis NB, Westhof E (2014) Self-assembled RNA nanostructures. *Science* 345(6198):732. <https://doi.org/10.1126/science.1257989>
143. Han D, Qi X, Myhrvold C, Wang B, Dai M, Jiang S, Bates M, Liu Y, An B, Zhang F, Yan H, Yin P (2017) Single-stranded DNA and RNA origami. *Science* 358(6369):eaao2648. <https://doi.org/10.1126/science.aao2648>
144. Praetorius F, Dietz H (2017) Self-assembly of genetically encoded DNA–protein hybrid nanoscale shapes. *Science* 355(6331):eaam5488. <https://doi.org/10.1126/science.aam5488>

Publisher's Note Springer Nature remains neutral with regard to jurisdictional claims in published maps and institutional affiliations.

Affiliations

Jinwei Duan^{1,2,3} · Xing Wang^{2,3,4} · Megan E. Kizer^{5,6}

¹ Department of Chemistry and Materials Science, College of Sciences, Chang'an University, Xi'an 710064, Shaanxi, People's Republic of China

² Department of Chemistry, University of Illinois at Urbana-Champaign, Urbana, IL 61801, USA

³ Holonyak Micro and Nanotechnology Laboratory, University of Illinois at Urbana-Champaign, Urbana, IL 61801, USA

⁴ Carl R. Woese Institute for Genomic Biology, University of Illinois at Urbana-Champaign, Urbana, IL 61801, USA

⁵ Department of Biology, Massachusetts Institute of Technology, Cambridge, MA 02139, USA

⁶ Department of Chemistry, Massachusetts Institute of Technology, Cambridge, MA 02139, USA



DNA-Driven Nanoparticle Assemblies for Biosensing and Bioimaging

Yuan Zhao^{1,2} · Lixia Shi¹ · Hua Kuang² · Chuanlai Xu²

Received: 14 October 2019 / Accepted: 18 January 2020 / Published online: 3 February 2020
© Springer Nature Switzerland AG 2020

Abstract

DNA molecules with superior flexibility, affinity and programmability have garnered considerable attention for the controllable assembly of nanoparticles (NPs). By controlling the density, length and sequences of DNA on NPs, the configuration of NP assemblies can be rationally designed. The specific recognition of DNA enables changes to be made to the spatial structures of NP assemblies, resulting in differences in tailorable optical signals. Comprehensive information on the fabrication of DNA-driven NP assemblies would be beneficial for their application in biosensing and bioimaging. This review analyzes the progress of DNA-driven NP assemblies, and discusses the tunable configurations determined by the structural parameters of DNA skeletons. The collective optical properties, such as chirality, fluorescence and surface enhanced Raman resonance (SERS), etc., of DNA-driven NP assemblies are explored, and engineered tailorable optical properties of these spatial structures are achieved. We discuss the development of DNA-directed NP assemblies for the quantification of DNA, toxins, and heavy metal ions, and demonstrate their potential application in the biosensing and bioimaging of tumor markers, RNA, living metal ions and phototherapeutics. We highlight possible challenges in the development of DNA-driven NP assemblies, and further direct potential prospects in the practical applications of macroscopical materials and photonic devices.

Keywords DNA · Nanoparticles · Assembly · Optical properties · Biosensing · Bioimaging

Chapter 9 was originally published as Zhao, Y., Shi, L., Kuang, H. & Xu, C. Topics in Current Chemistry (2020) 378: 18. <https://doi.org/10.1007/s41061-020-0282-z>.

✉ Yuan Zhao
zhaoyuan@jiangnan.edu.cn

¹ Key Laboratory of Synthetic and Biological Colloids, Ministry of Education, School of Chemical and Material Engineering, Jiangnan University, 214122 Wuxi, Jiangsu, China

² International Joint Research Laboratory for Biointerface and Biodetection, State Key Lab of Food Science and Technology, Jiangnan University, 214122 Wuxi, Jiangsu, China

1 Introduction

Biomolecules possess unique biological activity and specific recognition ability, and show potential applications for the modification of building blocks in the fabrication of functional nanomaterials [1–5]. In particular, nucleic acids, comprising DNA and RNA, possess programmed Watson–Crick base pairing and have become alternative candidates for the controllable functionalization and assembly of nanoparticles (NPs) [6–9]. Through designing the amount and length of DNA on the designed sites of each NP, NPs can be orderly arranged on hybridized DNA shapes and assembled into desired spatial configuration [10].

When NPs are in close proximity to each other, their respective surfaces are plasma coupled, resulting in a high electric field. Usually, these high electromagnetic (EM) fields are located in the gaps between NPs, and areas containing high electric fields are called hot spots. Acting as a linker, DNA can adjust the distances between NPs for the generation of strong EM fields, which would generate amplified optical properties, involving surface enhanced Raman scattering (SERS), chirality, photofluorescence enhancement, plasmon-enhanced absorption, and so on. These unique properties have led DNA-driven NP assemblies to be widely used in biosensing and bioimaging. Specific recognition of targets by DNA, or sequence-specific hybridization between base pairs induces disassembly of nanomaterials, and these changed structures affect the resulting optical properties [1]. There is a close relationship between the optical signals of assemblies and the concentration of targets. Sensitive and specific biosensors are being developed for various applications.

In this article, we review recent progress in the field of DNA-driven NP assemblies, and explore the engineered optical properties of these spatial structures with the aid of DNA. We also discuss the development of biosensors for the detection of traces of hazardous substrates in food and in the environment, and demonstrate the potential applications of biosensing and bioimaging to the sensitive, accurate and multiplex monitoring of analytes in the fields of medical science. Finally, we highlight possible challenges in the development of DNA-programmed NP assemblies, and further direct the potential prospects of DNA-based nanoassemblies for practical applications in macroscopic materials and photonic devices.

2 DNA-Programmed NP Assemblies

DNA molecules can program the synthesis, modification and assembly of NPs, and NPs can also be used as probes to explore the specific recognition of DNA molecules. If different NPs can be modified and assembled by DNA, NP assemblies will show synergetic and collective optical performances. In the process of programming NP assemblies, DNA molecules have excellent molecular recognition function, which make the assembly process highly selective. The most

important challenge to overcome in achieving this goal is how to precisely control the modified number of DNA and binding sites on NPs. Many researchers have researched this issue in depth. Here, we will discuss DNA programmed adaptable and switchable NP modification and self-assemblies, involving plasmonic NPs, fluorescence NPs, and carbon nanomaterial.

2.1 Plasmonic Metal NP Assemblies

Plasmonic metal NPs refer mainly to Au NPs and Ag NPs. By controlling the sizes, morphology and structures of plasmonic NPs, localized surface plasmon resonance (LSPR) peaks, which have extensive application prospects in biosensing and bio-imaging, can be adjusted. Various functional groups, such as $-SH$, $-NH_2$, $-COOH$, $-CHO$, can be modified on the end of DNA. Nowadays, the method used most widely is to modify the DNA with $-SH$ functional groups on the surface of plasmonic metal NPs, and ensure close interaction between DNA and NPs through covalent metal–SH bonds.

Assemblies were constructed by simple complementary base pairing between ssDNA modified NPs. For example, Chou et al. [7] achieved different sized Au NPs to form multilayer satellite-like assemblies using a long mother chain, and realized the transformation of Au NPs from a linear arrangement to spatial divergence. They used a core-satellite framework to construct a DNA-assembled superstructure in

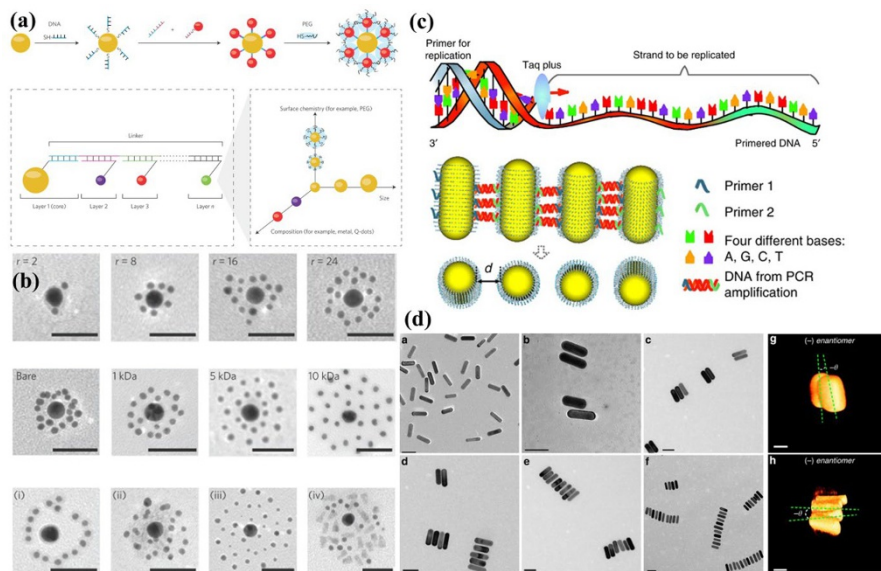


Fig. 1 **a, b** Schematic illustration and transmission electron microscopy (TEM) images of DNA programmed multilayered Au nanoparticle (NP) core-satellite assemblies. **c, d** Schematic illustration and TEM images of side-by-side Au nanorod (NR) assemblies prepared by polymerase chain reaction (PCR). Reprinted with permission from Refs. [7, 14]

which multilayered satellite-like NPs were arranged around central NPs (Fig. 1a). The total number of unique superstructures increased exponentially with increasing number of core–satellite layers and NP designs (Fig. 1b). The superstructures reduce retention and exhibit potential applications in tumor accumulation and whole-body elimination. Recently, Kuang and colleagues reviewed various plasmonic NP assemblies by using DNA as linkers [8]. By adjusting the numbers of DNA modified on NPs and designing the hybridized configuration, the geometry of assemblies can be controlled to form dimers, trimers, pyramids, core-satellite, chains, etc. The unique dipolar coupling between plasmonic NPs enables the enhancement of EM fields, including SERS and chirality, for the amplification of optical properties. The EM intensity of plasmonic NP assemblies is affected not only by the structural parameters of NPs (sizes, morphology, composition), but is also largely influenced by spatial order and interparticle gaps. Interparticle gaps can be controlled by adjusting the length of dsDNA and designing a Y-shaped DNA duplex, etc. [11]. Polymerase chain reaction (PCR) has been proposed for the programmable fabrication of NP assemblies by the modification of primers on NPs or nanorods (NRs) [12–14]. The number of primers on NPs can be adjusted to one for the production of dimers or two for the fabrication of chains [13, 15]. The yields of assemblies increased with increasing numbers of PCR cycles from 1 to 20 [13]. The located modification of primers on the side of anisotropic Au NRs enabled the assembly of side-by-side Au NR nanostructures (Fig. 1c) [16]. PCR cycles adjusted the number of Au NRs and the length of assemblies (Fig. 1d). By asymmetric modification of forward primers and reverse primers on different NPs, superstructures were obtained, becoming more complex with increasing PCR cycles for the generation of chiral signals [17]. The interparticle gaps of assemblies were optimized easily by designing the amplification length of primers. Consider the sensitive chiral signals of assemblies and the exponential amplification of PCR, PCR-driven assemblies showed potential applications for ultrasensitive DNA detection.

However, dsDNA was not rigid enough, the angles were still uncontrollable. DNA origami technology can accurately assemble NPs into multi-dimensional nanostructures, because of its controllable and programmable characteristics [18]. DNA origami could not only assemble Au NPs efficiently into the designed configuration, but also control accurately the position of NPs and the relative displacement between NPs. Au NS dimers were assembled on the surface of DNA origami, and the interparticle distances were controlled to be 7 nm and 13 nm. The SERS enhancement factors of Texas red were 2×10^{10} and 8×10^9 , respectively. This was beneficial for SERS-signal-dependent single-molecule detection [19]. DNA polyhedral wireframe nanocages were constructed and used as templates for the encapsulation of NPs into the internal space [20]. DNA nanostructures can control the relative position of Au NPs. By changing the configuration of DNA origami nanocages and designing the binding sites, molecule-like NP assemblies were accessible, such as CH_4 , SF_6 , $\text{W}(\text{CH}_3)_6$ and C_2H_6 (Fig. 2a–f) [20]. DNA tube structures were constructed by DNA origami, and regular Au NPs were assembled on them. Octahedron, decahedral and polyhedral DNA origami frames were constructed and NPs were assembled at each vertex [20, 21]. By adjusting the composition and arrangement of plasmonic NPs, the symmetry of assemblies could be programmed for the

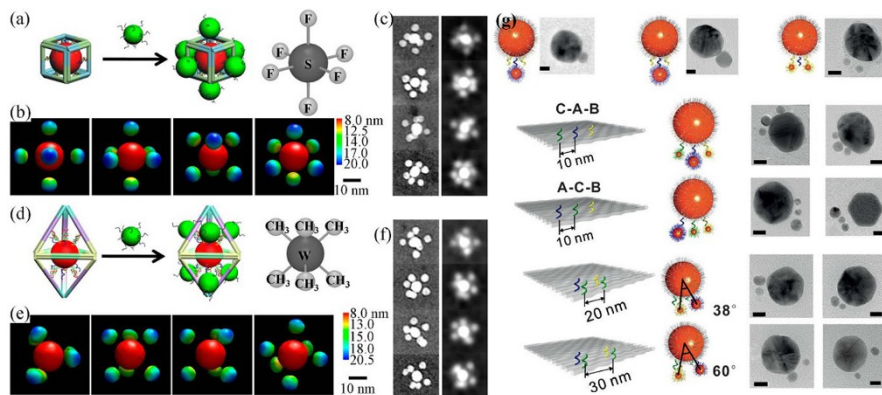


Fig. 2 Molecule-like NP assemblies by DNA origami nanocages. **a–c** SF_6 , **d–f** $\text{W}(\text{CH}_3)_6$, **g** DNA-origami-driven Au NP modification and assembly. Reprinted with permission from Refs. [20, 22]

generation of active chiroplasmonic properties. Interestingly, DNA origami enabled the precise modification of DNA on Au NPs with controlled number, angles and orientation. Fan groups placed DNA “set strands” on the predefined positions of DNA origami. By controlling the numbers, sequences and position of DNA “set strands”, DNA–Au NPs conjugations were obtained for the next assembly. In this way, Au NP heterodimers, trimers and tetramers were obtained (Fig. 2g). The angles between Au NPs can be regulated by alteration of the distance between DNA strands [22]. However, the commonly used plasmonic metal NPs were limited to expensive and unsustainable noble metal NPs, involving Au and Ag. It is necessary to explore cheap and abundant plasmonic metal NPs (such as Al, Cu) and tune the LSPR from ultraviolet (UV) to the near infrared (NIR) region by adjusting the sizes and shapes [23]. Suitable approaches should be further proposed for the efficient modification of DNA, and the optical activities of these assemblies need to be explored.

2.2 Fluorescent NP Assemblies

Fluorescent NPs exhibit unique fluorescent signals, long fluorescence lifetime and adjustable emission wavelengths. The fluorescence signals can be quenched due to the fluorescent resonance energy transfer (FRET) process, and amplified greatly due to plasmon resonance enhancement. Fluorescent NPs represent alternative candidates to replace fluorescent dyes and proteins for biosensing and bioimaging. Several kinds of fluorescent NPs have been fabricated and possess distinct fluorescence properties, including quantum dots (QDs), upconversion NPs (UCNPs), long-persistence NPs (PLNPs), carbon dots (CDs) and so on. In particular, QDs are made of semiconductor materials containing metallic elements such as Cd or Zn, and can be modified by SH–DNA through the formation of metal–SH covalent bonds. DNA binding sites on the surface of QDs can be controlled to between one and five using mercaptopropionic acid as a co-ligand to make the remaining sites passive [24]. DNA-programmed QD assemblies

were fabricated by using different QDs. Energy transfer occurred between various colored QDs at optimized interparticle distances by controlling the length of dsDNA and changing the dielectric environment around assemblies (Fig. 3a). This could pave the way for ordered fabrication of QDs with nanometer precision, which is another unachieved goal of nanotechnology.

The small sizes of QDs limit the purification of high-yield QDs assemblies. QDs still cannot be assembled at specific locations to precisely control sites and angles in DNA nanostructures. The assembly of QDs with metal NPs would increase the yield of assemblies and generated distinct optical properties owing to dipole–metal interactions. Plasmonic metal NPs featured with unique LSPR properties had a significant effect on the fluorescent activity of QDs. QDs are applied widely for the fabrication of plasmonic metal NP–QD hybrid assemblies using DNA as linkers. The density of DNA on Au NPs could be controlled to ~ 0.28 DNA per nm^2 , and about 35–40 DNA strands were modified on the surface of Au NPs [25]. QDs were assembled around Au NPs, and showed reduced luminescence lifetimes. About 63% of energy was transferred from QDs to Au NPs (Fig. 3b). By designing the DNA skeleton, plasmonic metal NP–QD hybrid assemblies were fabricated [26], including Au NP–QD dimers, Au NP–QD

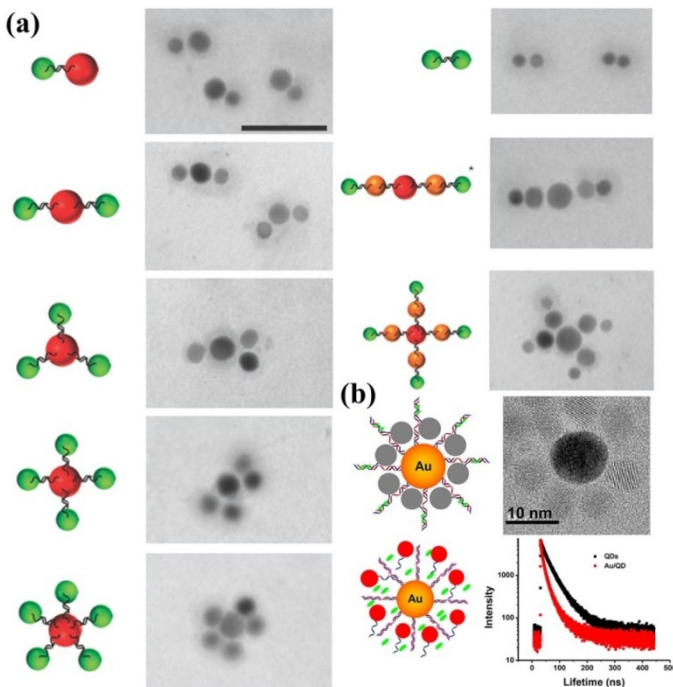


Fig. 3 a Schematic illustration and TEM images of different colored quantum dots (QDs) assembled by DNA. b, c Schematic illustration and TEM images of DNA driven Au NP-QD core-satellite assemblies and the fluorescence lifetimes of QDs. Reprinted with permission from Refs. [24, 25]

pyramids, Au NP–Ag NP–QD pyramids, Ag NP–QD dimers, etc. The chiral configuration of the DNA skeleton enabled NPs and QDs to locate at the designed position, which generated unique chiral activities.

In comparison to downconversion luminescence, upconversion luminescence is caused by continuous absorption of photons, and the emission wavelength is smaller than the excitation wavelength, which would cause little damage to biological systems [27]. However, UCNPs were poorly dispersed and insoluble in water systems. In order to expand the bioapplications of UCNPs, their surface modification and functionalization is particularly important but not changes the fluorescence properties. For example, oleic-acid-coated UCNPs were encapsulated by a polyacrylic acid (PAA) polymer shell by ligand exchanges [28, 29], and DNA molecules with amino groups were modified on the surface of UCNPs. In addition to polymers, silica shells are often used for UCNP surface modification and subsequent conjugate modification [30]. Although these conjugation methods have some advantages, DNA could not directly bind to UCNPs. A simple strategy was proposed to prepare water-soluble DNA–UCNPs [31]. DNA molecules replaced the oleic acid on UCNPs through a ligand exchange process.

DNA- or RNA-modified UCNPs can be used for the assembly with plasmonic NPs. Plasmonic NP–UCNP assemblies exhibited tailorable fluorescence properties and unique chiral activities, and could serve as phototherapy agents for bioapplications. The fluorescence of UCNPs could be quenched or enhanced in the presence of plasmonic NPs at optimized gaps by adjusting the length of dsDNA or designing the hybridized configurations of dsDNA. For example, NaGdF₄:Yb, Er UCNPs assembled with Au NPs by designing a DNA pyramid skeleton exhibited quenched fluorescence (Fig. 4a) [32]. The special DNA pyramids enabled the precise arrangements of NPs to show obvious chiral signals. UCNPs were assembled with Au NPs or Au NR dimers by designing DNA pyramid skeletons and core-satellite structures,

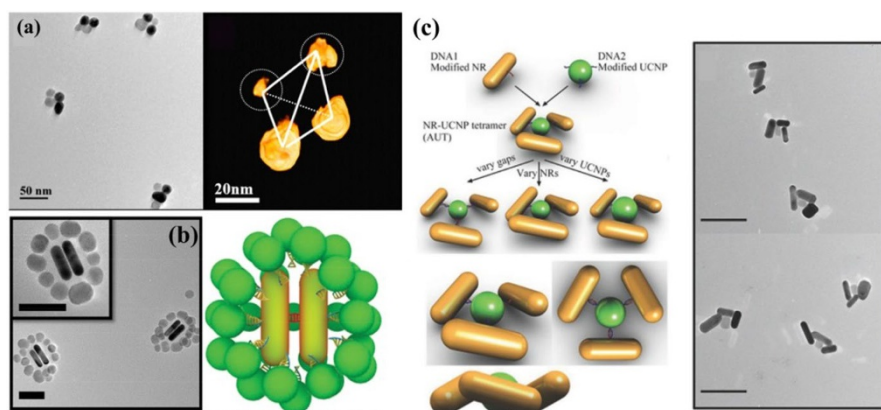


Fig. 4 a TEM images and tomography of DNA-engineered Au NP–upconversion (UC)NP pyramids. b Schematic illustration and TEM images of Au NR dimer–UCNP core-satellite assemblies. c Schematic illustration and TEM images of propeller-like Au NR–UCNP assemblies. Reprinted with permission from Refs. [32, 36, 37]

and exhibited quenched fluorescence (Fig. 4b) [33–36]. By adjusting the length of dsDNA between UCNPs and Au NRs, the fluorescence signals of UCNPs can also be greatly enhanced. DNA-driven propeller-like Au NR-UCNP assemblies showed decreased fluorescence signals when 11 and 18 bp DNA were used (Fig. 4c), but exhibited increased fluorescence intensity by using 24 bp, 30 bp, or 36 bp DNA as linkers [37]. The propeller-like configuration with varied gaps also induced shifts and amplification of the chiral signals. Despite numerous reports of DNA programmed fluorescent NP assemblies, each step of modification or the introduction of ligands may lead to changes in surface charges, which may induce aggregation of assemblies. The stability of these assemblies is still a main concern in complex physiologically relevant environments for the practical bioapplications. Besides QDs and UCNPs, other kinds of fluorescent NPs involving PLNPs and perovskite NPs have also been reported, and showed excellent fluorescence properties. The fluorescence properties of these NPs included assemblies that should be further studied for bioapplications.

2.3 Functional Carbon Material Assemblies

Carbon, a non-metallic element, participates in bonding in the form of sp , sp^2 , sp^3 and other hybrids, forming a large number of materials with peculiar structures and properties. The most representative carbon nanomaterials are graphene/graphene oxide (GO), CDs, graphene QDs (GQDs), and carbon nanotubes (CNTs), etc. Understanding the interaction between DNA molecules and carbon materials is particularly important when constructing functional carbon material assemblies.

The high density of π -electron-enabled carbon materials makes them alternative candidates for the attachment of ssDNA via π - π stacking interactions and hydrogen bonding [38]. However, dsDNA has a negatively charged phosphate backbone that would hinder the interactive force between nucleobases and carbon materials (Fig. 5a) [39]. The weak interaction enabled dsDNA-functionalized GO sheets to be in a solution state. By utilizing the transformation of dsDNA to ssDNA at 90 °C for 5 min, adjacent GO sheets were bridged by ssDNA via strong noncovalent interactions, resulting in the formation of multifunctional hydrogels [40]. ssDNA has become an efficient linker for the self-assembly of carbon materials. For example, FAM and Texas red functionalized ssDNA as well as Rox modified aptamers were assembled with graphene [39, 41]. ssDNA modified Au NPs were assembled with GO sheets (Fig. 5b) [42]. Aptamer-modified Au@gap@AgAu NPs and Ag/CdO NPs were assembled with GO sheets (Fig. 5c) [43, 44]. GO sheets exhibited efficient fluorescence quenching ability and could quench the fluorescence of fluorophores and fluorescent NPs due to the FRET process. DNA-driven fluorescent NP-GO sheet assemblies could be used for the detection of changes in fluorescence signals. GO not only possess fluorescence quench ability, but also exhibit unique Raman characteristic peaks, which could be applied to the fabrication of Raman sensors. Importantly, intrinsic Raman signals could be further enhanced in the presence of plasmonic NPs.

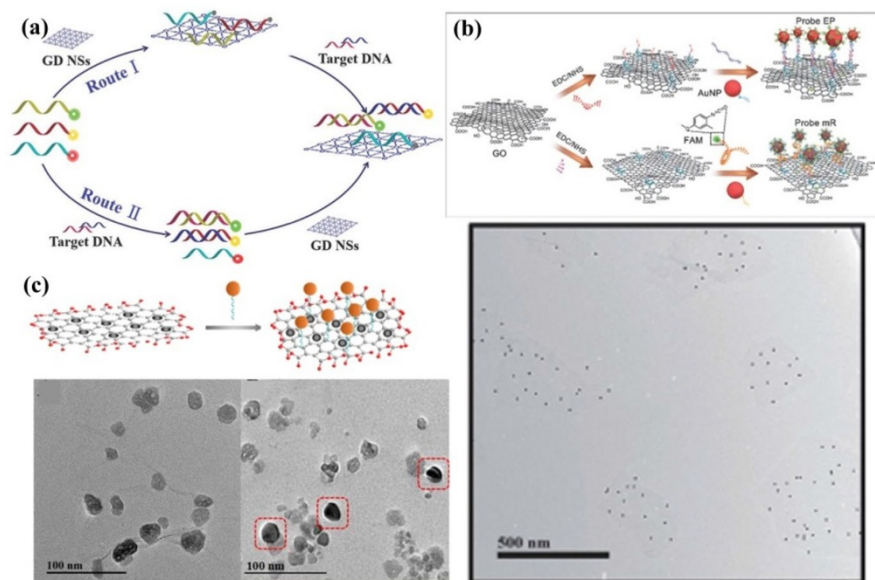


Fig. 5 **a** Graphdiyne (GD) based multiple DNA detection. **b** Schematic illustration and TEM images of graphene oxide (GO)–Au NP assemblies. **c** Schematic illustration and TEM images of GO–Ag/cadmium oxide (CdO) NP assemblies. Reprinted with permission from Refs. [39, 42, 43]

Besides graphene and GO sheets, CNTs were assembled using DNA as linkers. The non-covalent adsorption of DNA onto the surface of CNTs does not affect the electronic properties of CNTs. In order to achieve high-throughput preparation of ssDNA-modified CNTs, a simple and robust modification approach was proposed using surfactant-based exchange methods [45]. About 90% CNTs could be wrapped by ssDNA, increasing the yield of CNTs incorporated assemblies. Designing the binding sites and positions of DNA origami, CNTs were successfully assembled into 2D geometry using DNA origami as templates [46]. The length and sequence composition of ssDNA interrupted the interaction between chiral CNTs and DNA (Fig. 6a) [47], which could be applied in chiral selection of CNTs. ssDNA-functionalized CNTs were also assembled with other NPs with the aid of the hybridization of dsDNA. For example, ssDNA-functionalized CNTs were assembled with Au NPs modified by complementary DNA [48]. An amino-ssDNA was designed to modify the surface of carboxyl-CNTs, and biotin-ssDNA was modified on the surface of streptavidin-QDs. The hybridization of dsDNA enabled the self-assembly of CNTs and QDs (Fig. 6b) [49]. By adjusting the length of heterobifunctional dsDNA linkers, the interparticle distance between CNTs and QDs could be controlled. With increasing length of dsDNA, from 10 bp to 30 bp, QDs were quenched 63%, 52% and 47% (Fig. 6c), and the lifetimes of QDs were shortened correspondingly due to surface-guided charge transfer (Fig. 6d). DNA engineered adjustable gaps led to changes in the fluorescence intensity of QDs. Therefore, CNT-QD assemblies were applied for the detection of K^+ depending on the changes in dsDNA structures before and after recognition.

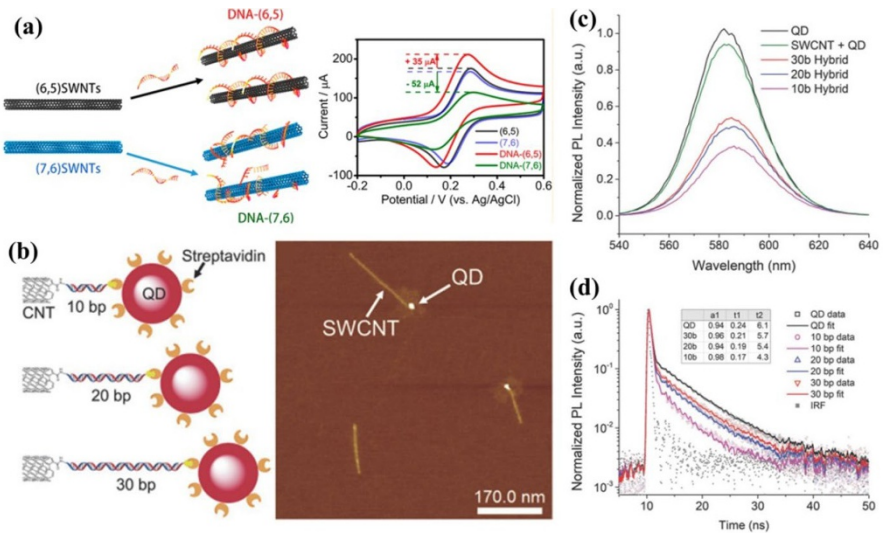


Fig. 6 **a** Interaction of chiral CNTs and ssDNA. **b** Schematic illustration and atomic force microscopy (AFM) images of carbon nanotube (CNT)-QD assemblies using different lengths of DNA. **c–e** Fluorescence spectra and fluorescence lifetimes of QDs after assembly with CNTs using different lengths of DNA. Reprinted with permission from Refs. [47, 49]

Unlike GO sheets and CNTs, CDs and GQDs are special carbon materials and exhibit unique fluorescence properties. The COOH groups of CDs and GQDs could be modified by NH_2 -DNA through carbodiimide bonding. CDs were assembled with organic dyes through the hybridization of dsDNA [50]. Photoinduced electron transfer from CDs to organic dyes enabled the fluorescence quenching of CDs. Aptamer-modified reduced GQDs were assembled on GO sheets through π - π stacking interaction and hydrogen bonding. The quenched fluorescence signals of reduced GQDs can be recovered owing to the formation of Pb^{2+} induced G-quadruplex DNA structures [51]. DNA-directed ratiometric fluorescent probes were assembled by using CDs and 5,7-dinitro-2-sulfo-acridone (DSA) [52]. Efficient FRET between CDs and DSA enabled the fluorescence quench of DSA. The presence of miRNA induced the disassembly of CDs and DSA, inducing changes in the fluorescence signals of both CDs and DSA.

Although DNA programmed carbon materials assemblies have shown different advantages in biosensing and bioimaging, there is still much room for improvement. The stability of carbon materials, the sensitivity of detection, the equilibrium times between probes and targets, and biocompatibility all affect the feasibility and sensitivity of biosensors. Due to chemical inertia and the strong hydrophobicity of the surface of carbon materials, the combination of carbon materials is achieved mainly through accumulation. The formation of large surface area carbon materials will lead to higher energy barriers and limit detection rates.

3 Optical Properties of Nanoassemblies

The development of nanoassemblies has been of special interest due to the tunable optical responses that they can introduce. These controllable optical properties, involving surface-enhanced Raman scattering (SERS), chirality, and photoluminescence (PL) properties, depend mainly on interparticle distance, size and morphology, the chemical composition of NPs, as well as the spatial configuration of the assembled NPs. DNA-driven assemblies exhibit strong optical activity and show potential applications for biosensing and bioimaging.

3.1 SERS Performance

SERS is capable of identifying unique fingerprint information [53, 54]. The wide application of SERS is attributed to its high sensitivity, nondestructive identification and multiplex detection capability [55]. The major contribution of SERS enhancement originates from the enhanced local EM field in the hot spots between neighboring metal NPs [56–58]. Nevertheless, the SERS signals of NPs are too weak for these applications, and uncontrolled aggregation would affect the reproducibility of SERS measurements [59]. In order to solve these problems, considerable interest has been shown in exploring SERS-active NP assemblies, which can greatly improve EM fields and consequently generate strong SERS signals [60]. Various NP assemblies have been reported using DNA as templates, including dimers [61, 62], trimers [63], tetramers [32, 64], chains [14, 65] and pyramids [26].

Plasmonic coupling between NPs of assemblies provides many new possibilities for the enhancement of local EM fields, which depend mainly on the interparticle distances between NPs, the compositions of NPs and the configurations of assemblies. For example, the strong EM fields between 80 nm Au NPs assembled on DNA origami achieved the quantization of single-molecule SERS [66]. The gaps between neighbor NPs were controlled by shell deposition. DNA-driven Au@Ag NR dimers were assembled and could significantly enhance the EM field after Ag shell coating [59]. Ag NPs with a higher SERS enhancement than Au NPs were demonstrated as perfect candidates for SERS probes. Multiple aptamer programmed Ag NP pyramids show potential for detection of multiplexed disease biomarkers (Fig. 7a, b) [59]. The structure of the pyramids was stable in high ionic-strength conditions, leading to potentially reproducible signals in complex systems. Hot spots between adjacent NPs in pyramids showed the maximum EM field intensity and thus enhanced SERS signals (Fig. 7c). Coupled with many intense EM hot spots from double plasmonic NPs, plasmonic Au NPs and Ag NPs assemblies were developed for the SERS application. A novel Ag NP ornamented-Au NP pyramid was fabricated using an aptamer-based self-assembly process (Fig. 7d, e) [67]. As-designed superstructures had intense EM hot spots, and showed potential for use as an ideal SERS substrates (Fig. 7f). Au NRs showed a huge enhancement of SERS signals because of the intense and aspect ratio-dependent longitudinal surface plasmon resonance. Au NR-Ag NP

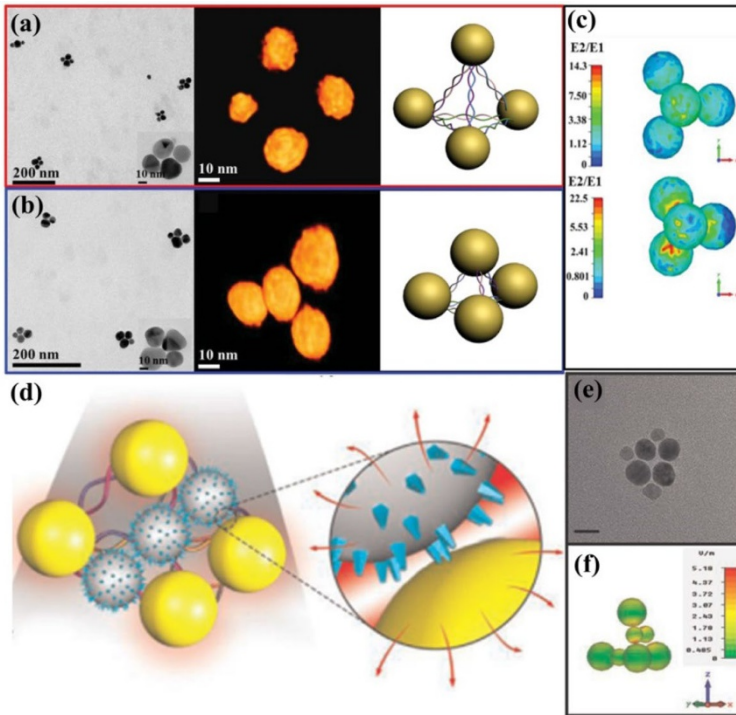


Fig. 7 a, b TEM images and tomography of Ag NP pyramids before and after the affinity of tumor markers. c Simulated electromagnetic (EM) fields of Ag NP pyramids. d–f Schematic illustration and TEM images of Ag NP ornamented-Au NP pyramids and simulated EM fields. Reprinted with permission from Refs. [67, 87]

core-satellite assemblies displayed obvious enhanced SERS performances and could be used for further detection. In order to enhance SERS signals, the anisotropic shape of Au NSs coupled with plasmons focused at the core, together with the tips of the NPs generated lots of “hotspots”, thus enabling enhancement of the EM field [19]. The excellent SERS performance made dimers a more prominent building block for SERS substrates than regular spherical particles dimers [19]. A self-assembled Au NS dimer was constructed by aptamers for Hg^{2+} detection [68].

Assemblies of UCNPs and plasmonic metal NPs combine two kinds of optical signals—luminescence and SERS—which inspires new designs for ultrasensitive detection of targets. Au NPs and Au NR dimers were assembled with UCNPs by using DNA as templates [36, 69]. Plasmonic NPs not only possess strong surface-enhanced spectroscopic effects for the amplification of SERS intensity, but also display fluorescence quenching ability. Plasmonic NP-UCNP assemblies showed outstanding SERS enhancement and fluorescence quenching effects, and show promise for accurate and sensitive dual-signal-dependent identification of targets. Graphene had already been shown to be an effective Raman enhancement

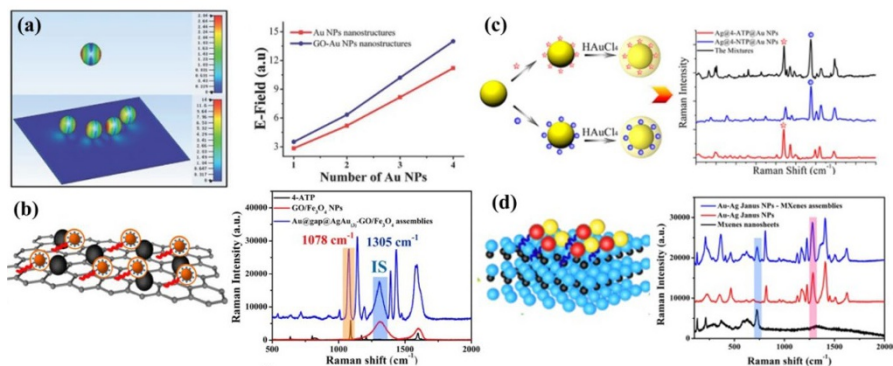


Fig. 8 a Simulated EM fields of Au NPs and GO–Au NP assemblies. b Schematic illustration and surface-enhanced Raman scattering (SERS) spectra of GO–Au@gap@AgAu NP assemblies. c SERS encoded Ag@Au CS NPs and the SERS spectra. d Schematic illustration and SERS spectra of MXenes–AuAg Janus NP assemblies. Reprinted with permission from Refs. [42, 44, 72, 73]

substrate because of its high electron mobility and low electrical resistivity [41, 70, 71]. DNA functionalized plasmonic NPs were assembled with GO sheets by π – π stacking interactions. Au NP–GO assemblies showed chiral properties and SERS activity, which can be attributed to the collective coupling between Au NPs and GO sheets (Fig. 8a) [42]. The intensity of the EM field enhanced with the increasing number of Au NPs assembled on GO sheets. GO sheets also possessed intrinsic Raman characteristic peaks that could serve as an internal standard (IS). Zhao et al. [44] designed aptamer-driven assemblies of Au@gap@AgAu NPs and GO sheets for the fabrication of SERS aptasensors (Fig. 8b). By embedding Raman molecules into the gaps of Au@gap@AgAu NPs, strong SERS signals were obtained, owing to the formation of hot spots in the interior gaps. SERS-active Au@gap@AgAu NPs served as detection tags, and GO sheets were applied as reference tags for the establishment of ratiometric SERS aptasensors. By changing Raman molecules into the junction of core and shell, various SERS tags can be obtained. Two types of Ag@Au CS NPs were encoded by 4-ATP and 4-NTP, and were used as SERS tags for the double detection of biotoxins (Fig. 8c) [72]. Similar to GO sheets, MXenes sheets also possessed intrinsic Raman signals and were applied as IS for the fabrication of ratiometric SERS aptasensors [73]. Au–Ag Janus NPs were fabricated under the guidance of 2-mercaptobenzoimidazole-5-carboxylic acid (MBIA). Au–Ag Janus NPs exhibited intrinsic SERS signals without extra modification of the Raman molecules, and were used as detection tags. Aptamer-modified SERS-active Au–Ag Janus NPs were assembled with MXenes sheets for the fabrication of ratiometric SERS aptasensors (Fig. 8d). SERS-active NP nanoassemblies have gained immense popularity. However, some problems remain, such as high cost, lack of uniformity, poor stability and biocompatibility, which seriously restrict the utilization of nanoassemblies in practical applications. There is still much potential for the development of nondestructive identification and multiplex detection capability.

3.2 Chiral Properties

DNA molecules as linkers can assemble plasmonic NPs into designed spatial configurations, which can endow NP assemblies with strong chirality [74]. DNA-driven heterodimers (including Au NP heterodimers, Au–Ag NP heterodimers, Au NR dimers, and Au NR–Au NP heterodimers, etc.) exhibit obvious chiral signals owing to the ellipsoidal shapes of plasmonic NPs and the formation scissor-like structures. The interparticle distance between adjacent NPs can be controlled by adjusting the length of DNA linkers, which further affected the EM fields for the adjustment of chiral signals. For example, chiral signals of Au NR–Au NP heterodimers became weaker with the increasing length of DNA from 15 to 80 bp due to the weak EM fields [75]. UCNPs and Au NRs were assembled to chiral propeller-like tetramers by using 11, 18, 24, 30, 36, 45 bp DNA [37]. It was noted that the chiral bands blue-shifted to short wavelengths by about 22 nm with the decreasing length of DNA from 45 to 11 bp (Fig. 9a). Besides the adjustment of DNA length, shell deposition provided another way to control the gaps between NPs [12, 13]. Deposition of the Ag shell on DNA engineered Au NP heterodimers further decreased the interparticle distances, which can be ascribed to the formation of a thick shell. The chiral signals of Au NP heterodimers were amplified, and the g -factor reached up to 1.21×10^{-2} . Due to the different plasmonic absorption of the Ag and Au shell, chiral Au NP heterodimers showed a blue-shifted CD peak at 418 nm after deposition of the Ag shell (Fig. 9b, c), and a red-shifted CD peak at 586 nm after deposition of the Au shell (Fig. 9d, e). Interestingly, the chiral signal returned to 525 nm after deposition of a double shell (Ag shell–Au shell or Au shell–Ag shell) [13]. Shell deposition not only reduced the interparticle distances between NPs for enhancement of the EM field, but also adjusted the position of chiral peaks at the designed positions.

Chiral nanoassemblies were fabricated by linear hybrid DNA chains. By asymmetric modification of DNA on different NPs, linear DNA can link NPs to form Au NP dimers, Au shell–Ag NP core–satellites, propeller-like Au NR–Au NP tetramers,

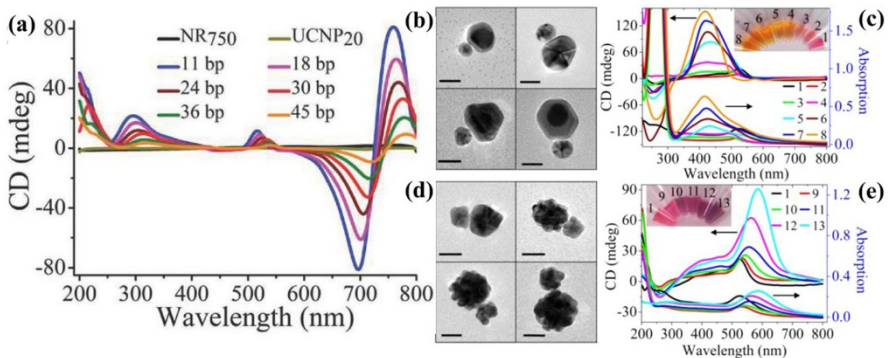


Fig. 9 a Circular dichromism (CD) spectra of propeller-like UCNP–Au NR assemblies using different lengths of DNA. b, c TEM images and CD spectra of Au dimers after Ag shell deposition. d, e TEM images and CD spectra of Au dimers after Au shell deposition. Reprinted with permission from Refs. [13, 37]

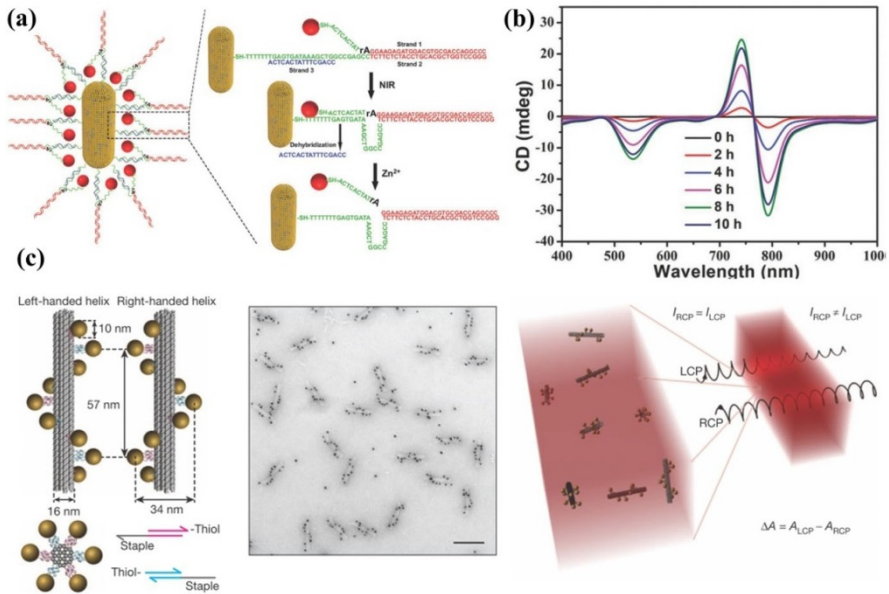


Fig. 10 **a** Au NR–Au NP core-satellites were assembled by a “Y”-shaped DNA hybrid skeleton. **b** CD spectra of Au NR–Au NP core-satellite assemblies at different times. **c** Au NR–UCNP assemblies for the detection of DNA. **d** Chiral Au NP helices assembled on DNA origami bundles. Reprinted with permission from Refs. [76, 77]

and so on. By designing the hybridization shapes of the DNA skeleton, various chiral spatial structures can be obtained. A “Y” shaped DNA hybrid skeleton was designed for the preparation of Au NR–Au NP core-satellites by using Zn^{2+} -specific DNA-cleaving DNase as a linker (Fig. 10a) [76]. The intracellular CD signal of chiral Au NR–Au NP core-satellites was recorded in the 520 nm and 700–800 nm regions (Fig. 10b). DNA pyramids possessed unique spatial configuration and could arrange building blocks into special structures. Chiral NP pyramids assembled by three types of NPs, including Au–Au–Au–Au pyramids, Au–Au–QD–QD pyramids and Au–Au–Ag–QD pyramids, were reported by Xu et al. [26]. Chiral Au NP–UCNP pyramids were assembled and showed an obvious chiral band at 521 nm [32]. DNA molecules can be assembled to DNA origami with designed sites and numbers. For example, DNA origami bundles and rectangular bifacial DNA origami were designed and used as templates for the preparation of chiral Au NP helices and chiral Au NP tetramer (Fig. 10c) [64, 77]. The chiral signals can be adjusted by changing the origami structures. By locating different sized Au NPs on the corner of octahedral DNA origami frames, chiral nanostructures were obtained [21].

PCR is a meaningful technique for the amplification of DNA with the aid of DNA polymerase and nucleotides. By modification of primers on NPs, the DNA amplification process can be performed on the interface of NPs, inducing programmed assembly of NPs. The yield and structures of NP assemblies can be controlled through the optimization of PCR cycles, primer density and appropriate temperatures. For example, chiral Au NP core-satellites can be assembled by PCR through

the modification different amounts of primers on NPs [17]. A high concentration of primers on large NPs enabled more small NPs to assemble around large NPs. If the modification of primers on each NP is symmetrical, chiral NP chains and web-like assemblies are formed. With increasing numbers of PCR cycles, high-yielding assemblies were obtained, and the chiral nanostructures become complex. By locating primers precisely on the side of Au NRs, side-by-side Au NR assemblies were obtained that display chiroplasmonic activity due to the unique 7° – 9° twist between the axes of Au NRs [14]. Aptamers were also DNA and RNA sequences, and also exhibited unique affinity towards their targets. Aptamer-directed chiral NP assemblies were also fabricated, using steps similar to those needed for DNA-dependent chiral nanostructures, including chiral dimers, chiral core-satellites and chiral pyramids, etc. For example, yolk-shell NPs were assembled into chiral pyramid nanostructures, and aptamer-modified UNCPCs were centralized in the middle positions [78]. These assemblies exhibited plasmonic-induced chirality and chiral conformation, and showed restored luminescence signals of UNCPCs by the recognition of aptamers towards targets.

3.3 Fluorescence Properties

Fluorescent NPs have attracted significant attention due to their natural advantages, such as simplicity, high sensitivity, anti-interference ability and fast responses. DNA-driven fluorescence NP assemblies have tailorable optical properties and could be applied for biosensing and bioimaging in the fields of environmental sciences, human health, food industries, etc. Organic fluorescent dyes, including fluorescein and rhodamine dyes, were first used as fluorescent probes in biomedical research. Au-NPs were assembled with Cy3 and Cy5 using dsDNA as a bridge [79]. The fluorescence of both Cy3 and Cy5 was quenched by Au NPs due to the FRET process. A similar principle was proposed for Cy5-DNA-directed Au@Ag NP and Au NR assemblies. In comparison to traditional organic dyes, fluorescent NPs have potential prospects for bioapplications owing to the advantages of their wide absorption spectrum, narrow emission spectrum and high fluorescence quantum yields. In particular, QDs exhibited size-dependent strong fluorescence signals, which could range from 450 nm to 780 nm. Major progress had been made in the application of DNA-driven QD assemblies. QDs with three different emission peaks were assembled by precise modification of DNA on the sites of QDs. The energy transfer was entirely reversible by adjusting the pH [24]. DNA molecules were used as linkers to assemble QDs with Au-NPs to form core-satellite assemblies (Fig. 11a) [80]. The fluorescence signals of QDs were quenched owing to the energy transfer from QDs to Au-NPs (Fig. 11b), and further restored when DNA-functionalized QDs dissociated from the surface of Au-NPs. In comparison to QDs emitting fluorescence in the visible region, Ag₂S QDs exhibited a fluorescence signal in the second-window near-infrared (NIR-II) region, causing little damage to normal tissues. DNA backbones were designed and applied as templates for the assembly of Ag₂S QDs and Au NRs@Pt nanostructures (Fig. 11c). The red-shifted LSPR peak enabled Au NRs@Pt

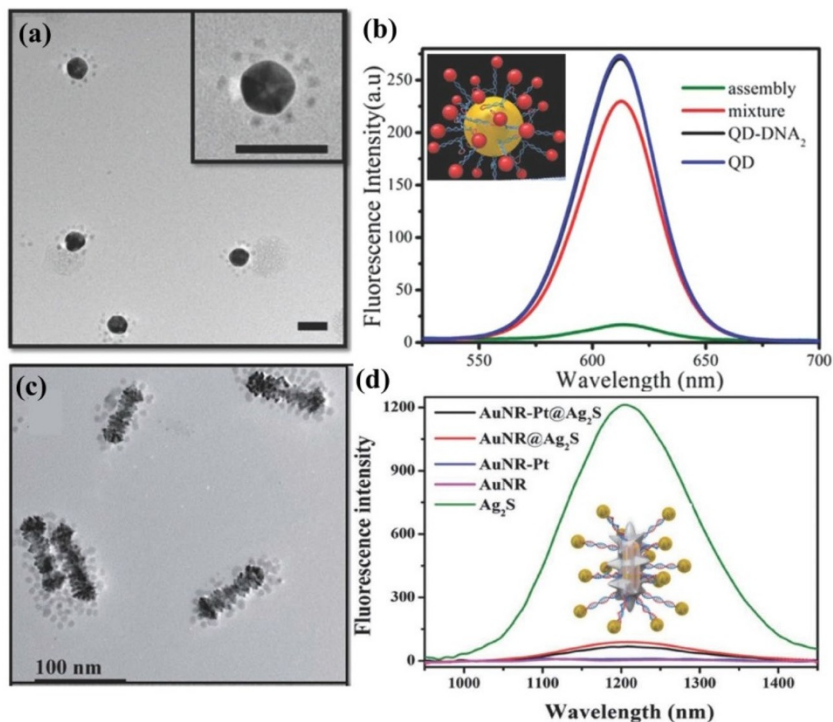


Fig. 11 **a, b** TEM images and fluorescence spectra of DNA driven Au NP-QD core-satellite assemblies. **c, d** TEM images and fluorescence spectra of DNA driven Au NR@Pt-QD core-satellite assemblies. Reprinted with permission from Refs. [80, 81]

nanostructures to quench the fluorescence signals of Ag₂S QDs (Fig. 11d) [81]. In comparison to QDs, CDs show excellent biocompatibility. DNA was used as a linker for the assembly of CDs and DSA. The fluorescence intensity of DSA was quenched by CDs due to the FRET process. CDs were disassembled from the structures due to reorganization of the microRNA. This would induce a decrease in the fluorescence intensity of CDs and the recovery of DSA [52]. The ratio of dual fluorescence signals were used for the detection of miRNA-21 without environmental fluctuations. In order to protect the fluorescence signals of QDs from photobleaching, QDs were designed to encode into SiO₂ NPs. The as-prepared QDs@SiO₂ core-shell NPs showed amplified fluorescence intensity and good stability. Importantly, the fluorescence signals of QDs@SiO₂ core-shell NPs could be encoded by using different colored QDs with distinct ratios. DNA modified QDs@SiO₂ core-shell NPs were used as detection probes for the multiplex detection of genetically modified organisms [82].

High-energy UV or visible light is usually required as an excitation source for QDs. Low tissue penetration, biological tissue destruction, and biological tissue autofluorescence interference may limit the bioapplications of QDs. Alternatively, UCNPs emit visible light under the excitation of near-infrared light,

and have unique advantages such as lower cytotoxicity and higher biocompatibility. UCNPs were widely modified by DNA and further assembled with plasmonic NPs. By designing the geometry of DNA backbones, plasmonic NP-UCNP assemblies can exhibit tunable fluorescence signals. The fluorescence signals of UCNPs are quenched by Au-NRs and Au-NR dimers by using DNA, RNA and aptamers as linkers, due to nonradiative energy transfer. The fluorescence properties of UCNPs can be controlled by adjusting the interparticle distances between plasmonic NPs and UCNPs. This can be achieved not only by coating polymers on NPs but also by using different lengths of dsDNA as linkers. Amphiphilic diblock copolymer polystyrene-block-poly (acrylic acid) (PS-*b*-PAA) was used as dense layer to coat Au-NR dimers. The stability of Au-NR dimers were greatly enhanced and the luminance quench ability was reduced. When the length of the dsDNA was kept below 24 bp, the close distances enabled the generation of the FRET process to quench fluorescence signals (Fig. 12a) [37]. However, fluorescence enhancement occurred between Au-NRs and UCNPs by adjusting the

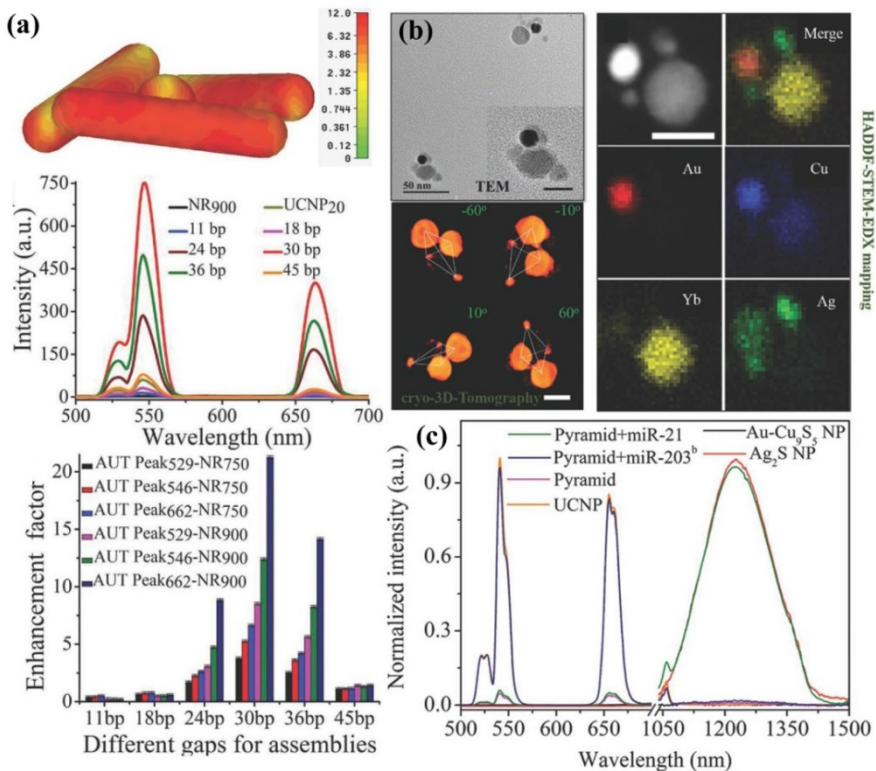


Fig. 12 **a** Fluorescence spectra of UCNP-Au NR assemblies at different lengths of DNA. **b** TEM images of Au-Cu₉S₅ NP-UCNP-Ag₂S NP pyramids. **c** Au NR-UCNP assemblies for the detection of DNA. **d** Fluorescence spectra of Au-Cu₉S₅ NP-UCNP-Ag₂S NP pyramids. Reprinted with permission from Refs. [33, 37]

length of dsDNA from 24 to 36 bp. Long distances (such as 45 bp DNA) would return fluorescence to the original intensity, due to the formation of a low level electric field.

DNA pyramids with special configuration were constructed for the location of plasmonic NPs and fluorescence NPs. The four corners of DNA pyramids enabled free positioning of distinct NPs. When two Au-NPs and two UCNPs were located, the fluorescence signals of UCNPs were quenched by Au-NPs. UCNPs and down-conversion NPs can both be located on the two corners of pyramids. The emission wavelengths, ranging from 500 nm to 1500 nm, enabled the exploration of plasmonic NPs with broad LSPR, which could overlap the emission peaks of fluorescence NPs. Recently, Kuang et al. [33, 37] reported novel pyramids consisting UCNPs, Ag₂S NPs and Au-Cu₉S₅ NPs for biosensing and bioimaging (Fig. 12b). Au-Cu₉S₅ NPs were proposed as quencher due to the unique LSPR peaks ranging from 500 nm to 1100 nm (Fig. 12c). The quenched fluorescence signals of UCNPs and Ag₂S NPs were both restored when they were released from the pyramids, attributing to high affinity between miRNA and their complementary DNA sequences.

Although various research goals have been achieved, some challenging problems still exist if these results are to be transferred to clinical practice, such as low luminous efficiency, poor biocompatibility and noted toxicity. Based on the advantages of high sensitivity and selectivity, development of fluorescent technology will still be of great value.

4 Applications for Biosensing and Bioimaging

The synthesis and assembly of NPs can be induced by DNA molecules, and NPs can also be used as probes to study the specific recognition of DNA molecules. DNA-driven NP assemblies showed multiple optical properties, which can be adjusted by rationally selecting assembly elements and designing DNA backbones. Taking advantage of the base complementary pairing principle of DNA and the specific affinity of aptamers, DNA-driven NP assemblies could be disassembled in the presence of targeted DNA or analysts. Changes in these nanostructures enabled the different optical responses of DNA-directed NP assemblies, which show potential applications in ultra-sensitive and highly specific biosensing and bioimaging.

4.1 Biosensing

4.1.1 DNA Biosensors

DNA molecules were used as templates to achieve the assembly of functional NPs, which generated unique optical responses. Changes in the structural parameters of DNA enabled changes in yields, geometry, and arrangements of assemblies, further affecting the optical signals. Therefore, optically active DNA-driven NP assemblies can be used for the detection of DNA, including targeted DNA, DNA concentration, DNA length, and even single base mismatches.

The highly sensitive and specific hybridization reaction between DNA and DNA complementary sequences enables the accurate detection of targeted DNA. DNA detection provides some critical information on genomic screening and medical diagnosis. By designing the detailed base sequences of DNA fragments, specific DNA can be detected. For example, QD-encoded SiO₂ NPs were used as fluorescence probes and modified on the end of probe DNAs, achieving detection of targeted DNA sequences in genetically modified organisms. SERS signals provide intrinsic information on DNA molecules. Iodide-modified Ag NPs were applied as substrates for the label-free detection of DNA with single-base sensitivity using the phosphate backbone signal as IS [83]. In comparison with noble metal NPs, non-noble metal NPs involving Al NPs and Cu NPs also exhibit distinct SERS activity. The phosphate backbone of ssDNA shows preferential affinity towards Al oxide surfaces [23]. More attention should be devoted to DNA-directed non-noble metal NP assemblies. Al-NP-dependent assemblies have not been prepared for the application of quantitative ssDNA analysis.

DNA-driven NP assemblies show unique CD signals in the visible region, originating from the transfer of chiral DNA molecules and the chiral geometry of assemblies. In comparison with other optical signals, chiral signals show better sensitivity and less interference [84]. This is because most matrixes are non-chiral or show only weak chiral signals in UV regions. Chiral-signal-dependent DNA detection exhibits high sensitivity and accuracy. DNA-engineered Au-NRs were assembled into chiral side-by-side structures, achieving attomolar DNA detection [14]. Chiral signals of Au-NP dimers were amplified after metal shell deposition, and were applied to

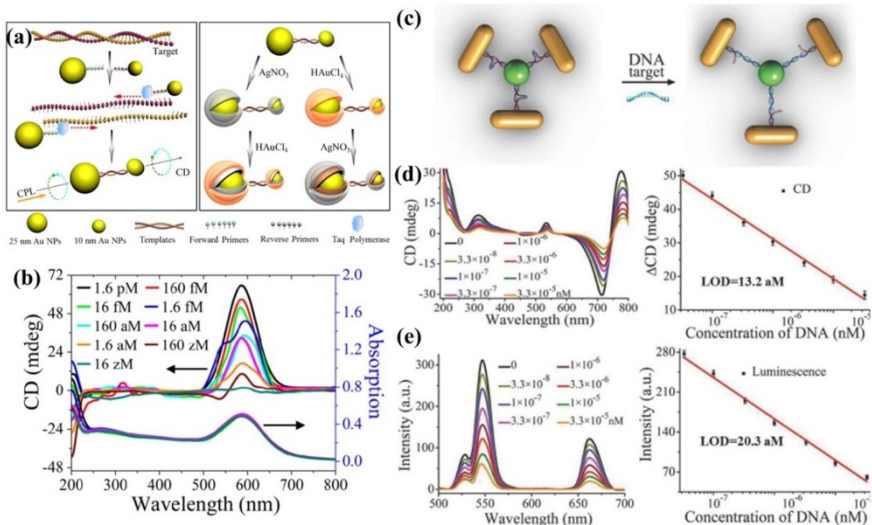


Fig. 13 **a** Shell-deposited chiral Au-NP dimers for the detection of DNA. **b** Chiral spectra of Au dimers@Au CS assemblies for the detection of DNA. **c** Au NR-UCNP assemblies for the detection of DNA. **d** Chiral signals dependent biosensors for the detection of DNA. **e** Fluorescence-signal-dependent biosensors for the detection of DNA. Reprinted with permission from Refs. [13, 37]

zeptomolar DNA detection with the aid of PCR techniques (Fig. 13a, b) [13]. In order to increase the accuracy of DNA detection, dual-model optical-signal-dependent biosensors were proposed for targeted gene detection. For example, DNA-engineered propeller-like Au-NR-UCNP assemblies were fabricated and exhibited strong chiral signals and amplified fluorescence signals (Fig. 13c) [37]. The presence of hepatitis A virus Vall7 polyprotein gene (HVA) enabled the opening of hairpin-like DNA strands, extending the interparticle distance between Au-NRs and UCNPs. A decreased chiral signal, together with a decreased fluorescence signal, was both observed with increasing concentration of DNA (Fig. 13d, e). The LODs were as low as 13.2 aM for chiral signals and 20.2 aM for fluorescence signals. Chiral signal-dependent DNA detection showed higher sensitivity than fluorescence signals.

4.1.2 Aptasensors for Biotoxins

Biotoxins with high biotoxicity could cause huge harm to public health, and their accurate detection methods have become a focus of research in recent years. A SERS aptasensor was established for aflatoxin B1 (AFB1) detection using SERS-active Au-NS-Ag-NP core-satellite nanostructures [85]. Aptamer-modified Ag satellites were dissociated from Au cores in the presence of AFB1, leading to a decreasing in SERS intensity. The long length of aptamers would induce large interparticle distances between NPs. In order to reduce the gaps, Y-shaped DNA hybridization was designed for NP assembly. For example, Au nanoflower (Au NF)-Ag NP core-satellites were assembled by designing aptamers of microcystin-LR (MC-LR) into Y shaped DNA hybridization. Interparticle distances were reduced from 19.8 nm to 4.0 nm [11]. The enhanced EM fields enabled SERS-active aptasensor for the ultra-sensitive detection of MC-LR.

SERS signals provide the possibility of multiplex detection by using SERS tags as detection probes. By embedding different Raman molecules into the junctions of core and shell, various SERS tags were obtained. A SERS-signal-dependent aptasensor was proposed for the dual detection of ochratoxin A (OTA) and AFB1 [72]. SERS-encoded Ag@Au CS NPs were designed and used as tags for detection. In the absence of targets, two types of SERS tags functionalized by different aptamers were assembled on the surface of magnetic NPs (MNPs), generating separate SERS signals. SERS tags would detach from MNPs because of the competitive combination of targets and aptamers. Embedding Raman molecules into the junctions of core-shell structures would protect Raman molecules from interference from the environment, thus increasing chemical stability for the accuracy detection of OTA and AFB1. To enhance reproducibility of detection, a ratiometric SERS aptasensor was proposed using the Raman characteristic peaks of 2D materials as internal standards. Recently, Zhao et al. [44] reported a ratiometric SERS aptasensor for MC-LR detection by using Au@gap@AgAu NPs as detection probes and GO sheets as reference probes. Raman molecules were embedded into the gaps of Au@gap@AgAu NPs for the amplification of SERS signals. GO sheets possessed D, G and 2D Raman vibrational modes at 1305 cm^{-1} , 1603 cm^{-1} and 2612 cm^{-1} . Aptamers modified Au@gap@AgAu NPs were assembled with GO sheets through $\pi-\pi$ stacking interactions, and would be dissociated into solution by the affinity of MC-LR.

Depending on the correction of IS Raman signals, reliable detection was achieved for MC-LR. Au–Ag Janus NPs as detection probes exhibited intrinsic SERS activity due to the MBIA as ligands for the guide growth of Ag islands [73]. Avoiding modification of Raman molecules on the nanostructures increased detection accuracy. With the aid of MXenes as reference probes, a ratiometric SERS aptasensor was fabricated for OTA detection.

4.1.3 Aptasensors for Heavy Metal Ions

Heavy metal ions are a potential threat to people's health. The aptamers were widely screened and showed high affinity towards heavy metal ions. Aptamer-directed NP assemblies were applied for sensitive heavy metal ion detections. Au-NSs possessed multiple tips, which was beneficial for the formation of strong hot spots. The enhanced EM fields generate amplified SERS activity. The affinity between aptamers and Pb^{2+} induced self-assembly of SERS-active Au NS dimers [68]. A SERS aptasensor was developed for the detection of Pb^{2+} . Aptamer-directed Au-NP trimers were assembled for the dual detection of Hg^{2+} and Ag^+ [63]. A “Y-shaped” DNA skeleton was designed using the aptamers of Hg^{2+} and Ag^+ . With the existence of Ag^+ or Hg^{2+} , Au NP dimers were assembled through the C– Ag^+ –C or T– Hg^{2+} –T mismatches, resulting in a highly enhanced Raman signal. The coexisting Ag^+ and Hg^{2+} induced assembly of Au NP trimers, and the resulting “hot-spots” caused enhanced SERS signal. This ideal Au NP trimer-based SERS sensor was first developed for the simultaneous detection of Hg^{2+} and Ag^+ . To increase detection accuracy, fluorescence and SERS signal-dependent aptasensors were established for the detection of Hg^{2+} [86]. Aptamers and Hg^{2+} driven Au@gap@AuAg NR assemblies were fabricated, and showed amplified fluorescence intensity and SERS activity, owing to the strong EM coupling between core and shell. Compared with fluorescence signals, SERS signal-dependent aptasensors exhibited higher sensitivity.

4.1.4 Aptasensors for Tumor Markers

The importance of detection and prevention of cancer is gradually attracting public attention. Aptamer-directed NP assemblies exhibit unique optical responses and could be applied to the detection of tumor markers. SERS signal-dependent aptasensors were widely developed for the sensitive detection of single, double and triple tumor markers. For example, Ag-NPs embedded Au-NP pyramids were designed and exhibited strong SERS signals attributing to the plasmonic coupling between Au-NPs and Ag-NPs. The affinity of vascular endothelial growth factor (VEGF) towards aptamers in the hybridization skeleton induced the dissociation of Ag-NPs from the assemblies, resulting in decreased SERS signal [67]. A negative linear correlation curve was established between the concentration of VEGF and SERS signals. The binding between aptamers and tumor markers could shorten the interparticle distances of NPs for the amplification of SERS intensity. There was a positive correlation between the concentration of tumor markers and SERS signals. For example, prostate-specific antigen (PSA) aptamer-incorporated DNA pyramids were applied as templates for the assembly of Ag-NPs. The reorganization of PSA

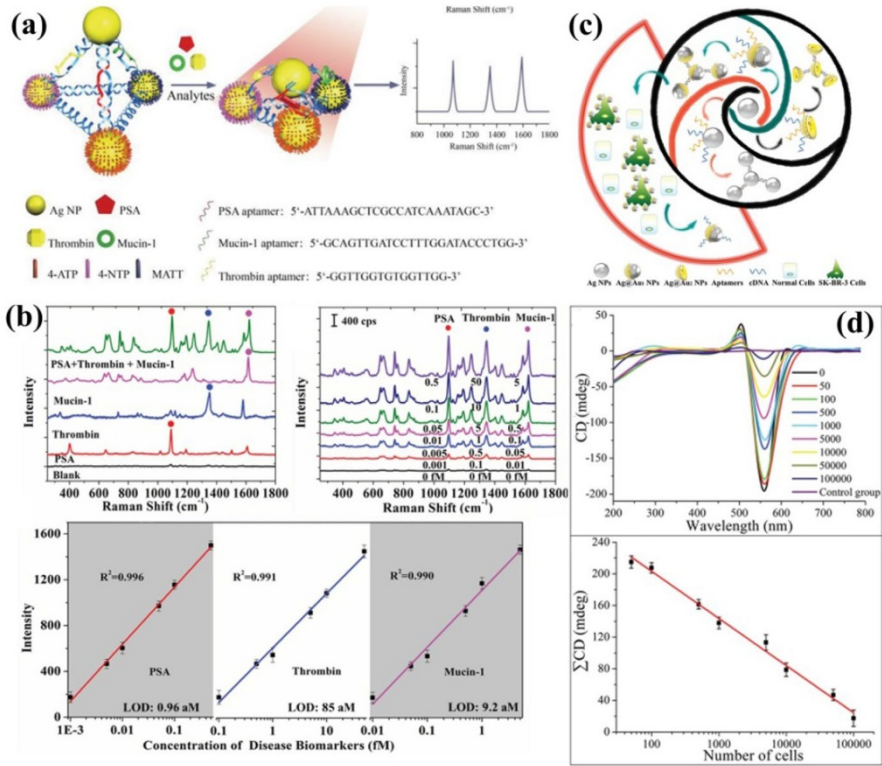


Fig. 14 **a** Aptamer-driven Ag-NP pyramids for the SERS signals based detection of prostate-specific antigen (PSA), thrombin and mucin-1. **b** Standard detection curves between the concentration of tumor markers and SERS signals of assemblies. **c** Aptamers driven chiral Ag@Au CS NP assemblies for the detection of cancer cells. **d** Chiral spectra of Ag@Au CS NP assemblies for the detection of cancer cells and standard curves. Reprinted with permission from Refs. [87, 90]

induced a decrease in the gaps between NPs for the enhancement of SERS responses (Fig. 14a) [87]. By designing three different aptamers into the three stands of the DNA skeleton, Ag-NP pyramids were used for the simultaneous monitoring of PSA, thrombin and mucin-1. The LODs were 0.96 aM, 85 aM, and 9.2 aM for PSA, thrombin, and mucin-1 (Fig. 14b).

Fluorescence signal-dependent aptasensors were also reported for the multiple recognition of three cancer biomarker (MUC1, CEA, CA125) [88]. Specifically, three kinds of aptamer-functionalized Ag and Ag/Au nanoclusters (NCs) were compiled, with the ability to specifically identify their corresponding targets. When GO appeared, the fluorescence of Ag NCs or Ag/AuNCs were quenched due to energy transfer from NCs to GO. During the detection process, once the tumor marker appeared, specific interactions between the tumor marker and its related aptamer occurred, resulting in the recovery of fluorescent signals. To increase the accuracy of detection, dual-mode optical signal-based aptasensors were proposed for the detection of tumor markers. For example, two types of aptamer-driven UCNP-Au

NP pyramids were assembled, which exhibited strong SERS signals and quenched fluorescence signals [89]. The presence of thrombin and PSA induced the dissociation of Au NPs and UCNPs, resulting in a decrease in SERS intensity and recovery of fluorescence signals.

Recently, aptamer-engineered chiral assemblies were reported and exhibited unique chiral responses in the visible regions. Chiral NP assembly-dependent aptasensors do not interfere with non-chiral substrates or chiral molecules with signals in the UV region, and show potential applications for sensitive and accurate tumor marker detection. Aptamer-driven chiral Ag assemblies were fabricated and transformed into chiral Ag@Au CS assemblies after Au shell deposition (Fig. 14c), which displayed obvious red-shifted, amplified and reverse chiral signals [90]. Chiral Ag@Au CS assemblies achieved the sensitive detection HER2 overexpressed on the surface of cancer cells (Fig. 14d). Au NRs were assembled to the chiral side-by-side nanostructures by using aptamers as templates [91]. Deposition of the Ag shell enabled the decrease of the interparticle gaps and further amplified the chiral signals. Chiral signal-based aptasensors were established for the sensitive detection of PSA.

4.2 Bioimaging

DNA molecules control the organization of NPs and switch assembly architectures. DNA-directed assemblies not only possessed unique optical responses for the interaction with analytes, but could also escape biological sequestration for the accumulation in cells or tissues [7]. DNA-directed assemblies showed potential prospects in bioimaging, including RNA imaging, living metal ions bioimaging, and phototherapeutics.

4.2.1 RNA Imaging

Distinct from messenger RNA (mRNA), microRNAs (miRNAs) are a class of short single-stranded, endogenous noncoding RNAs associated with early diagnosis and gene therapy. Fluorescence NPs included assemblies that showed adjustable fluorescence signals and can be applied to RNA imaging. DNA-driven Au-QD core-satellite assemblies were fabricated for ultrasensitive RNA bioimaging [25, 80]. Au-NPs as cores quenched the fluorescence of QDs due to the dipole-metal interaction. The affinity for RNA resulted in the separation of QDs from Au-NPs, and QDs regenerated fluorescent signals. DNA-driven Au-QD core-satellite assemblies achieved bioimaging of intracellular miRNA and mRNA. In comparison to QDs, UCNPs had the ability to convert NIR excitation light into visible emission light. UCNPs have many marvellous properties, including high photostability, low photodamage, and ideal signal-to-noise ratio [27], thus explaining why UCNP-incorporated assemblies have become potential luminescent nanomaterials for bioimaging. DNA-driven Au NR-UCNP core-satellite assemblies were applied to the double bioimaging of miRNA-21 and miRNA-200b [34]. The recognition of miRNA-21 and miRNA-200b induced dissociation of UCNPs-TAMRA conjugates and UCNPs-Cy5.5 conjugates,

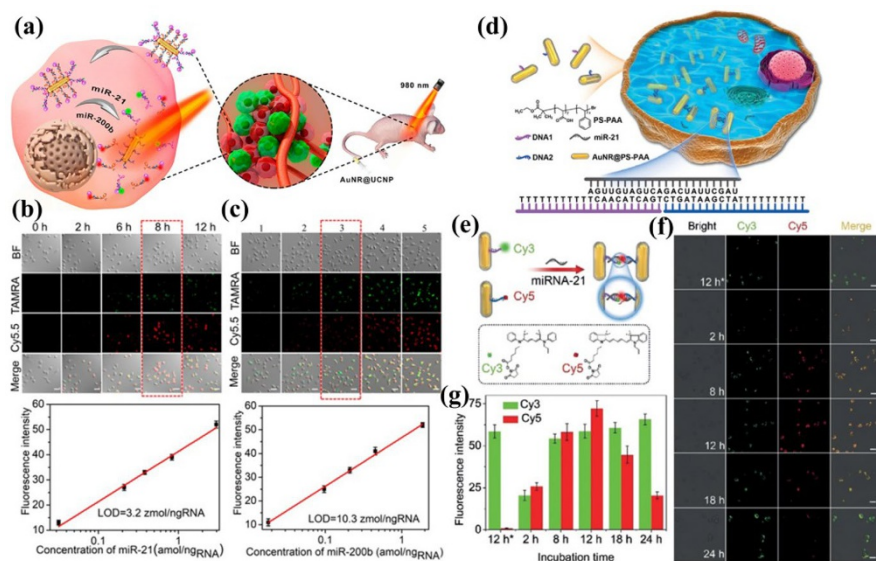


Fig. 15 a DNA programmed Au NR-UCNP core-satellite assemblies for bioimaging of microRNA (miRNA)-21 and miRNA-200b. **b, c** Bioimaging of miRNA-21 and miRNA-200b and the corresponding standard curves between miRNA concentration and emission intensity. **d** Intracellular miRNA driven Au NR dimers. **e–g** Intracellular Au NR dimer assembly for bioimaging of miRNA using FRET process. Reprinted with permission from Refs. [34, 53]

respectively (Fig. 15a). Under excitation at 980 nm, energy transfer from UCNPs and organic dyes enhanced signal from TAMRA and Cy 5.5. The LODs were 3.2 zmol ng^{-1} for miRNA-21 and $10.3 \text{ zmol ng}^{-1}$ for miRNA-200b, respectively (Fig. 15b, c). The use of DNA-engineered chiral Au-UCNP pyramids as intracellular nanoprobe has been reported. Intracellular miRNA in cells induced the disassembly of Au-NPs and UCNPs, resulting in a decrease in the CD spectra and the recovery of luminescence intensity of UCNPs under the excitation of 980 nm. Chiral-signal-together with luminescence-signal-dependent dual-mode sensors achieved accurate monitoring of intracellular miRNA [32]. Luminescence imaging in the NIR-II region was desirable for biological applications due to the low autofluorescence and deep tissue penetration. Recently, Ag_2S NPs were reported, and exhibited NIR-II emission under NIR excitation. Ag_2S NP-incorporated assemblies were also studied for the bioimaging of miRNA; however, the design of plasmonic nanostructures with LSPR peaks in the NIR region was critical for achievement of the LRET process. Au-NRs after Pt shell deposition and Au-NPs after growth of Cu_9S_5 NPs showed red-shifted adsorption peaks and were used to assemble with Ag_2S NPs [33, 81]. DNA-bridged Au@Pt NR- Ag_2S NP core-satellite assemblies were prepared, and served as intracellular probes for the bioimaging of miRNA-21 depending on the restoration of the luminescence signals of Ag_2S NPs [81]. Au/ Cu_9S_5 NPs were applied to quench the luminescence intensity of Ag_2S NPs and UCNPs [33]. Au/ Cu_9S_5 NP- Ag_2S NP-UCNP pyramids were fabricated by designing DNA pyramids as templates, and applied as intracellular probes for the bioimaging of miRNA-21

and miRNA-203. These previously reported studies focused on the application of assemblies as probes for the intracellular bioimaging of RNA. Recently, it was also reported that miRNA could induce the self-assembly of Au-NRs into dimers in living cells (Fig. 15d, e) [53]. Poly(styrene-*b*-acrylic acid) (PS-PAA) was capped on the surface of Au-NRs in order to increase their stability. Au-NR dimers demonstrated strong CD signals, SERS activity and obvious fluorescence intensity due to the FRET process from Cy3 to Cy5 on the end of DNA sequences (Fig. 15f, g). This study opened a way for the real-time bioimaging of miRNA in living cells.

4.2.2 Metal Ion Bioimaging

Metal ions in the living human body play an important role in many physiological processes. DNAzymes were screened widely and showed high affinity towards metal ions important in living organisms (such as Mg^{2+} , Cu^+ , Zn^{2+} and K^+). Thus, the research and detection of intracellular metal ions is of great significance. Wang and co-workers [92] designed a ratiometric probe for intracellular Zn^{2+} quantification and fluorescence imaging, based on the FRET between CDs and fluorescein (FAM). The CDs were conjugated with a Zn^{2+} aptamer, which improved selectivity of the fluorescent probe to Zn^{2+} , while the FAM was modified with the complementary DNA sequence. The FRET between CDs and FAM provide an ideal means of improving the sensitivity of detection. This approach has shown significant potential for the quantification and real-time tracing of Zn^{2+} in vivo by observing fluorescence images in vitro. Chiral-signal-based aptasensors exhibit good sensitivity and accuracy, and have been developed for the detection of metal ions in living systems. Zn^{2+} aptamer-directed Y shaped hybridization was designed for the assembly of Au@AgAu yolk-shell NRs and Au NPs. Strong chiral responses were obtained from the unique chiral geometry and the intrinsic chirality of the building block. Zn^{2+} induced the disassembly of structures together with decreased chiral intensity. The photothermal effects enabled the quantitative detection of Zn^{2+} in living cells [76]. Multiple metal ions were detected and imaged in living cells using DNAzymes-engineered Au@Pt NR-UCNP core-satellite assemblies [93]. The assemblies were activated by 980 nm left circular polarized light (CPL), and had the ability to analyze multiple divalent metal ions quantitatively in living cells. When the three target metal ions appeared, they recognized the binding sites, respectively. This would activate the DNAzymes and cleave the substrate DNA strands, resulting in the restoration of luminescence signals. The LODs were 1.1 nmol/ 10^6 cells, 1.02 nmol/ 10^6 cells and 0.45 nmol/ 10^6 cells for Zn^{2+} , Mg^{2+} , and Cu^{2+} , respectively, in living cells.

4.2.3 Photothermal Therapy and Photodynamic Therapy

DNA-engineered NP assemblies had desired NP arrangements and generated an enhanced EM field for the excitation of hot electrons, which was beneficial to the photothermal conversion efficiency. NP assemblies showed better photothermal conversion ability. For example, the heat transfer efficiency of Au NRs was 20.7%, while Au NR dimers could reach up to 42.3%, attributable to the intensive

plasmonic coupling [16]. Even though Au-Cu₉S₅ NPs displayed a high temperature increase, Au-Cu₉S₅ NPs incorporating pyramids by using DNA as templates showed better photothermal conversion ability [33]. The temperature was quickly increased to 55 °C within 4 min. This was not only because of the ideal sizes of pyramids for accumulation within tumors, but also caused by the wide adsorption range of the pyramids. DNA-engineered NP assemblies showed tailorable LSPR for the excitation and transfer of energy to ³O₂ for the generation of reactive oxygen species (ROS). DNA engineered NP assemblies showed potential applications for photodynamic therapy (PDT) in vitro and in vivo. For example, DNA-driven Au shell-Au NP core-satellite assemblies showed intensive chiral signals after modification of D-cys or L-cys (Fig. 16a) [94]. High ¹O₂ quantum yield was obtained for D-cys functionalized Au shell-Au NP core-satellite assemblies under right CPL irradiation. DNA-driven Au shell-Au NP core-satellite assemblies served as ¹O₂ generating agents were used successfully as PDT applications in vivo experiments without the use of organic photosensitizers (Fig. 16b). The generation of ROS was reported for

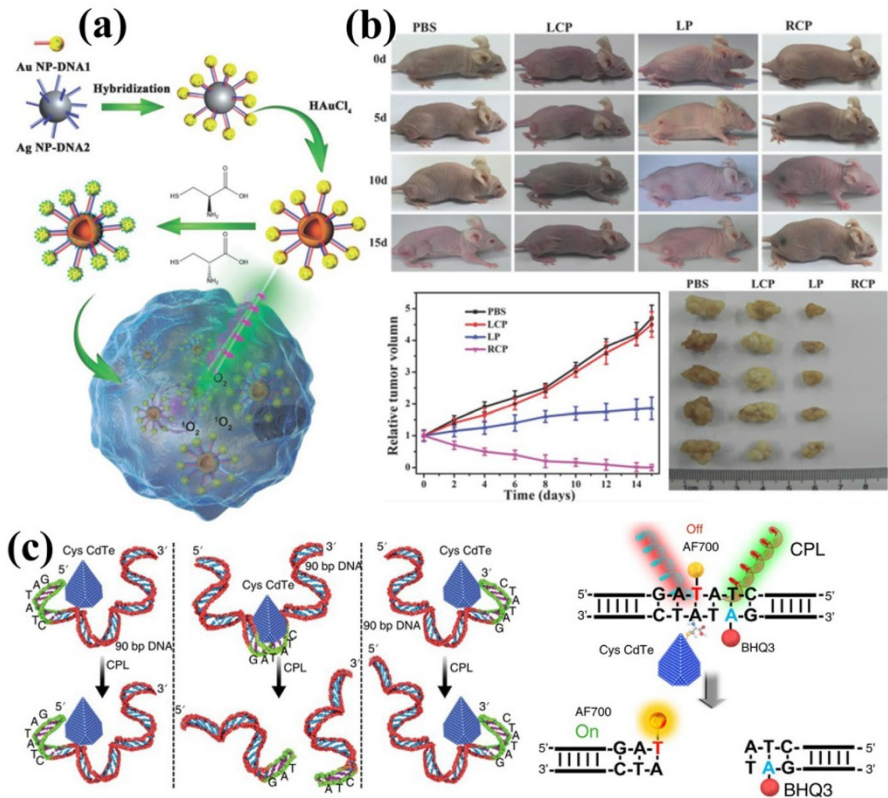


Fig. 16 a DNA-driven Au shell-Au NP core-satellite assemblies as photodynamic therapy (PDT) agents. b PDT applications of DNA driven Au shell-Au NP core-satellite assemblies in vivo. c The structural match of DNA and Cys-modified CdTe NPs for DNA shearing. Reprinted with permission from Refs. [94, 95]

the site-selective cleavage and profiling of DNA. Chiral Cys modified CdTe NPs were prepared and matched by the conformation of GAT'ATC sequences (Fig. 16c) [95]. Chiral Cys modified CdTe NPs could generate ROS under the illumination by CPL for the cleavage of sites between T and A.

5 Summary and Future Perspectives

DNA-driven NP assemblies had been developed for biosensing and bioimaging applications. Specific structural NP assemblies could be obtained by designing the number of DNAs modified on NPs and the hybrid DNA configurations. The structures of NP assemblies determines their optical properties, such as SERS, chirality, luminescence enhancement, plasmon-enhanced absorption, and so on. DNA-directed NP assemblies have made it possible to design specific assembled structures, and finally to obtain an assembly with satisfactory performance. The changed optical signals allows DNA-directed NP assemblies for biosensing and bioimaging. However, challenges remain in the practical application of DNA-driven NP assemblies, and further research is required. First of all, DNA-directed NP assemblies are sensitive to pH and ionic strength, and are unstable for application under harsh environmental conditions. Second, the modified number of DNA molecules on each NP was not uniform, and required complex purification steps for the preparation of NPs with precise amounts of DNA molecules. Third, DNA molecules were easily modified on the surface of metal NPs owing to stable metal-SH bonds, but efficient modified approaches should be explored for the attachment of DNA molecules on the surface of non-metallic NPs. Fourth, the fabrication and applications of DNA directed NP assemblies was limited mainly to microcosmic sizes. Dimensional scale-up macroscopic DNA-driven NP assemblies need to be developed for the fabrication of photonic devices. Finally, DNA molecules not only possessed unique recognition for biosensing and bioimaging, but also showed stimuli-controlled mechanical changes for applications in switchable electrocatalysis and actuators. With further development and improvement, some of the challenges will be solved, and NP assemblies with excellent biocompatibility, strong stability and higher sensitivity will be used in the field of macroscopical materials and photonic devices.

Acknowledgements This work was supported financially by the Natural Science Foundation of Jiangsu Province (BK20171136), National First-class Discipline Program of Food Science and Technology (JUFSTR20180302).

References

1. Zhang Y, Pal S, Srinivasan B, Vo T, Kumar S, Gang O (2015) Selective transformations between nanoparticle superlattices via the reprogramming of DNA-mediated interactions. *Nat Mater* 14(8):840–847. <https://doi.org/10.1038/nmat4296>
2. Zhao Y, Sun M, Ma W, Kuang H, Xu C (2017) Biological Molecules-governed plasmonic nanoparticle dimers with tailored optical behaviors. *J Phys Chem Lett* 8(22):5633–5642. <https://doi.org/10.1021/acs.jpcllett.7b01781>

3. Hu Y, Kahn JS, Guo W, Huang F, Fadeev M, Harries D, Willner I (2016) Reversible modulation of DNA-based hydrogel shapes by internal stress interactions. *J Am Chem Soc* 138(49):16112–16119. <https://doi.org/10.1021/jacs.6b10458>
4. Pu F, Ren J, Qu X (2018) Nucleobases, nucleosides, and nucleotides: versatile biomolecules for generating functional nanomaterials. *Chem Soc Rev* 47(4):1285–1306. <https://doi.org/10.1039/c7cs00673j>
5. Hu Q, Li H, Wang L, Gu H, Fan C (2019) DNA nanotechnology-enabled drug delivery systems. *Chem Rev* 119(10):6459–6506. <https://doi.org/10.1021/acs.chemrev.7b00663>
6. Wang Y, Zhu Y, Hu Y, Zeng G, Zhang Y, Zhang C, Feng C (2018) How to construct DNA hydrogels for environmental applications: advanced water treatment and environmental analysis. *Small* 14(17):e1703305. <https://doi.org/10.1002/smll.201703305>
7. Chou LY, Zagorovsky K, Chan WC (2014) DNA assembly of nanoparticle superstructures for controlled biological delivery and elimination. *Nat Nanotechnol* 9(2):148–155. <https://doi.org/10.1038/nnano.2013.309>
8. Wu X, Hao C, Kumar J, Kuang H, Kotov NA, Liz-Marzan LM, Xu C (2018) Environmentally responsive plasmonic nanoassemblies for biosensing. *Chem Soc Rev* 47(13):4677–4696. <https://doi.org/10.1039/c7cs00894e>
9. Liu X, Zhang F, Jing X, Pan M, Liu P, Li W, Zhu B, Li J, Chen H, Wang L, Lin J, Liu Y, Zhao D, Yan H, Fan C (2018) Complex silica composite nanomaterials templated with DNA origami. *Nature* 559(7715):593–598. <https://doi.org/10.1038/s41586-018-0332-7>
10. Maye MM, Kumara MT, Nykypanchuk D, Sherman WB, Gang O (2010) Switching binary states of nanoparticle superlattices and dimer clusters by DNA strands. *Nat Nanotechnol* 5(2):116–120. <https://doi.org/10.1038/nnano.2009.378>
11. Zhao Y, Yang X, Li H, Luo Y, Yu R, Zhang L, Yang Y, Song Q (2015) Au nanoflower-Ag nanoparticle assembled SERS-active substrates for sensitive MC-LR detection. *Chem Commun (Camb)* 51(95):16908–16911. <https://doi.org/10.1039/c5cc05868f>
12. Zhao Y, Xu L, Ma W, Liu L, Wang L, Kuang H, Xu C (2014) Shell-programmed Au nanoparticle heterodimers with customized chiroptical activity. *Small* 10(22):4770–4777. <https://doi.org/10.1002/smll.201401203>
13. Zhao Y, Xu L, Ma W, Wang L, Kuang H, Xu C, Kotov NA (2014) Shell-engineered chiroplasmonic assemblies of nanoparticles for zeptomolar DNA detection. *Nano Lett* 14(7):3908–3913. <https://doi.org/10.1021/nl501166m>
14. Ma W, Kuang H, Xu L, Ding L, Xu C, Wang L, Kotov NA (2013) Attomolar DNA detection with chiral nanorod assemblies. *Nat Commun* 4:2689. <https://doi.org/10.1038/ncomms3689>
15. Zhao Y, Xu L, Liz-Marzán LM, Kuang H, Ma W, Asenjo-García A, García de Abajo FJ, Kotov NA, Wang L, Xu C (2013) Alternating plasmonic nanoparticle heterochains made by polymerase Chain reaction and their optical properties. *J Phys Chem Lett* 4(4):641–647. <https://doi.org/10.1021/jz400045s>
16. Sun M, Qu A, Hao C, Wu X, Xu L, Xu C, Kuang H (2018) Chiral upconversion heterodimers for quantitative analysis and bioimaging of antibiotic-resistant bacteria in vivo. *Adv Mater* 30(50):e1804241. <https://doi.org/10.1002/adma.201804241>
17. Zhao Y, Xu L, Kuang H, Wang L, Xu C (2012) Asymmetric and symmetric PCR of gold nanoparticles: a pathway to scaled-up self-assembly with tunable chirality. *J Mater Chem* 22(12):5574. <https://doi.org/10.1039/c2jm15800k>
18. Hong F, Zhang F, Liu Y, Yan H (2017) DNA origami: scaffolds for creating higher order structures. *Chem Rev* 117(20):12584–12640. <https://doi.org/10.1021/acs.chemrev.6b00825>
19. Tanwar S, Haldar KK, Sen T (2017) DNA origami directed Au nanostar dimers for single-molecule surface-enhanced raman scattering. *J Am Chem Soc* 139(48):17639–17648. <https://doi.org/10.1021/jacs.7b10410>
20. Li Y, Liu Z, Yu G, Jiang W, Mao C (2015) Self-assembly of molecule-like nanoparticle clusters directed by DNA nanocages. *J Am Chem Soc* 137(13):4320–4323. <https://doi.org/10.1021/jacs.5b01196>
21. Tian Y, Wang T, Liu W, Xin HL, Li H, Ke Y, Shih WM, Gang O (2015) Prescribed nanoparticle cluster architectures and low-dimensional arrays built using octahedral DNA origami frames. *Nat Nanotechnol* 10(7):637–644. <https://doi.org/10.1038/nnano.2015.105>
22. Zhang Y, Chao J, Liu H, Wang F, Su S, Liu B, Zhang L, Shi J, Wang L, Huang W, Wang L, Fan C (2016) Transfer of two-dimensional oligonucleotide patterns onto stereocontrolled

- plasmonic nanostructures through DNA-origami-based nanoimprinting lithography. *Angew Chem* 55(28):8036–8040. <https://doi.org/10.1002/anie.201512022>
23. Tian S, Neumann O, McClain MJ, Yang X, Zhou L, Zhang C, Nordlander P, Halas NJ (2017) Aluminum nanocrystals: a sustainable substrate for quantitative SERS-based DNA detection. *Nano Lett* 17(8):5071–5077. <https://doi.org/10.1021/acs.nanolett.7b02338>
 24. Tikhomirov G, Hoogland S, Lee PE, Fischer A, Sargent EH, Kelley SO (2011) DNA-based programming of quantum dot valency, self-assembly and luminescence. *Nat Nanotechnol* 6(8):485–490. <https://doi.org/10.1038/nnano.2011.100>
 25. Zhang L, Jean SR, Li X, Sack T, Wang Z, Ahmed S, Chan G, Das J, Zaragoza A, Sargent EH, Kelley SO (2018) Programmable metal/semiconductor nanostructures for mRNA-modulated molecular delivery. *Nano Lett* 18(10):6222–6228. <https://doi.org/10.1021/acs.nanolett.8b02263>
 26. Yan W, Xu L, Xu C, Ma W, Kuang H, Wang L, Kotov NA (2012) Self-assembly of chiral nanoparticle pyramids with strong R/S optical activity. *J Am Chem Soc* 134(36):15114–15121. <https://doi.org/10.1021/ja3066336>
 27. Gorris HH, Wolfbeis OS (2013) Photon-upconverting nanoparticles for optical encoding and multiplexing of cells, biomolecules, and microspheres. *Angew Chem* 52(13):3584–3600. <https://doi.org/10.1002/anie.201208196>
 28. Kumar M, Zhang P (2009) Highly sensitive and selective label-free optical detection of DNA hybridization based on photon upconverting nanoparticles. *Langmuir* 25(11):6024–6027. <https://doi.org/10.1021/la900936p>
 29. Kumar M, Zhang P (2010) Highly sensitive and selective label-free optical detection of mercuric ions using photon upconverting nanoparticles. *Biosens Bioelectron* 25(11):2431–2435. <https://doi.org/10.1016/j.bios.2010.03.038>
 30. Sun M, Ma W, Xu L, Wang L, Kuang H, Xu C (2014) Chirality of self-assembled metal-semiconductor nanostructures. *J Mater Chem C* 2(15):2702–2706. <https://doi.org/10.1039/C4TC00040D>
 31. Li LL, Wu P, Hwang K, Lu Y (2013) An exceptionally simple strategy for DNA-functionalized up-conversion nanoparticles as biocompatible agents for nanoassembly, DNA delivery, and imaging. *J Am Chem Soc* 135(7):2411–2414. <https://doi.org/10.1021/ja310432u>
 32. Li S, Xu L, Ma W, Wu X, Sun M, Kuang H, Wang L, Kotov NA, Xu C (2016) Dual-mode ultra-sensitive quantification of microRNA in living cells by chiroplasmonic nanopyramids self-assembled from gold and upconversion nanoparticles. *J Am Chem Soc* 138(1):306–312. <https://doi.org/10.1021/jacs.5b10309>
 33. Li S, Xu L, Sun M, Wu X, Liu L, Kuang H, Xu C (2017) Hybrid nanoparticle pyramids for intracellular dual micrornas biosensing and bioimaging. *Adv Mater*. <https://doi.org/10.1002/adma.201606086>
 34. Qu A, Sun M, Xu L, Hao C, Wu X, Xu C, Kotov NA, Kuang H (2019) Quantitative zeptomolar imaging of miRNA cancer markers with nanoparticle assemblies. *Proc Natl Acad Sci USA* 116(9):3391–3400. <https://doi.org/10.1073/pnas.1810764116>
 35. Ma W, Fu P, Sun M, Xu L, Kuang H, Xu C (2017) Dual quantification of microRNAs and telomerase in living cells. *J Am Chem Soc* 139(34):11752–11759. <https://doi.org/10.1021/jacs.7b03617>
 36. Sun M, Xu L, Ma W, Wu X, Kuang H, Wang L, Xu C (2016) Hierarchical plasmonic nanorods and upconversion core-satellite nanoassemblies for multimodal imaging-guided combination phototherapy. *Adv Mater* 28(5):898–904. <https://doi.org/10.1002/adma.201505023>
 37. Wu X, Xu L, Ma W, Liu L, Kuang H, Kotov NA, Xu C (2016) Propeller-like nanorod-upconversion nanoparticle assemblies with intense chiroptical activity and luminescence enhancement in aqueous phase. *Adv Mater* 28(28):5907–5915. <https://doi.org/10.1002/adma.201601261>
 38. Tang L, Wang Y, Li J (2015) The graphene/nucleic acid nanobiointerface. *Chem Soc Rev* 44(19):6954–6980. <https://doi.org/10.1039/c4cs00519h>
 39. Parvin N, Jin Q, Wei Y, Yu R, Zheng B, Huang L, Zhang Y, Wang L, Zhang H, Gao M, Zhao H, Hu W, Li Y, Wang D (2017) Few-layer graphdiyne nanosheets applied for multiplexed real-time DNA detection. *Adv Mater*. <https://doi.org/10.1002/adma.201606755>
 40. Patil AJ, Vickery JL, Scott TB, Mann S (2009) Aqueous stabilization and self-assembly of graphene sheets into layered bio-nanocomposites using DNA. *Adv Mater* 21(31):3159–3164. <https://doi.org/10.1002/adma.200803633>
 41. Meng X, Wang H, Chen N, Ding P, Shi H, Zhai X, Su Y, He Y (2018) A graphene-silver nanoparticle-silicon sandwich SERS chip for quantitative detection of molecules and capture, discrimination, and inactivation of bacteria. *Anal Chem* 90(9):5646–5653. <https://doi.org/10.1021/acs.analchem.7b05139>

42. Ma W, Sun M, Fu P, Li S, Xu L, Kuang H, Xu C (2017) A chiral-nanoassemblies-enabled strategy for simultaneously profiling surface glycoprotein and microRNA in living cells. *Adv Mater*. <https://doi.org/10.1002/adma.201703410>
43. Zhao Y, Cui L, Sun Y, Zheng F, Ke W (2018) Ag/CdO NPs engineered magnetic electrochemical aptasensor for prostatic specific antigen detection. *ACS Appl Mater Interface*. <https://doi.org/10.1021/acsami.8b18887>
44. Zhao Y, Zheng F, Ke W, Zhang W, Shi L, Liu H (2019) Gap-Tethered Au@AgAu raman tags for the ratiometric detection of MC-LR. *Anal Chem* 91(11):7162–7172. <https://doi.org/10.1021/acs.analchem.9b00348>
45. Streit JK, Fagan JA, Zheng M (2017) A low energy route to DNA-wrapped carbon nanotubes via replacement of bile salt surfactants. *Anal Chem* 89(19):10496–10503. <https://doi.org/10.1021/acs.analchem.7b02637>
46. Maune HT, Han SP, Barish RD, Bockrath M, Goddard WA III, Rothmund PW, Winfree E (2010) Self-assembly of carbon nanotubes into two-dimensional geometries using DNA origami templates. *Nat Nanotechnol* 5(1):61–66. <https://doi.org/10.1038/nnano.2009.311>
47. He W, Dai J, Li T, Bao Y, Yang F, Zhang X, Uyama H (2018) Novel strategy for the investigation on chirality selection of single-walled carbon nanotubes with DNA by electrochemical characterization. *Anal Chem* 90(21):12810–12814. <https://doi.org/10.1021/acs.analchem.8b03323>
48. Chen Y, Liu H, Ye T, Kim J, Mao C (2007) DNA-directed assembly of single-wall carbon nanotubes. *J Am Chem Soc* 129:8696–8697
49. Freeley M, Attanzio A, Ceconello A, Amoroso G, Clement P, Fernandez G, Gesuele F, Palma M (2018) Tuning the coupling in single-molecule heterostructures: DNA-programmed and reconfigurable carbon nanotube-based nanohybrids. *Adv Sci (Weinh)* 5(10):1800596. <https://doi.org/10.1002/advs.201800596>
50. Gui R, He W, Jin H, Sun J, Wang Y (2018) DNA assembly of carbon dots and 5-fluorouracil used for room-temperature phosphorescence turn-on sensing of AFP and AFP-triggered simultaneous release of dual-drug. *Sens Actuators B* 255:1623–1630. <https://doi.org/10.1016/j.snb.2017.08.178>
51. Qian ZS, Shan XY, Chai LJ, Chen JR, Feng H (2015) A fluorescent nanosensor based on graphene quantum dots-aptamer probe and graphene oxide platform for detection of lead (II) ion. *Biosens Bioelectron* 68:225–231. <https://doi.org/10.1016/j.bios.2014.12.057>
52. Xia Y, Wang L, Li J, Chen X, Lan J, Yan A, Lei Y, Yang S, Yang H, Chen J (2018) A ratiometric fluorescent bioprobe based on carbon dots and acridone derivate for signal amplification detection exosomal microRNA. *Anal Chem* 90(15):8969–8976. <https://doi.org/10.1021/acs.analchem.8b01143>
53. Xu L, Gao Y, Kuang H, Liz-Marzan LM, Xu C (2018) MicroRNA-directed intracellular self-assembly of chiral nanorod dimers. *Angew Chem* 57(33):10544–10548. <https://doi.org/10.1002/anie.201805640>
54. Jiang X, Tan Z, Lin L, He J, He C, Thackray BD, Zhang Y, Ye J (2018) Surface-enhanced raman nanoprobe with embedded standards for quantitative cholesterol detection. *Small Methods*. <https://doi.org/10.1002/smt.201800182>
55. Zeng Y, Ren JQ, Shen AG, Hu JM (2018) Splicing nanoparticles-based “Click” SERS could aid multiplex liquid biopsy and accurate cellular imaging. *J Am Chem Soc* 140(34):10649–10652. <https://doi.org/10.1021/jacs.8b04892>
56. Zhao Y, Liu L, Kuang H, Wang L, Xu C (2014) SERS-active Ag@Au core-shell NP assemblies for DNA detection. *RSC Adv* 4(99):56052–56056. <https://doi.org/10.1039/c4ra11112e>
57. Zhang K, Wang Y, Wu M, Liu Y, Shi D, Liu B (2018) On-demand quantitative SERS bioassays facilitated by surface-tethered ratiometric probes. *Chem Sci* 9(42):8089–8093. <https://doi.org/10.1039/c8sc03263g>
58. Lin L, Zapata M, Xiong M, Liu Z, Wang S, Xu H, Borisov AG, Gu H, Nordlander P, Aizpurua J, Ye J (2015) Nanooptics of plasmonic nanomatryoshkas: shrinking the size of a core-shell junction to subnanometer. *Nano Lett* 15(10):6419–6428. <https://doi.org/10.1021/acs.nanolett.5b02931>
59. Tang L, Li S, Han F, Liu L, Xu L, Ma W, Kuang H, Li A, Wang L, Xu C (2015) SERS-active Au@Ag nanorod dimers for ultrasensitive dopamine detection. *Biosens Bioelectron* 71:7–12. <https://doi.org/10.1016/j.bios.2015.04.013>
60. Gao F, Liu L, Cui G, Xu L, Wu X, Kuang H, Xu C (2017) Regioselective plasmonic nano-assemblies for bimodal sub-femtomolar dopamine detection. *Nanoscale* 9(1):223–229. <https://doi.org/10.1039/c6nr08264e>

61. Wu X, Xu L, Liu L, Ma W, Yin H, Kuang H, Wang L, Xu C, Kotov NA (2013) Unexpected chirality of nanoparticle dimers and ultrasensitive chiroplasmonic bioanalysis. *J Am Chem Soc* 135(49):18629–18636. <https://doi.org/10.1021/ja4095445>
62. Osberg KD, Rycenga M, Harris N, Schmucker AL, Langille MR, Schatz GC, Mirkin CA (2012) Dispersible gold nanorod dimers with sub-5 nm gaps as local amplifiers for surface-enhanced Raman scattering. *Nano Lett* 12(7):3828–3832. <https://doi.org/10.1021/nl301793k>
63. Li S, Xu L, Ma W, Kuang H, Wang L, Xu C (2015) Triple raman label-encoded gold nanoparticle trimers for simultaneous heavy metal ion detection. *Small* 11(28):3435–3439. <https://doi.org/10.1002/sml.201403356>
64. Shen X, Asenjo-Garcia A, Liu Q, Jiang Q, Garcia de Abajo FJ, Liu N, Ding B (2013) Three-dimensional plasmonic chiral tetramers assembled by DNA origami. *Nano Lett* 13(5):2128–2133. <https://doi.org/10.1021/nl400538y>
65. Kun L, Zhihong N, Nana Z, Wei L, Michael R, Eugenia K (2010) Step-growth polymerization of inorganic nanoparticles. *Science* 329(5988):197–200
66. Fang W, Jia S, Chao J, Wang L, Duan X, Liu H, Li Q, Zuo X, Wang L, Wang L, Liu N, Fan C (2019) Quantizing single-molecule surface-enhanced Raman scattering with DNA origami meta-molecules. *Sci Adv* 5(eaau4506):1–8
67. Zhao S, Ma W, Xu L, Wu X, Kuang H, Wang L, Xu C (2015) Ultrasensitive SERS detection of VEGF based on a self-assembled Ag ornamented–Au pyramid superstructure. *Biosens Bioelectron* 68:593–597. <https://doi.org/10.1016/j.bios.2015.01.056>
68. Ma W, Sun M, Xu L, Wang L, Kuang H, Xu C (2013) A SERS active gold nanostar dimer for mercury ion detection. *Chem Commun (Camb)* 49(44):4989–4991. <https://doi.org/10.1039/c3cc39087j>
69. Qu A, Wu X, Xu L, Liu L, Ma W, Kuang H, Xu C (2017) SERS- and luminescence-active Au–Au–UCNP trimers for attomolar detection of two cancer biomarkers. *Nanoscale* 9(11):3865–3872. <https://doi.org/10.1039/c6nr09114h>
70. Lu Y, Ma Y, Zhang T, Yang Y, Wei L, Chen Y (2018) Monolithic 3D cross-linked polymeric graphene materials and the likes: preparation and their redox catalytic applications. *J Am Chem Soc* 140(37):11538–11550. <https://doi.org/10.1021/jacs.8b06414>
71. Zhang Y, Zeng GM, Tang L, Chen J, Zhu Y, He XX, He Y (2015) Electrochemical sensor based on electrodeposited graphene-Au modified electrode and nanoAu carrier amplified signal strategy for attomolar mercury detection. *Anal Chem* 87(2):989–996. <https://doi.org/10.1021/ac503472p>
72. Zhao Y, Yang Y, Luo Y, Yang X, Li M, Song Q (2015) Double detection of mycotoxins based on sers labels embedded Ag@Au core-shell nanoparticles. *ACS Appl Mater Inter* 7(39):21780–21786. <https://doi.org/10.1021/acsami.5b07804>
73. Zheng F, Ke W, Shi L, Liu H, Zhao Y (2019) Plasmonic Au–Ag janus nanoparticle engineered ratiometric surface-enhanced raman scattering aptasensor for Ochratoxin A detection. *Anal Chem* 91(18):11812–11820. <https://doi.org/10.1021/acs.analchem.9b02469>
74. Ma W, Xu L, de Moura AF, Wu X, Kuang H, Xu C, Kotov NA (2017) Chiral inorganic nanostructures. *Chem Rev* 117(12):8041–8093. <https://doi.org/10.1021/acs.chemrev.6b00755>
75. Hao C, Xu L, Ma W, Wang L, Kuang H, Xu C (2014) Assembled plasmonic asymmetric heterodimers with tailorable chiroptical response. *Small* 10(9):1805–1812. <https://doi.org/10.1002/sml.201303755>
76. Hao C, Xu L, Sun M, Ma W, Kuang H, Xu C (2018) Chirality on hierarchical self-assembly of Au@AuAg Yolk-Shell nanorods into core-satellite superstructures for biosensing in human cells. *Adv Funct Mater*. <https://doi.org/10.1002/adfm.201802372>
77. Kuzyk A, Schreiber R, Fan Z, Pardatscher G, Roller EM, Hoge A, Simmel FC, Govorov AO, Liedl T (2012) DNA-based self-assembly of chiral plasmonic nanostructures with tailored optical response. *Nature* 483(7389):311–314. <https://doi.org/10.1038/nature10889>
78. Sun M, Hao T, Li X, Qu A, Xu L, Hao C, Xu C, Kuang H (2018) Direct observation of selective autophagy induction in cells and tissues by self-assembled chiral nanodevice. *Nat Commun* 9(1):4494. <https://doi.org/10.1038/s41467-018-06946-z>
79. Yang L, Chen Y, Pan W, Wang H, Li N, Tang B (2017) Visualizing the conversion process of alcohol-induced fatty liver to steatohepatitis in vivo with a fluorescent nanoprobe. *Anal Chem* 89(11):6196–6201. <https://doi.org/10.1021/acs.analchem.7b01144>
80. Zhao X, Xu L, Sun M, Ma W, Wu X, Kuang H, Wang L, Xu C (2016) Gold-quantum dot core-satellite assemblies for lighting up microRNA in vitro and in vivo. *Small* 12(34):4662–4668. <https://doi.org/10.1002/sml.201503629>


81. Qu A, Xu L, Sun M, Liu L, Kuang H, Xu C (2017) Photoactive hybrid AuNR-Pt@Ag₂S core-satellite nanostructures for near-infrared quantitative cell imaging. *Adv Funct Mater* 27(46):1703408. <https://doi.org/10.1002/adfm.201703408>
82. Zhao Y, Hao C, Ma W, Yong Q, Yan W, Kuang H, Wang L, Xu C (2011) Magnetic bead-based multiplex DNA sequence detection of genetically modified organisms using quantum dot-encoded silicon dioxide nanoparticles. *J Phys Chem C* 115(41):20134–20140. <https://doi.org/10.1021/jp206443p>
83. Xu LJ, Lei ZC, Li J, Zong C, Yang CJ, Ren B (2015) Label-free surface-enhanced Raman spectroscopy detection of DNA with single-base sensitivity. *J Am Chem Soc* 137(15):5149–5154. <https://doi.org/10.1021/jacs.5b01426>
84. Ma W, Xu L, Wang L, Xu C, Kuang H (2019) Chirality-based biosensors. *Adv Func Mater*. <https://doi.org/10.1002/adfm.201805512>
85. Li A, Tang L, Song D, Song S, Ma W, Xu L, Kuang H, Wu X, Liu L, Chen X, Xu C (2016) A SERS-active sensor based on heterogeneous gold nanostar core-silver nanoparticle satellite assemblies for ultrasensitive detection of aflatoxinB1. *Nanoscale* 8(4):1873–1878. <https://doi.org/10.1039/c5nr08372a>
86. Yuan A, Wu X, Li X, Hao C, Xu C, Kuang H (2019) Au@gap@AuAg nanorod side-by-side assemblies for ultrasensitive SERS detection of mercury and its transformation. *Small*. <https://doi.org/10.1002/sml.201901958>
87. Xu L, Yan W, Ma W, Kuang H, Wu X, Liu L, Zhao Y, Wang L, Xu C (2015) SERS encoded silver pyramids for attomolar detection of multiplexed disease biomarkers. *Adv Mater* 27(10):1706–1711. <https://doi.org/10.1002/adma.201402244>
88. Wang Y, Wang S, Lu C, Yang X (2018) Three kinds of DNA-directed nanoclusters cooperating with graphene oxide for assaying mucin 1, carcinoembryonic antigen and cancer antigen 125. *Sens Actuators B* 262:9–16. <https://doi.org/10.1016/j.snb.2018.01.235>
89. Hao T, Wu X, Xu L, Liu L, Ma W, Kuang H, Xu C (2017) Ultrasensitive detection of prostate-specific antigen and thrombin based on gold-upconversion nanoparticle assembled pyramids. *Small*. <https://doi.org/10.1002/sml.201603944>
90. Zhao Y, Yang Y, Zhao J, Weng P, Pang Q, Song Q (2016) Dynamic chiral nanoparticle assemblies and specific chiroplasmonic analysis of cancer cells. *Adv Mater* 28(24):4877–4883. <https://doi.org/10.1002/adma.201600369>
91. Tang L, Li S, Xu L, Ma W, Kuang H, Wang L, Xu C (2015) Chirality-based Au@Ag nanorod dimers sensor for ultrasensitive PSA detection. *ACS Appl Mater Inter* 7(23):12708–12712. <https://doi.org/10.1021/acsami.5b01259>
92. Shu Y, Zheng N, Zheng A-Q, Guo T-T, Yu Y-L, Wang J-H (2019) Intracellular zinc quantification by fluorescence imaging with a FRET system. *Anal Chem* 91(6):4157–4163. <https://doi.org/10.1021/acs.analchem.9b00018>
93. Gao R, Xu L, Hao C, Xu C, Kuang H (2019) Circular polarized light activated chiral satellite nanoprobe for the imaging and analysis of multiple metal ions in living cells. *Angew Chem Interface Ed* 58(12):3913–3917. <https://doi.org/10.1002/anie.201814282>
94. Gao F, Sun M, Ma W, Wu X, Liu L, Kuang H, Xu C (2017) A singlet oxygen generating agent by chirality-dependent plasmonic shell-satellite nanoassembly. *Adv Mater*. <https://doi.org/10.1002/adma.201606864>
95. Sun M, Xu L, Qu A, Zhao P, Hao T, Ma W, Hao C, Wen X, Colombari FM, de Moura AF, Kotov NA, Xu C, Kuang H (2018) Site-selective photoinduced cleavage and profiling of DNA by chiral semiconductor nanoparticles. *Nat Chem* 10(8):821–830. <https://doi.org/10.1038/s41557-018-0083-y>

Publisher's Note Springer Nature remains neutral with regard to jurisdictional claims in published maps and institutional affiliations.



REVIEW

Aptamer-Functionalized DNA Nanostructures for Biological Applications

Xiaoyi Fu¹ · Fangqi Peng¹ · Jungyeon Lee² · Qi Yang² · Fei Zhang² · Mengyi Xiong¹ · Gezhi Kong¹ · Hong-min Meng³ · Guoliang Ke¹  · Xiao-Bing Zhang¹

Received: 31 October 2019 / Accepted: 17 January 2020 / Published online: 7 February 2020
© Springer Nature Switzerland AG 2020

Abstract

DNA nanostructures hold great promise for various applications due to their remarkable properties, including programmable assembly, nanometric positional precision, and dynamic structural control. The past few decades have seen the development of various kinds of DNA nanostructures that can be employed as useful tools in fields such as chemistry, materials, biology, and medicine. Aptamers are short single-stranded nucleic acids that bind to specific targets with excellent selectivity and high affinity and play critical roles in molecular recognition. Recently, many attempts have been made to integrate aptamers with DNA nanostructures for a range of biological applications. This review starts with an introduction to the features of aptamer-functionalized DNA nanostructures. The discussion then focuses on recent progress (particularly during the last five years) in the applications of these nanostructures in areas such as biosensing, bioimaging, cancer therapy, and biophysics. Finally, challenges involved in the practical application of aptamer-functionalized DNA nanostructures are discussed, and perspectives on future directions for research into and applications of aptamer-functionalized DNA nanostructures are provided.

Keywords Aptamer · DNA nanostructures · DNA origami · Biosensing · Bioimaging · Drug delivery

Chapter 10 was originally published as Fu, X., Peng, F., Lee J., Yang, Qi., Zhang, F., Xiong, M., Kong, G., Meng, H-m., Ke, G. & Zhang, X-B. Topics in Current Chemistry (2020) 378: 21. <https://doi.org/10.1007/s41061-020-0283-y>.

✉ Guoliang Ke
glke@hnu.edu.cn

¹ State Key Laboratory of Chemo/Biosensing and Chemometrics, College of Chemistry and Chemical Engineering, Hunan University, Changsha 410082, China

² Department of Chemistry, Rutgers University, 73 Warren Street, Newark, NJ 07102, USA

³ College of Chemistry, Zhengzhou University, Zhengzhou 450001, China

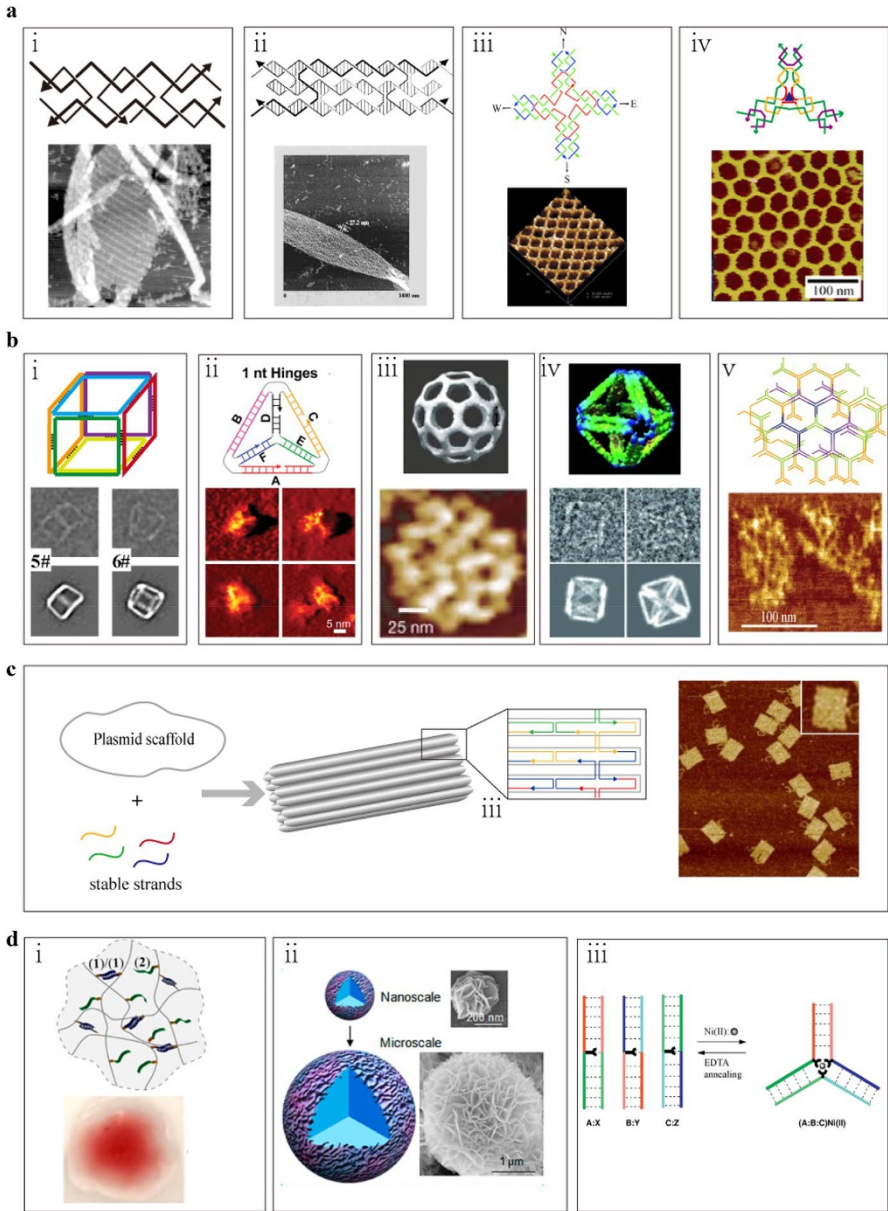
Fig. 1 Examples of representative classes of designed DNA nanostructures. **a** The building blocks of nanostructures: (i) double-crossover (DX) tiles (reproduced with permission from [7], copyright 1998 Springer Nature), (ii) triple-crossover (TX) tiles (reproduced with permission from [8], copyright 2000 American Chemical Society), (iii) 4×4 tiles (reproduced with permission from [9], copyright 2003 American Association for the Advancement of Science), (iv) three-point star tiles (reproduced with permission from [11], copyright 2005 American Chemical Society). **b** Higher-order DNA nanostructures constructed from tiles through bottom-up assembly: (i) DNA cube (reproduced with permission from [13], copyright 2009 American Chemical Society), (ii) DNA tetrahedron (reproduced with permission from [14], copyright 2005 American Association for the Advancement of Science), (iii) DNA polyhedron (reproduced with permission from [10], copyright 2008 Springer Nature), (iv) DNA octahedron (reproduced with permission from [16], copyright 2017 Chinese Chemical Society and Institute of Materia Medica, Chinese Academy of Medical Sciences), and (v) DNA dendrimer (reproduced with permission from [19], copyright 2014 American Chemical Society). **c** DNA origami-based structures (reproduced with permission from [20], copyright 2016 Wiley–VCH Verlag GmbH and Co. KGaA). **d** Other DNA nanostructures, including (i) DNA nanohydrogels produced by gelation (reproduced with permission from [21], copyright 2015 American Chemical Society), (ii) DNA nanoflowers prepared by rolling circle amplification-templated assembly (reproduced with permission from [22], copyright 2013 American Chemical Society), and (iii) metal-induced DNA assembly (reproduced with permission from [23], copyright 2015 Wiley–VCH)

1 Introduction

Nanotechnology, which utilizes various kinds of nanomaterials, has been widely applied in fields such as chemistry [1], biology [2], and medicine [3], among many others [4]. Nucleic acids (DNAs and RNAs), the genetic information carriers in living cells, are regarded as important building blocks for fabricating nanomaterials. Ever since Seeman first proposed the concept of structural DNA nanotechnology in 1982 [5], there has been increasing interest in fabricating DNA structures with controllability and versatility that can be applied in the field of nanobiotechnology. Compared to dsDNA helices, DNA nanostructures possess more complex and rigid structures due to the presence of immobile Holliday junctions. Various kinds of DNA nanostructures have been developed. The most basic DNA nanostructures are simple DNA tiles (Fig. 1a), such as double crossovers (DX) [6, 7], triple crossovers (TX) [8], 4×4 tiles [9], and three-point stars [10, 11].

Higher-order nanostructures can be assembled from the bottom up from DNA tiles (Fig. 1b). Such nanostructures include cubes [12, 13], tetrahedrons [14], polyhedrons [10], octahedrons [15, 16], and DNA dendrimers [17–19]. In 2006, Rothemund [24] reported DNA origami (Fig. 1c), in which DNA self-folds into pre-designed shapes. More specifically, hundreds of short synthetic DNA strands termed “staples” are employed to bind at particular sites on a long single-stranded scaffold DNA (such as M13 phage genomic DNA, ~7249 bp), causing the scaffold DNA to fold into the required shape. Other methods of preparing other kinds of DNA nanostructures (Fig. 1d), such as gelation-induced DNA nanohydrogels [25–27], rolling circle amplification-templated DNA nanoflowers [22], and metal-induced DNA assembly [28], have also been reported.

DNA nanostructures have many unique advantages over other nanomaterials. First, the Watson–Crick base pairing of nucleobases (A–T/U and G–C) via hydrogen bonding makes nucleic acids powerful and programmable materials for preparing nanostructures. Second, DNA nanostructures are predictable at the molecular level,



which enables us to fabricate well-defined and uniform DNA nanostructures [29]. Third, DNA binding can occur reversibly in response to various external stimuli such as temperature [30], pH [31], and ionic strength [32], and this response can be tuned by altering the length and sequence of DNA. Fourth, DNA interacts with various chemical and biochemical species such as metal ions [33], tool enzymes [34], and small molecules [35], which can therefore be used to control the construction

or binding abilities of DNA. Fifth, the biocompatibility of DNA nanostructures facilitates their application *in vitro* and *in vivo* [36]. Finally, DNA nanostructures can interact with functional nucleic acids (e.g., aptamers [37], DNazymes [38], and molecular beacons [39]) through simple Watson–Crick base pairing. All of these features mean that DNA nanostructures are attractive tools in fields such as cellular biophysics, medical diagnostics and therapeutics, and biomimetic systems.

Aptamers are short single-stranded nucleic acids that are isolated from a random-sequence library comprising 10^{12-15} different oligonucleotides of DNA or RNA through a process termed systematic evolution of ligands by exponential enrichment (SELEX) [40–42]. An aptamer that folds into a unique secondary or tertiary structure can be used to bind to a target of interest with high specificity and affinity. Aptamers have received increasing interest from researchers since they were first reported by the groups of Szastak and Gold in 1990, as they represent a useful alternative to antibodies. While the dissociation constants (K_d) of aptamers are comparable to those of antibodies (they are often regarded as “chemical antibodies”), aptamers possess many advantages over antibodies [43], such as easy synthesis and modification, small size, good stability, a wide variety of possible targets (ranging from small molecules to cells or even pathogens), and good biocompatibility. Therefore, considerable effort has been directed into identifying a variety of aptamers that can be applied in bioanalysis, diagnosis, and therapy.

Given the attraction of combining the unique characteristics of DNA nanostructures with the advantages of aptamers, it is not surprising that a great deal of research has focused on constructing a series of aptamer-functionalized DNA nanostructures for bioanalytical and biomedical applications (Fig. 2). The present review summarizes recent studies (particularly those from the last five years) of aptamer-functionalized DNA nanostructures. It mainly focuses on four representative types of DNA nanostructures: tile-based structures, DNA origami, DNA-based polymers such as dendrimers, micelles, and hydrogels, and DNA nanoflowers. Recent progress in research into these aptamer-functionalized DNA nanostructures is reviewed, as are their applications in the fields of biosensing, bioimaging, and nanomedicine (among others). Finally, the remaining challenges in this area of research and probable future trends in aptamer-functionalized DNA nanostructures are discussed.

2 Aptamer-Functionalized DNA Nanostructures for Biosensing Applications

Biosensors are useful analytical tools that include a biological sensing element. They have been widely applied in the pharmaceutical industry [44], disease diagnosis [45], food safety [46], and environmental monitoring [47]. Because the field of biosensors is undergoing phenomenal growth, an increasing number of novel analytical methods (e.g., nanomaterial-based probes) have been explored in this field in recent years [48]. Aptamers can specifically recognize various targets such as metal ions, proteins, small molecules, and even cells, which makes them promising analytical tools that can be incorporated into various sensing platforms [49]. Because it is possible to attach aptamers at nanometrically precise locations on DNA nanostructures,

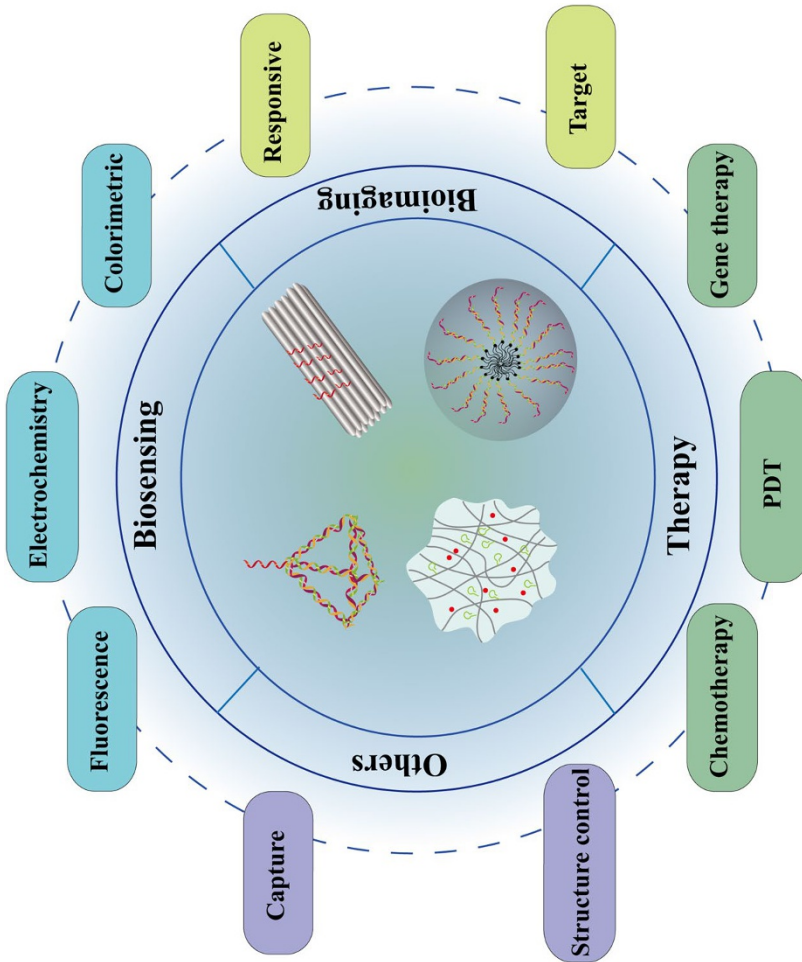


Fig. 2 Summary of the uses of aptamer-functionalized DNA nanostructures for biosensing, bioimaging, therapy, and other applications

aptamer-functionalized DNA nanostructures have great potential to detect targets through various sensing methods [50, 51]. Therefore, an increasing number of electrochemical and optical sensing platforms based on aptamer-functionalized DNA nanostructures have been exploited in recent years [52]. Here, we categorize these sensing methods into fluorescent biosensors, electrochemical biosensors, colorimetric biosensors, and other biosensors, based on the signal transduction mechanism involved.

2.1 Fluorescent Biosensors

Fluorescent biosensors make use of the physicochemical phenomenon known as fluorescence. When the analyte of interest is present, the emission characteristics (e.g., fluorescence intensity, fluorescence lifetime, and fluorescence isotropy) of the fluorophores used in the biosensor change. Below, we review the utilization of aptamer-functionalized DNA nanostructures in fluorescence biosensors employed for extracellular and intracellular biosensing.

2.1.1 Biosensing in a Tube

There are currently two ways to fabricate aptamer-functionalized DNA nanostructures for use as extracellular biosensors. The first approach is based on the rigidity and stability of DNA nanostructures. The fluorescent aptamer-based sensor is directly immobilized on a solid substrate [53, 54], thus expanding its range of biological applications. For example, Li et al. [53] immobilized a micrometer-sized DNA superstructure (“3D DNA”) on paper (Fig. 3a). They integrated a fluorescently labeled thrombin (or ATP) aptamer (i.e., an aptamer that binds to thrombin/ATP) into the 3D DNA superstructure using rolling circle amplification, leading to fluorescence enhancement in the presence of thrombin (or ATP). By combining the ability of 3D DNA to adhere to the surface of paper via physisorption with the features of functional DNA (aptamers or DNAzymes), assembled structures of this nature offer a strategy for designing high-density, surface-tethered nucleic acid probe (SNAP)-based paper sensors. Song et al. [54] constructed a DNA-tetrahedron-based fluorescent microarray platform for detecting various target types. By fabricating DNA tetrahedra on a glass substrate via amine–aldehyde interactions, it was possible to position capture probes with a specific alignment and with defined spacing of the probes at the vertices of tetrahedra, which provided the probes with a solution-phase-like environment for them to recognize the target. This strategy enabled the direct application of the fluorescent probe to the solid surface, facilitating high-throughput analysis. Appropriate design of the DNA nanostructure allowed various aptamers for specific biomolecules to be fixed indirectly to other solid surfaces in a specific orientation and with defined probe spacing.

The other way to fabricate aptamer-based sensors is through the rational design of DNA nanostructures that are intended for use in solution [55, 56]. For example, Wagenknecht et al. [55] put forward the concept of a “DNA traffic light” in solution. This design utilizes split aptamers as the recognition unit of a DNA origami tweezer

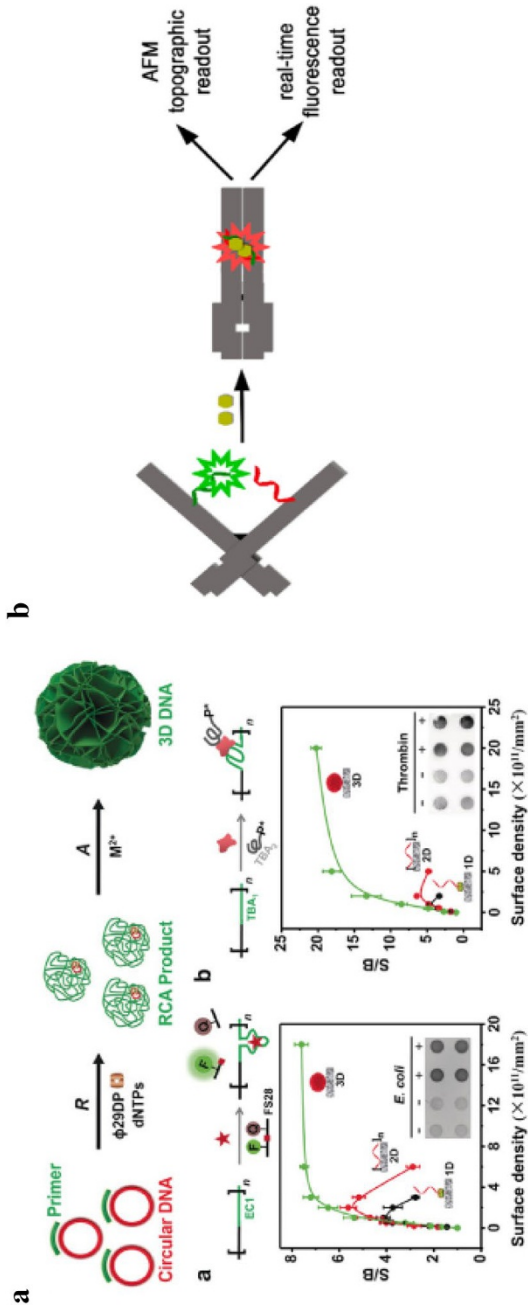


Fig. 3 Aptamer-functionalized DNA nanostructures for biosensing in a tube. **a** Schematic of the sensor based on 3D DNA on paper (reproduced with permission from [54], copyright 2018 Wiley-VCH Verlag GmbH and Co. KGaA). **b** Schematic of a “DNA traffic light” using a DNA origami tweezer with a split ATP aptamers in the presence of ATP (reproduced with permission from [55], copyright 2017 American Chemical Society)

that provides bicolor fluorescence readout (Fig. 3b). The stems of the split aptamers consist of donor and receptor fluorophores, respectively, which exhibit Förster resonance energy transfer (FRET) when the distance between the donor and the receptor is less than 10 nm. In the absence of ATP, the split aptamers are well separated, resulting in green fluorescence (the DNA origami is “open” and the FRET signal is off). When the DNA origami aptamers bind to ATP, the split aptamers move closer to each other, causing the fluorescence to change from green to red (the DNA origami is “closed” and the FRET signal is on). However, this assay can provide not only fluorescence readout but also topographic readout upon combining the DNA origami with AFM, representing a new strategy for bimodal sensor platforms. Tanner et al. [57] also reported an aptamer-functionalized DNA nanobox for the detection of the malaria biomarker protein *Plasmodium falciparum* lactate dehydrogenase (PfLDH) based on dual-modality (fluorescence and electron-microscopic) imaging. As well as small biomolecule detection, aptamer-functionalized DNA nanostructures can also be applied to detect whole cells [58].

2.1.2 Intracellular Biosensing

Aptamer-functionalized DNA nanostructures have also been successfully applied to detect biomolecules in cells, again making use of the rigidity and stability of these nanostructures [59]. For example, by modifying split aptamers with a DNA nanoprism, Huan et al. [60] developed an ATP-responsive biosensor for the stable, sensitive, and specific detection of ATP in living cells (Fig. 4a). In their design, the stems of the split aptamers are labeled with Cy3 and Cy5, leading to a FRET signal when the split aptamers bind to two ATP molecules. The use of the nanoprism in this design protects the probe from nuclease degradation.

In addition, some DNA aptamers (e.g., AS1411 and sgc-8) recognize proteins that are overexpressed on the surfaces of cancer cells and are internalized by cells. Thus, aptamers have been widely used as tools for transporting DNA nanoprobe into living cells. For example, Yang et al. [61] reported a DNA octahedron-based fluorescence nanoprobe for mRNA detection in living cells (Fig. 4b). Modification with the aptamer AS1411 allowed the DNA octahedron biosensor to be more efficiently internalized by cancer cells than normal cells, thus permitting the development of biosensors that facilitate specific cancer diagnoses or therapies. In order to enhance the detection sensitivity, Jie et al. [62] prepared a multifunctional DNA nanocage containing a nucleolin aptamer and fluorescent CdTe quantum dots for the fluorescence detection of human 8-oxoguanine DNA glycosylase 1 (hOGG1) with a detection limit of 0.001 U mL^{-1} .

2.2 Electrochemical Biosensors

Electrochemical biosensors have been widely applied in numerous fields, such as biomarker diagnosis [63], cancer cell screening [64], food safety [65], and environmental monitoring [66]. Compared to other aptamer-based biosensors, electrochemical methods possess the advantages of excellent sensitivity, high portability,

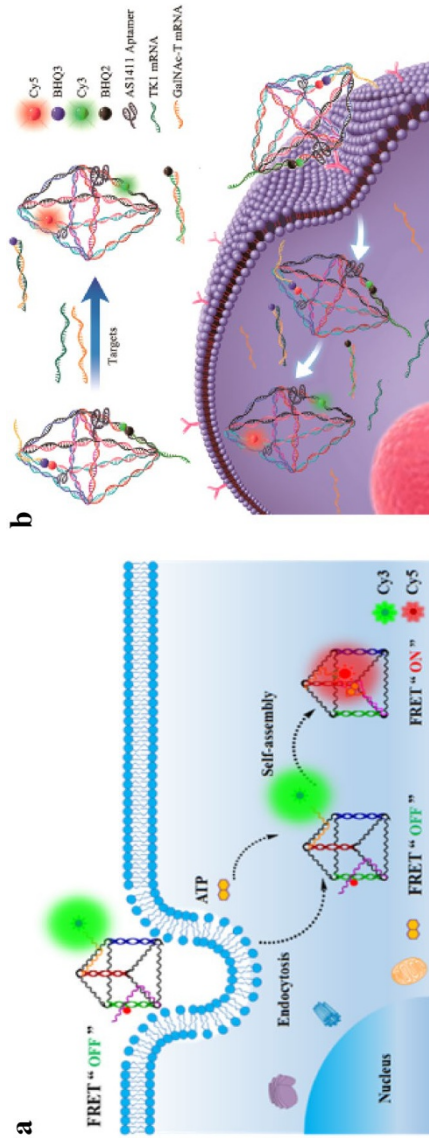


Fig. 4 Aptamer-functionalized DNA nanostructures for intracellular biosensing. **a** Schematic of split aptamers encapsulated in a DNA triangular prism for intracellular ATP sensing (reproduced with permission from [60], copyright 2017 American Chemical Society). **b** Schematic of the DNA octahedron that was integrated with the aptamer AS1411 for tumor-related mRNA detection in cells (reproduced with permission from [61], copyright 2018 American Chemical Society)

and rapid response. In an electrochemical aptasensor, the identification signal is converted to an electrical signal [67–69]. To date, most aptamer-functionalized DNA-nanostructure-based electrochemical biosensors have been based on labeled electrochemical biosensors in which the nucleic acids or aptamers are labeled with an electrochemically active substance or catalytically active inorganic/biological molecules such as ferrocene or peroxidase. Due to the mechanical rigidity and structural stability of DNA nanostructures, an electrochemical aptasensor can be anchored directly to an electrode surface, where it acts as an ultrasensitive and selective detector for a particular target. Electrochemical aptasensors can be divided into two classes according to the mode that causes the change in the electrical signal from the DNA nanostructure.

2.2.1 Immobilization-Based Electrochemical Aptasensors

In a traditional electrochemical aptamer sensor, the flexibility of the single-strand aptamers immobilized on the electrode surface results in a tendency for the aptamers to aggregate or entangle, affecting target recognition by the aptamer [52]. To overcome this limitation, 3D DNA nanostructures can be immobilized on the Au electrode surface to act as a scaffold for the aptamers. Given the mechanical rigidity, stability, and specific orientation of tetrahedral DNA nanostructures (TDNs), Fan et al. [52, 70] constructed a series of efficient electrochemical sensors based on DNA tetrahedra for the detection of nucleic acids, proteins, cell, small molecules, and so on. For example, a DNA tetrahedron structure with a recognition probe at one vertex for thrombin detection and thiol at the other three vertices was constructed on the Au surface through Au–S bonding (Fig. 5a) [70]. The thrombin recognition probe was a 15-nt aptamer that triggered the binding of any thrombin present to a 29-nt aptamer with avidin-HRP (horseradish peroxidase) at another site, resulting in the catalyzed electroreduction of hydrogen peroxide. It was demonstrated that this DNA-tetrahedron-based electrochemical biosensor was easily assembled on the Au surface with a specific orientation, well-controlled tetrahedron spacing, and high stability, leading to enhanced detection performance.

The detection of biological molecules is essential if we are to improve our understanding of their physiological and pathological functions and to diagnose diseases at an early stage. Various groups have recently applied an electrochemical detection strategy based on aptamer-functionalized DNA tetrahedra to detect a range of targets [71–75]. For example, Wei et al. [74] designed an electrochemical biosensor based on tetrahedral DNA nanostructures for detecting 8-hydroxy-2'-deoxyguanosine (8-OHdG), which is a key biomarker of oxidative damage and is widely distributed in various lesion tissues, urine, and exposed cells. The system obtained after immobilizing the TDN on the Au electrode surface and fixing an 8-OHdG aptamer to the vertex of the TDN was found to be almost 300-fold more sensitive to 8-OHdG than other electrochemical methods. Such enhanced sensitivity was also achieved for the detection of cancerous exosomes.

Exosomes [76] transport many macromolecules from their parent cells and are vital for intercellular communication. Dong et al. [77] developed a TDN-assisted aptasensor for the ultrasensitive detection of cancerous hepatocellular exosomes. In

this system, LZH8 aptamers that bind to HepG2 exosomes are affixed to TDNs distributed on a Au electrode surface, where the TDNs are separated by a defined nanometric distance (Fig. 5b). When an aptamer captures a HepG2 exosome, the redox signal would change. This assay made the aptamer strands individually at defined nanoscale distance on the gold electrode, which decreased the hindrance effect and maintained spatial orientation for improving identification of exosomes, leading to 100-fold greater sensitivity to exosomes than achieved with single-stranded aptamer sensors. As well as biomarker detection, electrochemical aptasensors based on DNA nanotetrahedra can be applied to monitor food safety. For instance, Chen et al. [78] constructed a system comprising aptamer-functionalized tetrahedral DNA nanostructures and macroporous MoS₂-AuNPs with three-dimensionally ordered structure for the detection of aflatoxin B1 (AFB1, a common contaminant in food). This detection system presented high linearity from 0.1 fg/mL to 0.1 µg/mL and a detection limit of 0.01 fg/mL.

2.2.2 Electrochemical Aptasensors Based on Conformational Switching

Some electrochemical biosensors utilize the change in electrical signal induced by DNA nanostructure self-assembly or disassembly for detection [79–86]. For example, a DNA-nanoladder-based electrochemical biosensor was recently used by Abnous et al. [80] to detect ampicillin (Fig. 6a). Their sensing strategy utilizes an ampicillin aptamer to form a ladder-shaped DNA and immobilize it on the surface of a gold electrode. The ladder-shaped DNA physically and electrostatically blocks [Fe(CN)₆]^{3-/4-} from reaching the surface of the gold electrode. However, in the presence of ampicillin, the DNA nanoladder dissociates from the electrode surface, allowing the [Fe(CN)₆]^{3-/4-} to access the electrode surface, which in turn increases the electrical signal from the electrode. This analytical approach presented a linear range of 7 pM to 100 nM and a detection limit of 1 pM for ampicillin. In another example, Wu et al. [79] developed a label-free impedimetric aptasensor based on DNA nanoladders. This was coupled with a peroxidase mimic to facilitate the amplified detection of nuclear factor kappa B (NF-κB).

In addition to simple two-dimensional DNA nanostructures, more complicated three-dimensional DNA nanostructures can be employed to create aptamer sensors based on more complex conformational switching. For example, Yin et al. [81] fabricated dendritic DNA structures on magnetic beads as a means to detect *Vibrio alginolyticus*. In this system, when *V. alginolyticus* is present, the dendritic DNA nanostructure disassembles, leading to a change in the electrical signal from the system. In order to enhance the detection sensitivity, Yuan et al. [82] utilized DNA dendrimers as nanocarriers of a novel electrochemiluminescence (ECL) indicator based on luminol. The system yielded a detection limit of 0.18 fg/mL for lipopolysaccharides (LPS) when LPS aptamers were incorporated for recognition purposes. This strategy of monitoring for changes in the electrical signal caused by DNA nanostructure assembly was also applied by Jie et al. [84], who developed an electrochemical/ECL assay based on the self-assembly of a DNA nanotube for Dam methylase (MTase) and aflatoxin B1 (AFB1) detection (Fig. 6b). In this assay, the DNA nanotube acts as the signal amplifier for the biosensor. As shown in Fig. 6b, when Dam MTase

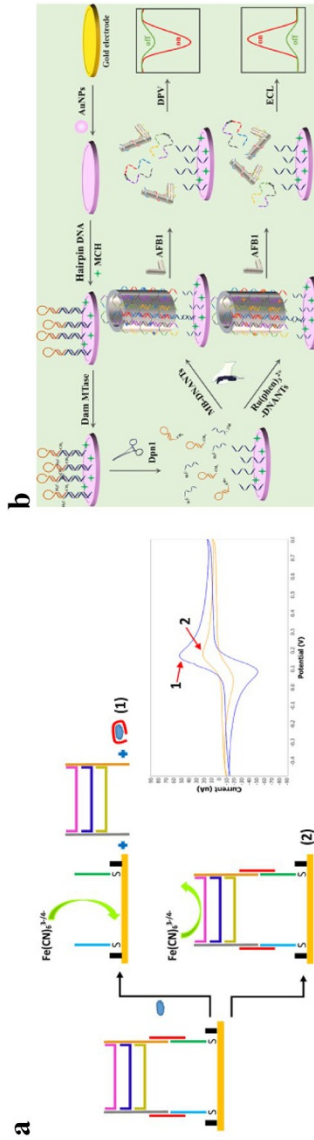


Fig. 6 Electrochemical aptasensors that utilize DNA nanostructures and conformational switching. **a** Schematic of a DNA-nanoladder-assisted electrochemical aptasensor for the detection of ampicillin (reproduced with permission from [80], copyright 2019 Elsevier B. V.). **b** Schematic of an electrochemical system that uses DNA nanotube assembly and disassembly and electrochemiluminescence (for signal amplification) to detect multiple targets (reproduced with permission from [84], copyright 2019 American Chemical Society)

is present, the hairpin DNA on the electrode is methylated and cleaved, inducing the assembly of the DNA nanotube. ECL or EC signal probes ($\text{Ru}(\text{phen})^{32+}$ and methylene blue) are then immobilized on the electrode as they hybridize with DNA nanotubes, leading to amplified ECL and EC signals. Moreover, the recognition of AFB1 by the aptamer S2 in DNA nanotubes was observed to induce the dissociation of the DNA nanotube from the electrode, resulting in decreased ECL and EC signals in the presence of AFB1.

2.3 Colorimetric Biosensors

Colorimetric assays possess the advantageous properties of simplicity, robustness, and low cost [87]. In particular, colorimetric methods can be performed without the need for any complicated instrumentation, which is a useful feature for point-of-care cancer diagnostics. The color changes utilized in colorimetric methods are usually due to the presence of colorimetric reagents such as gold nanoparticles (AuNPs) [88], enzymes [89], visible dyes [90], and polymers [91]. Many sensitive methods of converting aptamer–target binding events into color signals have been reported. These strategies are usually based on a DNA-nanostructure-based colorimetric biosensor and employ a DNA hydrogel to control the colorimetric reagent [92], which tend to be either gold nanoparticles or enzymes.

2.3.1 AuNP-Based Colorimetric Detection

Gold nanoparticle (AuNP)-based colorimetric probes have been widely used for colorimetric assays because their extinction coefficients are significantly higher than those of common organic dyes [93]. Two approaches are commonly used in the design of AuNP colorimetric sensors. In the first, the color change is obtained directly through the accumulation or dispersion of AuNPs. In an early example of this type of probe, Lu et al. used DNA-based interactions and aptamer recognition to control the aggregation of AuNPs, thus facilitating the colorimetric sensing of analytes [94]. A system utilizing an aptamer-containing polyacrylamide hydrogel was designed by Tan's group [95] for the colorimetric detection of adenosine. Tan's group also summarized the applications of aptamer-functionalized hydrogel systems in colorimetric detection, drug release, and targeted cancer therapy [96]. These hydrogels have been limited for sol-gel phase transitions because one molecule of specific biomolecular input could only cleave one site at the network, which need a large amount of biomolecular inputs. In order to promote the use of hydrogels, Oishi et al. [97] recently developed novel DNA hydrogels that are capable of responding to biological stimuli via DNA circuit systems. As shown in Fig. 7a, these DNA hydrogels were fabricated by integrating poly(ethylene glycol)-modified gold nanoparticles (PEG-NPs) for use as the colorimetric reagent into the hydrogel. The presence of catalyst DNA triggers the dissociation of crosslinking points and main chains, inducing the transition of the hydrogel from sol to gel. This releases the entrapped PEG-GNPs into a solution that consequently turns from colorless to red. Oishi et al. utilized this DNA hydrogel to realize the enzyme-free amplified

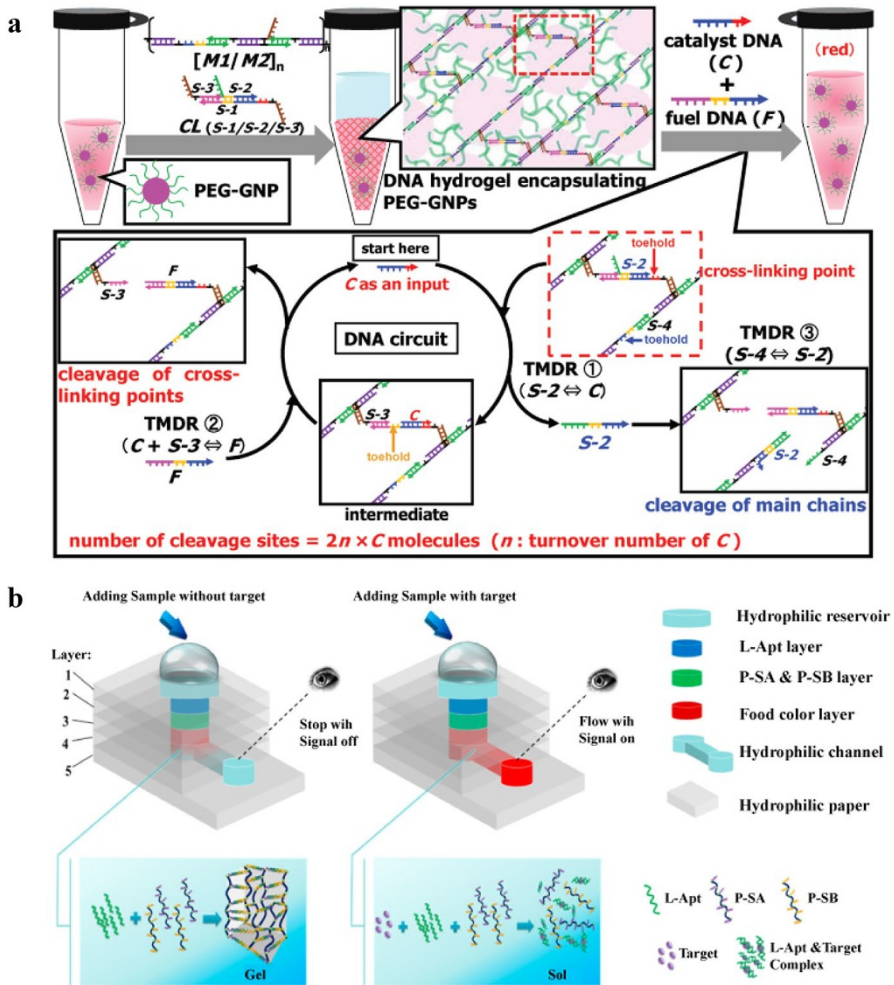


Fig. 7 AuNP-based aptamer-functionalized DNA hydrogels for colorimetric detection. **a** Schematic of a DNA-hydrogel-based colorimetric biosensor containing a DNA circuit system that responds to biological stimuli (reproduced with permission from [97], copyright 2019 Wiley–VCH Verlag GmbH and Co. KGaA). **b** Schematic of a microfluidic paper-based analytical device (μ PAD) for multisubstance colorimetric detection (reproduced with permission from [99], copyright 2015 American Chemical Society)

colorimetric detection of ATP by incorporating a structure-switching ATP aptamer. The resulting system was found to be more sensitive (capable of detecting $5.6 \mu\text{M}$ ATP within 30 min) than other DNA-hydrogel-based ATP-biosensing systems.

The second approach that is used to fabricate AuNP-based colorimetric systems is based on the mobility of the aggregation or dispersion in the presence of the analyte. For example, Lu et al. [98] developed a dipstick test for adenosine that is applicable to serum and is based on AuNP aggregation. Their adenosine-aptamer-based lateral flow device is placed into the solution to be tested. The color of the AuNPs

in the device changes from blue to red in the presence of the target. Yang et al. [99] also used aptamer-functionalized DNA hydrogels and AuNPs to develop another paper-based microdevice, a microfluidic paper-based analytic device (μ PAD) for multisubstance detection (Fig. 7b). Their device uses an aptamer as a crosslinker in the target-responsive hydrogel, gold nanoparticles or iodine staining as the colorimetric reagent, and a slipchip as the readout device. In the presence of the target, the aptamer-functionalized hydrogel changes from a solid to a mobile phase, which alters the flow in the μ PAD. Yang et al. utilized this platform to realize the simultaneous detection of multiple targets such as cocaine, adenosine, and Pb^{2+} .

2.3.2 Enzyme-Based Colorimetric Detection

Another way to observe a colorimetric reaction is to utilize enzymatic catalysis [100, 101]. Compared to other methods, enzymatic catalytic reactions can provide higher sensitivity when used as signal-amplifying elements. For example, Wang et al. [89] encapsulated HRP as a second signal amplification unit into an aptamer-functionalized DNA hydrogel with a target-switchable response to achieve the colorimetric detection of ochratoxin A (Fig. 8a). The DNA hydrogel was assembled from two kinds of DNA subunits: a Y-scaffold shape and an aptamer domain. In the presence of the target, the DNA hydrogel disassembles and releases the encapsulated HRP, which reacts with H_2O_2 and 2,2'-azinobis-(3-ethylbenzthiazoline-6-sulfonate) (ABTS^{2-}), inducing a color change. Instead of natural enzymes, screened DNA enzymes (e.g., a HRP-mimicking DNAzyme) can be used to develop enzyme-free colorimetric biosensors. For example, Ravan et al. [102] reported an isothermal amplification strategy to detect RNA (Fig. 8b). In their work, they combined a hybridized chain reaction (HCR) assay with a HRP-mimicking DNAzyme to increase target sensitivity. In the presence of the target, the HCR is triggered, leading to DNA concatemers. Upon adding hemin molecules, the inactive HRP-mimicking DNAzyme folds into its active configuration, changing the substrate from colorless to colored. This assay was found to have a sensitivity to the target RNA similar to that of RT-PCR, which has a LOD of 1 pM. Furthermore, Mohammadi et al. [103] used a colorimetric method based on a HRP-mimicking DNAzyme to detect cancer cells.

2.4 Other Biosensors

Recently, other methods have also been used in conjunction with DNA nanostructures to develop novel biosensors. Such methods include atomic force microscopy (AFM) [104], surface plasmon resonance (SPR) [105], surface-enhanced Raman scattering (SERS) [106, 107], circular dichroism (CD) [108, 109], and mechanochemistry [110]. Recent applications of aptamer-functionalized DNA nanostructures in these fields have generally made use of DNA origami. In contrast to inorganic materials, DNA origami permits precise spatial addressability and provides a wide range of sites for probe immobilization. For example, unlike oligonucleotides and proteins, the binding of small molecules with aptamers cannot cause significant

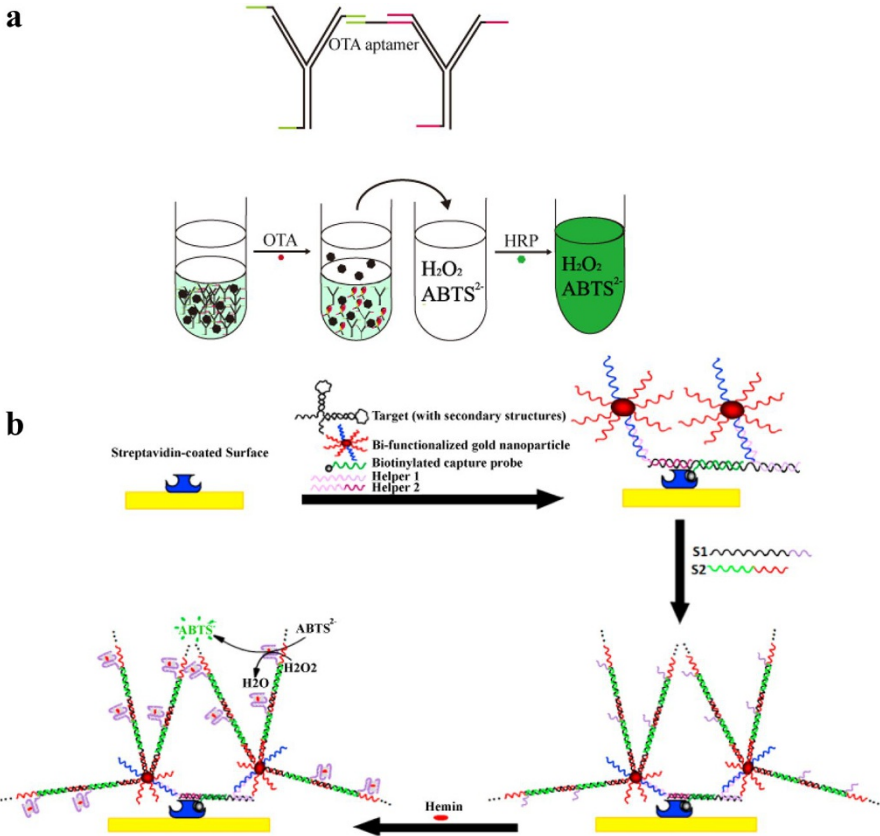


Fig. 8 Enzyme-based aptamer-functionalized DNA hydrogels for colorimetric detection. **a** Schematic of a DNA-hydrogel-based colorimetric biosensor with encapsulated HRP for the detection of ochratoxin A [89]. **b** Schematic of DNA concatemer assembly following HRP-mimicking DNAzyme activation in the isothermal amplified detection of RNA (reproduced with permission from [102], copyright 2016 Elsevier B.V.)

change in their elasticity and height, thus it is extremely hard to directly visualize the binding events of individual aptamer using AFM. To overcome this limitation, Lu et al. [111] constructed an aptamer-functionalized DNA origami biosensor for the AFM detection of small molecules such as aflatoxin B1 (AFB1) (Fig. 9a). In their biosensor, the aptamers attached to the DNA origami are initially bound to ssDNA-modified AuNPs. In the presence of the target (AFB1), the aptamer strands preferentially bind to the target and release the AuNPs, which are detected directly by AFM. In other methods, the DNA origami acts as a signal indicator. For example, Endo et al. [110] utilized the modular design of DNA origami to develop an expanded single-molecule mechanochemical sensor (Fig. 9b). Their design utilizes DNA origami with seven tiles, and the recognition elements are positioned next to the interlocks that connect the contiguous tiles. When present, the target binds to the recognition sites, breaking the interlocks and inducing a change in mechanical

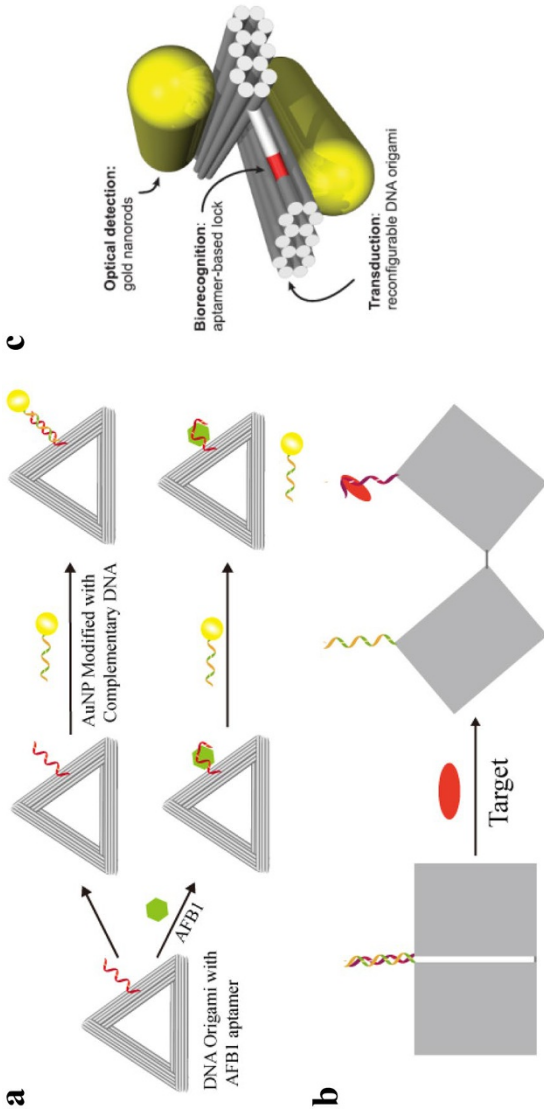


Fig. 9 Other biosensors that employ aptamer-functionalized DNA nanostructures. **a** Schematic of the aptamer-functionalized DNA origami used for target biosensing in conjunction with AFM [111]. **b** Schematic of a DNA-origami-based biosensor that monitors for changes in a mechanical signal [110]. **c** Schematic of a biosensor that employs CD spectroscopy and DNA origami with gold nanorods (reproduced with permission from [108], copyright 2018 American Chemical Society)

signal. The use of multiple recognition elements rather than just one reduces both the detection limit and detection time.

Furthermore, a biosensor that utilizes aptamer-functionalized DNA origami with two gold nanorods attached for optical detection based on CD spectroscopy has been developed (Fig. 9c) [108]. In this design, aptamer biorecognition is used as a molecular lock that controls the spatial configuration of DNA origami with two gold nanorods (AuNRs) attached. Aptamer biorecognition causes the two AuNRs to form a three-dimensional (3D) chiral plasmonic object that exhibits circular dichroism, which is detected via CD spectroscopy.

3 Aptamer-Functionalized DNA Nanostructures for Bioimaging Applications

It is important to monitor the distributions of biomolecules in cells, as this can enhance our understanding of cell function and pathology, improve disease diagnosis, and facilitate drug delivery. Various aptamer-based probes have been applied for bioimaging. In particular, the biocompatibility of aptamer-functionalized DNA nanostructures makes them attractive tools for bioimaging. Aptamer-functionalized DNA nanostructures employed for bioimaging can be divided into two classes depending on whether the aptamer is used as a responsive or a targeting element.

3.1 Aptamers as Responsive Elements

Many emerging intracellular and extracellular bioimaging methods based on DNA materials utilize aptamers as responsive units. For example, Tan et al. [112] proposed the use of switchable aptamer micelle nanostructures for ATP imaging in cells. However, it is important to consider the critical micelle concentration (CMC) of these micelle nanostructures when using them because they could dissociate at low concentrations. Therefore, researchers are interested in designing DNA nanostructures that are stable during cellular applications, especially at low concentrations. For example, Zhang et al. [18] designed an aptamer-functionalized DNA dendrimer for monitoring ATP in situ. Fan et al. [113] designed a DNA tetrahedral nanostructure which can be dynamically regulated by assembling an anti-ATP aptamer in one of the edges. The aptamer was modified with a pair of FRET fluorophores (Cy3 and Cy5), which would be close to each other to generate FRET signal through the conformational change of aptamer after recognizing ATP. This structure can be self-delivered into cells for monitoring the ATP in cells.

Recently, Li et al. [114] developed a series of framework nucleic acid (FNA) nanodevices for subcellular ATP imaging. They initially constructed a FNA nano-platform based on two tetrahedral nanostructures (TDNs) that was intended for use in lysosomes. As shown in Fig. 10a, the two TDNs have differently branched vertices, but both TDNs have a split ATP aptamer and a biomolecular i-motif at the vertex. When the TDNs enter intracellular acidic lysosomes, the acidic environment induces the TDNs to assemble (via an i-motif unit) into a heterodimeric structure.

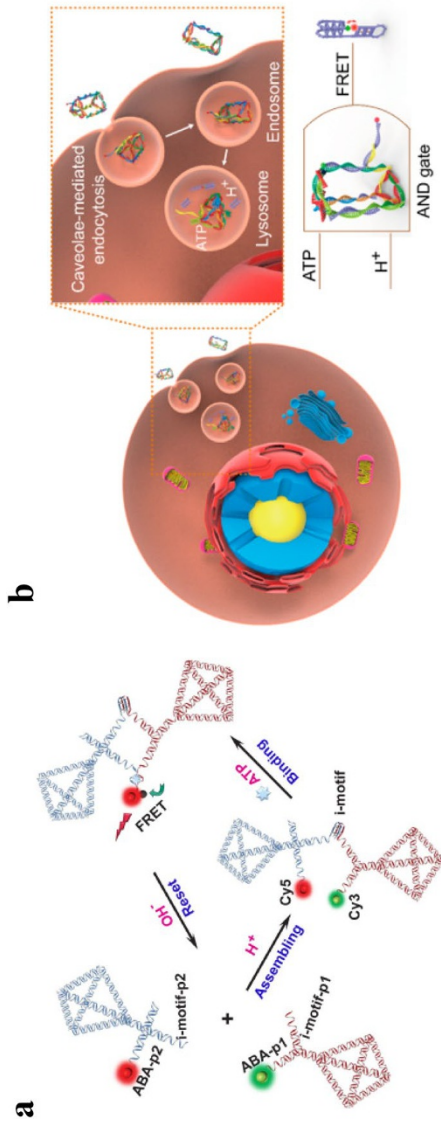


Fig. 10 The utilization of aptamers as responsive probes in bioimaging. **a** Schematic of a TDN-based framework nucleic acid (FNA) nanodevice for ATP imaging in lysosomes (reproduced with permission from [114], copyright 2019 Wiley-VCH Verlag GmbH and Co. KGaA). **b** Schematic of a DNA triangular prism used for the logic-based imaging of protons and ATP (reproduced with permission from [115], copyright 2019 American Chemical Society)

The formation of this large framework brings the split ATP aptamers on the two TDNs into close proximity, permitting ATP imaging within the lysosome via FRET. This i-motif-guided assembly of TDNs mimics the pH-responsive dimerization of natural silk proteins (spidroins). Li et al. subsequently used the same strategy to develop FNA-based logic nanodevices based on DNA triangular prisms for subcellular imaging (Fig. 10b) [115]. In this case, FRET (and therefore fluorescence) only occurs in the FNA-based logic device when both the pH and the ATP level change in the lysosome.

3.2 Aptamers as Targeting Elements

Targeting elements (e.g., aptamers, antibodies, peptides, or small molecules) are able to bind with biomarkers on targeted cells or tissues. Modifying the surfaces of nanomaterials with these targeted elements is an attractive method for realizing sensitive and selective bioimaging *in vitro* and *in vivo*. Among the various types of targeting elements, aptamers have attractive features such as easy synthesis and modification, small size, high stability, and good biocompatibility, which make them outstanding candidates for use in targeted imaging schemes [116]. Aptamer-functionalized DNA structures employed for target bioimaging are commonly based on synthetic biomacromolecules such as micelles [112, 117], nanoflowers [118], or dendrimers [119].

Ju et al. [117] developed a multifunctional nanomicelle for targeted imaging and photodynamic therapy *in vivo*. Although imaging *in vivo* was achieved using this nanomicelle, this imaging was limited by the instability of the nanomicelle at concentrations lower than the critical micelle concentration. In order to overcome this limitation, Tan et al. [120] recently reported the development of an aptamer-lipid micelle with internal photinduced crosslinking (Fig. 11a). The introduction of aptamers into micelle to give a DNA-lipid micelle (DLM) consisting of hydrophilic aptamer heads and hydrophobic lipid tails led to faster target-cell recognition. In addition, methacrylamide was incorporated as a layer of photinduced crosslinks between the DNA shell and the lipid core, enhancing the stability of the DLM in the cellular environment. On the other hand, in the absence of crosslinking, it should be possible to modify the lipid core or the aptamer shell of the aptamer-lipid micelle, making such micelles potentially useful in targeted cellular imaging, gene therapy, and drug delivery.

In addition to these large DNA nanostructures, conjugating aptamers with small DNA nanostructures such as a three-dimensional DNA tetrahedron can also improve aptamer targeting efficiency *in vitro*. Yang et al. [121] utilized a DNA tetrahedron as a phase-transfer agent for hydrophobic nanoparticles and transferred upconversion nanoparticles (UCNPs) for targeted cellular imaging using an aptamer-pendant DNA tetrahedron. Recently, Wu et al. [122] examined the effects of varying the number of MUC1 aptamers attached to a DNA tetrahedron on the efficiency and safety of this functionalized DNA tetrahedron when it was employed for targeted imaging and drug delivery (Fig. 11b). Their results showed that increasing the number of

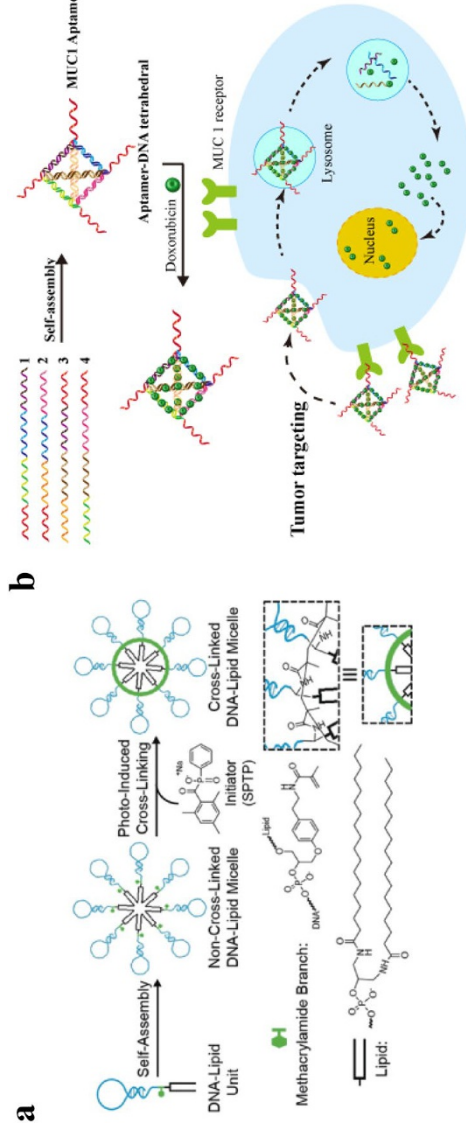


Fig. 11 The utilization of aptamers for targeted bioimaging in live cells and in vivo. **a** Schematic of a crosslinked DNA-methacrylamide-lipid micelle system (reproduced with permission from [120], copyright 2018 Wiley-VCH Verlag GmbH and Co. KGaA). **b** Schematic of a DNA tetrahedron conjugated with different numbers of MUC1 aptamers, allowing targeted drug delivery and in vivo imaging [122]

conjugated aptamers enhanced the specificity of the functionalized DNA tetrahedron for cancer cells.

4 Aptamer-Functionalized DNA Nanostructures for Cancer Therapy

Cancer is one of the most destructive diseases and a leading cause of human mortality. Current cancer treatment methods include surgery, chemotherapy, and radiotherapy. However, one of the major limitations of these therapeutic methods is their poor selectivity for cancer cells, which results in the destruction of normal, healthy cells and can lead to treatment failure and potentially death [123]. Aptamers are considered excellent candidates for use in targeted cancer therapies because they are small, easy to prepare, and show excellent target-specific recognition. Therefore, a wide variety of nanomaterials functionalized with aptamers have been produced for cancer treatments. Among these nanomaterials, DNA nanostructures are particularly popular for many biomedical applications because of their programmability, ease of modification, and high biocompatibility. In this section, we summarize recent progress in the development of aptamer-functionalized DNA nanostructures for use in various cancer treatment methods, including chemotherapy, photodynamic therapy, and gene therapy.

4.1 Chemotherapy

Chemotherapy is a widely used drug treatment for cancers. The drawbacks of using chemotherapeutic drugs are their toxic side effects, poor solubility, nonspecific distribution in the body, and systemic toxicity. However, the advantages of aptamer-functionalized DNA nanostructures—including a capacity for high drug loading, good biocompatibility, and specific recognition—make them attractive tools for bypassing these problems with chemotherapeutic drugs. Since chemotherapeutic agents can be conjugated with DNA through covalent [124] and noncovalent [125] bonding, DNA nanostructures are considered ideal candidates for drug delivery. Most aptamer-functionalized DNA nanostructures used in drug delivery are noncovalently conjugated with chemotherapeutic agents (e.g., doxorubicin, DOX). The aptamers most commonly used in this context are the mucin 1 protein (MUC1) aptamer, the nucleolin aptamer AS1411, and the aptamer sgc-8c.

MUC1 is a cell-surface glycoprotein that is overexpressed in many kinds of adenocarcinomas, making it an attractive target in anticancer drug delivery schemes [126]. Early in 2011, Huang et al. [127] attached a MUC1 aptamer to a DNA icosahedron and used the resulting system to efficiently and specifically deliver DOX to epithelial cancer cells for cancer therapy. Following that work, many groups utilized the MUC1 aptamer in TDN-based drug delivery systems [128, 129]. In addition to these small DNA nanostructures, the MUC1 aptamer can also guide relatively large DNA nanostructures into cells. For example, Ding et al. [130] attached the MUC1 aptamer to a triangular DNA origami–AuNR complex that permitted increased internalization of DOX and AuNRs (Fig. 12a). In their scheme, the first step is to

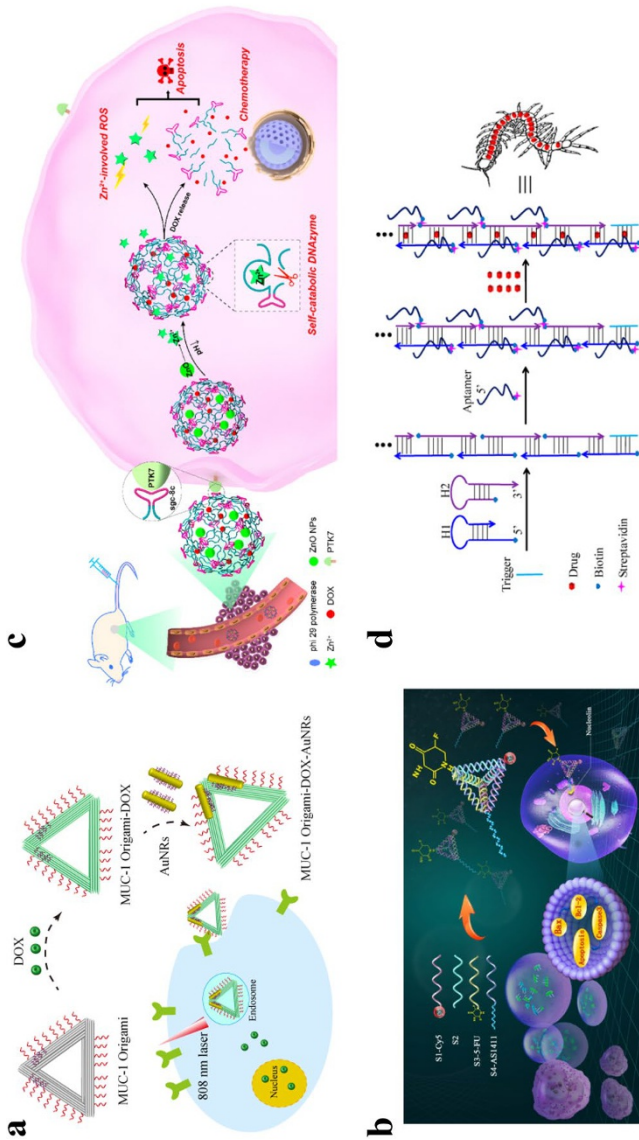


Fig. 12 Aptamer-functionalized DNA nanostructures used for chemotherapy. **a** Schematic of triangular DNA origami functionalized with the MUC-1 aptamer for drug delivery [130]. **b** Schematic of a DNA tetrahedron conjugated with the aptamer AS1411, which can be used for 5-fluorouracil (5-FU) delivery (reproduced with permission from [135], copyright 2019 American Chemical Society). **c** Schematic of yarn-like DNA nanospheres (NSs) used for drug delivery. These NSs encapsulate ZnO and the aptamer sgc-8c and incorporate DNzyme (reproduced with permission from [137], copyright 2019 American Chemical Society). **d** Schematic of the nanocapsule that is assembled via a HCR and has aptamer “legs” for cell-targeted drug delivery (reproduced with permission from [140], copyright 2016 American Chemical Society)

prepare the triangular DNA origami functionalized with the MUC1 aptamer. The DOX is then loaded into the DNA origami via an interaction between the DOX and GC-rich regions in DNA pairs. After that, two AuNRs are assembled on the origami template at a predesignated location. Guided by the MUC1 aptamer, the MUC1-DNA origami-DOX-AuNR (MODA) nanostructure is effectively internalized by cancer cells. This approach inhibits P-glycoprotein (multidrug resistance pump) expression, thus avoiding P-glycoprotein-mediated drug efflux and, in turn, increasing the sensitivity of multidrug-resistant breast cells to DOX. MCF-7/ADR cells can then be killed by a combination of DOX chemotherapy and hyperthermia induced by near-infrared (NIR) laser irradiation. Jiang et al. [131] developed a protein-scaffolded DNA nanohydrogel based on three types of streptavidin (SA)-based DNA tetrads and functionalized this nanohydrogel with the MUC1 aptamer. The resulting nanohydrogel, which can incorporate therapeutic agents, was found to facilitate activatable target imaging and therapy.

The aptamer AS1411 is a 26-mer DNA sequence with a G-rich region that can bind to nucleolin, a cell-surface protein that is overexpressed in tumor cells [132]. When the G-quadruplex structure of AS1411 is bound to nucleolin, the nucleolin can transfer the aptamer from cytomembrane to cytoplasm and nucleus. Furthermore, AS1411 possesses anticancer activity when it is present at high concentrations [133, 134]. There is therefore increasing interest in combining AS1411 with DNA nanostructures for targeted drug delivery. For example, Lin et al. [135] developed a DNA-based nanomedicine based on a AS1411-modified DNA tetrahedron for the targeted therapy of breast cancer cells (Fig. 12b). In their scheme, the anticancer drug 5-fluorouracil (5-FU) was inserted at the vertex of the DNA tetrahedron. Lin et al. demonstrated the importance of including AS1411 to facilitate targeted cell therapy through comparison with therapy based on free 5-FU. To further enhance the targeting of cancer cells, Chen et al. [129] simultaneously modified a DNA tetrahedron with the MUC1 aptamer and AS1411 in order to fabricate a system that targets both cancer cells and nucleolin.

Sgc-8c is another aptamer that is commonly used in anticancer drug delivery schemes. It has 41 oligonucleotides and specifically binds to the cell membrane protein tyrosine kinase 7 (PTK-7), which is overexpressed in CCRF-CEM (human T-cell acute lymphoblastic leukemia) [136] and other tumors (such as colon and gastric cancers). Therefore, sgc8 is commonly combined with DNA nanostructures when developing drug delivery systems that selectively target lymphoblastic leukemia. For example, Yang et al. [119] designed an sgc-8c-modified, DOX-loading DNA dendrimer that can selectively distinguish target cancer cells from normal cells and is internalized into CCRF-CEM and cervical cancer HeLa cells. Recently, Wang et al. [137] developed a drug delivery system based on a DNA hydrogel for smart targeted drug delivery (Fig. 12c). Their design involves the fabrication, through a method known as isothermal rolling circle amplification (RCA), of sgc-8c-functionalized, monodisperse, and sophisticated, yarn-like DNA nanosponges (NSs) that encapsulate ZnO and are bound to a DNase. The assembled DNA/ZnO NSs are designed to act as carriers for DOX. The sgc-8c guides the assembly into cancer cells, where intracellular acids trigger the conversion of the ZnO into Zn²⁺ ions, stimulating reactive oxygen species (ROS) generation. The Zn²⁺ also acts as

a cofactor in DNase digestion, leading to the digestion of the NSs and therefore the release of DOX.

There are also some DNA-nanostructure-based drug delivery systems in which other novel aptamers are applied. For example, Zhao et al. [138] site-specifically attached the novel aptamer C2NP [139], which is highly specific for the tumor cell marker CD30, to DNA origami for the purposes of targeted drug delivery. Also, Yang et al. [140] constructed a centipede-like DNA structure via a HCR to use for drug delivery in targeted therapy (Fig. 12d). In this scheme, the trunk of the nano-centipede is the DNA scaffold and the legs are aptamers that bind to SMMC-7721 cells (human hepatocellular carcinoma cells).

The anti-HER2 aptamer HApt specifically recognizes and binds to HER2, an epidermal growth factor receptor [28]. HApt can translocate HER2 to lysosomes for degradation, stimulating cell death and inhibiting cell growth. Lin et al. [141] recently reported that they had improved the stability and increased the blood circulation time of HApt by combining it with a tetrahedral nucleic acid framework.

4.2 Photodynamic Therapy

Photodynamic therapy (PDT) is a photochemistry-based method that utilizes light to activate chemicals that are cytotoxic in their activated state. PDT utilizes three components: a light source, a photosensitizer, and tissue oxygen [142]. When all three components are present, reactive oxygen species (ROS) are generated through an interaction between the photosensitizer and the tissue oxygen in the presence of radiation, and these ROS are toxic to cells. PDT is a highly efficient and noninvasive therapeutic method and is therefore an attractive treatment for malignant diseases [143]. PDT circumvents the problems of systemic therapies because the therapy is only applied at irradiated locations. Also, the photosensitizer used in PDT is selectively accumulated in cancer cells. Moreover, this method is inexpensive.

Aptamer-functionalized DNA nanostructures have also been used in PDT. There are three main ways to load the photosensitizer onto a DNA nanostructure: direct covalent modification, noncovalent binding, and encapsulation. Various strategies have been used to directly attach the photosensitizer to a DNA strand. One of the main advantages of this approach is that the resulting photosensitizer-modified DNA nanostructure can be integrated with a carrier. For example, Wang et al. [144] labeled a DNA tetrahedron (TDN) with the photosensitizer pyropheophorbide a, which activates the toxic species $^1\text{O}_2$ when it is irradiated with light. This system was then combined with a chemotherapeutic agent, thus facilitating the localized destruction of circulating tumor cells (CTCs) via simultaneous PDT and chemotherapy (Fig. 13a). In Wang et al.'s approach, the TDN-based system is first immobilized on a microchannel supporter by a hairpin aptamer switch at the vertex of the TDN, and the chemotherapeutic agent DOX is loaded into the dsDNA of the TDN. When CTCs enter the microchannel, the hairpin aptamer specifically recognizes and binds to them, releasing the TNA, which is internalized into the CTCs. DOX is therefore delivered into the target cells by the TDN, and PDT is realized by irradiating the photosensitizer with light.

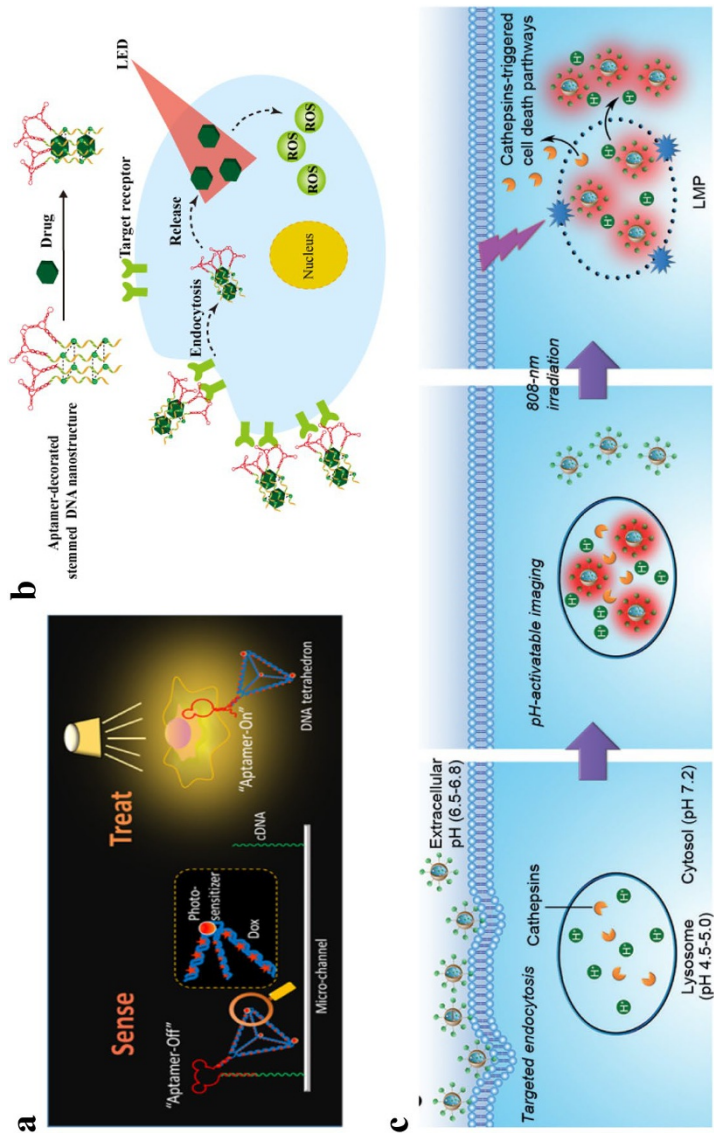


Fig. 13 Aptamer-functionalized DNA nanostructures for photodynamic therapy. **a** Schematic of a DNA tetrahedron labeled with a photosensitizer for photodynamic CTC therapy (reproduced with permission from [144], copyright 2016 American Chemical Society). **b** Schematic of an aptamer-based stemmed DNA nanostructure that loads a photosensitizer used for cell-specific therapy [145]. **c** Schematic of the utilization of a multifunctional nanomicelle encapsulating the fluorescent probe BDP-688 and a new photosensitizer for cell-targeted lysosome-based imaging and near-infrared PDT (reproduced with permission from [117], copyright 2014 Wiley-VCH Verlag GmbH and Co. KGaA)

Noncovalent binding strategies generally utilize the ability of the G-quadruplex of a DNA strand to load a photosensitizer such as methylene blue (MB) or 5,10,15,20-tetrakis(1-methylpyridinium-4-yl)porphyrin (TMPyP4). MB, a phenothiazine, is commonly used for cell staining, to treat methemoglobinemia, and to delineate the edge of a tumor during surgery. MB has also been widely used as a photosensitizer in PDT because it generates $^1\text{O}_2$ when irradiated at wavelengths between 620–670 nm. MB can also be loaded onto an aptamer-functionalized DNA nanostructure carrier as a means to improve the cell selectivity of PDT. For example, Shim et al. [145] developed a stemmed DNA nanostructure integrated with an aptamer (an aptamer-modified oligoguanine quadruplex) to load MB for PDT therapy with enhanced cell selectivity (Fig. 13b). In a similar way, TMPyP4, a porphyrin derivative, can be combined with a G-quadruplex-forming aptamer to improve cell selectivity. For example, Shieh et al. [146] utilized the guanine-rich aptamer AS1411 to selectively deliver TMPyP4 to breast cancer cells.

The third method of delivering a photosensitizer using a DNA nanostructure is encapsulation. For example, Yang et al. [117] developed a nanomicelle based on DNA that can simultaneously encapsulate the pH-activatable fluorescence probe BDP-688 and the NIR photosensitizer R16FPm, making it useful for cancer therapy (Fig. 13c). This system also uses the aptamer Apt S1 to specifically recognize and bind to human breast cancer cells (cell line MDA-MB-231). Results indicated that, after the nanomicelle had been internalized into the cells and transferred to lysosomes, the BDP-688 produced a fast and reversible fluorescence response to pH, allowing the pH in lysosomes to be monitored in real time. Irradiation with NIR caused the photosensitizer R16FP to generate ROS, inducing cell death. This strategy could allow cancer treatments to be visualized in vivo.

4.3 Gene Therapy

Gene therapy is an attractive approach for treating heritable or acquired diseases such as cancers, viral infections, and thalassemia. Among these, cancer is the most common gene therapy target, as it often has a genetic basis that is difficult to cure. DNA nanostructures are regarded as ideal nonviral vectors for nucleic acid delivery due to their high loading capacities and biocompatibilities. Generally speaking, these DNA-nanostructure-based therapeutic systems can be categorized into antisense, RNA interference (RNAi), and gene delivery approaches.

Antisense strands are single-stranded DNA or RNA sequences that are complementary to their target genes and knock them down, whereas RNAi is a method in which small interfering RNA (siRNA) or short hairpin DNA (shRNA) is used to recognize and cleave target messenger RNA (mRNA) [147]. However, it is difficult for siRNA, shRNA, and antisense strands to internalize into cells, so there is considerable interest in developing tools for delivering them into their targets. DNA nanostructures are outstanding candidates. For example, Tan et al. [148] developed an aptamer-based DNA nanohydrogel for delivering antisense oligonucleotides into A549 cells (Fig. 14a). Their design uses three building blocks for the hydrogel: a Y-shaped monomer (A) containing a DNAzyme, another Y-shaped monomer (B)

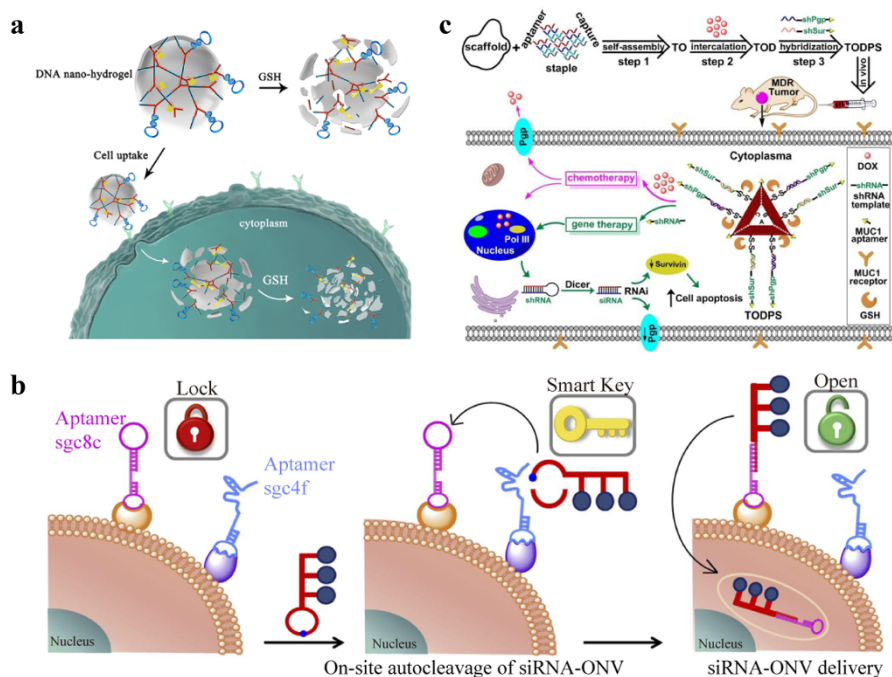


Fig. 14 Use of aptamer-functionalized DNA nanostructures in gene therapy. **a** Schematic of the application of a stimuli-responsive DNA nano-hydrogel to deliver antisense DNA into target cells for gene therapy (reproduced with permission from [148], copyright 2015 American Chemical Society). **b** Schematic of a DNA dual lock and key strategy for cell-subtype-specific binding and siRNA delivery (reproduced with permission from [149], copyright 2016 Springer Nature). **c** Schematic of a platform based on triangular DNA origami for delivering shRNA transcription templates and chemodrugs in vivo (reproduced with permission from [150], copyright 2018 Wiley–VCH Verlag GmbH and Co. KGaA)

containing an aptamer that is used as a cell-targeting unit, and a linker containing the antisense DNA. Disulfide linkages are incorporated into each block, which causes the DNA hydrogel to disassemble in the presence of the reducing agents found in cells. This strategy of incorporating various functional units into a DNA hydrogel was found to be highly effective from a therapeutic perspective.

Ju et al. [149] developed DNA logic nanotubes for the precise delivery of siRNA (Fig. 14b). These dual lock and key DNA nanotubes, which were modified with a self-cleavable hairpin structure, were considered to act as a “key” for two “locks,” which were two different aptamers (sgc-8c and sgc-4f) that specifically bind to the target cell membrane. This “dual lock and key” strategy avoids nonspecific siRNA adsorption and off-target toxicity. Qian et al. [128] recently investigated the utilization of a siRNA-loaded DNA nanoprism for gene therapy. They decorated the DNA nanoprism with two functional units: the siRNA Rab26 (the gene drug) and the aptamer MUC1 (the targeting unit). Targeting and drug loading was regulated by tuning the number of aptamers on the nanoprism. However, approaches such as these have the disadvantage that siRNA is easily degraded in complex biological

systems, reducing treatment efficacy. Therefore, strategies that enhance the stability of RNAi technology are of considerable interest. Ding et al. [150] recently proposed a method of maintaining the stability of shRNA transcription templates during their delivery to the target through the use of triangular DNA origami, thus allowing effective RNAi chemotherapy *in vitro* and *in vivo* (Fig. 14c). In their strategy, they attached two different shRNA transcription templates along with an aptamer used as a targeting unit to the triangular DNA origami through a stimuli-responsive and cleavable disulfide linkage. The chemotherapeutic drug DOX was then loaded through intercalation onto the DNA origami. This multifunctional DNA nanoplatform was found to permit both RNAi and chemotherapy at the same time, leading to enhanced therapeutic effects on antagonistic tumors *in vitro* and *in vivo*. They also applied this strategy to efficiently and simultaneously deliver the gene p53 and chemotherapeutic drugs to multidrug-resistant tumors [151].

4.4 Other Therapies

As well as the more common therapeutic methods discussed above, there are other promising strategies for treating diseases that make use of aptamer-functionalized DNA nanostructures. For instance, some proteins and enzymes are considered potential therapeutic agents [152–154]. Due to their molecular recognition and cell internalization abilities, aptamer-functionalized DNA nanostructures have been utilized to achieve the targeted delivery of these therapeutic agents [155–157]. For example, Zhao, Ding, Yan, and Nie et al. [155] recently constructed a DNA nanorobot that uses DNA origami as a carrier to transport thrombin to a tumor, where it coagulates (Fig. 15a). In their design, four thrombin molecules are attached to the inner surface of hollow tube-shaped DNA origami, which was then closed with pre-designed fastener DNA strands containing the aptamer AS1411. The AS1411 serves as both a targeting unit and a molecular switch that controls whether the DNA robot is open. The therapeutic activity of the thrombin molecules is activated when the aptamer interacts with nucleolin (a tumor vessel marker), meaning that the release of the thrombin leads to vascular infarction of the tumor (i.e., cancer treatment). In another application, Wang et al. [156] constructed aptamer-modified DNA super-sandwich assemblies that transport a catalase into cells. Once inside a cell, this catalase scavenges reactive oxygen species.

Another route to achieving a therapeutic effect is through the anticancer abilities of aptamers. Aptamers can combine directly and specifically with various proteins, some of which are potential therapeutic targets [158]. The anticancer aptamers that are most commonly combined with DNA nanostructures are AS1411 and thrombin aptamer. AS1411 is a G-rich oligonucleotide that inhibits NF- κ B signaling and reduces the expression of Bcl-2, so it has been explored as an anticancer agent in a phase 2 clinical trial [159]. By attaching this aptamer to a DNA nanostructure with an enhanced cell internalization ability, AS1411 can be efficiently delivered into cancer cells, inhibiting their growth [48]. For example, Lin et al. [48] attached AS1411 and drug molecules to TDN nanostructures (Fig. 15b), thus permitting the efficient delivery of both the aptamer and drugs to the target cells in a synergistic

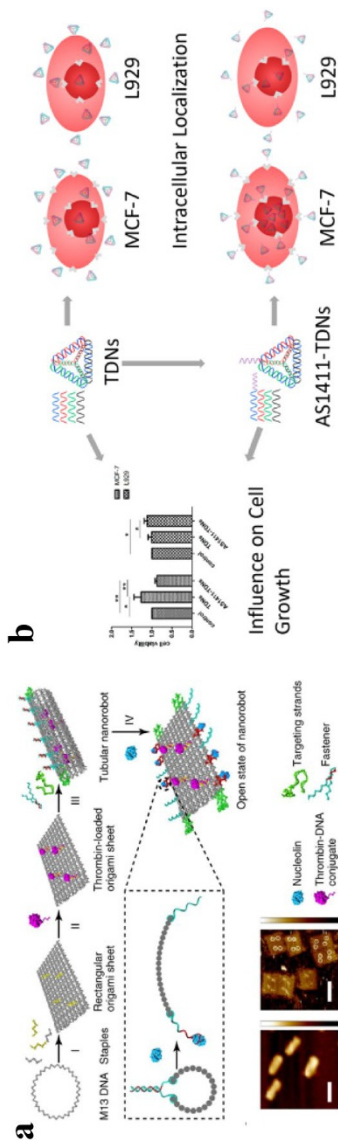


Fig. 15 Use of aptamer-functionalized DNA nanostructures in other therapeutic schemes. **a** Schematic of a DNA nanorobot that uses DNA origami as a carrier to transport thrombin for coagulation at the tumor site (reproduced with permission from [155], copyright 2018 Springer Nature). **b** Schematic of AS1411-modified TDN nanostructures for suppressing tumor cell growth (reproduced with permission from [48], copyright 2017 American Chemical Society)

cancer therapy scheme. Thrombin aptamer is reported to exhibit similar antithrombotic activity to anticoagulation drugs, and has therefore also been applied therapeutically [160]. For instance, Gianneschi et al. [161] recently developed polymeric micelles with thrombin aptamer for use as a nanoscale anticoagulant.

5 Aptamer-Functionalized DNA Nanostructures for Other Applications

Aside from biological applications, aptamer-functionalized DNA nanostructures have also been applied in fields such as protein or molecular immobilization and analysis (due to the addressable and programmable nature of DNA nanostructures) and structural control (due to the specific recognition abilities of aptamers). Because DNA nanostructures feature addressable decorations, allow high spatial resolution, and can be directly imaged using AFM, they are excellent candidates for biophysical research into aptamers. For example, the immobilization of a protein on a nanostructure can facilitate investigations of spatially precise biological interactions because biomolecular recognition events commonly happen at the nanoscale. In this context, in 2008, Yan et al. [162] performed the first investigation of the distance dependence of multivalent binding effects at the single-molecule level by immobilizing an aptamer at a precisely controlled position on a DNA nanostructure.

The application of an aptamer and a single-chain antibody against that aptamer has been shown to be an effective strategy for assembling proteins in a highly specific manner. Fabrega et al. [163] utilized DNA origami as an addressable support to investigate proteins at the single-molecule level (Fig. 16a). Using the ability of a thrombin aptamer to recognize and bind to α -thrombin, they were able to visualize via AFM, for the first time, the enzymatic activity of human O⁶-alkylguanine-DNA alkyltransferase (hAGT) while it was supported by the DNA origami platform. Recently, Seminario et al. [164] investigated the molecular dynamics of the interactions of the thrombin aptamers TBA26 and TBA29 with thrombin. In addition to protein immobilization, aptamer-functionalized DNA nanostructures have been used to investigate the biological functions of RNA [165] and cells [166].

Furthermore, an aptamer can be integrated into a DNA nanostructure as a building block that controls nanostructure formation. This method can be utilized to construct stimuli-responsive materials. For example, Mao et al. [167] constructed multilayered DNA nanocages where the formation of each layer was controlled by the binding of an aptamer to its target (Fig. 16b). ATP aptamers (blue strands) were embedded into the linkers between two tetrahedra by hybridization with a single strand (red strand) on the smaller tetrahedron. In the presence of ATP, the ATP aptamer bound to that ATP and separated from the red strand, triggering the dissociation of the two tetrahedra. Also, the macrostructure can be tuned by using a dynamic DNA structure containing an aptamer. Plaxco et al. [168] engineered a series of adenosine-responsive DNA hydrogels based on an aptamer. They investigated the response kinetics of these aptamer-based hydrogels at different length scales from nanometers to hundreds of microns (Fig. 16c). In their work, an adenosine-binding aptamer was incorporated into Y-shaped DNA hydrogel monomers

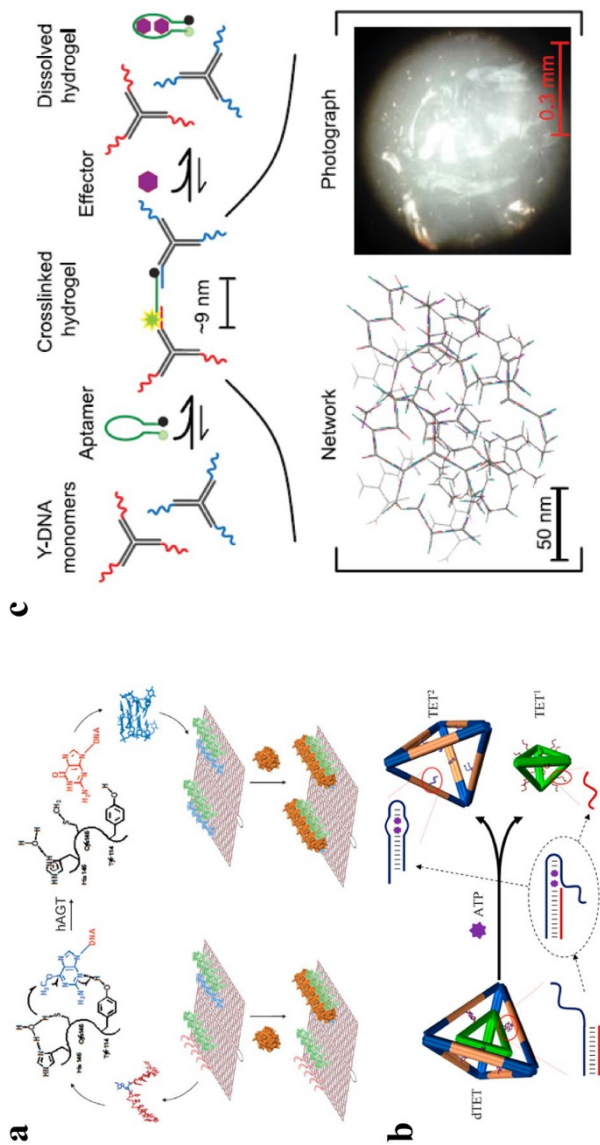


Fig. 16 Use of aptamer-functionalized DNA nanostructures for other applications. **a** Scheme in which α -thrombin is immobilized on DNA origami by binding the thrombin to a thrombin aptamer and the DNA repair activity is monitored by AFM (reproduced with permission from [163], copyright 2013 Wiley-VCH Verlag GmbH and Co. KGaA). **b** Schematic of the ATP-activated separation of multilayered DNA nanocages (reproduced with permission from [167], copyright 2015 American Chemical Society). **c** Schematic of the ATP-activated dissolution of a hydrogels at scales ranging from nanometers to hundreds of microns (reproduced with permission from [168], copyright 2017 American Chemical Society)

that were disrupted when the aptamer recognized adenosine. This dissolution of the DNA hydrogel could be monitored because the aptamer was fluorescently labeled. They then investigated the effect of modulating the aptamer-based crosslink stability on the DNA hydrogel. DNA hydrogel characteristics such as volume can also be controlled through schemes that incorporate DNA strand displacement. For example, Schulman et al. [169] incorporated a HCR into a macroscopic polyacrylamide-based hydrogel using DNA as a responsive crosslinker. The HCR caused the volume of the hydrogel to expand 100-fold. Schulman et al. later demonstrated that this change in the DNA hydrogel was induced by various molecular triggers, including ATP. When triggered by ATP, there was a change of fluorescence as well as DNA hydrogel swelling.

6 Conclusions and Perspectives

Over the past few decades, aptamer-functionalized DNA nanostructures have facilitated impressive advances in various fields. A range of strategies have been used to construct aptamer-functionalized DNA nanostructures, and these nanostructures have been widely used for biological applications due to their superior performance. In this review, we have summarized the most recent applications of aptamer-functionalized DNA nanostructures in biosensing, bioimaging, cancer therapy, and other promising fields. Despite the considerable achievements that such nanostructures have made possible, there are still issues with the use of aptamer-functionalized DNA nanostructures that need to be addressed.

The first of these issues is that some important targets don't have respective aptamers so far. Thus, it is necessary to screen more aptamers for these targets for broadening respective research (e.g., in studies of the interactions of aptamers with nonmammalian cells). Second, it is important to find a way to enhance the stability of aptamers in complex biological environments (e.g., serum), although some recent strategies for achieving this based on the electrostatic steric hindrance of nanoparticles [170] and the design of a circular aptamer [171] appear promising. Third, the preparation of DNA nanostructures via scalable methods [172] is crucial to facilitating their widespread application. To achieve this goal, Yan et al. [173] proposed a framework for designing and assembling a single DNA or RNA strand that self-folds into a predesigned complex unknotted structure and can be amplified by polymerases *in vitro* or by clonal production *in vivo*. Also, Dietz et al. [174] recently utilized the self-replicating ability of bacteriophages to produce macroscopic amounts of DNA origami. Furthermore, it is important to improve the purity of DNA nanostructures before applying them in any subsequent application [175]. Fourth, most bioanalytical schemes that use aptamer-functionalized DNA nanostructures are currently based on one-photon fluorescent imaging, which has a low penetration depth and has a problem with tissue autofluorescence. Using near-infrared (NIR) fluorescent imaging, photoacoustic imaging, and nuclear magnetic resonance imaging (NMRI) would further improve the accuracy and sensitivity of bioanalysis based on aptamer-functionalized DNA nanostructures. Fifth, in addition to the traditional biological applications mentioned above, aptamer-functionalized DNA nanostructures

present considerable potential for use in computing. For example, Bachelet et al. [176] developed DNA origami robots for computing in animals. Also, Tan et al. [177] engineered a 3D DNA nanostructure on a target cell membrane for logic computing. This appears to be a promising route to the creation of intelligent systems for molecular medicine and sensing. Lastly, the operation of aptamer-functionalized DNA nanostructures in vivo remains challenging due to the presence of numerous biological barriers during delivery. Although there are a few reports of attempts to apply aptamer-functionalized DNA nanostructures in vivo, the complex physiological environment makes such studies very difficult for a myriad of reasons: nuclease degradation, nonspecific adsorption of proteins, immunological rejection, and so on. Therefore, further mechanistic investigations of the fate of DNA nanostructures in vivo and the development of efficient methods to minimize interference from the physiological environment would drive the practical application of aptamer-functionalized DNA nanostructures in vivo.

Current developments in the construction and application of aptamer-functionalized DNA nanostructures indicate that there is great potential to improve their design, which should lead to important uses for these nanostructures in materials science and healthcare.

Acknowledgements This work is supported by the National Natural Science Foundation of China (grants 21705038, 21890744, 21521063, 21605038), the Natural Science Foundation of Hunan Province (2018JJ3029), and Rutgers University.

References

1. Pugazhendhi A, Shobana S, Nguyen DD, Banu JR, Sivagurunathan P, Chang SW, Ponnusamy VK, Kumar G (2019) Application of nanotechnology (nanoparticles) in dark fermentative hydrogen production. *Int J Hydrogen Energy* 44(3):1431–1440
2. Fan Y, Wang P, Lu Y, Wang R, Zhou L, Zheng X, Li X, Piper JA, Zhang F (2018) Lifetime-engineered NIR-II nanoparticles unlock multiplexed in vivo imaging. *Nat Nanotechnol* 13(10):941–946
3. Hu Q, Li H, Wang L, Gu H, Fan C (2019) DNA nanotechnology-enabled drug delivery systems. *Chem Rev* 119(10):6459–6506
4. Shulaker MM, Hills G, Park RS, Howe RT, Saraswat K, Wong HP, Mitra S (2017) Three-dimensional integration of nanotechnologies for computing and data storage on a single chip. *Nature* 547(7661):74–78
5. Seeman NC (1982) Nucleic acid junctions and lattices. *J Theor Biol* 99(2):237–247
6. Fu TJ, Seeman NC (1993) DNA double-crossover molecules. *Biochemistry* 32(13):3211–3220
7. Winfree E, Liu F, Wenzler LA, Seeman NC (1998) Design and self-assembly of two-dimensional DNA crystals. *Nature* 394(6693):539–544
8. LaBean TH, Yan H, Kopatsch J, Liu FR, Winfree E, Reif JH, Seeman NC (2000) Construction, analysis, ligation, and self-assembly of DNA triple crossover complexes. *J Am Chem Soc* 122(9):1848–1860
9. Yan H, Park SH, Finkelstein G, Reif JH, LaBean TH (2003) DNA-templated self-assembly of protein arrays and highly conductive nanowires. *Science* 301(5641):1882–1884
10. He Y, Ye T, Su M, Zhang C, Ribbe AE, Jiang W, Mao C (2008) Hierarchical self-assembly of DNA into symmetric supramolecular polyhedra. *Nature* 452(7184):198–201
11. He Y, Chen Y, Liu HP, Ribbe AE, Mao CD (2005) Self-assembly of hexagonal DNA two-dimensional (2D) arrays. *J Am Chem Soc* 127(35):12202–12203
12. Chen JH, Seeman NC (1991) Synthesis from DNA of a molecule with the connectivity of a cube. *Nature* 350(6319):631–633

13. Zhang C, Ko SH, Su M, Leng Y, Ribbe AE, Jiang W, Mao C (2009) Symmetry controls the face geometry of DNA polyhedra. *J Am Chem Soc* 131(4):1413–1415
14. Goodman RP, Schaap IAT, Tardin CF, Erben CM, Berry RM, Schmidt CF, Turberfield AJ (2005) Rapid chiral assembly of rigid DNA building blocks for molecular nanofabrication. *Science* 310(5754):1661–1665
15. Shih WM, Quispe JD, Joyce GF (2004) A 1.7-kilobase single-stranded DNA that folds into a nanoscale octahedron. *Nature* 427(6975):618–621
16. Wu X-R, Wu C-W, Ding F, Tian C, Jiang W, Mao C-D, Zhang C (2017) Binary self-assembly of highly symmetric DNA nanocages via sticky-end engineering. *Chin Chem Lett* 28(4):851–856
17. Hudson RHE, Damha MJ (1993) Nucleic acid dendrimers: novel biopolymer structures. *J Am Chem Soc* 115(6):2119–2124
18. Meng HM, Zhang XB, Lv YF, Zhao ZL, Wang NN, Fu T, Fan HH, Liang H, Qiu LP, Zhu G (2014) DNA dendrimer: an efficient nanocarrier of functional nucleic acids for intracellular molecular sensing. *ACS Nano* 8(6):6171–6181
19. Xuan F, Hsing IM (2014) Triggering hairpin-free chain-branching growth of fluorescent DNA dendrimers for nonlinear hybridization chain reaction. *J Am Chem Soc* 136(28):9810–9813
20. Song J, Arbona JM, Zhang Z, Liu L, Xie E, Elezgaray J, Aime JP, Gothelf KV, Besenbacher F, Dong M (2012) Direct visualization of transient thermal response of a DNA origami. *J Am Chem Soc* 134(24):9844–9847
21. Lu CH, Guo W, Hu Y, Qi XJ, Willner I (2015) Multitriggered shape-memory acrylamide-DNA hydrogels. *J Am Chem Soc* 137(50):15723–15731
22. Zhu G, Hu R, Zhao Z, Chen Z, Zhang X, Tan W (2013) Noncanonical self-assembly of multifunctional DNA nanoflowers for biomedical applications. *J Am Chem Soc* 135(44):16438–16445
23. Mandal S, Muller J (2017) Metal-mediated DNA assembly with ligand-based nucleosides. *Curr Opin Chem Biol* 37:71–79
24. Rothmund PWK (2006) Folding DNA to create nanoscale shapes and patterns. *Nature* 440(7082):297–302
25. English MA, Soenksen LR, Gayet RV, de Puig H, Angenent-Mari NM, Mao AS, Nguyen PQ, Collins JJ (2019) Programmable CRISPR-responsive smart materials. *Science* 365(6455):780–785
26. Shao Y, Jia H, Cao T, Liu D (2017) Supramolecular hydrogels based on DNA self-assembly. *Acc Chem Res* 50(4):659–668
27. Wang J, Chao J, Liu H, Su S, Wang L, Huang W, Willner I, Fan C (2017) Clamped hybridization chain reactions for the self-assembly of patterned DNA hydrogels. *Angew Chem Int Ed Engl* 56(8):2171–2175
28. Lim KS, Lee DY, Valencia GM, Won Y-W, Bull DA (2015) Nano-self-assembly of nucleic acids capable of transfection without a gene carrier. *Adv Funct Mater* 25(34):5445–5451
29. Dong Y, Chen S, Zhang S, Sodroski J, Yang Z, Liu D, Mao Y (2018) Folding DNA into a lipid-conjugated nanobarrel for controlled reconstitution of membrane proteins. *Angew Chem Int Ed Engl* 57(8):2072–2076
30. Zhang K, Zhu X, Jia F, Auyeung E, Mirkin CA (2013) Temperature-activated nucleic acid nanostructures. *J Am Chem Soc* 135(38):14102–14105
31. Amodio A, Adedeji AF, Castronovo M, Franco E, Ricci F (2016) pH-controlled assembly of DNA tiles. *J Am Chem Soc* 138(39):12735–12738
32. Zhu B, Zhao Y, Dai JB, Wang JB, Xing S, Guo LJ, Chen N, Qu XM, Li L, Shen JW, Shi JY, Li J, Wang LH (2017) Preservation of DNA nanostructure carriers: effects of freeze-thawing and ionic strength during lyophilization and storage. *ACS Appl Mater Interfaces* 9(22):18434–18439
33. Zhou W, Saran R, Liu J (2017) Metal sensing by DNA. *Chem Rev* 117(12):8272–8325
34. Silverman SK (2016) Catalytic DNA: scope, applications, and biochemistry of deoxyribozymes. *Trends Biochem Sci* 41(7):595–609
35. Li D, Song S, Fan C (2010) Target-responsive structural switching for nucleic acid-based sensors. *Acc Chem Res* 43(5):631–641
36. Surana S, Shenoy AR, Krishnan Y (2015) Designing DNA nanodevices for compatibility with the immune system of higher organisms. *Nat Nanotechnol* 10(9):741–747
37. Zhu G, Zheng J, Song E, Donovan M, Zhang K, Liu C, Tan W (2013) Self-assembled, aptamer-tethered DNA nanotrains for targeted transport of molecular drugs in cancer theranostics. *Proc Natl Acad Sci USA* 110(20):7998–8003

38. Zhou Y, Tang L, Zeng G, Zhang C, Zhang Y, Xie X (2016) Current progress in biosensors for heavy metal ions based on DNazymes/DNA molecules functionalized nanostructures: a review. *Sens Actuators B Chem* 223:280–294
39. Xie N, Huang J, Yang X, Yang Y, Quan K, Wang H, Ying L, Ou M, Wang K (2016) A DNA tetrahedron-based molecular beacon for tumor-related mRNA detection in living cells. *Chem Commun* 52(11):2346–2349
40. Tuerk C, Gold L (1990) Systematic evolution of ligands by exponential enrichment: RNA ligands to bacteriophage T4 DNA polymerase. *Science* 249(4968):505–510
41. Robertson DL, Joyce GF (1990) Selection in vitro of an RNA enzyme that specifically cleaves single-stranded DNA. *Nature* 344(6265):467–468
42. Ellington AD, Szostak JW (1990) In vitro selection of RNA molecules that bind specific ligands. *Nature* 346(6287):818–822
43. Lu D, He L, Zhang G, Lv A, Wang R, Zhang X, Tan W (2017) Aptamer-assembled nanomaterials for fluorescent sensing and imaging. *Nanophotonics* 6(1):109–121
44. Olaru A, Bala C, Jaffrezic-Renault N, Aboul-Enein HY (2015) Surface plasmon resonance (SPR) biosensors in pharmaceutical analysis. *Crit Rev Anal Chem* 45(2):97–105
45. Jayanthi V, Das AB, Saxena U (2017) Recent advances in biosensor development for the detection of cancer biomarkers. *Biosens Bioelectron* 91:15–23
46. Dong Y, Xu Y, Yong W, Chu X, Wang D (2014) Aptamer and its potential applications for food safety. *Crit Rev Food Sci Nutr* 54(12):1548–1561
47. Nguyen P-L, Sekhon SS, Ahn J-Y, Ko JH, Lee L, Cho S-J, Min J, Kim Y-H (2017) Aptasensor for environmental monitoring. *Toxicol Environ Health Sci* 9(2):89–101
48. Chen Y, Zhou S, Li L, Zhu J-j (2017) Nanomaterials-based sensitive electrochemiluminescence biosensing. *Nano Today* 12:98–115
49. Munzar JD, Ng A, Juncker D (2019) Duplexed aptamers: history, design, theory, and application to biosensing. *Chem Soc Rev* 48(5):1390–1419
50. Meng HM, Liu H, Kuai H, Peng R, Mo L, Zhang XB (2016) Aptamer-integrated DNA nanostructures for biosensing, bioimaging and cancer therapy. *Chem Soc Rev* 45(9):2583–2602
51. Huang R, He N, Li Z (2018) Recent progresses in DNA nanostructure-based biosensors for detection of tumor markers. *Biosens Bioelectron* 109:27–34
52. Lin M, Song P, Zhou G, Zuo X, Aldabahi A, Lou X, Shi J, Fan C (2016) Electrochemical detection of nucleic acids, proteins, small molecules and cells using a DNA-nanostructure-based universal biosensing platform. *Nat Protoc* 11(7):1244–1263
53. Liu M, Zhang Q, Kannan B, Botton GA, Yang J, Soleymani L, Brennan JD, Li Y (2018) Self-assembled functional DNA superstructures as high-density and versatile recognition elements for printed paper sensors. *Angew Chem Int Ed Engl* 57(38):12440–12443
54. Li Z, Zhao B, Wang D, Wen Y, Liu G, Dong H, Song S, Fan C (2014) DNA nanostructure-based universal microarray platform for high-efficiency multiplex bioanalysis in biofluids. *ACS Appl Mater Interfaces* 6(20):17944–17953
55. Walter HK, Bauer J, Steinmeyer J, Kuzuya A, Niemeyer CM, Wagenknecht HA (2017) “DNA Origami Traffic Lights” with a split aptamer sensor for a bicolor fluorescence readout. *Nano Lett* 17(4):2467–2472
56. Peng P, Shi L, Wang H, Li T (2017) A DNA nanoswitch-controlled reversible nanosensor. *Nucleic Acids Res* 45(2):541–546
57. Tang MSL, Shiu SC, Godonoga M, Cheung YW, Liang S, Dirkwager RM, Kinghorn AB, Fraser LA, Heddle JG, Tanner JA (2018) An aptamer-enabled DNA nanobox for protein sensing. *Nano-medicine* 14(4):1161–1168
58. Wang J, Dong HY, Zhou Y, Han LY, Zhang T, Lin M, Wang C, Xu H, Wu ZS, Jia L (2018) Immunomagnetic antibody plus aptamer pseudo-DNA nanocatenane followed by rolling circle amplification for highly-sensitive CTC detection. *Biosens Bioelectron* 122:239–246
59. Walsh AS, Yin H, Erben CM, Wood MJ, Turberfield AJ (2011) DNA cage delivery to mammalian cells. *ACS Nano* 5(7):5427–5432
60. Zheng X, Peng R, Jiang X, Wang Y, Xu S, Ke G, Fu T, Liu Q, Huan S, Zhang X (2017) Fluorescence resonance energy transfer-based DNA nanoprism with a split aptamer for adenosine triphosphate sensing in living cells. *Anal Chem* 89(20):10941–10947
61. Zhong L, Cai S, Huang Y, Yin L, Yang Y, Lu C, Yang H (2018) DNA octahedron-based fluorescence nanoprobe for dual tumor-related mRNAs detection and imaging. *Anal Chem* 90(20):12059–12066

62. Jie G, Gao X, Ge J, Li C (2019) Multifunctional DNA nanocage with CdTe quantum dots for fluorescence detection of human 8-oxoG DNA glycosylase 1 and doxorubicin delivery to cancer cells. *Mikrochim Acta* 186(2):85
63. Topkaya SN, Azimzadeh M, Ozsoz M (2016) Electrochemical biosensors for cancer biomarkers detection: recent advances and challenges. *Electroanalysis* 28(7):1402–1419
64. Hasanzadeh M, Shadjou N, de la Guardia M (2017) Early stage screening of breast cancer using electrochemical biomarker detection. *Trends Anal Chem* 91:67–76
65. Zeng Y, Zhu Z, Du D, Lin Y (2016) Nanomaterial-based electrochemical biosensors for food safety. *J Electroanal Chem (Lausanne)* 781:147–154
66. Mazzei F, Favero G, Bollella P, Tortolini C, Mannina L, Conti ME, Antiochia R (2015) Recent trends in electrochemical nanobiosensors for environmental analysis. *Int J Environ Health* 7(3):267–291
67. Yang J, Dou B, Yuan R, Xiang Y (2017) Aptamer/protein proximity binding-triggered molecular machine for amplified electrochemical sensing of thrombin. *Anal Chem* 89(9):5138–5143
68. Yang J, Dou B, Yuan R, Xiang Y (2016) Proximity binding and metal ion-dependent DNzyme cyclic amplification-integrated aptasensor for label-free and sensitive electrochemical detection of thrombin. *Anal Chem* 88(16):8218–8223
69. Jiang B, Li F, Yang C, Xie J, Xiang Y, Yuan R (2015) Aptamer pseudoknot-functionalized electronic sensor for reagentless and single-step detection of immunoglobulin E in human serum. *Anal Chem* 87(5):3094–3098
70. Pei H, Lu N, Wen Y, Song S, Liu Y, Yan H, Fan C (2010) A DNA nanostructure-based biomolecular probe carrier platform for electrochemical biosensing. *Adv Mater* 22(42):4754–4758
71. Sun D, Luo Z, Lu J, Zhang S, Che T, Chen Z, Zhang L (2019) Electrochemical dual-aptamer-based biosensor for nonenzymatic detection of cardiac troponin I by nanohybrid electrocatalysts labeling combined with DNA nanotetrahedron structure. *Biosens Bioelectron* 134:49–56
72. Wei M, Zhang W (2018) Ultrasensitive aptasensor with DNA tetrahedral nanostructure for ochratoxin A detection based on hemin/G-quadruplex catalyzed polyaniline deposition. *Sens Actuators B Chem* 276:1–7
73. Sun D, Lu J, Chen D, Jiang Y, Wang Z, Qin W, Yu Y, Chen Z, Zhang Y (2018) Label-free electrochemical detection of HepG2 tumor cells with a self-assembled DNA nanostructure-based aptasensor. *Sens Actuators B Chem* 268:359–367
74. Fan J, Liu Y, Xu E, Zhang Y, Wei W, Yin L, Pu Y, Liu S (2016) A label-free ultrasensitive assay of 8-hydroxy-2'-deoxyguanosine in human serum and urine samples via polyaniline deposition and tetrahedral DNA nanostructure. *Anal Chim Acta* 946:48–55
75. Poturnayová A, Šnejdárková M, Castillo G, Rybár P, Leitner M, Ebner A, Hianik T (2015) Aptamer-based detection of thrombin by acoustic method using DNA tetrahedrons as immobilisation platform. *Chem Pap* 69(1):221–226
76. Melo SA, Sugimoto H, O'Connell JT, Kato N, Villanueva A, Vidal A, Qiu L, Vitkin E, Perelman LT, Melo CA (2014) Cancer exosomes perform cell-independent microRNA biogenesis and promote tumorigenesis. *Cancer Cell* 26(5):707–721
77. Wang S, Zhang L, Wan S, Cansiz S, Cui C, Liu Y, Cai R, Hong C, Teng IT, Shi M, Wu Y, Dong Y, Tan W (2017) Aptasensor with expanded nucleotide using DNA nanotetrahedra for electrochemical detection of cancerous exosomes. *ACS Nano* 11(4):3943–3949
78. Peng G, Li X, Cui F, Qiu Q, Chen X, Huang H (2018) Aflatoxin B1 electrochemical aptasensor based on tetrahedral DNA nanostructures functionalized three dimensionally ordered macroporous MoS₂-AuNPs film. *ACS Appl Mater Interfaces* 10(21):17551–17559
79. Peng K, Zhao H, Xie P, Hu S, Yuan Y, Yuan R, Wu X (2016) Impedimetric aptasensor for nuclear factor kappa B with peroxidase-like mimic coupled DNA nanoladders as enhancer. *Biosens Bioelectron* 81:1–7
80. Taghdisi SM, Danesh NM, Nameghi MA, Ramezani M, Aliboland M, Abnous K (2019) An electrochemical sensing platform based on ladder-shaped DNA structure and label-free aptamer for ultrasensitive detection of ampicillin. *Biosens Bioelectron* 133:230–235
81. Zhao G, Ding J, Yu H, Yin T, Qin W (2016) Potentiometric aptasensing of *Vibrio alginolyticus* based on DNA nanostructure-modified magnetic beads. *Sensors (Basel)* 16(12):2052
82. Xie S, Dong Y, Yuan Y, Chai Y, Yuan R (2016) Ultrasensitive lipopolysaccharides detection based on doxorubicin conjugated *N*-(aminobutyl)-*N*-(ethylisoluminol) as electrochemiluminescence indicator and self-assembled tetrahedron DNA dendrimers as nanocarriers. *Anal Chem* 88(10):5218–5224

83. Wang YH, Chen YX, Wu X, Huang KJ (2018) Electrochemical biosensor based on Se-doped MWCNTs-graphene and Y-shaped DNA-aided target-triggered amplification strategy. *Colloids Surf B Biointerfaces* 172:407–413
84. Ge J, Zhao Y, Li C, Jie G (2019) Versatile electrochemiluminescence and electrochemical “on-off” assays of methyltransferases and aflatoxin B1 based on a novel multifunctional DNA nanotube. *Anal Chem* 91(5):3546–3554
85. Sheng Q, Liu R, Zhang S, Zheng J (2014) Ultrasensitive electrochemical cocaine biosensor based on reversible DNA nanostructure. *Biosens Bioelectron* 51:191–194
86. Lee T, Park SY, Jang H, Kim GH, Lee Y, Park C, Mohammadniaei M, Lee MH, Min J (2019) Fabrication of electrochemical biosensor consisted of multi-functional DNA structure/porous Au nanoparticle for avian influenza virus (H5N1) in chicken serum. *Mater Sci Eng C Mater Biol Appl* 99:511–519
87. Song Y, Wei W, Qu X (2011) Colorimetric biosensing using smart materials. *Adv Mater* 23(37):4215–4236
88. Fahimi-Kashani N, Hormozi-Nezhad MR (2016) Gold-nanoparticle-based colorimetric sensor array for discrimination of organophosphate pesticides. *Anal Chem* 88(16):8099–8106
89. Zhou L, Sun N, Xu L, Chen X, Cheng H, Wang J, Pei R (2016) Dual signal amplification by an “on-command” pure DNA hydrogel encapsulating HRP for colorimetric detection of ochratoxin A. *RSC Adv* 6(115):114500–114504
90. Sun QK, Chen MS, Liu ZW, Zhang HC, Yang WJ (2017) Efficient colorimetric fluoride anion chemosensors based-on simple naphthodipyrrolidone dyes. *Tetrahedron Lett* 58(28):2711–2714
91. Deng J, Ma W, Yu P, Mao L (2015) Colorimetric and fluorescent dual mode sensing of alcoholic strength in spirit samples with stimuli-responsive infinite coordination polymers. *Anal Chem* 87(13):6958–6965
92. Yin BC, Ye BC, Wang H, Zhu Z, Tan W (2012) Colorimetric logic gates based on aptamer-crosslinked hydrogels. *Chem Commun (Camb)* 48(9):1248–1250
93. Ghosh SK, Pal T (2007) Interparticle coupling effect on the surface plasmon resonance of gold nanoparticles: from theory to applications. *Chem Rev* 107(11):4797–4862
94. Liu J, Lu Y (2006) Preparation of aptamer-linked gold nanoparticle purple aggregates for colorimetric sensing of analytes. *Nat Protoc* 1(1):246–252
95. Yang H, Liu H, Kang H, Tan W (2008) Engineering target-responsive hydrogels based on aptamer-target interactions. *J Am Chem Soc* 130(20):6320–6321
96. Li J, Mo L, Lu CH, Fu T, Yang HH, Tan W (2016) Functional nucleic acid-based hydrogels for bioanalytical and biomedical applications. *Chem Soc Rev* 45(5):1410–1431
97. Oishi M, Nakatani K (2019) Dynamically programmed switchable DNA hydrogels based on a DNA circuit mechanism. *Small* 15(15):e1900490
98. Liu J, Mazumdar D, Lu Y (2006) A simple and sensitive “dipstick” test in serum based on lateral flow separation of aptamer-linked nanostructures. *Angew Chem Int Ed Engl* 45(47):7955–7959
99. Wei X, Tian T, Jia S, Zhu Z, Ma Y, Sun J, Lin Z, Yang CJ (2015) Target-responsive DNA hydrogel mediated “stop-flow” microfluidic paper-based analytic device for rapid, portable and visual detection of multiple targets. *Anal Chem* 87(8):4275–4282
100. Shi D, Sun Y, Lin L, Shi C, Wang G, Zhang X (2016) Naked-eye sensitive detection of alkaline phosphatase (ALP) and pyrophosphate (PPi) based on a horseradish peroxidase catalytic colorimetric system with Cu(II). *Analyst* 141(19):5549–5554
101. Xu J, Qian J, Li H, Wu Z-S, Shen W, Jia L (2016) Intelligent DNA machine for the ultrasensitive colorimetric detection of nucleic acids. *Biosens Bioelectron* 75:41–47
102. Ravan H (2016) Isothermal RNA detection through the formation of DNA concatemers containing HRP-mimicking DNazymes on the surface of gold nanoparticles. *Biosens Bioelectron* 80:67–73
103. Norouzi A, Ravan H, Mohammadi A, Hosseinzadeh E, Norouzi M, Fozooni T (2018) Aptamer-integrated DNA nanoassembly: a simple and sensitive DNA framework to detect cancer cells. *Anal Chim Acta* 1017:26–33
104. Wu N, Willner I (2017) Programmed dissociation of dimer and trimer origami structures by aptamer-ligand complexes. *Nanoscale* 9(4):1416–1422
105. Daems D, Pfeifer W, Rutten I, Sacca B, Spasic D, Lammertyn J (2018) Three-dimensional DNA origami as programmable anchoring points for bioreceptors in fiber optic surface plasmon resonance biosensing. *ACS Appl Mater Interfaces* 10(28):23539–23547

106. Fang W, Jia S, Chao J, Wang L, Duan X, Liu H, Li Q, Zuo X, Wang L, Wang L, Liu N, Fan C (2019) Quantizing single-molecule surface-enhanced Raman scattering with DNA origami meta-molecules. *Sci Adv* 5(9):eaau4506
107. Sun Y, Xu F, Zhang Y, Shi Y, Wen Z, Li Z (2011) Metallic nanostructures assembled by DNA and related applications in surface-enhancement Raman scattering (SERS) detection. *J Mater Chem B* 21(42):16675–16685
108. Huang Y, Nguyen MK, Natarajan AK, Nguyen VH, Kuzyk A (2018) A DNA origami-based chiral plasmonic sensing device. *ACS Appl Mater Interfaces* 10(51):44221–44225
109. Funck T, Liedl T, Bae W (2019) Dual aptamer-functionalized 3D plasmonic metamolecule for thrombin sensing. *Appl Sci* 9(15):3006
110. Koirala D, Shrestha P, Emura T, Hidaka K, Mandal S, Endo M, Sugiyama H, Mao H (2014) Single-molecule mechanochemical sensing using DNA origami nanostructures. *Angew Chem Int Ed Engl* 53(31):8137–8141
111. Lu Z, Wang Y, Xu D, Pang L (2017) Aptamer-tagged DNA origami for spatially addressable detection of aflatoxin B1. *Chem Commun (Camb)* 53(5):941–944
112. Wu C, Chen T, Han D, You M, Peng L, Cansiz S, Zhu G, Li C, Xiong X, Jimenez E (2013) Engineering of switchable aptamer micelle flares for molecular imaging in living cells. *ACS Nano* 7(7):5724–5731
113. Pei H, Liang L, Yao G, Li J, Huang Q, Fan C (2012) Reconfigurable three-dimensional DNA nanostructures for the construction of intracellular logic sensors. *Angew Chem Int Ed Engl* 51(36):9020–9024
114. Peng P, Du Y, Zheng J, Wang H, Li T (2019) Reconfigurable bioinspired framework nucleic acid nanoplatform dynamically manipulated in living cells for subcellular imaging. *Angew Chem Int Ed Engl* 58(6):1648–1653
115. Du Y, Peng P, Li T (2019) DNA logic operations in living cells utilizing lysosome-recognizing framework nucleic acid nanodevices for subcellular imaging. *ACS Nano* 13:5778–5784
116. Fan Z, Sun L, Huang Y, Wang Y, Zhang M (2016) Bioinspired fluorescent dipeptide nanoparticles for targeted cancer cell imaging and real-time monitoring of drug release. *Nat Nanotechnol* 11(4):388–394
117. Tian J, Ding L, Ju H, Yang Y, Li X, Shen Z, Zhu Z, Yu JS, Yang CJ (2014) A multifunctional nanomicelle for real-time targeted imaging and precise near-infrared cancer therapy. *Angew Chem Int Ed Engl* 53(36):9544–9549
118. Hu R, Zhang X, Zhao Z, Zhu G, Chen T, Fu T, Tan W (2014) DNA nanoflowers for multiplexed cellular imaging and traceable targeted drug delivery. *Angew Chem Int Ed Engl* 53(23):5821–5826
119. Zhang H, Ma Y, Xie Y, An Y, Huang Y, Zhu Z, Yang CJ (2015) A controllable aptamer-based self-assembled DNA dendrimer for high affinity targeting, bioimaging and drug delivery. *Sci Rep* 5:10099
120. Li X, Figg CA, Wang R, Jiang Y, Lyu Y, Sun H, Liu Y, Wang Y, Teng IT, Hou W, Cai R, Cui C, Li L, Pan X, Sumerlin BS, Tan W (2018) Cross-linked aptamer-lipid micelles for excellent stability and specificity in target-cell recognition. *Angew Chem Int Ed Engl* 57(36):11589–11593
121. Li J, Hong CY, Wu SX, Liang H, Wang LP, Huang G, Chen X, Yang HH, Shangguan D, Tan W (2015) Facile phase transfer and surface biofunctionalization of hydrophobic nanoparticles using Janus DNA tetrahedron nanostructures. *J Am Chem Soc* 137(35):11210–11213
122. Han X, Jiang Y, Li S, Zhang Y, Ma X, Wu Z, Wu Z, Qi X (2018) Multivalent aptamer-modified tetrahedral DNA nanocage demonstrates high selectivity and safety for anti-tumor therapy. *Nanoscale* 11(1):339–347
123. Allen TM (2002) Ligand-targeted therapeutics in anticancer therapy. *Nat Rev Cancer* 2(10):750
124. Zhang X-Q, Xu X, Lam R, Giljohann D, Ho D, Mirkin CA (2011) Strategy for increasing drug solubility and efficacy through covalent attachment to polyvalent DNA–nanoparticle conjugates. *ACS Nano* 5(9):6962–6970
125. Portugal J, Barcelo F (2016) Noncovalent binding to DNA: still a target in developing anticancer agents. *Curr Med Chem* 23(36):4108–4134
126. Da Pieve C, Blackshaw E, Missailidis S, Perkins AC (2012) PEGylation and biodistribution of an anti-MUC1 aptamer in MCF-7 tumor-bearing mice. *Bioconjug Chem* 23(7):1377–1381
127. Chang M, Yang CS, Huang DM (2011) Aptamer-conjugated DNA icosahedral nanoparticles as a carrier of doxorubicin for cancer therapy. *ACS Nano* 5(8):6156–6163

128. Liu Q, Wang D, Xu Z, Huang C, Zhang C, He B, Mao C, Wang G, Qian H (2019) Targeted delivery of Rab26 siRNA with precisely tailored DNA prism for lung cancer therapy. *ChemBioChem* 20(9):1139–1144
129. Tian Y, Huang Y, Gao P, Chen T (2018) Nucleus-targeted DNA tetrahedron as a nanocarrier of metal complexes for enhanced glioma therapy. *Chem Commun (Camb)* 54(68):9394–9397
130. Song L, Jiang Q, Liu J, Li N, Liu Q, Dai L, Gao Y, Liu W, Liu D, Ding B (2017) DNA origami/gold nanorod hybrid nanostructures for the circumvention of drug resistance. *Nanoscale* 9(23):7750–7754
131. Li N, Wang X-Y, Xiang M-H, Liu J-W, Yu R-Q, Jiang J-H (2019) Programmable self-assembly of protein-scaffolded DNA nanohydrogels for tumor-targeted imaging and therapy. *Anal Chem* 91(4):2610–2614
132. Bates PJ, Laber DA, Miller DM, Thomas SD, Trent JO (2009) Discovery and development of the G-rich oligonucleotide AS1411 as a novel treatment for cancer. *Exp Mol Pathol* 86(3):151–164
133. Rosenberg JE, Bambury RM, Van Allen EM, Drabkin HA, Lara PN, Harzstark AL, Wagle N, Figlin RA, Smith GW, Garraway LA (2014) A phase II trial of AS1411 (a novel nucleolin-targeted DNA aptamer) in metastatic renal cell carcinoma. *Investig New Drugs* 32(1):178–187
134. Holmboe S, Hansen PL, Thisgaard H, Block I, Müller C, Langkjaer N, Høiland-Carlsen PF, Olsen BB, Mollenhauer J (2017) Evaluation of somatostatin and nucleolin receptors for therapeutic delivery in non-small cell lung cancer stem cells applying the somatostatin-analog DOTATATE and the nucleolin-targeting aptamer AS1411. *PLoS One* 12(5):e0178286
135. Zhan Y, Ma W, Zhang Y, Mao C, Shao X, Xie X, Wang F, Liu X, Li Q, Lin Y (2019) DNA-based nanomedicine with targeting and enhancement of therapeutic efficacy of breast cancer cells. *ACS Appl Mater Interfaces* 11(17):15354–15365
136. Shangguan D, Cao Z, Meng L, Mallikaratchy P, Sefah K, Wang H, Li Y, Tan W (2008) Cell-specific aptamer probes for membrane protein elucidation in cancer cells. *J Proteome Res* 7(5):2133–2139
137. Wang J, Wang H, Wang H, He S, Li R, Deng Z, Liu X, Wang F (2019) Nonviolent self-catabolic DNAzyme nanosponges for smart anticancer drug delivery. *ACS Nano* 13(5):5852–5863
138. Sun P, Zhang N, Tang Y, Yang Y, Zhou J, Zhao Y (2018) Site-specific anchoring aptamer C2NP on DNA origami nanostructures for cancer treatment. *RSC Adv* 8(46):26300–26308
139. Parekh P, Kamble S, Zhao N, Zeng Z, Portier BP, Zu Y (2013) Immunotherapy of CD30-expressing lymphoma using a highly stable ssDNA aptamer. *Biomaterials* 34(35):8909–8917
140. Li H, Zhang K, Pi F, Guo S, Shlyakhtenko L, Chiu W, Shu D, Guo P (2016) Controllable self-assembly of RNA tetrahedrons with precise shape and size for cancer targeting. *Adv Mater* 28(34):7501–7507
141. Ma W, Zhan Y, Zhang Y, Shao X, Xie X, Mao C, Cui W, Li Q, Shi J, Li J, Fan C, Lin Y (2019) An intelligent DNA nanorobot with in vitro enhanced protein lysosomal degradation of HER2. *Nano Lett* 19(7):4505–4517
142. Chen J, Keltner L, Christopherson J, Zheng F, Krouse M, Singhal A, Wang SS (2002) New technology for deep light distribution in tissue for phototherapy. *Cancer J* 8(2):154–163
143. Agostinis P, Berg K, Cengel KA, Foster TH, Girotti AW, Gollnick SO, Hahn SM, Hamblin MR, Juzeniene A, Kessel D, Korbelik M, Moan J, Mroz P, Nowis D, Piette J, Wilson BC, Golab J (2011) Photodynamic therapy of cancer: an update. *CA Cancer J Clin* 61(4):250–281
144. Chen N, Qin S, Yang X, Wang Q, Huang J, Wang K (2016) “Sense-and-treat” DNA nanodevice for synergetic destruction of circulating tumor cells. *ACS Appl Mater Interfaces* 8(40):26552–26558
145. Jin H, Kim MG, Ko SB, Kim DH, Lee BJ, Macgregor RB Jr, Shim G, Oh YK (2018) Stemmed DNA nanostructure for the selective delivery of therapeutics. *Nanoscale* 10(16):7511–7518
146. Yen-An S, Shu-Jyuan Y, Ming-Feng W, Ming-Jium S (2010) Aptamer-based tumor-targeted drug delivery for photodynamic therapy. *ACS Nano* 4(3):1433–1442
147. Brummelkamp TR, Bernards R, Agami R (2002) A system for stable expression of short interfering RNAs in mammalian cells. *Science* 296(5567):550–553
148. Li J, Zheng C, Cansiz S, Wu C, Xu J, Cui C, Liu Y, Hou W, Wang Y, Zhang L, Teng IT, Yang HH, Tan W (2015) Self-assembly of DNA nanohydrogels with controllable size and stimuli-responsive property for targeted gene regulation therapy. *J Am Chem Soc* 137(4):1412–1415
149. Ren K, Liu Y, Wu J, Zhang Y, Zhu J, Yang M, Ju H (2016) A DNA dual lock-and-key strategy for cell-subtype-specific siRNA delivery. *Nat Commun* 7:13580


150. Liu J, Song L, Liu S, Zhao S, Jiang Q, Ding B (2018) A tailored DNA nanoplatform for synergistic RNAi-chemotherapy of multidrug-resistant tumors. *Angew Chem Int Ed Engl* 57(47):15486–15490
151. Liu J, Song L, Liu S, Jiang Q, Liu Q, Li N, Wang ZG, Ding B (2018) A DNA-based nanocarrier for efficient gene delivery and combined cancer therapy. *Nano Lett* 18(6):3328–3334
152. Biswas A, Joo KI, Liu J, Zhao M, Fan G, Wang P, Gu Z, Tang Y (2011) Endoprotease-mediated intracellular protein delivery using nanocapsules. *ACS Nano* 5(2):1385
153. Ran M, Tianyue J, Jin D, Wanyi T, Zhen G (2014) Emerging micro- and nanotechnology based synthetic approaches for insulin delivery. *Chem Soc Rev* 43(10):3595–3629
154. Yang W, Xia Y, Zou Y, Meng F, Zhang J, Zhong Z (2017) Bioresponsive chimaeric nanopolymer-somes enable targeted and efficacious protein therapy for human lung cancers in vivo. *Chem Mater* 29(20):8757–8765
155. Li S, Jiang Q, Liu S, Zhang Y, Tian Y, Song C, Wang J, Zou Y, Anderson GJ, Han JY, Chang Y, Liu Y, Zhang C, Chen L, Zhou G, Nie G, Yan H, Ding B, Zhao Y (2018) A DNA nanorobot functions as a cancer therapeutic in response to a molecular trigger in vivo. *Nat Biotechnol* 36(3):258–264
156. Chen Q, Zhou S, Li C, Guo Q, Yang X, Huang J, Liu J, Wang K (2019) DNA supersandwich assemblies as artificial receptors to mediate intracellular delivery of catalase for efficient ROS scavenging. *Chem Commun (Camb)* 55(29):4242–4245
157. Kim J, Kim D, Lee JB (2017) DNA aptamer-based carrier for loading proteins and enhancing the enzymatic activity. *RSC Adv* 7(3):1643–1645
158. Brody EN, Gold L (2000) Aptamers as therapeutic and diagnostic agents. *J Biotechnol* 74(1):5–13
159. Sridharan S, Weiwei C, Spicer EK, Nigel CL, Fernandes DJ (2008) The nucleolin targeting aptamer AS1411 destabilizes Bcl-2 messenger RNA in human breast cancer cells. *Cancer Res* 68(7):2358
160. Bock LC, Griffin LC, Latham JA, Vermaas EH, Toole JJ (1992) Selection of single-stranded DNA molecules that bind and inhibit human thrombin. *Nature* 355(6360):564
161. Roloff A, Carlini AS, Callmann CE, Gianneschi NC (2017) Micellar thrombin-binding aptamers: reversible nanoscale anticoagulants. *J Am Chem Soc* 139(46):16442–16445
162. Rinker S, Ke Y, Liu Y, Chhabra R, Yan H (2008) Self-assembled DNA nanostructures for distance-dependent multivalent ligand-protein binding. *Nat Nanotechnol* 3(7):418–422
163. Tintore M, Gallego I, Manning B, Eritja R, Fabrega C (2013) DNA origami as a DNA repair nanosensor at the single-molecule level. *Angew Chem Int Ed Engl* 52(30):7747–7750
164. Kumar N, Seminario JM (2018) Molecular dynamics study of thrombin capture by aptamers TBA26 and TBA29 coupled to a DNA origami. *Mol Simul* 44(9):749–756
165. Takeuchi Y, Endo M, Suzuki Y, Hidaka K, Durand G, Dausse E, Toulme JJ, Sugiyama H (2016) Single-molecule observations of RNA-RNA kissing interactions in a DNA nanostructure. *Biomater Sci* 4(1):130–135
166. Lin Y, Jiang L, Huang Y, Yang Y, He Y, Lu C, Yang H (2019) DNA-mediated reversible capture and release of circulating tumor cells with a multivalent dual-specific aptamer coating network. *Chem Commun (Camb)* 55(37):5387–5390
167. Liu Z, Tian C, Yu J, Li Y, Jiang W, Mao C (2015) Self-assembly of responsive multilayered DNA nanocages. *J Am Chem Soc* 137(5):1730–1733
168. Simon AJ, Walls-Smith LT, Freddi MJ, Fong FY, Gubala V, Plaxco KW (2017) Simultaneous measurement of the dissolution kinetics of responsive DNA hydrogels at multiple length scales. *ACS Nano* 11(1):461–468
169. Fern J, Schulman R (2018) Modular DNA strand-displacement controllers for directing material expansion. *Nat Commun* 9(1):3766
170. Zhao Z, Fan H, Zhou G, Bai H, Liang H, Wang R, Zhang X, Tan W (2014) Activatable fluorescence/MRI bimodal platform for tumor cell imaging via MnO₂ nanosheet-aptamer nanoprobe. *J Am Chem Soc* 136(32):11220–11223
171. Kuai H, Zhao Z, Mo L, Liu H, Hu X, Fu T, Zhang X, Tan W (2017) Circular bivalent aptamers enable in vivo stability and recognition. *J Am Chem Soc* 139(27):9128–9131
172. Zhang F, Yan H (2017) DNA self-assembly scaled up. *Nature* 552(7683):34–35
173. Han D, Qi X, Myhrvold C, Wang B, Dai M, Jiang S, Bates M, Liu Y, An B, Zhang F, Yan H, Yin P (2017) Single-stranded DNA and RNA origami. *Science* 358(6369):eaao2648
174. Praetorius F, Kick B, Behler KL, Honemann MN, Weuster-Botz D, Dietz H (2017) Biotechnological mass production of DNA origami. *Nature* 552(7683):84–87

175. Mathur D, Medintz IL (2017) Analyzing DNA nanotechnology: a call to arms for the analytical chemistry community. *Anal Chem* 89(5):2646–2663
176. Amir Y, Ben-Ishay E, Levner D, Ittah S, Abu-Horowitz A, Bachelet I (2014) Universal computing by DNA origami robots in a living animal. *Nat Nanotechnol* 9(5):353–357
177. Peng R, Zheng X, Lyu Y, Xu L, Zhang X, Ke G, Liu Q, You C, Huan S, Tan W (2018) Engineering a 3D DNA-logic gate nanomachine for bispecific recognition and computing on target cell surfaces. *J Am Chem Soc* 140(31):9793–9796

Publisher's Note Springer Nature remains neutral with regard to jurisdictional claims in published maps and institutional affiliations.



High-performance biosensing based on autonomous enzyme-free DNA circuits

Hong Wang¹ · Huimin Wang¹ · Itamar Willner² · Fuan Wang¹ 

Received: 31 October 2019 / Accepted: 17 January 2020 / Published online: 3 February 2020
© Springer Nature Switzerland AG 2020

Abstract

Nucleic acids are considered not only extraordinary carriers of genetic information but also are perceived as the perfect elemental materials of molecular recognition and signal transduction/amplification for assembling programmable artificial reaction networks or circuits, which are similar to conventional electronic logic devices. Among these sophisticated DNA-based reaction networks, catalytic hairpin assembly (CHA), hybridization chain reaction (HCR), and DNAzyme represent the typical nonenzymatic amplification methods with high robustness and efficiency. Furthermore, their extensive hierarchically cascade integration into multi-layered autonomous DNA circuits establishes novel paradigms for constructing more different catalytic DNA nanostructures and for regenerating or replicating diverse molecular components with specific functions. Various DNA and inorganic nanoscaffolds have been used to realize the surface-confined DNA reaction networks with significant biomolecular sensing and signal-regulating functions in living cells. Especially, the specific aptamers and metal-ion-bridged duplex DNA nanostructures could extend their paradigms for detecting small molecules and proteins in even living entities. Herein, the varied enzyme-free DNA circuits are introduced in general with an extensive explanation of their underlying molecular reaction mechanisms. Challenges and outlook of the autonomous enzyme-free DNA circuits will also be discussed at the end of this chapter.

Keywords Catalytic hairpin assembly · Hybridization chain reaction · DNAzyme · DNA circuit · Imaging · Biosensor

Chapter 11 was originally published as Wang, H., Wang, H., Willner, I. & Wang, F. Topics in Current Chemistry (2020) 378: 20. <https://doi.org/10.1007/s41061-020-0284-x>.

✉ Fuan Wang
fuanwang@whu.edu.cn

¹ College of Chemistry and Molecular Sciences, Wuhan University, Wuhan, People's Republic of China

² Institute of Chemistry, The Hebrew University of Jerusalem, Jerusalem, Israel

1 Introduction

In recent years, nucleic acids have substantially expanded their functions from natural bioinformation storage platforms to potent and designable tools for biosensing and bioengineering applications [1]. DNA represents the most powerful candidate for assembling artificial reaction networks for their intrinsic biocompatibility and programmability features. DNA reaction networks are composed of a series of successive strand displacement reactions and cascaded hybridization chain reactions, and they are especially appealing in investigating the signal pathways of more different cellular compartments, e.g., cytoplasm. As compared with the current artificial reaction networks, the advantage of DNA is overwhelmingly obvious for the following reasons. Firstly, DNA could be easily accommodated into different biological microenvironments without additionally complicating the information transmission between biological systems and electronic devices. Secondly, the directionality and programmability of DNA provides the most up-to-date powerful circuitry design and information storage based on the well-known Watson–Crick base-pairing interaction. Thirdly, more different functional DNAs, including aptamers and DNAzymes with their molecular recognition and signal transmission capabilities, could be facilely integrated into the present DNA-based artificial reaction networks. This allows the sensitive and selective sequence-specific analysis of nucleic acids, small molecules, and proteins, which is of great vitality for pathogen identification [2], medical diagnosis [3, 4], and environmental and food safety monitoring [5]. As a traditional nucleic acid amplification method, the polymerase chain reaction (PCR) shows a powerful capability to sensitively detect trace amounts of nucleic acids and other analytes [6, 7]. However, to guarantee the successful initiation of an efficient amplification, PCR needs complex and precise thermocycling procedures with specific polymerases, which may limit its applications in the detection of non-nucleic acid targets as well as in thermosensitive environments. As alternative tools, some isothermal signal amplification methods have thus been developed with more convenient and satisfying amplification capacity, including loop-mediated isothermal amplification (LAMP) [8], rolling circle amplification (RCA) [9, 10], as well as strand displacement amplification (SDA) [11, 12]. While these amplification methods are still bothered by the fragile biological enzymes. Enzyme-free isothermal detection methods are increasingly developed as alternative strategies for overcoming these limitations. The nonenzymatic DNA reaction networks provide the ideal candidate to fulfill these different requirements based on the versatile design out of protein enzyme. Then how to improve these nucleic acid amplification technologies that can compete with the current gold-standard enzyme-mediated amplification methods? Here, the topic of autonomous enzyme-free DNA reaction circuits will be discussed in this chapter by addressing the construction of different kinds of DNA reaction schemes and their effective integration with an adequate discussion of their potential applications.

2 Enzyme-Free DNA Circuit

Nucleic acid reaction networks have attracted increasing attention in the fields of analytical chemistry and biochemistry, and have been explored for sensitive detection of various target molecules. Enzyme-free signal amplification methods are especially appealing for the development of more robust and low-cost point-of-care diagnostics [13]. Among these different enzyme-free DNA reaction circuits, catalyzed hairpin assembly (CHA) [14] and hybridization chain reaction (HCR) [15] are emerging as typical amplification strategies that depend only on autonomous hybridization and strand-displacement reactions to achieve efficient signal amplifications [16]. Figure 1 exemplifies the well-known toehold-mediated strand displacement [17]. During this process, the initial DNA duplex is elongated with an exposed single-stranded domain, namely toehold that can hybridize partially with the input DNA primer. Then the sequential branch migration proceeds, and the input gradually displaces one primer that is partially (or fully) complemented to the other primer of the duplex, yielding a new and more stable DNA duplex structure. As shown in Fig. 1a, the primers P1 and P2 are connected by the hybridization of a – a^* (domain x corresponds to a Watson–Crick base-pairing with x^* .) that is elongated with a toehold sequence a_t . The DNA complex P1/P2 hybridizes with the input DNA P3 by toehold binding of a_t^* – a_t , after which the a^* – a -mediated sequential branch migration leads to the ultimate assembly of P1/P3 product with the simultaneous generation of P2 strand. Interestingly, the kinetics (rate constant) of these strand-displacement reactions varied with the base numbers and species of toehold domains (Fig. 1b), and the G–C-rich toehold leads to a higher strand displacement reaction rate than that of the A–T counterpart.

Based on this mechanism, various research has been carried out to address the strand-displacement process and to extend their broader applications. Among these different works, CHA and HCR have been well developed and have attracted more

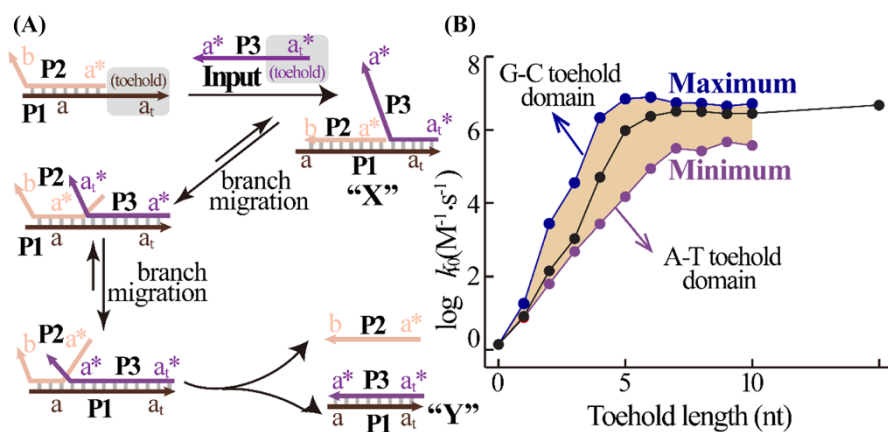


Fig. 1 a Schematic illustration of DNA strand-displacement principle. b Kinetics models of DNA strand-displacement reaction that were affected by the number and species of bases in the toehold domain. Reprinted with permission from Ref. [17]. Copyright 2009 American Chemical Society

attention for their isothermal and autonomous hybridization reaction properties. In a typical CHA process, the initiator acts as a special key to cyclically open their corresponding hairpin locks without consuming the input strand itself. CHA mediates the target-catalyzed hybridization and strand-displacement of hairpins for assembling numerous dsDNA products, which are especially useful in amplifying and transducing the input DNA at the terminus of nucleic acid amplifications. Indeed, CHA is facilely conjugated with other amplification procedures to achieve an improved sensing performance. As for the HCR, the input primer promotes the autonomous cascade cross-hybridization of hairpin reactants, yielding long nicked dsDNA copolymers through an easy and programmable operation. Also, the generated long dsDNA nanowire products are not only encoded with various functional DNA sequences but are also utilized as powerful nanocarriers for accommodating small guest molecules [18]. Meanwhile, DNazymes are emerged with fascinating catalytic functions of protein enzymes that can catalyze various biological and chemical reactions, including DNA ligation and cleavage. These enzyme-mimicking functionalities with multiple turnover rates allow DNazymes to be ideal candidates for high-performance signal amplification applications. All of these enzyme-free DNA circuits have prominent and modular amplification features—that is, their signal gain performance could be improved by integrating with other amplification methods in more extended application fields. These nonenzymatic amplification strategies have been used to detect various important analytes (nucleic acids [19, 20], proteins [21], small molecules [22], and metal ions [23]) with different transduction approaches, such as fluorescence [24, 25], colorimetry [26], chemiluminescence (CL) [27], and electrochemical approaches [28].

2.1 Catalytic Hairpin Assembly (CHA)

The analyte-activated isothermal autonomous catalytic hairpin assembly (CHA) was initially proposed by Pierce et al. [14]. It provides a versatile free-energy-driven amplification procedure to stimulate the catalytic generation of stable linear or branched duplex DNA nanostructures. The mechanism of CHA is presented in Fig. 2a. A characteristic CHA reaction consists of two hairpins, H_A and H_B . The sequence a_t – a of H_A is complementary to domain a^* – a_t^* of trigger T , and hairpin H_B is designed to hybridize with H_A from b_t^* . T opens hairpin H_A to generate the DNA assembly “I” based on toehold-mediated displacement of sequence a^* – a_t^* . The released domain b – b_t of H_A hybridizes with hairpin H_B , generating an intermediate structure “II”. The newly released H_B initiates the branch migration procedure and gradually stimulates the strand displacement of T to form numerous dsDNA product “III”. The regenerated trigger strand allows the continuous activation of CHA circuit that stimulates the successive hybridizations between hairpins H_A and H_B . Similarly, more different hairpins can be assembled by CHA to generate a “Y-shaped” model with three hairpin reactants or “X-shaped” model with four hairpin reactants.

The trigger-induced CHA-mediated cross-opening of nucleic acid hairpins could also enhance the complexities of DNA nanostructures. As shown in Fig. 2b, the cascaded cross-opening of three hairpins leads to the formation of a three-arm branched

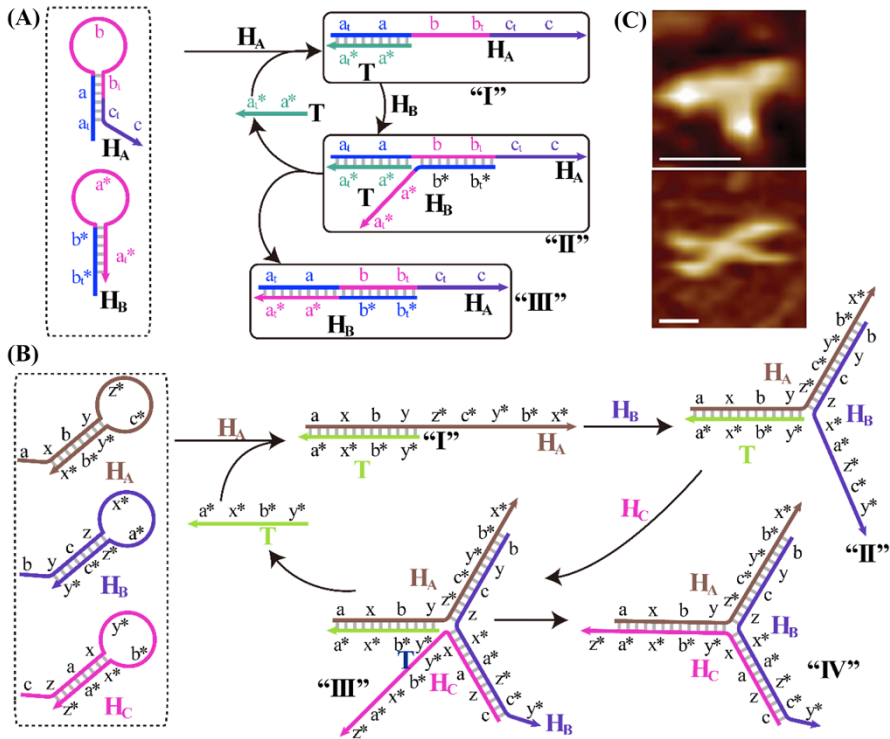


Fig. 2 Schematic illustration of conventional CHA. **a** CHA-assembled linear dsDNA nanostructure, which is induced by trigger-catalyzed assembly of hairpins H_A and H_B . **b** CHA-assembled Y-shaped DNA nanostructure that is generated by cross-opening of hairpins H_A , H_B , and H_C . **c** AFM images of the CHA-assembly of “Y-shaped” (upper AFM image) and “X-shaped” (lower AFM image) dsDNA nanostructures, respectively. Scale bar indicates 10 nm. Reprinted with permission from Ref. [14]. Copyright 2008 Nature Publishing Group

junction structure. The initiator T hybridizes with hairpin H_A to generate dsDNA product “I”, and the toehold of “I” opens H_B to generate structure “II”. The exposed toehold in “II” opens H_C to form an intermediate structure “III”. The newly released strand of H_C initiates the branch migration and displaces T to form the three-arm branched junction structure “IV”. The released initiator subsequently stimulates the successive hybridizations among hairpins H_A , H_B , and H_C to generate “Y-shaped” DNA nanostructures. Similarly, the four-arm branched junction structure could be programmed through the catalytic self-assembly of four hairpins, as demonstrated in Fig. 2c. The autonomous regeneration of trigger with the cross-opening hairpin-mediated hybridization method represents an isothermal enzyme-free amplification method for the analysis of trigger DNA.

The as-demonstrated CHA system can be extended as a powerful sensing platform for analyzing nucleic acids and more different analytes via fluorescence transduction [29]. In Fig. 3a, trigger T hybridizes with hairpin H_{CP} to generate the actual initiator T- H_{CP} with a newly exposed toehold sequence (light blue), and

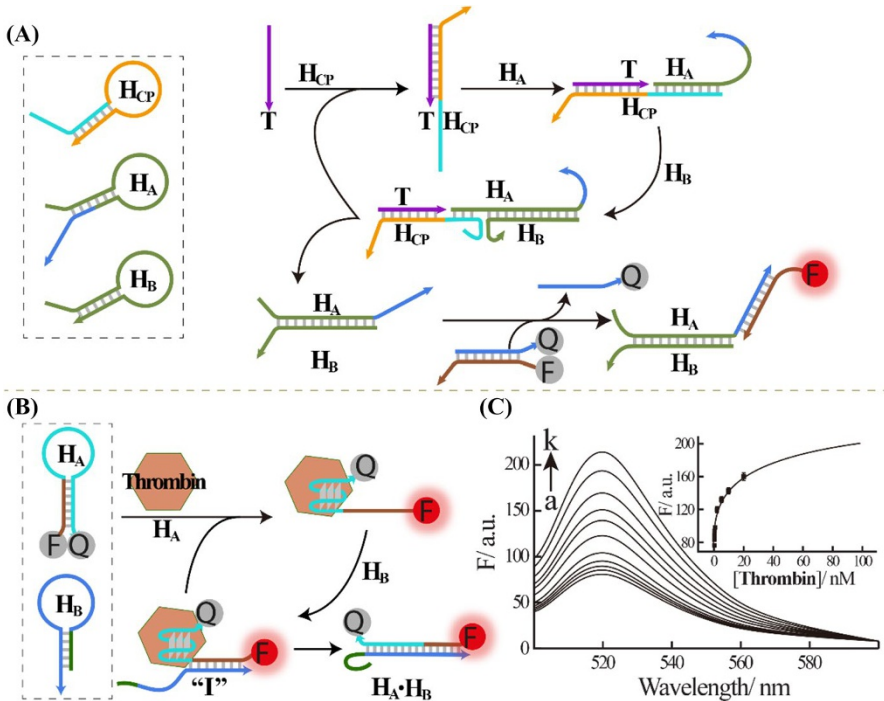


Fig. 3 **a** Schematic illustration of an isothermal autonomous CHA amplifier for analyzing target DNA with the aid of an auxiliary sensing module H_{CP} . **b** Schematic illustration of the analysis of thrombin based on the CHA-mediated transduction of an aptamer recognition module. **c** Fluorescence spectrum of the CHA-amplified thrombin detection system by incubating with different concentrations of thrombin: a–k: 0 , 2.0×10^{-11} , 5.0×10^{-11} , 2.0×10^{-10} , 5.0×10^{-10} , 2.0×10^{-9} , 5.0×10^{-9} , 1.0×10^{-8} , 2.0×10^{-8} , 5.0×10^{-8} , and 1.0×10^{-7} M. (Inset) Derived calibration curve. Reprinted with permission from Ref. [30]. Copyright 2012 Elsevier

then the T - H_{CP} initiator catalyzes the cross-opening of H_A and H_B to implement the CHA reaction, yielding a duplex H_A - H_B with a single-strand domain (dark blue) that could displace a fluorophore/quencher-modified duplex and generate fluorescence readout for detecting DNA targets [30]. Apart from DNA detection, CHA could also be applied for protein detection with the specifically designed aptamer that was encoded into one of these two hairpin reactants (H_A and H_B), Fig. 3b. Here, H_A contains a thrombin–aptamer sequence in the loop region and is attached with a fluorophore/quencher pair on each end. In the presence of thrombin, H_A is opened to form the thrombin–aptamer complex with a toehold (brown), which then opens H_B to generate an intermediate structure “I”. The exposed toehold of H_B competitively binds the aptamer region associated with thrombin and releases the thrombin analyte for continuously triggering the CHA system. The formation of H_A - H_B leads the efficient separation of fluorophore and quencher, and generates high fluorescence signal for analyzing thrombin down to 20 pM (Fig. 3c).

Apart from the programmed catalytic assembly of different DNA nanostructures, the CHA reaction could be facily engineered as a stochastic DNA walker that utilizes hybridization reactions to traverse a microparticle surface. Figure 4a exemplifies the initiator-catalyzed successive cross-opening of surface-immobilized H_1 and FAM-functionalized H_2 on microparticles [31]. The catalyst DNA can open the surface-bound H_1 through toehold-mediated strand-displacement reaction. Then, a newly released tether of H_1 hybridizes to the toehold of FAM-modified H_2 for initiating a branch migration reaction, resulting in the generation of an intermediate structure consisting of H_1 , H_2 , and the catalyst. Along with the strand displacement process, the catalyst DNA is displaced from the duplex structure of H_1 - H_2 . The regenerate catalyst then continuously participates in the nearby CHA reaction cycle. Through the CHA process, the nanoscale movements of the walker (catalyst) lead to the immobilization of fluorescent strands on the surface of the microparticle.

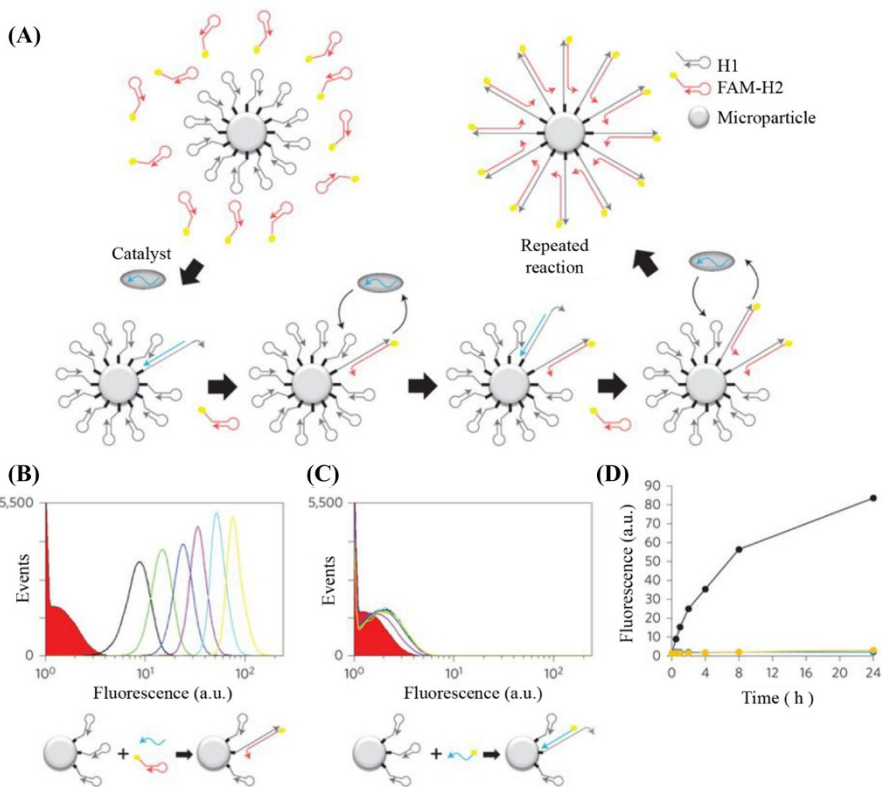


Fig. 4 **a** Schematic illustration of the microparticle-confined CHA based on the catalytic hybridization reaction between surface-anchored H_1 and non-anchored FAM-modified H_2 . **b** Flow cytometry characterization of the microparticle-confined CHA over different time intervals (0, 0.5, 1, 2, 4, 8, 24 h, from left to right). **c** Flow cytometry characterization of the negative CHA control experiment without the involvement of H_2 . **d** Summary of the mean fluorescence intensity from the flow cytometry assay over time (black for catalytic system; blue and yellow for non-catalytic and no-catalyst controls, respectively). Reprinted with permission from Ref. [31]. Copyright 2016 Nature Publishing Group

An obvious fluorescence change over different time intervals has demonstrated the successful capture of FAM-H₂ on microparticles through the as-suggested CHA process (Fig. 4b). The H₂-absent negative control experiment was carried out with substantially lower fluorescence readout and thus exemplified the amplification performance of CHA (Fig. 4c). This signal difference could be easily observed from the summarized flow cytometry assay, as shown in Fig. 4d. The walking system offers new insights into the analytical and diagnostic applications, as well as biomaterials development.

By using the underlying nanoparticles as nanocarriers, the CHA system could also be applied towards sensitive detection of intracellular RNA, e.g., manganese superoxide dismutase (MnSOD) mRNA in living cells [32]. Subsequently, other functional nanostructures, e.g., tetrahedron DNA, are also supplemented versatile tools to deliver DNA primers into living cells, considering that the homologous DNA could be assembled into suitable size and shape for delivering DNA probes. An entropy-driven three-dimensional DNA amplifier (EDTD) has been constructed for delivering DNA probes into living cells where a specific intracellular mRNA analyte triggers the EDTD-involvement CHA process [33]. As illustrated in Fig. 5a, the first module of EDTD corresponds to an entropy tetrahedron (ET) module that is constructed with six DNA primers and elongated an important dsDNA toehold. Here, the quencher-modified P5 and the fluorophore-modified P6 are assembled together with no fluorescence readout. The other key module of EDTD is the fuel tetrahedron (FT) module (Fig. 5b). Similar to ET, the FT uses four DNA primers to construct the same tetrahedral backbone. Different from P4, here part of P7 toehold acts as fuel sequence (yellow) in the CHA process. The tetrahedron amplifier could be quickly activated by target mRNA which hybridizes with the exposed region 4*

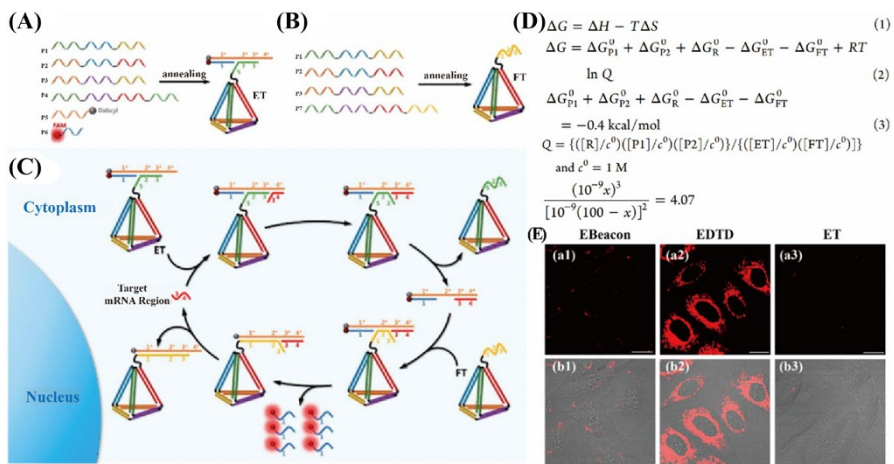


Fig. 5 Schematic illustration of the assembly of the entropy tetrahedron (ET) module (a), the fuel tetrahedron (FT) module (b), and the EDTD principle in living cells (c). **d** Theoretical simulation of the EDTD reaction. **e** EDTD-mediated intracellular imaging of TK1 mRNA in HepG2 cells that were treated with different systems. Scale bar 20 μm. Reprinted with permission from Ref. [33]. Copyright 2018 American Chemical Society

of ET to initiate the toehold-mediated strand displacement, resulting in an immediate T–P5–P6 product (Fig. 5c). The as-achieved T–P5–P6 structure binds to the exposed domain 2* of FT to release target mRNA and P6 with the formation of a waste tetrahedron FT–P5 product. The regenerate mRNA and P6 can take part in the next cycle of CHA reaction to realize an effective signal amplification. Therefore, the fluorescence of P6 can directly reflect the amount of intracellular mRNA. Different from the cross-opening of convenient CHA reaction, this new strategy is free from hairpin reactants and is driven by entropy as demonstrated by theoretical simulations (Fig. 5d). Benefiting from this special structure and the exclusive driving force, this DNA nanostructure could be operated in living cells for a high-performance mRNA detection (Fig. 5e). This entropy-driven 3D DNA nano-amplifier might provide a more reliable sensing platform for living entities.

2.2 Hybridization Chain Reaction (HCR)

Another characteristic isothermal non-enzymatic nucleic acid reaction, hybridization chain reactions (HCR), is achieved by successive cross-opening of two hairpins to assemble dsDNA copolymeric nanowires [15]. As shown in Fig. 6a, H_1 consists of the programmed sequences a–b and c–b*, which are complementary to the sequence b*–a* of initiator I and b–c* of H_2 , respectively. The rest sequence of H_2 corresponds to domain b*–a*, an analog sequence of I, which can subsequently hybridize to domain a–b of H_1 . These hairpins stay in a kinetically trapped situation without initiator. Based on the toehold-mediated displacement process, initiator

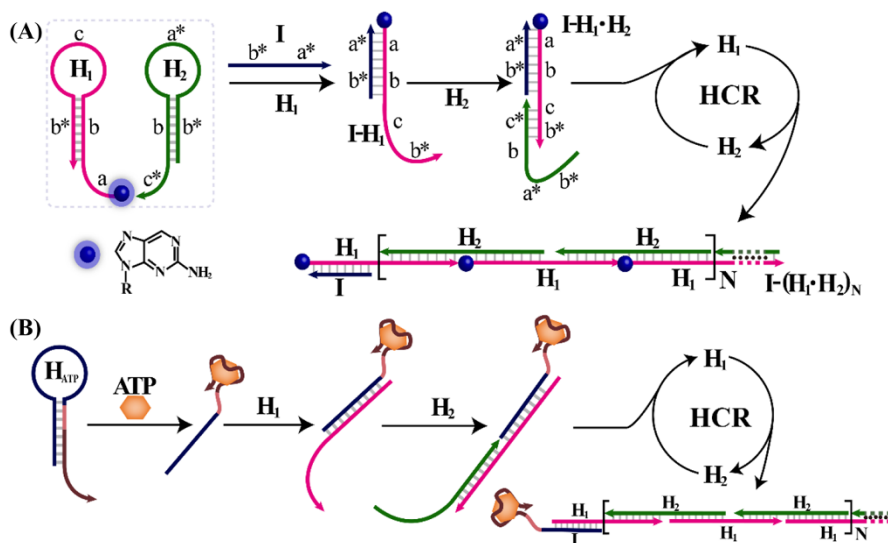


Fig. 6 a Schematic illustration of the HCR circuit where the initiator I triggers the autonomous cross-opening of H_1 and H_2 to generate dsDNA nanowires. b Amplified ATP detection by integrating HCR amplification with functional hairpin H_{ATP}

I opens hairpin H_1 to generate $I \cdot H_1$ duplex. The released domain $c-b^*$ in $I \cdot H_1$ opens H_2 to form an immediate product $I \cdot H_1 \cdot H_2$ of which the exposed sequence b^*-a^* initiates the following new round of hybridization cycle, resulting in the generation of long dsDNA polymeric nanowires. Here, H_1 is functionalized with 2-amino purine, which shows high fluorescence in the single-stranded configuration of the hairpin structure, while it is quenched by stacking in the duplex DNA nanowire structure. More importantly, the HCR circuit could be served as an easily adapted amplifier for extensive sensing applications, e.g., aptasensors (Fig. 6b).

The HCR system could also be considered as a more versatile sensing platform when the HCR reactants H_1 and H_2 were labeled with two pyrene moieties on each end (Fig. 7a) [34]. Without target DNA, both hairpins are in the closed form, and the two pyrene moieties are separated far away from each other through the sticky end, leading to the observation of the monomer emission spectra. Target DNA can open H_1 through a strand-displacement reaction. The newly released toehold of H_1

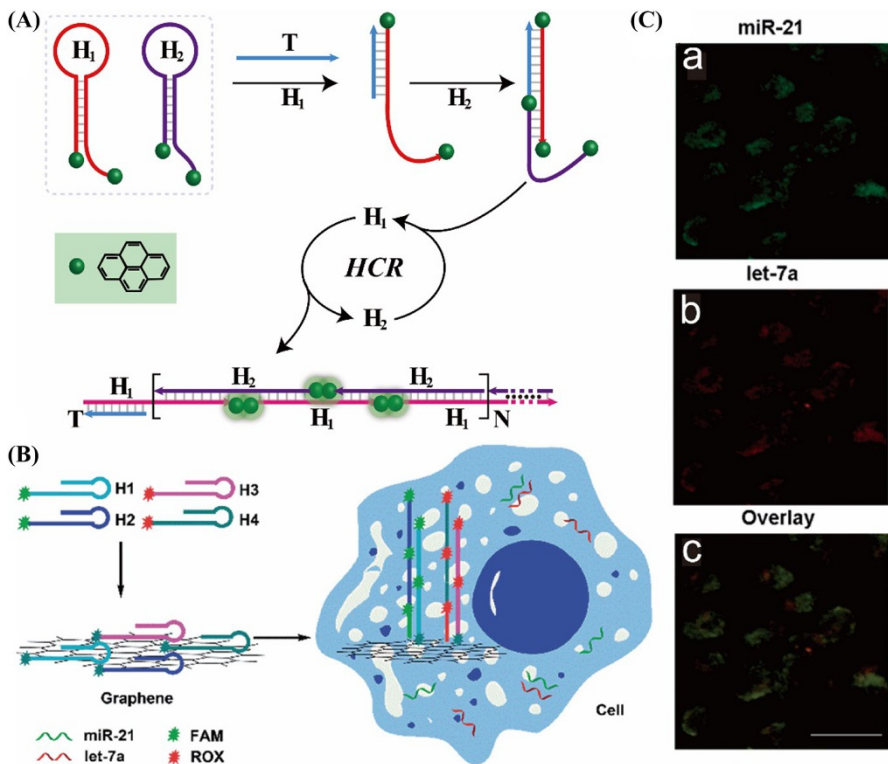


Fig. 7 **a** The autonomous HCR system based on the target-induced cross-hybridization of H_1 and H_2 that were functionalized with pyrene units in two ends, resulting in the generation of long dsDNA nanowires with exciplex emission of pyrene. **b** Schematic illustration of the intracellular multicolor miRNA imaging based on the HCR reaction on graphene oxide (GO). **c** Two-color confocal fluorescence imaging of miR-21 and let-7a analytes in MCF-7 cells. The scale bar indicates 50 μm . Reprinted with permission from Ref. [36]. Copyright 2017 Royal Society of Chemistry

nucleates at the tether end of H_2 and opens H_2 to expose another target analog. Thus, the target can propagate a successive cross-opening of two hairpins to yield long dsDNA nanowires. In this HCR product, the pyrene moieties are brought into close proximity, thus generating numerous pyrene excimers with an emission at approximately 485 nm. Therefore, the target can be sensitively detected by the varied emissions of pyrene monomers and the corresponding excimers.

Two-dimensional nanomaterials, including graphene oxide (GO) [35], molybdenum disulfide (MoS_2), and manganese dioxide (MnO_2), could also be integrated with HCR amplifier for intracellular mRNA imaging, originating from their excellent capability of ssDNA adsorbing and fluorescence quenching. Figure 7b exemplified the simultaneous detection of two intracellular miRNAs by using GO-supported HCR circuit [36]. Here, H_1 and H_2 were functionalized with fluorophore FAM for miR-21 detection while H_3 and H_4 were modified with fluorophore ROX for let-7a detection. These hairpins were physically adsorbed on the surface of GO through noncovalent π - π stacking interaction and all fluorophores were efficiently quenched. These hairpin probes were transported into living cells by GO via a non-destructive clathrin-mediated endocytosis process. Then the miR-21 target could initiate the successive hybridization between H_1 and H_2 , yielding long dsDNA $(H_1/H_2)_n$ nanowires. These nanowires were then detached from the surface of GO with fluorescence recovery of FAM, which is originated from the weak interaction between dsDNA and GO. Similarly, the let-7a analyte could trigger the sequential hybridization of H_3 and H_4 for obtaining a remarkable higher fluorescence of ROX. The amplified green and red fluorescence signal represented the corresponding miRNAs in living cells, and thus providing a novel tool for sensitive intracellular imaging of multiple biomarkers (Fig. 7c).

Besides graphene oxide, gold nanoparticles (AuNPs) could also be utilized for transducing the HCR system via a colorimetric or fluorescent bioassay. Figure 8a illustrates the colorimetric detection system based on AuNPs transduction of HCR system consisting of two hairpins H_1 and H_2 [37]. Domains I and II of H_1 are designed to be complementary to domains I' and II' of H_2 . Without target, the ssDNA tethers of HCR hairpins are adsorbed on the surface of AuNPs, and thus avoid the salt-induced aggregation of AuNPs. The introduced target can hybridize with domain I of H_1 and open H_1 through strand displacement reaction (step 1). The newly exposed tether II of H_1 then hybridizes to domain II' of H_2 and opens H_2 (step 2). The as-released domain I' is encoded with the same sequence of target for triggering the efficient opening of H_1 (step 3). With the repeat operation of steps 2 and 3, the sequential hybridization of H_1 and H_2 leads to the efficient assembly of long dsDNA nanowires. Under this circumstance, these as-achieved nanowires are detached from the AuNPs, resulting in the aggregation of AuNPs under high-salt concentrations with immediate color transition. This method achieves a simple yet convenient colorimetric detection of DNA and could sensitively and selectively discriminate single base-pair mismatches of the target (Fig. 8a inset).

For HCR transduction, AuNPs were not only acting as colorimetric transduction agent, but were also considered as a versatile fluorescence quencher [38]. The combination of AuNPs with HCR circuit has also been applied for intracellular mRNA imaging. The target survivin mRNA is known to be overexpressed in

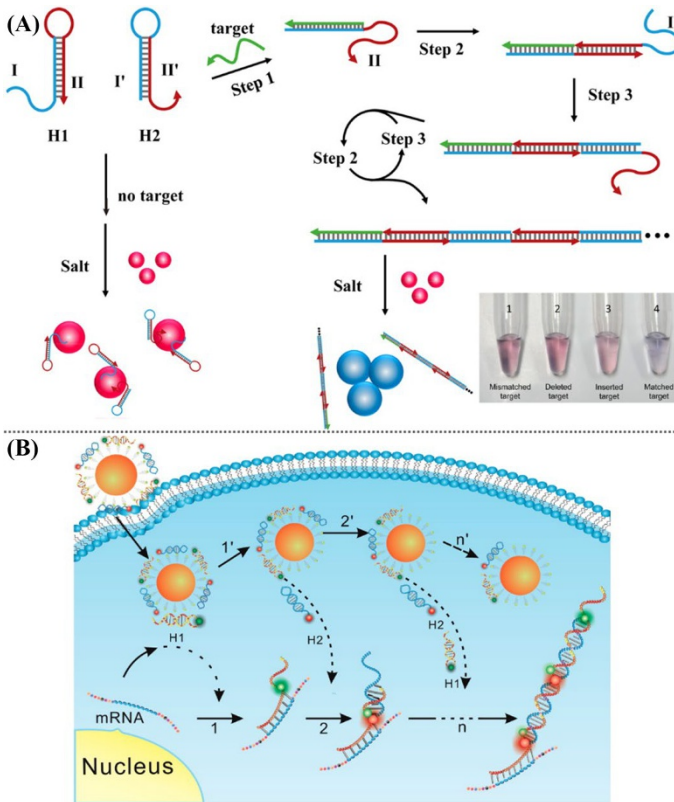


Fig. 8 **a** Schematic illustration of the colorimetric detection of DNA target through AuNPs-mediated transduction of HCR amplifier. Inset shows the corresponding photographs of AuNPs solutions that were introduced with different reactants. Reprinted with permission from Ref. [37]. Copyright 2013 American Chemical Society. **b** Scheme of the fluorescent detection of mRNA target using AuNPs-supported HCR amplification. Reprinted with permission from Ref. [39]. Copyright 2015 American Chemical Society

most cancer cells [39]. In Fig. 8b, two hairpin reactants H_1 and H_2 are designed to recognize and amplify the target mRNA. Here, H_1 and H_2 are functionalized with a fluorescence donor (FAM) and a fluorescence acceptor (TMR), respectively, and are steadily assembled on the surface of cationic peptide-coated AuNPs. These fluorescence signals are thus effectively quenched by AuNPs. The survivin mRNA opens hairpin H_1 with the exposure of an ssDNA tether. This tether sequence then hybridizes with hairpin H_2 and releases the same sequence of target. Then the alternative hybridization of H_1 and H_2 generates dsDNA nano-wires with rigid conformation, resulting in the dissociation of these HCR nano-wires from the surface of AuNPs. The dissociated product brings two fluorophores FAM and TMR into close proximity for generating an efficient Förster resonance energy transfer (FRET) signal. The gold particles-DNA nanoassembly enables high performance to deliver into living cells and to quench the DNA probes, thus offering high sensitivity and specificity for intracellular mRNA imaging. The

nanoassembly might provide a novel strategy for low-abundance biomolecule detection and regulation in cell biology studies.

The confined HCR reaction on AuNPs could similarly be extended to DNA nanostructures, e.g., rolling circle polymerized one-dimensional RCA nanowires. This DNA-confined HCR system is proposed as a powerful tool for realizing intracellular sensing applications (Fig. 9a) [40]. Based on an accelerated HCR system on the RCA track product, the DNA “nano string light” (DNSL) achieved high-performance intracellular mRNA imaging. This system was designed by interval immobilizing functional hairpins H_1 and H_2 on RCA-produced DNA nanowires. The fluorophore/quencher-modified hairpin H_1 was conjugated with folic acid (FA) for targeting HeLa cells. The intracellular survivin mRNA initiates the cascade cross-opening of the alternatively arranged H_1 and H_2 along the DNA nanowire, which could enhance the fluorescence of DNSL (Fig. 9b). In comparison with the non-confined catalytic amplification and successive DNA hybridization, the DNSL includes

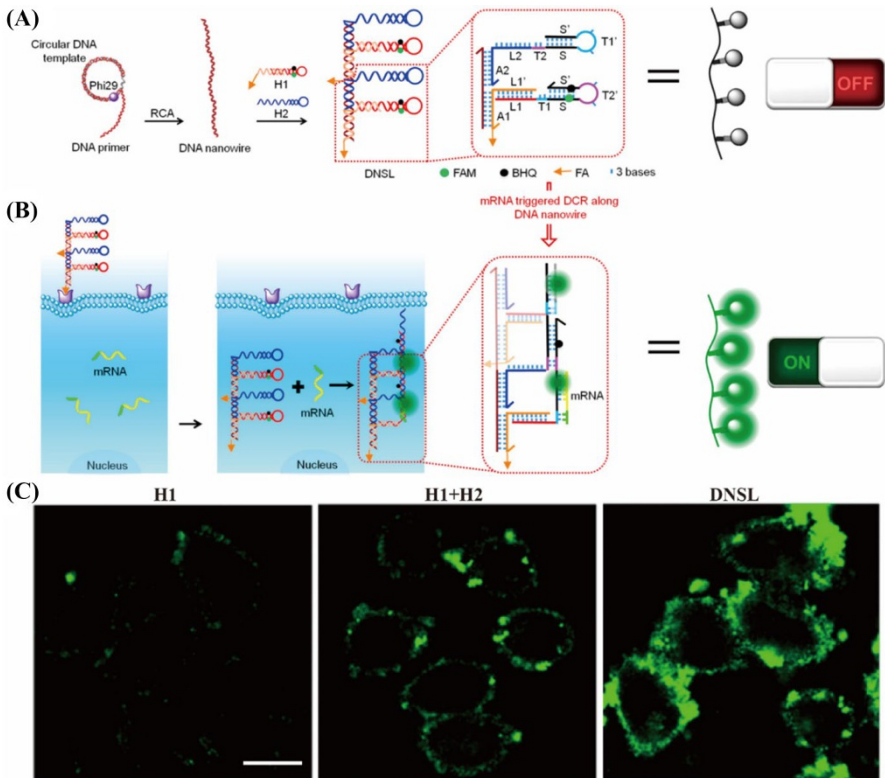


Fig. 9 Schematic illustration of the one-dimensional DNA scaffold-confined HCR reaction through the alternative arrangement of hairpins H_1 and H_2 on the RCA-produced nanowire. **a** DNSL synthesis procedure and **b** the targeting delivery of DNSL into living cells for imaging target mRNA. **c** Confocal images of HeLa cells that were treated with H_1 , mixture of H_1 and H_2 , and DNSL, respectively. Scale bar 20 μm . Reprinted with permission from Ref. [40]. Copyright 2018 American Chemical Society

numerous H_1 and H_2 that were alternately arranged with designed space, to accelerate hybridization reaction and strand-displacement with enhanced sensing performance. The biocompatible DNSL further facilitated the efficient delivery of HCR probes into living cells (Fig. 9c). It thus introduces a potential intracellular mRNA imaging platform for various disease diagnostics and therapies.

2.3 DNAzyme

DNAzymes are referred to as catalytic ssDNAs that are obtained via the *in vitro* selection. They usually require indispensable cofactors for executing an efficient catalytic DNA or RNA cleavage, DNA hydrolyzation, DNA ligation, and so on. One of the most commonly used DNAzymes is the metal ion-dependent RNA-cleaving DNAzyme, which requires the involvement of metal ion cofactors, such as Mg^{2+} [41], Cu^{2+} [42], Ni^{2+} [43], Hg^{2+} [44], Zn^{2+} [45], Pb^{2+} [46], and so on. The DNAzyme-based biocatalysis reactions have been extensively described in a series of review articles [47, 48]. As shown in Fig. 10a, the DNAzyme (blue strand) can specifically bind to the riboadenine (rA, yellow)-containing DNA substrate (purple strand) through Watson–Crick base pairing hybridization. The DNAzyme folds into the catalytic active structure with metal ions for cleaving substrate at “rA” site, releasing two fragments of the cleaved substrate. Here, the cleavage of RNA

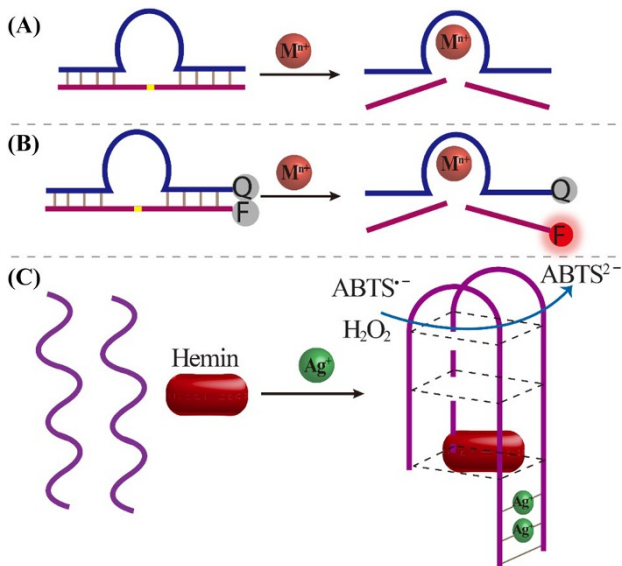


Fig. 10 **a** Schematic illustration of the DNAzyme-mediated RNA-cleavage with the aid of indispensable cofactors. **b** The design of fluorescent DNAzyme biosensors based on the fluorophore/quencher-modified DNAzyme and substrate. Reprinted with permission from Ref. [49]. Copyright 2017 American Chemical Society. **c** The specific Ag^+ -involved assembly of cytosine- Ag^+ -cytosine bridges for constructing hemin/G-quadruplex HRP-mimicking DNAzyme. Reprinted with permission from Ref. [52]. Copyright 2009 American Chemical Society

is mostly initiated by the attacking of 2'-OH group to the scissile phosphate. The released DNAzyme then moves to the cyclic cleavage of another substrate, thus achieving the amplified catalytic process. The substrate could be labeled with a F/Q pair for transducing the DNAzyme reaction process [49]. Figure 10b shows that the DNAzyme catalytically cleaves the FAM-labeled substrate with metal ion cofactors. The cleaved substrate fragments detached from the quencher-functionalized DNAzyme, resulting in the recovery of FAM fluorescence. Another widely used DNAzyme is the hemin/G-quadruplex horseradish peroxidase (HRP)-mimicking DNAzyme, which could mimic the catalytic functions of peroxidase for catalyzing the oxidation of ABTS or TMB with color changes, and the chemiluminescence of luminol with H_2O_2 [50, 51]. Since the cytosine–cytosine (C–C) gap of dsDNA can specifically capture Ag^+ ions to generate C– Ag^+ –C bridge, a DNA-based Ag^+ sensor was then constructed [52]. Figure 10c depicts the hemin/G-quadruplex DNAzyme-mediated colorimetric detection of Ag^+ ions. Without Ag^+ , these hemin/G-quadruplex strands are separated with each other with no DNAzyme activity. The Ag^+ ions can initiate the generation of C– Ag^+ –C base pairs for assembling hemin/G-quadruplex DNAzyme. The as-achieved DNAzyme can catalyze the ABTS– H_2O_2 reaction and give rise to a colorimetric assay. This Ag^+ -mediated DNAzyme switch system could be used for sensitive detection of Ag^+ with a detection limit of 2.5 nM.

Since the surface plasmon resonance absorption of AuNPs is affected by their size and distance, AuNPs are widely used in assembling various colorimetric sensors. This property is especially appealing for producing DNAzyme biosensors via the DNAzyme-conjugated AuNPs [53]. As shown in Fig. 11a, the AuNPs were modified with DNAzyme/substrate strands through Au–S bond. The DNAzyme-hybridized substrate was elongated to capture AuNPs, leading to the aggregation of AuNPs with blue color in solution. In the presence of Pb^{2+} cofactor, the DNAzyme was activated to cleave the substrate and led to the dissociation of gold nanoassembly with red color of the dispersed AuNPs. Not only metal ion cofactors, but other factors could also be considered as the specific analytes for their influence on the compact DNAzyme structure. With the help of AuNPs and aptamer-involved recognitions and activations, an amplified aptazyme–AuNPs biosensor was assembled for intracellular ATP detection [54]. Here, the aptazyme is designed with two major regions: ATP aptamer-recognition domain and DNAzyme transduction region. As shown in Fig. 11b, the ATP aptazyme and its substrate are both immobilized on AuNPs. Meanwhile, the ATP aptazyme is labeled with a quencher (BHQ-2) unit and the substrate is labeled with a fluorophore unit. In that case, the fluorophore would be effectively quenched by AuNPs and BHQ-2. Thus, the ATP aptazyme sensors are catalytic inactive without fluorescence readout. The ATP could specifically combine with aptazyme and favor the assembly of DNAzyme microenvironment for activating the cleavage reaction of DNAzyme substrate. After cleavage, the fluorophore-labeled DNA fragment is separated from the substrate strand and moves far from the quencher units, thus yielding a high fluorescence signal. The AuNPs surface-confined DNAzyme reaction leads to an efficient DNAzyme reaction as mentioned before. Thus, the free aptazyme keeps active to hybridize with other substrate strands on AuNPs for new cycles of DNAzyme cleavages, resulting in highly sensitive ATP

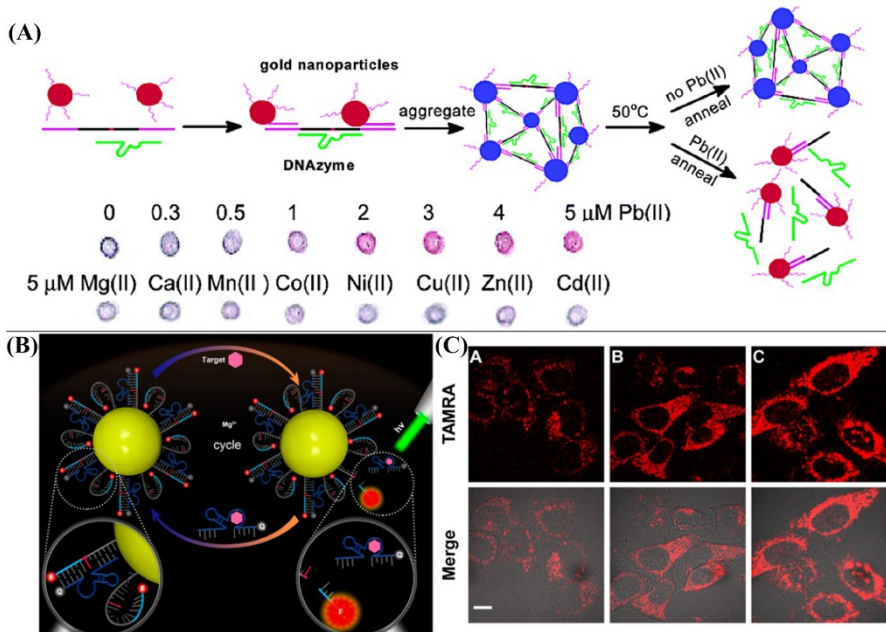


Fig. 11 **a** The colorimetric assay of lead ions based on the integration of DNAzyme biocatalysis with AuNPs labels. Reprinted with permission from Ref. [53]. Copyright 2003 American Chemical Society. **b** Schematic illustration of the AuNPs-confined aptazyme sensing platform for ATP assay. **c** Intracellular imaging of ATP by AuNPs-confined aptazyme reaction in HeLa cells that were treated with different systems: A, 10 μg/ml oligomycin and 5 mM 2-deoxy-D-glucose; B, intact control; C, 5 mM Ca²⁺. Scale bar 10 μm. Reprinted with permission from Ref. [54]. Copyright 2016 American Chemical Society

detecting performance. Moreover, this strategy can further be applied for intracellular imaging of various targets in living cells (Fig. 11c). Similarly, based on the remarkable affinity difference between GO and ssDNA, the GO surface-confined DNAzyme has also been introduced for selective and amplified Pb²⁺ detection [55].

Apart from AuNPs integration, DNAzymes can also be applied to cascade with the endonucleases, which could realize a more sensitive enzymatic recycling cleavage strategy. The molecular recognition element was facily integrated with a signal reporter element with improved sensitivity. As shown in Fig. 12a, the dual loop hairpin H_{ip} is composed of DNAzyme and substrate that were connected by a poly-T sequence. In the presence of L-histidine, the intramolecular cleavage reaction releases a trigger sequence T. Then the reporter MB is opened by trigger T to form the double-stranded recognition site for Nicking enzyme, realizing the second cycle of cleavage. The cascade DNAzyme-Nicking enzyme system undergoes sequential and successive cleavage of MB probe, providing a high fluorescence readout (Fig. 12b). This cascade-catalytic sensing strategy affords a sensitive L-histidine assay down to 200 nM [56]. Except for cofactors detection, a ligase-regulated DNAzyme system was similarly developed to probe DNA ligase

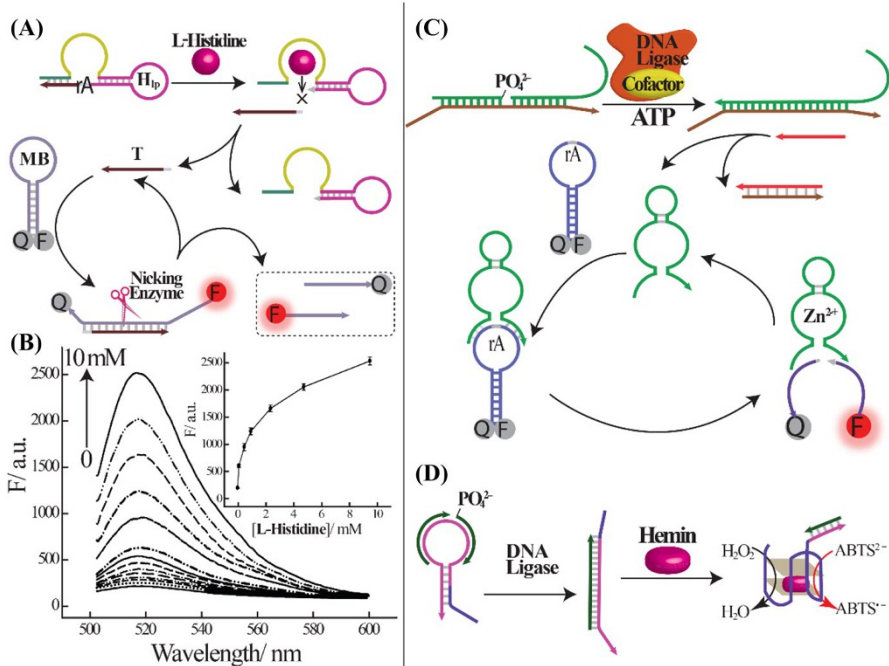


Fig. 12 **a** Schematic illustration of the cascade from L-Histidine-DNAzyme to nicking enzyme biocatalysis. **b** Fluorescence monitoring of the cascade DNAzyme system for histidine detection. Inset: Derived calibration curve. Reprinted with permission from Ref. [56]. Copyright 2011 American Chemical Society. **c** Schematic illustration of a coupled ligase/DNAzyme cascade for ATP detection. Reprinted with permission from Ref. [57]. Copyright 2011 American Chemical Society. **d** Schematic illustration of a coupled ligase/hemin/G-quadruplex for detecting ligase activity

activity [57]. One of the feasible examples is based on an allosteric DNAzyme-containing hairpin probe (HDP). With the help of DNA ligase, DNAzymes could be synthesized as “products” to achieve a more sensitive bioassay. As illustrated in Fig. 12c, the ligase-mediated ligation of two DNAzyme fragments activate the assembly of new DNAzyme. Only with ATP, then the ligase is active to assemble a new DNAzyme for cleaving the F/Q-labeled substrate, resulting in the generation of a high fluorescence signal. In another study, the DNAzyme domain is partially caged on the stem domain of a hairpin, Fig. 12d. [58]. Once the ligase repairs the nicking site and forms a more stable duplex DNA, then the hemin/G-quadruplex DNAzyme could be activated with peroxidase-like activity.

2.4 Integration

These catalytic CHA, cross-hybridization-involved HCR, and functional DNAzyme have shown great performance for amplified biosensing, yet are constrained with low signal gain. To make full use of these different enzyme-free circuits, the sophisticated cascading integration of these amplifiers was proposed to realize a

more readily quantitative detection as well as the assembly of exquisite DNA nanostructures [1]. Only through the corrected executions of individual reaction pathways, then the integrated multiple or cross-initiated enzyme-free amplifiers could be engineered for precisely detecting both nucleic acids and other analytes, leading to a higher amplification efficiency with delicate hierarchical DNA nanostructures [59]. The catalyzed translation of CHA leads to the assembly of numerous dsDNA by the preceding initiator.

For cascaded integration of catalytic hairpin assembly (CHA), the two-layered and three-layered CHA reactions have been engineered to further improve the signal amplification [60]. The integration depth of CHA was further promoted by using a cross-catalytic hairpin assembly (cross-CHA) circuit that consists of three CHA units, CHA-1, CHA-2, and CHA-3 (Fig. 13) [14]. Here, CHA-1 is composed of two hairpins H_A and H_B , which is initiated by trigger T to realize the assembly of H_A-H_B duplex through the catalyzed hairpin hybridization. The newly exposed single-stranded initiator of duplex H_A-H_B product can catalyze CHA-2 to assemble the H_C-H_D duplex from H_C and H_D reactants. Interestingly, the single-stranded region of duplex H_C-H_D is encoded with the same initiator sequence I that can reversely activate CHA-1 to generate another catalytic circuit “CHA-3”. Therefore, the CHA-1 and CHA-2 circuits could mutually trigger each other by the intermediary “CHA-3” circuit, yielding an autocatalytic module for substantially promoting the cross-CHA-mediated exponential amplification.

The exposed single-stranded tether of CHA product could be utilized as a versatile trigger for motivating other DNA circuit, e.g., HCR circuit for generating long dsDNA polymers [61–64]. As shown in Fig. 14, the upstream catalytic CHA generates numerous dsDNA structures that each is decorated with an analogous sequence of T trigger for downstream HCR circuit. During this process, the low amount of

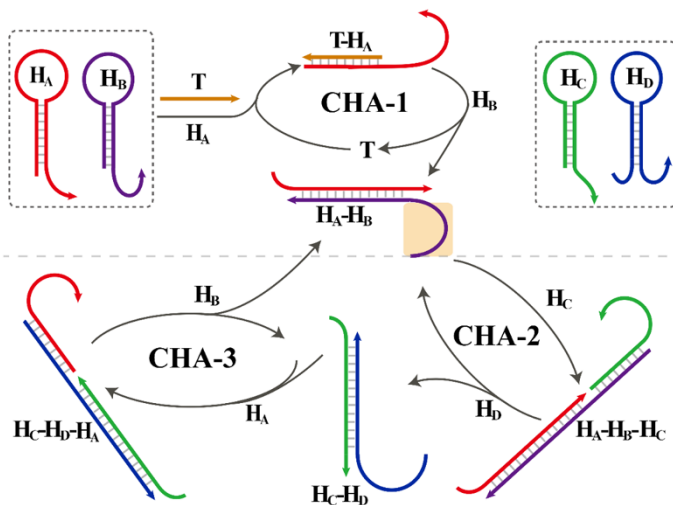


Fig. 13 Schematic illustration of the trigger T -driven cross-CHA circuit for yielding an exponential signal amplification

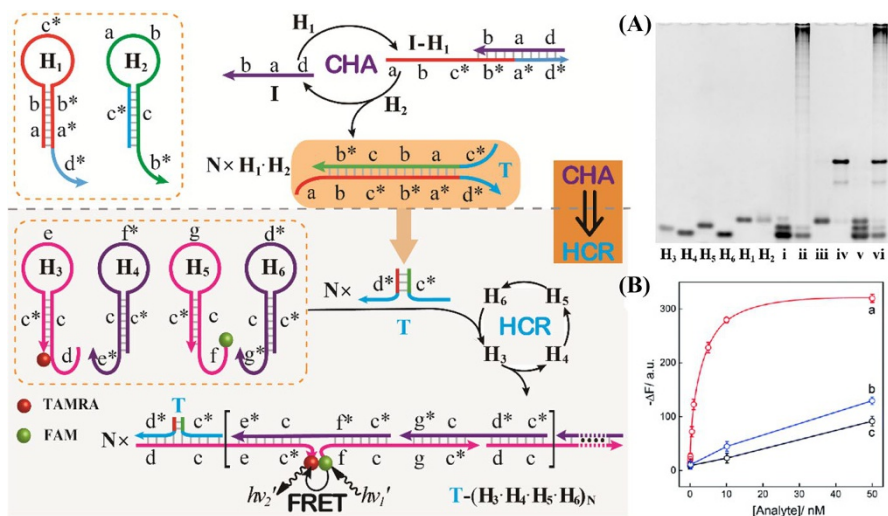


Fig. 14 Schematic illustration of the CHA–HCR system; **a** Gel–PAGE demonstration of the feasibility of CHA–HCR strategy: i/ii for HCR without/with T; iii/iv for CHA without/with I; v/vi for intact CHA–HCR without/with I. **b** Different calibration curves: (a) CHA–HCR, (b) HCR, and (c) CHA methods for analyzing different concentrations of analytes. Reprinted with permission from Ref. [65]. Copyright 2018 Royal Society of Chemistry

initiator **I** is transduced with the assembly of numerous duplex H₁–H₂ products, of which the newly exposed trigger **T** motivates the downstream HCR-driven sequential cross-hybridization among H₃, H₄, H₅, and H₆. This leads to the efficient assembly of plenty of long dsDNA copolymeric nanowires with the CHA trigger than that of HCR initiator (Fig. 14a). Then the respective FAM and TAMRA fluorophores of H₃ and H₅ are brought into close proximity, yielding a remarkably FRET signal [65]. This successive cascade hybridization between CHA and HCR realizes a sensitive detection of analytes. As shown in Fig. 14b, the CHA–HCR system showed a higher sensing-performance than the conventional CHA or HCR system, generating a significant synergistic amplification capacity.

The CHA circuit could also be translated into the assembly of DNAzyme catalyst. The integrated CHA–DNAzyme circuits showed great potential in high-performance biosensing applications [66, 67]. The sequential amplification feature of CHA–DNAzyme circuit could be further improved by using a cyclic-catalytic CHA–DNAzyme circuit where the DNAzyme biocatalysis could also trigger the initial CHA circuit (Fig. 15a) [68]. In the initial CHA scheme, initiator **T** catalyzes the cross-hybridization between H₁ and the fluorophore donor/acceptor-bearing H₂, yielding a “turn-on” fluorescence readout. The as-achieved H₁–H₂ duplex product carries an active DNAzyme that can cleave the T-caged S–L substrates to generate new trigger strands for reversely initiating the CHA circuit. Based on the programmable and modular characteristics, the cross-catalytic CHA–DNAzyme method is decomposed into two simplified basic reaction pathways, which are verified by theoretical simulations and experimental demonstrations (Fig. 15b, c, respectively).

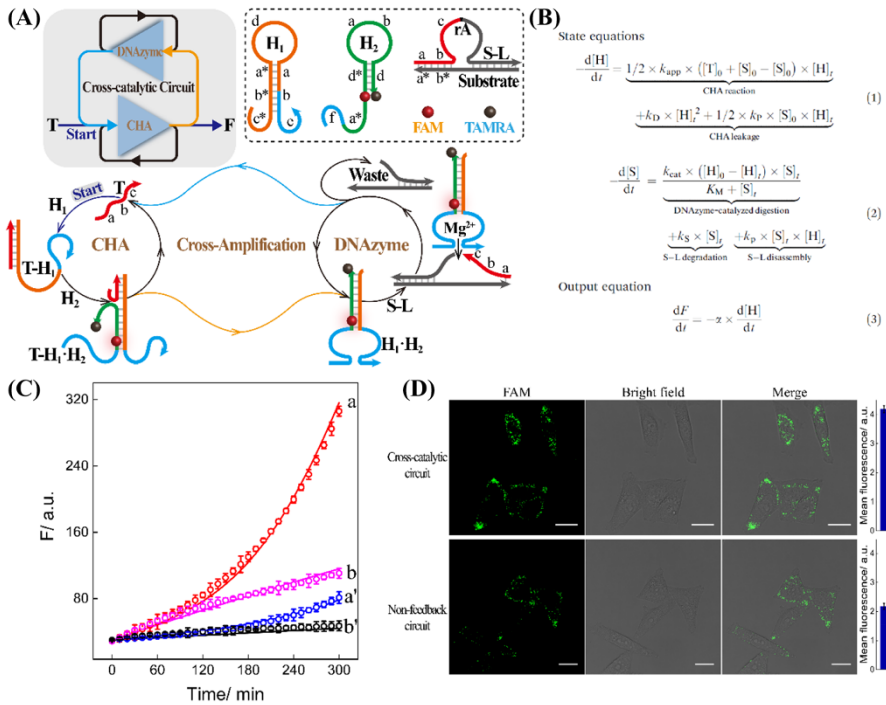


Fig. 15 Schematic illustration of the cross-catalytic CHA–DNAzyme circuit. **b** The mathematical model for cross-catalytic CHA–DNAzyme reaction simulation. **c** The fluorescence changes (solid lines represent for simulation results while circle dots represent for experimental data) of the cross-catalytic (a/a') and non-feedback systems (b/b') with/without input. Error bars \pm SD ($n=3$). **d** CLSM imaging of miRNA in MCF-7 cells with the cross-catalytic and non-feedback-catalytic CHA–DNAzyme methods. Scale bars 20 μ m. Reprinted with permission from Ref. [68]. Copyright 2019 Royal Society of Chemistry

Through the feedback DNAzyme loop, the newly exposed CHA initiators can essentially promote the assembly of numerous CHA products with high fluorescence readout. This isothermal cross-catalytic DNA circuit was then utilized as a general sensing strategy for amplified intracellular imaging of microRNA in living cells, which revealed a tremendously higher fluorescence readout than the conventional CHA–DNAzyme cascade (Fig. 15d).

Similarly, by precise design, the triple-layered CHA–HCR–DNAzyme circuit can also be integrated for amplified biosensing [61]. This isothermal autonomous enzyme-free DNA circuit system is constructed from the sequential integration of CHA, HCR, and DNAzyme amplifiers (Fig. 16a) [69]. The analyte-triggered CHA amplifier leads to the assembly of numerous dsDNA products in the first amplification stage. Here, the dsDNA products are encoded with HCR trigger sequence that can stimulate the cross-hybridization of HCR hairpins. Along with the generation of HCR copolymers, the DNAzyme biocatalysts are simultaneously activated for sustainably cleaving its fluorophore/quencher-labeled DNAzyme substrates, yielding an

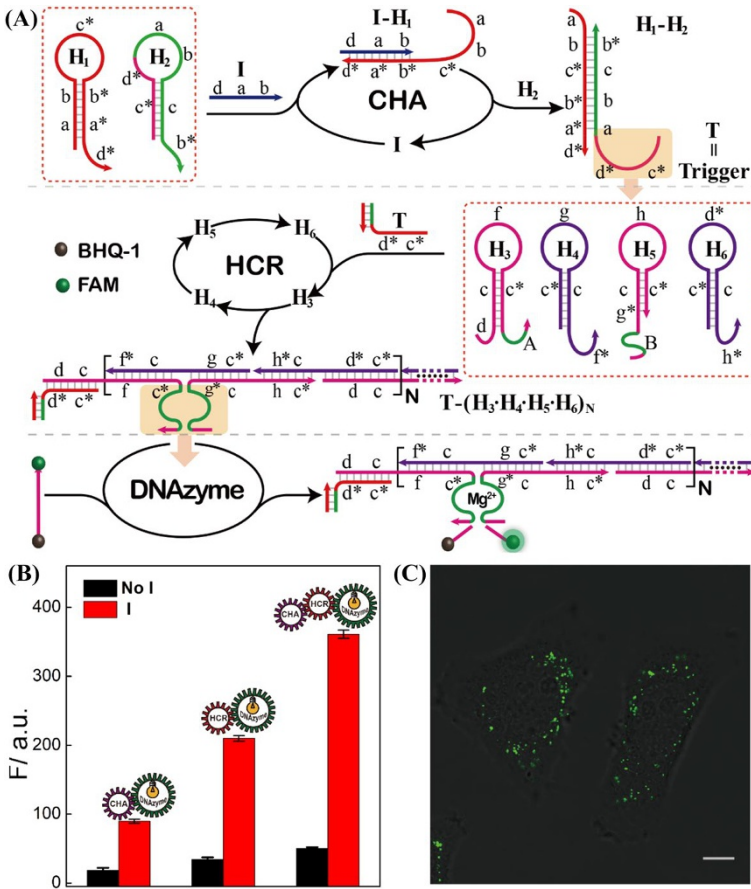


Fig. 16 **a** Scheme of the CHA–HCR–DNAzyme circuit. **b** The fluorescence monitoring the dual or triple DNA circuits initiated by their corresponding analytes. **c** Confocal imaging of miR-21 in MCF-7 cells through the CHA–HCR–DNAzyme system. Scale bar: 20 μm. Reprinted with permission from Ref. [69]. Copyright 2019 Royal Society of Chemistry

amplified fluorescence readout. As shown in Fig. 16b, the triple CHA–HCR–DNAzyme strategy realizes a more synergistic amplification performance than the dual CHA–DNAzyme and HCR–DNAzyme control circuits. This system was facily introduced into living cells for intracellular imaging of microRNA with high signal gain and accuracy (Fig. 16c). Furthermore, the HRP-mimicking DNAzyme has also integrated with a cross-CHA circuit for amplified DNA detection with increased sensing performance by three orders of magnitude than traditional CHA [70].

As mentioned before, the HCR circuit could be heterogeneously integrated with a different CHA system. In fact, the HCR could also be integrated with a homologous HCR system to construct a cascade HCR system, where the initial HCR copolymer product could be elongated with new functional DNA branches through a sequential hybridization reaction [71]. The two-layered enzyme-free C-HCR circuit

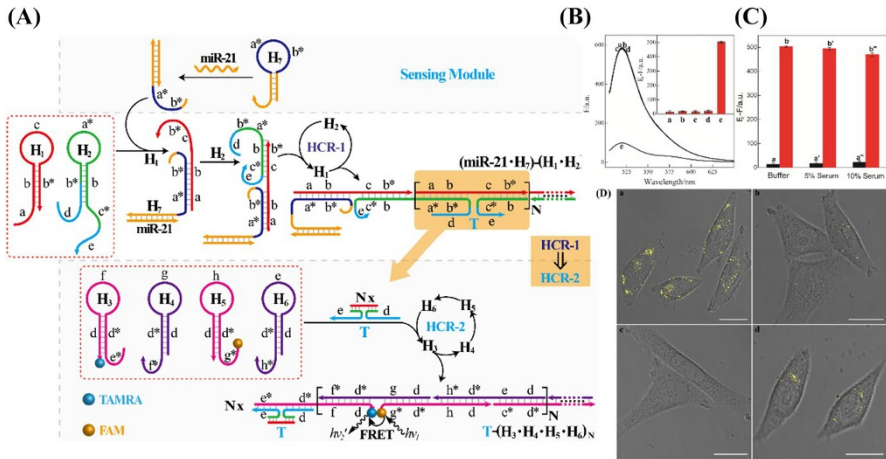


Fig. 17 Schematic illustration of the cascaded HCR circuit with a miR-21 sensing module. **b** Specific detection with the cascaded HCR system: a-e for no analyte, β -actin mRNA, let-7a, son DNA, and miR-21, respectively. Inset: summary of these fluorescence intensity readout. **c** The stability study of cascaded HCR-mediated miR-21 sensing system in serum buffer. **bd** Confocal imaging of miR-21 with FRET transduction (in the form of F_A/F_D) in (a/d) MCF-7/Hela cells by cascaded HCR amplifier, (b) MCF-7 cells by conventional HCR amplifier and (c) miR-21-inhibited MCF-7 cells by cascaded HCR amplifier. Scale bars 20 μ m. Reprinted with permission from Ref. [72]. Copyright 2018 Royal Society of Chemistry

is composed of HCR-1 and HCR-2 circuits, which allows the first HCR-1 layer to be cascaded into the other HCR-2 circuit as shown in Fig. 17a [72]. Without initiator I, all hairpin reactants coexist metastable in the initial state. The initiator I triggers the successive cross-hybridization reaction between hairpins H_1 and H_2 in upstream HCR-1 for generating long dsDNA HCR-1 nanowires that concomitantly assemble the tandem trigger T. Here, the system realizes the first amplification stage by converting the limited amount of initiator into thousands of triggers through the successful cross-hybridization of upstream HCR-1. Subsequently, the newly generated T triggers HCR-2 to assemble dsDNA copolymers in the as-achieved HCR-1 DNA nanowires, where the fluorophore donor/acceptor pair is brought into close proximity for enabling the FRET process. This two-layered C-HCR circuit realizes a remarkably effective detection of microRNA with an improved anti-interference ability (Fig. 17b, c). Meanwhile, this amplification strategy has been further applied for miR-21 detection in living cells by coupling with a “plug-and-play” sensing module, whose promoted signal amplification capacity was demonstrated as compared with the conventional HCR system (Fig. 17d).

The facile design of HCR facilitates the assembly of tandem colocalized DNA sequences with more different decorations, e.g., DNazymes. The HCR–DNAzyme amplification paradigm introduced a sensitive HCR-assembled DNAzyme amplification platform, Fig. 18a [73]. The HCR scheme is merely composed of two hairpins, which are grafted with two split functional DNAzyme subunits. The split DNAzyme stays in a catalytic inactive state for the absence of a favorable DNAzyme micro-environment. Once the analyte induces the assembly of two hairpins into dsDNA

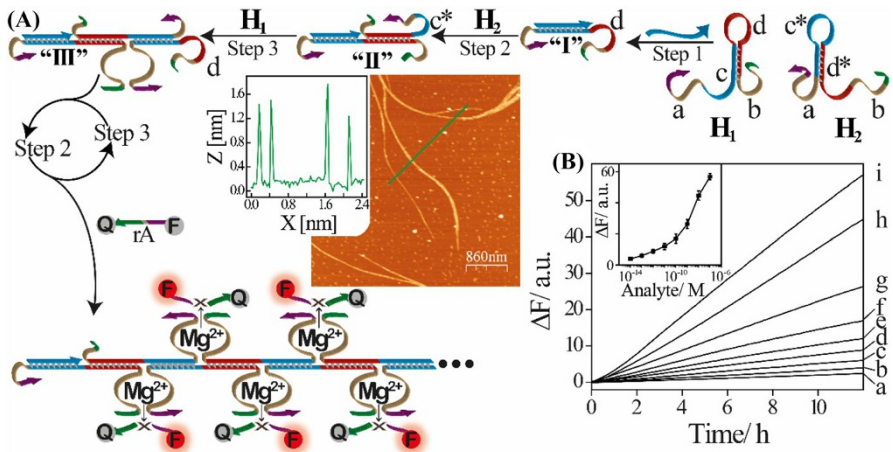


Fig. 18 **a** Schematic illustration of the HCR–DNAzyme cascade. Inset: AFM characterization of HCR copolymer nanowires. **b** Dynamic fluorescence changes of the HCR–DNAzyme system for detecting target with different concentrations: a–i for 0 , 1×10^{-14} , 1×10^{-13} , 1×10^{-12} , 1×10^{-11} , 1×10^{-10} , 1×10^{-9} , 4×10^{-8} , and 2×10^{-7} M, respectively. Inset: Derived calibration curve. Reprinted with permission from Ref. [73]. Copyright 2011 American Chemical Society

polymer nanowires, the split DNAzyme subunits would be brought into close proximity on the HCR backbone, resulting in the assembly of a compact tandem DNAzyme nanostructures. These DNAzymes would be activated in the presence of their corresponding cofactors, leading to the cyclic cleavage of the F/Q-labeled DNAzyme substrate with a tremendously amplified fluorescence readout (Fig. 18b).

Many excellent systems have shown the merits of the cascade sensing features of synergistic HCRs, and sensitive HCR–DNAzyme systems [74]. Similarly, these previous cascaded HCR systems could also be integrated with the DNAzyme biocatalysis amplifier, Fig. 19a [75]. This triple-layered cascaded HCR–DNAzyme circuit is designed in a more compact and precise format. In the presence of an initiator, the preceding HCR-1 produces numerous analogous sequence T to motivate the following HCR-2, which concomitantly promotes the assembly of numerous tandem DNAzyme biocatalysts on the HCR-2 copolymer backbone. As demonstrated by AFM, large amounts of linear dsDNA copolymers are observed for the initiator-triggered HCR-1 system (Fig. 19b). As anticipated, micrometer-long dsDNA branches were observed after the initiation of CHCR–DNAzyme process with a height of ~ 2 nm. By incorporating a flexibly sensing module, this sophisticated CHCR–DNAzyme system extends its broad application for miRNAs detection in EVs.

Besides these different DNA hybridization networks, the varied DNAzymes could also be integrated for amplified sensing applications. As functional catalytic DNA strands, DNAzymes require the involvement of cofactors for executing an efficient biocatalysis and signal transduction. This property could be utilized for sensitively and selectively analyzing their corresponding cofactors by using the different DNAzyme or cascade DNAzyme systems. For example, the Pb^{2+} - or L-histidine-dependent DNAzyme could be initially applied to activate the assembly of two

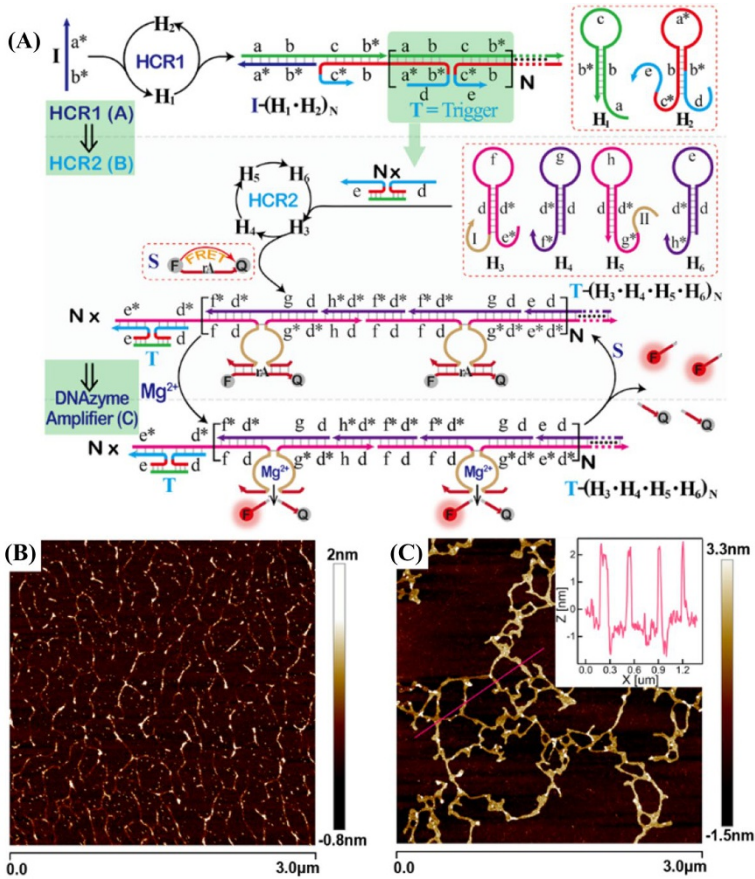


Fig. 19 **a** Schematic illustration of the cascade HCR–DNAzyme strategy. **b** AFM images of the HCR-1-assembled linear dsDNA polymers and **c** the cascade HCR-assembled branched dsDNA products. Reprinted with permission from Ref. [75]. Copyright 2019 American Chemical Society

hemin/G-quadruplex HRP-mimicking DNAzyme through the catalyzed disassembly of two cooperatively stabilized duplexes (Fig. 20a). Only with their corresponding cofactors, the DNAzyme substrate could be cleaved for releasing the hemin/G-quadruplex DNAzyme that enabled the colorimetric or chemiluminescence detection of Pb^{2+} or L-histidine (Fig. 20b, c) [76]. Here, the compact DNAzyme could be easily reconfigured into other metal ions or amino acid-dependent DNAzyme sequences, e.g., Pb^{2+} -DNAzyme (Fig. 20d), thus providing a universal and facile toolbox for more different bioassays.

DNAzymes also show great sensing performance through regenerating the target initiator by themselves [77], Fig. 21a. The autocatalytic DNAzyme system consists of two caged DNAzyme subunits and an initiator sequence-containing hairpin, which is functionalized with a F/Q pair in the stem's ends and a ribonucleobase (rA) in the loop. Target DNA induces the assembly of an

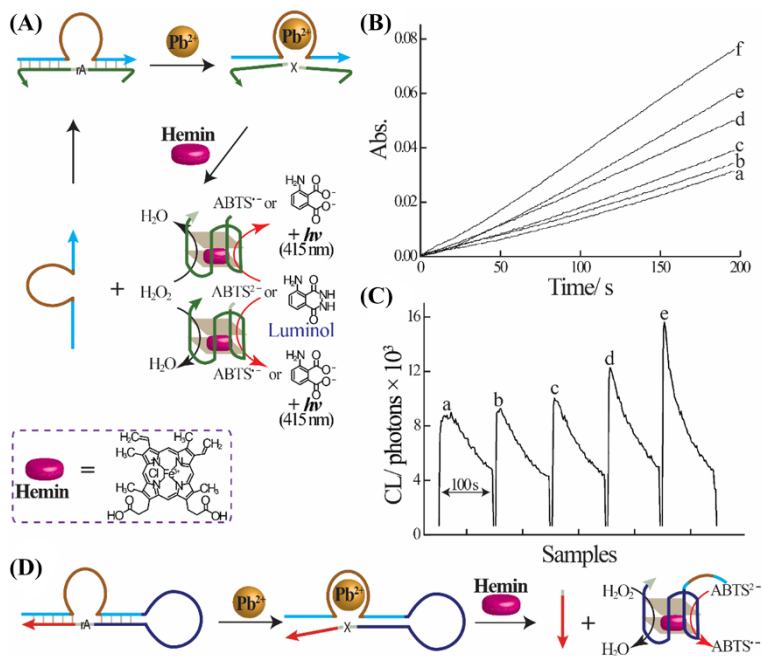


Fig. 20 **a** Schematic illustration of the cascade DNAzyme-(HRP) DNAzyme circuit for Pb²⁺ ions detection. **b** Absorbance and **c** chemiluminescence behaviors of DNAzyme cascade circuit for Pb²⁺ ions detection: a–f for 0, 1 × 10⁻⁸, 1 × 10⁻⁷, 5 × 10⁻⁷, 1 × 10⁻⁶, and 1 × 10⁻⁵ M, respectively. Reprinted with permission from Ref. [76]. Copyright 2008 Royal Society of Chemistry. **d** Schematic illustration of the cascade DNAzyme-(HRP) DNAzyme circuit with one compact DNA nanoprobe

inactive DNAzyme to specifically cleave the functional hairpin substrate with an enhanced fluorescence readout. Meanwhile, the cleaved fragment contains the same sequence of target DNA, thus inducing the initial assembly of DNAzymes for capturing and cleaving the substrate. Based on this catabolic replication method, this isothermal regenerating DNAzyme system realizes a significant signal amplification. Here, the RNA-cleaving DNAzyme could be replaced with a ligation DNAzyme, resulting in the assembly of an enzyme-free self-replication DNAzyme machinery. This cascade ligation DNAzyme was developed for detecting analyte, Fig. 21b [78]. Herein, target DNA hybridizes with the caged DNAzyme primer for generating a high fluorescence output and a new catalytic active ligation DNAzyme unit. With Zn²⁺-cofactor, the ligation DNAzyme catalyzes the ligation of two fragments to form a similar strand of target DNA. The newly assembled target could be utilized for realizing ultrasensitive target DNA detection with the catalyzed assembly of more DNAzyme units.

In general, by taking advantage of these different amplification means, various integrated isothermal amplification strategies have provided more possibilities for realizing the more sensitive and selective detection of different analytes. These cascade DNA circuits could be considered as general amplification modules and

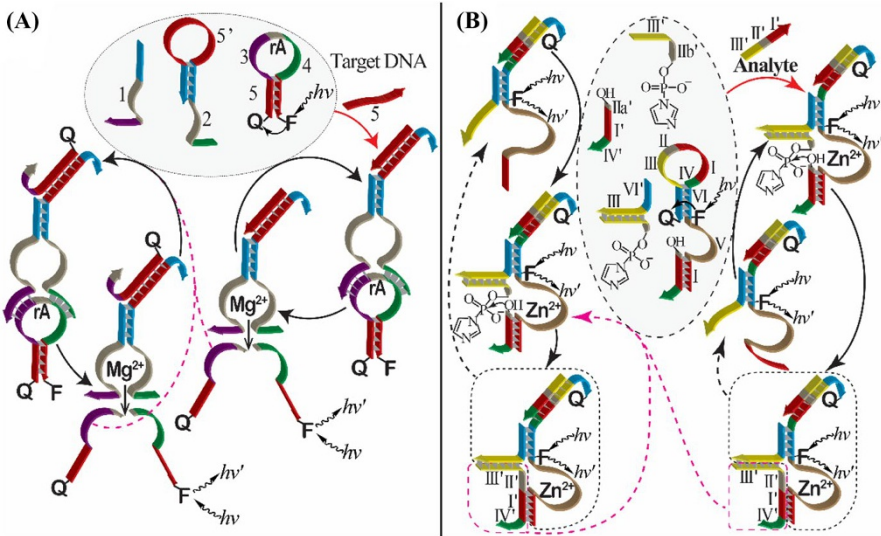


Fig. 21 **a** Scheme of the autocatalytic DNazyme system based on the catabolic DNazyme reaction. Reprinted with permission from Ref. [77]. Copyright 2011 Wiley–VCH. **b** Schematic illustration of a ligation DNazyme-mediated replication DNazyme machinery circuit. Reprinted with permission from Ref. [78]. Copyright 2012 American Chemical Society

further applied to parallelly detect various biomarkers with the help of other recognition elements, for example, aptamers [79], methylation [80, 81], uracil-DNA glycosylase [82], and special recognition sequence, e.g., C–Ag–C [83] or T–Hg–T [84] bridge. It is also interesting to develop a parallel analysis for more different targets with one cascaded catalytic machinery. In cells, the catalytic circuitry-based logic gates also contribute to the accurate analysis of more different biologically important targets in a complicated environment [85, 86]. The cascade DNA circuits could be applied for stimulating other signal transfer and complex signaling pathways that are involved with selective branching and feedback mechanisms, which can facilitate an in-depth and comprehensive understanding about the magical nature of living entities.

3 Conclusions and Future Perspectives

This chapter has discussed the different autonomous enzyme-free DNA circuits, including, catalytic hairpin assembly (CHA), hybridization chain reaction (HCR), catalytic functional nucleic acids (DNazymes), and the integrated DNA reaction circuits in solution or on different nanoscaffolds (DNA, GOs [87] and AuNPs [88]). Based on the Watson–Crick base pairing, these enzyme-free amplification techniques have been successfully introduced for imaging intracellular mRNA [89, 90] or microRNA [91–94], and some interesting works also reported on surface-confined HCR on cells surface by the specific aptamer recognizing element (e.g.,

sgc8 aptamer binding PTK protein) with tremendously amplified transductions [95, 96]. Meanwhile, CHA, HCR, and DNAzyme could be integrated into a versatile and powerful toolbox with special functions through the cascade reaction format, which is especially suitable for isothermal conditions without special enzymes. Moreover, most of these circuits have been implemented in serum biological environments after a moderate modification of these DNA probes. The integration of DNA circuits could achieve improved sensitivity and selectivity for sensing applications in living entities. It is expected that these methods can be implemented with multiple sensing transductions, and show extensive potential for clinical diagnosis and prognosis.

Despite this progress, several challenges are still ahead of us. It is more appealing to realize intracellular analysis and to construct portable devices for POCT-based diagnosis, even though some commercial products have emerged. The intracellular amplified analyses of mRNA or microRNA are developed and non-nucleic acid biomolecules could also be converted into nucleic acid amplification events by introducing more configurable sensing modules [97]. Yet these systems are still confronted with more challenges, e.g., fragile and easy disturbance by the complicate bio-environment despite with relatively high stability. They are vulnerable to non-specific adsorption and degradation in living animals. Single-layered enzyme-free circuits are relatively easy to be delivered into living cells by nanoparticles while cascade DNA circuits are more sophisticated with more DNA participants. This requires more efficient carriers to protect and transfer DNA primers to target tissues and cells. The specific and targeted delivery of DNA probes also represents a great challenge, so that the sophisticated DNA circuits could realize their functions as expected. What's more, all the reactants of DNA circuits need longer sensing durations. A promising route might be the utilization of intracellular cicerone to deliver them so that they can accumulate on a specific bio-compartments in a more efficient way. At the same time, some alternative nanomaterials could be introduced to ensure the proportional delivery of DNA probes and DNAzyme cofactors for DNAzyme-involved DNA reaction circuits.

Furthermore, based on the corrected executions of individual pathways, the autonomous DNA circuits have more significantly scientific implications far beyond biosensing. They might yield new properties and functions for the integration of diagnosis and immediate therapy. For example, the conjugation of gene-silencing functional DNAzyme with CHA or HCR can construct multiplexed catalytic DNA circuits with dual functions of sensing and disease treatment [98]. What's more, short-interfering RNAs are well developed to suppress gene expressions through a highly regulated enzyme-mediated process [99]. It is also a promising strategy to conjugate autonomous programmed cascade DNA circuits with siRNAs operations. In general, there is still much room for autonomous DNA circuits to implement. We hope this chapter will provide an overview of the autonomous enzyme-free DNA circuits for readers and inspire their interest to develop more strategies and discoveries in this interesting research field.

Acknowledgements This work is supported by National Natural Science Foundation of China (no. 21874103), National Basic Research Program of China (973 Program, 2015CB932601), and Fundamental Research Funds for the Central Universities (nos. 2042018kf0210 and 2042019kf0206).

References

1. Wang F-A, Lu CH, Willner I (2014) From cascaded catalytic nucleic acids to enzyme-DNA nanostructures: controlling reactivity, sensing, logic operations, and assembly of complex structures. *Chem Rev* 114:2881–2941
2. Lam B, Das J, Holmes RD, Live L, Sage A, Sargent EH, Kelley SO (2013) Solution-based circuits enable rapid and multiplexed pathogen detection. *Nat Commun* 4:2001
3. Benenson Y, Gil B, Ben-Dor U, Adar R, Shapiro E (2004) An autonomous molecular computer for logical control of gene expression. *Nature* 429:423–429
4. Maojo V, Martin-Sanchez F, Kulikowski C, Rodriguez-Paton A, Fritts M (2010) Nanoinformatics and DNA-based computing: catalyzing nanomedicine. *Pediatr Res* 67:481–489
5. Jo M, Ahn JY, Lee J, Lee S, Hong SW, Yoo JW, Kang J, Dua P, Lee DK, Hong S, Kim S (2011) Development of single-stranded DNA aptamers for specific bisphenol A detection. *Oligonucleotides* 21:85–91
6. Edwards K, Johnstone C, Thompson C (1991) A simple and rapid method for the preparation of plant genomic DNA for PCR analysis. *Nucleic Acids Res* 19:1349
7. Livak KJ, Schmittgen TD (2001) Analysis of relative gene expression data using real-time quantitative PCR and the $2^{-\Delta\Delta Ct}$ method. *Methods* 25:402–408
8. Tomita N, Mori Y, Kanda H, Notomi T (2008) Loop-mediated isothermal amplification (lamp) of gene sequences and simple visual detection of products. *Nat Protoc* 3:877–882
9. Wang J, Wang HM, Wang H, He SZ, Li RM, Deng Z, Liu XQ, Wang F-A (2019) Nonviolent self-catabolic DNAzyme nanosponges for smart anticancer drug delivery. *ACS Nano* 13:5852–5863
10. Zhang LR, Zhu GC, Zhang CY (2014) Homogeneous and label-free detection of microRNAs using bifunctional strand displacement amplification-mediated hyperbranched rolling circle amplification. *Anal Chem* 86:6703–6709
11. Walker GT, Fraiser MS, Schram JL, Little MC, Nadeau JG, Malinowski DP (1992) Strand displacement amplification—an isothermal, in vitro DNA amplification technique. *Nucleic Acids Res* 20:1691–1696
12. Zhou WH, Hu L, Ying LM, Zhao Z, Chu PK, Yu XF (2018) A CRISPR-cas9-triggered strand displacement amplification method for ultrasensitive DNA detection. *Nat Commun* 9:5012
13. Zhao YX, Chen F, Li Q, Wang LH, Fan CH (2015) Isothermal amplification of nucleic acids. *Chem Rev* 115:12491–12545
14. Yin P, Choi HM, Calvert CR, Pierce NA (2008) Programming biomolecular self-assembly pathways. *Nature* 451:318–322
15. Dirks RM, Pierce NA (2004) Triggered amplification by hybridization chain reaction. *Proc Natl Acad Sci USA* 101:15275–15278
16. Lai W, Xiong XW, Wang F, Li Q, Li L, Fan CH, Pei H (2019) Nonlinear regulation of enzyme-free DNA circuitry with ultrasensitive switches. *ACS Synth Biol* 8:2106–2112
17. Zhang DY, Winfree E (2009) Control of DNA strand displacement kinetics using toehold exchange. *J Am Chem Soc* 131:17303–17314
18. Xuan F, Hsing IM (2014) Triggering hairpin-free chain-branching growth of fluorescent DNA dendrimers for nonlinear hybridization chain reaction. *J Am Chem Soc* 136:9810–9813
19. Ying ZM, Wu Z, Tu B, Tan WH, Jiang JH (2017) Genetically encoded fluorescent RNA sensor for ratiometric imaging of microRNA in living tumor cells. *J Am Chem Soc* 139:9779–9782
20. Zhang KY, Song ST, Huang S, Yang L, Min QH, Wu XC, Lu F, Zhu JJ (2018) Lighting up microRNA in living cells by the disassembly of lock-like DNA-programmed UCNPS-AUNPS through the target cycling amplification strategy. *Small* 14:1802292–1802302
21. Zhang B, Liu BQ, Tang DP, Niessner R, Chen G, Knopp D (2012) DNA-based hybridization chain reaction for amplified bioelectronic signal and ultrasensitive detection of proteins. *Anal Chem* 84:5392–5399
22. Zhou YJ, Yang L, Wei J, Ma K, Gong X, Shang JH, Yu SS, Wang F-A (2019) An autonomous nonenzymatic concatenated DNA circuit for amplified imaging of intracellular ATP. *Anal Chem* 91:15229–15234
23. Liu NN, Hou RZ, Gao PC, Lou XD, Xia F (2016) Sensitive Zn^{2+} sensor based on biofunctionalized nanopores via combination of DNAzyme and DNA supersandwich structures. *Analyst* 141:3626–3629

24. Deng Y, Nie J, Zhang XH, Zhao MZ, Zhou YL, Zhang XX (2014) Hybridization chain reaction-based fluorescence immunoassay using DNA intercalating dye for signal readout. *Analyst* 139:3378–3383
25. Pan M, Liang M, Sun JL, Liu XQ, Wang F-A (2018) Lighting up fluorescent silver clusters via target-catalyzed hairpin assembly for amplified biosensing. *Langmuir* 34:14851–14857
26. Quan K, Huang J, Yang XH, Yang YJ, Ying L, Wang H, He Y, Wang KM (2015) An enzyme-free and amplified colorimetric detection strategy via target-aptamer binding triggered catalyzed hairpin assembly. *Chem Commun* 51:937–940
27. Jo EJ, Mun H, Kim SJ, Shim WB, Kim MG (2016) Detection of ochratoxin A (OTA) in coffee using chemiluminescence resonance energy transfer (CRET) aptasensor. *Food Chem* 194:1102–1107
28. Liang MJ, Pan M, Hu JL, Wang F-A, Liu XQ (2018) Electrochemical biosensor for microRNA detection based on cascade hybridization chain reaction. *Chemelectrochem* 5:1380–1386
29. Li BL, Ellington AD, Chen X (2011) Rational, modular adaptation of enzyme-free DNA circuits to multiple detection methods. *Nucleic Acids Res* 39:e110
30. Zheng AX, Wang JR, Li J, Song XR, Chen GN, Yang HH (2012) Enzyme-free fluorescence aptasensor for amplification detection of human thrombin via target-catalyzed hairpin assembly. *Biosens Bioelectron* 36:217–221
31. Jung C, Allen PB, Ellington AD (2016) A stochastic DNA walker that traverses a microparticle surface. *Nat Nanotechnol* 11:157–163
32. Wu CC, Cansiz S, Zhang LQ, Teng I, Qiu LP, Li J, Liu Y, Zhou CS, Hu R, Zhang T, Cui C, Cui L, Tan WH (2015) A nonenzymatic hairpin DNA cascade reaction provides high signal gain of mRNA imaging inside live cells. *J Am Chem Soc* 137:4900–4903
33. He L, Lu DQ, Liang H, Xie S, Zhang XB, Liu QL, Yuan Q, Tan WH (2018) mRNA-initiated, three-dimensional DNA amplifier able to function inside living cells. *J Am Chem Soc* 140:258–263
34. Huang J, Wu YR, Chen Y, Zhu Z, Yang XH, Yang CY, Wang KM, Tan WH (2011) Pyrene-excimer probes based on the hybridization chain reaction for the detection of nucleic acids in complex biological fluids. *Angew Chem Int Ed* 50:401–404
35. Shi ZL, Zhang XF, Cheng R, Li BX, Jin Y (2016) Sensitive detection of intracellular RNA of human telomerase by using graphene oxide as a carrier to deliver the assembly element of hybridization chain reaction. *Analyst* 141:2727–2732
36. Li L, Feng J, Liu HY, Li QL, Tong LL, Tang B (2016) Two-color imaging of microRNA with enzyme-free signal amplification via hybridization chain reactions in living cells. *Chem Sci* 7:1940–1945
37. Liu P, Yang XH, Sun S, Wang Q, Wang KM, Huang J, Liu JB, He LL (2013) Enzyme-free colorimetric detection of DNA by using gold nanoparticles and hybridization chain reaction amplification. *Anal Chem* 85:7689–7695
38. Zou L, Li RM, Zhang MJ, Luo YW, Zhou N, Wang J, Ling LS (2017) A colorimetric sensing platform based upon recognizing hybridization chain reaction products with oligonucleotide modified gold nanoparticles through triplex formation. *Nanoscale* 9:1986–1992
39. Wu Z, Liu GQ, Yang XL, Jiang JH (2015) Electrostatic nucleic acid nanoassembly enables hybridization chain reaction in living cells for ultrasensitive mRNA imaging. *J Am Chem Soc* 137:6829–6836
40. Ren KW, Xu YF, Liu Y, Yang M, Ju HX (2018) A responsive “nano string light” for highly efficient mRNA imaging in living cells via accelerated DNA cascade reaction. *ACS Nano* 12:263–271
41. Breaker RR, Joyce GF (1994) A DNA enzyme that cleaves RNA. *Chem Bio* 1:223–229
42. Carmi N, Balkhi SR, Breaker RR (1998) Cleaving DNA with DNA. *Proc Natl Acad Sci USA* 95:2233–2237
43. Liu ZJ, Mei SHJ, Brennan JD, Li YF (2003) Assemblage of signaling DNA enzymes with intriguing metal-ion specificities and pH dependences. *J Am Chem Soc* 125:7539–7545
44. Liu JW, Lu Y (2007) Rational design of “turn-on” allosteric DNzyme catalytic beacons for aqueous mercury ions with ultrahigh sensitivity and selectivity. *Angew Chem Int Ed* 46:7587–7590
45. Santoro SW, Joyce GF, Sakthivel K, Gramatikova S, Barbas CF (2000) RNA cleavage by a DNA enzyme with extended chemical functionality. *J Am Chem Soc* 122:2433–2439
46. Liang G, Man Y, Li A, Jin XX, Liu XH, Pan LG (2017) DNzyme-based biosensor for detection of lead ion: a review. *Microchem J* 131:145–153
47. McGhee CE, Loh KY, Lu Y (2017) DNzyme sensors for detection of metal ions in the environment and imaging them in living cells. *Curr Opin In Biotech* 45:191–201
48. Zhou WH, Saran R, Liu JW (2017) Metal sensing by DNA. *Chem Rev* 117:8272–8325

49. Li J, Lu Y (2000) A highly sensitive and selective catalytic DNA biosensor for lead ions. *J Am Chem Soc* 122:10466–10467
50. Golub E, Freeman R, Willner I (2011) A hemin/g-quadruplex acts as an NADH oxidase and NADH peroxidase mimicking DNzyme. *Angew Chem Int Ed* 50:11710–11714
51. Pavlov V, Xiao Y, Gill R, Dishon A, Kotler M, Willner I (2004) Amplified chemiluminescence surface detection of DNA and telomerase activity using catalytic nucleic acid labels. *Anal Chem* 76:2152–2156
52. Li T, Shi LL, Wang EK, Dong SJ (2009) Silver-ion-mediated DNzyme switch for the ultrasensitive and selective colorimetric detection of aqueous Ag⁺ and cysteine. *Chemistry* 15:3347–3350
53. Liu JW, Lu Y (2003) A colorimetric lead biosensor using DNzyme-directed assembly of gold nanoparticles. *J Am Chem Soc* 125:6642–6643
54. Yang YJ, Huang J, Yang XH, Quan K, Wang H, Ying L, Xie N, Ou M, Wang KM (2016) Aptzyme-gold nanoparticle sensor for amplified molecular probing in living cells. *Anal Chem* 88:5981–5987
55. Zhao XH, Kong RM, Zhang XB, Meng HM, Liu WN, Tan WH, Shen GL, Yu RQ (2011) Graphene-DNzyme based biosensor for amplified fluorescence “turn-on” detection of Pb²⁺ with a high selectivity. *Anal Chem* 83:5062–5066
56. Kong RM, Zhang XB, Chen Z, Meng HM, Song ZL, Tan WH, Shen GL, Yu RQ (2011) Unimolecular catalytic DNA biosensor for amplified detection of L-histidine via an enzymatic recycling cleavage strategy. *Anal Chem* 83:7603–7607
57. Lu LM, Zhang XB, Kong RM, Yang B, Tan Wh (2011) A ligation-triggered DNzyme cascade for amplified fluorescence detection of biological small molecules with zero-background signal. *J Am Chem Soc* 133:11686–11691
58. He KY, Li W, Nie Z, Huang Y, Liu ZL, Nie LH, Yao SZ (2012) Enzyme-regulated activation of DNzyme: a novel strategy for a label-free colorimetric DNA ligase assay and ligase-based biosensing. *Chemistry* 18:3992–3999
59. Li BL, Jiang Y, Chen X, Ellington AD (2012) Probing spatial organization of DNA strands using enzyme-free hairpin assembly circuits. *J Am Chem Soc* 134:13918–13921
60. Dai JY, He HF, Duan ZJ, Guo Y, Xiao D (2017) Self-replicating catalyzed hairpin assembly for rapid signal amplification. *Anal Chem* 89:11971–11975
61. Feng CJ, Zhu J, Sun JW, Jiang W, Wang L (2015) Hairpin assembly circuit-based fluorescence cooperative amplification strategy for enzyme-free and label-free detection of small molecule. *Talanta* 143:101–106
62. Quan K, Huang J, Yang XH, Yang YJ, Ying L, Wang H, Xie NL, Ou M, Wang KM (2016) Powerful amplification cascades of FRET-based two-layer nonenzymatic nucleic acid circuits. *Anal Chem* 88:5857–5864
63. Wei YL, Zhou WJ, Li X, Chai YQ, Yuan R, Xiang Y (2016) Coupling hybridization chain reaction with catalytic hairpin assembly enables non-enzymatic and sensitive fluorescent detection of microRNA cancer biomarkers. *Biosens Bioelectron* 77:416–420
64. Wu XY, Chai YQ, Yuan R, Zhuo Y, Chen Y (2014) Dual signal amplification strategy for enzyme-free electrochemical detection of microRNAs. *Sensors Actuators B-Chem* 203:296–302
65. Wang HM, Li CX, Liu XQ, Zhou X, Wang F-A (2018) Construction of an enzyme-free concatenated DNA circuit for signal amplification and intracellular imaging. *Chem Sci* 9:5842–5849
66. Liu SF, Cheng CB, Gong HW, Wang L (2015) Programmable Mg²⁺-dependent DNzyme switch by the catalytic hairpin DNA assembly for dual-signal amplification toward homogeneous analysis of protein and DNA. *Chem Commun* 51:7364–7367
67. Yang L, Wu Q, Chen YQ, Liu XQ, Wang F-A, Zhou X (2019) Amplified microRNA detection and intracellular imaging based on an autonomous and catalytic assembly of DNzyme. *ACS Sens* 4:110–117
68. Zou LN, Wu Q, Zhou YJ, Gong X, Liu XQ, Wang F-A (2019) A DNzyme-powered cross-catalytic circuit for amplified intracellular imaging. *Chem Commun* 55:6519–6522
69. Wang H, Wang HM, Wu Q, Liang MJ, Liu XQ, Wang F-A (2019) A DNzyme-amplified DNA circuit for highly accurate microRNA detection and intracellular imaging. *Chem Sci* 10:9597–9604
70. Yue SZ, Zhao TT, Qi HJ, Yan YC, Bi S (2017) Cross-catalytic hairpin assembly-based exponential signal amplification for CRET assay with low background noise. *Biosens Bioelectron* 94:671–676
71. Bi S, Chen M, Jia XQ, Dong Y, Wang ZH (2015) Hyperbranched hybridization chain reaction for triggered signal amplification and concatenated logic circuits. *Angew Chem Int Ed* 54:8144–8148

72. Wei J, Gong X, Wang Q, Pan M, Liu XQ, Liu J, Xia F, Wang F-A (2018) Construction of an autonomously concatenated hybridization chain reaction for signal amplification and intracellular imaging. *Chem Sci* 9:52–61
73. Wang F-A, Elbaz J, Orbach R, Magen N, Willner I (2011) Amplified analysis of DNA by the autonomous assembly of polymers consisting of DNAzyme wires. *J Am Chem Soc* 133:17149–17151
74. He DG, Hai L, Wang HZ, Wu R, Li HW (2018) Enzyme-free quantification of exosomal microRNA by the target-triggered assembly of the polymer DNAzyme nanostructure. *Analyst* 143:813–816
75. Wu Q, Wang H, Gong KK, Shang JH, Liu XQ, Wang F-A (2019) Construction of an autonomous nonlinear hybridization chain reaction for extracellular vesicles-associated microRNAs discrimination. *Anal Chem* 91:10172–10179
76. Elbaz J, Shlyahovsky B, Willner I (2008) A DNAzyme cascade for the amplified detection of pb(2+) ions or L-histidine. *Chem Commun* 13:1569–1571
77. Wang F-A, Elbaz J, Teller C, Willner I (2011) Amplified detection of DNA through an autocatalytic and catabolic DNAzyme-mediated process. *Angew Chem Int Ed* 50:295–299
78. Wang F-A, Elbaz J, Willner I (2012) Enzyme-free amplified detection of DNA by an autonomous ligation DNAzyme machinery. *J Am Chem Soc* 134:5504–5507
79. Zhang ZX, Sharon E, Freeman R, Liu XQ, Willner I (2012) Fluorescence detection of DNA, adenosine-5'-triphosphate (ATP), and telomerase activity by zinc(II)-protoporphyrin ix/g-quadruplex labels. *Anal Chem* 84:4789–4797
80. Li CX, Wang HM, Shang JH, Liu XQ, Yuan B, Wang F-A (2018) Highly sensitive assay of methyltransferase activity based on an autonomous concatenated DNA circuit. *ACS Sens* 3:2359–2366
81. Wang Q, Pan M, Wei J, Liu XQ, Wang F-A (2017) Evaluation of DNA methyltransferase activity and inhibition via isothermal enzyme-free concatenated hybridization chain reaction. *ACS Sens* 2:932–939
82. Wang J, Pan M, Wei J, Liu XQ, Wang F-A (2017) A C-HCR assembly of branched DNA nanostructures for amplified uracil-DNA glycosylase assays. *Chem Commun* 53:12878–12881
83. Liu L, Li Q, Tang LJ, Yu RQ, Jiang JH (2016) Silver nanocluster-lightened hybridization chain reaction. *RSC Adv* 6:57502–57506
84. Chen PP, Wu P, Zhang YX, Chen JB, Jiang XM, Zheng CB, Hou XD (2016) Strand displacement-induced enzyme-free amplification for label-free and separation-free ultrasensitive atomic fluorescence spectrometric detection of nucleic acids and proteins. *Anal Chem* 88:12386–12392
85. Gong X, Wei J, Liu J, Li RM, Liu XQ, Wang F-A (2019) Programmable intracellular DNA biocomputing circuits for reliable cell recognitions. *Chem Sci* 10:2989–2997
86. Orbach R, Willner B, Willner I (2015) Catalytic nucleic acids (DNAzymes) as functional units for logic gates and computing circuits: from basic principles to practical applications. *Chem Commun* 51:4144–4160
87. Hong C, Kim DM, Baek A, Chung H, Jung W, Kim DE (2015) Fluorescence-based detection of single-nucleotide changes in RNA using graphene oxide and DNAzyme. *Chem Commun* 51:5641–5644
88. Chen XP, Wang L, Sheng SC, Wang T, Yang J, Xie GM, Feng WL (2015) Coupling a universal DNA circuit with graphene sheets/polyaniline/AUNPS nanocomposites for the detection of BCR/ABL fusion gene. *Anal Chim Acta* 889:90–97
89. Huang J, Wang H, Yang XH, Quan K, Yang YJ, Ying L, Xie NL, Ou M, Wang KM (2016) Fluorescence resonance energy transfer-based hybridization chain reaction for in situ visualization of tumor-related mRNA. *Chem Sci* 7:3829–3835
90. Wang SF, Ding JS, Zhou WH (2019) An aptamer-tethered, DNAzyme-embedded molecular beacon for simultaneous detection and regulation of tumor-related genes in living cells. *Analyst* 144:5098–5107
91. Bi S, Ye JY, Dong Y, Li HT, Cao W (2016) Target-triggered cascade recycling amplification for label-free detection of microRNA and molecular logic operations. *Chem Commun* 52:402–405
92. Deng RJ, Zhang KX, Li JH (2017) Isothermal amplification for microRNA detection: from the test tube to the cell. *Accounts Chem Res* 50:1059–1068
93. Wu H, Liu YL, Wang YL, Wang HY, Wu J, Zhu FF, Zou P (2016) Label-free and enzyme-free colorimetric detection of microRNA by catalyzed hairpin assembly coupled with hybridization chain reaction. *Biosens Bioelectron* 81:303–308
94. Yang L, Liu CH, Ren W, Li ZP (2012) Graphene surface-anchored fluorescence sensor for sensitive detection of microRNA coupled with enzyme-free signal amplification of hybridization chain reaction. *ACS Appl Mater Interfaces* 4:6450–6453

95. Chang X, Zhang C, Lv C, Sun Y, Zhang MZ, Zhao YM, Yang LL, Han D, Tan WH (2019) Construction of a multiple-aptamer-based DNA logic device on live cell membranes via associative threshold activation for accurate cancer cell identification. *J Am Chem Soc* 141:12738–12743
96. Yuan BY, Chen YY, Sun YQ, Guo QP, Huang J, Liu JB, Meng XX, Yang XH, Wen XH, Li ZH, Li L, Wang KM (2018) Enhanced imaging of specific cell-surface glycosylation based on multi-FRET. *Anal Chem* 90:6131–6137
97. Wu PW, Hwang KV, Lan T, Lu Y (2013) A DNzyme-gold nanoparticle probe for uranyl ion in living cells. *J Am Chem Soc* 135:5254–5257
98. Feng J, Xu Z, Liu F, Zhao Y, Yu WQ, Pan M, Wang F-A, Liu XQ (2018) Versatile catalytic deoxyribozyme vehicles for multimodal imaging-guided efficient gene regulation and photothermal therapy. *ACS Nano* 12:12888–12901
99. Brummelkamp TR, Bernards R, Agami R (2002) A system for stable expression of short interfering RNAs in mammalian cells. *Science* 296:550–553

Publisher's Note Springer Nature remains neutral with regard to jurisdictional claims in published maps and institutional affiliations.



DNA Strand Displacement Reaction: A Powerful Tool for Discriminating Single Nucleotide Variants

Weiyang Tang¹ · Weiye Zhong¹ · Yun Tan¹ · Guan A. Wang² · Feng Li^{2,4} · Yizhen Liu^{1,3}

Received: 7 October 2019 / Accepted: 6 December 2019 / Published online: 2 January 2020
© Springer Nature Switzerland AG 2019

Abstract

Single-nucleotide variants (SNVs) that are strongly associated with many genetic diseases and tumors are important both biologically and clinically. Detection of SNVs holds great potential for disease diagnosis and prognosis. Recent advances in DNA nanotechnology have offered numerous principles and strategies amenable to the detection and quantification of SNVs with high sensitivity, specificity, and programmability. In this review, we will focus our discussion on emerging techniques making use of DNA strand displacement, a basic building block in dynamic DNA nanotechnology. Based on their operation principles, we classify current SNV detection methods into three main categories, including strategies using toehold-mediated strand displacement reactions, toehold-exchange reactions, and enzyme-mediated strand displacement reactions. These detection methods discriminate SNVs from their wild-type counterparts through subtle differences in thermodynamics, kinetics, or response to enzymatic manipulation. The remarkable programmability of dynamic DNA nanotechnology also allows the predictable design and flexible operation of diverse strand displacement probes and/or primers. Here, we offer a systematic survey of current strategies, with an emphasis on the molecular mechanisms and their applicability to *in vitro* diagnostics.

Keywords DNA · Single nucleotide variants · Toehold-mediated strand displacement · Toehold-exchange reaction · DNA polymerases mediated primer extension reaction

Electronic supplementary material The online version of this article (<https://doi.org/10.1007/s41061-019-0274-z>) contains supplementary material, which is available to authorized users.

Weiyang Tang, Weiye Zhong, Yun Tan and Guan A. Wang contributed equally to this work.

Chapter 12 was originally published as Tang, W., Zhong, W., Tan, Y., Wang, G. A., Li, F. & Liu, Y. Topics in Current Chemistry (2020) 378: 10. <https://doi.org/10.1007/s41061-019-0274-z>.

✉ Feng Li
fli@brocku.ca

✉ Yizhen Liu
yzliu@szu.edu.cn

Extended author information available on the last page of the article

1 Introduction

A single nucleotide variant (SNV) is a genetic variation in a single nucleotide. SNVs occur at a frequency of 1 every 100–300 bases in the human genome, which may have important clinical consequences. Genetic SNV at coding regions are closely related to the causes of many somatic diseases such as cancer, Alzheimer's disease, and many others [1–4]. Therefore, disease-related SNVs found in the blood circulation, such as circulating tumor DNA (ctDNA) and microRNAs, may serve as important disease biomarkers for *in vitro* diagnosis, and can be used to monitor the development of the disease [5–9]. However, many important disease-related nucleic acids only present in trace levels. For example, the abundance of ctDNA was estimated to be only 1% or even 0.01% of the entire circulating DNA. Discrimination of SNVs in such low abundant nucleic acid markers is often challenged by interference from the large excess of wild-type counterparts. Therefore, techniques capable of discriminating rare SNVs with high sensitivity and specificity in liquid biopsies are highly desired and hold great promise for disease diagnosis and prognosis.

Current techniques for analyzing SNVs rely mainly on polymerase chain reaction (PCR) and nucleic acid sequencing [10–13]. However, both techniques are challenged by tedious and lengthy operation procedures, the need for expensive infrastructure and special expertise, and high error-rate for discriminating SNVs. The use of nucleic acid hybridization probes, such as molecular beacons [14, 15] and Taqman probes [16, 17], have helped improve assay speed and accuracy through exquisite Watson–Crick base pairing rules, but are generally difficult to design and operate, and extensive experimental validation and optimization are required. This is because the thermodynamic difference between a SNV and its wild-type counterpart is only a few kcal mol⁻¹, the discrimination of which requires a delicate balance between hybridization yield and sequence selectivity. Moreover, coexisting nucleic acids with high sequence similarity in liquid biopsies are often at concentrations 100–10,000 times higher than those of target SNVs. As high sequence interference may further comprise the analytical performance of hybridization probes, alternative strategies that are highly programmable and robust are thus urgently needed for the detection of SNVs over high abundance interfering sequences in real clinical samples.

Facing these challenges, DNA nanotechnology offers unique solutions for analyzing SNVs with high sensitivity, specificity, programmability and robustness. Specifically, DNA strand displacement reactions mediated by a short sticky end, known as the toehold, have shown remarkable tunability at both thermodynamic and kinetic levels [18]. As such, *in silico* sequence design becomes possible for generating strand displacement beacons or even more sophisticated strategies capable of isolating or enriching rare SNVs. DNA strand displacement can also be triggered or controlled using enzymes, which offer several unique mechanisms that facilitate signal amplification while maintaining high sequence specificity. In this review, we will summarize recent advances in SNV detection techniques that harness DNA strand displacement. We will first give a brief introduction of

the fundamental basis of varying strand displacement principles, and then discuss various SNV detection techniques based on three classes of strand displacement, including toehold-mediated DNA strand displacement, toehold-exchange, and DNA polymerase-mediated primer extension reaction.

2 Fundamental Basis of DNA Strand Displacement

Strand displacement reactions, such as toehold-mediated strand displacement and toehold-exchange, have been used widely as basic building blocks in DNA nanotechnology for the design of reconfigurable structures [19–21], logic gates, [22–26] DNA machines, [27–30] and biosensors [31–33]. Compared with other nucleic acid hybridization probes, such as molecular beacons, strand displacement reactions offer much higher design-level and operation-level flexibility. Leveraging strand displacement reactions, diverse DNA nanostructures or devices can be tailored into powerful tools to amplify the sensitivity and specificity for the detection of SNVs. Here, we will first discuss the fundamental basis of various DNA strand displacement reactions with an emphasis on their potential for SNV analysis. Their applications in DNA nanotechnology have been reviewed elsewhere [34, 35].

2.1 Toehold-Mediated Strand Displacement

Toehold-mediated strand displacement was first introduced by Yurke et al. [36] in their seminal work in creating DNA tweezers. As shown in Fig. 1a, toehold-mediated strand displacement between a single-stranded input and a duplex substrate is initiated at a short complementary single-stranded domains on the substrate (referred to as toeholds), and progresses through a branch migration process that resembles a random walk. As more base pairs are formed, the reaction is thermodynamically favored. When the hybrid domain is short, the kinetics of strand displacement are determined mainly by the length and sequence of the toehold domain. Depending on the binding strength of the toehold (length and GC content), the rate constant may vary from 1 to $6 \times 10^6 \text{ M}^{-1}\text{s}^{-1}$ [22]. When a point mutation occurs at or close to the toehold domain, it may significantly alter the kinetics of a strand displacement. Such a kinetic difference may be used to design assays that discriminate SNVs from wild-type counterparts. To guide the design of such assays, the rate of toehold-mediated strand displacement reactions in the presence of varying mutations can be predicted theoretically using an intuitive energy landscape model (IEL model) established by Srinivas and Winfree [37].

Toehold-mediated strand displacement also inspired the development of several other types of toehold designs capable of fine-tuning the thermodynamics or kinetics of strand displacement reactions. For example, the remote toehold, where a spacer is introduced between the toehold domain and branch migration domain, can be used to control the kinetics of strand displacement with a higher precision than the normal toehold (Fig. 1b) [38]. The allosteric toehold can increase the flexibility of regulating strand displacement reactions by splitting the toehold domain and the

Fig. 1 **a** Schematic of the toehold-mediated strand displacement reaction. Input *A* hybridizes with the complementary toehold of complex *X* to initiate branching migration, and then *A* displaces *B* to form a new complex *Y* [36]. **b** Schematic of remote toehold-mediated strand displacement. The toehold and displacement domains on both the duplex substrate and a single-stranded input strand are separated by spacer domains. Bounding of the duplex substrate and the input strand by hybridization of the toehold domains is followed by an internal diffusion step, initiating the branch migration reaction by which the short strand of the substrate is displaced [38]. **c** Schematic of allosteric toehold-mediated strand displacement. A short strand *R* first reacts with *CP* to form a reaction intermediate *CPR*, and the invading region of *R* exposes a short segment of *C* that serves as a secondary toehold to drive the strand-exchange between *X* and *CPR* to form *XC* and *RP* [39]. **d** Schematic of the toehold exchange reaction. Hybridization of the duplex substrate to the input *X* strand is initiated at the 5' toehold of the substrate, proceeds through a branch migration process, and is completed via the spontaneous dissociation of the 3' base pairs of the substrate to release single-stranded protector *Y*. The toeholds allow the forward and reverse reactions to proceed with fast kinetics [41]. **e** Schematic of the primer extension reaction mediated by DNA polymerases. Conformation of the probe is changed by hybridization of the probe with the target DNA, and then the target DNA is displaced in the process of the polymerization reaction and then hybridized to another probe [42]

branch migration domain (Fig. 1c) [39]. Such advanced toehold designs have also been adapted to create unique assays for discriminating SNVs [40].

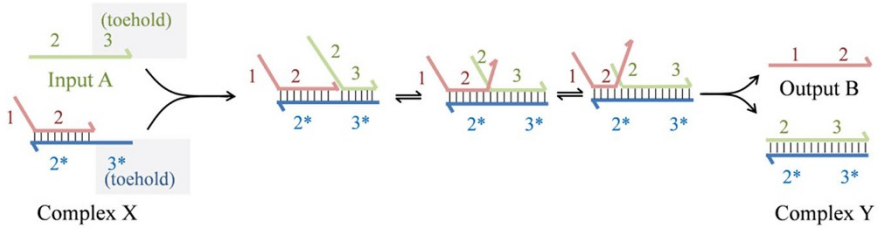
2.2 Toehold-Exchange

Of all toehold designs, toehold-exchange is one of the most powerful and widely used strategies for designing assays and probes that discriminate SNVs (Fig. 1d). This reaction, which was first introduced by Zhang et al. [41], involves a reverse toehold introduced into the duplex substrate. By simply tuning the length of the forward and reverse toehold, one can control the thermodynamics of the reaction with high precision. Moreover, the toehold-exchange principle also effectively decouples the thermodynamics and kinetics of the strand displacement, allowing the reaction to progress rapidly regardless of the thermodynamics. To better describe the kinetics of toehold-exchange, Zhang and Winfree [18] established a three-step reaction model, through which the kinetics can be predicted using a flow chart (Fig. 2). For a given toehold-exchange reaction, *n* and *m* represent the length of the forward and reverse toeholds, respectively. The reaction rate constant of this reaction can be determined roughly based on the numeric values of *n* and *m*. One of the most remarkable applications of toehold-exchange is to discriminate SNVs through fine-tuning the thermodynamics, i.e., the Gibbs free energy, of the reaction, which will be detailed in the section on [SNV detection using toehold-exchange](#).

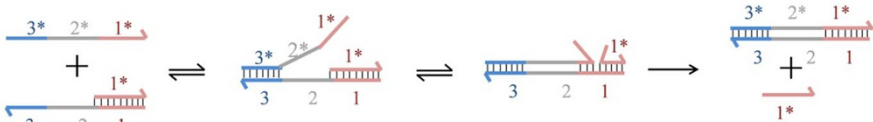
2.3 DNA Polymerase-Mediated Primer Extension Reaction

Strand displacement may also be triggered through a primer extension reaction mediated by DNA polymerases possessing high displacement activities (Fig. 1e) [42]. Enzyme-assisted DNA strand displacement has been used widely for isothermal nucleic acid amplification as well as for the development of enzyme-mediated DNA machinery. For example, strand displacement amplification that combines enzyme-assisted DNA strand displacement and a nicking endonuclease has been widely

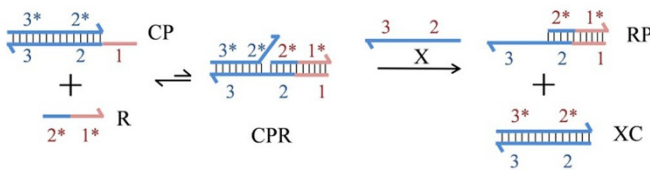
A. Toehold mediate strand displacement



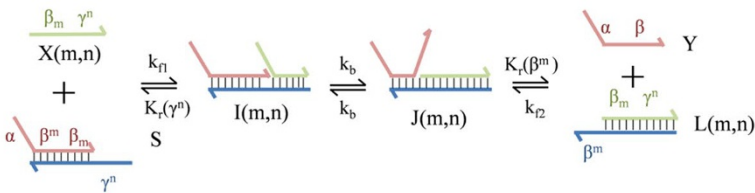
B. Remote toehold mediate strand displacement



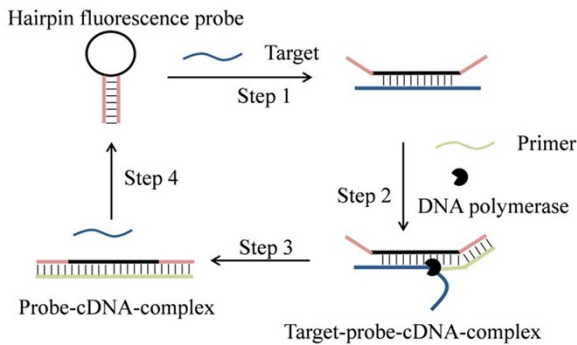
C. Allosteric toehold mediate strand displacement



D. Toehold Exchange mediate strand displacement



E. Primer extension reaction mediated by DNA polymerases



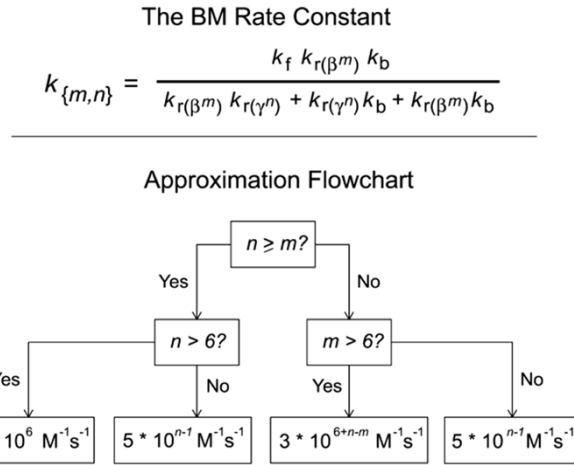


Fig. 2 Predicting the rate of toehold-mediated strand displacement reaction using a flow chart of three-step reaction model (reprinted with permission from [18])

adopted as an isothermal alternative to polymerase chain reactions [43, 44]. Further integration of strand displacement amplification with DNA hairpins also led to the development of beacon-assisted detection amplification [43]. Enzyme-assisted DNA strand displacement has also been incorporated as a signal amplification component into various assays for discriminating SNVs [45]. Sequence specificity can be achieved through the differential response to enzymes or through the integration of well-designed probes, primers, or other strand displacement techniques.

3 Discrimination of SNVs Using Strand Displacement Reactions

DNA strand displacement technology provides numerous tools for SNV detection, such as toehold-mediated strand displacement reactions, strand exchange reactions, and enzyme-assisted strand displacement reactions. These tools can be used to determine the presence or absence of SNV from a thermodynamic and kinetic perspective. Disease progression can be monitored by diagnosing the presence and concentration of SNV. The practical application of the above-mentioned related tools in SNV will be described in detail below.

3.1 SNV Detection Using Toehold-Mediated Strand Displacement Reaction

Current research on the detection of SNVs based on the strand displacement reaction relies mainly on reaction kinetics to achieve SNV detection [46–48]. When a point mutation occurs at, or near, the toehold region, the rate of strand displacement reaction is significantly reduced, thereby allowing the mutation to be distinguished from the wild type kinetically. Li [49] proposed a new SNV detection method using double-stranded probes to identify SNVs, improving the low specificity of direct

hybridization of single-stranded probes. The double-stranded probe overcomes the small difference in free energy between the single-stranded probe–wild type and the single-stranded probe–SNV direct binding, thereby enhancing the specificity of the recognition probe (see Fig. 3a, b). The length of the double-stranded probe toehold is also found to have a significant influence on the specificity of SNV recognition. When the toehold length is 6 or 7 nt, wild type and SNV can exhibit significant kinetic reaction rate differences, which is beneficial to the identification of SNV. For SNV detection in rare SNVs, Li introduced other double-stranded probes corresponding to the non-target SNV to shield from interference of the non-target SNV, thereby ensuring specific recognition of the target SNV (see Fig. 3c). Since then, SNV detection technology based on toehold-mediated strand displacement has mushroomed.

With the rapid development of the application of toehold-mediated strand displacement reaction in SNV detection, researchers were not satisfied with the SNV recognition specificity achieved by conventional linear probes. Therefore, how to improve the specificity of SNV detection method is now the focus of research. As shown in Fig. 4, most researchers studied probe structure with a view to increasing the difficulty of the strand displacement reaction between SNV sequences and probes by increasing the thermal stability of the probes, so as to enhance the difference in reaction kinetics between wild type and SNV and further improve specificity. Y-type [50] and X-type [51] probes are widely favored because their thermal stability is much higher than that of linear probes [52]. In addition to optimization of probe structure, locked-nucleic acid (LNA) can be used in strand displacement to improve the specificity of detection methods because

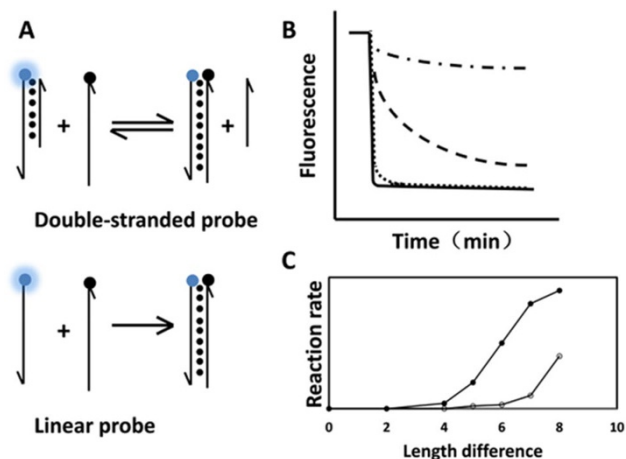


Fig. 3 **a** Labeling scheme for comparing double-stranded probe with linear probes. **b** Comparison of reaction kinetics of double-stranded probe with linear probes with matched and mismatched targets. While linear probes react equally with matched (solid line) and mismatched (dotted line) targets, double-stranded probes react well with matched (dashed line) but not with mismatched (dot-dash line) targets. **c** Dependence of the reaction rate on the difference in length between the long and short strands in the presence of the perfectly match (solid circle) and the single mismatch oligonucleotide (open circle) [49]

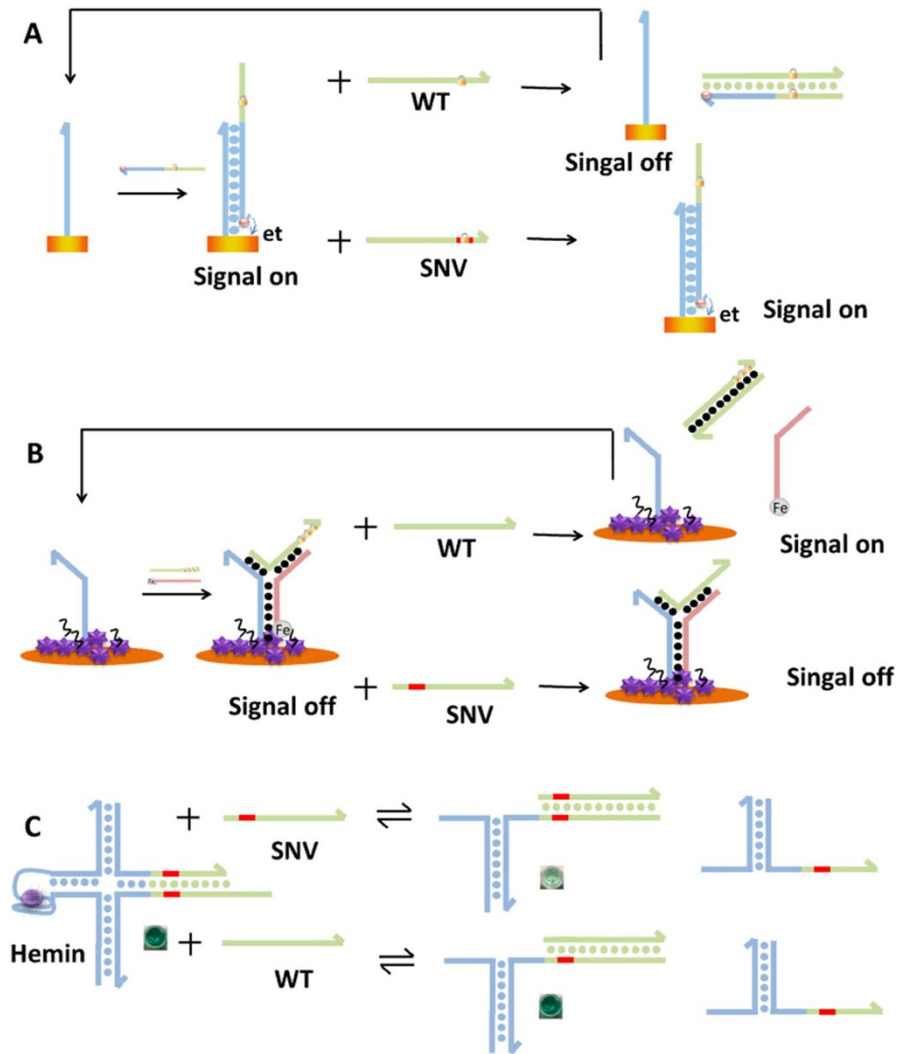


Fig. 4 Application of the double-stranded probe (a) [53], Y probe (b) [51], and (c) X-probe in single nucleotide variant (SNV) recognition [52]

of its function in amplifying the destabilization of mutations in double-stranded DNA. LNA contains a methylene linkage between the 2'-O atom and 4'-C atom of the ribose ring [53, 54], leading to restricted ribose conformations, resulting in a higher melting temperature of double-stranded with LNA [55, 56]. Therefore, the affinity between wild type and probe, and the repulsion between SNV and probe, can both be enhanced by replacing natural nucleotides with LNA at mutation sites. As a result, the reaction efficiency of the probe with the wild type was improved, while that with SNV was weakened, so as to expand the kinetic difference and enhance the specificity.

Typical toehold-mediated strand displacement reaction is limited by the toehold length of the hybridization probe. The toehold strand displacement rates of wild type and SNV are not much different when the toehold length is too long, resulting in poor recognition specificity. Therefore, Li et al. [57] proposed the one-sided remote toehold design based on a toehold-mediated strand displacement and internal diffusion driven branch migration mechanism [38] (Fig. 5a). In this design, a spacer region was added between the toehold and branch migration regions to introduce the internal diffusion step. In this way, one-sided remote toehold strategy increases the energy threshold of the strand displacement reaction to increase the difficulty of the reaction. By increasing the spacer length, the rate of the SNV reaction can be greatly reduced, while that of the complementary reaction changes little, thereby increasing the kinetic difference and the detection specificity.

A single binding event resulting from a single target binding domain of the probe may cause only small thermodynamic constraints for SNV. Compared with the overall reaction thermodynamics, this constraint has little effect on the reaction results of wild type and SNV, resulting in poor recognition specificity. Therefore, Liu et al. [58] increased thermodynamic limitations by designing probes with two

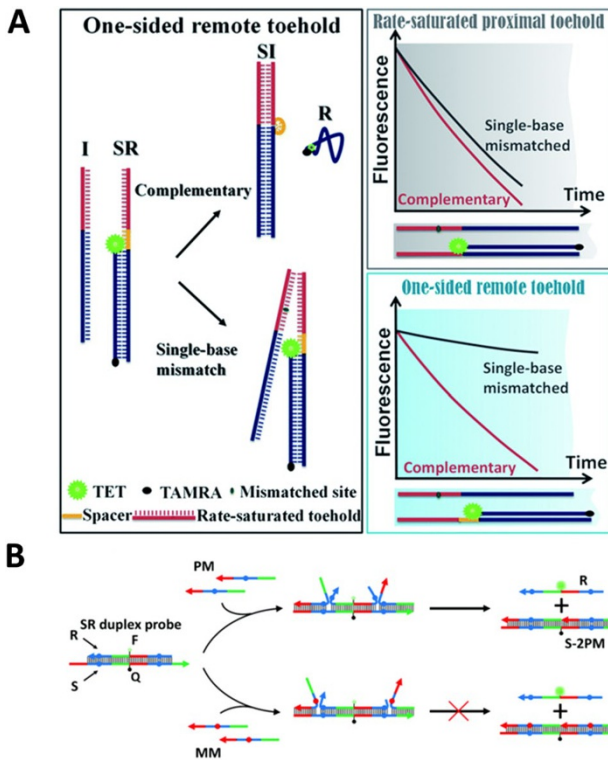


Fig. 5 **a** Schematic diagram of SNV discrimination based on the one-sided remote toehold-mediated strand displacement reaction response. Reprinted with permission from [57]. **b** Schematic diagram of SNV discrimination method based on cooperativity system (Reprinted with permission from [58])

target binding domains (as shown in Fig. 5b). Liu et al. [58] achieved the diagnosis of KRAS-G12D mutations by combining this design with PCR amplification. In this design, the SR double-stranded probe reacts with the target to achieve two binding events with synergistic effects [59, 60]. If the target contains SNV, two mismatched bubbles will be generated during the reaction, increasing the thermodynamic constraints. Thermodynamically, the probe with the double toehold has higher thermodynamic constraints, resulting in increased specificity. The system can also be combined with an isolation system to develop a highly specific dual discrimination strategy.

In addition to these tools, a framework nucleic acid (FNA) acting as a detection platform is also an important method to increase sensitivity and specificity. The probe-based FNA not only spatially segregates neighboring probes avoiding molecular entanglements but also molecular diffusion and convection is expected to be faster than at smooth macroscopic sites, which improves sensitivity of sensors greatly [61]. Zhang et al. [62] combined FNA with a DNA strand displacement reaction to develop a sensing platform for detecting SNPs. The probe marker with streptavidin captures the target nucleic acid by a strand displacement reaction, and, if a SNP is present, the process is aborted (Fig. 6a) [62]. Seeman et al. [63] also developed a DNA origami chip for SNP genotyping. This rectangular DNA tile harbors a pattern of alphabetic characters representing the four nucleotides (i.e., A, T, G, and C) that enable AFM imaging with a symbolic display. In the presence of complementary sequences, the corresponding probe can trigger DNA strand displacement and remove the symbolic character while other toehold-based migrations would be inhibited by a single-base mismatch (Fig. 6b).

Moreover, a defect of the toehold-mediated strand displacement reaction method is that it can judge only whether nucleic acids have a mutation, but not mutation location. To solve this problem, Liu et al. [39] proposed using the logic judgment function of DNA logic circuit to identify the location of SNV. As shown in Fig. 7a, The 4-to-2 encoder was constructed based on the allosteric toehold-mediated strand displacement reaction, which can be used to specifically determine SNVs and their positions [64]. There are two recognition elements in the encoder, B-C and G-L, which distinguish mutations of region 1* and 2* and region 2* and 3* of the sequence, respectively. After the SNV sequence is recognized by the circuit, the encoder will output different signal combinations according to the region where the SNV site is located. As Fig. 7b shows, when the first number is 1, the analyte has no SNV in domains 1* and 3*. When the second number is 1, the analyte has no SNV in domains 3* and 2*. Thus, SNV sites can be located precisely in an exact domain. Although this circuit is a useful SNV recognition circuit, it has some limitations in the recognition of rare SNVs. Therefore, the circuit is hopefully cascaded with the amplification circuit to achieve a lower detection limit.

3.2 SNV Detection Using Toehold-Exchange

Although the toehold-mediated displacement reaction can be used to differentiate SNVs, it suffers from the limitation that the SNV needs to be in the vicinity of the

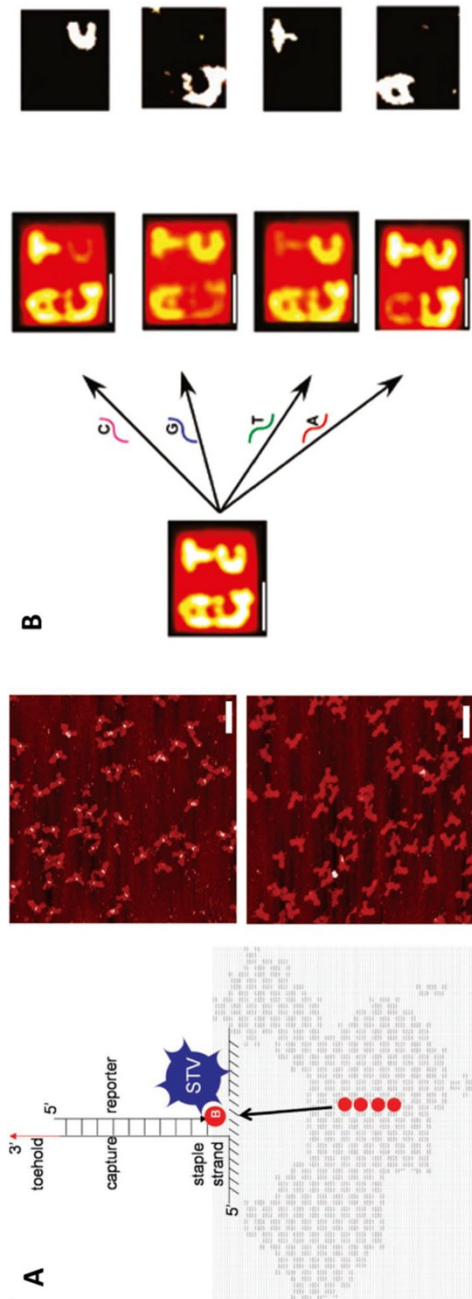


Fig. 6 **a** DNA framework nucleic acid (FNA) origami-based toehold-mediated SNP detection. Reprinted with permission from [62]. **b** Alphabetic patterned origami structure for SNP detection. (reprinted with permission from [63])

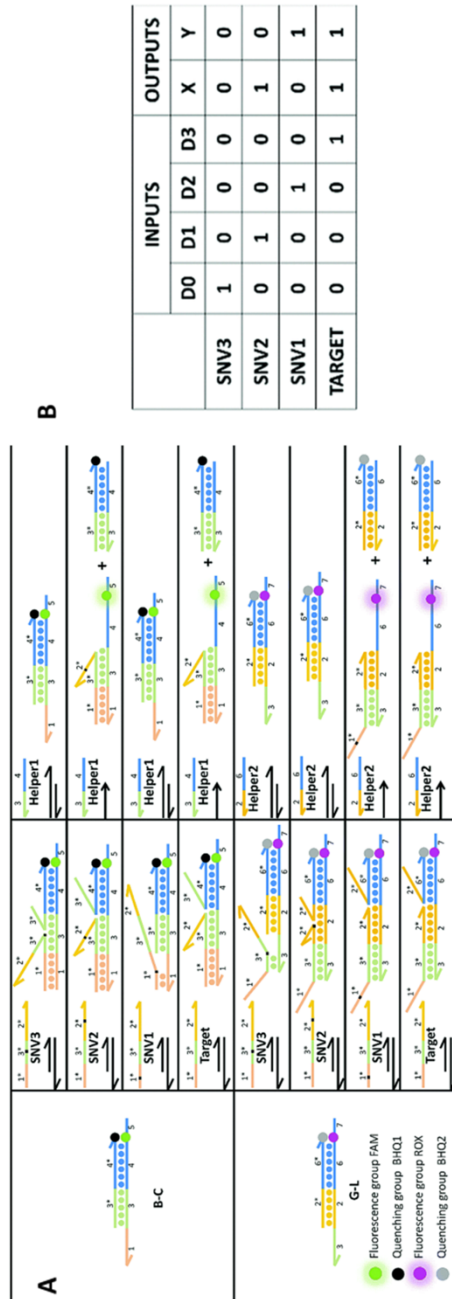


Fig. 7 a SNV recognition method based on a 4-to-2 encoder. **b** Truth table of the 4-to-2 encoder (reprinted with permission from [64])

toehold area. This strand displacement reaction also shows poor performance on SNVs that are very close in thermodynamic energy to the wild type. These limitations can be overcome by probes operated using toehold-exchange principles [65]. The reversible nature of toehold-exchange makes it very sensitive to subtle changes in thermodynamic difference caused by SNVs. Reaction yield and discrimination factors (DFs) can be predicted accurately and tuned by altering the lengths of the forward and reverse toeholds. It is also possible to further improve the specificity for discriminating rare SNVs by introducing competitive “sink” probes [66]. This “sink” strategy takes advantage of both kinetics and thermodynamics to enhance hybridization specificity, making it possible to detect a minute amount of SNVs with a large excess of wild-type interference. Zhang et al. [65] achieved in vitro diagnosis of mutant nucleic acids such as EGFR-L858R by this strategy with a large excess of wild-type interference.

The fundamental basis of discriminating SNVs using toehold-exchange was first established by Zhang and colleagues in 2012 (Fig. 8) [65]. The standard Gibbs free energy (ΔG°) of a toehold-exchange reaction between an input X and duplex CP was found to be tunable by altering the length of the forward and reverse toehold. When ΔG° is highly negative, this reaction has a high reaction yield but low sequence specificity (DF is close to 1). However, when ΔG° is tuned to be near 0, the reaction yield approaches 50% and the DF increases dramatically. Hybridization probes making use of toehold exchange were also found to be highly robust, and resistant to changes in assays conditions such as buffer saline and temperature. In addition to toehold length, it is also possible to further fine-tune the toehold-exchange through auxiliary probes such as the protector probe (*P*) in Fig. 8. Because thermodynamic parameters of toehold-exchange probes are readily available, it is possible to achieve the in silico design of such probes without the need for experimental optimization. Such simulation-guided designs and operations of toehold-exchange probes make them highly attractive for practical application in SNV analyses. Zhang et al. [65] detected the let 7 g and other SNV nucleic acids through this design.

One inherent restriction of typical toehold exchange reaction is that the hybridization probes can only recognize single-stranded targets with mutations sites. Therefore, Zhang et al. further expanded the target to double-stranded nucleic acids through the development of an X-probe (Fig. 9) [67]. In this design, two different toeholds are created at the same end of each complementary strand in a duplex. Upon binding with the probe, a quadruplex DNA structure will be formed. If the target contained a base pair of SNVs, two mismatch bubbles will be generated in the produced duplexes. Thermodynamically, SNVs in the double-toehold exchange reaction are less favorable than that in a single-toehold counterpart, resulting in the enhancement in specificity.

Despite excellent performance for discriminating SNVs using toehold-exchange, it remains analytically challenging to detect rare SNVs in the presence of a large excess of somatic nucleic acids. To address the need for discriminating rare mutations, Zhang et al. [66] introduced a “sink” strategy, which dramatically improved the specificity of toehold-exchange probes. Because of the complexity in the reaction network, they built a model to simulate and predict the yield and DF distribution as a function of probe and sink reaction free energy. The basic principle is to

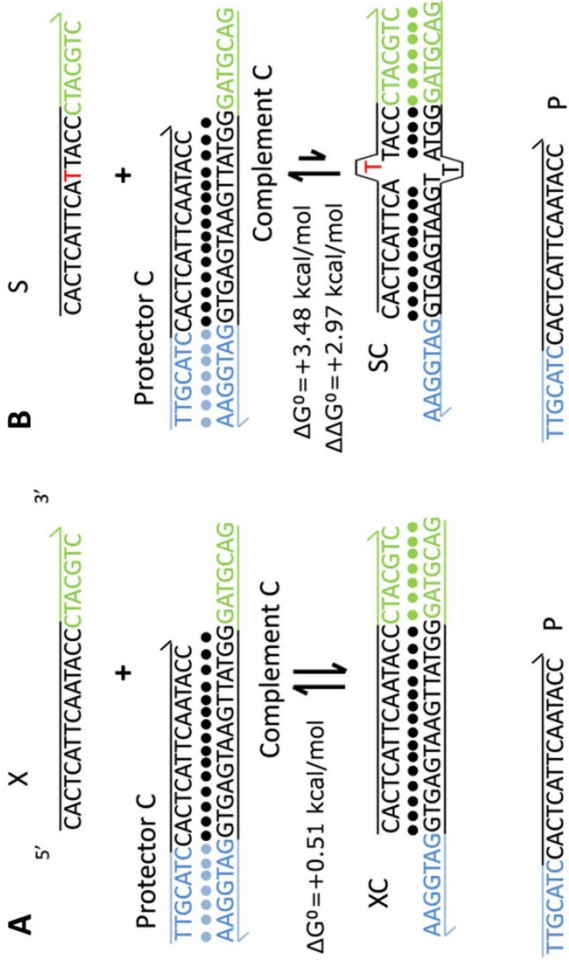


Fig. 8 Toehold exchange probes for SNV identification. **a** The probe reacts with an incorrect target X to release protector strand P. In this process, the standard free energy of the reaction is close to zero. **b** Hybridization of a spurious target S with one base change is thermodynamically less favorable by +2.97 kcal mol⁻¹ [65]

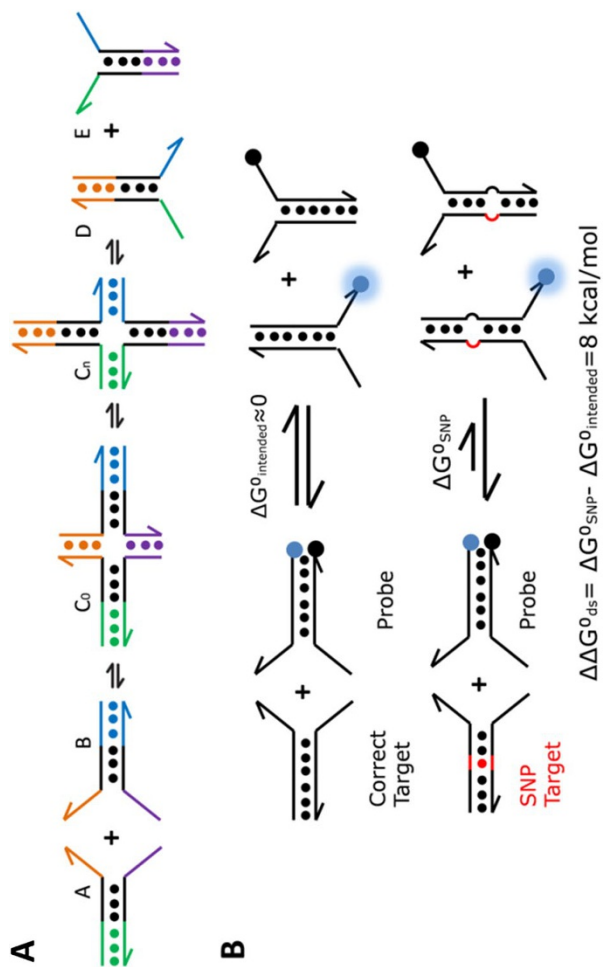
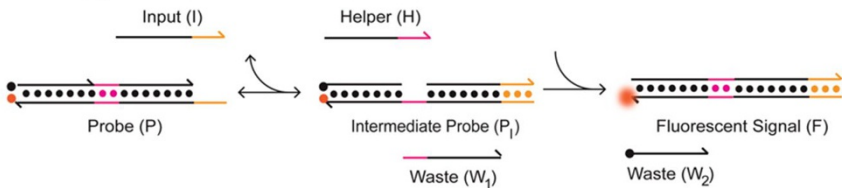


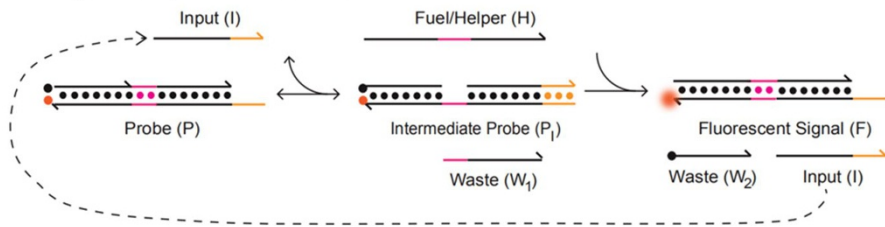
Fig. 9 Schematic representation of the double-stranded toehold exchange mechanism. **a** Reversible branch migration process of double-chain toehold exchange. **b** Highly specific variants identification based on double-stranded toehold exchange. The reaction with the intended target has $\Delta G^{\circ}_{intended}$ is close to zero. The reaction between the probe and the SNP target will result in two mismatch bubbles, and the reaction ΔG°_{SNP} will be about 8 kcal mol⁻¹ [67]

reduce the reaction potential between unexpected spurious targets and signal-generating probes by splitting the target-probe hybridization process. The perfect match target-probe pairs have faster kinetics than that with a SNV mismatch. Therefore, unwanted wild-type target will be annihilated by the sink instead of competing the SNV target to generate a signal. Seelig et al. [68] further improve the sensitivity of the Sink design by introducing two fuel strands (Fig. 10). Using this strategy, both the sensitivity and specificity can be enhanced. In addition to linear probes, DNA hairpins may also be used as competitive “sink” probes to enhance the sequence

A Two-step probe mechanism



B Amplification probe mechanism



C Amplification with Competition (two-step mechanism)

(i) DNA realization

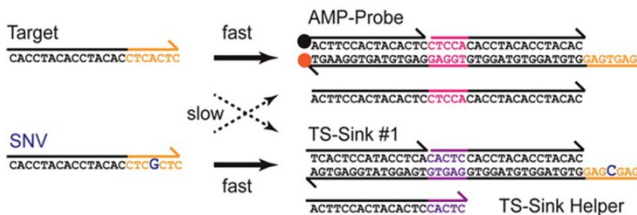


Fig. 10 Using an engineered two step sink and catalytic probe, SNVs in any position of the input can be reliably identified. **a** Two-step reaction mechanism. The first reaction step is a reversible toehold exchange reaction between the input strand (*I*) and the waste strand (*W1*). In the second step, an auxiliary helper molecule (*H*) competes with *W1* for binding to the magenta toeholds. Binding of *H* makes the overall reaction irreversible. **b** An amplification probe mechanism. Binding of the input strand is reversible, exactly as for the two step probe. In the second reaction step, the longer helper (or fuel) sequence hybridizes to the bottom strand using the pink toehold and displaces not only the waste strand *W2* but also the input irreversibly. After the input is released, it can react with another probe to initiate the next catalytic cycle. **c** An amplification circuit with a competitive two-step sink exhibits dramatically increased specificity and sensitivity for SNVs (reprinted with permission from [68])

specificity [69]. For example, Liu and coworkers combined hairpin competitor and asymmetric PCR amplification with *in vitro* diagnostics. Eventually, they successfully detected mutant nucleic acids (KRAS-G12D) with only 0.2% abundance [58] (Fig. 11).

When discriminating SNVs using toehold-exchange reaction, a tradeoff between assay sensitivity and specificity often occurs. Integration of toehold-exchange probes with nucleic acid amplification can help address this intrinsic trade-off. PCR and isothermal nucleic acid amplification was often used to pre-amplify the target sequence before the SNV analysis. It is also possible to amplify the detection signal during toehold-exchange process by introducing catalytic DNA circuits. Recently, Li and coworkers [70] explored the possibility of post-SNV-recognition amplification through the integration of toehold-exchange with a three-dimensional (3D) DNA nanomachine (Fig. 12). The 3D DNA nanomachine was designed by co-conjugating a toehold exchange probe with hundreds of signal reporters on a single gold nanoparticle. In the presence of the target, the nanomachine was activated through toehold-exchange and then cleaved signal reporters processive through nicking recognition and cleavage. As a result, each target could trigger the release of hundreds of fluorogenic signal reporters and the signal could thus be amplified by over 100 times. This strategy was shown to be fully compatible with toehold-exchange, allowing simulation-guided sequence designs and high sequence specificity. In addition to enzyme-powered DNA nanomachine, signal amplifications can also be achieved through enzyme-free strand displacement networks, which will be detailed in the next section.

3.3 Amplified SNV Detection Using Enzyme-Free Strand Displacement Networks

An enzyme-free strand displacement network [71] is often used in conjunction with strand displacement probes to amplify detection signals to address the trade-off in sensitivity and specificity [40, 72, 73]. The target can be used as a promoter for the amplification network or recognized by a recognition mechanism to induce an amplification mechanism. Both can amplify the target signal and distinguish it from SNV. For example, catalytic hairpin assembly (CHA), as an isothermal and enzyme-free signal amplification DNA network, plays an important role in recognition of SNV due to its remarkable inhibition of catalytic activity in the catalytic strand [74]. As shown in Fig. 13a, in the early stage of the reaction, the wild type as the catalytic strand undergo a CHA reaction, rapidly amplifying the signal in a short time, and expanding the signal difference with the SNV, thereby increasing DF [71]. Signal amplification can be achieved through target recycling. Similarly, Chen et al. [73] also achieved signal amplification by re-releasing the target into the DNA tetrahedron, which was based on FNA, thereby achieving an increase in specificity and sensitivity (as shown in Fig. 13b). The recognition probe modified on the tetrahedron limits the freedom of single-stranded DNA, providing a rigid platform to facilitate the strand displacement amplification process. In addition to the reuse of targets on an amplification network, mass amplification has also been used as a novel amplification method (Fig. 13c). In this design, only wild type can be captured

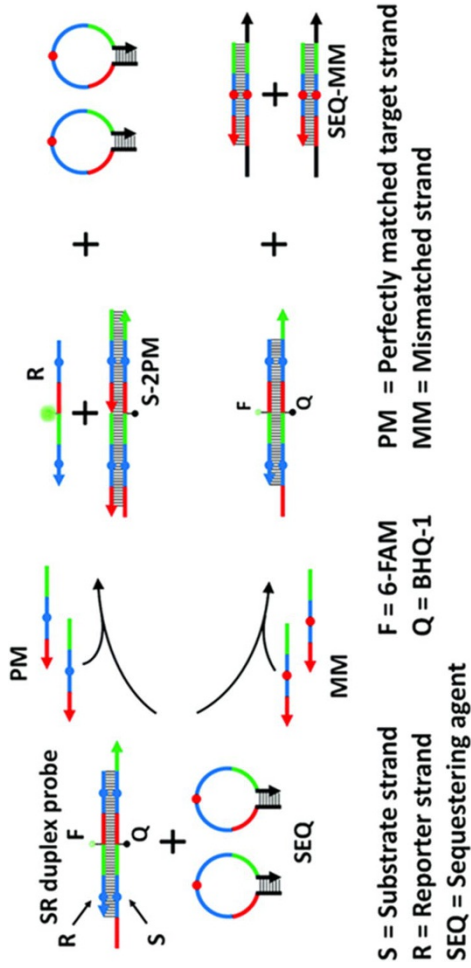


Fig. 11 Schematic representation of the proposed SNV discrimination methods based on cooperativity and combining cooperativity with sequestration (reprinted with permission from [58])

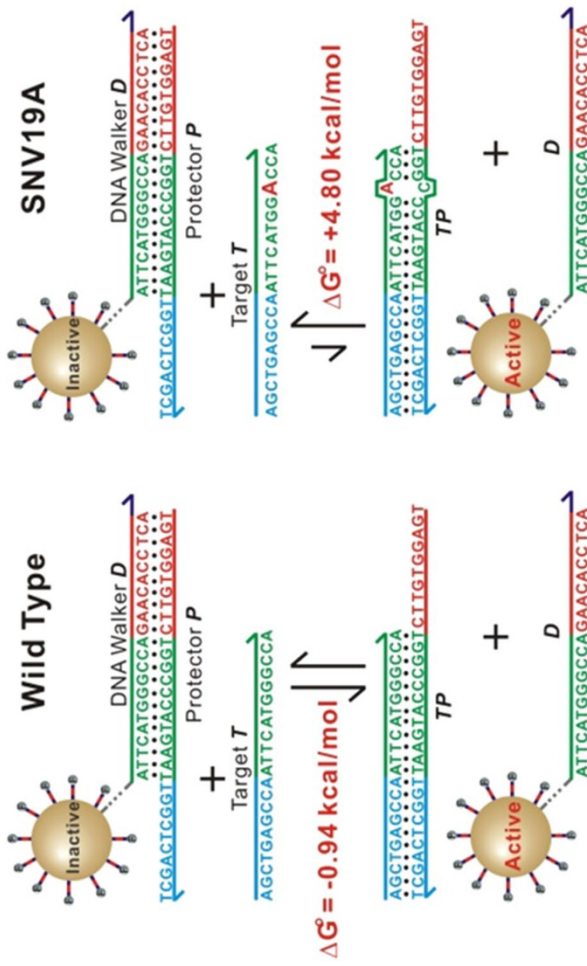


Fig. 12 Enhancing both sensitivity and specificity for discriminating SNVs by integrating toehold-exchange with a three-dimensional (3D) DNA nanomachine [70]

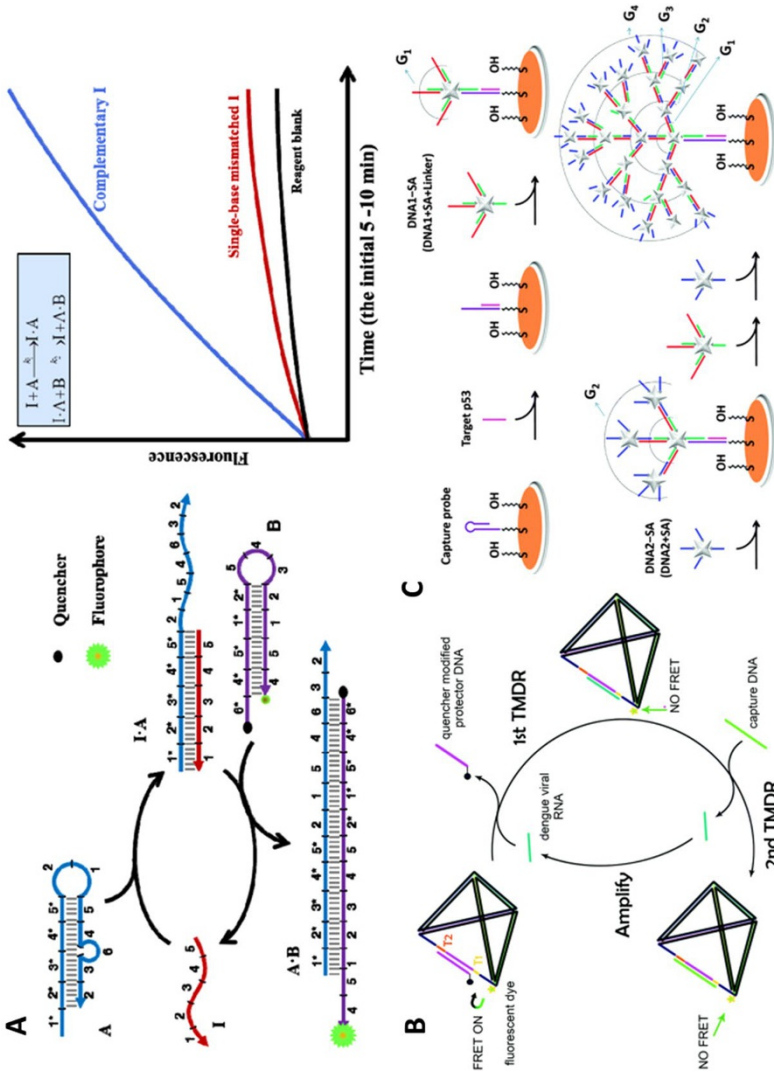


Fig. 13 a Schematic diagram of SNV recognition based on the initial reaction rate of the CHA circuit. Reprinted with permission from [74]. b Schematic diagram of SNV detection method based on the cascade of strand displacement and strand displacement amplification technology. Reprinted with permission from [73]. c Schematic diagram of SNV detection principle based on DNA-SA dendrimer nanostructure-amplified quartz microbalance sensing platform. Reprinted with permission from [75]

by probes modified on the quartz crystal microbalance to assemble dendrimer nanostructures, increasing mass and changing the signal frequency shift response [75]. Among them, Streptavidin's special four binding sites allow one DNA1-SA to bind to three DNA2-SAs, and one DNA2-SA can be binded to three DNA1-SAs, so the probe mass is increasing violently, achieving amplification. Furthermore, the complementary target signal is significantly amplified and the SNV signal does not, which result in significant kinetic signal differences and increases DF. The use of this enzyme-free strand displacement amplification network can improve the sensitivity and specificity of the recognition technology, which has broad application prospects in SNV applications.

3.4 SNV Detection Using DNA Polymerase-Mediated Primer Extension Reaction

DNA polymerase-mediated primer extension reaction can be used as a signal amplification component or as a terminal mutation recognition component, which plays an important role in SNV detection [45, 76–78]. The reaction was originally proposed by Guo et al. [42] and the relevant principles were clarified in 2009. DNA polymerase-mediated primer extension reaction is divided into four steps. Steps 1 and 2 are commonly used for SNV detection. As shown in Fig. 14a, when the target is identified based on step 1, the wild-type DNA can fold the hairpin and the signal cannot be recovered [44]. The mutant DNA can unfold the hairpin to initiate an enzyme-assisted strand-displacement reaction, which in turn releases the target and reuses it for signal amplification. Based on isothermal strand-displacement polymerase reactions, Liu et al. [45] realized the detection of mutations R156H and R156C which will be causing epidermolytic hyperkeratosis (EHK). This further extends the signal difference between the SNV and the target. When the SNV is identified based on the step 2, the target to be tested is usually set as a primer (Fig. 14b). At this time, a polymerase such as Klenow enzyme functions. Such enzymes have the 5' → 3' polymerase activity and 3' → 5' exonuclease activity of normal polymerases, but lack the 5' → 3' exonuclease activity of intact polymerase. This means that such enzymes cannot cleave mutant bases when they encounter an SNV site during polymerization, so that polymerization still occurs but the reaction rate becomes extremely slow, forming a significant kinetic difference with the complementary target [79]. This special property makes the detection of terminal mutations feasible. In addition, the polymerase-assisted strand displacement reaction can also form a two-step recognition mechanism with the toehold exchange reaction, which has high specificity recognition and can achieve low abundance detection as low as 0.3% within 5 min (Fig. 14c). In this system, DNA polymerase-mediated primer extension reaction calibrates the products of the first-order discrimination reaction and determines whether to continue the reaction [80]. Since the products of the first-order discrimination reaction of the non-target nucleic acid are not completely complementary, when the reaction proceeds, it is terminated by incomplete matching. This mechanism allows SNV to cause significant deviations in conversion rates and achieve high specificity for low abundance detection. Zhao et al. [77] detected mutant nucleic acids (BRAF V600E) with only 1% abundance using this mechanism.

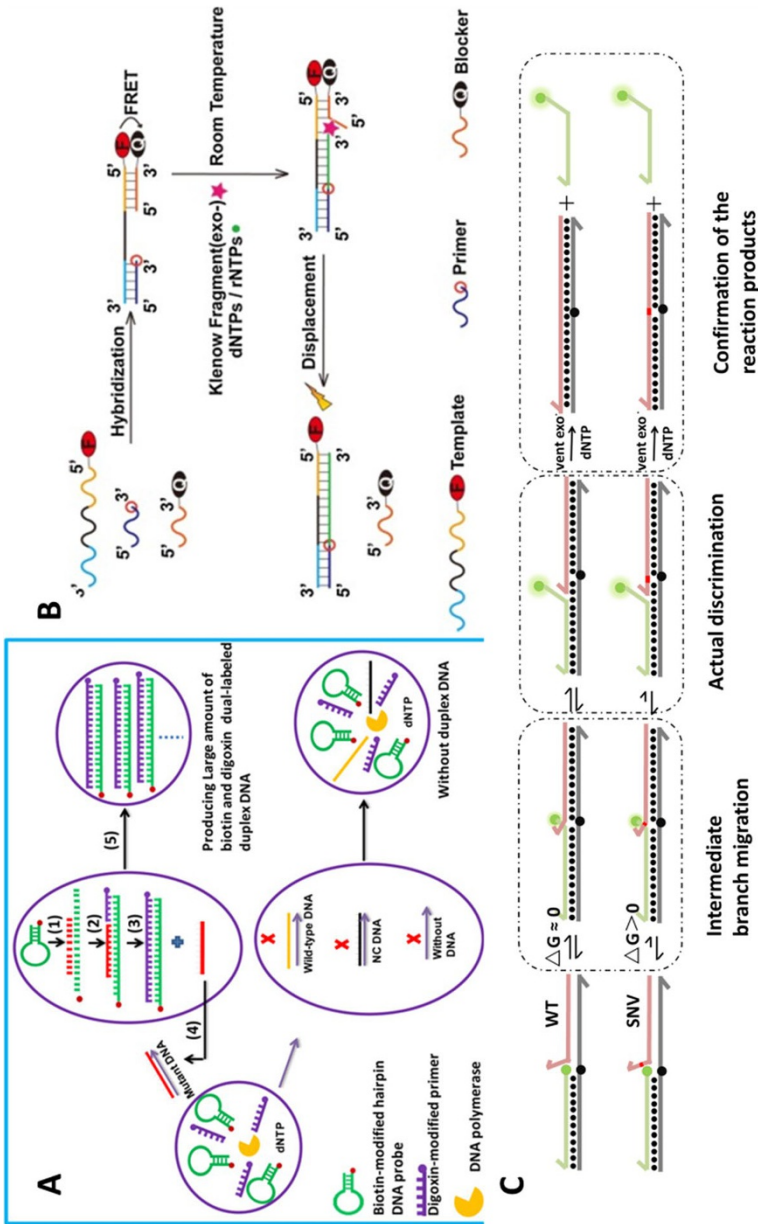


Fig. 14 a The schematic diagram of target DNA signal amplification based on the DNA polymerases mediated primer extension reaction. Reprinted with permission from [44]. **b** The scheme of using fluorescence resonance energy transfer method to measure primer extension kinetics catalyzed by Klenow fragments (exo-). The red circle highlights the single nucleotide substitution in the primer sequence. Reprinted with permission from [79]. **c** The schematic diagram of a two-step recognition mechanism combines toehold exchange reaction and the DNA polymerases mediated primer extension reaction [80]

Table 1 Discrimination factor (DF) values of different mutation identification methods

Discrimination format	Discrimination factor (DF)	Reference
Toehold-mediated strand displacement		
Quartz crystal microbalance biosensor based on toehold mediated strand displacement reaction	63 (G > C substitution)	[46]
Amplified quartz crystal microbalance platform	17–72 (3 SNVs)	[75]
Competition and catalytic amplification	23 (A > G substitution)	[68]
Combining cooperativity with sequestration	67–618, median = 194 (12 SNVs)	[58]
DNA polymerases mediated primer extension reaction		
The droplet-based microfluidic platform	100–550	[79]
Toehold exchange mediated strand displacement		
Competitive and amplification assisted by exonuclease III	33–44	[81]
Energy driven cascade recognition	45–109, median = 70 (6 SNVs)	[82]
A branch-migration based fluorescent probe	89–311	[80]
Enzyme-powered 3D DNA nanomachine	7–26, median = 12 (9 SNVs)	[70]
Conditionally fluorescent molecular probes	Median = 43	[67]
Simulation-guided DNA probe and sink design	Median β = 890c (44 SNVs)	[66]
Optimizing the specificity of nucleic acid hybridization	3–100, median = 26	[65]

3.5 The performance evaluation index of SNV detection method

Specificity and sensitivity are commonly used as indicators of detection in SNV detection. Sensitivity, or detection limit, refers to the lowest analytical concentration detectable by the detection system. Specificity is usually assessed using the DF, indicating the discrimination degree of the method against false targets. The calculation formula of specificity and sensitivity is as follows: [66]

$$\text{Specificity (DF)} = \frac{\chi_T}{\chi_N} \cong \frac{\frac{[T \cdot \text{Probe}]}{[T]_0}}{\frac{[N \cdot \text{Probe}]}{[N]_0}} \text{ or } \text{DF} = \frac{\chi_T}{\chi_N} \cong \frac{\Delta F_T}{\Delta F_N},$$

$$\text{Sensitivity (yield)} = \frac{[T \cdot \text{Probe}]}{[T]_0}$$

where T and N represent the target and non-target molecules, respectively. χ is the hybridization yield. $[T]_0$ and $[N]_0$ represent the initial concentration of T and N molecules, respectively. $[T \cdot \text{Probe}]$ and $[N \cdot \text{Probe}]$ represent the product concentration of T and N molecules reaction, respectively. ΔF is the net increment of the signal.

The literature recognizing mutation based on strand displacement reactions and explicitly calculated DF values is listed in Table 1.

Although the DF index can be applied to most scenarios, there is an error in the evaluation of DF in actual sample detection. Because the SNV target usually has a low abundance, the tradeoff between sensitivity and specificity becomes extremely

significant. In order to solve this problem, Zhang et al. [66] introduced a new metric, the normalized multiple change β , mathematically expressed as:

$$\beta \cong \frac{(T \cdot \text{Probe})/\text{VAF}}{\text{background} + (N \cdot \text{Probe})}$$

Variant allele frequency (VAF) is defined as the $\text{VAF} \cong \frac{[T]_0}{[N]_0}$.

This equation also takes into account the influence of the background, which is a constant, representing a collection of all sources of unavoidable detection signals (e.g., detector dark current, autofluorescence, ambient noise, etc.). It is worth noting that when the background is equal to 0, β is the same as DF, so β explains the specificity. When the background is positive, the minimum signal required for the detection mechanism increases, resulting in an increase in detection limit, a decrease in sensitivity, and a decrease in β value. Therefore, the β value also explains the sensitivity. Since it can explain the specificity and the sensitivity, the β value has a more accurate and comprehensive evaluation index than the DF value in the detection environment of the low abundance target.

As shown in Fig. 15, Zhang et al. [66] used X-probes to detect SNV. When $\text{VAF}=1\%$, the mutant nucleic acid EGFR L858R was low in abundance. In this case, the background signal is not negligible. In this system, $\beta=145$ when $\text{VAF}=1\%$. Further, they proposed using a competitor to detect SNV to improve the specificity of the detection method. When $\text{VAF}=1\%$, $\beta=560$, when $\text{VAF}=0.1\%$, $\beta=2420$; when $\text{VAF}=0.01\%$, $\beta=5460$. In the lower VAF experiments, the β value is higher because of the relatively small contribution of background fluorescence. In addition, the β value takes into account the non-target signal interference under low abundance conditions, and can more accurately judge the specificity of the method.

4 Conclusion and Prospects

Techniques that can detect SNVs with high specificity and high sensitivity are of great value for both fundamental research and clinical applications. Recent advances in DNA strand displacement provide ever finer tools to develop sensitive methods for SNV detection. In this review, we highlighted different strand displacement techniques that are universal and can be generalized to most nucleic acid targets of interest. Therefore, they hold great application potential. These techniques generally rely on the specificity of Watson–Crick complementary base pairing, and each strategy has its own advantages and disadvantages. For SNV detection based on toehold-mediated strand displacement reaction, the discrimination factor based on the initial data response rate detection mode is much higher than that based on the maximum strength detection mode. Moreover, the method is sensitive only to mutations occurring in and near the toehold region, and is insensitive to SNVs that are far away from the toehold. For SNV detection based on toehold exchange, it can specifically identify SNV in any region but with the disadvantage of low hybridization yield and long reaction time. The DNA polymerase-mediated primer extension reaction is involved in recognition of SNV as an amplification component or as a sensitive

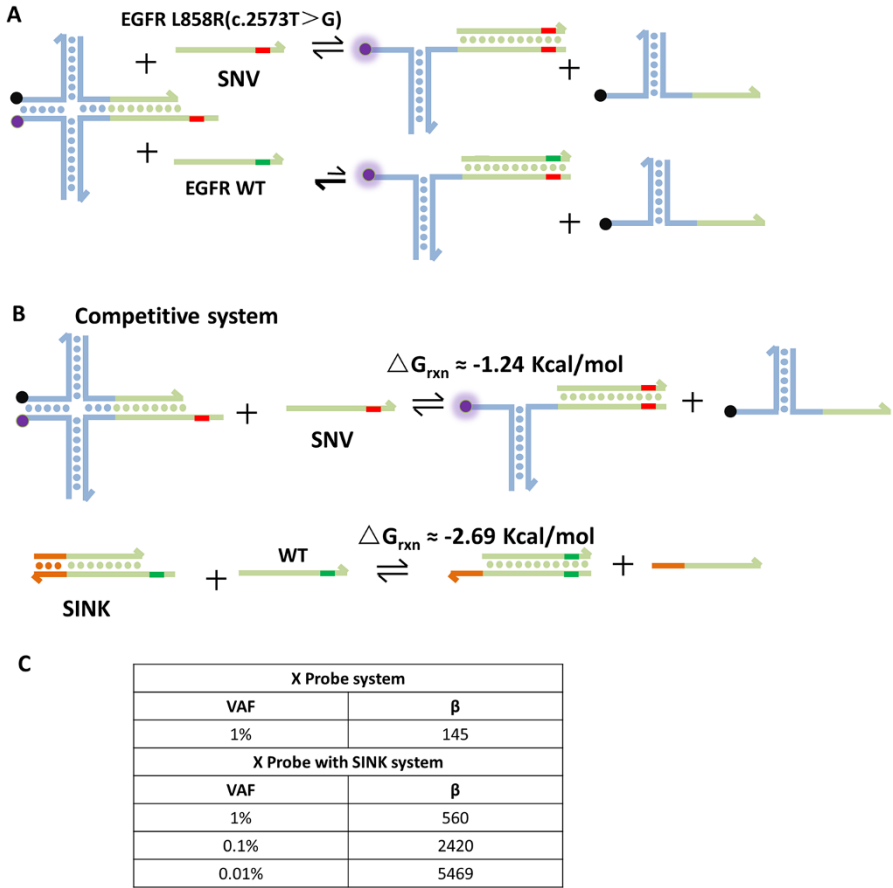


Fig. 15 **a** SNV detection based on X probe. **b** Competitive composition here consists of a target-specific X-Probe and a WT-specific Sink, with near-optimal ΔG° rxn values (kcal mol^{-1}). **c** Different variant allele frequencies (VAF) of the target [66]

detection method for the 3'-end mutation, supplementing the defect of terminal mutation detection.

To further expand the ultrasensitive SNV detection techniques for actual samples, several challenges remain to be addressed. First, it is known that mutant nucleic acids in an actual sample are low-abundance, and samples usually contains a large number of highly homologous sequences. Thus, methods with high selectivity and high specificity are desirable. Priority enrichment methods have been developed to increase the collision probability between the probe and the target to increase specificity. Or, through competitive separation strategies, unexpected reactions in the mixture can be eliminated, ensuring probe selection and improved recognition specificity. These methods are designed to ensure the probe prefers to react with target, thereby increasing specificity and selectivity. Second, many analytical methods

require the design of an equal number of probes to identify multiple different SNVs, which results in unnecessary manual checks and increased system complexity. Therefore, DNA logic circuits are very promising in the application of multiple SNVs identification. Third, the combination of multiple strategies is a good solution when conventional detection methods fail to provide the required performance. For example, more SNV recognition strategies in series can obtain high specificity. The combination of recognition strategy and amplification strategy can address the trade-offs of specificity and sensitivity. Towards these challenges, we anticipate that the unique properties of DNA strand displacement techniques will be continuously explored, generating powerful analytical tools for nucleic acid analysis and clinical diagnosis in the near future.

Acknowledgment This work was supported by the National Natural Science Foundation of China (21605104) and the Shenzhen Science and Technology Foundation (JCYJ20170817101123812).

Compliance with Ethical Standards

Conflict of interest The authors declare that they have no conflict of interest.

References

- Xu Q, Huang S-q, Ma F, Tang B, Zhang C-y (2016) Controllable mismatched ligation for bioluminescence screening of known and unknown mutations. *Anal Chem* 88:2431–2439
- Gilissen C, Hehir-Kwa JY, Thung DT, van de Vorst M, van Bon BWM, Willemsen MH, Kwint M, Janssen IM, Hoischen A, Schenck A et al (2014) Genome sequencing identifies major causes of severe intellectual disability. *Nature* 511:344–347
- Poznik GD, Xue Y, Mendez FL, Willems TF, Massaia A, Sayres MAW, Ayub Q, McCarthy SA, Narechania A, Kashin S et al (2016) Punctuated bursts in human male demography inferred from 1,244 worldwide Y-chromosome sequences. *Nat Genet* 48:593–599
- Khurana E, Fu Y, Chakravarty D, Demichelis F, Rubin M, Gerstein M (2016) Role of non-coding sequence variants in cancer. *Nat Rev Genet* 17:93–108
- Diehl F, Schmidt K, Choti MA, Romans K, Goodman S, Li M, Thornton K, Agrawal N, Sokoll L, Szabo SA et al (2008) Circulating mutant DNA to assess tumor dynamics. *Nat Med* 14:985–990
- Bettegowda C, Sausen M, Leary RJ, Kinde I, Wang Y, Agrawal N, Bartlett BR, Wang H, Luber B, Alani RM et al (2014) Detection of circulating tumor DNA in early- and late-stage human malignancies. *Sci Transl Med* 6:224ra224
- Lu J, Getz G, Miska EA, Alvarez-Saavedra E, Lamb J, Peck D, Sweet-Cordero A, Ebet BL, Mak RH, Ferrando AA et al (2005) MicroRNA expression profiles classify human cancers. *Nature* 435:834–838
- Calin GA, Croce CM (2006) MicroRNA signatures in human cancers. *Nat Rev Cancer* 6:857–866
- Esquela-Kerscher A, Slack FJ (2006) Oncomirs—microRNAs with a role in cancer. *Nat Rev Cancer* 6:259–269
- Mardis ER (2008) Next-generation DNA sequencing methods. *Annu Rev Genomics Hum Genet* 9:387–402
- Loman NJ, Misra RV, Dallman TJ, Constantinidou C, Gharbia SE, Wain J, Pallen MJ (2012) Performance comparison of benchtop high-throughput sequencing platforms. *Nat Biotechnol* 30:562
- Hashimoto M, Barany F, Xu F, Soper SA (2007) Serial processing of biological reactions using flow-through microfluidic devices: coupled PCR/LDR for the detection of low-abundant DNA point mutations. *Analyst* 132:913–921

13. Hamada M, Shimase K, Tsukagoshi K, Hashimoto M (2014) Discriminative detection of low-abundance point mutations using a PCR/ligase detection reaction/capillary gel electrophoresis method and fluorescence dual-channel monitoring. *Electrophoresis* 35:1204–1210
14. Jash B, Scharf P, Sandmann N, Guerra CF, Megger DA, Mueller J (2017) A metal-mediated base pair that discriminates between the canonical pyrimidine nucleobases. *Chem Sci* 8:1337–1343
15. Guo Q, Bai Z, Liu Y, Sun Q (2016) A molecular beacon microarray based on a quantum dot label for detecting single nucleotide polymorphisms. *Biosens Bioelectron* 77:107–110
16. Miotke L, Lau BT, Rumma RT, Ji HP (2014) High sensitivity detection and quantitation of DNA copy number and single nucleotide variants with single color droplet digital PCR. *Anal Chem* 86:2618–2624
17. Jiang YS, Bhadra S, Li B, Wu YR, Milligan JN, Ellington AD (2015) Robust strand exchange reactions for the sequence-specific, real-time detection of nucleic acid amplicons. *Anal Chem* 87:3314–3320
18. Zhang DY, Winfree E (2009) Control of DNA strand displacement kinetics using toehold exchange. *J Am Chem Soc* 131:17303–17314
19. Zhang Y, Pan V, Li X, Yang X, Li H, Wang P, Ke Y (2019) Dynamic DNA structures. *Small* 15:e1900228
20. Choi Y, Choi H, Lee AC, Lee H, Kwon S (2018) A reconfigurable DNA accordion rack. *Angew Chem Int Edit* 57:2811–2815
21. He K, Li Y, Xiang B, Zhao P, Hu Y, Huang Y, Li W, Nie Z, Yao S (2015) A universal platform for building molecular logic circuits based on a reconfigurable three-dimensional DNA nanostructure. *Chem Sci* 6:3556–3564
22. Seelig G, Soloveichik D, Zhang DY, Winfree E (2006) Enzyme-free nucleic acid logic circuits. *Science* 314:1585–1588
23. Bi S, Yue S, Wu Q, Ye J (2016) Initiator-catalyzed self-assembly of duplex-looped DNA hairpin motif based on strand displacement reaction for logic operations and amplified biosensing. *Biosens Bioelectron* 83:281–286
24. Liu Y, Dong B, Wu Z, Fang W, Zhou G, Shen A, Zhou X, Hu J (2014) Toehold-mediated DNA logic gates based on host-guest DNA-GNPs. *Chem Commun* 50:12026–12029
25. Tang W, Huang Q, Wang Z, Zheng Q, Wang L, Zhang J, Chen L, Zhou X, Liu Y, Hu J (2017) A DNA kinetics competition strategy of hybridization chain reaction for molecular information processing circuit construction. *Chem Commun* 53:1789–1792
26. Tang W, Zhong W, Fan J, Tan Y, Huang Q, Liu Y (2019) Addressable activated cascade DNA sequential logic circuit model for processing identical input molecules. *Chem Commun* 55:6381–6384
27. Song C, Wang ZG, Ding B (2013) Smart nanomachines based on DNA self-assembly. *Small* 9:2382–2392
28. Cox AJ, Bengtson HN, Rohde KH, Kolpashchikov DM (2016) DNA nanotechnology for nucleic acid analysis: multifunctional molecular DNA machine for RNA detection. *Chem Commun* 52:14318–14321
29. Thubagere AJ, Li W, Johnson RF, Chen Z, Doroudi S, Lee YL, Izatt G, Wittman S, Srinivas N, Woods D et al (2017) A cargo-sorting DNA robot. *Science* 357:6558
30. Yao D, Li H, Guo Y, Zhou X, Xiao S, Liang H (2016) A pH-responsive DNA nanomachine-controlled catalytic assembly of gold nanoparticles. *Chem Commun* 52:7556–7559
31. Monserud JH, Macri KM, Schwartz DK (2016) Toehold-mediated displacement of an adenosine-binding aptamer from a DNA duplex by its ligand. *Angew Chem Int Ed* 55:13710–13713
32. Ge Z, Lin M, Wang P, Pei H, Yan J, Shi J, Huang Q, He D, Fan C, Zuo X (2014) Hybridization chain reaction amplification of microRNA detection with a tetrahedral DNA nanostructure-based electrochemical biosensor. *Anal Chem* 86:2124–2130
33. Kang D, White RJ, Xia F, Zuo X, Vallée-Bélisle A, Plaxco KW (2012) DNA biomolecular-electronic encoder and decoder devices constructed by multiplex biosensors. *NPG Asia Mater* 4:e1
34. Zhang DY, Seelig G (2011) Dynamic DNA nanotechnology using strand-displacement reactions. *Nat Chem* 3:103–113
35. Seeman NC, Sleiman HF (2018) DNA nanotechnology. *Nat Rev Mater* 3:17068
36. Yurke B, Turberfield AJ, Mills AP, Simmel FC, Neumann JL (2000) A DNA-fuelled molecular machine made of DNA. *Nature* 406:605–608

37. Srinivas N, Ouldrige TE, Sulc P, Schaeffer JM, Yurke B, Louis AA, Doye JPK, Winfree E (2013) On the biophysics and kinetics of toehold-mediated DNA strand displacement. *Nucleic Acids Res* 41:10641–10658
38. Genot AJ, Zhang DY, Bath J, Turberfield AJ (2011) Remote toehold: a mechanism for flexible control of DNA hybridization kinetics. *J Am Chem Soc* 133:2177–2182
39. Yang X, Tang Y, Traynor SM, Li F (2016) Regulation of DNA strand displacement using allosteric DNA toehold. *J Am Chem Soc* 138:14076–14082
40. Li S, Liu X, Pang S, Lu R, Liu Y, Fan M, Jia Z, Bai H (2018) Voltammetric determination of DNA based on regulation of DNA strand displacement using an allosteric DNA toehold. *Mikrochim Acta* 185:433–439
41. Zhang DY, Turberfield AJ, Yurke B, Winfree E (2007) Engineering entropy-driven reactions and networks catalyzed by DNA. *Science* 318:1121–1125
42. Guo Q, Yang X, Wang K, Tan W, Li W, Tang H, Li H (2009) Sensitive fluorescence detection of nucleic acids based on isothermal circular strand-displacement polymerization reaction. *Nucleic Acids Res* 37:e20–e20
43. Du Y, Guo S, Dong S, Wang E (2011) An integrated sensing system for detection of DNA using new parallel-motif DNA triplex system and graphene–mesoporous silica–gold nanoparticle hybrids. *Biomaterials* 32:8584–8592
44. He Y, Zeng K, Zhang S, Gurung AS, Baloda M, Zhang X, Liu G (2012) Visual detection of gene mutations based on isothermal strand-displacement polymerase reaction and lateral flow strip. *Biosens Bioelectron* 31:310–315
45. Liu W, Zhu M, Liu H, Wei J, Zhou X, Xing D (2016) Invading stacking primer: a trigger for high-efficiency isothermal amplification reaction with superior selectivity for detecting microRNA variants. *Biosens Bioelectron* 81:309–316
46. Wang D, Tang W, Wu X, Wang X, Chen G, Chen Q, Li N, Liu F (2012) Highly selective detection of single-nucleotide polymorphisms using a quartz crystal microbalance biosensor based on the toehold-mediated strand displacement reaction. *Anal Chem* 84:7008–7014
47. Khodakov DA, Khodakova AS, Linacre A, Ellis AV (2013) Toehold-mediated nonenzymatic DNA strand displacement as a platform for DNA genotyping. *J Am Chem Soc* 135:5612–5619
48. Wang DZ, Chen GJ, Wang HM, Tang W, Pan W, Li N, Liu F (2013) A reusable quartz crystal microbalance biosensor for highly specific detection of single-base DNA mutation. *Biosens Bioelectron* 48:276–280
49. Li QQ, Luan GY, Guo QP, Liang JX (2002) A new class of homogeneous nucleic acid probes based on specific displacement hybridization. *Nucleic Acids Res* 30:e5
50. Zhang X, Zhang J, Wu D, Liu Z, Cai S, Chen M, Zhao Y, Li C, Yang H, Chen J (2014) Ultrasensitive electrochemiluminescence biosensor based on locked nucleic acid modified toehold-mediated strand displacement reaction and junction-probe. *Analyst* 139:6109–6112
51. Chen X, Zhou D, Shen H, Chen H, Feng W, Xie G (2016) A universal probe design for colorimetric detection of single-nucleotide variation with visible readout and high specificity. *Sci Rep* 6:20257–20263
52. Gao ZF, Ling Y, Lu L, Chen NY, Luo HQ, Li NB (2014) Detection of single-nucleotide polymorphisms using an ON-OFF switching of regenerated biosensor based on a locked nucleic acid-integrated and toehold-mediated strand displacement reaction. *Anal Chem* 86:2543–2548
53. Veedu RN, Wengel J (2009) Locked nucleic acid nucleoside triphosphates and polymerases: on the way towards evolution of LNA aptamers. *Mol Biosyst* 5:787–792
54. Kaur H, Babu BR, Maiti S (2007) Perspectives on chemistry and therapeutic applications of Locked Nucleic Acid (LNA). *Chem Rev* 107:4672–4697
55. Bondensgaard K, Petersen M, Singh SK, Rajwansi VK, Kumar R, Wengel J, Jacobsen JP (2000) Structural studies of LNA: RNA duplexes by NMR: Conformations and implications for RNase H activity. *Chem Eur J* 6:2687–2695
56. Natsume T, Ishikawa Y, Dedachi K, Tsukamoto T, Kurita N (2007) Effect of base mismatch on the electronic properties of DNA-DNA and LNA-DNA double strands: density-functional theoretical calculations. *Chem Phys Lett* 446:151–158
57. Li CX, Li YX, Chen Y, Lin RY, Li T, Liu F, Li N (2016) Modulating the DNA strand-displacement kinetics with the one-sided remote toehold design for differentiation of single-base mismatched DNA. *RSC Adv* 6:74913–74916
58. Hu SC, Li N, Liu F (2018) Combining cooperativity with sequestration: a novel strategy for discrimination of single nucleotide variants. *Chem Commun* 54:3223–3226

59. Zhang DY (2011) Cooperative hybridization of oligonucleotides. *J Am Chem Soc* 133:1077–1086
60. Simon AJ, Vallee-Belisle A, Ricci F, Watkins HM, Plaxco KW (2014) Using the population-shift mechanism to rationally introduce “Hill-type” cooperativity into a normally non-cooperative receptor. *Angew Chem Int Edit* 53:9471–9475
61. Squires TM, Messinger RJ, Manalis SR (2008) Making it stick: convection, reaction and diffusion in surface-based biosensors. *Nat Biotechnol* 26:417–426
62. Zhang Z, Zeng D, Ma H, Feng G, Hu J, He L, Li C, Fan C (2010) A DNA-Origami chip platform for label-free SNP genotyping using toehold-mediated strand displacement. *Small* 6:1854–1858
63. Subramanian HK, Chakraborty B, Sha R, Seeman NC (2011) The label-free unambiguous detection and symbolic display of single nucleotide polymorphisms on DNA origami. *Nano Lett* 11:910–913
64. Zhong W, Tang W, Fan J, Zhang J, Zhou X, Liu Y (2017) A domain-based DNA circuit for smart single-nucleotide variant identification. *Chem Commun* 55:842–845
65. Zhang DY, Chen SX, Yin P (2012) Optimizing the specificity of nucleic acid hybridization. *Nat Chem* 4:208–214
66. Wang JS, Zhang DY (2015) Simulation-guided DNA probe design for consistently ultraspecific hybridization. *Nat Chem* 7:545–553
67. Chen SX, Zhang DY, Seelig G (2013) Conditionally fluorescent molecular probes for detecting single base changes in double-stranded DNA. *Nat Chem* 5:782–789
68. Chen SX, Seelig G (2016) An engineered kinetic amplification mechanism for single nucleotide variant discrimination by DNA hybridization probes. *J Am Chem Soc* 138:5076–5086
69. Hu S, Tang W, Zhao Y, Li N, Liu F (2017) Ultra-specific discrimination of single-nucleotide mutations using sequestration-assisted molecular beacons. *Chem Sci* 8:1021–1026
70. Li Y, Wang GA, Mason SD, Yang X, Yu Z, Tang Y, Li F (2018) Simulation-guided engineering of an enzyme-powered three dimensional DNA nanomachine for discriminating single nucleotide variants. *Chem Sci* 9:6434–6439
71. Jung C, Ellington AD (2014) Diagnostic applications of nucleic acid circuits. *Acc Chem Res* 47:1825–1835
72. Zhu D, Lu B, Zhu Y, Ma Z, Wei Y, Su S, Wang L, Song S, Zhu Y, Wang L et al (2019) Cancer-specific MicroRNA analysis with a non-enzymatic nucleic acid circuit. *ACS Appl Mater Inter* 11:11220–11226
73. Gao MX, Daniel D, Zou HY, Jiang SX, Lin S, Huang CZ, Hecht SM, Chen SX (2018) Rapid detection of a dengue virus RNA sequence with single molecule sensitivity using tandem toehold-mediated displacement reactions. *Chem Commun* 54:968–971
74. Li CX, Li YX, Xu X, Wang XY, Chen Y, Yang XD, Liu F, Li N (2014) Fast and quantitative differentiation of single-base mismatched DNA by initial reaction rate of catalytic hairpin assembly. *Biosens Bioelectron* 60:57–63
75. Zhao Y, Wang H, Tang W, Hu S, Li N, Liu F (2015) An in situ assembly of a DNA-streptavidin dendrimer nanostructure: a new amplified quartz crystal microbalance platform for nucleic acid sensing. *Chem Commun* 51:10660–10663
76. Xu XT, Liang KY, Zeng JY (2015) Portable and sensitive quantitative detection of DNA based on personal glucose meters and isothermal circular strand-displacement polymerization reaction. *Biosens Bioelectron* 64:671–675
77. Zhou X, Xing D (2012) Amplified electrochemiluminescence detection of nucleic acids by hairpin probe-based isothermal amplification. *Analyst* 137:4188–4192
78. Cui M, Xiao X, Zhao M, Zheng B (2017) Detection of single nucleotide polymorphism by measuring extension kinetics with T7 exonuclease mediated isothermal amplification. *Analyst* 143:116–122
79. Cui M, Feng H, Guo D, Wang D, Zheng B (2017) A droplet-based microfluidic platform for kinetics-based detection of single nucleotide variation at room temperature with large discrimination factors. *Sensor Actuat B-Chem* 253:731–737
80. Xiao X, Wu T, Xu L, Chen W, Zhao M (2017) A branch-migration based fluorescent probe for straightforward, sensitive and specific discrimination of DNA mutations. *Nucleic Acids Res* 45:e90
81. Zhang Z, Hsing IM (2017) Nucleic acid self-assembly circuitry aided by exonuclease III for discrimination of single nucleotide variants. *Anal Chem* 89:12466–12471
82. Zhang Z, Li JL, Yao J, Wang T, Yin D, Xiang Y, Chen Z, Xie G (2016) Energy driven cascade recognition for selective detection of nucleic acids with high discrimination factor at room temperature. *Biosens Bioelectron* 79:488–494

Publisher's Note Springer Nature remains neutral with regard to jurisdictional claims in published maps and institutional affiliations.

Affiliations

Weiyang Tang¹ · Weiye Zhong¹ · Yun Tan¹ · Guan A. Wang² · Feng Li^{2,4} · Yizhen Liu^{1,3}

¹ College of Chemistry and Environmental Engineering, Shenzhen University, Shenzhen, Guangdong, People's Republic of China

² Department of Chemistry, Centre for Biotechnology, Brock University, 1812 Sir Isaac Brock Way, St. Catharines, ON L2S 3A1, Canada

³ Key Laboratory of Analytical Chemistry for Biology and Medicine (Ministry of Education), Wuhan University, Wuhan, China

⁴ College of Chemistry, Sichuan University, Chengdu 610064, China